# BALANCING INTERMOLECULAR INTERACTIONS IN THE DESIGN AND SYNTHESIS OF SUPERMOLECULES

by

NATHAN C. SCHULTHEISS

B.Sc., Missouri State University, 2002
M.Sc., Missouri State University, 2003

AN ABSTRACT OF A DISSERTATION

submitted in partial fulfillment of the requirements for the degree

DOCTOR OF PHILOSOPHY

Department of Chemistry
College of Arts and Sciences

KANSAS STATE UNIVERSITY
Manhattan, Kansas

2007

# Abstract

The directed-assembly of small molecular building-blocks into discrete supermolecules or extended networks through non-covalent intermolecular interactions is an on-going challenge in the field of crystal engineering. This synthetic challenge may be overcome by identifying or establishing a hierarchy of intermolecular interactions which, in turn, may facilitate a modular supramolecular assembly process producing final products in high yields.

A family of three 3-pyridine/amino-pyrimidine supramolecular reactants (SR's) was prepared and allowed to react with aromatic carboxylic acids producing nine 1:1 molecular co-crystals and four 1:1 ionic salts through heteromeric O-H···N/N-H···O or charge-assisted $N–H^{+}\cdots O^{-}$/$N–H\cdots O^{-}$ hydrogen bonds with the amino-pyrimidine binding site. We introduced a Q-value, based on AM1 calculations, to show that the amino-pyrimidine moiety is a superior hydrogen-bond acceptor for an incoming carboxylic acid. The amino-pyrimidine/carboxylic acid synthon resulted 13/13 times (100 % yield) even in the presence of other potentially disruptive intermolecular interactions. However, reacting a 4-pyridine/amino-pyrimidine SR and a carboxylic acid in a 1:2 ratio, resulted in structures containing both acid/amino-pyrimidine and acid/pyridine synthons.

The same family of pyridine/amino-pyrimidine SR's were allowed to react with halogentated benzoic acids in which the amino-pyrimidine/carboxylic acid synthon formed 7/7 times (100 % yield) and halogen bonds (N···I or N···Br) extended the SR/acid dimers into polymeric networks 4/7 times (57 %). These results were rationalized through a hierarchical view of intermolecular interactions consisting of hydrogen and halogen bonds.

Four bifunctional 3-pyridine/amino-pyrimidine or amino-pyridine SR's were reacted with neutral metal complexes producing thirteen crystal structures in which the pyridyl moiety coordinates to the metal center 13/13 times (100 % yield) and amino-pyrimidine···amino-pyrimidine hydrogen bonds link the neighboring metal-ligand complexes 10/13 times (77 % yield) into 1-D or 2-D extended architectures.

Finally, we synthesized and characterized a series of tetra-substituted hydrogen bond donor and acceptor functionalized, *i.e.* pyridyl, amino-pyridine, carboxylic acid, resorcinarene-based cavitands forming deep-walled cavitands through amino-pyridine···carboxylic acid heteromeric synthons and a heterodimeric molecular capsule through pyridyl···carboxylic acid hydrogen bonds. The heterodimeric capsule is only one of three, of its type, characterized crystallographically.

# BALANCING INTERMOLECULAR INTERACTIONS IN THE DESIGN AND SYNTHESIS OF SUPERMOLECULES

by

NATHAN C. SCHULTHEISS

B.Sc., Missouri State University, 2002
M.Sc., Missouri State University, 2003

A DISSERTATION

submitted in partial fulfillment of the requirements for the degree

DOCTOR OF PHILOSOPHY

Department of Chemistry
College of Arts And Sciences

KANSAS STATE UNIVERSITY
Manhattan, Kansas

2007

Approved by:

Major Professor
Dr. Christer Aakeröy

# Abstract

The directed-assembly of small molecular building-blocks into discrete supermolecules or extended networks through non-covalent intermolecular interactions is an on-going challenge in the field of crystal engineering. This synthetic challenge may be overcome by identifying or establishing a hierarchy of intermolecular interactions which, in turn, may facilitate a modular supramolecular assembly process producing final products in high yields.

A family of three 3-pyridine/amino-pyrimidine supramolecular reactants (SR's) was prepared and allowed to react with aromatic carboxylic acids producing nine 1:1 molecular co-crystals and four 1:1 ionic salts through heteromeric O-H···N/N-H···O or charge-assisted $N–H^{+}\cdots O^{-}$/$N–H\cdots O^{-}$ hydrogen bonds with the amino-pyrimidine binding site. We introduced a Q-value, based on AM1 calculations, to show that the amino-pyrimidine moiety is a superior hydrogen-bond acceptor for an incoming carboxylic acid. The amino-pyrimidine/carboxylic acid synthon resulted 13/13 times (100 % yield) even in the presence of other potentially disruptive intermolecular interactions. However, reacting a 4-pyridine/amino-pyrimidine SR and a carboxylic acid in a 1:2 ratio, resulted in structures containing both acid/amino-pyrimidine and acid/pyridine synthons.

The same family of pyridine/amino-pyrimidine SR's were allowed to react with halogentated benzoic acids in which the amino-pyrimidine/carboxylic acid synthon formed 7/7 times (100 % yield) and halogen bonds (N···I or N···Br) extended the SR/acid dimers into polymeric networks 4/7 times (57 %). These results were rationalized through a hierarchical view of intermolecular interactions consisting of hydrogen and halogen bonds.

Four bifunctional 3-pyridine/amino-pyrimidine or amino-pyridine SR's were reacted with neutral metal complexes producing thirteen crystal structures in which the pyridyl moiety coordinates to the metal center 13/13 times (100 % yield) and amino-pyrimidine···amino-pyrimidine hydrogen bonds link the neighboring metal-ligand complexes 10/13 times (77 % yield) into 1-D or 2-D extended architectures.

Finally, we synthesized and characterized a series of tetra-substituted hydrogen bond donor and acceptor functionalized, *i.e.* pyridyl, amino-pyridine, carboxylic acid, resorcinarene-based cavitands forming deep-walled cavitands through amino-pyridine···carboxylic acid heteromeric synthons and a heterodimeric molecular capsule through pyridyl···carboxylic acid hydrogen bonds. The heterodimeric capsule is only one of three, of its type, characterized crystallographically.

# Table of Contents

# List of Figures

# List of Tables

# Acknowledgements

Although only my name appears on the cover of this dissertation, many individuals made it possible for such a piece to be put into production and thus, I am indebted to have been surrounded by such a supporting cast of great scientific minds and encouraging attitudes. These last four years will not quickly be forgotten.

I would like to first thank my Ph. D. advisory committee Professor Eric Maatta, Professor Chris Culbertson, Professor Chris Sorenson, and Professor Larry Glasgow for your valuable time, energy, and insight into making this dissertation as exceptional as possible.

Much of the research, displayed within this dissertation, comes from single-crystal X-ray data, which thanks to Dr. John Desper is generated with a great deal of care and expertise. John is not only a reliable and passionate crystallographer, but also a friend. I also thank Curtis Moore, a friend and graduate student at Wichita State University for collecting ~30 data sets for me over the last year and a half.

I would like to thank the many 'behind-the-scenes' people who made my research and life at KSU easier, Dr. Yasmin Patell, Ms. Earline Dikeman, Mr. Jim Hodgson, Mr. Richard Bachamp, Mr. Tobe Eggers, Mr. Arlon Meek, Ms. Connie Cusimano, and Ms. Donna Wright.

And finally, I would like to express my deepest gratitude to my advisor professor Christer Aakeröy for his continual guidance, patience, and care during my time at KSU. I believe, he is one of the rare advisors that every graduate student dreams of having. I hope that one day I will be as good of a mentor as Christer has been to me.

# Dedication

I would like to dedicate this dissertation to the large scientific family of supramolecular chemists and crystal engineers that have inspired me over the years as well as my family and friends for inspiration outside of the lab and academic arena.

Listed are a few of my scientific heroes that I have gained insight from through publications or presentations, Professor Makoto Fujita, Professor Jean-Marie Lehn, Professor Gautam Desiraju, Professor Julius Rebek Jr., Professor Eric Bosch, and Professor Christer Aakeröy. Each of these individuals has in some manner, grown my excitement and passion for supramolecular chemistry.

Finally and most importantly, thanks be to God…the author and perfecter of my faith, who for the joy set before him endured the cross, scorning its shame, and sat down at the right hand of the throne of God.

Hebrews 12:2

Quoting Dr. Henry F. Schaefer, who's words I could not say better, "The significance and joy in my science comes in those occasional moments of discovering something new and saying to myself, 'So that's how God did it!' My goal is to understand a little corner of God's plan."

# Preface

Research carried out at Kansas State University for this dissertation led to the following publications in scientific journals.

Aakeröy, Christer B.; Schultheiss, Nate; Desper, John. "Synthesis and hydrogen-bond capabilities of an amino-pyridine functionalized cavitand", *CrystEngComm*, **2007**, *9*, 211.

Aakeröy, Christer B.; Schultheiss, Nate; Desper, John, Moore, Curtis. "Balancing intermolecular hydrogen-bond interactions for the directed assembly of binary 1:1 co-crystals", *New Journal of Chemistry*, **2006**, *30*, 1452.

Aakeröy, Christer B.; Schultheiss, Nate; Desper, John. "A pyridyl-functionalized cavitand: Starting point for hydrogen-bond driven assembly of heterodimeric capsules", *CrystEngComm*, **2006**, *8*, 502.

Aakeröy, Christer B.; Schultheiss, Nate; Desper, John. "C-pentyltetra(3-pyridyl)cavitand: A versatile building block for the directed-assembly of hydrogen-bonded heterodimeric capsules", *Organic Letters*, **2006**, *8*, 2607.

Aakeröy, C.B.; Schultheiss, N. Assembly of molecular solids via non-covalent interactions, in "Making Crystals by Design - from molecules to molecular materials, methods, techniques, applications", Wiley-VCH, Eds. F. Grepioni and D. Braga. **2006**.

Aakeröy, Christer B.; Schultheiss, Nate; Desper, John. "Directed supramolecular assembly of Cu(II)-based "paddlewheels" into infinite 1-D chains using structurally bifunctional ligands", *Journal of Chemical Society, Dalton Transactions*, **2006**, *13*, 1627.

Aakeröy, Christer B.; Schultheiss, Nate; Desper, John. "Directed supramolecular assembly of infinite 1-D M(II)-containing chains (M = Cu, Co, Ni) using structurally bifunctional ligands", *Inorganic Chemistry*, **2005**, *44*, 4983.

# CHAPTER 1 - Assembly of molecular solids via non-covalent interactions

## 1.1 Introduction

### *1.1.1 How do we design and build a molecular crystal?*

A central aspect of crystal engineering, which in itself can be viewed as a sub-discipline of supramolecular chemistry, concerns the construction of crystalline materials from discrete molecular building blocks using non-covalent interactions.[1,2] An overriding goal for such efforts is to acquire and develop reliable and practical means for the synthesis of molecular materials with specific and tunable properties.[3] For example, we may want to design materials that can perform chemical separations, or that have non-linear optical,[4] magnetic,[5] or catalytic properties.[6] In order to obtain non-linear optical materials, individual molecules must be organized in a non-centrosymmetric arrangement with appropriately aligned dipole moments, for magnetic materials they must be positioned so that communication between spins is facilitated and optimized, and for chemical separations the host-material must be able to selectively entrap molecules or ions. In other words, if we wish to build functional materials, we must be able to control *how* molecular building blocks can be assembled into architectures with desirable connectivity and precisely defined metrics. Supramolecular synthesis is a pro-active process – molecular building blocks are typically designed such that directional intermolecular interactions are expressed as specific structural consequences and it may therefore be more appropriate to describe targeted supramolecular synthesis as "directed-assembly" instead of "self-assembly".

### *1.1.2 The power of covalent synthesis*

For more than a century, synthetic chemists have devised a vast number of reactions allowing more and more complicated compounds to be made using elaborate processes.[7] Today we are capable of making extraordinary molecules that rival some of Nature's best efforts when it comes to structural complexity.[8,9] Covalent synthesis has become such a powerful discipline[8,9] partly because organic chemists have been able to establish reproducible links between molecular structure, reactivity, and reaction pathways through systematic studies of organic

reactions. The explicit correspondence between molecular structure and function has provided a plethora of "named reactions" that collectively create an invaluable toolbox for covalent synthesis. Individual reactions can often be described in a brief, yet fully comprehensive manner -- "…this is the transformation of A into B, by treatment with X and Y". These recipes, often involving specific catalysts and reagents that facilitate coupling reactions between two different molecular fragments through the making and breaking of covalent bonds, play an essential role in every aspect of synthetic chemistry. In contrast, supramolecular synthesis[8] has yet to reach the same level of sophistication,[2,10,11] and despite much progress we do not yet have access to a 'dictionary' that allows us to translate from molecular structure to supramolecular assembly.

Chemistry is the science of communication and change, and these interrelated processes are primarily initiated and controlled by reversible interactions between molecules. Consequently, the behavior of an assembly of molecules, be it in solution or in the solid phase, is determined by cooperative intermolecular communication. Unfortunately, our understanding of many fundamental physical properties as displayed by relatively simple crystalline materials, *e.g.* color, solubility, and thermal stability, is still rudimentary. This lack of comprehension and control stems from an incomplete insight into the forces that determine molecular recognition, binding, and multi-molecular association.[12,13,14,15,16] Crystal engineering is still at the stage where much experimentation is concerned with *how* to control assembly.[10,17] Thus, predicting and controlling the competition between intermolecular forces such as weak and strong hydrogen bonds, halogen-halogen interactions, π···π contacts, van der Waals forces, etc. are part of every crystal engineering effort. The challenge comes down to the following: how do we unravel the bundle of often inter-related interactions and identify strong, directional, reliable non-covalent interactions? How do we develop a reliable synthetic protocol for supramolecular synthesis?

### *1.1.3 The case for supramolecular chemistry*

*"...the emerging science of supramolecular chemistry represents a natural extension of the science of molecular chemistry".*[18]

Nicholas J. Turro

Despite the inherent difficulties with using weak forces as primary synthetic tools, considerable progress has been made, and the preponderance of strategies for supramolecular

synthesis prompted Desiraju[19] to introduce the term "supramolecular synthon". Synthons describe the precise recognition events that take place when molecules assemble into supermolecules and provide an important illustration of the conceptual similarities between retrosynthetic organic synthesis and supramolecular assembly.[20]

Identifying supramolecular synthons is clearly as important to crystal engineering as is an understanding of reaction mechanisms and reagents in conventional covalent synthesis. It is essential to find the limits and conditions under which intermolecular recognition can be used to reliably assemble structures with specific topologies. Such insight is most effectively obtained through systematic structural studies, and recent developments in crystallography/diffraction hardware and software have provided unprecedented access to structural information both in terms of sheer numbers of new crystal structures and the type (size/quality) of samples that can be examined.

This introductory Chapter outlines some advances that have been made specifically through the use of hydrogen-bond interactions in the directed assembly of organic molecular solids with desirable and well-defined supramolecular connectivity.[21] However, the scope of this Chapter allows us to mention but a fraction of the many efforts that have been put forth, and the main focus will be on extended networks and infinite architectures; directed assembly of discrete entities has been reviewed extensively elsewhere.[22]

This Chapter is broadly divided into two subject areas. First, an overview of strategies for the directed assembly of homomeric 0-D, 1-D, 2-D, and 3-D molecular architectures with specific, pre-determined, and desirable connectivities and metrics is offered. Second, a description of some design principles that have been devised and tested for the assembly of heteromeric molecular solids, is given.

### *1.1.4 Supramolecular synthesis*

Conventional synthesis relies on covalent bonds, which makes it possible to devise assembly processes composed of several independent steps performed in a sequential manner, *e.g.* protection of active groups, followed by coupling reaction, then deprotection, etc. In supramolecular synthesis, on the other hand, the desired product is typically held together by reversible intermolecular interactions[2,10,11] and solution-phase supramolecular chemistry is therefore normally restricted to one-pot processes. A supramolecular “intermediate” cannot

ordinarily be prepared, isolated and then added to another solution in order to perform sequential synthesis and herein lies a challenge at the core of supramolecular synthesis: How to devise reliable synthetic pathways towards sophisticated supramolecular structures if we are frequently confined to one-pot reactions? Is it somehow possible to develop a 'dictionary' that allows us to translate from molecular structure to supramolecular assembly?[19]

## 1.2 Directed assembly of homomeric molecular solids

### *1.2.1 Hydrogen-bond interactions – Essential tools for constructing molecular solids*

The intermolecular interaction that lends itself most readily to chemical or geometric fine-tuning is, arguably, the hydrogen bond, and the strength and directionality of this interaction, as compared to most other intermolecular forces, account for its significance in supramolecular synthesis of molecular solids.[23,24] Many design strategies have relied upon hydrogen-bond complementarity,[2,7,11,10,13,14,15,16,25] which can involve both geometric factors and a suitable balance between the number of hydrogen-bond donors and hydrogen-bond acceptors. Self-complementary homomeric interactions have been studied extensively and they include the well-known carboxylic acid dimer, although other homomeric synthons have also been employed in crystal engineering, Figure 1.1.

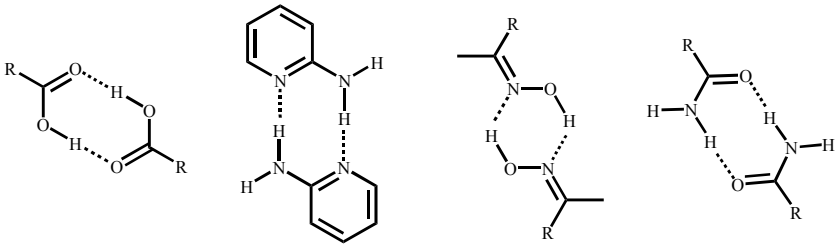

**Figure 1.1** Examples of self-complementary (homomeric) hydrogen-bond interactions.

Not only do these synthons bring molecules together, they also constrain the relative orientation of those components in much the same way as carbon-carbon double bonds impart specific stereochemistry to individual molecules. An increased degree of complementarity (triple,[26] quadruple,[27] or quintuple[28]) will increase selectivity but may also present considerable covalent synthetic challenges; a balance has to be struck in order to develop cost-effective and versatile supramolecular synthesis.

The importance of complementary hydrogen bonds for providing selectivity and specificity in biological processes is also well documented. A crucial consequence of the

commonly occurring eight-membered hydrogen-bonded rings in such systems is that the participating molecules only fit together in one orientation, thereby providing a mechanism for coding and encoding information onto the resulting assembly (*cf.* base pairing in DNA).

## *1.2.2 Hydrogen-bond based assemblies*

### *1.2.2.1 Homomeric 0-D assemblies constructed from hydrogen-bonds*

Carboxylic acids, oximes, diones, and amino-pyridines can all form homomeric 0-D motifs through self-complementary and frequently, symmetry-related hydrogen-bond interactions, Figure 1.2.

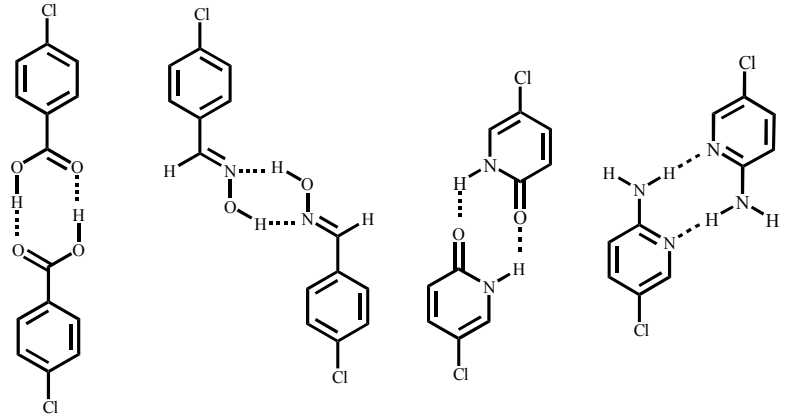

**Figure 1.2** Homomeric 0-D motifs formed from acid, oxime, pyridone, and amino-pyridine dimers.

4-Chlorophenylcarboxylic acid produces a dimer through O-H···O hydrogen bonds,[29] while 4-chlorophenyloxime dimerizes through O-H···N hydrogen bonds.[30] Similarly, 5-chloro-2-pyridone forms a dimer through N-H···O hydrogen bonds,[31] while 2-amino-5-chloropyridine forms a dimer through N-H···N hydrogen bonds.[32] In the absence of other strong hydrogen-bond donors or acceptors such as a pyridine or an –OH moiety, these interactions can be relied upon to appear regardless of the overall shape and size of the molecule to which they are covalently attached. All four functionalities could, in principle, also lead to infinite 1-D assemblies without altering hydrogen-bond connectivities, but such aggregates are generally far less common than their dimeric counterparts. One exemption is noteworthy however. If the oxime is equipped with a strongly electron-withdrawing group on the imine moiety (such as -C≡N) the most likely motif is a 1-D chain (O-H···N≡C-) instead of a dimeric motif involving the imine nitrogen atom as the hydrogen-bond acceptor.

### *1.2.2.2 Hydrogen-bonded homomeric 1-D architectures*

Amides,[33] pyrimidines,[34] dicarboxylic acids,[35] dioximes,[36,37] and dipyridones[38] can all form homomeric 1-D motifs through self-complementary interactions, Figure 1.3.

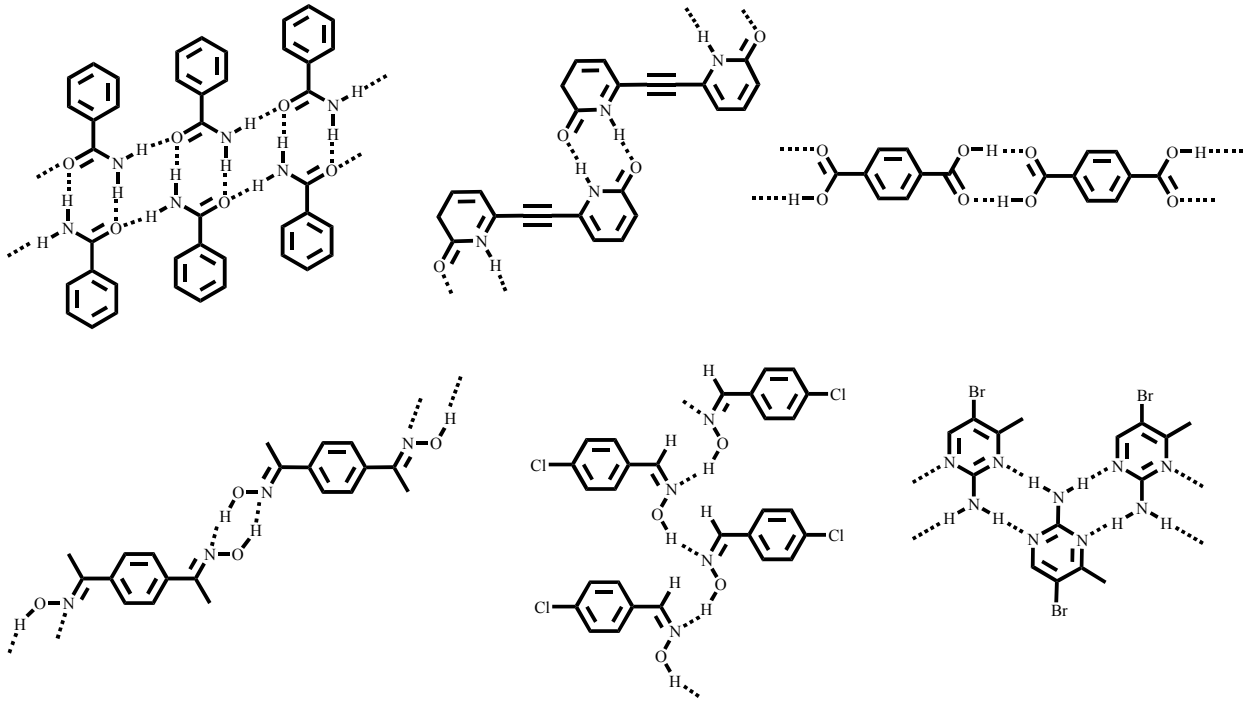

**Figure 1.3** Homomeric 1-D motifs formed from a variety of hydrogen-bond synthons.

Amides frequently combine two unique structural motifs, dimers and catemers, into a well-known 1-D ribbon-like structure. The dimer is constructed from self-complementary N-H···O hydrogen bonds, while the catemeric N-H···O hydrogen bonds result from the *anti*-proton of the amine and the bifurcated carbonyl oxygen atom.

Symmetric dipyridones form 1-D arrays through pairs of N-H···O interactions. Similarly, diacids, both aliphatic and aromatic, commonly produce infinite 1-D chains in the absence of competitive hydrogen-bond acceptors.

Oxime functionalities have the capability of forming either dimers or catemers, both of which result from O-H···N hydrogen bonds. The balance between the two types of motifs is subtle which is illustrated by the fact that 4-chlorophenylaldoxime, which is known to be dimorphic, appears both in a dimeric as well as in a catemeric version in the solid state.[30,37] A search through the CSD of aromatic molecules containing the oxime fragment, revealed approximately twenty 1-D chain motifs, two cyclic motifs, and forty-five dimeric motifs, in the absence of competing moieties.

### *1.2.2.3 Hydrogen-bonded homomeric 2-D architectures*

Any supramolecular synthon can, in principle, provide the basis for molecular building blocks capable of creating extended 2-D architectures. For example, trimesic acid (benzene-1,3,5-tricarboxylic acid) forms hexagonal networks with the aid of self-complementary O-H···O hydrogen bonds,[39] Figure 1.4. These hexagonal sheets are catenated leading to an interpenetrated 3-D framework. Extended 2-D arrays are produced from a variety of symmetrical and unsymmetrical substituted urea and oxalamidecarboxylic acids utilizing acid-acid dimers to form the 1-D chains while further propagation is achieved in two-dimensions through multiple N-H···O hydrogen bonds,[24,40] Figure 1.4. Not surprising, when the acid moiety of the symmetrical substituted ureas and oxalamides is changed to a phenol group, a 2-D sheet is once again formed through a series of O-H···O and N-H···O hydrogen bonds.[41] It has also been shown that pyrazinecarboxamide forms 2-D architectures through multiple N-H···O and C-H···N hydrogen bonds.[42]

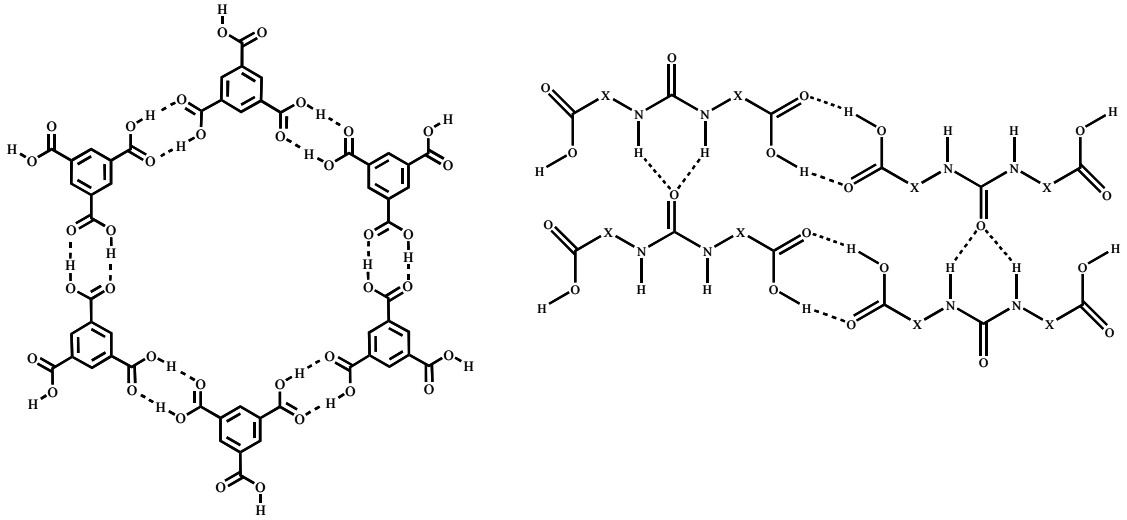

**Figure 1.4** Hydrogen-bonded 2-D architectures comprised of multiple O-H···O and N-H···O hydrogen bonds.

### *1.2.2.4 Hydrogen-bonded homomeric 3-D architectures*

Carboxylic acids, such as adamantane-1,3,5,7-tetracarboxylic acid[43] and tetrapyridones (silane and carbon based),[44,45] have been employed in the construction of 3-D diamondoid networks through self-complementary interactions, Figure 1.5.

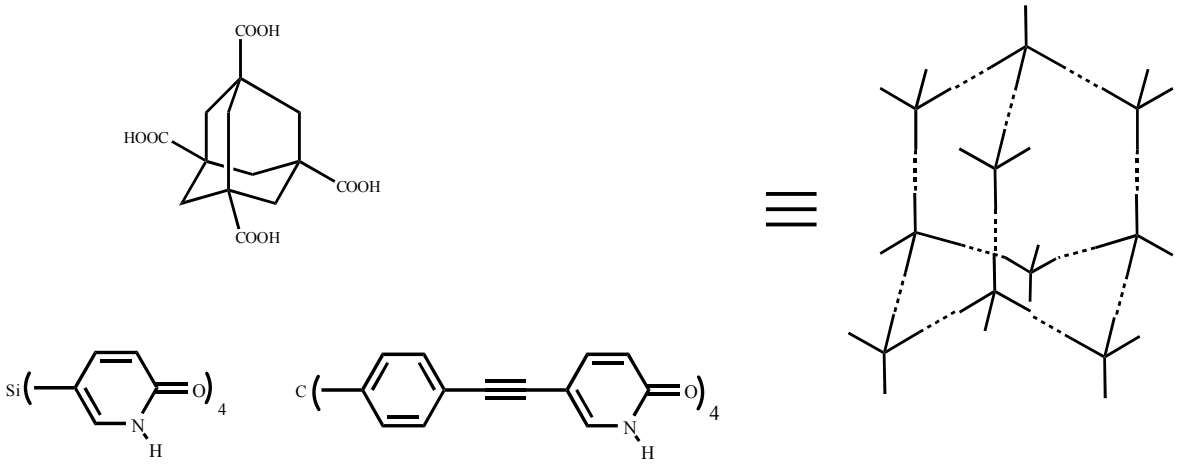


**Figure 1.5** Examples of molecules that form 3-dimensional self-complementary hydrogen-bonded networks.

### *1.2.3 Halogen-bond based assembly strategies*

This section covers structures and assemblies that have been constructed principally through X···X , N···X, and C≡N···X (where X is either Br or I). For information on the nature of such interactions, see recent review articles.[46]

#### *1.2.3.1 Halogen bonds through N···X (X = Br or I)*

4-Iodobenzonitrile and 4-bromobenzonitrile form head-to-tail chains through C≡N···X interactions, Figure 1.6.[47,48]

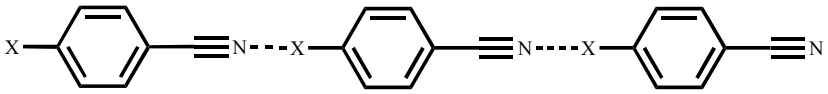


X=I, Br

**Figure 1.6** Homomeric 1-D chains formed from nitrile···halogen interactions.

Fluorination of 4-iodobenzonitrile or 4-bromobenzonitrile molecules leads to shorter C≡N···X distances. This is expected, since the Lewis acidity of the halogen atoms increases due to the electron-withdrawing effects of the four fluorine substituents on the phenyl ring. In changing the halogen to a chloro group, the nitrile···chloro interaction does not form, even with the ring being flourinated.

4-iodopyridine forms 1-D head-to-tail chains through N···I interactions, Figure 1.7.[49] Similarly, 4'-bromo-2',3',5',6'-tetrafluorostilbazole forms 1-D head-to-tail chains through N···Br interactions, Figure 1.7.[50] The N···I and N···Br interactions are fundamentally similar, but the former are significantly stronger. Calculated bond dissociation energies (kcal) display a 2-fold increase for interactions between 1,4-diiodotetrafluorobenzene and a nitrogen containing heterocycle compared to the 1,4-dibromotetrafluorobenzene analog.[51]

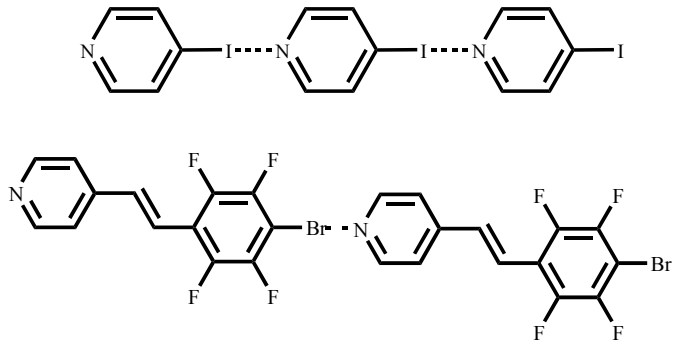


**Figure 1.7** Homomeric 1-D chains formed from nitrogen···iodo or bromo interactions.

### *1.2.3.2 Halogen···halogen interactions*

A variety of halogen···halogen interactions have been used to guide the orientation of molecular building blocks in homomeric solids. For example, 1,4-dihalogenated aryls (X = Cl, Br, I) often give rise to two-dimensional sheets through bifurcated halogen···halogen interactions, Figure 1.8.[52,53,54]

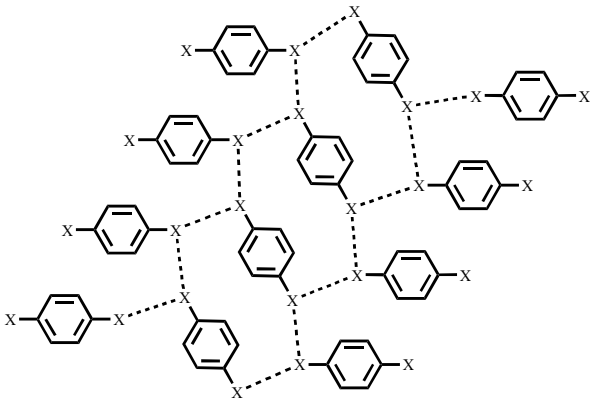


**Figure 1.8** Extended 2-D sheets produced from bifurcated halogen···halogen interactions.

Fluorinated compounds do behave much differently compared to their heavier congeners. Desiraju has proposed that F···F interactions are unlikely to play a structure-directing role and, instead, fluorine atoms prefer to interact weakly with neighboring C-H protons forming C-H···F

interactions.[55] Interestingly, Dunitz has reported, based on molecular modeling and CSD searches, that organic fluorine atoms hardly ever accept a hydrogen atom to form C-H···F interactions and therefore, should not be regarded as a weak hydrogen bond.[56]

Halogen···halogen interactions have also been used to design more complex architectures, and the crystal structure determination of 1,3,5,7-tetraiodoadamantane reveals the presence of a 3-D diamondoid-like network established through multiple iodo···iodo interactions.[57,58]

## 1.3 Design and synthesis of heteromeric solids

### *1.3.1 Co-crystals: Solid-state targets for non-covalent synthesis*

What is the most likely outcome when a solution containing different molecular solutes is allowed to evaporate to dryness? Unless a chemical reaction driven by the formation of covalent bonds takes place between the solutes, one would normally expect the appearance of separate molecular solids. This is a demonstration of the innate structural selfishness of molecules,[59] and it is utilized every time recrystallization is employed as a method of purification. Recrystallizations are performed on a daily basis in every synthetic laboratory around the world but in the supramolecular laboratory, however, the very same process provides the supramolecular chemist with an opportunity to move in a completely different direction. A co-crystallization is an attempt at bringing together different molecular species within one periodic crystalline lattice without making or breaking covalent bonds. Recrystallization and co-crystallization processes are essentially only distinguishable by their intents. The goal of the former is a homomeric product, whereas the latter procedure strives for a heteromeric product. In general, the odds are stacked firmly in favor of the former, Figure 1.9, so how do we go about developing reliable, effective, and versatile synthetic methods for the directed assembly of molecular co-crystals?

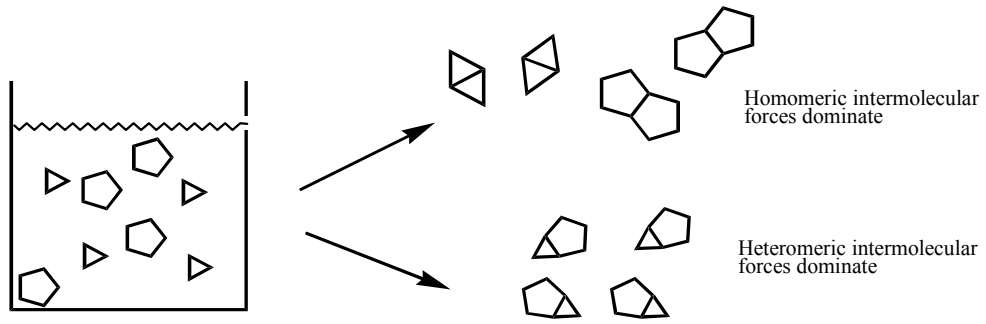


**Figure 1.9** Recrystallization (homomeric) or co-crystallization (heteromeric)?

Since a crystalline material can be constructed in an enormous number of ways, these recognition mechanisms are extraordinarily selective and, consequently, each crystal structure contains important information about the way in which intermolecular forces compete and collaborate and eventually create an energetically balanced system. The use of co-crystallizations for studying hydrogen-bond motifs and intermolecular forces, was brought to the forefront by Etter and co-workers.[60,61,62,63] By introducing several molecular species to the same solution, followed by systematic structural studies, one can begin to identify patterns of behavior, structural selectivity, and trends in recognition and binding that will furnish an improved understanding of the balance between solvent-solute and solute-solute interactions.

### *1.3.1.1 Nomenclature*

Crystal engineering is a highly interdisciplinary area, which to some extent explains why unambiguous definitions and systematic nomenclatures have yet to be fully developed. The term co-crystal is not well-defined, and the existing literature contains terms such as molecular complexes, co-crystals, molecular adducts, molecular salts, clathrates, inclusion compounds, etc., that are often meant to describe one and the same family of chemical compounds. The purpose of this Chapter is not to suggest definitions or to comment on the recent debate on nomenclature,[64] but it is necessary to define the scientific scope of this overview. Thus, the primary subject matter of this next section will be delineated with the aid of the following provisions:

1. Only compounds constructed from discrete neutral molecular species will be considered as co-crystals and solids containing ions, including complex transition-metal ions, are excluded from this overview.

2. Co-crystals are made from reactants that are solids at ambient conditions.[65] Therefore all hydrates and other solvates are excluded which, in principle, eliminates compounds that are typically classified as clathrates or inclusion compounds (where the guest is a solvent or a gas molecule).
3. A co-crystal is a structurally homogeneous crystalline material that contains two or more neutral building blocks that are present in definite stoichiometric amounts.

At this point we are essentially left with two families of compounds: binary charge-transfer complexes and hydrogen-bonded or halogen-bonded co-crystals. This section will focus almost exclusively upon representatives from the latter categories.[66] The terms "binary/ternary supermolecule" indicates a discrete species with predictable and desirable connectivity, constructed from two/three different molecular species and assembled via directional non-covalent forces.[67,68,69,70,71,72,73,74,75,76,77]

Despite the abundance of papers dealing with all aspects of design and assembly of organic extended networks with desirable connectivities and shapes, it remains exceedingly difficult to bring more than two different molecular species into one crystalline lattice, without making or breaking covalent bonds.

### *1.3.2 Developing hydrogen-bond design strategies for synthesis of co-crystals*

The reliability of and competition between synthons are most effectively determined through systematic database studies,[42,78,79] not through detailed analyses of individual structures. Etter and co-workers[62,80] were pioneers in this area, and after extensive studies of preferential hydrogen-bond patterns in organic crystals they presented the following empirical 'rules' as a guide to the deliberate design of hydrogen-bonded solids;

(i) All good proton donors and acceptors are involved in hydrogen bonding.[81]
(ii) Six-membered ring intramolecular hydrogen bonds form in preference to intermolecular hydrogen bonds.
(iii) The best proton donor and acceptor remaining after intramolecular hydrogen bond formation will form intermolecular hydrogen bonds.

These guidelines are based upon observed correlations between hydrogen-bond patterns and functional groups and generally, as a proton increases in acidity, its donor properties will improve. The second rule derives from competition studies showing that intramolecular

hydrogen bonds are more difficult to break than comparable intermolecular bonds formed from similar donors. The third rule can be illustrated by examining the structure of 2-aminopyrimidine/carboxylic acid co-crystals, where the best donors (acidic proton) are paired with the best acceptors (ring nitrogen atom),[60] Figure 1.10.

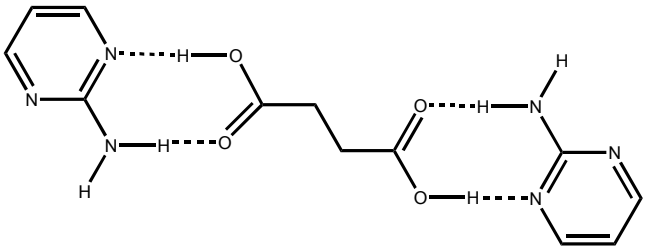

**Figure 1.10** The primary hydrogen bonds in co-crystals of 2-aminopyrimidine and dicarboxylic acids.

### *1.3.2.1 Examples of binary hydrogen-bonded co-crystals*

There are, strictly speaking, no "discrete" aggregates within a solid-state framework but it is nevertheless convenient to classify an assembly as being 0-D, 1-D, 2-D, or 3-D depending upon the type of intermolecular interactions that are present between and within an array of molecules.

Some examples of 0-D assemblies, Figure 1.11, in co-crystals include heteromeric carboxylic acid:carboxylic acid dimers (1:1),[82] pyridine:carboxylic acid dimers (1:1),[83] 2-aminopyrimidine:carboxylic acid trimers (1:2),[84] pyridine:dihydroxybenzene trimers (2:1),[85] bipyridine:carboxylic acid trimers (1:2),[72] 2-aminopyrimidine:carboxylic acid tetramers (2:2),[84,86] bipyridine:resorcinol tetramers (2:2),[73] 3,5-dinitrobenzoic acid:nicotinic acid tetramers (2:2),[87] *iso*nicotinamide:carboxylic acid tetramers (2:2),[88] 2-pyridone:carboxylic acids pentamers (4:1),[89] melamine:thymine tetramers (1:3),[90] melamine:barbital hexamers (3:3),[91] and tripenylphosphine oxide with a variety of hydrogen-bond donors (1:1).[61,92,93]

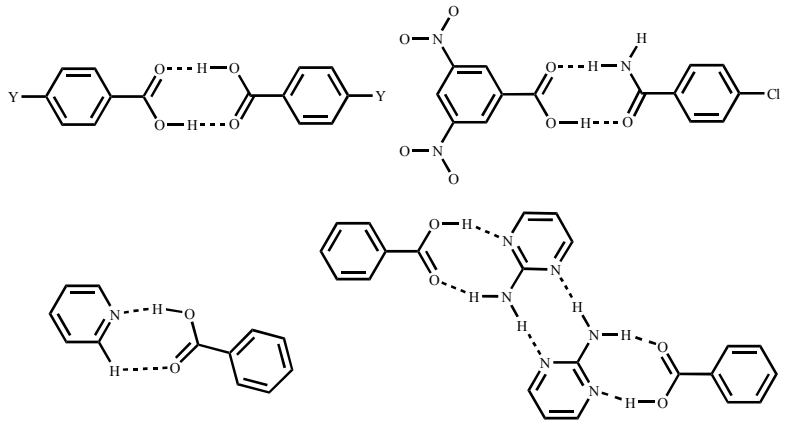

**Figure 1.11** Four 0-D motifs found in co-crystals created by heteromeric hydrogen-bond interactions.

Examples of co-crystals containing chains, ribbons, and other infinite 1-D motifs, Figure 1.12, include: bipyridine:dihydroxybenzene,[94] melamine:cyanuric acid,[95] bipyridine:(fluorinated)dibromobenzene,[96] bipyridine:(diiodobenzene, tetraiodoethylene or diiodine),[97] 2-aminopyridine:dicarboxylic acids,[98] triaminopyrimidine:barbituric acid,[71] 2-aminopyrimidine:dicarboxylic acid,[60] 1,2,3-trihydroxybenzene:hexamethylenetetramine,[99] diols:diamines,[100] *bis*-benzimidazole:dicarboxylic acids,[101] and 2-amino-5-nitropyrimidine:2-amino-3-nitropyridine.[102]

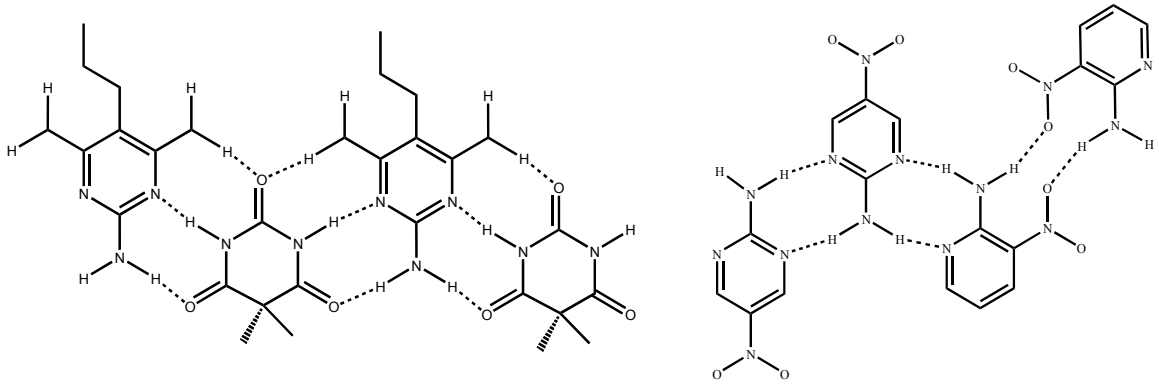

**Figure 1.12** Examples of 1-D motifs generated by heteromeric hydrogen-bond interactions.

Many infinite 2-D assemblies have also been constructed including (but not limited to): piperazine:carboxylic acid,[103] trithiocyanuric:bipyridine,[104] pyridyloxamide:dicarboxylic acid,[105] picolylaminocyclohexenone:dicarboxylic acid,[106] triazine:uracil,[107] *tris*-(4-

pyridyl)triazine:trimesic acid,[108] bipyridine:ureylene dicarboxylic acid,[75] and *iso*nicotinamide:dicarboxylic acid,[88,109] Figure 1.13.

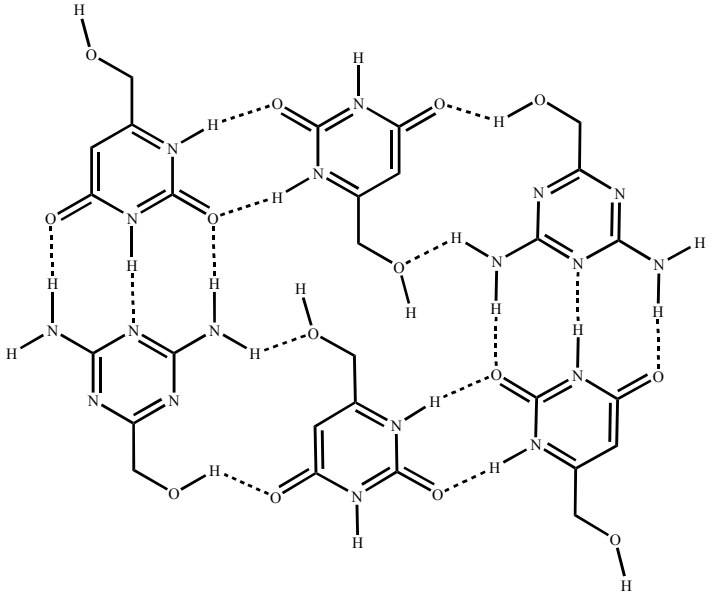

**Figure 1.13** A central hexameric motif in the hydrogen-bonded 2-D network in a diaminotriazine:uracil co-crystal.[107]

Finally, carbamazepine:tetracarboxylic acid-adamantane[110] represents one of the few examples of clearly defined and predictable 3-D motif observed in a hydrogen-bond based binary co-crystal.

### *1.3.3 Heteromeric halogen-bonded co-crystals*

Intermolecular interactions of the type D···X-C, where D = electron donor/halogen-bond acceptor and X = halogen atom/halogen-bond donor, are known to be reliable supermolecular synthons. The strength of the halogen-bond increases with the increase of the Lewis acidity of the acceptor atom, thus I > Br > Cl. Likewise, an increase of the electron density on the electron donor, will strengthen its donor ability, as a result N > O > S. Additionally, many halogen-bond acceptor molecules will contain fluorine atoms; this enhances the acceptor strength of the halogen nuclei, thus strengthening the overall halogen-bond. As shown previously, nitrile moieties can also act as halogen-bond acceptors. An example of this is shown in the 1:1 binary co-crystal of 1,4-dicyanobutane and diiodoperfluorohexane, Figure 1.14.[111]

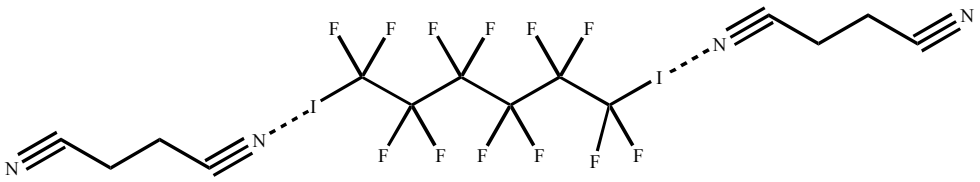

**Figure 1.14** The primary halogen bonds in co-crystals of dicyanoalkyls and diiodoperfluoroalkanes.

4,4'-Bipyridine and 1,4-diiodobenzene crystallize in a 1:1 ratio forming 1-D chains through nitrogen-iodine interactions with N···I distances of 3.023 Å.[51] Similarly, 4,4'-bipyridine and 1,4-diiodotetafluorobenzene produce 1-D chains with N···I distances of 2.851 Å, which is considerably shorter than for the non-fluorinated derivative. Not surprisingly, 4,4'-bipyridine and 1,4-dibromotetrafluorobenzene also form a 1:1 co-crystal containing 1-D chains constructed from nitrogen-bromine interactions with N···Br distances of 2.878 and 2.979 Å, respectively, Figure 1.15.[96]

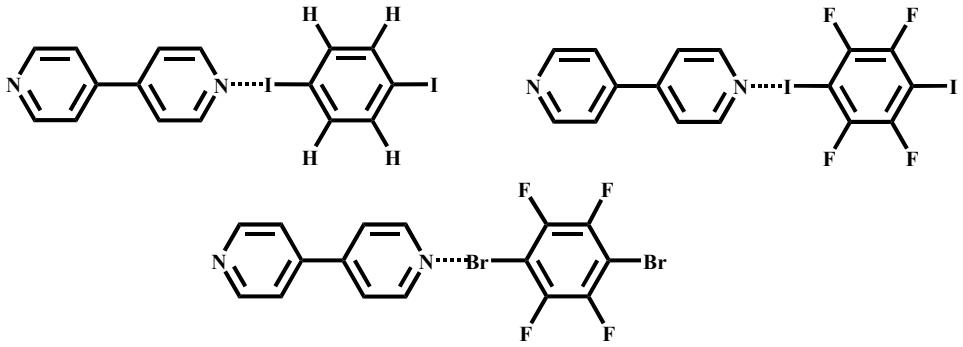

**Figure 1.15** 1-D motifs in co-crystals of 4,4'-bipyridine and 1,4-dihalogenated aryls.

The number of co-crystals assembled primarily through nitrile-halogen or nitrogen-halogen interactions is still small. A search through the CSD showed a total of ten co-crystals containing C≡N···X (X=Br or I) interactions, thirteen with Br···N interactions and fifty-three co-crystals containing N···I contacts.

Finally, some examples of 3-D motifs in halogen-based binary co-crystals include tetrabromoadamantane:hexamethylenetetramine[112] and iodoform:hexamethylenetetramine.[113]

### *1.3.4 Synthesis of co-crystals and the supramolecular yield*

The fact that in the crystal structures of 4-bromo-4'-cyanobiphenyl[114] and 4-bromobenzonitrile[115] the molecular components are aligned in a head-to-tail fashion with

relatively short Br···N contacts indicates that there are stabilizing intermolecular interactions between cyano and bromo moieties,[116] Figure 1.16. However, there is still no example of successful synthesis of binary co-crystals driven by CN···Br interactions. Such interactions can organize molecules within a lattice but have yet to bring about the assembly of heteromeric co-crystals. There is clearly a difference between observing a large number of short-contacts in molecular crystal structures composed of only one type of building blocks and translating such interactions into useful synthetic tools for constructing *heteromeric* architectures.

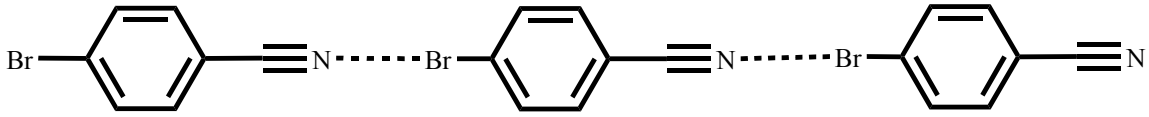


**Figure 1.16** A chain of 4-bromobenzonitrile molecules organized in a head-to-tail manner.

Much current work in organic crystal engineering is now geared towards synthesizing co-crystals using supramolecular reactions based upon reliable synthons and, so far, the vast majority of organic molecular co-crystals has been assembled via conventional, strong hydrogen bonds.[117,118] Weaker hydrogen bonds and many other intermolecular interactions such as nitro···iodo, cyano···nitro, halogen···halogen, *etc.*, have not yet been found to be useful tools for constructing co-crystals. The success and efficiency for any set of supramolecular reactions can be judged by the frequency of occurrence of desired intermolecular interactions and connectivities in the resulting solid. The probability that a certain motif will appear in a crystalline lattice is, in many ways, a measure of the *yield of a supramolecular reaction*. Just as a covalent synthetic chemist searches for ways in which a specific reaction can be promoted or prevented, a supramolecular chemist tries to identify the experimental regime where a synthon prevails despite competition from other non-covalent forces.

### *1.3.5 Heteromeric interactions are better than homomeric interactions*

A survey of hydrogen bonded co-crystals in the CSD[119] reveals that most of them have been prepared using strategies that utilize suitable combinations of chemical entities (or functional groups) located on different molecules, such that they would prefer to interact and bind heteromerically, Figure 1.17, rather than with themselves.[70,74,76,77,120]

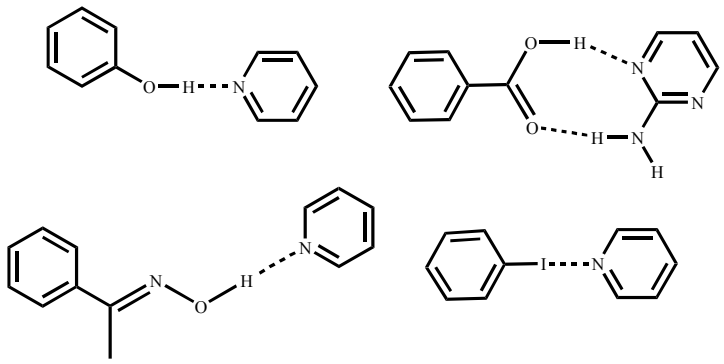

**Figure 1.17** Four dimeric motifs constructed via heteromeric intermolecular interactions.

The most widely used synthons for the directed assembly of binary co-crystals have contained a carboxylic acid in combination with a suitable N-containing heterocycle. For example, there are currently three co-crystals in the CSD with pyrazine,[121] seven with phenazine,[122] sixteen with 4,4'-bipyridine,[123] one with pyrimidine,[124] and nine co-crystals with either azapyrine, quinoline, phenantroline[125] and a benzoic acid-based counterpart. In every case, the expected/intended carboxylic acid···N(heterocycle), O-H···N, hydrogen bond is present. For slightly more complex heterocycles (*i.e.* with added substituents capable of hydrogen bonding) the results are still very consistent; 11 of 12 carboxylic acid:isonicotinamide co-crystals contain an acid···pyridine interaction[126] – a good example of a high-yielding supramolecular reaction.

There are, in fact, very few occurrences of binary hydrogen-bond based co-crystals that do not contain a primary intermolecular interaction between the two different molecules. Two such examples include 4-nitrobenzamide:pyrazinecarboxamide (1:1)[69] and 3,5-dintrobenzoic acid:4-(*N,N*-dimethylamino)benzoic acid (1:1).[127] The latter is a rare example of a carboxylic acid···carboxylic acid co-crystal that contains two homomeric dimers instead of one heteromeric dimer.[128]

The overriding conclusion from the extensive data available in the CSD is clear. In order to convince two different discrete chemical species to coexist in a molecular co-crystal there needs to be some specific molecular-recognition based reason for their solid-state union.[88] Although individual structures that defy rationalization will appear from time to time, there is no doubt that the important 'big picture' reveals structural trends, patterns of behavior, and

reproducible motifs that, when combined, can be developed into a library of high-yielding supramolecular reactions.

## 1.4 Functional materials from supramolecular chemistry

### *1.4.1 Co-crystalline Active Pharmaceutical Ingredients (API's)*

Drug bioavailability is governed by solubility, tableting behavior, filterability, and bulk density of a drug, which are determined by size and particle shape, and all these aspects are related to the internal structure of the solid. Thus, developing versatile approaches for modulating the internal structure of solid-API's, without compromising the overall structural integrity through breaking or forming covalent bonds, is advantageous. Such approaches have traditionally included crystal form manipulations *i.e.* polymorph, hydrate, and salt formations in order to improve physiochemical properties.[129] Another technique, although in its infancy, is the engineering of pharmaceutical co-crystals, through directed-supramolecular synthesis.[130] Forming API containing co-crystals has a number of potential advantages over the previously mentioned approaches, in which a few are listed; (1) potentially all API's (basic, acidic, and non-ionizable) may be used within a co-crystalline reaction, not just ionizable species which are necessary in salt-formation, (2) products obtained from a co-crystallization experiment are often controllable and reliable, while the formation of polymorphs, hydrates, and solvates are usually serendipitous, and (3) a large number of non-toxic co-crystal formers (chemicals included within the GRAS, Generally Recognized As Safe, list)[131] can be incorporated within the crystalline or amorphous solid.

Thus, co-crystallization reactions between predesigned, inexpensive, and readily available small molecules (co-crystal formers), combined with API's may allow for subtle changes in bulk-physical properties, *i.e.* solubility, morphology, and stability, without altering the inherent biological activity in the API. Furthermore, the following case study displays how co-crystalline products formed from various API's and suitable co-crystal formers alter the overall physiochemical properties of the bulk starting material.

#### *1.4.1.1 Improving caffeine hydration stability through co-crystals*

Caffeine (1,3,7-trimethyl-1*H*-purine-2,6(3*H*,7*H*)-dione) is a central nervous system and metabolic stimulant, which can temporarily increase alertness and reduce fine motor

coordination. This particular compound exhibits instability, with regards to humidity, changing from either of the anhydrous forms (α or β) to the nonstoichiometric hydrate when the relative humidity (RH) is between 75 and 98 %.[132] Therefore, atmospheric moisture is of considerable concern and must be controlled throughout each stage of processing, formulation, packaging, and storage in order not to jeopardize the desired solid drug substance.

Pure caffeine is known to exist in two anhydrous crystal forms and one crystalline nonstoichiometric hydrate form.[133] Furthermore, one pharmaceutically acceptable caffeine salt has been generated, a hydrochloride dihydrate,[134] as well as several pharmaceutically active co-crystals (1:1 caffeine:sulfacetamide,[135] 1:1 caffeine:sulfaproxyline,[136] and a 1:1 caffeine:barbital).[137] Recently, a systematic study was carried out to test the stability of co-crystals containing caffeine and pharmaceutically acceptable co-crystal formers, upon exposure to various RH percentages. Anhydrous caffeine was allowed to co-crystallize with di-aliphatic carboxylic acids, Figure 1.18, and their RH stability was determined.

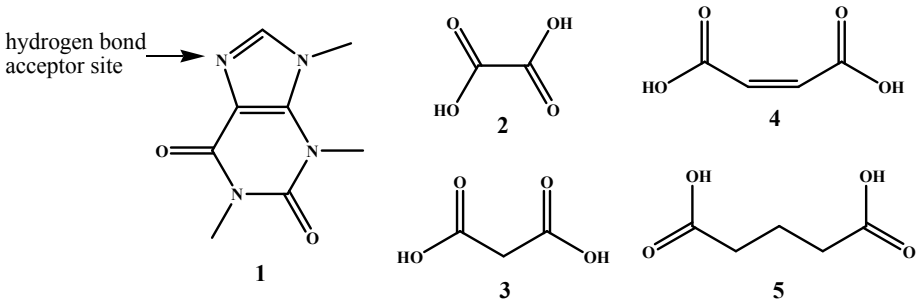


**Figure 1.18** API, caffeine 1 (showing hydrogen bonding acceptor site), alongwith co-crystal formers oxalic acid 2, malonic acid 3, maleic acid 4, and glutaric acid 5.

Co-crystals, caffeine:oxalic acid **A** and caffeine:malonic acid **B** crystallized in a 2:1 stoichiometric ratio, while caffeine:maleic acid **C** and caffeine:glutaric acid **D** crystallized in a 1:1 ratio. RH stability results were carried out on each co-crystal **A**-**D** and compared to the standard anhydrous β-caffeine sample. Pure caffeine exhibits instability between 75 and 98 % RH after just one day, however, co-crystal **A** showed a high stability even after 7 weeks at 98% RH. Co-crystalline product **B**, displayed a slightly improved stability compared to pure caffeine, whereas **C** and **D** did not improve the overall moisture absorption, compared to anhydrous caffeine.

### *1.4.2 Porous materials*

Up to this point, the focus has been on assembling purely-organic based building blocks into solid-state architectures through robust hydrogen bond interactions, however the metal-ligand coordination bond is another type of interaction utilized in binding and organizing individual entities into supermolecules. Over the past several decades porous supramolecular networks have been extensively studied,[138] and potential properties for such networks lie in, but are not limited to, molecular storage or separations, magnetism, conductivity, and catalysis.[139] Porous architectures have primarily been constructed through connecting ligands (linkers) to metal ions (nodes), forming the desired discrete or extended topological product. This type of design rational becomes very powerful, due to the vast variety of ligand designs, *i.e.* placement and number of donor atoms on the linkers, and the large number of metal ions and clusters at ones disposal.

A decade ago, Fujita *et. al* constructed a $M_6L_4$ discrete octahedron complex[140] from four exo-tridentate triangular ligands, 2,4,6-*tris*(4-pyridyl)-1,3,5-triazine, and six *cis*-capped square planar units, [enPd$X_2$] (en = ethylenediamine, X = Cl, $NO_3$ etc.), Figure 1.19. This compound is now commercially available,[141] and has found applications in size-selective molecular storage[142] and catalysis.[143]

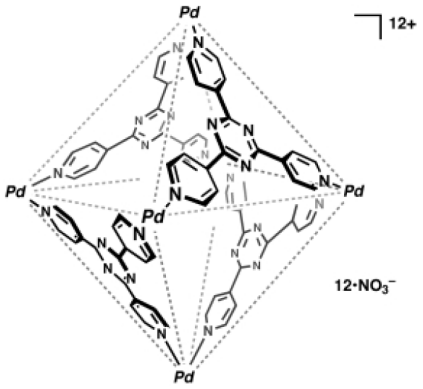


**Figure 1.19** Cartoon displaying the structural arrangement of the four 2,4,6-*tris*(4-pyridyl)-1,3,5-triazine ligands and the six *cis*-capped palladium units within the octahedron complex.

In 1998, Yaghi reported his first crystalline porous metal-organic framework (MOF).[144] MOF's are very attractive compounds due to their high surface area 2000-7000 $m^2/g$, stability at high temperatures > 450 °C, isolation in high yields using inexpensive starting materials, and ability to capture gases, such as $CH_4$, $CO_2$, $N_2$, $H_2$, and Ar.[145] More recently, Yaghi's group

constructed crystalline metal-organic polyhedra (MOP) where the pore size and functionality can be systematically varied. The design strategy includes the directed-assembly of sulfate-capped oxygen-centered iron-carboxylate trimers, $Fe_3O(CO_2)_3(SO_4)_3$ as nodes and either phenyl, biphenyl, tetrahydropyrene, or terphenyl as the organic linker, Figure 1.20.

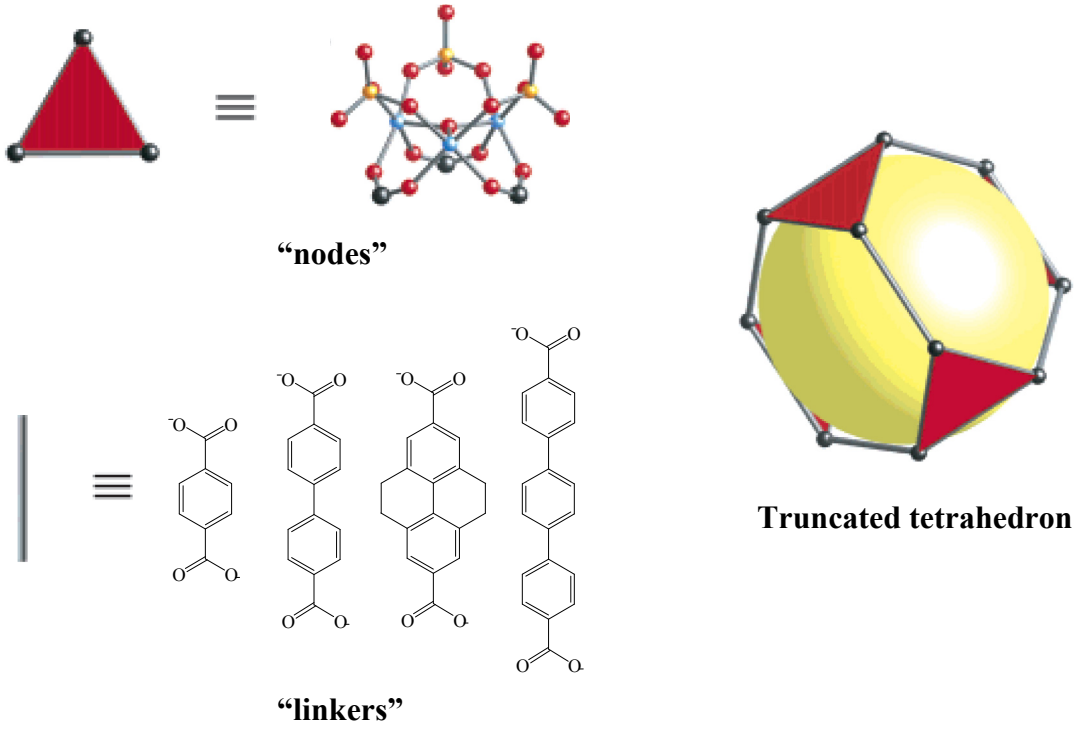


**Figure 1.20** Formation of a truncated tetrahedron upon mixing a stoichiometric ratio of nodes and linkers.

It is reported that the total open space (including inside the pore and between pores) in these crystals ranges from 46.3 to 76.4 %![146]

Even within the crystalline phase, coordination networks can exhibit dynamic porosity, Figure 1.21, due to their construction not only through coordinate covalent bonds, but also in combination with much weaker intermolecular interactions *e.g.* hydrogen bonds, π-π stacking etc.

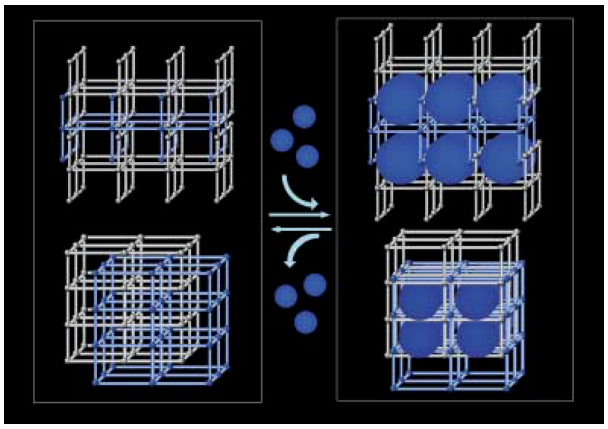

**Figure 1.21** An example of a dynamic framework. In the top example, the gaps are created with respect to the incoming guest molecules, while in the bottom example the framework interunit space depends solely on the guest molecules.

One such 3-dimensional network, consisting of $Cu^{II}$, benzene-1,4-dicarboxylate, and 4,4'bipyridine, reported by Kitagawa *et al*., displays dynamic porous properties upon gas-adsorption ($CO_2$, $CH_4$, $O_2$, and $N_2$) and desorption.[147,148]

Although less abundant, purely organic-based porous assemblies have also been constructed, primarily through self-complementary hydrogen-bonds. Wuest *et al*. have designed a series of tetrasubstituted silanes, Figure 1.22, which form 3-dimensional porous networks.[149]

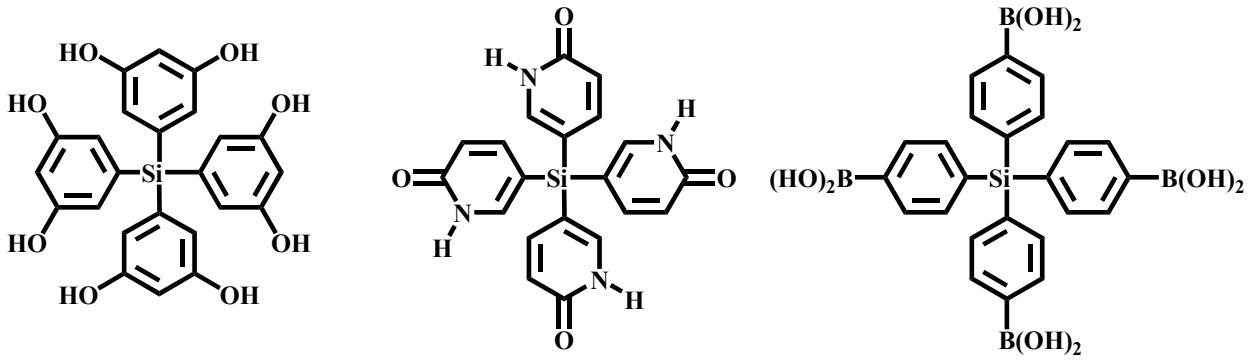


**1** **2** **3**

**Figure 1.22** Three tetrasubstituted silanes: **1** *tetrakis*(3,5-dihydroxyphenyl)silane, **2** *tetrakis*(4-pyridone)silane, **3** *tetrakis*(4-phenylboronic acid)silane.

Upon recrystallization, **1** forms an open diamondiod framework in which 45 % of the crystalline volume is accessible to guests, while **2** has ~60 % and **3** has 64 % of its internal volume accessible to guest molecules, Figure 1.23.

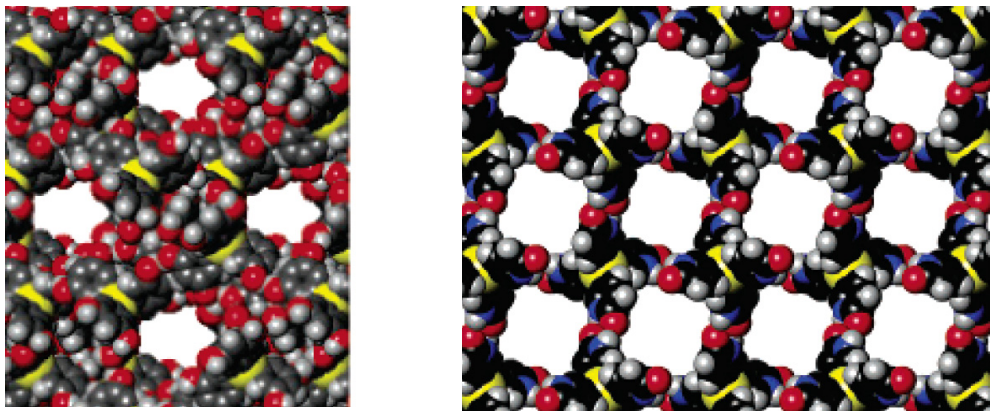

**Figure 1.23** Open frameworks constructed through recrystallization of ligand **1** (left) and ligand **2** (right).

## 1.5 In summary…

Even though molecular recognition is typically associated with molecules in solution, such interactions are also responsible for organizing molecules in the solid state. Translating principles of molecular recognition to solid-state assembly of heteromeric molecular solids is of key importance to the development of versatile and reliable strategies for practical supramolecular synthesis. In this Chapter we have tried to present some transferable supramolecular design strategies based upon a hierarchy of intermolecular interactions. The effectiveness of these strategies can eventually be evaluated and quantified using the supramolecular yield, Figure 1.24.

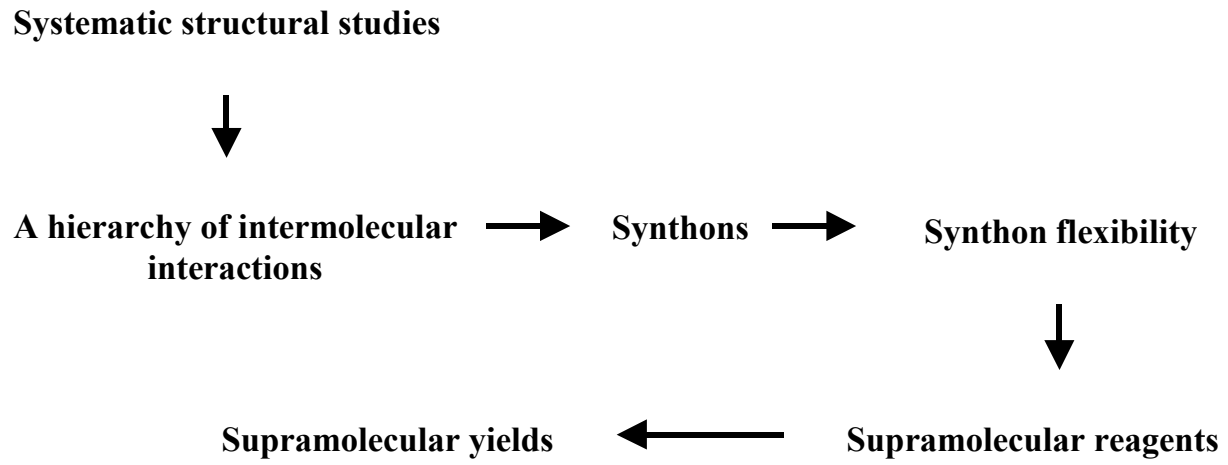


**Figure 1.24** Design, implementation, and evaluation of supramolecular synthesis.

Inevitably, any supramolecular synthetic strategy will fail at some point, but through the power of covalent synthesis we have access to refined tools for modulating the electronic and geometric details of each binding site on a supramolecular reagent such that a variety of chemical functionalities can be targeted for binding. By carefully examining the connections between molecular chemistry and supramolecular reactivity, it may be possible to build a library of SR's that, collectively, is capable of affecting the assembly of new supermolecules with a high degree of specificity and reliability. If we can clear a path towards practical and transferable guidelines for versatile supramolecular synthesis through an improved awareness of the balance and competition between intermolecular interactions, then it is inevitable that much more complex supermolecules and higher-order co-crystals will be synthesized.

### *1.5.1 Goals*

The goals of this thesis center on predictably organizing molecular building-blocks into supermolecules through reliable and robust intermolecular interactions. A theme throughout the following Chapters will be to establish a better understanding of the directed-assembly process as it pertains to: 1) supramolecular synthetic strategies based upon a hierarchy of hydrogen-bond driven patterns, 2) establishing a hierarchical assembly approach through hydrogen and halogen bonding, 3) constructing inorganic-organic hybrid materials, and 4) designing hydrogen-bond functionalized cavitand-based capsules.

#### *1.5.1.1 Supramolecular synthetic strategies based upon a hierarchy of hydrogen-bond driven patterns*

One of Etters rules states that all hydrogen bonds will form in a hierarchical fashion *i.e.* best-donor to best acceptor, second-best donor to second best-acceptor, etc. We plan to examine the competition and balance between a family of ditopic pyridine/amino-pyrimidine based molecular SR's and their hydrogen bonding ability with various aromatic mono-carboxylic acids (Chapters 2 and 3). This study will allow us to determine hydrogen-bond preferences in the presence of multiple competing synthons.

#### *1.5.1.2 Establishing a hierarchical assembly approach through hydrogen and halogen bonding*

A hierarchical approach must be established in order to rationally design any supramolecular product in which multiple and thus competing synthons exist. Within the literature, only one example exists of an architecture in which its assembly is driven by the formation of primary hydrogen bonds and secondary halogen interactions. We will employ the family of pyridine/amino-pyrimidine SR's in attempts to form predictable supermolecular products through combinations of both hydrogen and halogen bonds (Chapter 4). Within these systems, we want to determine if iodine acts as a better halogen bond donor than bromine, as well as if binding abilities increase upon fluorination of the aryl ring.

#### *1.5.1.3 Constructing inorganic-organic hybrid materials*

Directed assembly of linear M(II)-complexes (M = Cu, Co and Ni) into infinite chains by combining anionic chelating ligands (for controlling the coordination geometry) with bi-functional ligands containing a metal-coordinating pyridyl moiety and a self-complementary amino-pyrimidine hydrogen-bonding moiety will be explored (Chapter 5). We plan to employ anionic ligands for the four equatorial-coordination sites leaving room for the bi-functional ligand to coordinate in the two axial positions, while further extending the ligand-metal complex into infinite 1-D chains through amino-pyrimidine/amino-pyrimidine self-complementary hydrogen bonds.

#### *1.5.1.4 Designing hydrogen-bond functionalized cavitand-based capsules*

Molecular capsules containing enforced cavities possess many useful properties within host-guest chemistry namely: catalysis, molecular sensing, molecular transport, stabilization of reactive intermediates, et cetera. The construction of cavity-bearing compounds has primarily been achieved through metal-ligand interactions or hydrogen bonds, although the latter has been much less explored. Cavitands are a class of rigid, bowl-shaped molecules, which will be appended with hydrogen bond functionalities and utilized in the building of heteromeric nano-sized molecular capsules (Chapter 6 and 7).

# References


[1] (a) Lehn, J.-M. *Angew. Chem. Int. Ed. Engl.* **1990**, *29,*1304; (b) Desiraju, G. R. *Crystal Engineering: The Design of Organic Solids*, Elsevier, Amsterdam, 1989; (c) Sharma, C. V. K. *J. Chem. Ed.* **2001**, *78*, 617; (d) Atwood, J. L.; Davies, J. E. D.; MacNicol, D. D.; Vögtle, F.; Suslick, K. S. (Eds.), *Comprehensive Supramolecular Chemistry,* Elsevier, Oxford, 1996; (e) Steed, J. W.; Atwood, J. L. Supramolecular Chemistry: An Introduction, J.Wiley & Sons, Chichester, 2000.

[2] Aakeröy, C. B. Acta Crystallogr. **1997**, *B53*, 569.

[3] (a) Desiraju, G. R. *Nature* **2001**, *412*, 397; (b) Coronado, E.; Galan-Mascaros, J. R.; (c) Gomez-Garcia, C. J.; Laukhin, V. *Nature* **2000**, *408,* 447.

[4] (a) Muthuraman, M.; Masse, R.; Nicoud, J.-F.; Desiraju, G. R. *Chem. Mater.* **2001**, *13*, 1473; (b) König, O.; Burgi, H.-B.; Armbruster, T.; Hulliger, J.; Weber, T. *J. Am. Chem. Soc.* **1997**, *119*, 10632.

[5] (a) Kahn, O. *Acc. Chem. Res.* **2000**, *33*, 1; (b) Miller, J. S. *Inorg. Chem.* **2000**, *39*, 4392.

[6] (a) Aoyama, Y. *Topics Curr. Chem*. **1998**, *198*, 131; (b) Bassani, B. M.; Darcos, V.; Mahony, S.; Desvergne, J.-P. *J. Am.Chem. Soc.* **2000**, *122*, 8795.

[7] Lehn, J.-M. *Supramolecular Chemistry*, VCH, Weinheim, 1995.

[8] Corey, E. J. *Chem. Soc. Rev*. **1988**, *17*, 111.

[9] Nicolaou, K. C.; Sorensen, E. J. *Classics in total synthesis*, Wiley-VCH, Weinheim, 1996.

[10] Moulton, B.; Zaworotko, M. J. *Chem. Rev*. **2001**, *101*, 1629.

[11] Desiraju, G. R. *Acc. Chem. Res*. **2002**, *35*, 565.

[12] Holman, K. T.; Pivovar, A. M.; Swift, J. A.; Ward, M. D. *Acc. Chem. Res*. **2001**, *34*, 107; *Crystal engineering: From molecules and crystals to materials*, A NATO Advanced Study Institute and a Euroconference, (Eds. D. Braga, F. Grepioni and A.G. Orpen) Erice,Italy, 1999, *58*.

[13] Aakeröy, C. B.; Beatty, A. M. *Aus. J. Chem.* **2001**, *54*, 409.

[14] Hosseini, M. W. *CrystEngComm* **2004**, *6*, 318.

[15] MacGillivray, L. *CrystEngComm* **2004**, *6*, 77.

[16] Brammer, L. *Chem. Soc*. *Rev*. **2004**, *33*, 476.

[17] (a) Prins, L. J.; Reinhoudt, D. N.; Timmerman, P. *Angew. Chem. Int. Ed.* **2001**, *40*, 2382; (b) Sherrington, D. C.; Taskinen, K. A.; *Chem. Soc. Rev.* **2001**, *30*, 83; (c) Whitesides, G. M.; Simanek, E. E.; Mathias, J. P.; Seto, C. T.; Chin, D. N.; Mammen, M.; Gordon, D. M. *Acc. Chem. Res.* **1995**, *28*, 37.

[18] Turro, N. J. *Chem. Commun.* **2002**, 2279.

[19] Desiraju, G. R. *Angew. Chem. Int. Ed. Engl.* **1995**, *34*, 2311.

[20] Nangia, A.; Desiraju, G. R. *Acta Crystallogr.* **1998**, *A54*, 934.

[21] An extensive discussion on 'weaker' or unconventional hydrogen bonds is provided by Steiner, T.; Desiraju, G. R. in 'The Weak Hydrogen Bond in Structural Chemistry and Biology', Oxford University Press, New York, 1999.

[22] (a) Conn, M. M.; Rebek, J. *Chem. Rev.* **1997**, *97*, 1647; (b) Lawrence, D. S.; Jiang, T.; Levett, M. *Chem. Rev.* **1995**, *95*, 2229; (c) Stang, P.; Olenyuk, B. *Acc. Chem. Res.* **1997**, *30*, 502; (d) Fujita, M. *Chem. Soc. Rev*. **1998**, *27*, 417; (e) Linton, B.; Hamilton, A. D. *Chem. Rev.* **1997**, *97*, 1669.

[23] (a) Seto, C. T.; Whitesides, G. M. *J. Am. Chem. Soc.* **1991**, *113,* 712; (b) Aakeröy, C. B.; Seddon, K. R. *Chem. Soc. Rev.* **1993**, *22*, 397; (c) Subramanian, S.; Zaworotko, M. J. *Coord. Chem. Rev.* **1994**, *137,* 357; (d) Lehn, J.-M.; Mascal, M.; DeCian, A.; Fischer, J. *J. Chem. Soc., Perkin Trans. 2*, **1992**, 461.

[24] Zhao, X.; Chang, Y.-L.; Fowler, F. W.; Lauher, J. W. *J. Am. Chem. Soc.* **1990**, *112*, 6627.

[25] (a) Caulder, D. L.; Raymond, K. N. *Acc. Chem. Res.* **1999**, *32*, 975; (b) Reinhoudt, D. N.; Crego-Calama, M. *Science* **2002**, *295*, 2403; (c) Lehn, J.-M. *Science* **2002**, *295*, 2400.

[26] Marsh, A.; Silvestri, M.; Lehn, J.-M. *Chem. Commun*. **1996**, 1527.

[27] Beijer, F. H.; Kooijman, H.; Spek, A. L.; Sijbesma, R. P.; Mejer, E. W. *Angew. Chem. Int. Ed. Engl.* **1998**, *37*, 75.

[28] Jaunky, W.; Hosseini, M. W.; Planeix, J. M.; De Cian, A.; Kyritsakas, N.; Fischer, J. *Chem. Commun.* **1999**, 2313.

[29] (a) Toussaint, J. *Acta Crystallogr*. **1951**, *4*, 71; (b) Miller, R. S.; Paul, I. C.; Curtin, D. Y. *J. Am. Chem. Soc.* **1974**, *96*, 6334; (c) Colapietro, M.; Domenicano, A. *Acta Crystallogr. Sect. B.* **1982**, *38*, 1953; (d) Takazawa, H.; Ohba, S.; Saito, Y. *Acta Crystallogr. Sect. B*. **1989**, *45*, 432.

[30] (a) Folting, K.; Lipscomb, W. M.; Jerslev, B. *Acta Crystallogr*. **1964**, *17*, 1263; (b) Arte, E.; Declercq, J. P.; German, G.; van Meerssche, M. *Bull. Soc. Chim. Belg*. 1980, *89*, 155.

[31] Kvick, Å.; Booles, S. S. *Acta Crystallogr. Sect. B*. **1972**, *28*, 3405.

[32] (a) Kvick, Å.; Backeus, M. *Acta Crystallogr. Sect. B*. **1974**, *30*, 474; (b) Kvick, Å.; Thomas, R.; Koetzle, T. F. *Acta Crystallogr. Sect. B*. **1976**, *32*, 224.

[33] Penfold, B. R.; White, J. C. B. *Acta. Crystallogr*. **1959**, *12*, 130.

[34] Aakeröy, C. B.; Desper, J.; Elisabeth, E.; Helfrich, B. A.; Levin, B.; Urbina, J. F. *Z. Kristallogr*. **2005**, *220*, 325.

[35] Bailey, M.; Brown, C. J. *Acta. Crystallogr*. **1967**, *22*, 387.

[36] Burton, E. A.; Brammer, L.; Pigge, F. C.; Aakeröy, C. B.; Leinen, D. *New. J. Chem.* **2003**, *27*, 1084.

[37] Jensen, K. G. *Acta. Chem. Scand*. **1970**, *24*, 3293.

[38] Ducharme, Y.; Wuest, J. D. *J. Org. Chem*. **1988**, *53*, 5787.

[39] Duchamp, D. J.; Marsh, R. E. *Acta. Crystallogr., Sect. B*. **1969**, *25*, 5.

[40] (a) Chang, Y.-H.; West, M.-A.; Fowler, F. W. Lauher, J. W. *J. Am. Chem. Soc*. **1993**, *115*, 5991; (b) Coe, S.; Kane, J. J.; Nguyen, T. L.; Toledo, L. M.; Wininger, E.; Fowler, F. W.; Lauher, J. W. *J. Am. Chem. Soc*. **1997**, *119*, 86.

[41] Nguyen, T. L. Scott, A.; Dinkelmeyer, B.; Fowler, F. W. Lauher, J. W. *New J. Chem*. **1998**, *2*, 129.

[42] Leiserowitz, L. *Acta Crystallogr*. **1976**, *B32*, 775.

[43] Ermer, O. *J. Am. Chem. Soc*. **1998**, *110*, 3747.

[44] Saied, O.; Maris, T.; Wuest, J. D. *J. Am. Chem. Soc*. **2003**, *125*, 14956.

[45] (a) Wang, X.; Simard, M.; Wuest, J. D. *J. Am. Chem. Soc*. **1994**, *116*, 12119; (b) Simard, M.; Su, D.; Wuest, J. D. *J. Am. Chem. Soc*. **1991**, *113*, 4696.

[46] (a) Metrangolo, P.; Neukirch, H.; Pilati, T.; Resnati, G. *Acc. Chem. Res*. **2005**, *38*, 386; (b) Metrangolo, P.; Resnati, G. *Chem.--Eur. J*. **2001**, *12*, 2511.

[47] Desiraju, G. R.; Harlow, R. L. *J. Am. Chem. Soc*. **1989**, *111*, 6757.

[48] Bond, A. D.; Griffiths, J.; Rawson, J. M.; Hulliger, J. *Chem Commun*. **2001**, 2488.

[49] Ahrens, B.; Jones, P. G. *Acta Crystallogr., Sect. C. Cryst. Struct. Commun*. **1999**, *55*, 1308.

[50] Lucassen, A. C. B. Vartanian, M.; Leitus, G.; van der Boom, M. *Cryst. Growth Des*. **2005**, *5*, 1671.

[51] Walsh, R. B.; Padgett, C. W.; Metrangolo, P.; Resnati, G.; Hanks, T. W.; Pennington, W. T. *Cryst. Growth Des*. **2001**, *1*, 165.

[52] Hinchliffe, A.; Munn, R. W.; Pritchard, R. G.; Spicer, C. J. *J. Mol. Struct*. **1985**, *130*, 93.

[53] Maiga, A.; Haget, Y.; Cuevas-Diarte, M. A. *J. Appl. Crystallogr.* **1984**, *17*, 210.

[54] Estop, E.; Alvarez-larena, A.; Belaaraj, A.; Solans, X.; Labrador, M. *Acta Cryst. C*, **1997**, *53*, 1932.

[55] Thalladi, V. R.; Weiss, H.-C.; Blaser, D.; Boese, R.; Nangia, A.; Desiraju, G. R. *J. Am. Chem. Soc*. **1998**, *120*, 8702.

[56] (a) Dunitz, J. D. *ChemBioChem*. **2004**, *5*, 614; (b) Dunitz, J. D.; Schweizer, W. B. *Chem. Eur. J*. **2006**, 12, 6804.

[57] Bremer, M.; Gregory, P. S.; Schleyer, P. V. R. *J. Org. Chem*. **1989**, *54*, 3796.

[58] Pedireddi, V. R.; Reddy, D. S.; Goud, B. S.; Craig, D. C.; Rae, A. D.; Desiraju, G. R. *J. Chem. Soc. Perkin Trans. 2* **1994**, 2353.

[59] Dunitz, J. D. in *Perspectives in Supramolecular Chemistry: The Crystal as a Supramolecular Entity*, ed. G.R. Desiraju, Wiley, Amsterdam, 1995.

[60] Etter, M. C.; Adsmond, D. A. *J. Chem. Soc., Chem. Commun.* **1990**, 589.

[61] Etter, M. C.; Baures, P. W. *J. Am. Chem. Soc.***1988**, *110*, 639.

[62] Etter, M. C. *Acc. Chem. Res.* **1990**, *23*, 120.

[63] Etter, M. C. *J. Phys. Chem*. **1991**, *95*, 4601.

[64] (a) Desiraju, G. R. *CrystEngComm*, **2003**, *5*, 466; (b) Dunitz, J. D. *CrystEngComm*, **2003**, *5*, 506.

[65] This requirement may be deemed overly restrictive but it does offer an important distinction between solvates and co-crystals. However, in same cases, notably in the work by Boese and co-workers, it is clear that in their elegant work using low-temperature crystallizations they intentionally prepare co-crystals with a very clear and deliberate strategy (see e.g. Kirchner, M. T.; Boese, R.; Gehrke, A.; Blaeser, D. *CrystEngComm*. **2004**, *6*, 360.)

[66] For information about charge-transfer compounds, see (a) Okamoto, Y.; Brenner, W. *Organic Semiconductors*, Rheinhold, 1964; (b) Akamatsu, H.; Inokuchi, H.; Matsunaga, Y. *Nature* **1954**, *173*, 168; (c) Sun, D.; Rosokha, S. V.; Kochi, J. K. *Angew. Chem., Int. Ed*. **2005**, *44*, 5133.

[67] (a) Shan, S.; Batchelor, E.; Jones, W. *Tet. Lett.* **2002**, *43*, 8721; (b) Vishweshwar, P.; Thaimattam, R.; Jaskolski, M.; Desiraju, G. R. *Chem. Commun.* **2002**, 1830; (c) Vishweshwar, P.; Nangia, A.; Lynch, V. M. *CrystEngComm*. **2003**, *5*; (d) Almarsson, Ö.; Zaworotko, M. J. *Chem. Commun.* **2004**, 1889.

[68] (a) Desiraju, G. R.; Sarma, J. A. R. P. *Chemical Comm*. **1983**, 45; (b) Pan, F.; Wong, W. S.; Gramlich, V.; Bosshard, C.; Gunter, P. *Chem. Commun.* **1996**, 2; (c) Pedireddi, V. R.; Jones, W.; Chorlton, A. P.; Docherty, R. *Chem. Commun*. **1996**, 997; (d) Dale, S. H.; Elsegood, M. R. J.; Hemmings, M.; Wilkinson, A. L. *CrystEngComm* **2004**, *6*, 207; (e) Pedireddi, V. R.; PrakashaReddy, J.; Arora, K. K. *Tet. Lett.* **2003**, *44*, 4857.

[69] Aakeröy, C. B.; Desper, J.; Helfrich, B. A. *CrystEngComm* **2004**, *6,* 19.

[70] Aakeröy, C. B.; Beatty, A. M.; Nieuwenhuyzen, M.; Zou, M.; *Tetrahedron* **2000**, *56*, 6693.

[71] Lehn, J.-M.; Mascal, M.; DeCian, A.; Fischer, J. *J. Chem. Soc., Chem. Commun.* **1990**, 479.

[72] Bailey Walsh, R. D.; Bradner, M. W. Fleischman, S.; Morales, L. A.; Moulton, B.; Rodriguez-Hornedo, N.; Zaworotko, M. J. *Chem. Commun*. **2003**, 186.

[73] MacGillivray, L. R.; Reid, J. L.; Ripmeester, J. A. *J. Am. Chem. Soc.* **2000**, *122*, 7817.

[74] Zerkowski, J. A.; MacDonald, J. C.; Whitesides, G. M. *Chem. Mater*. **1997**, *9*, 1933.

[75] Kane, J. J.; Liao, R.-F.; Lauher, J. W.; Fowler, F. W. *J. Am. Chem. Soc.* **1995**, *117*, 12003.

[76] Vishweshwar, P.; Nangia, A.; Lynch, V. M. *J. Org. Chem.* **2002**, *67*, 556.

[77] Huang, C.; Leiserowitz, L.; Schmidt, G. M. *J. Chem. Soc., Perkin Trans. 2* **1973**, 503.

[78] Allen, F. A.; Raithby, P. R.; Shields, G. P.; Taylor, R. *Chem. Commun*. **1998**, 1043.

[79] (a) Ermer, O.; Neudörfl, J. *Helv. Chim. Acta.* **2001**, *84*, 1268; (b) Leiserowitz, L.; Tuval, M. *Acta Crystallogr.* **1978**, *B34*, 1230.

[80] Etter, M. C.; Frankenbach, G. M. *Chem. Mater.* **1989**, *1*, 10.

[81] This observation was first made by Donohue J. *J. Phys. Chem.* **1952**, *56*, 502.

[82] Sarma, J. A. R. P.; Desiraju, G. R. *J. Chem. Soc., Perkin Trans. 2* **1985**, 1905.

[83] Sugiyama, T.; Meng, J.; Matsuura, T. *J. Mol. Struct.* **2002**, *611*, 53.

[84] Lynch, D. E.; Smith, G.; Freney, D.; Byriel, K. A.; Kennard, C. H. L. *Aust. J. Chem.* **1994**, *47*, 1097.

[85] Nassimbeni, L. R.; Su, H.; Weber, E.; Skobridis, K. *Cryst. Growth Des.* **2004**, *4*, 85.

[86] Lynch, D. E.; Latif, T.; Smith, G.; Byriel, K. A.; Kennard, C. H. L.; Parsons, S. *Aust. J. Chem.* **1998**, *51*, 403.

[87] Zhu, J.; Zheng, J.-M. *Chin. J. Struct. Chem*. **2004**, *23*, 417.

[88] Aakeröy, C. B.; Beatty, A. M.; Helfrich, B. A. *J. Am. Chem. Soc.* **2002**, *124*, 14425.

[89] Aakeröy, C. B.; Beatty, A. M.; Zou, M. *Cryst. Eng.* **1998**, *1*, 225.

[90] Lange, R. F. M.; Beijer, F. H.; Sijbesma, R. P.; Hooft, R. W. W.; Kooijman, H.; Spek, A. L.; Kroon, J.; Meijer, E. W. *Angew. Chem., Int. Ed,* **1997**, *36*, 969.

[91] Zerkowski, J. A.; Seto, C. T.; Whitesides, G. M. *J. Am. Chem. Soc*. **1992**, *114*, 5473.

[92] (a) Antipin, M. Y.; Akhmedov, A. I.; Struchkov, Y. T.; Matrosov, E. I.; Kabachnik, M. I. *Zh. Strukt. Khim.* **1983**, *24*, 86; (b) Lynch, D. E.; Smith, G.; Byriel, K. A.; Kennard, C. H. L. *Acta Crystallogr., Sect. C: Cryst. Struct. Commun.* **1993**, *49*, 718.

[93] Etter, M. C.; Panunto, T. W. *J. Am. Chem. Soc.* **1988**, *110*, 5896.

[94] Glidewell, C.; Ferguson, G.; Gregson, R. M.; Lough, A. J. *Acta Crystallogr., Sect. C: Cryst. Struct. Commun.* **1999**, *55*, 2133.

[95] Ranganathan, A.; Pedireddi, V. R.; Rao, C. N. R. *J. Am. Chem. Soc.* **1999**, *121*, 1752.

[96] De Santis, A.; Forni, A.; Liantonio, R.; Metrangolo, P.; Pilati, T.; Resnati, G. *Chem.--Eur. J.* **2003**, *9*, 3974.

[97] Walsh, R. B.; Padgett, C. W.; Metrangolo, P.; Resnati, G.; Hanks, T. W.; Pennington, W. T. *Cryst. Growth Des.* **2001**, *1*, 165.

[98] Garcia-Tellado, F.; Geib, S. J.; Goswami, S.; Hamilton, A. D. *J. Am. Chem. Soc.* **1991**, *113*, 9265.

[99] Tremayne, M.; Glidewell, C. *Chem. Commun.* **2000**, 2425.

[100] Ermer, O.; Eling, A. *J. Chem. Soc., Perkin Trans. 2* **1994**, 925.

[101] Aakeröy, C. B.; Desper, J.; Leonard, B.; Urbina, J. F. *Cryst. Growth Des.* **2005**, *3*, 865.

[102] Aakeröy, C. B.; Beatty, A. M.; Helfrich, B. A.; Nieuwenhuyzen, M. *Cryst. Growth Des.* **2003**, *3*, 159.

[103] Luo, T.-J. M.; Palmore, G. T. R. *Cryst. Growth Des*. **2002***, 2*, 337.

[104] Pedireddi, V. R.; Chatterjee, S.; Ranganathan, A.; Rao, C. N. R. *J. Am. Chem. Soc.* **1997**, *119*, 10867.

[105] Nguyen, T. L.; Fowler, F. W.; Lauher, J. W. *J. Am. Chem. Soc.* **2001**, *123*, 11057.

[106] Xiao, J.; Yang, M.; Lauher, J. W.; Fowler, F. W. *Angew. Chem., Int. Ed.* **2000**, *39*, 2132.

[107] Beijer, F. H.; Sijbesma, R. P.; Vekemans, J. A. J. M.; Meijer, E. W.; Kooijman, H.; Spek, A. L. *J. Org. Chem.* **1996**, *61*, 6371.

[108] Ma, B.-Q.; Coppens, P. *Chem. Commun.* **2003**, 2290.

[109] Vishweshwar, P.; Nangia, A.; Lynch, V. M. *Cryst. Growth Des.* **2003**, *3*, 783.

[110] Fleischman, S. G.; Kuduva, S. S.; McMahon, J. A.; Moulton, B.; Walsh, R. D. B.; Rodriguez-Hornedo, N.; Zaworotko, M. J. *Cryst. Growth Des*. **2003**, *3*, 909.

[111] Metrangolo, P.; Pilati, T.; Resnati, G.; Stevenazzi, A. *Chem. Commun*. **2004**, 1492.

[112] Reddy, D. A.; Craig, D. C.; Desiraju, G. R. *Chem. Commun*. **1994**, 1457.

[113] Dahl, T.; Hassel, O. *Acta Chem. Scand*. **1970**, *24*, 377.

[114] Kronenbusch, P.; Gleson, W. B.; Britton, D. *Cryst. Struct. Commun.* **1976**, *5*, 17.

[115] Britton, D.; Konnert, J.; Lam, S. *Cryst. Struct. Commun.* **1977**, *6*, 45.

[116] Quast, H.; Gorlach, Y.; Peters, E.-M.; Peters, K.; von Schnering, H. G.; Jackman, L. M.; Ibar, G.; Freyer, A. J. *Chem. Ber*. **1986**, *119*, 1801.

[117] Charge-transfer complexes are not included in this discussion.

[118] Several co-crystals have been constructed from heterocycles like bipyridine or pyrazine and activated iodo-containing compounds; see refs. 51 and 96 in this Chapter.

[119] Allen, F. A. *Acta Crystallogr. Section B* **2002**, *58*, 380.

[120] (a) Pan, F.; Wong, W. S.; Gramlich, V.; Bosshard, C.; Gunter, P. *Chem. Commun.* **1996**, 2; (b) Zerkowski, J. A.; MacDonald, J. C.; Whitesides, G. M. *Chem. Mater*. **1997**, *9*, 9; (c) Liao, R.-F.; Lauher, J. W.; Fowler, F. W. *Tetrahedron*, **1996**, *52*, 3153; (d) Shan, N.; Bond, A. D.; Jones, W.; *Cryst. Eng*. **2002**, *5*, 9; (e) Pedireddi, V. R.; Jones, W.; Chorlton, A. P.; Docherty, R. *Chem. Commun*. **1996**, 997.

[121] CSD codes: OCAYUM, OCASAT, and POFPAB.

[122] CSD codes: GURVOE, GURVUK, LUDFUL, UNECAR, ZUPKUQ, and ZUPLAX.

[123] CSD codes: BEQWAV, FIHYEA, FIJCIK, FIJCUW, HUPPOX, MUFNIK, NOPXIZ, OJENIA, PULWUO, RAPHAR, SUXVOW, UDUZIC, UDOZOI, UHELUO, XUNGIW, and XUNGOC.

[124] CSD code: POFPEF.

[125] CSD codes: CUFSET, LUSWEB, PANYIM, PANZEJ, PAPDIT, PAPFOB, UNEBOE, WUKREZ, and WUKROJ.

[126] CSD codes: AJAKEB, AJAKIF, ASAXOH, ASAXUN, BUDWEC, BUDZUV, BUFBIP, BUFQAU, LUNMEM, LUNMIC, LUNMOW, and VAKTOR.

[127] Sharma, C. V. K.; Panneerselvam, K.; Pilati, T.; Desiraju, G. R. *J. Chem. Soc., Perkin Trans. 2* **1993**, 2209.

[128] Pedireddi, V. R.; Prakash Reddy, J. *Tetrahedron Lett.* **2002**, *43*, 4927.

[129] (a) Stahl, P. H.; Nakano, M. Pharmaceutical aspects of the drug salt form. In *Handbook of Pharmaceutical Salts: Properties, Selection, and Use*; Stahl, P. H., Wermuth, C. G., Eds.; Wiley-VCH/VCHA: New York, 2002; (b) Byrn, S. R.; Pfeiffer, R. R.; Stowell, J. G. *Solid-State Chemistry of Drugs*; SSCI: West Lafayette, IN, 1999; (c) Rodríguez-Spong, B.; Price, C. P.; Jayasankar, A.; Matzger, A. J.; Rodríguez-Hernedo, N. *Adv. Drug. Deliv. Rev.* **2004**, *56*, 241.

[130] (a) Walsh, R. D. B.; Bradner, M. W.; Fleischman, S.; Morales, L. A.; Moulton, B.; Rodríguez-Hernedo, N.; Zaworotko, M. J. *Chem. Commun.* **2003**, 186; (b) Oswald, I. D. H.; Allen, D. R.; McGregor, P. A.; Motherwell, W. D. S.; Parsons, S.; Pulham,C. R. *Acta Crystallogr*. **2002**, *B58*, 1057; (c) Remenar, J. F.; Morissette, S. L., Peterson, M. L.; Moulton, B.; MacPhee, J. M.; Guzman, H. R.; Almarsson, Ö. *J. Am. Chem. Soc*. **2003**, *125*, 8456; (d) Bučar, D. –K.; Henry, R. F.; Lou, X.; Borchardt, T. B.; Zhang, G. G. Z. *Chem. Commun*. **2007**, ASAP.

[131] http://vm.cfsan.fda.gov/~dms/eafus.html

[132] Trask, A. V.; Motherwell, W. D. S.; Jones, W. *Cryst. Growth Des*. **2005**, *5*, 1013.

[133] (a) Griesser, U. J.; Burger, A. *Int. J. Pharm*. **1995**, *120*, 83; (b) Bothe, H.; Cammenga, H. K. *Thermochim. Acta* **1980**, *40*, 29.

[134] Mercer, A.; Trotter, J. *Acta Crystallogr.* **1978**, *B34*, 450.

[135] Leger, J. M., Alberola, S.; Carpy, A. *Acta Crystallogr.* **1977**, *B33*, 1455.

[136] Ghosh, M.; Basak, A. K.; Mazumbar, S. K.; Sheldrick, B. *Acta Crystallogr*. **1991**, *C47*, 577.

[137] Craven, B. M.; Gartland, G. L. *Acta Crystallogr.* **1974**, *B30*, 1191.

[138] (a) Braga, D.; Desiraju, G. R.; Miller, J. S.; Orpen, A. J.; Price, S. L. *CrystEngComm* **2002**, 500-509; (b) Tashiro, S.; Tominaga, M.; Kusukawa, T.; Kawano, M.; Sakamoto, S.; Yamaguchi, K.; Fujita, M. *Angew. Chem., Int. Ed*. **2003**, *42*, 3267-3270; (c) Wu, C-.D.; Lin, W. *Dalton Trans*. **2006**, 4563; (d) Campbell, K.; Kuehl, C. J.; Ferguson, M. J.; Stang, P. J.; Tykwinski, R. R. *J. Am. Chem. Soc*. **2002**, *124*, 7266; (e) Welbes, L. L.; Borovik, A. S. *Acc. Chem. Res*. **2005**, *38*, 765; (f) Batten, S. R.; Robson, R. *Angew. Chem., Int. Ed.* **1998**, *37*, 1460; (g) Moulton, B.; Zaworotko, M. J.; *Chem. Rev*. **2001**, *101*, 1629.

[139] (a) Rowsell, J. L. C.; Yaghi, O. M. *Microporous and Mesoporous Materials* **2004**, *73*, 3; (b) Rowsell, J. L. C.; Millward, A. R.; Park, K. S.; Yaghi, O. M. *J. Am. Chem. Soc*. **2004**, *126*, 5666; (c) Atwood, J. L.; Barbour, L. J.; Dalgarno, S. J.; Hardie, M. J.; Raston, C. L.; Webb, H. R. *J. Am. Chem. Soc.* **2004**, *126*, 13170; (d) Kahn, O. *Acc. Chem. Res*. **2000**, *33*, 1; (e) Chapman, M. E.; Ayyappan, P.; Foxman, B. M.; Yee, G. T.; Lin, W. *Cryst. Growth Des*. **2001**, *2*, 159; (f) Berry, J. F.; Cotton, F. A.; Lei, P.; Murillo, C. A. *Inorg. Chem*. **2003**, *42*, 377; (g) Gumienna-Kontecka, E.; Rio, Y.; Bourgogne, C.; Elhabiri, M.; Louis, R.; Albrecht-Gary, A.-M.; Nierengarten, J.-F. *Inorg. Chem*. **2004**, *43*, 3200; (h) Noveron, J. C.; Arif, A. M.; Stang, P. *J. Chem. Mater*. **2003**, *15*, 372.

[140] Fujita, M.; Oguro, D.; Miyazawa, M.; Oka, H.; Yamaguchi, K.; Ogura, K. *Nature* **1995**, *378*, 469.

[141] Wako Co. Ltd.

[142] (a) Kusukawa, T.; Fujita, M. *Angew Chem., Int. Ed*. **1998**, *37*, 3142; (b) Tashiro, S.; Tominaga, M.; Kawano, M.; Therrien, B.; Ozeki, T.; Fujita, M. *J. Am. Chem. Soc*. **2007**, *127*, 4546; (c) Kusukawa, T., Fujita, M. *J. Am. Chem. Soc*. **1999**, *121*, 1397; (d) Kusukawa, T.; Fujita, M. *J. Am. Chem. Soc*. **2002**, *124*, 13576.

[143] (a) Ito, H.; Kusukawa, T.; Fujita, M. *Chem. Lett*. **2000**, 598; (b) Yoshizawa, M.; Takeyama, Y.; Kusukawa, T.; Fujita, M. *Angew. Chem., Int. Ed*. **2002**, *41*, 1347; (c) Yoshizawa, M.; Takeyama, Y.; Okano, T.; Fujita, M. *J. Am. Chem. Soc*. **2003**, *125*, 3243; (d) Kawano, M.; Kobayashi, Y.; Ozeki, T.; Fujita, M. *J. Am. Chem. Soc*. **2006**, *128*, 6558; (e) Kusukawa, T.; Yoshizawa, M.; Fujita, M. *Angew. Chem., Int. Ed*. **2001**, *40*, 1879.

[144] (a) Li, H.; Davis, C. E.; Groy, T. L.; Kelley, D. G.; Yaghi, O. M. *J. Am. Chem. Soc*. **1998**, *120*, 2186; (b) Li, H.; Eddaoudi, M.; Groy, T. L.; Yaghi, O. M. *J. Am. Chem. Soc*. **1998**, *120*, 8571.

[145] Eddaoudi, M.; Moler, D. B.; Li, H.; Chen, B.; Reineke, T. M.; O'Keeffe, M.; Yaghi, O. M. *Acc. Chem. Res*. **2001**, *34*, 319.

[146] Sudik, A. C.; Millward, A. R.; Ockwig, N. W.; Côté, A. P.; Kim, J.; Yaghi, O. M. *J. Am. Chem. Soc*. **2005**, *127*, 7110.

[147] Kitagawa, S.; Uemura, K. *Chem. Soc. Rev.* **2005**, *34*, 109.

[148] Kitaura, R.; Seki, K.; Akiyama, G.; Kitagawa, S. *Angew. Chem., Int. Ed*. **2003**, *42*, 428.

[149] (a) Saied, O.; Maris, T.; Wang, X.; Simard, M.; Wuest, J. D. *J. Am. Chem. Soc*. **2005**, *127*, 10008; (b) Saied, O.; Maris, T.; Wuest, J. D. *J. Am. Chem. Soc*. **2003**, *125*, 14956; (c) Fournier, J-.H.; Maris, T.; Wuest, J. D.; Guo, W.; Galoppini, E. *J. Am. Chem. Soc*. **2003**, *125*, 1002.

# CHAPTER 2 - Bifunctional pyridine/amino-pyrimidine supramolecular reagents used for designing binary and ternary co-crystals

## 2.1 Introduction

When it comes to the assembly of purely organic supramolecular architectures, synthetic strategies including, but not limited to, hydrogen bonding,[1] halogen bonding,[2] π- stacking,[3] have been employed. The hydrogen bond is a particularly powerful tool due to its strength and directionality, but it can also be fine-tuned electronically and geometrically.[4] For example, a systematic IR study of a series of carboxylic acid···pyridine complexes (in chloroform) showed that even the weakest acid in this sequence, acetic acid, forms a 1:1 dimer with pyridine held together by a short O-H···N hydrogen bond.[5] The potential energy of this hydrogen bond is described by a highly asymmetrical double-minimum curve. With increasing acidity the O-H···N hydrogen bond becomes stronger and the potential energy curve has a more symmetric appearance. For intermolecular interactions of this type, correct qualitative interpretations and trends within related chemical systems can frequently be extracted from a relatively simple electrostatic description of the hydrogen bond.[6]

Etter suggested,[7] that in a system with multiple hydrogen-bond donors and acceptors, the best hydrogen donor will interact with the best hydrogen bond acceptor, and the second-best donor will interact with the second-best acceptor and so forth. To further develop this idea into versatile and reliable synthetic strategies, we have examined the structural reactivity and behavior of a family of new supramolecular reagents (SR's) containing two competing and tunable hydrogen-bonding sites, Figure 2.1. In each case, one end of the molecule contains a pyridine or methoxy-substituted pyridine moiety while the other end contains an amino-pyrimidine functionality.

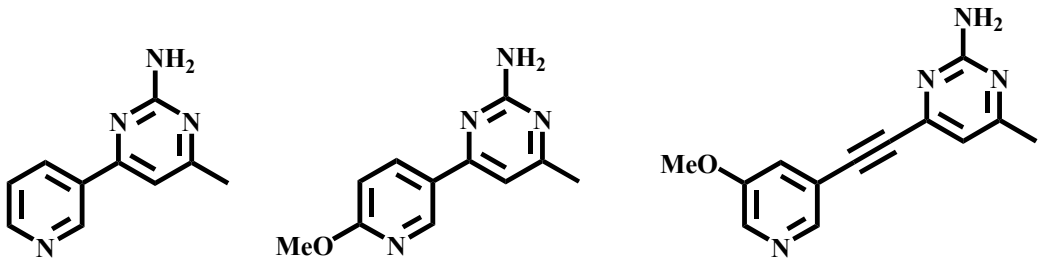


**1** **2** **6**

**Figure 2.1** A series of bifunctional ligands with two distinctly different hydrogen-bonding moieties.

Pyridine is significantly more basic than both pyrimidine and 2-aminopyrimidine, Figure 2.2, and consequently, the former would be expected to form stronger N···H-O hydrogen bonds with an incoming carboxylic acid.

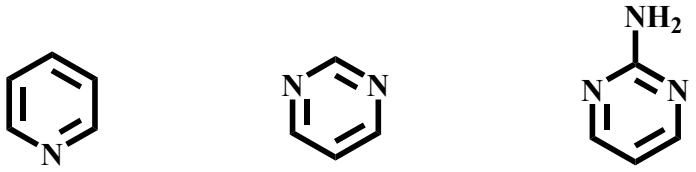


| p$K_a$ | **5.17** | **1.23** | **3.45** |
|---|---|---|---|

**Figure 2.2** Three nitrogen-containing heterocycles, pyridine, pyrimidine and 2-aminopyrimidine, and their experimental p$K_a$ values.[8]

However, since an approaching carboxylic acid can also interact with the hydrogen-bond donor adjacent to the heterocylic nitrogen atom (C-H in the case of pyridine and N-H in the case of 2-aminopyrimidine) it is important to try to quantify the combined effect of both the donor and the acceptor within each hydrogen-bonding functionality. Since hydrogen bonds are primarily electrostatic in nature, the magnitude of the charge on each participating atom is expected to play an important role in determining the structural outcome of any intermolecular event where a variety of different hydrogen-bond interactions may form.

Electrostatic potential surface calculations offer readily available information about the relative differences in charge in the vicinity of all atoms within a molecule, and such data may provide a better indicator than p$K_a$ values for ranking relative hydrogen-bonding abilities of a series of related chemical moieties.[6] For example, AM1-based calculations of the electrostatic potential surfaces of pyridine and 2-aminopyrimidine, Figure 2.3, indicate that the nitrogen atoms in both molecules display electrostatic minima at around -275 kJ/mol, which would make

them equally attractive as hydrogen-bond acceptors. However, if the positive potential for the hydrogen atom on the auxillary hydrogen-bond donor is taken into account (71 kJ/mol for the C-H group on pyridine, and 133 kJ/mol for the N-H proton on 2-aminopyrimidine), the latter functionality has, overall, a significant advantage and would offer a better binding site for any approaching carboxylic acid.

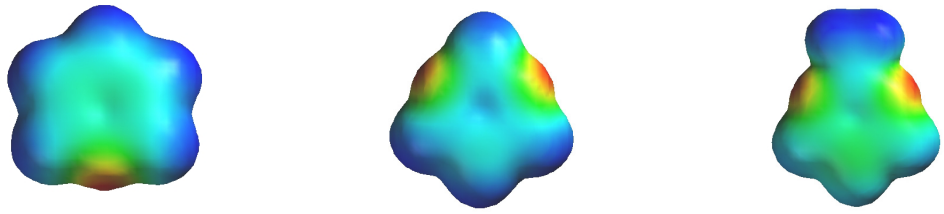

| $E_{min}$ | **-275 kJ/mol** | **-263 kJ/mol** | **-275 kJ/mol** |
|---|---|---|---|

**Figure 2.3** AM1 calculated electrostatic potential surfaces of pyridine (left), pyrimidine (center), and 2-aminopyrimidine (right).

Based on an electrostatic argument pyridine is expected to form significantly stronger N···H-O hydrogen bonds with an incoming carboxylic acid than is pyrimidine. There is, in fact, only one reported co-crystal that has been constructed using an O-H···N hydrogen bond between a carboxylic acid and unsubstituted pyrimidine,[9] whereas there are more than one hundred co-crystals in the CSD that have been synthesized primarily via an carboxylic acid···pyridine synthon.[10] However, if the less basic nitrogen atom in pyrimidine is accompanied by a strong hydrogen-bond donor, such as an amino group, in the appropriate location, it may become a better hydrogen-bonding moiety than a pyridine nitrogen atom only supported by an adjacent C-H donor.

To further probe the electrostatic nature of the two individual hydrogen bonding sites, *i.e.* pyridine/adjacent C-H and pyrimidine/amino-group, we assigned a relative hydrogen-bonding ability value, Q, to each site. This value can be compared in families of compounds with closely related functional groups containing well-defined donor/acceptor sites. The Q-value is based on calculated electrostatic potential surfaces, as indicated in Equation 2.1, where $A_1$ is the maximum positive potential, and $A_2$ is the minimum negative potential.

$$Q = A_1 - (A_2) \qquad (2.1)$$

In order to determine the limits and limitations of the best-donor/best-acceptor concept and the Q-value in the context of supramolecular assembly, we have allowed three SR's **1**, **2**, and

**6** to react with a range of substituted aromatic carboxylic acids in a variety of stoichiometric ratios. Calculated electrostatic potential surfaces were employed to rank the hydrogen-bond ability of the different binding sites on **1**, **2**, and **6** and single-crystal structure determinations were carried out in order to establish if the proposed modular supramolecular strategy provides an effective guideline for constructing supermolecules with predictable connectivity.

## 2.2 Experimental

### *2.2.1 Synthesis*

All chemicals, unless otherwise noted, were purchased from Aldrich and used without further purification. The catalyst, *bis*(triphenylphosphine)palladium(II) dichloride, was purchased from Strem chemicals. Trimethylsilylacetylene was purchased from GFS chemicals. 3-Pyridylboronic acid was synthesized according to previous literature.[11] 3,5-Dibromopyridine was purchased from Acros chemicals. Column chromatography was carried out on silica gel (150 Å pore size) from Analtech Inc. Melting points were determined on a Fisher-Johns melting point apparatus and are uncorrected. $^{1}H$ and $^{13}C$ NMR spectra were recorded on a Varian Unity plus 400 MHz or 200 MHz spectrometer in $CDCl_3$ or $D_6$-DMSO. Compounds were prepared for infrared spectroscopic (IR) analysis as a mixture in KBr. Electrospray Ionization – Ion-Trap Mass Spectrometry (ESI-IT-MS) was carried out on a Bruker Daltonics Esquire 3000 Plus. MALDI-TOF / TOF-MS was carried out on a Bruker Daltonics Ultraflex TOF/TOF.

#### *2.2.1.1 Synthesis of 3-(2-amino-4-methylpyrimidin-6-yl)pyridine, 1*

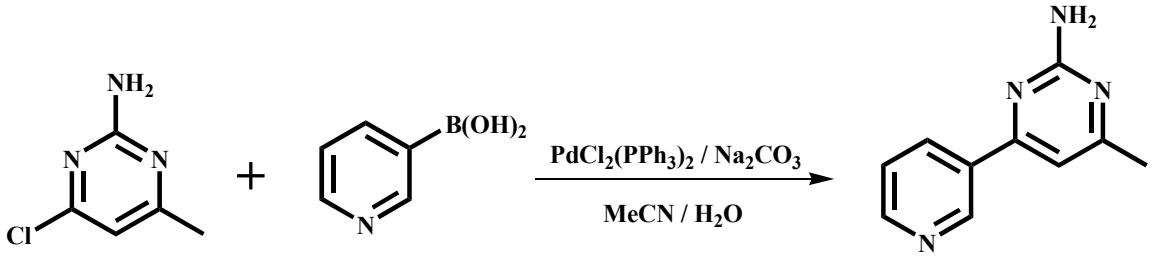


A mixture of 2-amino-4-chloro-6-methylpyrimidine (1.468 g, 10.3 mmol), 3-pyridyl boronic acid (1.403 g, 11.41 mmol), sodium carbonate (0.600 g, 5.66 mmol), and *bis*(triphenylphosphine)palladium(II) dichloride (180 mg, 0.256 mmol, 2.5 mol %) were added to a round bottom flask. Acetonitrile (35 mL) and water (35 mL) were added and dinitrogen

bubbled through the resultant mixture for 10 minutes. A condenser was attached and the mixture heated at 70 ˚C under a dinitrogen atmosphere. The reaction was monitored by TLC and allowed to cool to room temperature on completion (48 hours). The solution was then diluted with ethyl acetate (150 mL), washed with water (3 x 100 mL) then washed with saturated aqueous sodium chloride (1 x 100 mL). The organic layer was separated and dried over magnesium sulfate. The solvent was removed on a rotary evaporator and the residue chromatographed on silica with a hexanes/ethyl acetate mixture (1/1) as the eluant. The product was isolated as a light yellow/white solid. The product **1** was then recrystallized from an ethanol/chloroform mixture as colorless block-shaped crystals, (1.40 g, 74 %). M.p. 192 – 194 ºC; $^{1}$H NMR ($\delta_H$; 400 MHz, $D_6$-DMSO): 9.18 (d, J = 2Hz, 1H), 8.63 (dd, J = 4.8Hz, J = 1.6Hz, 1H), 8.33 (dt, J = 8Hz, J = 1.6Hz, 1H), 7.48 (dd, J = 8Hz, J = 4.8Hz, J = 0.8Hz, 1H), 7.09 (s, 1H), 6.65 (s, 2H), 2.28 (s, 3H); $^{13}$C NMR ($\delta_C$; 400 MHz, $D_6$-DMSO): 168.52, 163.61, 161.43, 150.88, 147.89, 134.05, 132.66, 123.64, 105.41, 23.66; IR (KBr pellet): $\upsilon$ 3324, 3154, 1576, 1345 cm$^{-1}$, MALDI-TOF / TOF-MS *m/z* 187 ([**1** + H]$^{+}$).

***2.2.1.2 Synthesis of 4-methoxy-3-(2-amino-4-methylpyrimidin-6-yl)pyridine, 2***

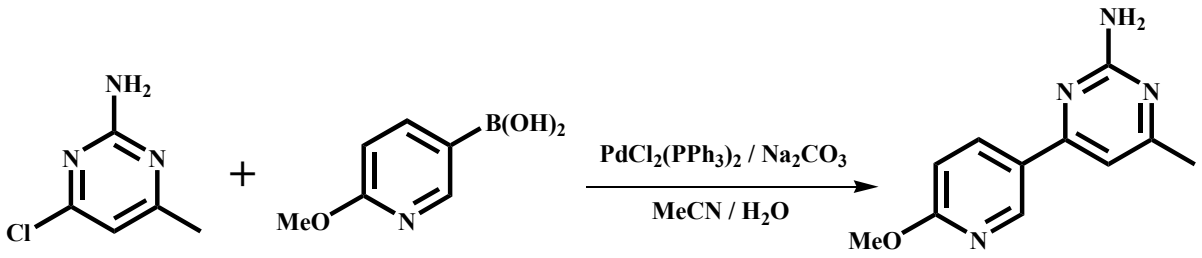


A mixture of 2-amino-4-chloro-6-methylpyrimidine (1.534 g, 10.73 mmol), 2-methoxy-5-pyridylboronic acid (1.90 g, 12.42 mmol), sodium carbonate (0.700 g, 6.60 mmol), and *bis*(triphenylphosphine)palladium(II) dichloride (180 mg, 0.256 mmol, 2.4 mol %) were added to a round bottom flask. Acetonitrile (35 mL) and water (35 mL) were added and dinitrogen bubbled through the resultant mixture for 10 minutes. A condenser was attached and the mixture heated at 65 ˚C under a dinitrogen atmosphere. The reaction was monitored by TLC and allowed to cool to room temperature on completion (24 hours). A portion of the product precipitated from the reaction mixture, thus the precipitate was filtered and the remaining reaction mixture worked up accordingly. The solution was diluted with

ethyl acetate (150 mL), washed with water (3 x 100 mL) then washed with saturated aqueous sodium chloride (1 x 100 mL). The organic layer was separated and dried over magnesium sulfate. The solvent was removed on a rotary evaporator and the residue chromatographed on silica with a hexane/ethyl acetate mixture (1/3) as the eluant. The isolated product was then combined with the filtered portion. The tan solid **2** was then recrystallized from ethanol as colorless bar-shaped crystals, (1.44 g 64 %). M.p. 163 - 165 ºC; $^{1}$H NMR ($\delta_H$; 400 MHz, $CDCl_3$): 8.74 (d, J = 2.8Hz, 1H), 8.22 (dd, J =8.8Hz, J = 2.4Hz, 1H), 6.87 (s, 1H), 6.82 (d, J = 8.8Hz, 1H), 5.11 (s, 2H), 4.00 (s, 3H), 2.41 (s, 3H); $^{13}$C NMR ($\delta_C$; 400 MHz, $CDCl_3$): 168.62, 165.55, 163.14, 162.93, 146.33, 137.26, 126.51, 110.83, 106.30, 53.75, 24.13; IR (KBr pellet): $\upsilon$ 3449, 3317, 1583, 1367, 1290, 1013 cm$^{-1}$, MALDI-TOF / TOF-MS *m/z* 203 ([**2** + H]$^{+}$).

### *2.2.1.3 Synthesis of 3-methoxy-5-bromopyridine, 3*[12]

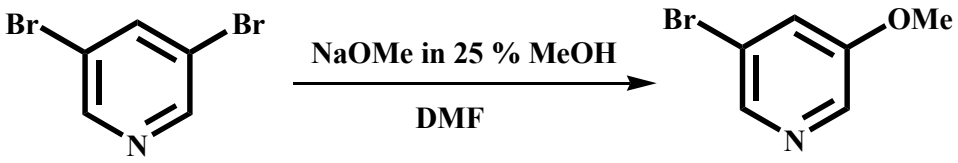


A solution of sodium methoxide in 25% methanol (6.83 mL, 31.6 mmol) was combined with DMF (anhydrous 20 mL) under an inert $N_2$ atmosphere in a round bottom flask. 3,5-Dibromopyridine (5.00 g, 21.1 mmol) was then added and stirred at 65 ºC for 24 hours. An additional equivalent of sodium methoxide in 25% methanol (2.33 mL) was added after 4 hours. The reaction was monitored by TLC and allowed to cool to room temperature upon completion. The reaction was then diluted with water (50 mL) and extracted with diethyl ether (3 x 50 mL). The organic extractions were combined and washed with brine then dried over magnesium sulfate. The solvent was removed on a rotary evaporator and the residue chromatographed on silica with a hexanes/ethyl acetate mixture (1:1) as the eluant. The product **3** was isolated as a yellow oil. Hexanes (20 mL) was then added to the product and placed in the refrigerator. Colorless crystals precipitated from the mother liquor, which were isolated and dried, (2.82 g, 71 %). M.p. 27 – 29 ºC; $^{1}$H NMR ($\delta_H$; 400 MHz, $CDCl_3$): 8.29 (d, J = 1.6Hz, 1H), 8.25 (d, J = 2.4Hz, 1H), 7.36 (dd, J = 2.6Hz, J = 1.8Hz, 1H), 3.86 (s, 3H); $^{13}$C NMR ($\delta_C$; 400 MHz, $CDCl_3$): 155.83, 142.70, 136.01, 123.01, 120.18, 55.61 cm$^{-1}$.

### *2.2.1.4 Synthesis of 3-methoxy-5-trimethylsilanylethynylpyridine, 4*

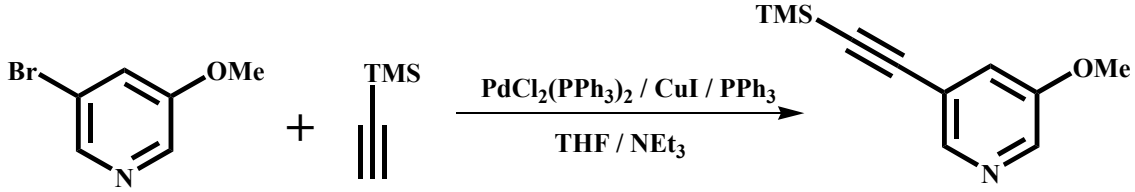


A mixture of **3** (3.26 g, 17.31 mmol), trimethylsilylacetylene (2.05 g, 20.9 mmol), copper(I) iodide (0.100 g, 0.590 mmol), triphenylphosphine (0.420 g, 1.60 mmol), and *bis*(triphenylphosphine)palladium(II) dichloride (0.360 g, 0.510 mmol) were added to a round bottom flask. Tetrahydrofuran (75 mL) and triethylamine (75 mL) were added and dinitrogen bubbled through the resultant mixture for 10 minutes. A condenser was attached and the mixture heated at 65 ˚C under a dinitrogen atmosphere. The reaction was monitored by TLC and allowed to cool to room temperature on completion (26 hours). The solution was then diluted with ethyl acetate (100 mL), washed with water (3 x 100 mL) then washed with saturated aqueous sodium chloride (1 x 100 mL). The organic layer was separated and dried over magnesium sulfate. The solvent was removed on a rotary evaporator and the residue chromatographed on silica with *n*-pentane as the eluant. The product **4** was isolated as a light yellow oil, (4.25 g, 86 %). $^1$H NMR ($\delta_H$; 200 MHz, $CDCl_3$): 8.27 (d, 1.6Hz, 1H), 8.21 (d, J = 5.2Hz, 1H), 7.20 (dd, J = 6Hz, J = 2.8, 1H), 3.81 (s, 3H), 0.24 (s, 9H).

### *2.2.1.5 Synthesis of 3-methoxy-5-ethynylpyridine, 5*

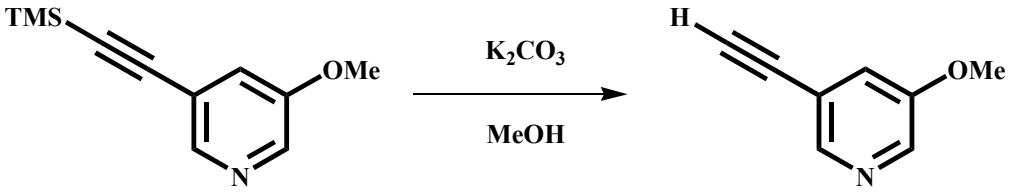


A mixture of **4** (4.25 g, 14.9 mmol) and potassium carbonate (3.00 g, 21.7 mmol) were stirred in methanol (80 mL) at room temperature for 1 hour. The solution was then diluted with ethyl ether (100 mL) and washed with water (4 x 100 mL). The solvent was removed on a rotary evaporator and the residue chromatographed on silica with a *n*-pentane/ethyl acetate (10:1) as eluant. The product **5** was isolated as a white solid, (1.72 g, 87 %). $^1$H NMR ($\delta_H$; 200 MHz,

$CDCl_3$): 8.21 (d, J = 2.8Hz, 1H), 8.16 (d, J = 4Hz, 1H), 7.15 (dd, J =5.8Hz, J = 3Hz, 1H), 3.72 (s, 3H), 3.17 (s, 1H).

***2.2.1.6 Synthesis of 1-(2-amino-4-methylpyrimidin-6-yl)-2-(3-methoxypyridin-5-yl)ethyne, 6***

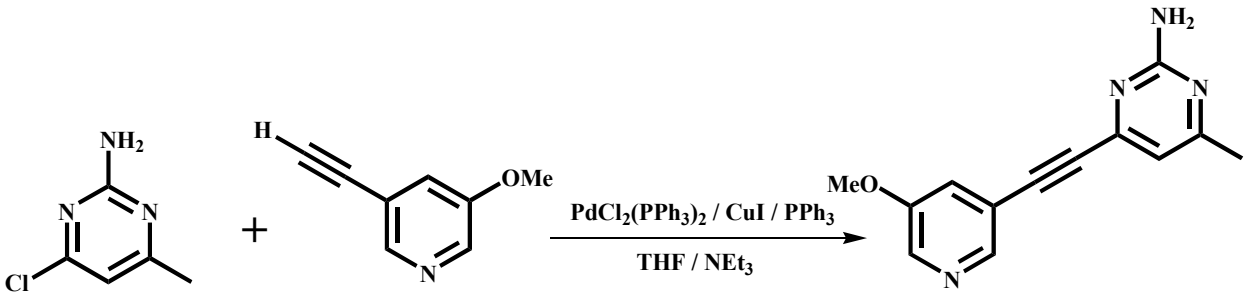


A mixture of 2-amino-4-chloro-6-methylpyrimidine (360 mg, 2.50 mmol), **5** (400 mg, 3.01 mmol), copper(I) iodide (12.0 mg, 0.0710 mmol), triphenylphosphine (50.0 mg, 0.191 mmol), and *bis*(triphenylphosphine)palladium(II) dichloride (50.0 mg, 0.071 mmol) were added to a round bottom flask. Tetrahydrofuran (12 mL) and triethylamine (12 mL) were added and dinitrogen bubbled through the resultant mixture for 10 minutes. A condenser was attached and the mixture heated at 70 ˚C under a dinitrogen atmosphere. The reaction was monitored by TLC and allowed to cool to room temperature upon completion (48 hours). The solution was then diluted with ethyl acetate (50 mL), washed with water (3 x 100 mL) then washed with saturated aqueous sodium chloride (1 x 100 mL). The organic layer was separated and dried over magnesium sulfate. The solvent was removed on a rotary evaporator and the residue chromatographed on silica with a hexanes/ethyl acetate mixture (1:1) as the eluant. The product **6** was isolated as a light brown solid and recrystallized from chloroform producing colorless block shaped crystals, (426 mg, 72 %). M.p. 171-173 ºC; $^1$H NMR ($\delta_H$; 400 MHz, $CDCl_3$): 8.39 (d, J = 2Hz, 1H), 8.30 (d, J = 2.8Hz, 1H), 7.36 (dd, J = 3Hz, J = 1.4Hz, 1H), 6.70 (s, 1H), 5.43 (s, 2H), 3.85 (s, 3H), 2.35 (s, 3H), $^{13}$C NMR ($\delta_C$; 400 MHz, $CDCl_3$): 168.88, 162.83, 154.99, 150.37, 144.92, 138.72, 122.61, 118.80, 113.48, 89.78, 87.66, 55.60, 23.81; IR (KBr pellet): $\upsilon$ 3326, 3171, 2229, 1652, 1558, 1423 cm$^{-1}$, MALDI-TOF / TOF-MS *m/z* 241 ([**6** + H]$^+$).

## *2.2.2 Synthesis of co-crystals and salts*

***2.2.2.1 Synthesis of 3-(2-amino-4-methylpyrimidin-6-yl)pyridine:4-nitrobenzoic acid, 1a***

3-(2-Amino-4-methylpyrimidin-6-yl)pyridine (19 mg, 0.10 mmol) and 4-nitrobenzoic acid (17 mg, 0.10 mmol) were placed in a vial containing ethanol (6 mL) and heated until a clear homogeneous solution was obtained. After four days of slow evaporation, colorless rod-shaped crystals were obtained. M.p. 188-190 °C; IR (KBr pellet): $\upsilon$ 3308 and 3083 $cm^{-1}$ ($NH_2$, m), 2254 and 1900 $cm^{-1}$ (O-H···N, br), 1696 $cm^{-1}$ (C=O, m).

***2.2.2.2 Synthesis of 3-(2-amino-4-methylpyrimidin-6-yl)pyridine:pentamethylbenzoic acid, 1b***

3-(2-Amino-4-methylpyrimidin-6-yl)pyridine (10 mg, 0.05 mmol) and pentamethylbenzoic acid (21 mg, 0.10 mmol) were placed in a vial containing an ethanol/ethyl acetate mixture (5:5 mL) and heated until a clear homogeneous solution was obtained. After two days of slow evaporation, yellow/orange prism-shaped crystals were obtained. M.p. 155-157 °C; IR (KBr pellet): $\upsilon$ 3331 and 3198 $cm^{-1}$ ($NH_2$, m), 2442 and 1912 $cm^{-1}$ (O-H···N, br), 1635 $cm^{-1}$ (C=O, m).

***2.2.2.3 Synthesis of 3-(2-amino-4-methylpyrimidin-6-yl)pyridine:4-hydroxybenzoic acid, 1c***

3-(2-Amino-4-methylpyrimidin-6-yl)pyridine (11 mg, 0.06 mmol) and 4-hydroxybenzoic acid (16 mg, 0.12 mmol) were placed in a vial containing ethanol (10 mL) and heated until a clear homogeneous solution was obtained. After two days of slow evaporation, yellowish/orange cube-shaped crystals were obtained. M.p. 195-197 °C; IR (KBr pellet): $\upsilon$ 3432 (OH, s), 3314 and 3191 $cm^{-1}$ ($NH_2$, m), 2494 and 1875 $cm^{-1}$ (O-H···N, br), 1655 $cm^{-1}$ (C=O, m).

***2.2.2.4 Synthesis of 3-(2-amino-4-methylpyrimidinium-6-yl)pyridine:2,6-difluorobenzoate, 1d***

3-(2-Amino-4-methylpyrimidin-6-yl)pyridine (13 mg, 0.07 mmol) and 2,6-difluorobenzoic acid (22 mg, 0.14 mmol) were placed in a vial containing methanol/ethyl acetate (3:6 mL) and heated until a clear homogeneous solution was obtained. After four days of slow evaporation, orange plate-shaped crystals were obtained. M.p. 168-170 °C; IR (KBr pellet): $\upsilon$ 3339 and 3001 $cm^{-1}$ ($NH_2$, m), 2423 and 1957 $cm^{-1}$ (O-H···N, br), 1684 $cm^{-1}$ (C=O, m).

***2.2.2.5 Synthesis of 4-methoxy-3-(2-amino-4-methylpyrimidin-6-yl)pyridine:4-N,N-dimethylaminobenzoic acid, 2a***

4-Methoxy-3-(2-amino-4-methylpyrimidin-6-yl)pyridine (10 mg, 0.05 mmol) and 4-*N*,*N*-dimethylaminobenzoic acid (8 mg, 0.05 mmol) were placed in a vial containing ethyl acetate (10 mL) and heated until a clear homogeneous solution was obtained. After one day of slow

evaporation, colorless cube-shaped crystals were obtained. M.p. 173-175 °C; IR (KBr pellet): $\upsilon$ 3317 and 3204 $cm^{-1}$ ($NH_2$, m), 2455 and 1872 $cm^{-1}$ (O-H···N, br), 1705 $cm^{-1}$ (C=O, m).

#### *2.2.2.6 Synthesis of 4-methoxy-3-(2-amino-4-methylpyrimidin-6-yl)pyridine:2,4-difluorobenzoic acid, 2b*

4-Methoxy-3-(2-amino-4-methylpyrimidin-6-yl)pyridine (10 mg, 0.05 mmol) and 2,4-difluorobenzoic acid (15 mg, 0.10 mmol) were placed in a vial containing methanol (10 mL) and heated until a clear homogeneous solution was obtained. After two days of slow evaporation, colorless rod-shaped crystals were obtained. M.p. 165-167 °C; IR (KBr pellet): $\upsilon$ 3350 and 3191 $cm^{-1}$ ($NH_2$, m), 2372 and 1880 $cm^{-1}$ (O-H···N, br), 1685 $cm^{-1}$ (C=O, m).

#### *2.2.2.7 Synthesis of 4-methoxy-3-(2-amino-4-methylpyrimidin-6-yl)pyridine: pentamethylbenzoic acid, 2c*

4-Methoxy-3-(2-amino-4-methylpyrimidin-6-yl)pyridine (13 mg, 0.06 mmol) and pentamethylbenzoic acid (23 mg, 0.12 mmol) were placed in a vial containing ethanol (6 mL) and heated until a clear homogeneous solution was obtained. After two days of slow evaporation, colorless rod-shaped crystals were obtained. M.p. 181-183 °C; IR (KBr pellet): $\upsilon$ 3385 and 3206 $cm^{-1}$ ($NH_2$, m), 2429 and 1926 $cm^{-1}$ (O-H···N, br), 1653 $cm^{-1}$ (C=O, m).

#### *2.2.2.8 Synthesis of 4-methoxy-3-(2-amino-4-methylpyrimidinium-6-yl)pyridine:3,5-dinitrobenzoate, 2d*

4-Methoxy-3-(2-amino-4-methylpyrimidin-6-yl)pyridine (10 mg, 0.05 mmol) and 3,5-dinitrobenzoic acid (19 mg, 0.09 mmol) were placed in a vial containing ethyl acetate (6 mL) and heated until a clear homogeneous solution was obtained. After two days of slow evaporation, colorless rod-shaped crystals were obtained. Dec. 195 °C; IR (KBr pellet): $\upsilon$ 3298 and 3099 $cm^{-1}$ ($NH_2$, m), 2356 and 1977 $cm^{-1}$ (O-H···N, br), 1701 $cm^{-1}$ (C=O, m).

#### *2.2.2.9 Synthesis of 4-methoxy-3-(2-amino-4-methylpyrimidinium-6-yl)pyridine:2,5-dichlorobenzoate, 2e*

4-Methoxy-3-(2-amino-4-methylpyrimidin-6-yl)pyridine (10 mg, 0.05 mmol) and 2,5-dichlorobenzoic acid (18 mg, 0.09 mmol) were placed in a vial containing methanol (10 mL) and heated until a clear homogeneous solution was obtained. After two days of slow evaporation,

colorless plate-shaped crystals were obtained. M.p. 167-169 °C; IR (KBr pellet): $\upsilon$ 3334 and 3063cm$^{-1}$ ($NH_2$, m), 2366 and 1972 cm$^{-1}$ (O-H···N, br), 1665 cm$^{-1}$ (C=O, m).

### *2.2.2.10 Synthesis of 1-(2-amino-4-methylpyrimidin-6-yl)-2-(3-methoxypyridin-5-yl)ethyne:3,5-dinitrobenzoic acid, 6a*

1-(2-Amino-4-methylpyrimidin-6-yl)-2-(3-methoxypyridin-5-yl)ethyne (10 mg, 0.04 mmol) and 3,5-dinitrobenzoic acid (9 mg, 0.04 mmol) were placed in a vial containing an ethanol/ethyl acetate mixture (15:15 mL) and heated until a clear homogeneous solution was obtained. After one day of slow evaporation, colorless plate-shaped crystals were obtained. M.p. 235-237 °C; IR (KBr pellet): $\upsilon$ 3314 and 3145 cm$^{-1}$ ($NH_2$, m), 2479 and 1890 cm$^{-1}$ (O-H···N, br), 2223 cm$^{-1}$ (C≡C), 1690 cm$^{-1}$ (C=O, m).

### *2.2.2.11 Synthesis of 1-(2-amino-4-methylpyrimidin-6-yl)-2-(3-methoxypyridin-5-yl)ethyne:4-nitrobenzoic acid, 6b*

1-(2-Amino-4-methylpyrimidin-6-yl)-2-(3-methoxypyridin-5-yl)ethyne (10 mg, 0.04 mmol) and 4-nitrobenzoic acid (14 mg, 0.08 mmol) were placed in a vial containing an ethanol/ethyl acetate mixture (10:10 mL) and heated until a clear homogeneous solution was obtained. After one day of slow evaporation, colorless plate-shaped crystals were obtained. M.p. 196-198 °C; IR (KBr pellet): $\upsilon$ 3385 and 3304 cm$^{-1}$ ($NH_2$, m), 2428 and 1885 cm$^{-1}$ (O-H···N, br), 2222 cm$^{-1}$ (C≡C), 1697 cm$^{-1}$ (C=O, m).

### *2.2.2.12 Synthesis of 1-(2-amino-4-methylpyrimidin-6-yl)-2-(3-methoxypyridin-5-yl)ethyne:3-N,N-dimethylaminobenzoic acid, 6c*

1-(2-Amino-4-methylpyrimidin-6-yl)-2-(3-methoxypyridin-5-yl)ethyne (12 mg, 0.06 mmol) and 3-*N*,*N*-dimethylaminobenzoic acid (18 mg, 0.12 mmol) were placed in a vial containing ethanol (6 mL) and heated until a clear homogeneous solution was obtained. After three days of slow evaporation, yellow block-shaped crystals were obtained. M.p. 168-170 °C; IR (KBr pellet): $\upsilon$ 3324 and 3140 cm$^{-1}$ ($NH_2$, m), 2413 and 1895 cm$^{-1}$ (O-H···N, br), 2228 cm$^{-1}$ (C≡C), 1655 cm$^{-1}$ (C=O, m).

### *2.2.2.13 Synthesis of 1-(2-amino-4-methylpyrimidinium-6-yl)-2-(3-methoxypyridin-5-yl)ethyne:pentafluorobenzoate, 6d*

1-(2-Amino-4-methylpyrimidin-6-yl)-2-(3-methoxypyridin-5-yl)ethyne (10 mg, 0.04 mmol) and pentafluorobenzoic acid (9 mg, 0.04 mmol) were placed in a vial containing ethyl aceate / ethanol (6:3 mL) and heated until a clear homogeneous solution was obtained. After three days of slow evaporation, colorless rod-shaped crystals were obtained. M.p. 176-178 °C; IR (KBr pellet): $\upsilon$ 3283 and 3048 $cm^{-1}$ ($NH_2$, m), 2433 and 1952 $cm^{-1}$ (O-H···N, br), 2223 $cm^{-1}$ (C≡C), 1701 $cm^{-1}$ (C=O, m).

### *2.2.3 AM1 Calculations*

Ligands **1**, **2**, and **6**, pyridine, pyrimidine, and 2-aminopyrimidine (Figure 2.3) molecular structures were constructed using Spartan '04 (Wavefunction, Inc. Irvine, CA). All six molecules were optimized using AM1, with the maxima and minima in the electrostatic potential surface (0.002 e/au isosurface) determined using a positive point charge in the vacuum as a probe.

## 2.3 Results

A summary of the crystallographic information for **1**, **2**, **6**, **1a-1d**, **2a-2e**, and **6a-6d** is displayed in Table B.1 and all hydrogen-bond geometries for **1**, **2**, **6**, **1a-1d**, **2a-2e**, and **6a-6d** are listed in Table 2.1.

**Table 2.1** Hydrogen-Bond Geometries for **1**, **2**, **6**, **1a-1d**, **2a-2e**, and **6a-6d**

| Structure | D-H•••H | d(D-H)/Å | d(H•••A)/Å | d(D•••A)/Å | <(DHA)/º |
|---|---|---|---|---|---|
| **1**[i] | N(12)-H(12A)...N(21)#1 | 0.892(18) | 2.154(19) | 3.0450(17) | 176.4(15) |
| | N(12)-H(12B)...N(11)#2 | 0.897(18) | 2.206(19) | 3.1013(17) | 175.3(14) |
| **2**[ii] | N(12)-H(12A)...O(26)#1 | 0.97(3) | 2.10(3) | 3.062(3) | 170(2) |
| | N(12)-H(12B)...N(11)#2 | 0.88(3) | 2.17(3) | 3.047(3) | 177(3) |
| **6**[iii] | N(12)-H(12A)...N(21)#1 | 0.88 | 2.12 | 2.993(2) | 171.5 |
| | N(12)-H(12B)...N(11)#2 | 0.88 | 2.21 | 3.086(2) | 172.7 |
| **1a**[iv] | N(12)-H(12B)...O(32) | 0.90(2) | 2.14(2) | 3.034(2) | 170.9(19) |
| | N(12)-H(12A)...N(21)#1 | 0.87(2) | 2.14(2) | 3.015(2) | 177.4(19) |
| | O(31)-H(31)...N(11) | 1.17(2) | 1.36(2) | 2.5274(18) | 174.4(19) |
| **1b**[v] | O(41)-H(41)...N(11) | 0.90(3) | 1.72(3) | 2.599(2) | 164(3) |
| | N(12)-H(12A)...O(42) | 0.87(3) | 2.15(3) | 3.013(2) | 176(3) |
| | N(12)-H(12B)...N(21)#1 | 0.88(3) | 2.46(3) | 3.112(3) | 132(2) |
| **1c**[vi] | N(12)-H(12A)...O(32) | 0.83(4) | 2.08(4) | 2.906(3) | 170(3) |
| | N(12)-H(12B)...O(34)#1 | 0.93(3) | 2.28(4) | 3.163(3) | 157(3) |
| | O(31)-H(31)...N(11) | 0.91(4) | 1.75(4) | 2.656(3) | 173(3) |
| | O(34)-H(34)...N(21)#2 | 0.93(3) | 1.80(4) | 2.728(3) | 169(3) |
| **1d**[vii] | N(11)-H(11)...O(31) | 0.88(2) | 1.78(2) | 2.6608(17) | 178(2) |
| | N(12)-H(12A)...O(32) | 0.88(2) | 1.94(2) | 2.8161(18) | 175.7(19) |
| | N(12)-H(12B)...N(21)#1 | 0.91(2) | 2.29(2) | 2.9888(19) | 132.9(17) |
| **2a**[viii] | O(31)-H(31)...N(11) | 0.951(17) | 1.690(17) | 2.6321(14) | 170.0(15) |
| | N(12)-H(12A)...O(32) | 0.894(17) | 2.026(17) | 2.9173(15) | 174.3(14) |
| | N(12)-H(12B)...O(32)#1 | 0.862(16) | 2.110(16) | 2.8925(15) | 150.8(14) |
| **2b**[ix] | N(12)-H(12A)...O(32) | 0.92(3) | 2.02(3) | 2.925(3) | 170(2) |
| | N(12)-H(12B)...N(11)#1 | 0.94(3) | 2.16(3) | 3.085(3) | 172(2) |
| | O(31)-H(31)...N(13) | 0.91(3) | 1.70(3) | 2.604(3) | 174(3) |
| **2c**[x] | N(12)-H(12A)...O(42) | 0.91(2) | 2.05(2) | 2.9519(19) | 173.1(19) |
| | N(12)-H(12B)...N(21)#1 | 0.85(2) | 2.25(2) | 3.080(2) | 165.3(19) |
| | O(41)-H(41)...N(11) | 0.90(2) | 1.77(2) | 2.6515(18) | 167(2) |
| **2d**[xi] | N(13)-H(13)...O(31) | 0.97(3) | 1.60(3) | 2.569(3) | 173(3) |
| | N(12)-H(12A)...O(32) | 0.91(4) | 1.92(4) | 2.833(4) | 176(3) |
| | N(12)-H(12B)...N(21)#1 | 0.86(4) | 2.22(4) | 3.060(4) | 163(3) |
| **2e**[xii] | N(11)-H(11)...O(31) | 0.94(2) | 1.62(2) | 2.5486(19) | 174(2) |
| | N(12)-H(12A)...O(32) | 0.91(2) | 2.03(2) | 2.932(2) | 173.2(19) |
| | N(12)-H(12B)...N(21)#1 | 0.83(2) | 2.36(2) | 3.008(2) | 136(2) |
| **6a**[xiii] | N(12)-H(12A)...O(32) | 0.88 | 2.19 | 3.049(9) | 165.6 |
| | N(12)-H(12B)...N(13)#1 | 0.88 | 2.24 | 3.121(12) | 175.3 |
| | O(31)-H(31)...N(11) | 0.84 | 1.84 | 2.633(9) | 157.2 |
| **6b**[xiv] | N(12)-H(12A)...O(32) | 0.91(3) | 2.22(3) | 3.109(3) | 168(2) |
| | O(31)-H(31)...N(11) | 0.99(3) | 1.67(3) | 2.652(3) | 173(3) |
| | N(12)-H(12B)...N(13)#1 | 0.90(3) | 2.24(3) | 3.122(3) | 168(2) |
| **6c**[xv] | O(31)-H(31)...N(11) | 0.96(4) | 1.67(4) | 2.625(3) | 170(3) |
| | N(12)-H(12A)...O(32) | 0.99(3) | 1.92(3) | 2.908(4) | 177(3) |
| | N(12)-H(12B)...N(21)#1 | 0.95(3) | 2.09(3) | 3.023(4) | 171(3) |
| **6d**[xvi] | N(12)-H(12A)...O(32) | 0.925(17) | 1.933(17) | 2.8551(15) | 174.4(15) |
| | N(12)-H(12B)...N(13)#1 | 0.888(17) | 2.216(18) | 3.0941(16) | 170.2(15) |

i) #1 -x+2,-y+1,-z+1 #2 -x+1,-y+1,-z ii) #1 -x,y-1/2,-z+1/2 #2 -x,-y,-z+1 iii) #1 -x+2,-y+2,-z+1 #2 -x+1,-y+1,-z iv) #1 -x,-y,-z+1 v) #1 x+1,y+1,z vi) #1 x,y,z-1 #2 x+1,y-1,z+1 vii) #1 x+1,y,z+1 viii) #1 -x+1,-y+1,-z+1 ix) #1 -x+1,y,-z+1/2 x) #1 -x+1,-y+2,-z+1 xi) #1 -x,-y+1,-z-1 xii) #1 x,y,z+1 xiii) #1 -x+2,-y+1,-z+1 xiv) #1 -x+1,-y,-z+1 xv) #1 -x,y-1/2,-z+1/2 xvi) #1 -x+1,-y,-z+1

As mentioned earlier, p$K_a$/p$K_b$ values have been used quite successfully for predicting and rationalizing hydrogen bonding patterns in the crystalline solid-state.[13] However, in order to apply predictable supramolecular strategies to a wider range of chemical functionalities under a variety of reaction conditions, it would be extremely useful if we could find a more satisfactory way of ranking intermolecular hydrogen-bond interactions that would take into account the many different factors that influence the molecular recognition behavior in any system. Accordingly, electrostatic potential surfaces for SR's **1**, **2**, and **6** were calculated using, Equation 2.1, and the Q values for each binding site were determined. Ligand **1** has two amino-protons ($H_1$), two pyrimidine nitrogen atoms ($N_1$), one pyridine nitrogen atom ($N_2$) and two *ortho*-protons ($H_2$ and $H_6$) nearest the pyridyl-nitrogen, that are of particular interest. Both the amino protons, both $H_2$ and $H_6$ on the pyridyl moiety, and both pyrimidine nitrogen atoms display similar values, respectively, so only one atom in each pair will be discussed, Figure 2.4.

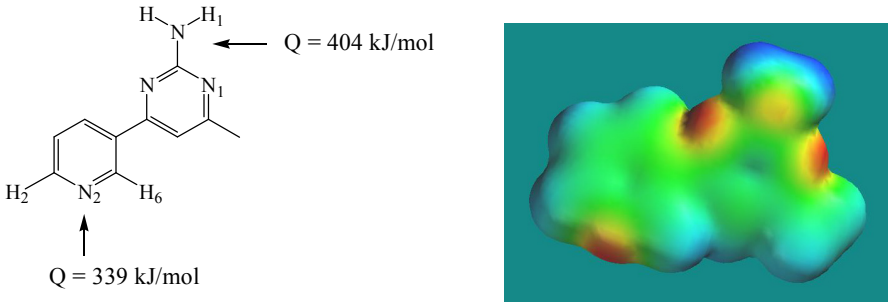


**Figure 2.4** Molecular structure and the electrostatic potential surface map of ligand **1**.

The basic nitrogen atom sites in both pyrimidine and pyridine, display similar numerical values ~ -266 and -268 kJ/mol, respectively. The positive potentials on the auxillary hydrogen-bond donors, N-H and C-H, were calculated at 138 and 71 kJ/mol, respectively. Consequently, the Q values for the two binding sites are 404 and 339 kJ/mol for the pyrimidine and pyridine sites, respectively, Table 2.2. Based upon these results, it is expected that the former moiety would be a more effective hydrogen-bonding site, and therefore a better competitive match for an approaching carboxylic acid.

**Table 2.2** Calculated electrostatic potentail values (kJ/mol) of ligands **1**, **2**, and **6** using AM1

| Ligand | $N_1$ | $H_1$ | $N_2$ | $H_2$ | Q ($N_1$ + $H_1$) | Q ($N_2$ + $H_2$) |
|---|---|---|---|---|---|---|
| **1** | -266 | 138 | -268 | 71 | 404 | 339 |
| **2** | -255 | 142 | -251 | 55 | 397 | 301 |
| **6** | -272 | 134 | -251 | 75 | 406 | 326 |

A similar analysis of the two binding sites in **2** again shows that there is a significant difference between the two binding sites, Figure 2.5.

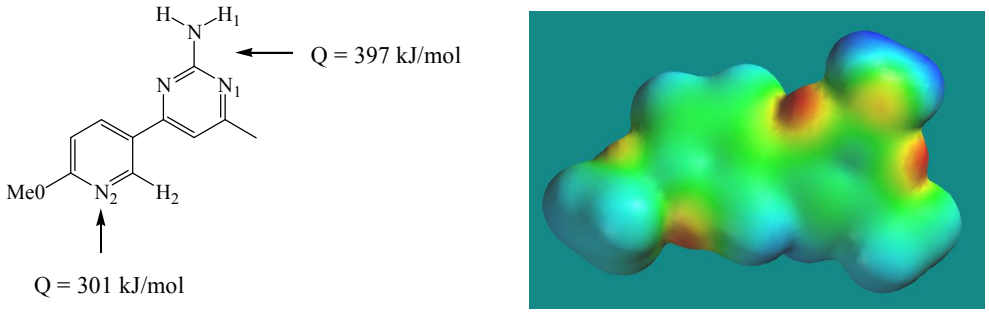


**Figure 2.5** Molecular structure and the electrostatic potential surface map of ligand **2**.

For this SR, the Q-value for the N/N-H moiety on pyrimidine is 397 kJ/mol, whereas the value for the N/C-H moiety on the pyridine site is only 301 kJ/mol, Table 2.2. The addition of a methoxy-substituent, next to the pyridyl nitrogen atom, reduces its negative charge and this is also as reflected by the p*K*a value 3.25 (compared to 5.17 for pyridine).[8] Again, these calculations indicate that the amino-pyrimidine site should offer a more favorable match than the pyridyl moiety.

SR **6** is structurally similar to **1**, with the exception that a triple bond is now connecting the two aromatic rings and the methoxy group has been moved to the meta-position, Figure 2.6. However, neither of these changes significantly alter the overall electrostatic balance between the two binding sites. The pyrimidine moiety, N/N-H, has a Q-value of 406 kJ/mol, whereas the pyridine, N/C-H, site has a Q-value of 326 kJ/mol. Again, the former moiety is expected to be the more effective and competitive hydrogen-bonding site on **6**.

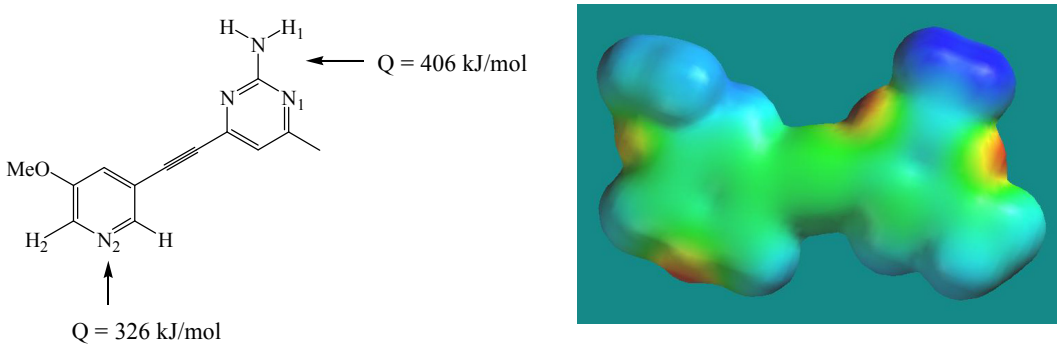


**Figure 2.6** Molecular structure and the electrostatic potential surface map of ligand **6**.

In all three SR's, **1**, **2**, and **6** the overall electrostatic charges show that the amino-pyrimidine moiety is a superior hydrogen-bond site, compared to either the pyridine or the methoxy-substituted pyridine site. This hypothesis only holds true if electrostatics are playing a dominant role in the assembly process.

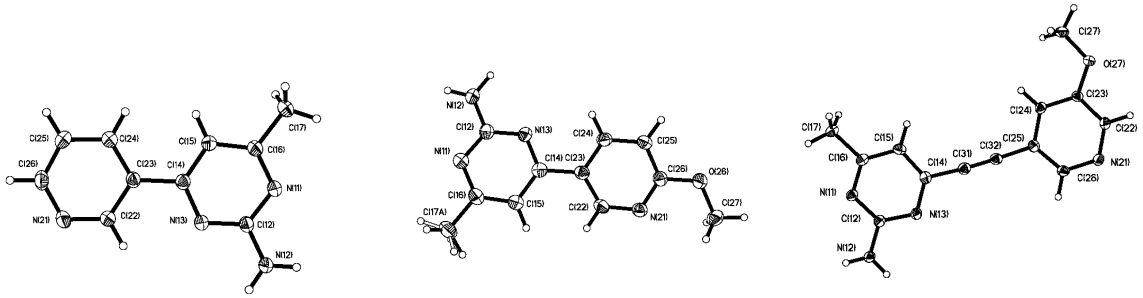

**1** **2** **6**

**Figure 2.7** Thermal-ellipsoids plots (50% probability level) of ligands **1**, **2**, and **6**.

### *2.3.1 Crystal structure of 3-(2-amino-4-methylpyrimidin-6-yl)pyridine, 1*

The crystal structure of **1** displays one molecule within the asymmetric unit and extension of the architecture shows individual ligands forming a 1-D strand through multiple N-H···N hydrogen bonds. The amino-pyrimidine moiety forms self-complementary N-H···N hydrogen bonds (N12···N11, 3.1013(17) Å) with a neighboring ligand producing a dimeric unit, which is further extended by secondary N-H···N hydrogen bonds from the *anti*-amino proton to the pyridyl nitrogen atom (N12···N21, 3.0450(17) Å) in a head-to-tail arrangement, Figure 2.8.

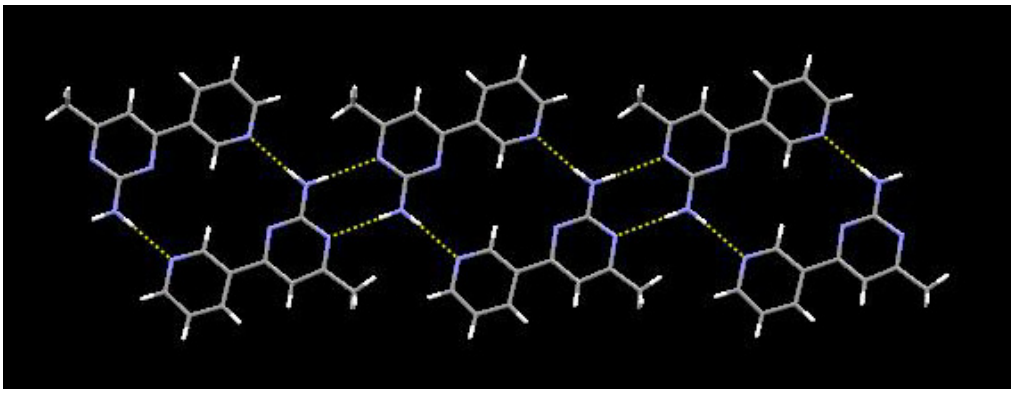

**Figure 2.8** 1-D strands formed through multiple N-H···N hydrogen bonds of ligand **1**.

### *2.3.2 Crystal structure of 4-methoxy-3-(2-amino-4-methylpyrimidin-6-yl)pyridine, 2*

The crystal structure of **2** displays one molecule within the asymmetric unit, orientated with the two heterocycles in a relatively planar fashion. Individual molecules form dimeric units through self-complementary amino-pyrimidine N-H···N/N···H-N (N12···N11, 3.047(3) Å) hydrogen bonds, Figure 2.9. The motif is extended into a 2-D sheet through N-H···O hydrogen bonds from the *anti*-amino proton and the oxygen atom of the methoxy group with an N(12)···O(26) distance of 3.062(3) Å.

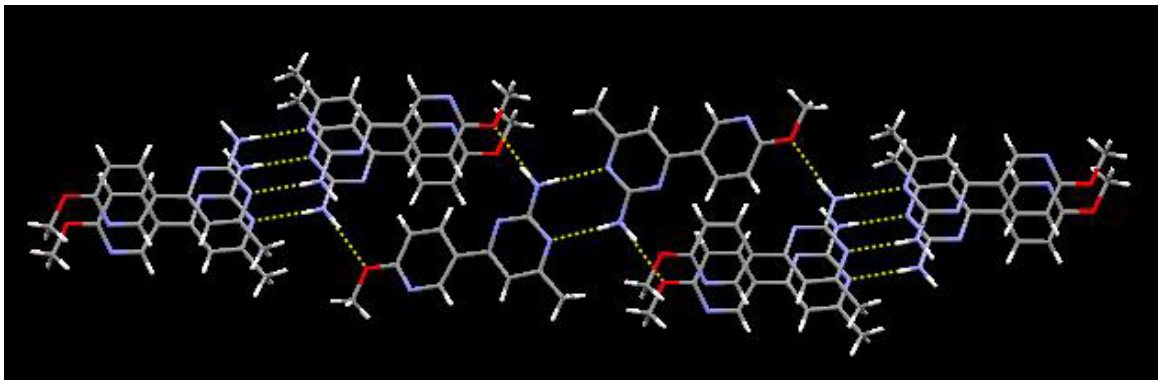

**Figure 2.9** 1-D strand formed through self-complementary amino-pyrimidine N-H···N hydrogen bonds.

### *2.3.3 Crystal structure of 1-(2-amino-4-methylpyrimidin-6-yl)-2-(3-methoxypyridin-5-yl)ethyne, 6*

The crystal structure of **6** displays one ligand and a 0.5 dichloromethane molecule within the asymmetric unit, with the two heterocycles orientated in a relatively planar fashion. Extension of the architecture reveals connectivities similar to that of structure **1**, Figure 2.10.

The amino-pyrimidine moiety forms self-complementary N-H···N hydrogen bonds (N12···N11, 3.086(2) Å) with a neighboring ligand producing a dimeric unit, which is further extended by secondary N-H···N hydrogen bonds from the *anti*-amino proton to the pyridyl nitrogen atom (N12···N21, 2.993(2) Å) in a head-to-tail arrangement.

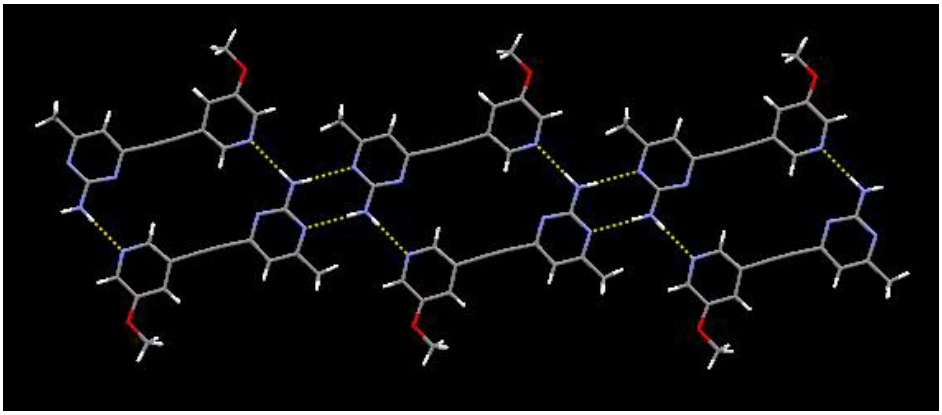

**Figure 2.10** 1-D strands formed through multiple N-H···N hydrogen bonds of ligand **6**.

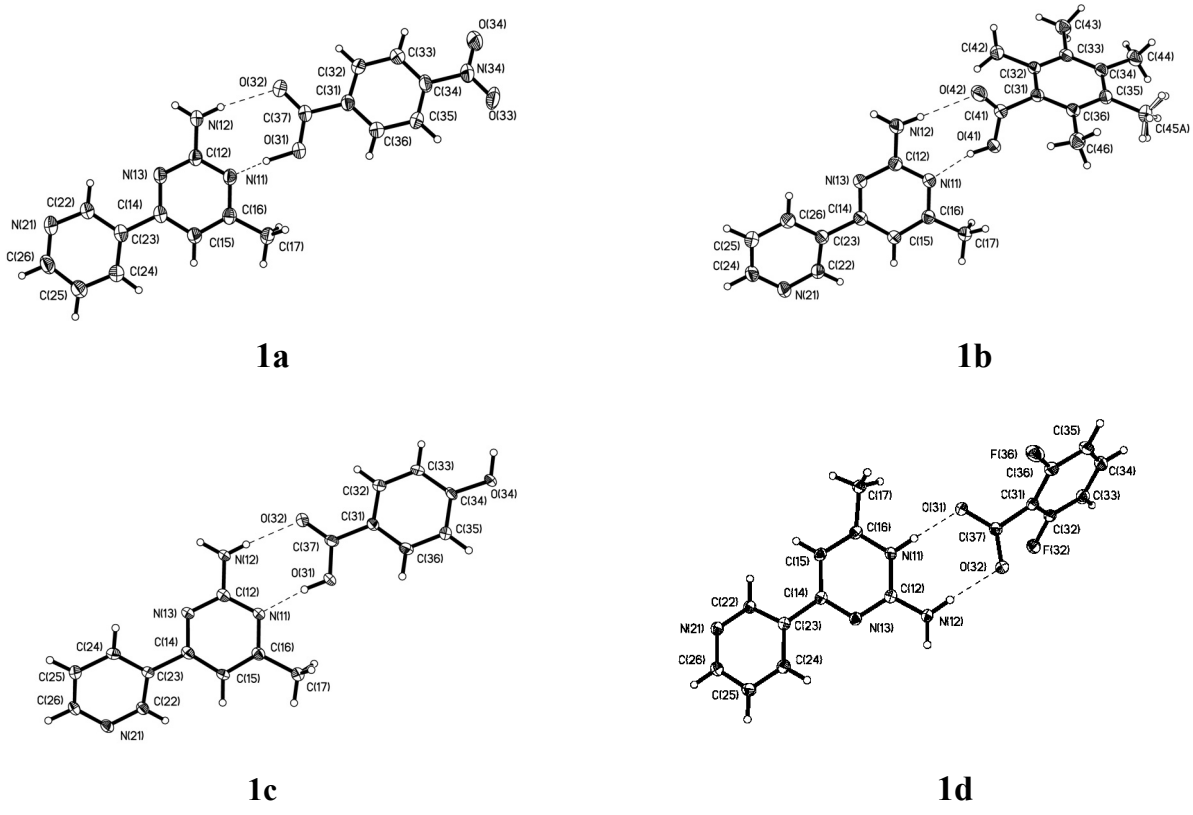


**Figure 2.11** Thermal ellipsoid plots (50 % probabilities) and labeling schemes for **1a-1d**.

### *2.3.4 Crystal structure of 3-(2-amino-4-methylpyrimidin-6-yl)pyridine:4-nitrobenzoic acid, 1a*

The primary motif in the crystal structure of **1a** is composed of SR **1** and one 4-nitrobenzoic acid molecule connected through the acid and amino-pyrimidine moieties. The primary synthons are O–H···N and N–H···O hydrogen bonds with O31···N11 and N12···O32 distances of 2.5274(18) Å and 3.034(2) Å respectively, Table 2.1. Secondary N–H···N hydrogen bonds, N12···N21, 3.015(2) Å, formed from the *anti*-amino proton and the pyridyl nitrogen atom extend the architecture into a four-component supermolecule, Figure 2.12.

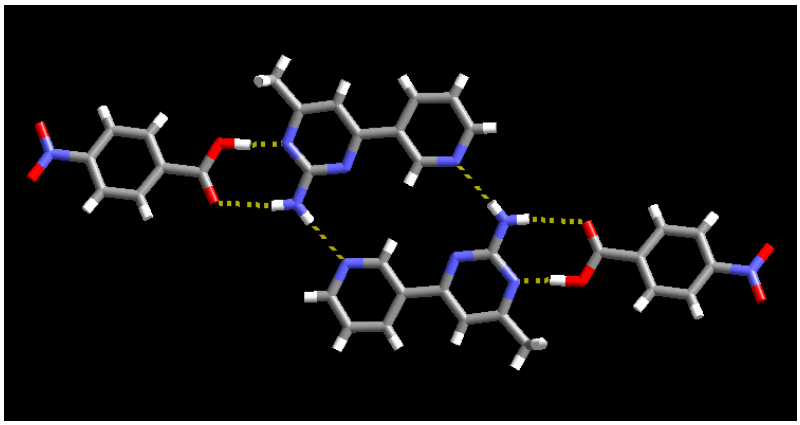

**Figure 2.12** A four-component supermolecule in **1a** formed through multiple O–H···N, N–H···O and N–H···N hydrogen bonds.

### *2.3.5 Crystal structure of 3-(2-amino-4-methylpyrimidin-6-yl)pyridine:pentamethylbenzoic acid, 1b*

The primary motif in the crystal structure of **1b** contains SR **1** and one pentamethylbenzoic acid molecule, interconnected through the acid and amino-pyrimidine moieties.. The primary synthons are O–H···N and N–H···O hydrogen bonds with O41···N11 and N12···O42 distances of 2.599(2) Å and 3.013(2) Å, respectively. Secondary N–H···N hydrogen bonds, N12···N21, 3.112(3) Å, between the *anti*-amino proton and the pyridyl nitrogen atom extend the architecture into a 1-D strand, Figure 2.13.

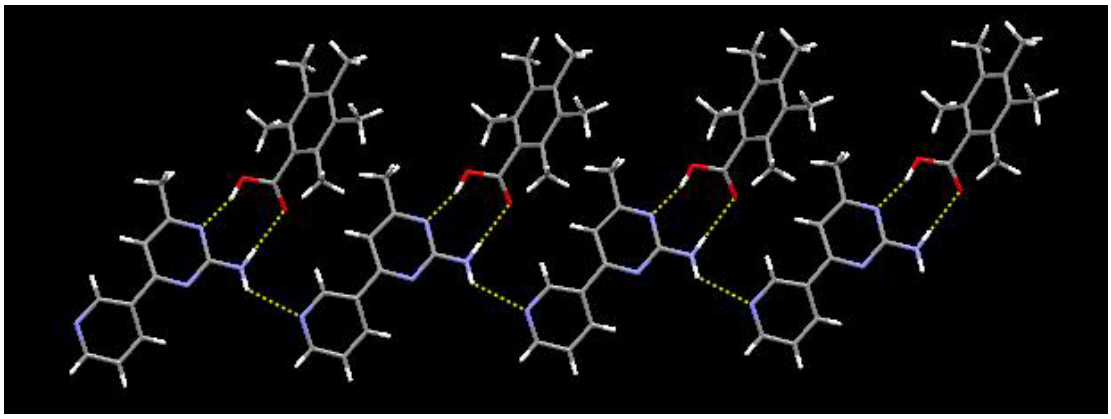

**Figure 2.13** 1-D strand formed through secondary N–H···N hydrogen bonds from 1:1 ligand:acid dimers of **1b**.

### *2.3.6 Crystal structure of 3-(2-amino-4-methylpyrimidin-6-yl)pyridine:4-hydroxybenzoic acid, 1c*

In the crystal structure of **1c** the main motif consists of SR **1** and one 4-hydroxybenzoic acid molecule, assembled via a complementary hydrogen-bond interaction between the carboxylic acid and the amino-pyrimidine moiety. The primary hydrogen bonds are O–H···N and N–H···O interactions with O31···N11 and N12···O32 distances of 2.656(3) Å and 2.906(3) Å, respectively. Secondary O–H···N hydrogen bonds, O34···N21, 2.728(3) Å, formed through the hydroxyl proton and the pyridyl nitrogen atom extend the architecture into a 1-D chain, Figure 2.14.

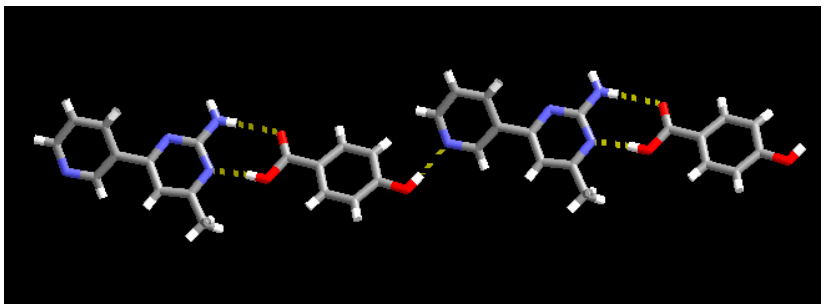

**Figure 2.14** Infinite 1-D chains formed through acid/amino-pyrimidine and hydroxy/pyridine hydrogen bonds in **1c**.

### *2.3.7 Crystal structure of 3-(2-amino-4-methylpyrimidinium-6-yl)pyridine:2,6-difluorobenzoate, 1d*

The 1:1 ionic salt of **1d** shows the primary motif composed of a protonated SR **1** and one 3,5-dinitrobenzoate ion, interlinked through the carboxylate and the amino-pyrimidinium moieties. The primary synthons in this structure are charge-assisted N–$H^{+}\cdots O^{-}$ and N–H$\cdots O^{-}$ hydrogen bonds, with $N^{+}11\cdots O^{-}31$ and N12$\cdots O^{-}32$ distances of 2.6608(17) Å and 2.8161(18) Å, respectively. The 1:1 ion pairs are linked into a 1-D zig-zag chain through N–H$\cdots$N hydrogen bonds, N12$\cdots$N21, 2.9888(19) Å, from the *anti*-amino proton and the pyridyl nitrogen atom, Figure 2.15.

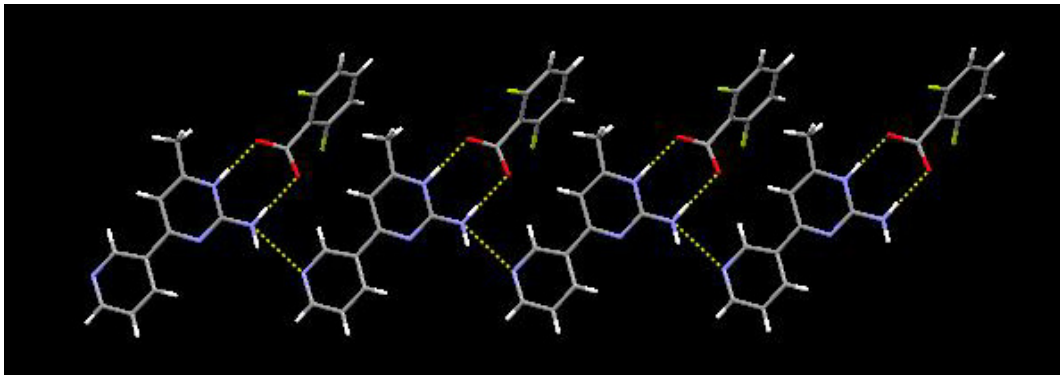

**Figure 2.15** 1-D strand formed through secondary N–H$\cdots$N hydrogen bonds from 1:1 ligand:acid dimers of **1d**.

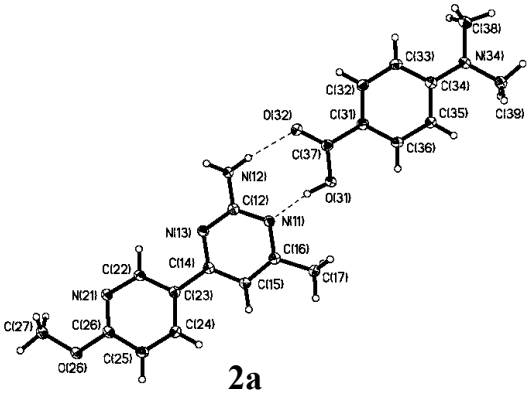


**2a**

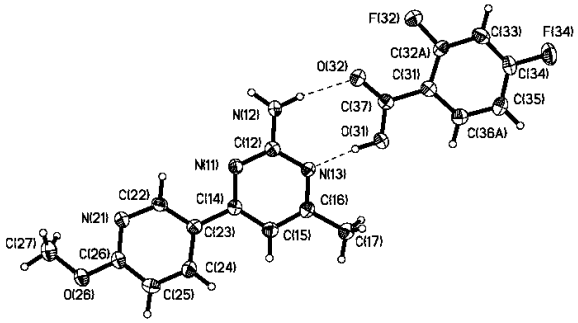


**2b**

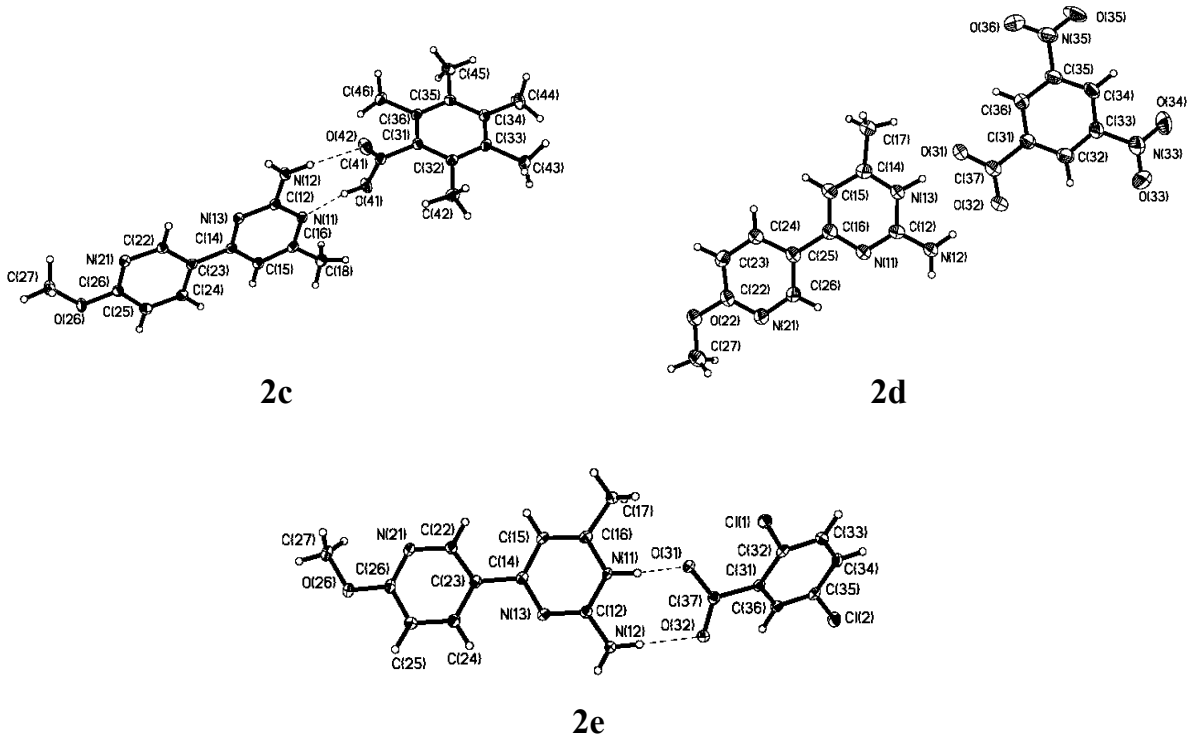


**Figure 2.16** Thermal ellipsoid plots (50 % probabilities) and labeling schemes for **2a-2e**.

### *2.3.8 Crystal structure of 4-methoxy-3-(2-amino-4-methylpyrimidin-6-yl)pyridine:4-N,N-dimethylaminobenzoic acid, 2a*

The primary supermolecule in the crystal structure of **2a** consists of SR **2** and one 4-*N,N*-dimethylaminobenzoic acid molecule; the two molecules are again connected through the acid and amino-pyrimidine moieties. The primary synthons in this structure are O–H···N and N–H···O hydrogen bonds with O31···N11 and N12···O32 distances of 2.6321(14) Å and 2.9173(15) Å, respectively. Secondary N–H···O hydrogen bonds, N12···O32, 2.8925(15) Å, formed from the *anti*-amino proton and the carboxylic acid oxygen atom extend the structure into a four-component supermolecule, Figure 2.17.

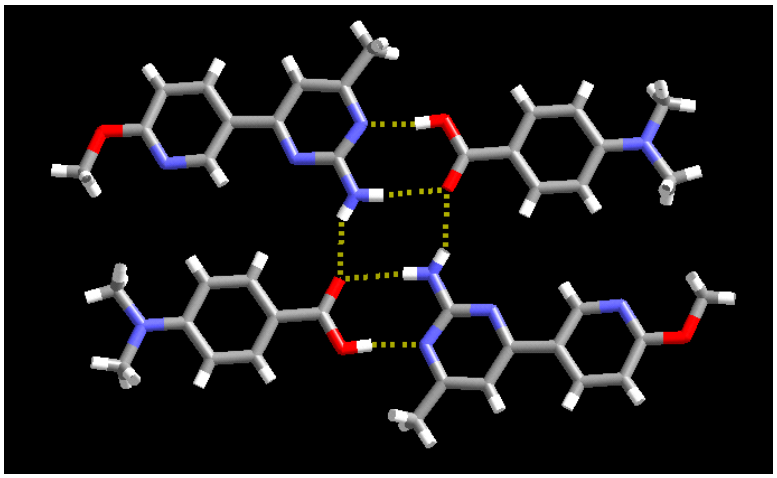

**Figure 2.17** Four-component supermolecule in **2a** formed through a series of O–H···N and N–H···O hydrogen bonds.

### *2.3.9 Crystal Structure of 4-methoxy-3-(2-amino-4-methylpyrimidin-6-yl)pyridine:2,4-difluorobenzoic acid, 2b*

In the crystal structure of **2b**, SR **2** and one 2,4-difluorobenzoic acid molecule form the primary hydrogen bonds between the carboxylic acid and amino-pyrimidine moieties. The primary synthons in this structure are O–H···N and N–H···O hydrogen bonds with O31···N13 and N12···O32 distances of 2.604(3) Å and 2.925(3) Å, respectively. Secondary N–H···N hydrogen bonds, N12···N11, 3.085(3) Å, between the *anti*-amino proton and the second pyrimidine nitrogen atom lead to a four-component supermolecule, Figure 2.18.

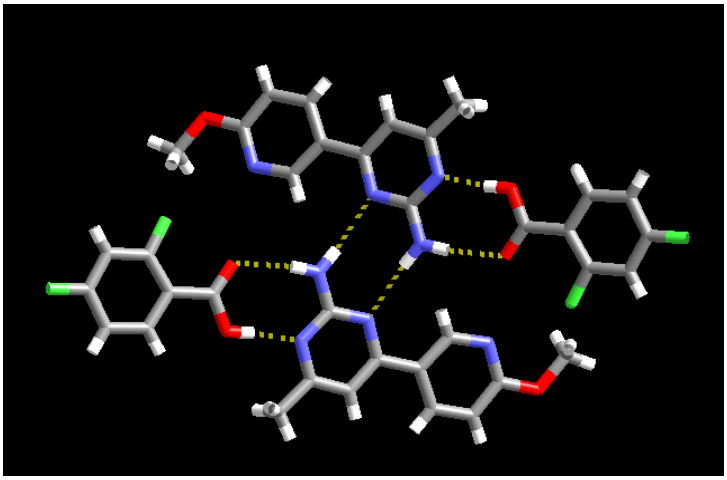

**Figure 2.18** Tetrameric supermolecule in **2b** formed through a series of O–H···N, N–H···O, and N–H···N hydrogen bonds.

### *2.3.10 Crystal structure of 4-methoxy-3-(2-amino-4-methylpyrimidin-6-yl)pyridine:pentamethylbenzoic acid, 2c*

The 1:1 co-crystal of **2c** shows a primary motif composed of SR **2** and one pentamethylbenzoic acid molecule, which are interlinked through the carboxylic acid and the amino-pyrimidine moieties. The primary synthons in this structure are O–H···N and N–H···O hydrogen bonds with O41···N11 and N12···O32 distances of 2.6515(18) Å and 2.9519(19) Å, respectively. Secondary N–H···N hydrogen bonds, N12···N11, 3.080(2) Å, between the *anti*-amino proton and the pyridyl nitrogen atom extend the architecture into a four-component supermolecule, Figure 2.19.

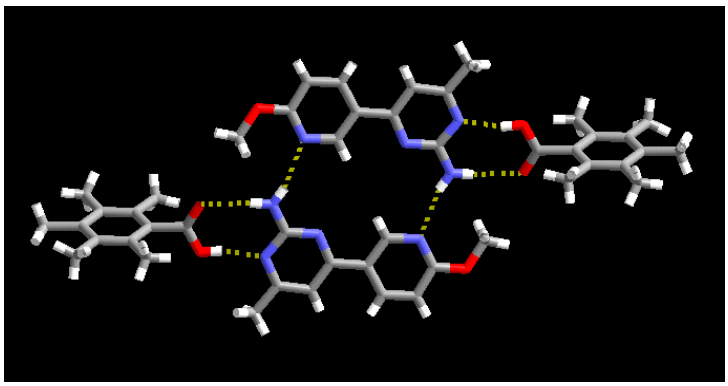

**Figure 2.19** Four-component supermolecule in **2c** formed through a series of O–H···N, N–H···O, and N–H···N hydrogen bonds.

### *2.3.11 Crystal structure of 4-methoxy-3-(2-amino-4-methylpyrimidinium-6-yl)pyridine:3,5-dinitrobenzoate, 2d*

The primary motif in the crystal structure of **2d** is composed of a protonated SR **2** and one 3,5-dinitrobenzoate ion connected through the benzoate and amino-pyrimidinium moieties. The primary synthons are charge-assisted $N–H^{+}\cdots O^{-}$ and $N–H\cdots O^{-}$ hydrogen bonds, with $N^{+}13\cdots O^{-}31$ and $N12\cdots O^{-}32$ distances of 2.569(3) Å and 2.833(4) Å, respectively. Secondary N–H···N hydrogen bonds, N12···N21, 3.060(4) Å, formed from the *anti*-amino proton and the pyridyl nitrogen atom extend the architecture into a four-component supermolecule, Figure 2.20.

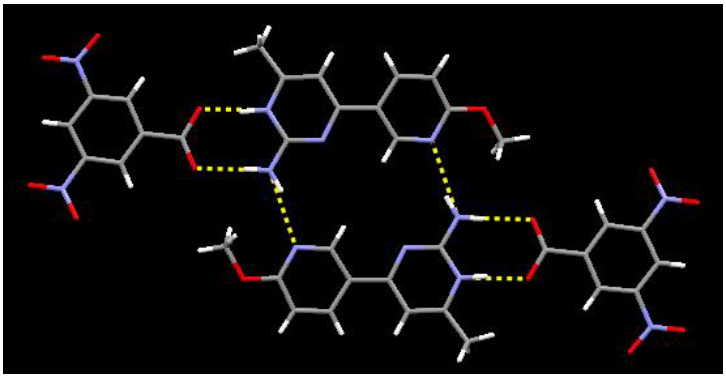

**Figure 2.20** A four-component supermolecule in **2d** formed through multiple charge-assisted and neutral hydrogen bonds.

### *2.3.12 Crystal structure of 4-methoxy-3-(2-amino-4-methylpyrimidinium-6-yl)pyridine:2,5 dichlorobenzoate, 2e*

The 1:1 ionic salt of **2e** shows the primary motif composed of a protonated SR **2** and one 2,5-dichlorobenzoate ion, interlinked through the carboxylate and the amino-pyrimidinium moieties. The primary synthons in this structure are charge-assisted $N–H^{+}\cdots O^{-}$ and $N–H\cdots O^{-}$ hydrogen bonds, with $N^{+}11\cdots O^{-}31$ and $N12\cdots O^{-}32$ distances of 2.5486(19) Å and 2.932(2) Å, respectively. The 1:1 ion pairs are linked into 1-D zig-zag chain through N–H···N hydrogen bonds, N12···N21, 3.008(2) Å, from the *anti*-amino proton and the pyridyl nitrogen atom, Figure 2.21.

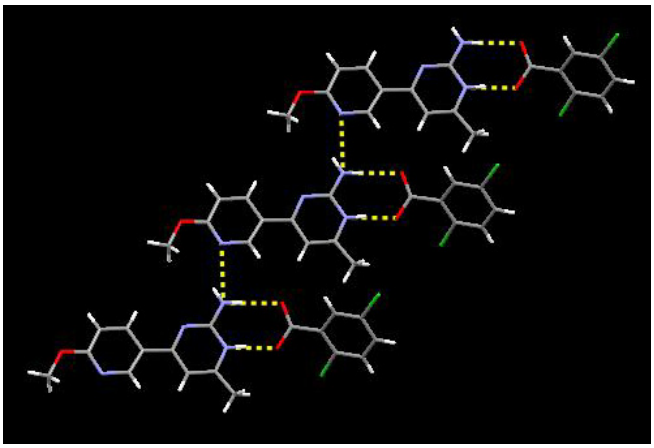

**Figure 2.21** 1-D strand formed through secondary N–H···N hydrogen bonds from 1:1 ionic ligand:carboxylate dimers of **2e**.

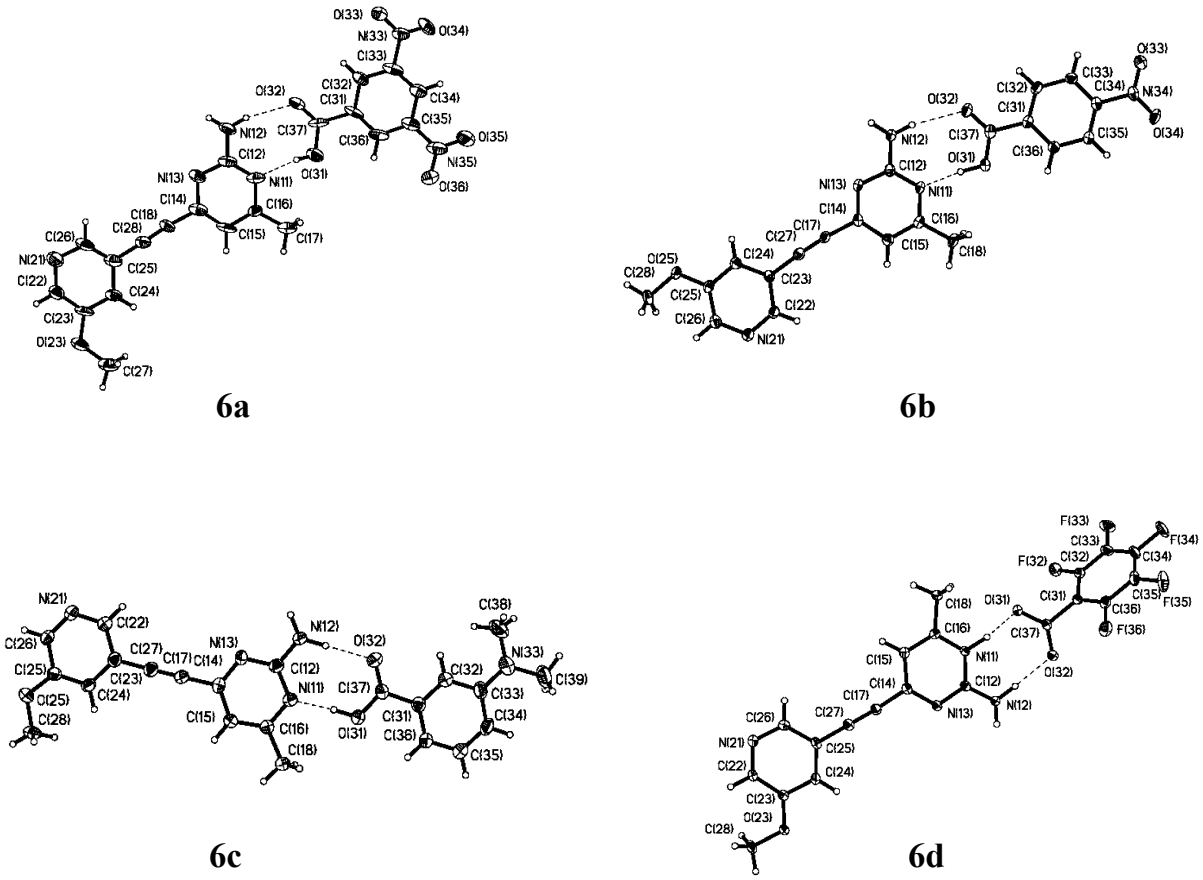


**Figure 2.22** Thermal ellipsoid plots (50 % probabilities) and labeling schemes for **6a-6d**.

### *2.3.13 Crystal structure of 1-(2-amino-4-methylpyrimidin-6-yl)-2-(3-methoxypyridin-5-yl)ethyne:3,5-dinitrobenzoic acid, 6a*

The central motif in the crystal structure of **6a** contains SR **6** and one 3,5-dinitrobenzoic acid molecule, constructed with complementary hydrogen bonds between the carboxylic acid and the amino-pyrimidine moieties. The primary synthons in this structure are O–H···N and N–H···O hydrogen bonds with O31···N11 and N12···O32 distances of 2.633(9) Å and 3.049(9) Å, respectively. Secondary N–H···N hydrogen bonds, N12···N13, 3.121(12) Å, between the *anti*-amino proton and second pyrimidine nitrogen atom extend the structure into a four-component supermolecule, Figure 2.23.

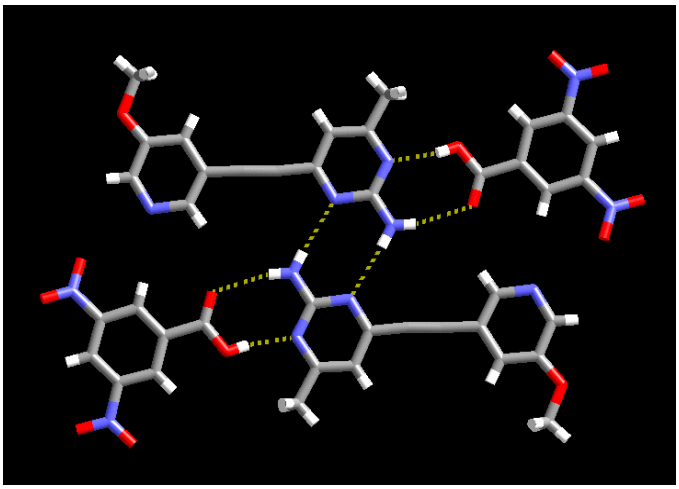

**Figure 2.23** Four-component supermolecule in **6a** formed through O–H···N, N–H···O, and N–H···N hydrogen bonds.

### *2.3.14 Crystal structure of 1-(2-amino-4-methylpyrimidin-6-yl)-2-(3-methoxypyridin-5-yl)ethyne:4-nitrobenzoic acid, 6b*

The crystal structure of **6b** contains SR **6** and one 4-nitrobenzoic acid molecule that are linked through hydrogen bonds between the carboxylic acid and the amino-pyrimidine moieties. The primary synthons are O–H···N and N–H···O hydrogen bonds with O31···N11 and N12···O32 distances of 2.652(3) Å and 3.109(3) Å, respectively. Secondary N–H···N hydrogen bonds, N12···N13, 3.122(3) Å, between the *anti*-amino proton and second pyrimidine nitrogen atom extend the structure into a four-component supermolecule, Figure 2.24.

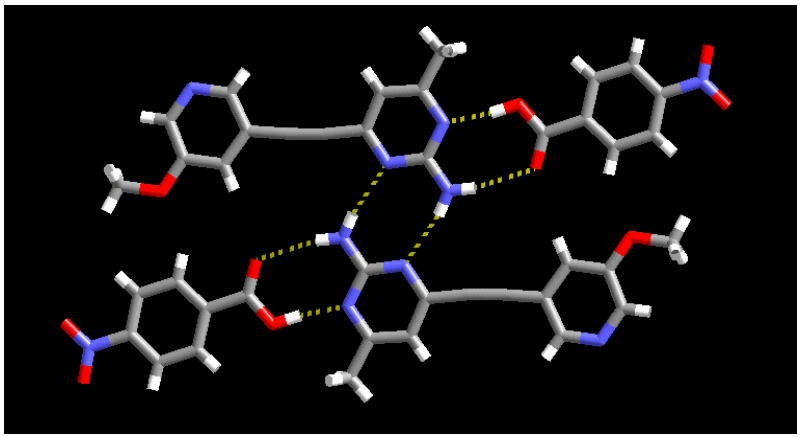

**Figure 2.24** Four-component supermolecule in **6b** formed through a series of O–H···N, N–H···O, and N–H···N hydrogen bonds.

### *2.3.15 Crystal structure of 1-(2-amino-4-methylpyrimidin-6-yl)-2-(3-methoxypyridin-5-yl)ethyne:3-N,N-dimethylaminobenzoic acid, 6c*

The crystal structure of **6c** contains a supermolecule constructed with SR **6** and one 3-*N*,*N*-dimethylaminobenzoic acid molecule, held together with hydrogen bonds between the carboxylic acid and the amino-pyrimidine site. The primary synthons are O–H···N and N–H···O hydrogen bonds with O31···N11 and N12···O32 distances of 2.625(3) Å and 2.908(4) Å, respectively. Secondary N–H···N hydrogen bonds, N12···N21, 3.023(3) Å, between the *anti*-amino proton and pyridine nitrogen atom extend the structure into a 1-D strand, Figure 2.25.

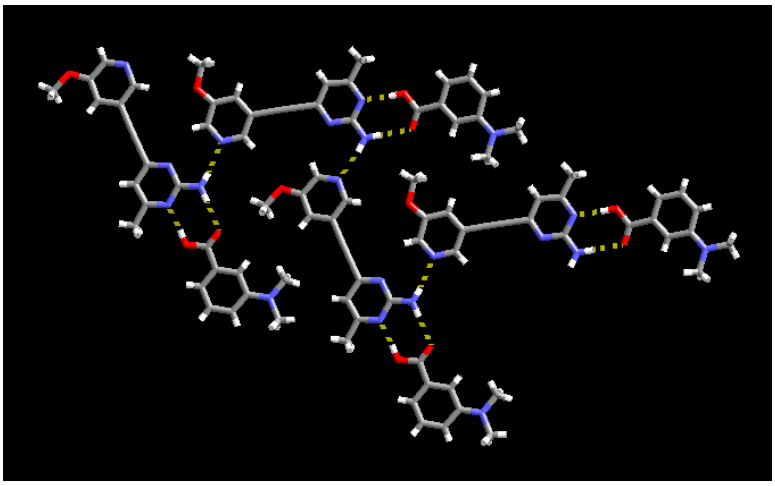

**Figure 2.25** 1-D strand in **6c** formed through secondary N–H···N hydrogen bonds between the *anti*-amino proton and the pyridine nitrogen atom.

### *2.3.16 Crystal structure of 1-(2-amino-4-methylpyrimidinium-6-yl)-2-(3-methoxypyridin-5-yl)ethyne:pentafluorobenzoate, 6d*

The crystal structure of **6d** contains a protonated SR **6** and one pentamethylbenzoate ion that are linked through charge-assisted hydrogen bonds between the carboxylate and the amino-pyrimidinium moieties. The primary synthons are charge-assisted $N–H^{+}\cdots O^{-}$ and $N–H\cdots O^{-}$ hydrogen bonds, with $N^{+}11\cdots O^{-}31$ and $N12\cdots O^{-}32$ distances of 2.597(17) Å and 2.8551(15) Å, respectively. Secondary N–H···N hydrogen bonds, N12···N13#1, 3.0941(16) Å, between the *anti*-amino proton and second pyrimidine nitrogen atom extend the structure into a four-component supermolecule, Figure 2.26.

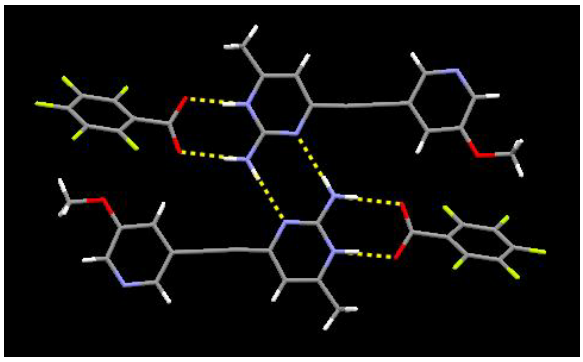

**Figure 2.26** Tetrameric supermolecule in **6d** formed through multiple charge-assisted and neutral hydrogen bonds.

## 2.4 Discussion

### *2.4.1 Formation of py-pym/carboxylic acid co-crystals and salts*

In every one of the nine co-crystals containing SR's **1**, **2**, or **6** and a carboxylic acid that we have obtained so far, the intermolecular interaction responsible for the construction of the main supramolecular assembly, is a pairwise O-H···N/N-H···O motif between the carboxylic acid and the amino-pyrimidine moieties. While the four ionic salts that were generated, between SR's **1**, **2**, or **6** and a carboxylic acid, formed a pairwise charge-assisted N–$H^{+}$···$O^{-}$ and N–H···$O^{-}$ motif between the amino-pyrimidinium and carboxylate moieties, Figure 2.27.

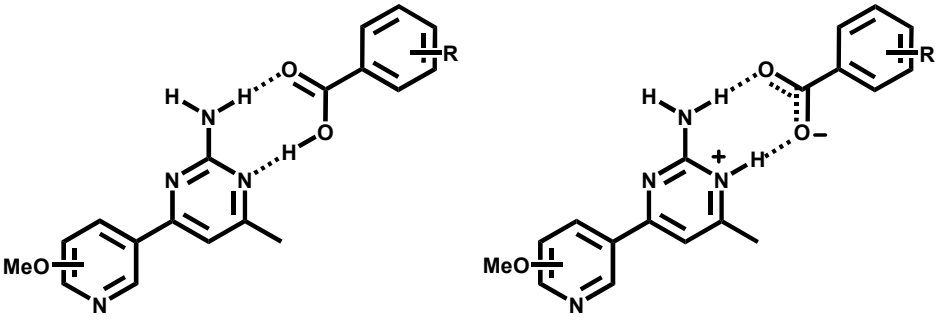


| | | |
|---|---|---|
| co-crystals or salts | 9 | 4 |
| primary synthon | amino-pyrimidine / carboxylic acid | amino-pyrimidinium / carboxylate |
| # of occurances | 9/9 | 4/4 |
| supramolecular yield | 100 % | 100 % |

**Figure 2.27** Summary of primary hydrogen bonding between SR's **1**, **2**, and **6** and various aromatic carboxylic acids.

It is possible that SR **2** did not form hydrogen bonds at the pyridyl site because the nitrogen atom is somewhat sterically hindered by the neighboring methoxy-group, potentially blocking an incoming carboxylic acid. However upon moving the methoxy-group to the *meta*-position, thereby removing any possibility of steric congestion, the approaching carboxylic acid still binds to the amino-pyrimidine moiety.

It is worth emphasizing that the carboxylic acid···pyridine interaction is a very effective tool for the assembly of molecular co-crystals,[14] and a search of the CSD[10] reveals that twenty-one such co-crystals, assembled via complementary carboxylic acid···amino-pyrimidine interactions, exist.[15] Clearly, both synthons are suitable supramolecular tools, capable of bringing together a variety of discrete molecular building blocks into heteromeric molecular co-crystals. The competition between the two types of synthons has not yet not been examined in a systematic manner, but the structural results presented herein, clearly demonstrate that the amino-pyrimidine site is much more competitive for a carboxylic acid than is a pyridine moiety.

### *2.4.2 Secondary hydrogen bonding motifs*

Beyond the primary interactions that take place between the carboxylic acid or carboxylate and 2-aminopyrimidine or 2-aminopyrimidinium (the dominating receptor in this study), we have identified four types of motifs in this series of compounds, Figure 2.28. For simplicity only the carboxylic acid/amino-pyrimidine synthon will be drawn as the model.

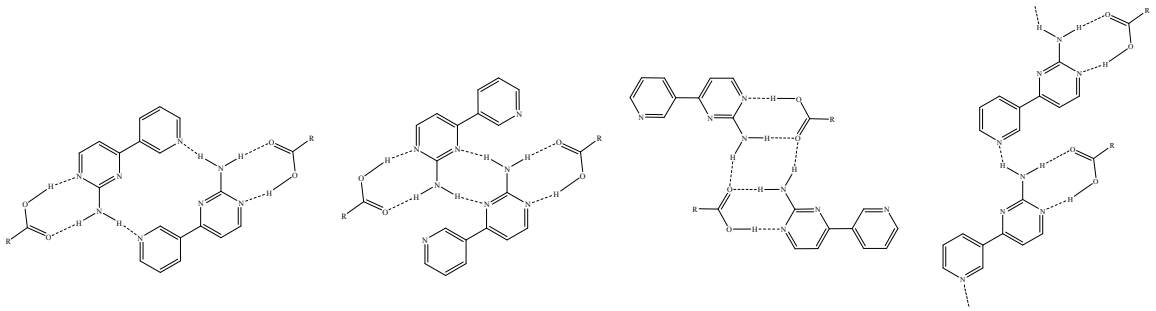

**I** **II** **III** **IV**

**Figure 2.28** Observed motifs between supramolecular dimers in co-crystals obtained from reactions between SR's **1**, **2**, and **6** and a carboxylic acid.

The frequency of occurrence of each type of motif is summarized in Table 2.3. The crystal structure of **2f** is somewhat different because the pyridine nitrogen atom is acting as an

acceptor for the O-H substituent of the carboxylic acid, which leaves the *anti*-$NH_2$ proton as a donor for the same hydroxyl group. However, in seven out of the twelve remaining structures, the *anti*-proton prefers to interact with the pyridine nitrogen atom. On one occasion, the pyridine nitrogen atom is engaged in a hydrogen bond with a C-H moiety located next to a nitro groups (in **6a**). The pyridine site is left alone on four occasions (in **2a**-**2b**, **6b**, and **6d**) with no short contacts to any C-H group.

**Table 2.3** Summary of secondary structural motifs

| SR | Carboxylic acid or Carboxylate | Structure | Secondary structural motif |
|---|---|---|---|
| 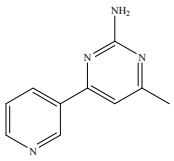 | 4-Nitrobenzoic acid | **1a** | **I** |
| | Pentamethylbenzoic acid | **1b** | **IV** |
| | 4-Hydroxybenzoic acid | **1c** | ---- |
| | 2,6-Difluorobenzoate | **1d** | **IV** |
| 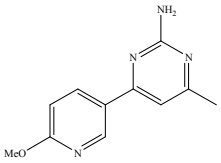 | 4-*N*,*N*-Dimethylaminobenzoic acid | **2a** | **III** |
| | 2,4-Difluorobenzoic acid | **2b** | **II** |
| | Pentamethylbenzoic acid | **2c** | **I** |
| | 3,5-Dinitrobenzoate | **2d** | **I** |
| | 2,4-Dichlorobenzoate | **2e** | **IV** |
| 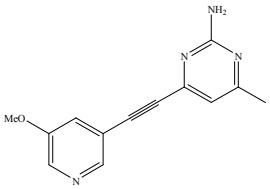 | 3,5-Dinitrobenzoic acid | **6a** | **II** |
| | 4-Nitrobenzoic acid | **6b** | **II** |
| | 3-*N*,*N*-Dimethylaminobenzoic acid | **6c** | **IV** |
| | Pentafluorobenzoate | **6d** | **I** |

### *2.4.3 Q-value determination through AM1 calculations*

We have been able to rationalize the observed structural behavior through a comparative analysis of the calculated electrostatic potential surfaces of the two binding sites. By simply subtracting the negative potential of the hydrogen-bond acceptor from the positive potential of

the hydrogen-bond donor in each binding site, a numerical value, Q, which represents overall hydrogen-bond capability is obtained, Equation 2.1. A comparison of the two numbers show significant differences between the amino-pyrimidine and pyridine sites and indicates that the former is likely to be the most effective hydrogen-bonding functionality in all three supramolecular reagents **1**, **2**, and **6**, Figure 2.29

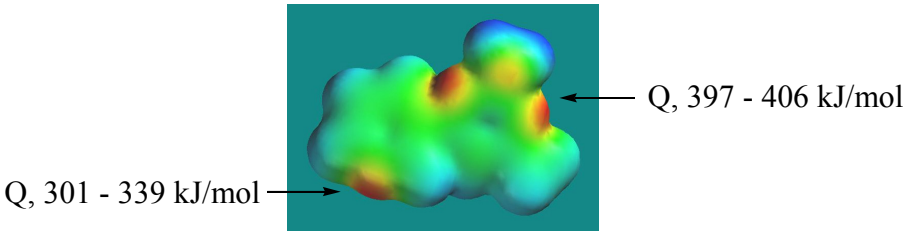


**Figure 2.29** Electrostatic potential surface displaying the Q-value ranges of SR's **1**, **2**, and **6**.

This ranking of binding sites is reflected by the structural preferences that we have observed in nine co-crystals and four ionic salts based upon **1**, **2**, and **6**. In fact, we have yet to find any exceptions to the expected behavior, which equates to a high supramolecular yield.

### *2.4.4. Product determination through IR spectroscopy*

In addition to determining the hydrogen bonding preference of an incoming acid, attempts were also made to characterize the supramolecular products, *i.e.* neutral co-crystal or salt, through infrared spectroscopy (IR), by observing specific stretches and band shifts within the spectrum. The classic neutral O-H···N stretches formed between a nitrogen containing heterocycle and an –OH group, give rise to pronounced bands in the regions of 2500 and 1900 $cm^{-1}$. Unfortunately, specific analysis was inconclusive since all products **1a-1d**, **2a-2e**, and **6a-6d** display stretches around 2500 and 1900 $cm^{-1}$, regardless if the final product was a co-crystal or salt.

We also attempted to track the shift of the carbonyl stretch. A typical monomeric C=O stretching band of a carboxylic acid, when on an aromatic ring, appears around 1760 $cm^{-1}$, while the acid dimeric C=O stretching mode absorbs at a lower frequency in the 1720-1706 $cm^{-1}$ region. The carboxylate ion displays a strong asymmetrical stretching band around 1650-1550 $cm^{-1}$ and a weaker symmetric stretch ~1400 $cm^{-1}$.[16] A summary of the observed carbonyl stretches from **1a-1d**, **2a-2e**, and **6a-6d** are displayed in Table 2.4. The results do not directly

correlate with what is expected based on previously reported data, however some trends within this set of compounds are identified.[16]

The IR spectra of ionic compounds **1d**, **2d**, **2e** and **6d**, in which a carboxylate is present, all display a strong stretching band around 1700 $cm^{-1}$, instead of in the 1650 – 1550 $cm^{-1}$ region. Furthermore, neutral structures, containing a relatively strong acid *i.e.* **1a**, **2b**, **6a**, and **6b**, also show an increase in wavenumbers of the carbonyl stretch compared to those of weaker acids.

**Table 2.4** Summary of IR data for compounds **1a-1d**, **2a-2e**, and **6a-6d**

| Compound | **1a** | **1b** | **1c** | **1d** | **2a** | **2b** | **2c** | **2d** | **2e** | **6a** | **6b** | **6c** | **6d** |
|---|---|---|---|---|---|---|---|---|---|---|---|---|---|
| Observed stretch ($cm^{-1}$) | 1696 | 1635 | 1655 | 1700 | 1605 | 1685 | 1653 | 1701 | 1700 | 1690 | 1696 | 1655 | 1700 |
| Product | C | C | C | S | C | C | C | S | S | C | C | C | S |

Note: product = C, co-crystal; product = S, salt

It seems, within this system, that the IR data was inconclusive in accurately determining whether proton-transfer has occurred or not. Furthermore, an explanation cannot be given at this time as to why the structures containing a carboxylate ion have distinct bands at higher wavenumbers (~1700) than a neutral carbonyl moiety.

Finally, we have been able to establish differences in hydrogen-bond capacity of related binding sites by combining readily available and computationally inexpensive semi-empirical methods with systematic structural data. The calculated numbers themselves are not likely to offer strict correlations with intermolecular bond-energies or other measurable physical quantities. However, they do offer a very useful tool for establishing hydrogen-bond preferences in series of related compounds which, in turn, can allow us to predict connectivities, stoichiometries and dimensionalities of supramolecular architectures.

# References


[1] (a) Desiraju, G. R. *Angew. Chem., Int. Ed. Engl*. **1995**, *34*, 2311; (b) Desiraju, G. R. *Acc. Chem. Res*. **2002**, *35*, 565; (c) Moulton, B.; Zaworotko, M. J. *Chem. Rev*. **2001**, *101*, 1629; (c) MacGillivray, L.; *CrystEngComm* **2004**, *6*, 77; (d) Lehn, J.-M. *Science* **2002**, *295*, 2400.

[2] (a) Walsh, R. B.; Padgett, C. W.; Metrangolo, P.; Resnati, G.; Hanks, T. W.; Pennington, W. T. *Cryst. Growth Des.* **2001**, *1*, 165; (b) Metrangolo, P.; Pilati, T.; Resnati, G.; Stevenazzi, A. *Chem. Commun*. **2004**, 1492; (c) De Santis, A.; Forni, A.; Liantonio, R.; Metrangolo, P.; Pilati, T.; Resnati, G. *Chem. Eur. J*. **2003**, *9*, 3974; (d) Metrangolo, P.; Neukirch, H.; Pilati, T.; Resnati, G. *Acc. Chem. Res.* **2005**, *38*, 386.

[3] Motohiro, N. *CrystEngComm* **2004**, *6*, 130 and references within.

[4] (a) Shattock, T. R.; Vishweshwar, P.; Wang, Z.; Zaworotko, M. J. *Cryst. Growth. Des*. **2005**, *5*, 2046; (b) Aakeröy, C. B.; Desper, J.; Urbina, J. F. *CrystEngComm* **2005**, *31*, 193; (c) Braga, D.; Grepioni, F. *Chem. Commun*. **2005**, 3635; (d) Saha, B. K.; Nangia, A.; Jaskolski, M. *CrystEngComm* **2005**, 335; (e) Basavoju, S.; Nangia, A. *Cryst. Growth. Des*. **2005**, *5*, 1683; (f) Varaghese, S.; Pedireddi, V. R. *Chem.-Eur. J*. **2006**, *12*, 1597; (g) Aakeröy, C. B.; Beatty, A. M.; Helfrich, B. A. *J. Am. Chem. Soc.* **2002**, *124*, 14425.

[5] Langner, R.; Zundel, C. J. *Chem. Soc. Faraday Trans.* **1995**, *91*, 3831.

[6] (a) Hunter, C. A. *Angew. Chem. Int. Ed*. **2004**, *43*, 5310; (b) Henry, M.; Hosseini, M. W. *New J. Chem*. **2004**, *28*, 897.

[7] (a) Etter, M. C. *Acc. Chem. Res*. **1990**, *23*, 120; (c) Etter, M. C. *J. Phys. Chem*.**1991**, *95*, 4601.

[8] Dissociation constants of organic bases in aqueous solutions, ed. D. D. Perrin, International Union of Pure and Applied Chemistry, London, Butterworths, 1965.

[9] Valiyaveettil, S.; Enkelmann, V.; Mullen, K. *Chem. Commun*. **1994**, 2097.

[10] Cambridge Structural Database ConQuest version 1.8.

[11] Li, W.; Nelson, D. P.; Jensen, M. S.; Hoerner, R. S.; Cai, D.; Larsen, R. D.; Reider, P. J. *J. Org. Chem*. **2002**, *67*, 5394.

[12] Comins, D. L.; Killpack, M. O. *J. Org. Chem*. **1990**, *55*, 69.

[13] (a) Aakeröy, C. B.; Desper, J.; Urbina, J. F. *Chem. Commum*. **2005**, 2820; (b) Aakeröy, C. B.; Desper, J.; Scott, B. M. T. *Chem. Commun*. **2006**, 1445; (c) Aakeröy, C. B.; Beatty, A. M.; Helfrich, B. A. *Angew. Chem. Int. Ed*. **2001**, *40*, 3240.

[14] (a) Shan, N.; Bond, A. D.; Jones, W. *New J. Chem*. **2003**, *2*, 365; (b) Arora, K. K.; Pedireddi, V. R. *J. Org. Chem*. **2003**, *67*, 556; (c) Sugiyama, T.; Meng, J.; Matsuura, T. *J. Mol. Struct*. **2002**, *611*, 53; (d) Shan, N.; Batchelor, E.; Jones, W. *Tetrahedron Lett*. **2002**, *43*, 8721; (e) Bhogala, B. R.; Nangia, A. *Cryst. Growth Des*. **2002**, *2*, 325; (f) Zaworotko, M. J. *Chem. Commun*. **2001**, 1.

[15] (a) Chinnakali, K.; Fun, H.-K.; Goswami, S.; Mahapatra, A. K.; Nigam, G. D. *Acta. Cryst*. **1999**, *C55*, 399; (b) Goswami, S.; Mahapatra, A. K.; Ghosh, K.; Nigam, G. D.; Chinnakali, K.; Fun, H.-K. *Acta. Cryst*. **1999**, *C55*, 87; (c) Lynch, D. E.; Smith, G.; Byriel, K. A.; Kennard, C. H. L. *Aust. J. Chem*. **1998**, *51*, 403; (d) Smith, G.; Gentner, J. M.; Lynch, D. E.; Byriel, K. A.; Kennard, C. H. L. *Aust. J. Chem*. **1995**, *48*, 1151.

[16] Silverstein, R. M.; Bassler, G. C.; Morrill, T. C. Spectroscopic Identification of Organic Compounds, John Wiley and Sons: New York, 1991.

# CHAPTER 3 - Balancing intermolecular hydrogen-bond interactions for the directed assembly of ternary co-crystals utilizing a 4-pyridyl-aminopyrimidine supramolecular reagent

## 3.1 Introduction

The design of synthetic methodologies, involves not only optimization of the reaction conditions *i.e.* solvent, temperature, reaction time etc., but also an examination of the scope and/or limitations of a specific chemical reaction.[1] Expansion of the reaction scope usually involves subtle modifications to a range of reactants including but not limited to, addition or subtraction of electron donating or withdrawing groups and steric modifications, within the reactants. These details can have dramatic effects on formation and yields of the desired products.

The goal of any supramolecular synthesis is a specific target that can be defined in terms of its connectivity and function, while the limits/limitations of a specific supramolecular strategy can be determined by a range of reaction conditions.

One such example, of expanding the supramolecular reaction scope, was outlined in Chapter 2, with the design and synthesis of three pyridyl/amino-pyrimidine (py-pym) SR's. In each case the 2-amino-4-methylpyrimidin-6-yl fragment remained unchanged, however on SR **2** a methoxy group was appended to the pyridine ring in the *ortho*-position, while on SR **6** the methoxy substituent was in the *meta*-position on the pyridine ring. Within this supramolecular reaction system, subtle covalent modifications, *i.e.* addition of methoxy functional groups, were used to increase the electron density on the pyridyl nitrogen atom. However, the hydrogen bonding capabilities of the pyridyl nitrogen atom, with respect to incoming aromatic carboxylic acid, remained unaffected by the addition. In each case (13/13, 100% supramolecular yield) the 1:1 product was constructed through the robust amino-pyrimidine···carboxylic acid or amino-pyrimidinium···carboxylate synthons, independent of the introduction of an electron-donating methoxy substituent.[2]

A search through the CSD for structures containing pyridine···carboxylic acid synthons revealed one 1:1 co-crystal of a pyridine/amino-pyrimidine ligand and an aromatic carboxylic acid,[3] Figure 3.1.

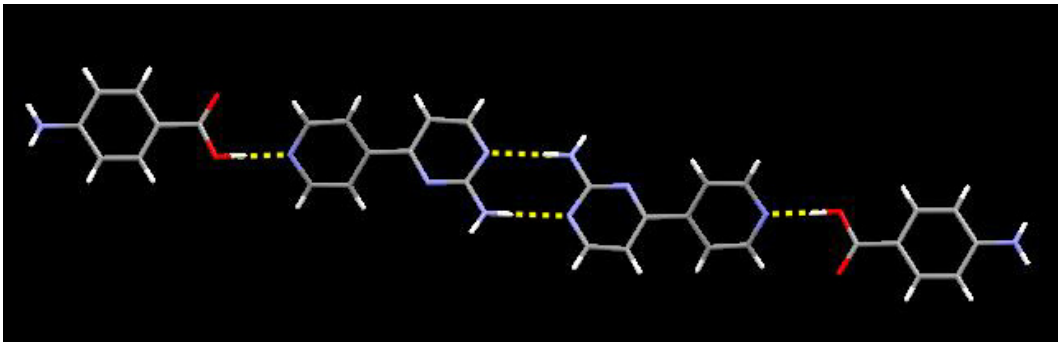

**Figure 3.1** 1:1 Tetrameric supermolecule formed through acid···pyridine and amino-pyrimidine···amino-pyrimidine synthons.

Surprisingly, compared to our results from Chapter 2, the carboxylic acid forms an O-H···N hydrogen bond with the 4-pyridyl moiety, leaving the amino-pyrimidine moieties to engage in self-complementary N-H···N hydrogen bonds. The hydrogen bonding connectivities within the crystal structure, differ from what we observed in our py-pym SR/carboxylic acid systems.

To further probe our supramolecular reaction scope between py-pym SR's and aromatic carboxylic acids, we decided to synthesize a structural analog of **1**, Figure 3.2. Supramolecular reagent **7** has a similar chemical make-up to SR's **1**, **2**, and **6** however the pyridyl nitrogen atom has been moved to the 4-position, with respect to the amino-pyrimidine ring, and the methoxy substituents have been removed.

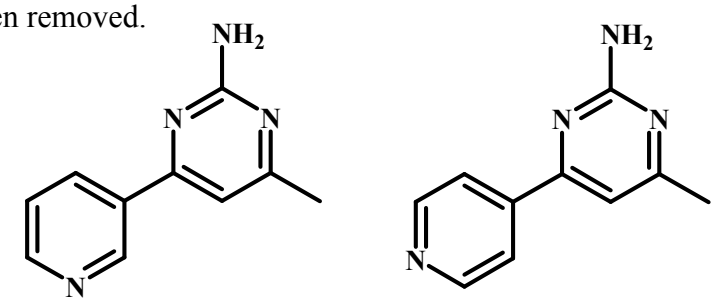


**1** **7**

**Figure 3.2** Two different SR's, 3-(2-amino-4-methylpyrimidin-6-yl)pyridine (left) and 4-(2-amino-4-methylpyrimidin-6-yl)pyridine (right), based purely on the placement of the pyridine nitrogen atom.

This chapter attempts to answer the following questions, (1) does the overall hydrogen-bond accepting ability increase in strength, within the py-pym/carboxylic acid systems, if the pyridyl-nitrogen is moved from the 3- to the 4-position, and (2) does addition or subtraction of the methyl-group on the amino-pyrimidine ring play a role in forming amino-pyrimidine/carboxylic acid interactions? These questions will be addressed through semi-empirical AM1 calculations and single-crystal X-ray analysis of molecular co-crystals and salts formed from SR **7** and a variety of aromatic carboxylic acids.

## 3.2 Experimental

### *3.2.1 Synthesis*

All chemicals were purchased from Aldrich and used without further purification. 4-Pyridylboronic acid was purchased from COMBI-BLOCKS and used as is. Melting points were determined on a Fisher-Johns melting point apparatus and are uncorrected. Compounds were prepared for infrared spectroscopic (IR) analysis as a mixture in KBr. $^{1}H$ and $^{13}C$ NMR spectra were recorded on a Varian Unity plus 400 MHz spectrometer in $CDCl_3$. Electrospray Ionization – Ion-Trap Mass Spectrometry (ESI-IT-MS) was carried out on a Bruker Daltonics Esquire 3000 Plus.

#### *3.2.1.1 Synthesis of 4-(2-amino-4-methylpyrimidin-6-yl)pyridine, 7*

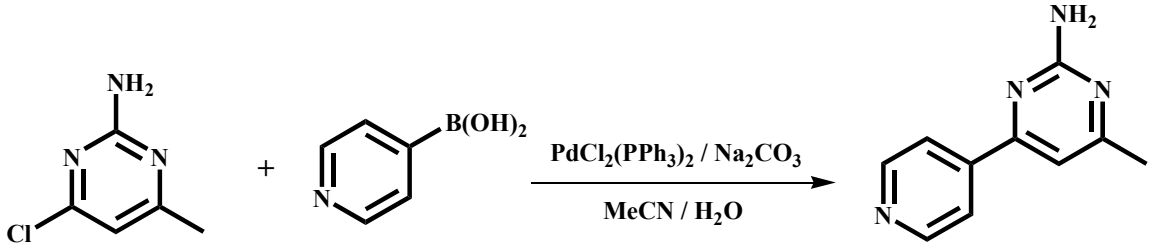


A mixture of 2-amino-4-chloro-6-methylpyrimidine (1.20g, 8.39 mmol), 4-pyridylboronic acid (1.14g, 9.27 mmol), sodium carbonate (0.500g, 6.03 mmol), *bis*(triphenylphosphine)palladium(II) dichloride (180mg, 0.256 mmol, 2.5 mol %) was added to a round bottom flask. Acetonitrile (50 mL) and water (50 mL) were added and dinitrogen bubbled through the resultant mixture for 10 minutes. A condenser was attached and the mixture heated at 80 ˚C under a dinitrogen atmosphere. The reaction was monitored by TLC and allowed

to cool to room temperature on completion (48 hours). The solution was then diluted with ethyl acetate (150 mL), washed with water (3 x 100 mL) then washed with saturated aqueous sodium chloride (1 x 100 mL). The organic layer was separated and dried over magnesium sulfate. The solvent was removed on a rotary evaporator and the residue chromatographed on silica with ethyl acetate as the eluant. The product was isolated as a light yellow/white solid. The product **7** was then recrystallized from an ethanol/chloroform mixture as colorless plate-shaped crystals, (1.1g, 71 %). M.p: 179-181 ºC; $^{1}$H NMR ($\delta_H$; 400 MHz, $CDCl_3$): 8.74 (dd, J = 4.4Hz, J = 2Hz, 2H), 7.84 (dd, J = 4.4Hz, J = 2Hz, 2H), 6.97 (s, 1H), 5.18 (s, 2H), 2.45 (s, 3H); $^{13}$C NMR ($\delta_C$; 200 MHz, $CDCl_3$):169.6, 163.4, 162.7, 150.5, 144.7, 121.0, 107.5, 24.2; IR (KBr): 3318, 3151, 1581, 1376. ESI-IT-MS *m/z* 187 ([**7** + H]$^+$).

### *3.2.2 Synthesis of co-crystals and salts*

#### *3.2.2.1 Synthesis of 4-(2-amino-4-methylpyrimidin-6-yl)pyridine:4-hydroxybenzoic acid, 7a*

4-(2-Amino-4-methylpyrimidin-6-yl)pyridine (10 mg, 0.05 mmol) and 4-hydroxybenzoic acid (7 mg, 0.05 mmol) were placed in a vial containing ethanol (6 mL) and heated until a clear homogeneous solution was obtained. After one day of slow evaporation, colorless block-shaped crystals were obtained. M.p. 243-245 °C; IR (KBr pellet) $\upsilon$ 3334 and 3160 cm$^{-1}$ ($NH_2$, m), 2479 and 1875 cm$^{-1}$ (O-H···N, br), 1670 cm$^{-1}$ (C=O, m).

#### *3.2.2.2 Synthesis of 4-(2-amino-4-methylpyrimidin-6-yl)pyridine:3-hydroxybenzoic acid, 7b*

4-(2-Amino-4-methylpyrimidin-6-yl)pyridine (10 mg, 0.05 mmol) and 3-hydroxybenzoic acid (7 mg, 0.05 mmol) were placed in a vial containing ethanol (6 mL) and heated until a clear homogeneous solution was obtained. After one day of slow evaporation, colorless block-shaped crystals were obtained. M.p. 230-232 °C; IR (KBr pellet) $\upsilon$ 3329 and 3211 cm$^{-1}$ ($NH_2$, m), 2694 and 1910 cm$^{-1}$ (O-H···N, br), 1623 cm$^{-1}$ (C=O, m).

#### *3.2.2.3 Synthesis of 4-(2-amino-4-methylpyrimidinium-6-yl)pyridine:3,5-dinitrobenzoate, 7c*

4-(2-Amino-4-methylpyrimidin-6-yl)pyridine (10 mg, 0.05 mmol) and 3,5-dinitrobenzoic acid (11 mg, 0.05 mmol) were placed in a beaker containing ethanol (5 mL). The beaker was heated until a clear homogeneous solution was obtained. After three days, yellow rod-shaped

crystals formed. Dec 208 °C; IR (KBr pellet) $\upsilon$ 3447 and 3176 $cm^{-1}$ ($NH_2$, m), 1696 $cm^{-1}$ (C=O, m).

#### *3.2.2.4 Synthesis of 4-(2-amino-4-methylpyrimidin-6-yl)pyridine:3-bromo-4-methylbenzoic acid, 7d*

4-(2-Amino-4-methylpyrimidin-6-yl)pyridine (10 mg, 0.05 mmol) and 3-bromo-4-methylbenzoic acid (23 mg, 0.11 mmol) were placed in a vial containing acetonitrile (6 mL) and heated until a clear homogeneous solution was obtained. After two days of slow evaporation, yellow prism-shaped crystals were obtained. M.p. 190-192 °C; IR (KBr pellet) $\upsilon$ 3380 and 3196 $cm^{-1}$ ($NH_2$, m), 2387 and 1916 $cm^{-1}$ (O-H···N, br), 1690 $cm^{-1}$ (C=O, m).

#### *3.2.2.5 Synthesis of 4-(2-amino-4-methylpyrimidinium-6-yl)pyridine:3,5-dinitrobenzoate, 7e*

4-(2-Amino-4-methylpyrimidin-6-yl)pyridine (10 mg, 0.05 mmol) and 3,5-dinitrobenzoic acid (22 mg, 0.10 mmol) were placed in a beaker containing ethanol (5 mL). The beaker was heated until a clear homogeneous solution was obtained. After three days, yellow block-shaped crystals formed. M.p. 237-239 °C; IR (KBr pellet) $\upsilon$ 3391 and 3170 $cm^{-1}$ ($NH_2$, m), 2443 and 1916 $cm^{-1}$ (O-H···N, br), 1696 $cm^{-1}$ (C=O, m).

#### *3.2.2.6 Synthesis of 4-(2-amino-4-methylpyrimidinium-6-yl)pyridine:pentamethylbenzoic acid:pentafluorobenzoate, 7f*

4-(2-Amino-4-methylpyrimidin-6-yl)pyridine (10 mg, 0.05 mmol), pentamethylbenzoic acid (11 mg, 0.06 mmol), and pentafluorobenzoic acid (12 mg, 0.06 mmol) were placed in a beaker containing ethanol (5 mL). The beaker was heated until a clear homogeneous solution was obtained. After two days, block-shaped crystals formed. M.p. 136-138 °C; IR (KBr pellet) $\upsilon$ 3370 and 3083 $cm^{-1}$ ($NH_2$, m), 1675 $cm^{-1}$ (C=O, m).

### *3.2.3 AM1 Calculations*

Molecular structures of SR's **7**, 2-amino-4-(3-pyridyl)pyrimidine and 2-amino-4-(4-pyridyl)pyrimidine were constructed using Spartan '04 (Wavefunction, Inc. Irvine, CA). The geometris of all three molecules were optimized using AM1, with the maxima and minima in the electrostatic potential surface (0.002 e/au isosurface) determined using a positive point charge in the vacuum as a probe.

## 3.3 Results

Crystallographic information for **7**, **7(1)**, and **7a-7f** displayed in Tables B.2 and hydrogen-bond geometries for **7**, **7(1)**, and **7a-7f** are listed in Table **3.1**

**Table 3.1** Hydrogen-Bond Geometries for **7**, **7(1)**, and **7a-7f**

| Structure | D-H•••H | d(D-H)/Å | d(H•••A)/Å | d(D•••A)/Å | <(DHA)/º |
|---|---|---|---|---|---|
| **7**[i] | N(12)-H(12A)...N(11)#1 | 0.93(2) | 2.17(2) | 3.052(2) | 159.3(18) |
| | N(12)-H(12B)...N(13)#2 | 0.85(2) | 2.29(2) | 3.1222(19) | 166.0(19) |
| **7(1)**[ii] | N(12-1)-H(12B-1)...N(11-2) | 0.86 | 2.23 | 3.067(4) | 164.4 |
| | N(12-1)-H(12A-1)...N(21-3) | 0.86 | 2.20 | 3.033(4) | 161.8 |
| | N(12-2)-H(12B-2)...N(11-1) | 0.86 | 2.20 | 3.042(4) | 168.2 |
| | N(12-2)-H(12A-2)...N(21-4) | 0.86 | 2.18 | 3.008(5) | 162.6 |
| | N(12-3)-H(12A-3)...N(21-1)#1 | 0.86 | 2.19 | 3.013(5) | 160.3 |
| | N(12-3)-H(12B-3)...N(11-4)#2 | 0.86 | 2.22 | 3.047(4) | 160.9 |
| **7a**[iii] | O(31)-H(31)...N(11) | 0.98(2) | 1.76(2) | 2.732(2) | 173(2) |
| | N(12)-H(12A)...O(32) | 0.89(2) | 1.94(2) | 2.824(2) | 172(2) |
| | N(12)-H(12B)...N(13)#1 | 0.94(2) | 2.14(2) | 3.069(2) | 172.6(18) |
| | O(34)-H(34)...N(21)#2 | 0.86(2) | 1.88(2) | 2.724(2) | 166(2) |
| **7b**[iv] | O(31)-H(31)...N(11) | 1.10(3) | 1.56(3) | 2.646(3) | 169(3) |
| | N(12)-H(12A)...O(32) | 0.97(3) | 1.94(3) | 2.887(4) | 165(3) |
| | N(12)-H(12B)...O(33)#1 | 0.94(3) | 2.09(3) | 2.975(4) | 156(3) |
| | O(33)-H(33)...N(21)#2 | 0.99(3) | 1.71(3) | 2.702(3) | 172(3) |
| **7c**[v] | N(11)-H(11)...O(31) | 0.88 | 1.77 | 2.646(6) | 175.2 |
| | N(12)-H(12A)...O(42) | 0.88 | 1.91 | 2.783(6) | 174.2 |
| | N(12)-H(12B)...N(21)#1 | 0.88 | 2.12 | 2.962(7) | 158.6 |
| **7d**[vi] | N(12)-H(12B)...O(42) | 0.88 | 2.08 | 2.948(7) | 168.7 |
| | N(12)-H(12A)...O(32)#1 | 0.88 | 2.14 | 2.959(9) | 154.9 |
| | O(31)-H(31)...N(21) | 0.84 | 1.77 | 2.600(8) | 170.7 |
| | O(41)-H(41)...N(11) | 0.84 | 1.79 | 2.620(7) | 167.5 |
| **7e**[vii] | N(11)-H(11)...O(42) | 1.032(16) | 1.507(16) | 2.5341(14) | 172.5(15) |
| | N(12)-H(12A)...O(41) | 0.889(18) | 2.169(18) | 3.0559(15) | 176.3(16) |
| | N(12)-H(12B)...O(41)#1 | 0.850(18) | 2.115(18) | 2.8515(16) | 144.8(15) |
| | O(31)-H(31)...O(21) | 0.996(17) | 1.603(17) | 2.5983(14) | 177.6(16) |
| **7f**[viii] | N(11)-H(11)...O(31) | 0.94(3) | 1.72(4) | 2.655(4) | 173(3) |
| | N(12)-H(12A)...O(32) | 0.92(4) | 1.97(4) | 2.875(4) | 172(3) |
| | N(12)-H(12B)...O(32)#1 | 0.91(4) | 2.18(4) | 2.939(4) | 140(3) |
| | O(51)-H(51)...O(31) | 0.80(4) | 1.88(4) | 2.654(4) | 162(4) |

i) #1 -x,y+1/2,-z+1/2 #2 -x,y-1/2,-z+1/2 ii) #1 x-1,y,z #2 x-1,y,z+1 iii) #1 -x+1,-y+2,-z+1 #2 x-3/2,-y+3/2,z+1/2 iv) #1 -x,-y+1,-z+2, #2 x, y+1, z+1 v) #1 –x-1,y+1/2,-z-1/2 vi) #1 –x+1,y-1/2,-z+1 vii) #1 x+1,y,z+1 viii) #1 -x+1,-y+1,-z+1

In order to probe the electrostatic nature of SR **7**, semi-empirical AM1 calculations were carried out and the Q-value determined (eqn. 2.1). The structure of ligand **7** is very similar to that of **1**, with the pyridyl nitrogen atom moved from the 3- to the 4-position. Ligand **7** has two amino-protons ($H_1$), two pyrimidine nitrogen atoms ($N_1$), one pyridine nitrogen atom ($N_2$) and

two ortho-protons ($H_2$ and $H_3$) nearest the pyridyl-nitrogen, that are of particular interest. Both the amino protons, both $H_2$ and $H_3$ on the pyridyl moiety, and both pyrimidine nitrogen atoms display similar values, respectively, so only one atom in each pair will be discussed, Figure 3.3.

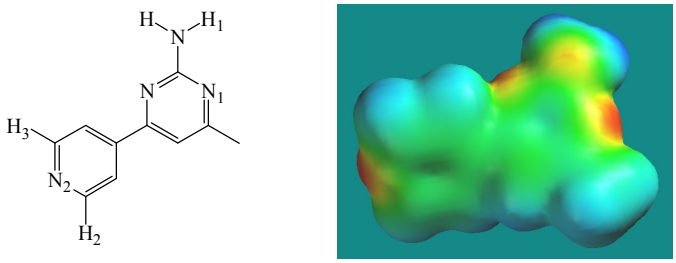


**Figure 3.3** Molecular structure and the electrostatic potential surface map of ligand **7**.

The basic nitrogen atom sites in both pyrimidine and pyridine, display similar numerical values ~ -260 and -276 kJ/mol, respectively. The positive potentials on the auxillary hydrogen-bond donors, N-H and C-H, were calculated at 140 and 65 kJ/mol, respectively. Consequently, the Q values for the two binding sites are 400 and 341 kJ/mol for the amino-pyrimidine and pyridine sites compared to 404 and 339 kJ/mol for ligand **1**, respectively, Figure 3.4. Based upon these results, the former moiety is expected to be the more effective hydrogen-bonding site for an approaching carboxylic acid.

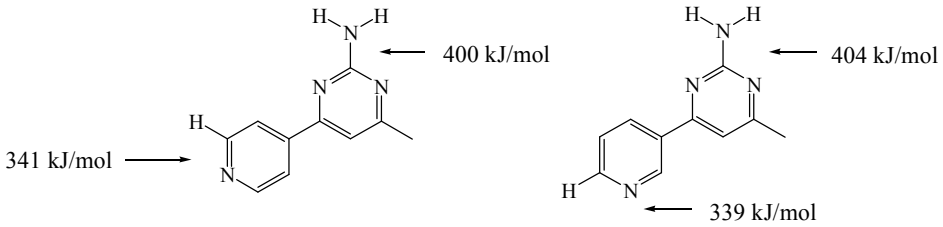


**(7)** **(1)**

**Figure 3.4** A comparison of the Q-values determined for the amino-pyrimidine and pyridine binding sites of SR's **1** and **7**.

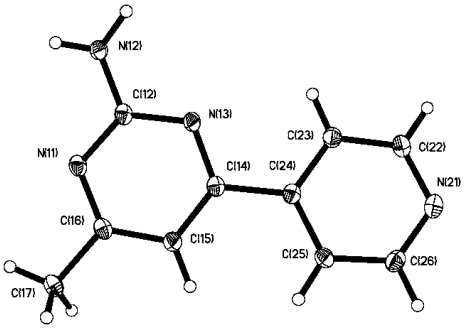
N(12)
C(12)
N(13)
N(11)
C(14)
C(24)
C(23)
C(22)
N(21)
C(16)
C(15)
C(25)
C(26)
C(17)

**7**

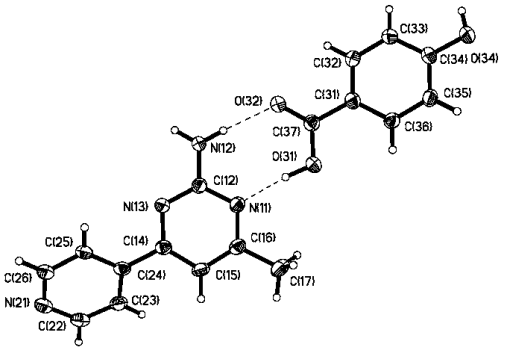
C(33)
C(32)
C(34)
O(34)
O(32)
C(31)
C(35)
C(37)
C(36)
N(12)
O(31)
C(12)
N(13)
N(11)
C(25)
C(14)
C(16)
C(26)
C(24)
C(15)
C(17)
N(21)
C(23)
C(22)

**7a**

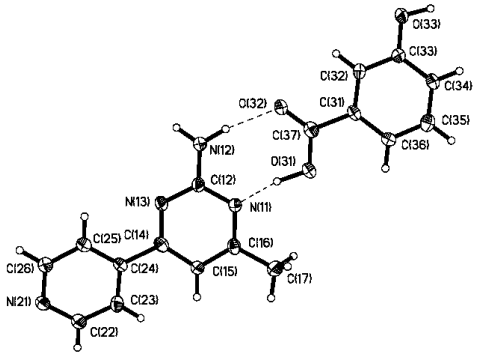
O(33)
C(33)
C(32)
C(34)
O(32)
C(31)
C(35)
C(37)
C(36)
N(12)
O(31)
C(12)
N(13)
N(11)
C(25)
C(14)
C(16)
C(26)
C(24)
C(15)
C(17)
N(21)
C(23)
C(22)

**7b**

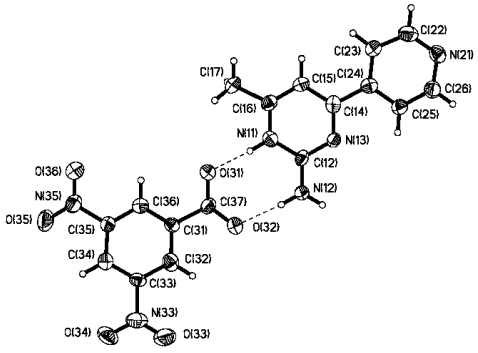
C(22)
C(23)
N(21)
C(17)
C(15)
C(24)
C(26)
C(16)
C(14)
C(25)
N(11)
N(13)
C(12)
O(36)
O(31)
N(35)
C(36)
N(12)
O(35)
C(35)
C(37)
C(31)
O(32)
C(34)
C(32)
C(33)
N(33)
O(34)
O(33)

**7c**

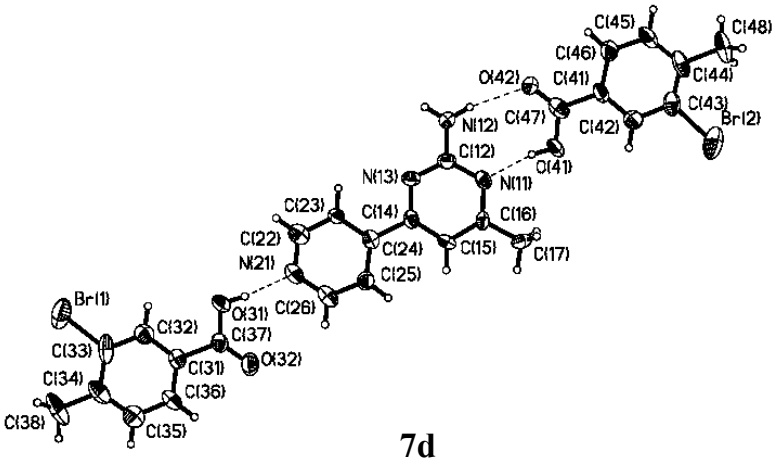
C(45)
C(48)
C(46)
O(42)
C(41)
C(44)
C(43)
C(47)
Br(2)
N(12)
C(42)
C(12)
O(41)
N(13)
N(11)
C(23)
C(14)
C(16)
C(22)
C(24)
C(15)
C(17)
N(21)
C(25)
Br(1)
O(31)
C(26)
C(32)
C(37)
C(33)
C(31)
O(32)
C(34)
C(36)
C(38)
C(35)

**7d**

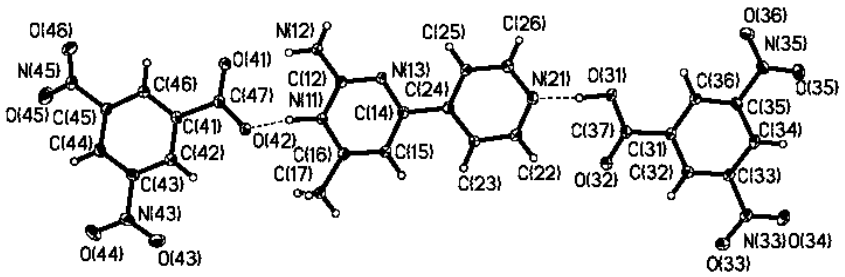


**7e**

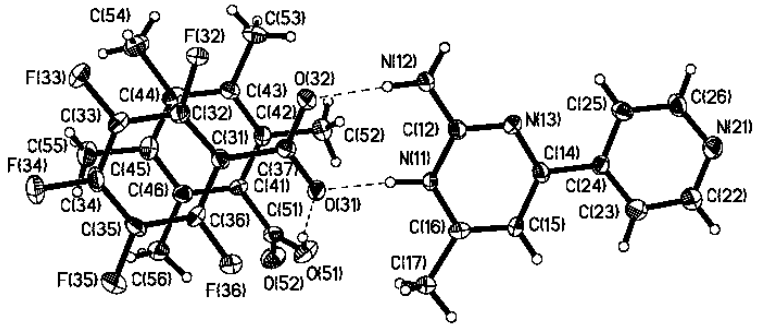


**7f**

**Figure 3.5** Thermal-ellipsoids plots (50% probability level) of ligands **7** and **7a-7f**

### *3.3.1 Crystal structure of 4-(2-amino-4-methylpyrimidin-6-yl)pyridine,7*

The crystal structure of **7** displays one molecule within the asymmetric unit, orientated with the two heterocycles in a relatively planar fashion. Extension of the architecture shows individual ligands forming a 1-D strand through multiple self-complementary amino-pyrimidine N-H···N (N12···N11, 3.052(2) Å and N12···N13, 3.1222(19) Å) hydrogen bonds, Figure 3.6. Within this arrangement, the pyridine moiety is not participating in hydrogen bonding, possibly due to the shortage of hydrogen bond donors.

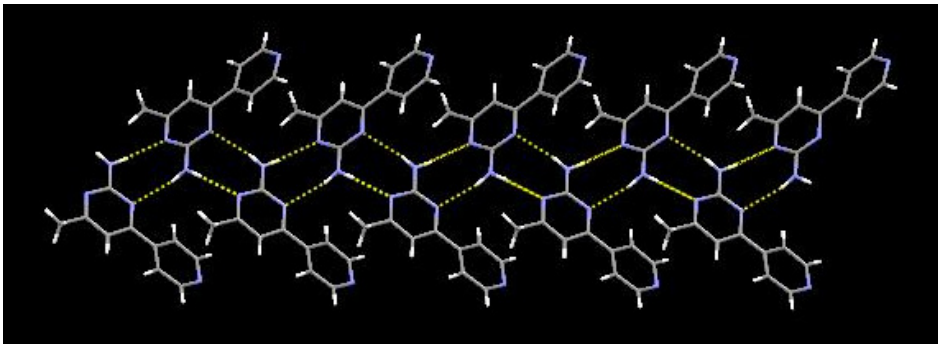

**Figure 3.6** 1-D strand formed through self-complementary amino-pyrimidine N-H···N hydrogen bonds.

### *3.3.2 Crystal structure of 4-(2-amino-4-methylpyrimidin-6-yl)pyridine, 7(1)*

A polymorph of **7**, **7(1)** displays four molecules within the asymmetric unit, orientated in a planar fashion, Figure 3.7.

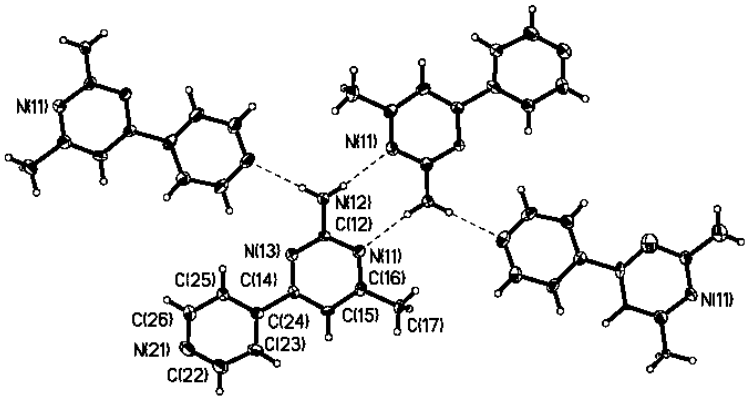


**Figure 3.7** Thermal-ellipsoids plot (50% probability level) of **7(1)**.

Multiple N-H···N hydrogen bonds extend the architecture into a 2-D sheet, Figure 3.8. The N-H···N hydrogen bonds include a pairwise self-complementary amino-pyrimidine/amino-pyrimidine (N12-2···N11-1, 3.042(4) Å, N12-1···N11-2, 3.067(4) Å) motif, two different amino-proton/pyridine (N12-1···N21-3, 3.033(4) Å, N12-2···N21-4, 3.008(5) Å) and two different amino-proton/pyrimidine (N12-3···N11-4, 3.047(4) Å, N12-3···N21-1, 3.013(5) Å) interactions.

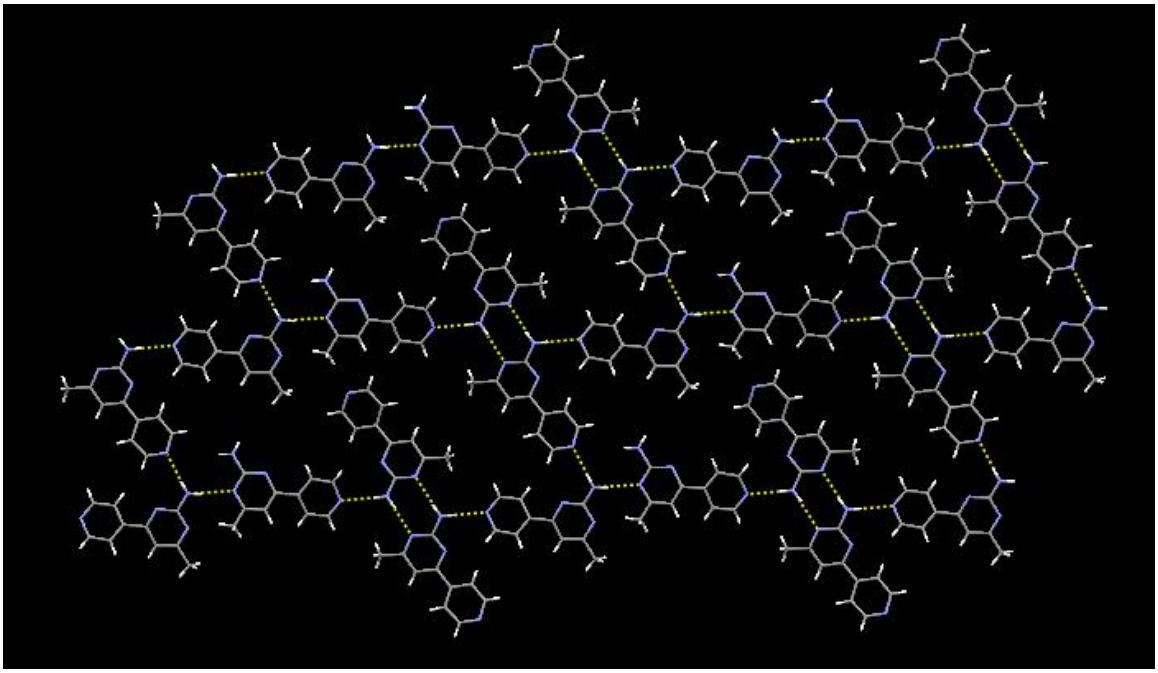

**Figure 3.8** Extended architecture of polymorph **7(1)**.

### *3.3.3 Crystal structure of 4-(2-amino-4-methylpyrimidin-6-yl)pyridine:4-hydroxybenzoic acid, 7a*

In the crystal structure of **7a** the main motif consists of SR **7** and one 4-hydroxybenzoic acid molecule, assembled *via* a complementary hydrogen-bond interaction between the carboxylic acid and the amino-pyrimidine moieties. The primary hydrogen bonds are O–H···N and N–H···O interactions with O31···N11 and N12···O32 distances of 2.732(2) Å and 2.824(2) Å respectively. Secondary O–H···N hydrogen bonds, O34···N21, 2.724(2) Å, formed through the hydroxyl proton and the pyridyl nitrogen atom extend the architecture into a one-dimensional chain. The 1-D strands are propagated into 2-D sheets through self-complementary N-H···N hydrogen bonds, N12···N13, 3.069(2) Å, from the *anti*-amino proton to the second pyrimidine nitrogen atom, Figure 3.9.

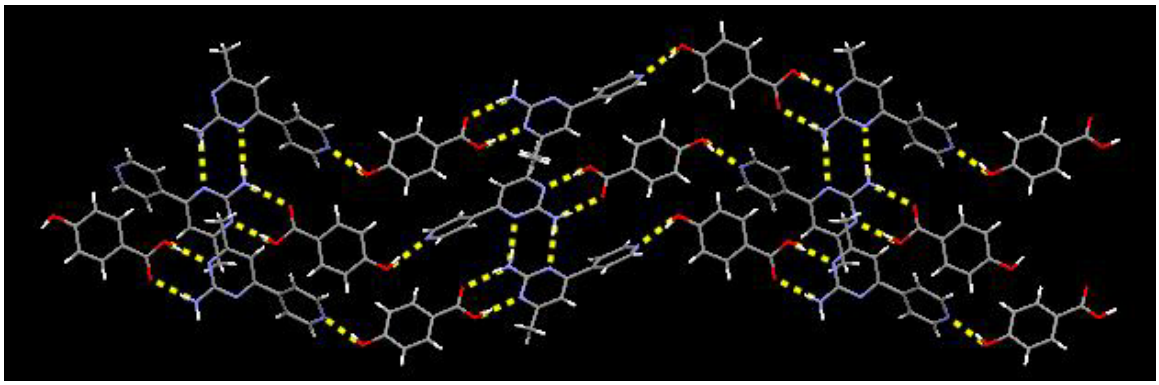

**Figure 3.9** Extended 2-D sheet of **7a** formed through a series of O-H···N, N-H···O, and N-H···N hydrogen bonds.

### *3.3.4 Crystal structure of 4-(2-amino-4-methylpyrimidin-6-yl)pyridine:3-hydroxybenzoic acid, 7b*

The primary motif in the crystal structure of **7b** contains SR **7** and one 3-hydroxybenzoic acid molecule, interconnected through the carboxylic acid and the amino-pyrimidine moieties. The primary synthons are O–H···N and N–H···O interactions with O31···N11 and N12···O32 distances of 2.646(3) Å and 2.887(4) Å respectively. Secondary O–H···N hydrogen bonds, O34···N21, 2.702(3) Å, formed through the hydroxyl proton and the pyridyl nitrogen atom extend the architecture into a one-dimensional chains which are linked into a double-strand arrangement with adjacent chains through additional N–H···O hydrogen bonds, N12···O33, 2.975(4) Å, from the *anti*-amino proton and the hydroxyl oxygen atom, Figure 3.10.

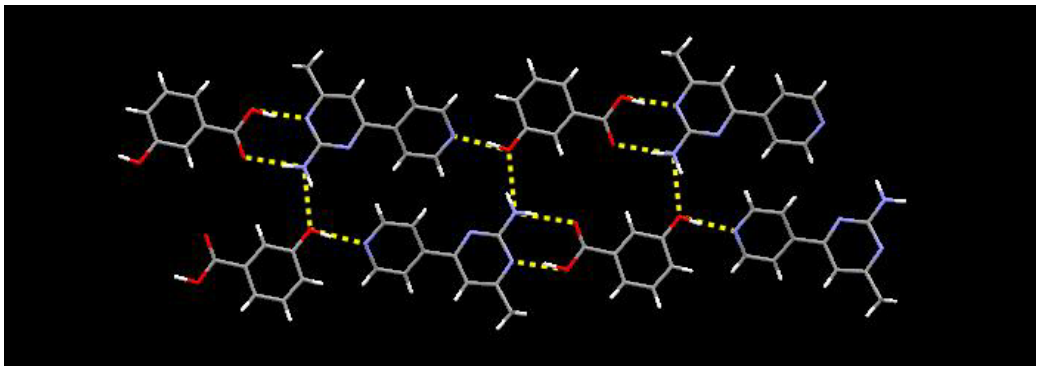

**Figure 3.10** Infinite 1-D strand formed through acid···amino-pyrimidine and hydroxy···pyridine hydrogen bonds in **7b**.

### *3.3.5 Crystal structure of 4-(2-amino-4-methylpyrimidinium-6-yl)pyridine:3,5-dinitrobenzoate, 7c*

The 1:1 salt **7c** shows the primary motif composed of a protonated SR **7** and one 3,5-dinitrobenzoate ion, which are interlinked through the carboxylate and the amino-pyrimidinium moieties. The primary synthons in this structure are charge-assisted N–$H^{+}$···$O^{-}$ and N–H···$O^{-}$ hydrogen bonds, with N···O distances of 2.646(6) Å and 2.783(6) Å, respectively. Ion pairs are linked into a 1-D zig-zag chain through N–H···N hydrogen bonds, N12···N21, 2.962(7) Å, from the *anti*-amino proton and the pyridyl nitrogen atom, Figure 3.11.

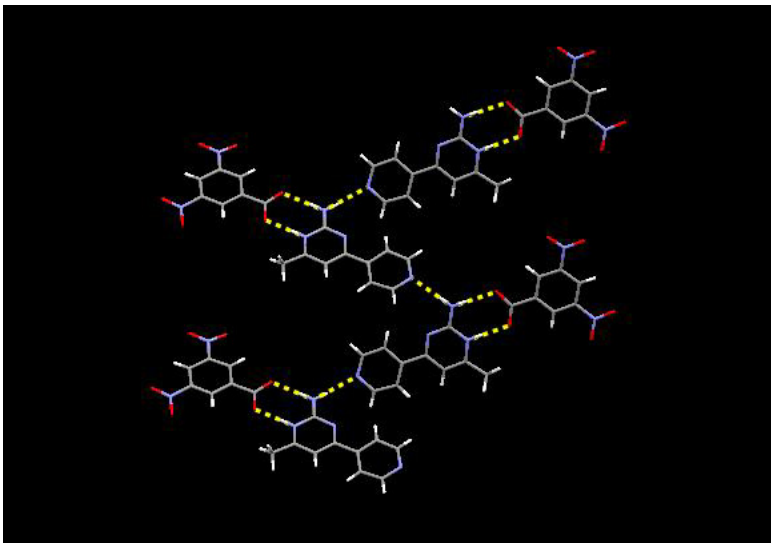

**Figure 3.11** 1-D strand in **7c** formed through secondary N-H···N hydrogen bonds between the *anti*-amino proton and the pyridine nitrogen atom.

### *3.3.6 Crystal structure of 4-(2-amino-4-methylpyrimidinium-6-yl)pyridine:3,5-dinitrobenzoate, 7d*

The central motif in the crystal structure of **7d** is the result of charge-assisted and neutral hydrogen-bond interactions between the carboxylic acid and the amino-pyrimidine and the pyridine moieties. The primary synthons in this structure are charge-assisted N–$H^{+}$···$O^{-}$ and N–H···$O^{-}$ and neutral O-H···N hydrogen bonds, with N···O distances of 2.5342(14) Å and 3.0559(15) Å, formed through the amino-pyrimidinium and carboxylate moieties, while a neutral O-H···N hydrogen bond, O31···N21, 2.5979(14) Å, is formed from the second carboxylic acid moiety to the pyridine group. The 1:2 ligand-acid trimer is extended into a hexameric

supermolecule through secondary charge assisted N–H···$O^-$ hydrogen bonds with N12···$O^-$41 distances of 2.8517(16) Å, Figure 3.12.

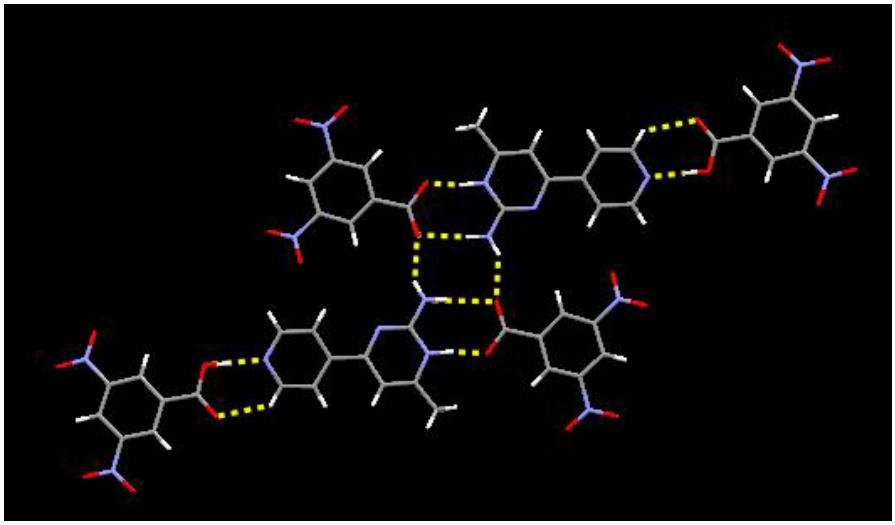

**Figure 3.12** Hexameric supermolecule of **7d** formed through multiple charge-assisted and neutral hydrogen bonds.

### *3.3.7 Crystal structure of 4-(2-amino-4-methylpyrimidin-6-yl)pyridine:3-bromo-4-methylbenzoic acid, 7e*

The primary supermolecule in the crystal structure of **7e** consists of SR **7** and two 3-bromo-4-methylbenzoic acid molecules, constructed through acid···amino-pyrimidine, N12···O42, 2.948(7) Å; O41···N11, 2.620(7) Å, and acid···pyridine O31···N21, 2.600(8) Å synthons. The 1:2 ligand-acid trimer is further connected into a polymeric network through a secondary N–H···O hydrogen bond with a N12···O32 distance of 2.959(9) Å, Figure 3.13.

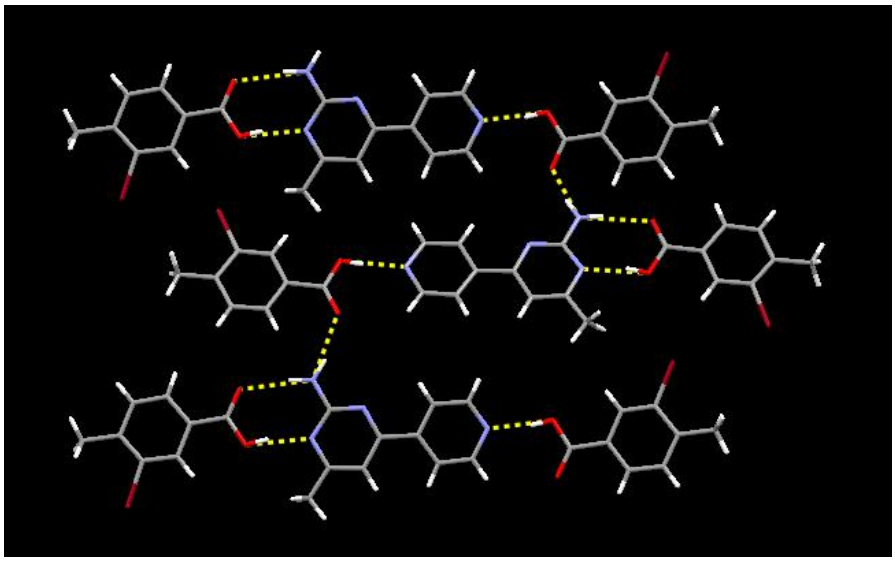

**Figure 3.13** One-dimensional zig-zag chain of **7e** connected through secondary N-H···O hydrogen bonds.

### *3.3.8 Crystal structure of 4-(2-amino-4-methylpyrimidinium-6-yl)pyridine:pentamethylbenzoic acid:pentafluorobenzoate, 7f*

The asymmetric unit of **7f** contains a protonated SR **7**, one pentafluorobenzoate ion, and one pentamethylbenzoic acid molecule constructed through charge-assisted hydrogen-bond interactions. The primary synthons in this structure are charge-assisted N–$H^{+}$···$O^{-}$, N–H···$O^{-}$, and O-H···$O^{-}$ hydrogen bonds, with $N^{+}11$···$O^{-}31$ and N12···$O^{-}32$ distances of 2.655(4) Å and 2.875(4) Å, formed through the amino-pyrimidinium and carboxylate moieties, while a charge-assisted O-H···$O^{-}$ hydrogen bond, O51···$O^{-}31$, 2.654(4) Å, is formed from the pentamethylbenzoic moiety to the carboxylate group of the anion, Figure 3.14.

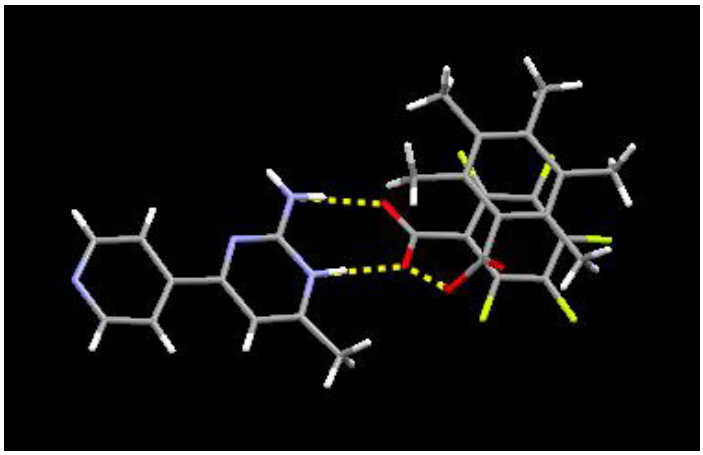

**Figure 3.14** Three component ionic supermolecule formed through multiple charge-assisted hydrogen bonds

The three-component ionic complex is further extended into a six-component supermolecule through secondary charge-assisted N–H···$O^-$ hydrogen bonds from the *anti*-amino proton to a carboxylate oxygen of the pentafluorobenzoate molecule, Figure 3.15.

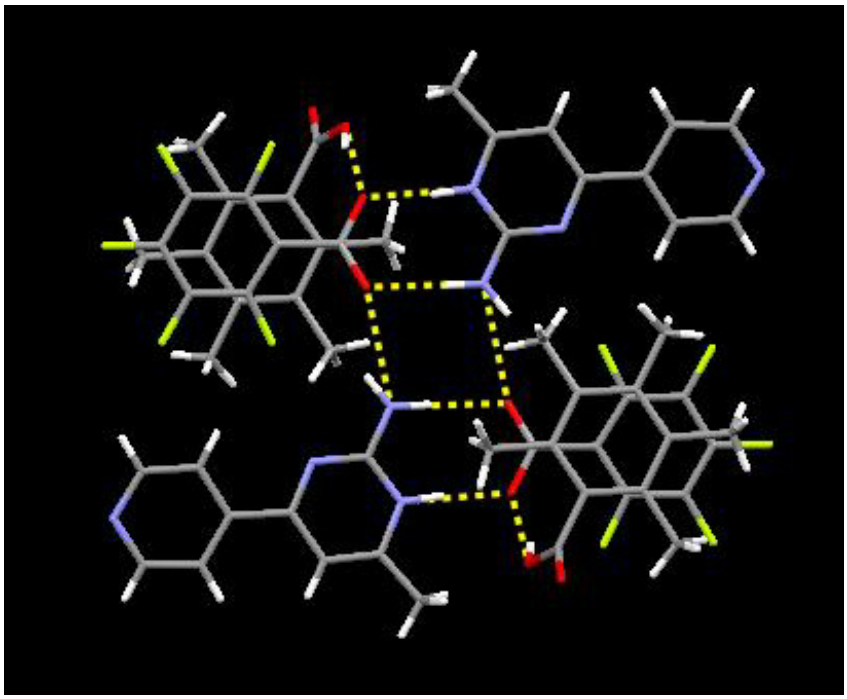

**Figure 3.15** Six-component supermolecule formed through secondary ionic hydrogen bonds.

## 3.4 Discussion

### *3.4.1 Characterization of polymorph 7(1) through powder XRD*

Crystals of **7** were grown from 200 proof ethanol, while **7(1)** were grown from ethyl acetate as a co-crystallization reaction between SR **7** and benzoic acid. We were interested in determining if the solvent *i.e.* ethanol or ethyl acetate or the benzoic acid additive produced one polymorph over another. Thus crystals were grown from ethyl acetate, examined using powder XRD, and compared to simulated powder patterns of **7** and **7(1)**. The simulated powder patterns of **7** and **7(1)** are displayed in Figure 3.16.

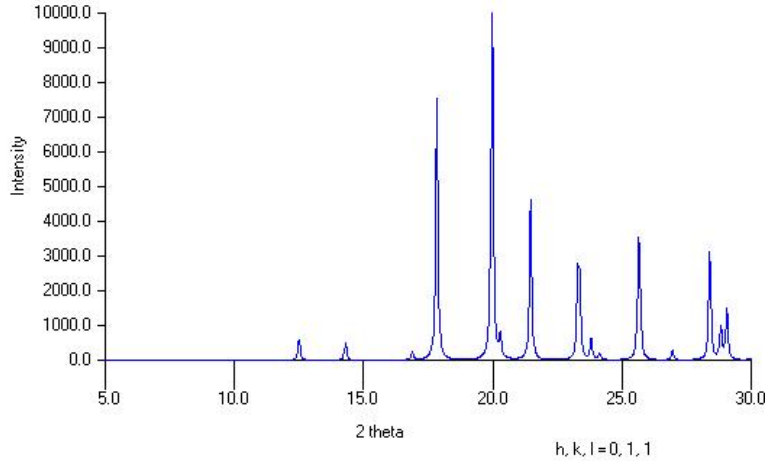


**(7)**

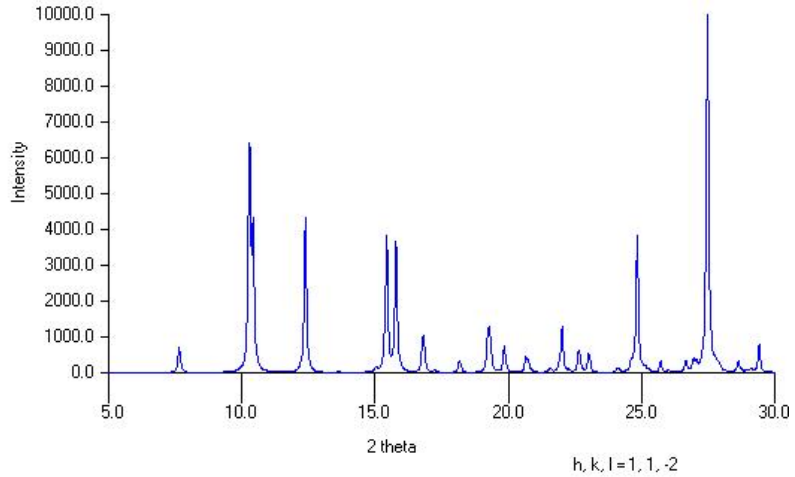


**7(1)**

**Figure 3.16** Powder XRD patterns for **7** (simulated) and **7(1)** (simulated).

The powder pattern, of the sample grown from ethyl acetate, matched very closely to the simulated powder pattern of **7**, Figure 3.17. Thus, the conclusion was made that crystal packing

in structure **7** occurs independent of solvent choice, however the benzoic acid additive must be contributing to the packing arrangement within **7(1)**.

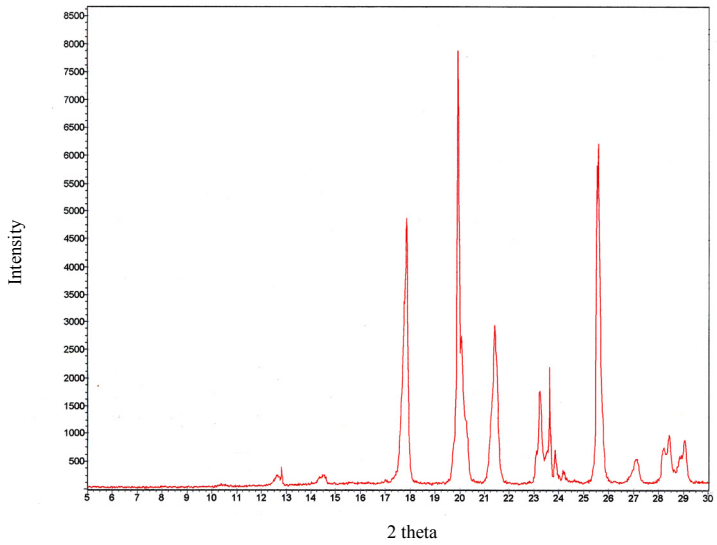


**Figure 3.17** Powder XRD pattern of SR **7** grown from ethyl acetate (experimental).

### *3.4.2 Formation of 4-py-pym/carboxylic acid co-crystals and salts*

SR **7** was prepared in good yields (71 %) through the palladium catalyzed Suzuki-Miyaura reaction, by cross-coupling 4-pyridylboronic acid and 2-amino-4-methyl-6-chloro pyrimidine under basic conditions. Both SR's **1** and **7** have similar molecular structures with the only difference being the placement of the pyridyl nitrogen atom. However, this small structural variation in **7** made a significant difference in the outcome of the products produced.

Each of the structures **7a-7f** were obtained upon mixing SR **7** with various aromatic carboxylic acids in polar solvents. In every structure the primary intermolecular interaction is a pairwise O-H···N/N-H···O or $N–H^{+}\cdots O^{-}$/$N–H\cdots O^{-}$ motif between the carboxylic acid or carboxylate and the amino-pyrimidine or amino-pyrimidinium moieties, Figure 3.18.

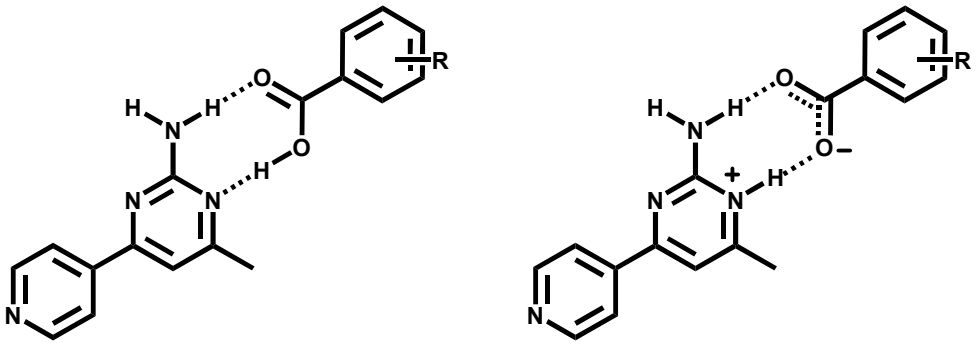

**Figure 3.18** Primary hydrogen bonding interactions between SR **7** and an incoming carboxylic acid molecule.

In structures **7a-7c** the connectivities support the results obtained from the AM1-calculations, in which the Q-value of the amino-pyrimidine moiety (400 kJ/mol) significantly outweighs the 4-pyridyl/auxillary C-H site (341 kJ/mol) as the dominating primary hydrogen bonding site. Additionally, structures **7a-7c** match those of Chapter 2, **1a-1d**, **2a-2e**, and **6a-6d**, where 1:1 stoichiometric products were produced through carboxylic acid/amino-pyrimidine or carboxylate/amino-pyrimidinium synthons.

Upon increasing the acid:ligand mixing ratio from 1:1 to 2:1, a 2:1 acid:ligand product **7d** and **7e** form. The 2:1 acid:ligand complexes are held together through the conventional hydrogen bonding pattern at the amino-pyrimidine site, while a second acid molecule hydrogen bonds to the 4-pyridyl nitrogen through O-H···N interactions, Figure 3.19. These two results are quite different from what was seen in Chapter 2, when the product was a 1:1 dimer, regardless of stoichiometric mixing ratios.

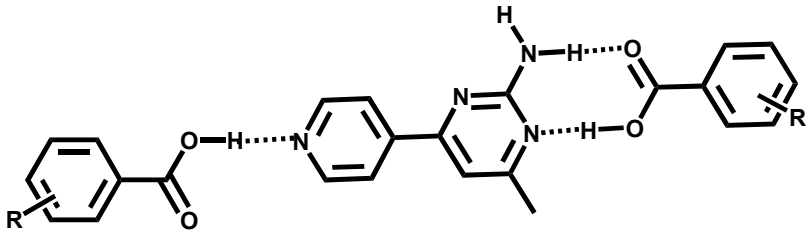

**Figure 3.19** Pictorial description of the hydrogen bonding synthons seen between SR **7** and a carboxylic acid upon mixing in a 2:1 acid/SR stoichiometric ratio.

It is conceivable that only two of the three sites *i.e.* 1 and 2 on SR **7** are accessible for an approaching carboxylic acid, since site 3 is slightly sterically hindered by the neighboring

pyridyl ring, Figure 3.20. In fact, every example in which a carboxylic acid is hydrogen bound to a py-pym SR, the acid preferentially binds at site 1 and never at site 3.

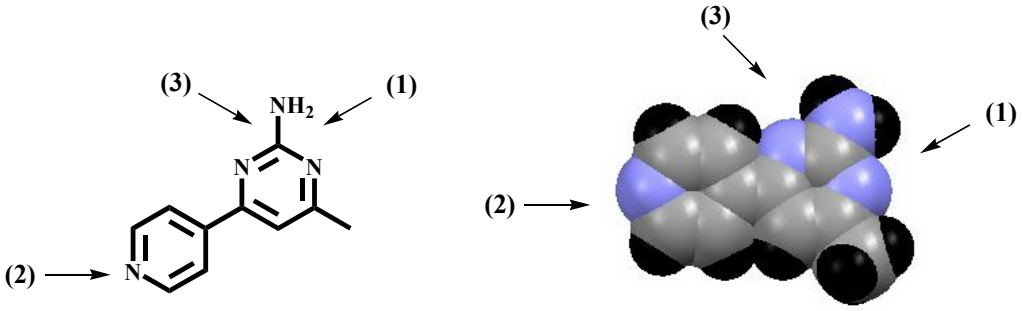


**Figure 3.20** (left) Schematic and space-filling model of SR **7** displaying the three potential hydrogen bonding sites (1-3) for an incoming carboxylic acid.

Clearly, both hydrogen bond acceptor sites *i.e.* amino-pyrimidine and 4-pyridyl are suitable supramolecular tools, capable of bringing together multiple carboxylic acids into a single crystalline lattice. Thus, SR **7** was used as a 'supramolecular-hub' in attempts to form ternary co-crystals with two different carboxylic acids. One ternary complex **3f** was produced however the overall connectivities of the species was unexpected. The stronger pentafluorobenzoic acid was expected to bind to the amino-pyrimidine site, the strongest base, while the weaker pentamethylbenzoic acid was expected to bind to pyridine. The stronger pentafluorobenzoic acid molecule does indeed hydrogen bond with the strongest base, however, proton-transfer to a pyrimidine nitrogen atom occurs, resulting in charge assisted $N–H^{+}\cdots O^{-}$/$N–H\cdots O^{-}$ interactions. Thus a competition, between the pyridyl nitrogen and the carboxylate oxygen of the pentafluorobenzoate molecule occurs, for the remaining pentamethylcarboxylic acid. Possibly due to the carboxylate oxygen being the second best hydrogen bond acceptor, paired with strong $\pi\cdots\pi$ stacking between pentamethyl and pentafluoro rings (~3.5 Å), the carboxylic acid moiety prefers a charge-assisted $O\text{-}H\cdots O^{-}$ hydrogen bond motif instead of the pyridyl nitrogen atom.

### *3.4.3 Q-value determinations through AM1 calculations*

AM1 electrostatic potential surfaces were calculated in order to determine if the methyl-substituent, on the amino-pyrimidine ring, plays a role in directing the supramolecular assembly.

Each molecule (**1**, **7**, **a**, and **b**) has two separate Q-values, pyrimidine nitrogen atoms + amino-protons (●) and pyridine nitrogen atoms + auxiliary C-H protons (□), Figure 3.21.

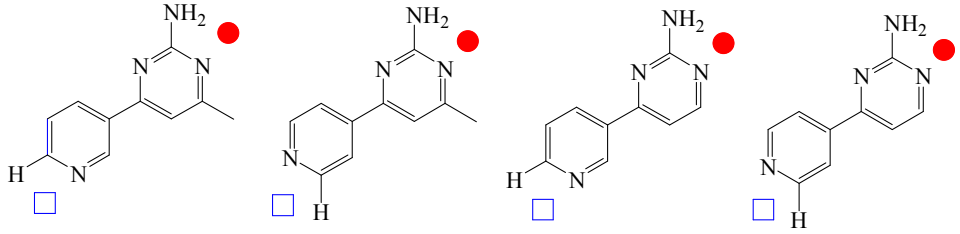

| | **(1)** | **(7)** | **(a)** | **(b)** |
|---|---|---|---|---|
| ● kJ/mol | 404 | 400 | 402 | 383 |
| □ kJ/mol | 339 | 341 | 350 | 330 |

**Figure 3.21** Calculated electrostatic potential surfaces for a variety of pyridine/amino-pyrimidine SR's.

These calculations show that the methyl-group does not play a significant role in altering the electronics of the amino-pyrimidine or pyridine ring. In fact, the Q-value of the amino-pyrimidine moiety in **b** decreases upon removing the methyl group, correlating to a weaker hydrogen bonding site, compared to SR's **1** and **7**. The connectivity displayed in the 1:1 co-crystal, Figure 3.1, fails to correlate with our calculated and structural data for similar systems. This clearly demonstrates the need for multiple crystal structures, within a particular study, if one is to draw strict conclusions on connectivity and stoichiometry of the final products.

### *3.4.4 Co-crystal or salt; is it predictable based on $pK_a$ values?*

Is it possible to determine if proton transfer is going to occur, upon mixing a carboxylic acid and N-containing base, before conducting the actual experiment? Some guidelines based upon solid-state and solution infrared spectroscopy have been reported.[4] The rule simply states, that if the $\Delta pK_a$ is >3.75, the system is favorable for proton transfer.[5] We decided to examine if our results could be explained against this background.

Since a titration experiment of py-pym **7** would be difficult to carry out, we relied on theoretical calculations to generate the necessary $pK_a$ values.[6] Relevant $pK_a$ values, for the carboxylic acids contained in this study were obtained from reported literature values.[7] Our findings for this study are displayed in Table 3.2.

**Table 3.2** Determination of $\Delta pK_a$ for structures **3c-3h**

| Co-crystal | Salt | Benzoic acid | SR **7** ($pK_a$) N / $NH_2$ | Acid ($pK_a$) | $\Delta pK_a$ |
|---|---|---|---|---|---|
| **7a** | ---- | 4-hydroxybenzoic acid | 1.83 | 4.58 | 2.75 |
| **7b** | ---- | 3-hydroxybenzoic acid | 1.83 | 4.06 | 2.23 |
| ---- | **7c** | 3,5-dinitrobenzoic acid | 1.83 | 2.82 | 0.99 |
| **7e** | ---- | 3-bromo-4-methylbenzoic acid | 1.83 | 3.87 | 3.04 |
| ---- | **7f** | pentafluorobenzoic acid | 1.83 | 1.73 | 0.10 |

Interestingly, co-crystals **7a**, **7b**, and **7e** produce the largest $\Delta pK_a$, while salts **7c** and **7f** display small $\Delta pK_a$ difference although proton transfer has occurred. No doubt, these guidelines will work for some hydrogen bond donor/acceptor pairs, however in our py-pym/carboxylic acid system, the $\Delta pK_a$ results do not offer any reliable guidelines. The drawbacks with this type of comparison are numerous, *e.g.* varying types of reaction conditions, instrumentation, and scientific advances, all of which could lead to misinterpreted data and conclusions.

This study has displayed how subtle molecular modifications can have dramatic effects on the overall supramolecular assembly process. The difference, in product outcome, was observed when SR **7** versus SR **1** was allowed to react with aromatic carboxylic acids. From these results, SR **7** should provide an ideal environment for the construction of ternary supermolecules, between aromatic carboxylic acids of different strength and/or other hydrogen bond donor moieties *i.e.* oxime, hydroxy, or acetamide. This study also serves to underscore some of the similarities between the development of non-covalent and covalent synthetic methodologies. In each case, the driving force is a specific goal. Within supramolecular synthesis the goal is an assembly of molecules with predictable connectivities and stoichiometries, while successful covalent synthesis is based on the organization of individual atoms. For instance, the supramolecular chemist might rely on the placement of individual atoms to direct the overall assembly, while the organic chemist might rely on the directing effects of substituents *i.e. ortho*, *meta*, and *para*, when carrying out an electrophilic aromatic substitution reaction on substituted benzenes. The efficiency of the supramolecular synthesis can be improved by systematically altering reaction conditions or by making deliberate changes to the supramolecular reagent.

## References:


[1](a) Nicolaou, K. C.; Sorensen, E. J. 1996. *Classics in Total Synthesis*. New York: VCH; (b) March, J.; Smith, D. 2001. *Advanced Organic Chemistry, 5th ed*. New York: Wiley; (c) Corey, E. J.; Cheng, X-M. 1995. *The Logic of Chemical Synthesis*. New York: Wiley.

[2] Aakeröy, C. B.; Schultheiss, N.; Desper, J.; Moore, C. *New J. Chem*. **2006**, *30*, 1452.

[3] Lynch, D. E.; McClenaghan, I. *Acta Cryst*. **2001**, *C57*, 830.

[4] Lindemann, R.; Zundel, G. *J. Chem. Soc., Faraday Trans. 2*, **1977**, *73*, 788.

[5] Johnson, S. L.; Rumon, K. A. *J. Phys. Chem*. **1965**, *69*, 74.

[6] Theoretical p$K_a$ values were calculated using pKalc3.2 from PALLAS2.1, Lynch, D. E.; McClenaghan, I. *Acta Cryst*. **2001**, *C57*, 830.

[7] Tehan, B. G.; Lloyd, E. J.; Wong, M. G.; Pitt, W. R.; Montana, J. G.; Manallack, D. T.; Gancia, E. *Quant. Struct.-Act. Relat.* **2002**, *21*, 457.

# CHAPTER 4 - Combining hydrogen and halogen bonding in the construction of polymeric supermolecules

## 4.1 Introduction

Heteromeric synthons such as carboxylic acid···pyridine[1] and carboxylic acid···amide[2] are well-established and dependable partners within crystal engineering, however synthons such as amino-pyrimidine···carboxylic acid[3] and nitrogen···halogen (I or Br)[4] have been utilized far less frequently, although they can form discrete and/or extended supramolecular architectures, Figure 4.1

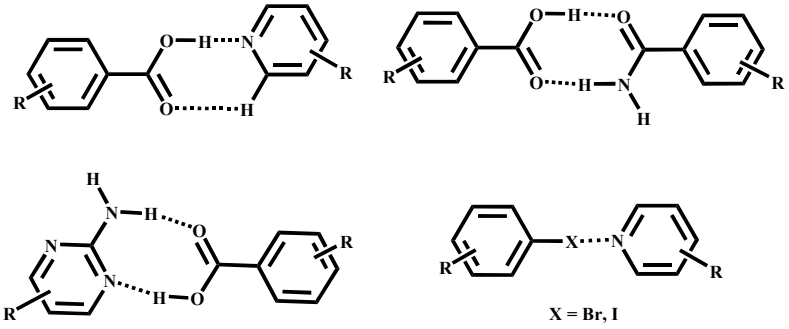


**Figure 4.1** A variety of heteromeric synthons employed in crystal engineering.

Designing and constructing supermolecular products from two individual entities, which contain only one complementary moiety each, is often predictable due to the limited number of synthons that could form between the reactants. However, predictability becomes inherently more difficult upon increasing the number of potentially interactive moieties on each reactant leading to an increase in possible synthons that might form. In this chapter, we will be focus on the design and synthesis of supramolecular architectures formed through combinations of both hydrogen and halogen bonds in a systematic manner.

There is one example in the literature of an assembly deliberately formed through combinations of both hydrogen and halogen bonds.[5] In this example, 4-nitrobenzoic acid and 4-iodopyridine assemble into 1-D tapes through acid···pyridine and nitro···iodo heteromeric synthons, Figure 4.2.

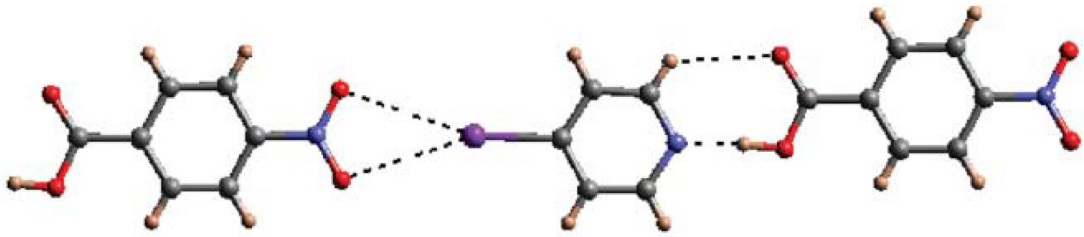

**Figure 4.2** 1-D strands formed through combinations of both hydrogen and halogen bonding.

Within this system, two molecules containing a total of four different functional groups are allowed to react, in which (based on electrostatics) the acid/pyridine heterosynthon is the most favorable primary interaction (9.9 kcal/mol),[6] while the iodo/nitro heterosynthon forms as a secondary interaction (2.5 kcal/mol).[7] Calculations were also carried out for the acid/acid dimer and iodo/pyridine interaction which shows energy values lower (7.8 and 3.4 kcal/mol) than the primary acid/pyridine synthon.

A suitable bifunctional ligand for selective hydrogen and halogen bonding would need to contain a robust chemical functionality capable of forming hydrogen bonds even in the presence of other potential disruptive moieties, coupled with a functional group that would prefer to interact with a halogen atom through N···X (X = I or Br) halogen bonds.

Conventional halogen bonds are typically formed through a suitable halogen bond donor *i.e.* iodine or bromine and a halogen bond acceptor, a nitrogen containing heterocycle. Furthermore, the halogen bond donor can be strengthened upon fluorination of the molecule, which leads to a dramatic increase in the electron-acceptor ability of the iodine or bromine atoms.[8]

In Chapter 2 we demonstrated how ditopic pyridine/amino-pyrimidine functionalized SR's selectively interact and bind aromatic carboxylic acids utilizing a hierarchical approach through hydrogen bond strength and synthon complementarity. In all cases (13/13), when the 3-pyridyl functionalized SR's were allowed to react with aromatic carboxylic acids, the result was a 1:1 co-crystal or salt assembled through an amino-pyrimidine/carboxylic acid or amino-pyrimidinium/carboxylate heterosynthon, Figure 4.3.

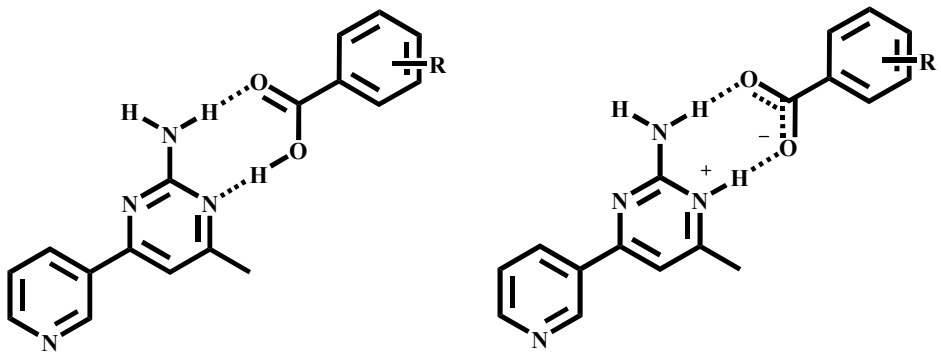

**Figure 4.3** Results obtained by mixing carboxylic acids with 3-pyridine/amino-pyrimidine SR's.

These results show that our py/pym based SR's provide ideal molecular recognition sites for promoting both hydrogen and halogen bonding in a controllable and predictable manner. By introducing a halogen-bonding atom (Br or I) on an aromatic carboxylic acid, we can take advantage of the complementarity between the amino-pyrimidine and carboxylic acid moieties, while allowing the 1:1 dimer to assemble into an infinite network through pyridyl-iodine or -bromine halogen bonding, Figure 4.4.

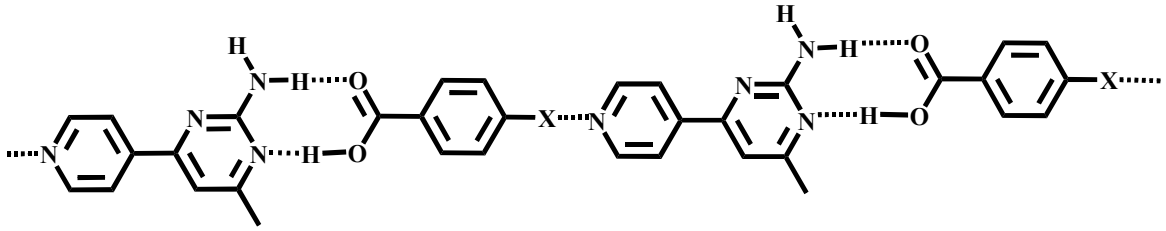

**Figure 4.4** A postulated network formed through a series of hydrogen and halogen bonds (X = I, Br).

With these goals in mind, we decided to target three py/pym SR's **1**, **6**, and **7** and three halogenated benzoic acids **8**, **13**, and **14**, Figure. 4.5.

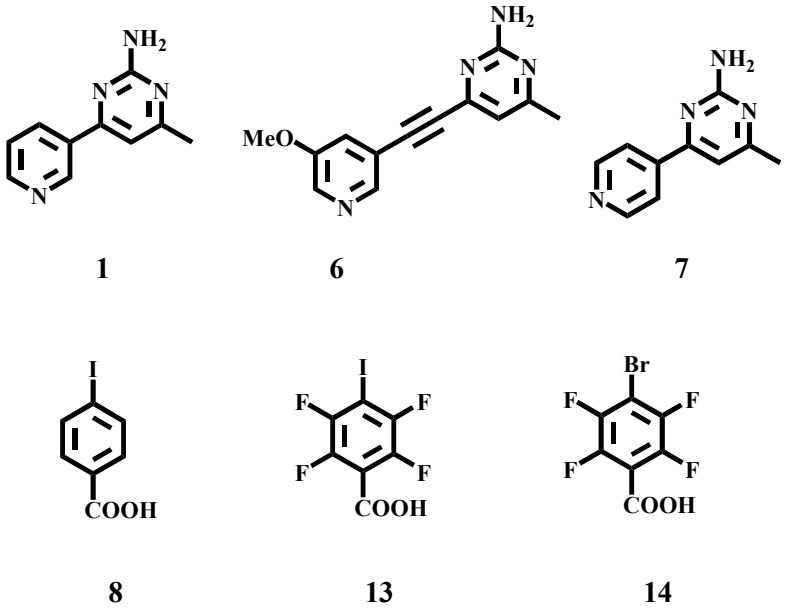


**1** **6** **7**

**8** **13** **14**

**Figure 4.5** Three bifunctional SR's **1**, **6**, and **7**, possessing two distinctly different hydrogen-bonding moieties *i.e.* pyridine and amino-pyrimidine and three halogenated aromatic carboxylic acids **8**, **13**, and **14**.

In order to study the limits and limitations of the hierarchical approach to supramolecular synthesis through hydrogen and halogen bonding, py-pym SR's **1**, **6**, and **7** were allowed to react with either 4-iodobenzoic acid **8**, 1-iodo-2,3,5,6-tetrafluorobenzoic acid **13**, or 1-bromo-2,3,5,6-tetrafluorobenzoic acid **14** in a 1:1 ratio. This chapter will attempt to address the following questions:

- Can combinations of hydrogen and halogen bonds be utilized, in a hierarchical fashion to construct predictable assemblies?
- Is iodine a better halogen bond donor than bromine?
- Does the Lewis acidity of halogen nuclei increase upon fluorination of the aryl ring?

## 4.2 Experimental

### *4.2.1 Synthesis*

All chemicals, unless noted, were purchased from Aldrich and used without further purification. 1,2,4,5-tetrafluorobenzene was purchased from Apollo Scientific Inc. Column chromatography was carried out on silica gel (150 Å pore size) from Analtech Inc. Melting

points were determined on a Fisher-Johns melting point apparatus and are uncorrected. $^{1}H$ and $^{13}C$ NMR spectra were recorded on a Varian Unity plus 400 MHz or 200 MHz spectrometer in $CDCl_3$ or $D_6$-DMSO. Compounds were prepared for infrared spectroscopic (IR) analysis as a mixture in KBr. Electrospray Ionization – Ion-Trap Mass Spectrometry (ESI-IT-MS) was carried out on a Bruker Daltonics Esquire 3000 plus. MALDI-TOF / TOF-MS was carried out on a Bruker Daltonics Ultraflex TOF/TOF.

### *4.2.1.1 Synthesis of 1,2,4,5-tetrafluoro-3-(1,3-dioxol-2-yl)benzene, 9*[9]

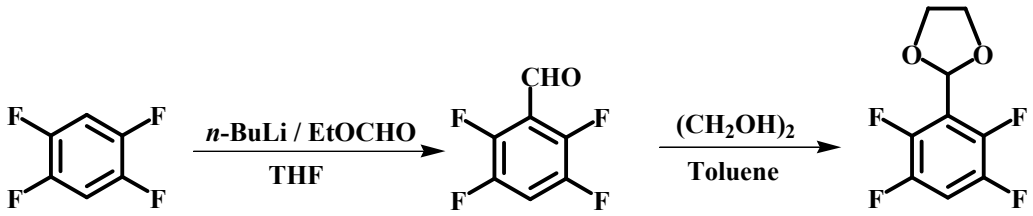


**9**

Under a dinitrogen atmosphere, a single neck round-bottom flask containing dry THF (65 mL) was cooled to –78 °C (dry ice/acetone). Upon cooling, *n*-BuLi (1.6 M, 21.25 mL) was added to the stirred solution. 1,2,4,5-Tetrafluorobenzene (5 g, 0.033 mol) was added and allowed to stir at –78 ° for 1h. After 1h ethyl formate (5.0 g, excess) was added in one portion and the reaction was allowed to reach room temperature. The mixture was then diluted with saturated $NaHCO_3$(aq) (45 mL), separated, dried over $MgSO_4$ and the solvent removed on a rotary evaporator. The mixture was then transferred to a round-bottom flask containing ethylene glycol (5.0 g, excess) and toluene (35 mL). 4-Toluenesulfonic acid (40 mg) was added and a dean-stark trap was attached and the mixture was refluxed for 2h. After cooling to room temperature, the reaction mixture was washed with $NaHCO_3$(aq) (45 mL), separated, dried over $MgSO_4$ and the solvent removed on a rotary evaporator. The residue was chromatographed on silica with hexanes as the eluant. The product **9** was isolated as a colorless oil, which solidified upon standing, (5.4 g, 74 %). M.p. 38-40 ºC; $^{1}H$ NMR ($\delta_H$; 200 MHz, $CDCl_3$): 7.17-7.00 (m, 1H), 6.24 (s, 1H), 4.26-4.01 (m, 4H); IR (KBr pellet): υ 3078, 2914, 1511, 1403, 1260, 1178, 1132, 989, 937, 851, 702, 615, 559 $cm^{-1}$.

### *4.2.1.2 Synthesis of 2-(2,3,5,6-tetrafluoro-4-iodo-phenyl)-[1,3]dioxolane, 10*[10]

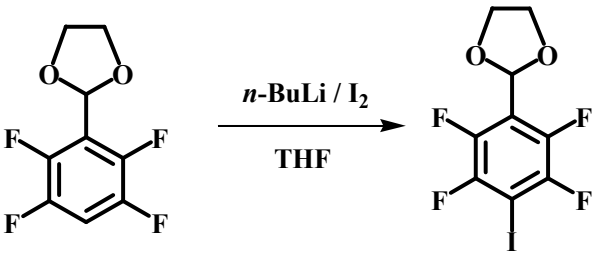


**9** **10**

Under a dinitrogen atmosphere, a single neck round-bottom flask containing dry THF (22 mL) and 1,2,4,5-Tetrafluoro-3-(1,3-dioxol-2-yl)benzene **9** (1.5 g, 6.73 mmol) was cooled to –78 °C (dry ice/acetone bath). Upon cooling, *n*-BuLi (1.6 M, 4.65 mL) was added dropwise to the stirred solution. After 1h, a solution of iodine (1.88 g, 7.41 mmol) in THF (6 mL) was added by syringe all at once. The reaction was allowed to reach room temperature, upon which THF (20 mL) was added. The reaction mixture was washed with aqueous $NaHCO_3$(aq) (5 mL), then 0.5 M aqueous $Na_2S_2O_3$, dried over $MgSO_4$ and the solvent removed on a rotary evaporator. The off-white solid residue was recrystallized from dissolving in boiling *n*-pentane and placed in the refrigerator affording colorless plate-shaped crystals of **10**, (1.90 g, 81 %). M.p. 92-94 ºC; $^1$H NMR ($\delta_H$; 200 MHz, $CDCl_3$): 6.23 (s, 1H), 4.26-4.01 (m, 4H); IR (KBr pellet): υ 2981, 2904, 1640, 1481, 1399, 1271, 1112, 994, 922, 758, 723, 630 cm$^{-1}$.

### *4.2.1.3 Synthesis of 1-iodo-2,3,5,6-tetrafluorobenzaldehyde, 11*[10]

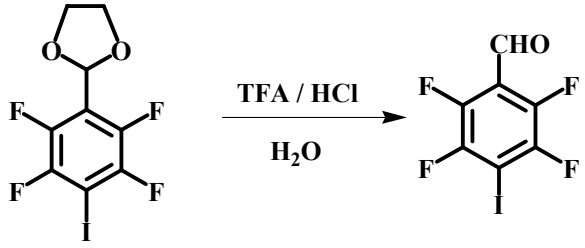


**10** **11**

In a round-bottom flask, 2-(2,3,5,6-tetrafluoro-4-iodo-phenyl)-[1,3]dioxolane **10** (800 mg, 2.29 mmol) and trifluoroacetic acid (2.5 mL) were allowed to stir. To the solution, water (7 mL) was added, followed by HCl (1.5 mL, 37 %), affording a white precipitate. The reaction mixture was heated to 70 °C for 2h. Upon cooling, the mixture was washed with chloroform (3 x 25 mL) and the organic layer washed with water, separated, and dried over $MgSO_4$. The

solvent was removed on a rotary evaporator and the residue dissolved in dichloromethane. This solution was then poured into hexanes and cooled to 0 ºC. The white precipitate **11** was filtered and dried, (610 mg, 88 %). M.p. 108-110 ºC; $^1$H NMR ($\delta_H$; 200 MHz, $CDCl_3$): 10.31-10.30 (m, 1H); IR (KBr pellet): υ 1696, 1629, 1470, 1414, 1373, 1265, 1030, 963, 769, 620 cm$^{-1}$.

***4.2.1.4 Synthesis of 1-bromo-2,3,5,6-tetrafluorobenzaldehyde, 12***[11]

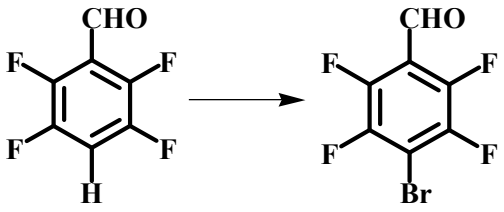


**12**

Pentafluorbenzaldehyde (12.0 g, 61.22 mmol), anhydrous lithium bromide beads (6.0 g, 69.0 mmol) and *N*-methylpyrrolidone (36 mL) were added to a round bottom flask and heated to 160 ºC under a dinitrogen atmosphere for 2h. Upon cooling the mixture was poured into water and the brown precipitate filtered and dried in a dessicator over phosphorus pentoxide. The solid was subject to silica gel column chromatography with hexanes as the eluent, affording a white solid. This solid was further purified by recrystallization from hexanes, yielding **12** as colorless crystals, (6.6 g, 42 %). M.p. 93-95 ºC; $^1$H NMR ($\delta_H$; 200 MHz, $CDCl_3$): 10.31 (s, 1H); IR (KBr pellet): υ 1703, 1636, 1487, 1415, 1391, 1274, 1036, 971, 830, 777, 626 cm$^{-1}$.

***4.2.1.5 Synthesis of 1-iodo-2,3,5,6-tetrafluorobenzoic acid, 13***

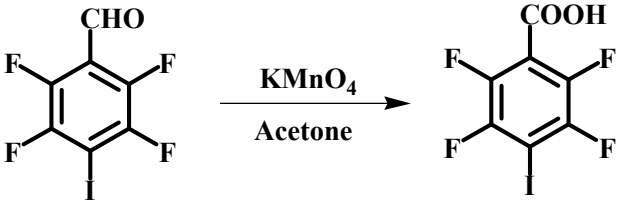


**11** **13**

A solution of 1-iodo-2,3,5,6-tetrafluoro benzaldehyde **11** (1.52 g, 5.0 mmol) in acetone (50 mL) was brought to reflux, when a saturated aqueous solution of $KMnO_4$ (1.67 g, 10.57 mmol) was added. The reaction was kept under reflux for 18h. Upon completion the reaction mixture was filtered hot and the precipitate washed with acetone. The filtrate and the acetone wash were combined and concentrated by rotary evaporator. The residue was treated with dilute

HCl (5 %) and extracted into dichloromethane. The organic layer was washed with water, dried over magnesium sulfate and evaporated on a rotary evaporator yielding a white solid **13**, (1.29 g, 81 %). Dec. 140 ºC; $^1$H NMR ($\delta_H$; 200 MHz, $CDCl_3$): 8.173 (br s); ESI-IT-MS *m/z* 318 ([**13 -** H]$^-$); IR (KBr pellet): υ 2996, 1700, 1475, 979, 718 cm$^{-1}$.

#### *4.2.1.6 Synthesis of 1-bromo-2,3,5,6-tetrafluorobenzoic acid, 14*

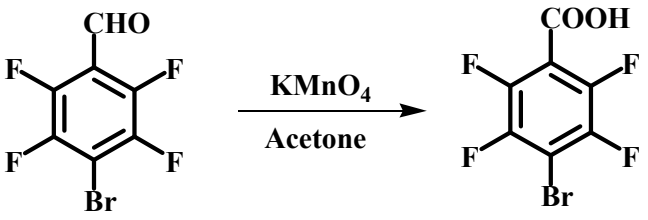


**12** **14**

A solution of 1-bromo-2,3,5,6-tetrafluoro benzaldehyde **12** (1.54 g, 6.0 mmol) in acetone (60 mL) was brought to reflux, when a saturated aqueous solution of $KMnO_4$ (2.01 g, 12.72 mmol) was added. The reaction was kept under reflux for 18h. Upon completion the reaction mixture was filtered hot and the precipitate washed with acetone. The filtrate and the acetone wash were combined and concentrated by rotary evaporator. The residue was treated with dilute HCl (5 %) and extracted into dichloromethane. The organic layer was washed with water, dried over magnesium sulfate and evaporated on a rotary evaporator yielding a white solid **14**, (1.32 g, 81 %). M.p. 128 - 130 ºC; $^1$H NMR ($\delta_H$; 200 MHz, $CDCl_3$): 10.16 (br s); ESI-IT-MS *m/z* 270 ([**14 -** H]$^-$); IR (KBr pellet): υ 2996, 1711, 1475, 979, 712 cm$^{-1}$.

### *4.2.2 Synthesis of co-crystals and salts*

#### *4.2.2.1 Synthesis of 3-(2-amino-4-methylpyrimidin-6-yl)pyridine:4-iodobenzoic acid, 8a*

3-(2-Amino-4-methylpyrimidin-6-yl)pyridine (10 mg, 0.05 mmol) and 4-iodobenzoic acid (13 mg, 0.05 mmol) were placed in a beaker containing an ethyl acetate/toluene (2:1) mixture and heated until a clear homogeneous solution was obtained. After two days of slow evaporation, colorless rod-shaped crystals were obtained. M.p. 152-154 °C; IR (KBr pellet) *υ* 3329 and 3083 cm$^{-1}$ ($NH_2$, m), 2413 and 1921 cm$^{-1}$ (O-H···N, br), 1685 cm$^{-1}$ (C=O, m).

#### *4.2.2.2 Synthesis of 3-(2-amino-4-methylpyrimidin-6-yl)pyridine:1-iodo-2,3,5,6-tetrafluorobenzoic acid, 13a*

3-(2-Amino-4-methylpyrimidin-6-yl)pyridine (10 mg, 0.05 mmol) and 1-iodo-2,3,5,6-tetrafluorobenzoic acid (17 mg, 0.05 mmol) were placed in a beaker containing ethanol (6 mL) and heated until a clear homogeneous solution was obtained. After two days of slow evaporation, colorless rod-shaped crystals were obtained. M.p. 196-198 °C; IR (KBr pellet) $\upsilon$ 3334 and 3104 $cm^{-1}$ ($NH_2$, m), 2407 and 1972 $cm^{-1}$ (O-H···N, br), 1680 $cm^{-1}$ (C=O, m), 963 $cm^{-1}$.

#### *4.2.2.3 Synthesis of 4-(2-amino-4-methylpyrimidin-6-yl)pyridine:4-iodobenzoic acid, 8b*

4-(2-Amino-4-methylpyrimidin-6-yl)pyridine (10 mg, 0.05 mmol) and 4-iodobenzoic acid (13 mg, 0.05 mmol) were placed in a vial containing acetonitrile (6 mL) and heated until a clear homogeneous solution was obtained. After two days of slow evaporation, orange block-shaped crystals were obtained. M.p. 181-183 °C; IR (KBr pellet) $\upsilon$ 3334 and 3176 $cm^{-1}$ ($NH_2$, m), 2428 and 1895 $cm^{-1}$ (O-H···N, br), 1660 $cm^{-1}$ (C=O, m).

#### *4.2.2.4 Synthesis of 4-(2-amino-4-methylpyrimidinium-6-yl)pyridine:1-iodo-2,3,5,6-tetrafluorobenzoate, 13b*

3-(2-Amino-4-methylpyrimidin-6-yl)pyridine (10 mg, 0.05 mmol) and 1-iodo-2,3,5,6-tetrafluorobenzoic acid (17 mg, 0.05 mmol) were placed in a vial containing ethanol/ethyl acetate (3:2) and heated until a clear homogeneous solution was obtained. After one day of slow evaporation, colorless rod-shaped crystals were obtained. Dec. 210 °C; IR (KBr pellet) $\upsilon$ 3350 and 2996 $cm^{-1}$ ($NH_2$, m), 2387 and 1967 $cm^{-1}$ (O-H···N, br), 1690 $cm^{-1}$ (C=O, m)

#### *4.2.2.5 Synthesis of 4-(2-amino-4-methylpyrimidinium-6-yl)pyridine:1-bromo-2,3,5,6-tetrafluorobenzoate, 14a*

3-(2-Amino-4-methylpyrimidin-6-yl)pyridine (10 mg, 0.05 mmol) and 1-bromo-2,3,5,6-tetrafluorobenzoic acid (17 mg, 0.05 mmol) were placed in a vial containing nitromethane/acetonitrile (5:1) and heated until a clear homogeneous solution was obtained. After one day of slow evaporation, colorless rod-shaped crystals were obtained. M.p. 204-206 °C; IR (KBr pellet) $\upsilon$ 3340 and 3044 $cm^{-1}$ ($NH_2$, m), 2361 and 1962 $cm^{-1}$ (O-H···N, br), 1696 $cm^{-1}$ (C=O, m).

#### *4.2.2.6 Synthesis of 1-(2-amino-4-methylpyrimidin-6-yl)-2-(3-methoxypyridin-5-yl)ethyne:4-iodobenzoic acid, 8c*

1-(2-Amino-4-methylpyrimidin-6-yl)-2-(3-methoxypyridin-5-yl)ethyne (10 mg, 0.04 mmol) and 4-iodobenzoic acid (12 mg, 0.04 mmol) were placed in a vial containing a methanol/nitromethane solution (2:1) and heated until a clear homogeneous solution was obtained. After four days of slow evaporation, colorless rod-shaped crystals were obtained. M.p. 188-190 °C; IR (KBr pellet) $\upsilon$ 3257 and 3037 $cm^{-1}$ ($NH_2$, m), 2361 and 1957 $cm^{-1}$ (O-H···N, br), 1690 $cm^{-1}$ (C=O, m), 2218 $cm^{-1}$ (-C≡C-, m).

#### *4.2.2.7 Synthesis of 1-(2-amino-4-methylpyrimidinium-6-yl)-2-(3-methoxypyridin-5-yl)ethyne:1-bromo-2,3,5,6-tetrafluorobenzoate, 14b*

1-(2-Amino-4-methylpyrimidin-6-yl)-2-(3-methoxypyridin-5-yl)ethyne (10 mg, 0.04 mmol) and 1-bromo-2,3,5,6-tetrafluorobenzoic acid (12 mg, 0.04 mmol) were placed in a vial containing ethanol (6 mL) and heated until a clear homogeneous solution was obtained. After four days of slow evaporation, colorless rod-shaped crystals were obtained. M.p. 188-190 °C; IR (KBr pellet) $\upsilon$ 3257 and 3037 $cm^{-1}$ ($NH_2$, m), 2361 and 1957 $cm^{-1}$ (O-H···N, br), 1690 $cm^{-1}$ (C=O, m), 2218 $cm^{-1}$ (-C≡C-, m).

## 4.3 Results

A summary of the crystallographic information for **14**, **8a-8c**, **13a-13b**, and **14a-14b** displayed in Tables B.3 and all hydrogen-bond geometries for are listed in Table 4.1

**Table 4.1** Hydrogen-Bond Geometries for **14**, **8a-8c**, **13a-13b**, and **14a-14b**

| Structure | D-H···H | d(D-H)/Å | d(H···A)/Å | d(D···A)/Å | <(DHA)/º |
|---|---|---|---|---|---|
| **14**[i] | O(1)-H(1)...O(2)#1 | 0.84 | 1.82 | 2.663(6) | 175.4 |
| **8a**[ii] | O(31)-H(31)...N(11) | 0.98(2) | 1.59(3) | 2.5607(19) | 168(2) |
| | N(12)-H(12A)...O(32) | 0.84(2) | 2.21(2) | 3.035(2) | 168(2) |
| | N(12)-H(12B)...N(21)#1 | 0.83(2) | 2.12(2) | 2.951(2) | 177(2) |
| **13a**[iii] | O(31)-H(31)...N(11) | 0.84 | 1.77 | 2.589(7) | 165.0 |
| | N(12)-H(12A)...O(32) | 0.88 | 2.06 | 2.924(8) | 168.6 |
| | N(12)-H(12B)...O(32)#1 | 0.88 | 2.05 | 2.855(8) | 150.9 |
| **8b** | N(11)-H(12A)...O(32) | 0.88 | 1.95 | 2.818(4) | 167.9 |
| | O(31)-H(31)...N(11) | 0.84 | 1.84 | 2.675(3) | 172.6 |
| **13b**[iv] | N(11)-H(11)...O(31) | 0.85(6) | 1.81(6) | 2.646(5) | 167(5) |
| | N(12)-H(12A)...O(32) | 0.88 | 1.94 | 2.801(5) | 164.7 |
| | N(12)-H(12B)...O(32)#1 | 0.88 | 2.07 | 2.808(5) | 141.4 |
| **14a**[v] | N(11)-H(11)...O(31) | 0.82(2) | 1.83(2) | 2.6430(19) | 173(2) |
| | N(12)-H(12A)...O(32) | 0.84(2) | 1.99(2) | 2.823(2) | 172(2) |
| | N(12)-H(12B)...O(32)#1 | 0.89(2) | 2.07(2) | 2.812(2) | 140(2) |
| **8c**[vi] | O(31)-H(31)...N(11) | 0.97(9) | 1.71(9) | 2.643(8) | 162(7) |
| | N(12)-H(12A)...O(32) | 0.86 | 2.14 | 2.987(8) | 169(3) |
| | N(12)-H(12B)...N(13)#1 | 0.86 | 2.28 | 3.108(8) | 160.3 |
| **14b**[vii] | N(11)-H(11)...O(31) | 0.94(3) | 1.68(3) | 2.605(2) | 169(2 ) |
| | N(12)-H(12A)...O(32) | 0.93(3) | 1.90(3) | 2.832(2) | 173(2) |
| | N(12)-H(12B)...N(13)#1 | 0.74(3) | 2.34(3) | 3.073(2) | 170(3) |

i) #1 -x,-y+1,-z+1 ii) #1 -x,-y+2,-z+1 iii) #1 -x+2,-y+1,-z+2 iv) #1 -x+1,-y+1,-z+1 v) #1 -x+1,-y+2,-z+2 vi) #1 -x,-y+1,-z vii) #1 -x+1,-y,-z+1

### *4.3.1 Crystal structure of 1-bromo-2,3,5,6-tetrafluorobenzoic acid, 14*

Crystals of 1-bromo-2,3,5,6-tetrafluorobenzoic acid **14** were grown at room temperature by slow evaporation of a saturated dichloromethane solution. As expected the acid moieties form head-to-head dimers through self-complementary O-H···O (O1 ···O2, 2.663(6)) hydrogen bonds, Figure 4.6. Bromine···bromine contacts were not observed.

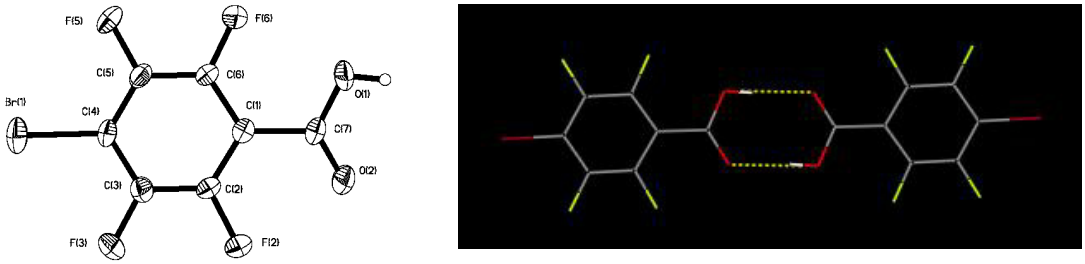


**(a)** **(b)**

**Figure 4.6** a) Thermal-ellipsoids plot (50% probability level) of 1-bromo-2,3,5,6-tetrafluorobenzoic acid; b) acid···acid dimer produced from two molecules of **14**.

### *4.3.2 Crystal structure of 3-(2-amino-4-methylpyrimidin-6-yl)pyridine:4-iodobenzoic acid, 8a*

The primary motif in the crystal structure of **8a** is composed of SR **1** and 4-iodobenzoic acid **8**, assembled via a complementary hydrogen-bond interaction between the carboxylic acid and the amino-pyrimidine moieties, Figure 4.7. The primary hydrogen bonds are O–H···N and N–H···O with O31···N11 and N12···O32 distances of 2.5607(19) Å and 3.035(2) Å, respectively. Secondary N-H···N hydrogen bonds, N12-N21, 2.951(2) Å, formed from the *anti*-amino and the pyridyl nitrogen atom extend the architecture into a four-component supermolecule, Figure 4.8. No halogen···nitrogen or halogen···halogen interactions are observed.

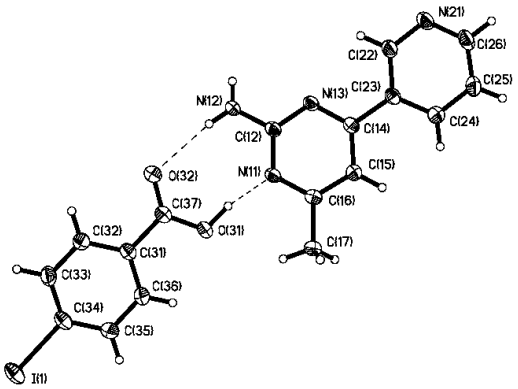


**Figure 4.7** Thermal-ellipsoids plot (50% probability level) of the 1:1 co-crystal **8a**.

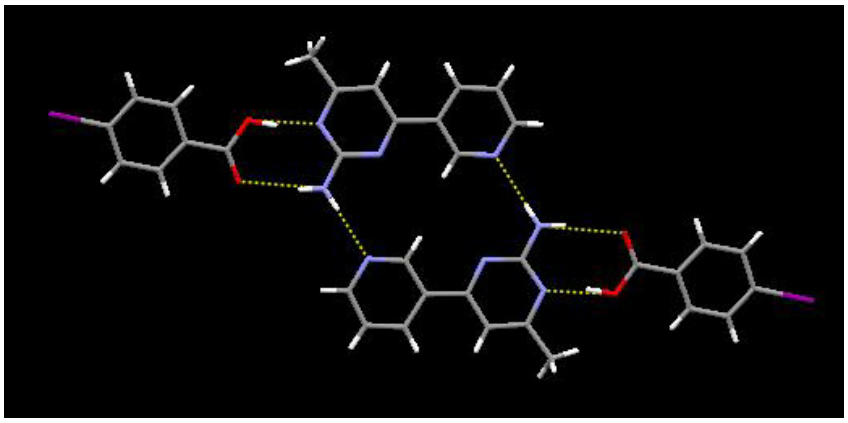

**Figure 4.8** Four-component supermolecule of **8a** comprised of N-H···O, O-H···N, and N-H···N hydrogen bonds. The toluene solvent molecule has been omitted for clarity.

### *4.3.3 Crystal structure of 3-(2-amino-4-methylpyrimidin-6-yl)pyridine:1-iodo-2,3,5,6-tetrafluorobenzoic acid, 13a*

In the crystal structure of **13a** the main motif consists of SR **1** and 1-iodo-2,3,5,6-tetrafluorobenzoic acid **13**, assembled via a complementary hydrogen-bond interaction between the carboxylic acid and the amino-pyrimidine moieties, Figure 4.9. The primary hydrogen bonds are O–H···N and N–H···O interactions with O31···N11 and N12···O32 distances of 2.589(7) Å and 2.924(8) Å, respectively. Halogen bonding formed through the iodine atom and the pyridyl nitrogen atom extend the architecture into one-dimensional chains with a N···I distance of 2.941 Å. The 1-D chains are connected into a two-dimensional wave-like pattern through additional N–H···O interactions (N12···O32, 2.855(8) Å) from the *anti*-proton of the amino-functionality to the carbonyl oxygen of the halogenated benzoic acid, Figure 4.10.

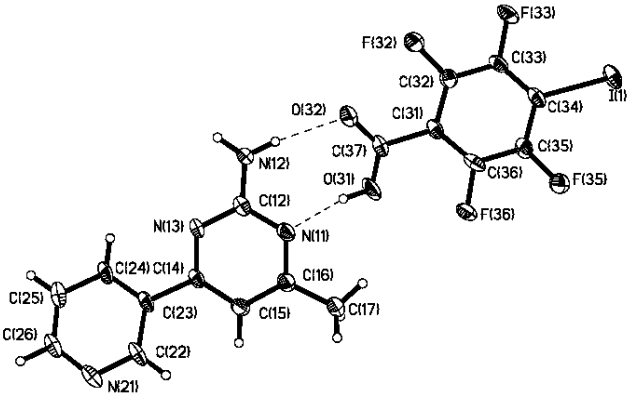


**Figure 4.9** Thermal-ellipsoids plot (50% probability level) of the 1:1 binary co-crystal of **13a**.

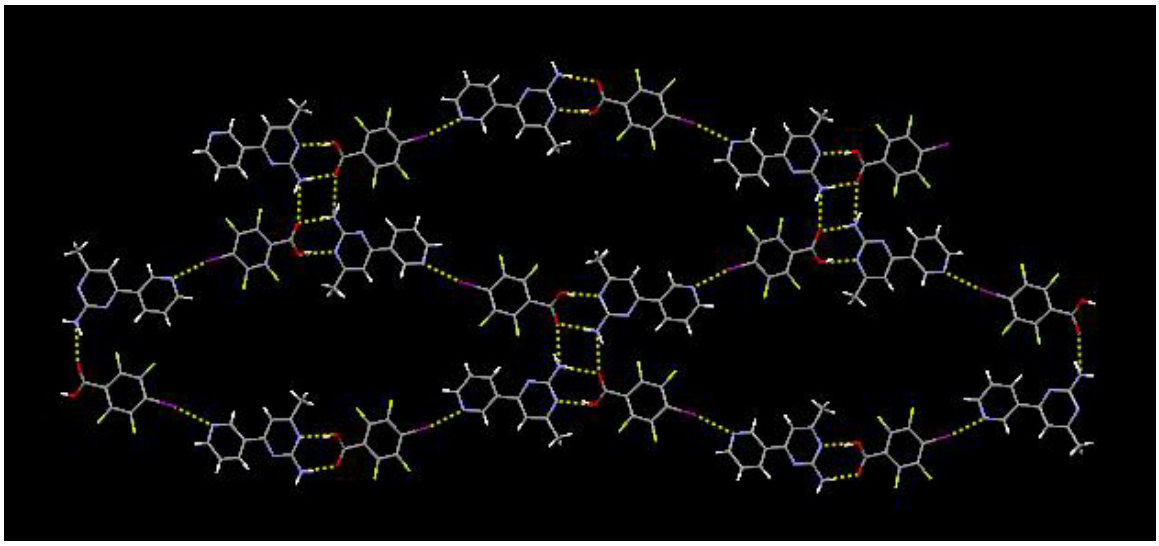

**Figure 4.10** Extended motif of **13a**, displaying the combinations of O–H···N and N–H···O hydrogen bonds as well as N···I halogen bonds.

### *4.3.4 Crystal structure of 4-(2-amino-4-methylpyrimidin-6-yl)pyridine:4-iodobenzoic acid, 8b*

In the crystal structure of **8b** the main motif consists of SR **7** and 4-iodobenzoic acid **8**, assembled via a complementary hydrogen-bond interaction between the carboxylic acid and the amino-pyrimidine moieties, Figure 4.11. The primary hydrogen bonds are O–H···N and N–H···O interactions with O31···N11 and N12···O32 distances of 2.675(3) Å and 2.818(4) Å, respectively. Halogen bonding extends the architecture into 1-D chains with a N···I distance of 3.004 Å. Adjacent chains are connected through self-complementary N–H···N hydrogen bonds with N12···N13 distances of 2.250 Å, Figure 4.12.

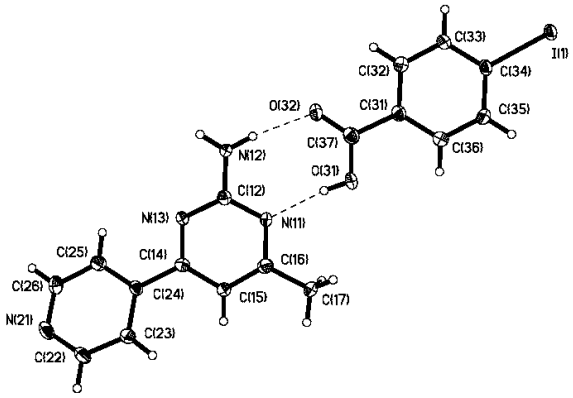


**Figure 4.11** Thermal-ellipsoids plot (50% probability level) of the 1:1 binary co-crystal of **8b**.

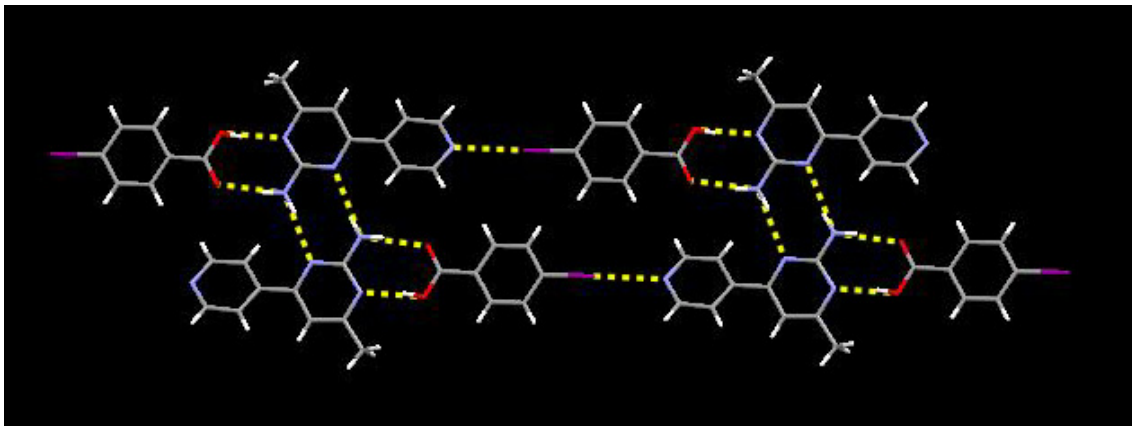

**Figure 4.12** Extended motif of **8b**, displaying combinations of O–H···N, N–H···O, and N–H···N hydrogen bonds as well as N···I halogen bonds.

### *4.3.5 Crystal structure of 4-(2-amino-4-methylpyrimidinium-6-yl)pyridine:1-iodo-2,3,5,6-tetrafluorobenzoate, 13b*

In the crystal structure of **13b** the main motif consists of a protonated SR **7** and one 1-iodo-2,3,5,6-tetrafluorobenzoate ion, assembled via charge-assisted hydrogen-bond interactions between the carboxylate and the amino-pyrimidinium moieties, Figure 4.13. The primary hydrogen bonds are $N–H^{+}\cdots O^{-}$ and $N\text{-}H\cdots O^{-}$ interactions with $N^{+}11\cdots O^{-}31$ and $N12\cdots O^{-}32$ distances of 2.675(3) Å and 2.818(4) Å, respectively. Halogen bonding extends the architecture into 1-D chains with a N···I distance of 2.812 Å. The 1:1 ionic chains are linked into a ladder motif through secondary $N\text{-}H\cdots O^{-}$ hydrogen bonds (N12···O32, 2.812(2)), from the *anti*-amino proton and the carboxylate oxygen atom, Figure 4.14.

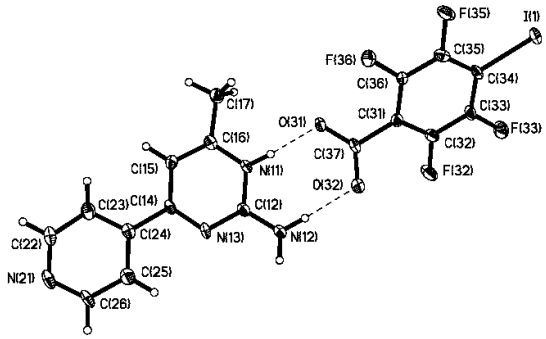


**Figure 4.13** Thermal-ellipsoids plot (50% probability level) of the 1:1 ionic dimer of **13b**.

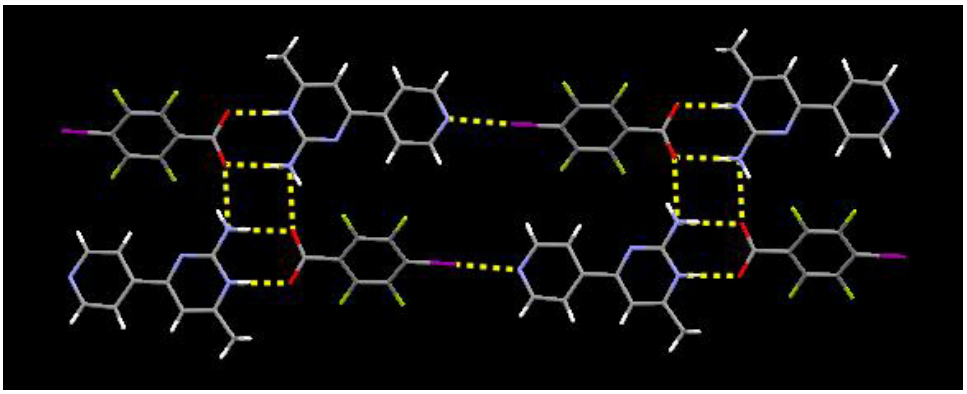

**Figure 4.14** 1-D strands formed through a series of hydrogen bonds and halogen bonds.

### *4.3.6 Crystal structure of 4-(2-amino-4-methylpyrimidinium-6-yl)pyridine:1-bromo-2,3,5,6-tetrafluorobenzoate, 14a*

In the crystal structure of **14a** the main motif consists of one protonated SR **7** and one 1-bromo-2,3,5,6-tetrafluorobenzoate ion, assembled via charge-assisted hydrogen-bond interactions between the carboxylate and the amino-pyrimidinium moieties, Figure 4.15, with $N^{+}11\cdots O^{-}31$ and $N^{+}12\cdots O^{-}32$ distances of 2.6430(19) Å and 2.823(2) Å, respectively. Halogen bonds extend the architecture into 1-D chains with an N···Br distance of 2.840 Å, while the *anti*-proton of the amino group forms an N–H···$O^{-}$ hydrogen bond (N12···$O^{-}$32, 2.812(2) Å) with a neighboring carboxylate oxygen atom generating a ladder motif, Figure 4.16.

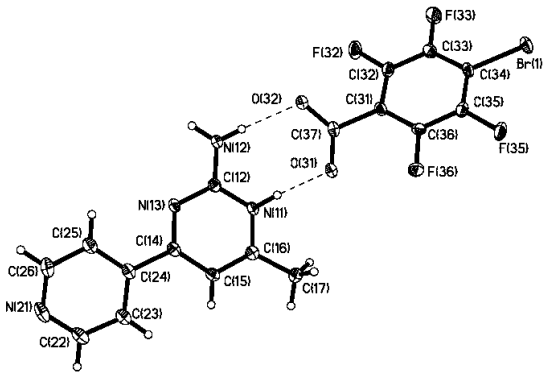


**Figure 4.15** Thermal-ellipsoids plot (50% probability level) of the 1:1 dimer **14a**.

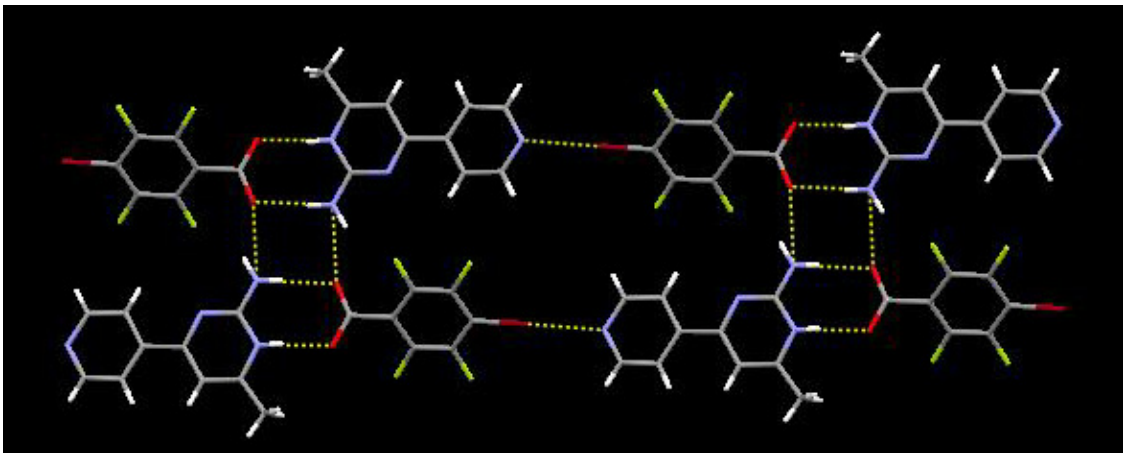

**Figure 4.16** 1-D strands formed through a series of hydrogen bonds and halogen bonds.

### *4.3.7 Crystal structure of 1-(2-amino-4-methylpyrimidin-6-yl)-2-(3-methoxypyridin-5-yl)ethyne:4-iodobenzoic acid, 8c*

The primary motif in the crystal structure of **8c** consists of O–H···N and N–H···O interactions with O31···N11 and N12···O32 distances of 2.643(8) and 2.987(8) Å, respectively, Figure 4.17. The *anti*-proton of the amino group forms self-complementary N–H···N hydrogen bonds (N12···N13, 3.108(8) Å) with a pyrimidine nitrogen of a neighboring 1-D strand generating a tetrameric supermolecule, Figure 4.18.

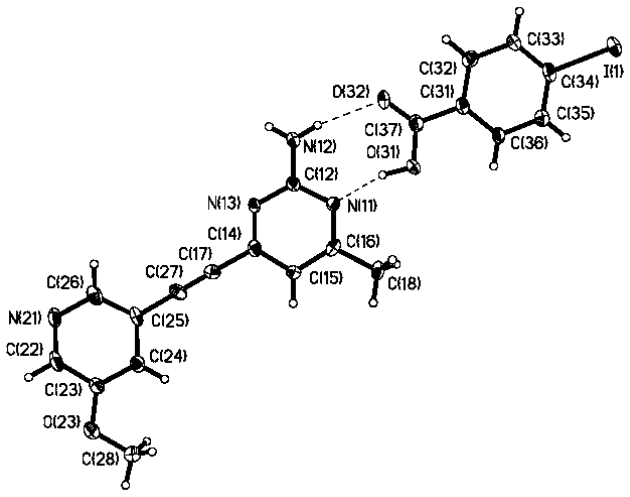


**Figure 4.17** Thermal-ellipsoids plot (50% probability level) of the 1:1 binary co-crystal of **8c**.

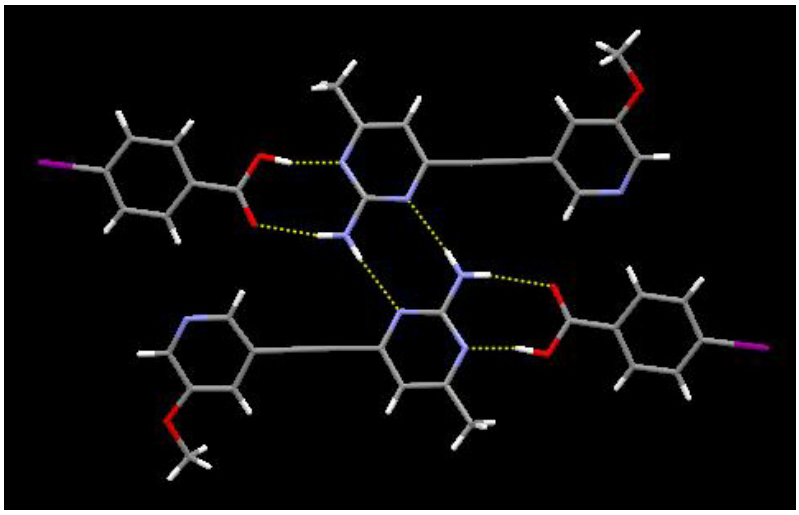

**Figure 4.18** Tetrameric supermolecule **8c** formed through a series of hydrogen bonds.

### *4.3.8 Crystal structure of 1-(2-amino-4-methylpyrimidinium-6-yl)-2-(3-methoxypyridin-5-yl)ethyne:1-bromo-2-3-5-6-tetrafluorobenzoate, 14b*

In the crystal structure of **14b** the main motif comprises hydrogen-bonding interactions between the carboxylate and the amino-pyrimidinium moieties, with $N^{+}11\cdots O^{-}31$ and $N12\cdots O^{-}32$ distances of 2.605(2) Å and 2.832(2) Å, respectively. Adjacent ions are connected through self-complementary N–H···N hydrogen bonds with N12···N13 distances of 3.073(2) Å, producing a four-component supermolecule, Figure 4.20. No short Br···N or Br···Br interactions were observed.

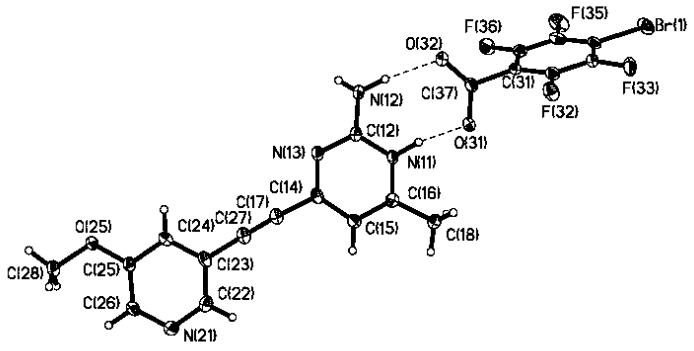


**Figure 4.19** Thermal-ellipsoids plot (50% probability level) of the 1:1 dimer **14b**.

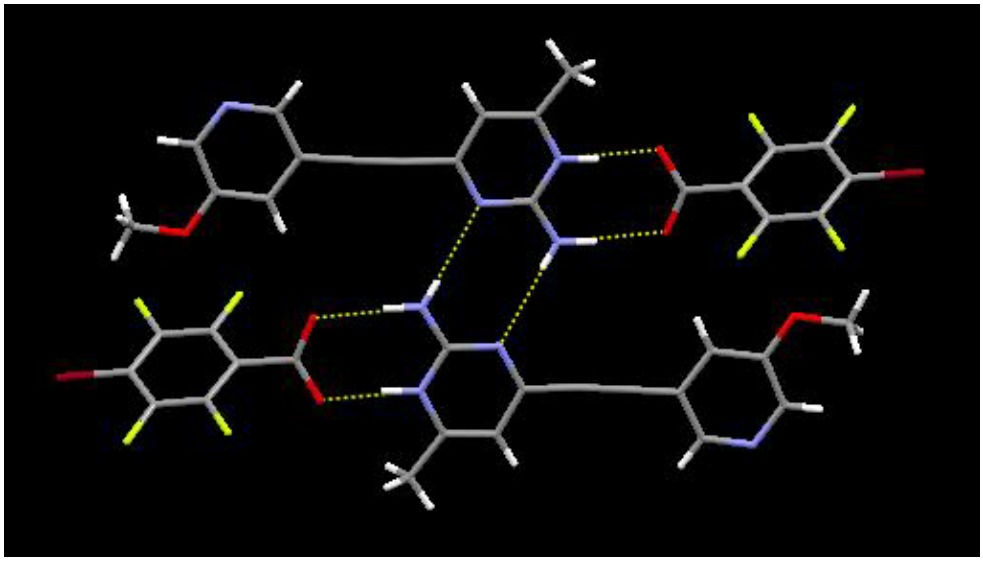

**Figure 4.20** Four-component supermolecule **14b** constructed through charge-assisted and neutral hydrogen bonds.

## 4.4 Discussion

### *4.4.1 Can a hierarchy through hydrogen and halogen bonds be established?*

Each of the four co-crystals obtained so far, possesses the robust and reliable amino-pyrimidine···carboxylic acid heterosynthon. Additionally, the same connectivities are observed in the three ionic salts, through pairwise N-$H^{+}$···$O^{-}$ and N-H···$O^{-}$ charge-assisted hydrogen bonds between the amino-pyrimidinium and the carboxylate moieties. Unfortunately, suitable crystals for single-crystal X-ray crystallography were not obtained for compounds 3-(2-amino-4-methylpyrimidin-6-yl)pyridine:1-bromo-2,3,5,6-tetrafluorobenzoic acid and 1-(2-amino-4-methylpyrimidin-6-yl)-2-(3-methoxypyridin-5-yl)ethyne:1-iodo-2-3-5-6-tetrafluorobenzoic acid.

In four of the seven structures **13a-13b**, **8b**, and **14a** halogen bonds *i.e.* N···I or N···Br extend the acid/SR dimers into polymeric networks. The halogen bonding patterns and distances for each crystal structure is displayed in Table 4.2.

**Table 4.2** Halogen bonding patterns observed in crystal structures **8a-8c**, **13a-13b**, and **14a-14b**

| SR | Acid | Structure # | Halogen bonds | Type of Halogen bond | Halogen bond Distance (Å) |
|---|---|---|---|---|---|
| **1** | I-BA | **8a** | No | ---- | **----** |
| **1** | I-$F_4$BA | **13a** | Yes | N···I | 2.941 |
| **7** | I-BA | **8b** | Yes | N···I | 3.004 |
| **7** | I-$F_4$BA | **13b** | Yes | N···I | 2.812 |
| **7** | Br-$F_4$BA | **14a** | Yes | N···Br | 2.840 |
| **6** | I-BA | **8c** | No | ---- | ----- |
| **6** | Br-$F_4$BA | **14b** | No | ---- | **-----** |

**Note**: I-BA = 4-iodobenzoic acid, I-$F_4$BA = 1-iodo-2,3,5,6-tetrafluorobenzoic acid, and Br-$F_4$BA = 1-bromo-2,3,5,6-tetrafluorobenzoic acid.

### *4.4.2 Characterization of halogen bonding through IR spectroscopy*

Attempts were made at detecting whether or not an actual N···I or N···Br halogen bond had formed through changes in the C-X (X = I or Br) stretch in the IR spectrum. If halogen bonding takes place, then shifts to lower wavenumbers should occur for the C-X (X = I or Br) stretch. In "free" 1,4-diiodotetrafluorobenzene, the C-I stretch is observed around 945 $cm^{-1}$, however upon complexation (with a N-heterocycle) the C-I stretch shifts to lower wavenumbers around 940 $cm^{-1}$.

We assigned the band at 979 $cm^{-1}$ to the C-I stretch of "free" halogenated benzoic acid **13** to 979 $cm^{-1}$, however upon complexation, structures **13a** and **13b**, that band had shifted to around 963 and 968 wavenumbers, respectively. Attempts to monitor the change in the C-I stretch of benzoic acid **8**, *i.e.* uncomplexed vs. complexed were unsuccessful. The uncomplexed C-I stretch occurs ~1010 $cm^{-1}$, however we observed C-I stretches at lower wavenumbers, *i.e.* 1004, 1009, and 1004 $cm^{-1}$ for compounds **8a**, **8b**, and **8c**, even though complexation did not take place (based upon crystallography). This may be explained based on attempting to track band shifts between relatively weak interactions, which would produce very small changes in the IR spectra. Additionally, we were unable to identify the C-Br stretching band for halogenated benzoic acid **14**, and thus characterization of whether or not complexation, based on IR data had occurred, was not possible.

### *4.4.3 Does the Lewis acidity of the halogen nuclei increase upon fluorination?*

As expected, comparing structures **13a** and **8b**, the halogen bond distance becomes shorter upon fluorination of the aryl ring. Furthermore, structure **13a** also displays a shorter halogen bond distance compared to that of the bromo analog, **14a**, which is consistent with aryl iodides being stronger Lewis acid's than aryl bromides.

It is possible that SR's **1** and **6** only formed the desired halogen bonding connectivities 1 out of 4 times, due to the location of the pyridyl nitrogen atom *i.e.* 3- vs. 4-pyridyl. Although upon fluorination of the carboxylic acid, structure **13a** displays the desired hydrogen and halogen bonding arrangement and connectivity, while **8a** failed to produce halogen bonds.

### *4.4.4. Effects of the halogen (I or Br) on the directed-assembly*

Due to the limited number of crystal structures, it is difficult to draw direct conclusions about the binding effects of iodine vs. bromine as a more suitable electron-pair acceptor atom within our py-pym SR/carboxylic acid systems. However, upon observation of the halogen bond distances, Table 4.2, **13b** displays a shorter N···I distance, 2.812 Å, compared to **14a**, which has an N···Br distance of 2.840 Å, even though the size of iodine (1.32 Å) is larger than bromine (1.14 Å). Furthermore, a search through the CSD revealed only thirteen structures containing N···Br interactions, however fifty-three contained N···I contacts.

This Chapter has described a strategy for designing and constructing supermolecules through combinations of hydrogen bonds and halogen bonds. In all seven structures the amino-pyrimidine···carboxylic acid synthon was utilized to 'lock' two individual molecules into a correct orientation and arrangement, in which secondary N···I or N···Br halogen bonds, in four cases, extended the architecture. We were also able to display how the electron-pair accepting ability of the 4-iodobenzoic acid molecule was increased upon fluorination in comparing structures **13a** and **13b**.

## References:


[1] (a) Hguyen, T. L.; Fowler, F. W.; Lauher, J. W. *J. Am. Chem. Soc*. **2001**, *123*, 11057. (b) Bhogala, B. R.; Nangia, A. *Cryst. Growth Des.* **2003**, *3*, 547. (c) Bensemann, I.; Gdaniec, M.; Lakomecka, K.; Milewska, M. J.; Polonski, T. *Org. Biomol. Chem*. **2003**, *1*, 1425. (d) Mei, X.; Wolf, C. *Eur. J. Org. Chem.* **2004**, 4340. (e) Dale, S. H.; Elsegood, M. R. J.; Hemmings, M.; Wilkinson, A. L. *CrystEngComm*. **2004**, *6*, 207. (f) Lynch, D. E.; Chatwin, S.; Parsons, S. *Crystal Eng*. **1999**, *2*, 137.

[2] (a) Aakeröy, C. B.; Desper, J.; Helfrich, B. A. *CrystEngComm*. **2004**, *6*, 19. (b) Aakeröy, C. B.; Desper, J.; B. M. T. Scott. *Chem. Commun*. **2006**, 1445. (c) Aakeröy, C. B.; Beatty, A. M.; Helfrich, B. A.; Nieuwenhuyzen, M. *Cryst. Growth Des*. **2003**, *3*, 159. (d) Reddy, L. S.; Nangia, A.; Lynch, V. M. *Cryst. Growth Des*. **2004**, **4**, 89. (e) Ito, Y.; Hosomi, H.; Ohba, S. *Tetrahedron*, **2000**, *56*, 6833. (f) Vishweshwar, P.; McMahon, J. A.; Peterson, M. L.; Hickey, M. B. Shattock, T. R.; Zaworotko, M. J. *Chem. Commun*. **2005**, 4601.

[3] (a) Aakeröy, C. B.; Schultheiss, N.; Desper, J.; Moore, C. *New J. Chem*. **2006**, *30*, 1452. (b) Thanigaimani, K; Muthiah, P. T.; Lynch, D. E. *Acta Cryst*. **2006**, E*62*, 2976. (c) Balasubramani, K; Muthiah, P. T.; Lynch, D. E. *Acta Cryst*. **2006**, E*62*, 2907. (d) Smith, G.; Gentner, J. M.; Lynch, D. E.; Byriel, K. A.; Kennard, C. H. L. *Aust*. *J. Chem*. **1995**, *48*, 1151. (e) Etter, M. C.; Adsmond, D. A. *Chem. Commun*. **1990**, 589.

[4] (a) Walsh, R. B.; Padgett, C. W.; Metrangolo, P.; Resnati, G.; Hanks, T. W.; Pennington, W. T. *Cryst. Growth Des*. **2001**, *1*, 165. (b) Metrangolo, P.; Pilati, T.; Resnati, G.; Stevenazzi, A. *Chem. Commun*. **2004**, 1492. (c) De Santis, A.; Forni, A.; Liantonio, R.; Metrangolo, P.; Pilati, T.; Resnati, G. *Chem*. *Eur*. *J*. **2003**, *9*, 3974. (d) Metrangolo, P.; Neukirch, H.; Pilati, T.; Resnati, G. *Acc*. *Chem*. *Res*. **2005**, *38*, 386.

[5] Saha, B. K.; Nangia, A.; Jaskólski, M. *CrystEngComm* **2005**, *7*, 355.

[6] Vishweshwar, P.; Nangia, A.; Lynch, V. M. *J. Org. Chem*. **2002**, *67*, 556.

[7] (a) Allen, F. H.; Lommerse, J. P. M.; Hoy, V. J.; Howard, J. A. K.; Desiraju, G. R. *Acta. Crystallogr*. **1997**, *B53*, 1006. (b) Lommerse, J. P. M.; Stone, A. J.; Taylor, R.; Allen, F. H. *J. Am. Chem. Soc*. **1996**, *118*, 3108.

[8] Weiss, R.; Schwab, O.; Hampel, F. *Chem.-Eur. J.* **1999**, *5*, 968.

[9] Krebs, F. C.; Jensen, T. *Journal of Fluorine Chemistry*, **2003**, *120*, 77-84.

[10] Leroy, J.; Schollhorn, B.; Syssa-Magale, J.-L.; Boubekeur, K.; Palvadeau, P. *Journal of Fluorine Chemistry*, **2004**, *125*, 1379-1382.

[11] Robson, M. J.; Williams, J. European Patent, #EP 0 196 156 B1, 1986.

# CHAPTER 5 - Directed supramolecular assembly of M(II)-containing complexes (M = Co, Cu, Ni) into infinite 1-D chains using structurally bifunctional ligands

## 5.1 Introduction

The design and synthesis of inorganic:organic hybrid materials through supramolecular synthesis, is a rapidly emerging field within crystal engineering.[1] The ability to translate the inherent dimensionality and geometry of any coordination complex into extended architectures with specific (and tunable) metrics is critical for producing materials with desired chemical and physical properties.[2] The use of coordinate covalent bonds for the assembly of coordination polymers is well established,[3] whereas synthetic strategies that utilize non-covalent (*i.e.* hydrogen bonds,[4] π-π interactions,[5] etc.) and metal-ligand interactions within the same network are far less developed.[6] Composite hybrid materials are of crucial importance in natural systems[7] and they have also found numerous uses in synthetic high-tech applications.[8] Since the physical properties of any solid are influenced by the communication and interactions between molecules or complex ions, it is important, from the point of view of tuning properties, to be able to alter specific metrics (*e.g.* distance between metal ions) without inducing dramatic changes to the overall crystal structure. Thus, the design of versatile bifunctional ligands that are capable of coordinating to a metal ion whilst providing the means for organizing such complex ions into extended networks in a predictable manner is an important aspect of current structural inorganic chemistry.

We are specifically interested in developing reliable and versatile supramolecular routes for the directed assembly of metal ions and multi-functional organic ligands into infinite 1-D chains, which means that we need to (a) carefully control the geometry of the complex ion and, (b) eliminate the need for potentially disruptive counterions. This is particularly important when targeting metal ions with diverse and unpredictable coordination modes such as Cu(II). In order to reach this specific supramolecular goal it is essential that the synthetic process is designed such that the number of potentially structural interfering components present, or introduced, during the assembly process is kept to a minimum. In essence, the reaction conditions need to be

optimized in the same way that reaction conditions for covalent synthesis are selected for maximum yield.

With this in mind, a variety of structurally bifunctional organic ligands containing a metal-ion coordinating moiety and a hydrogen bonding functionality were synthesized with the specific supramolecular goal of organizing a variety of M(II)-based complex ions (M = Co, Cu, Ni) into infinite 1-D chains. Dinuclear Cu(II) complexes incorporating four carboxylate moieties ($Cu^{II}_2L_4$, where L = acetate or 2-fluorobenzoate) provides a reasonable starting point since the four monoanionic functional groups bridge two copper(II) centers thereby creating a neutral "paddlewheel" complex, Figure 5.1a. Each copper ion is in an arrangement where four of the equatorial positions are coordinated by the anions, leaving a vacant axial position accessible for the supramolecular ligand.

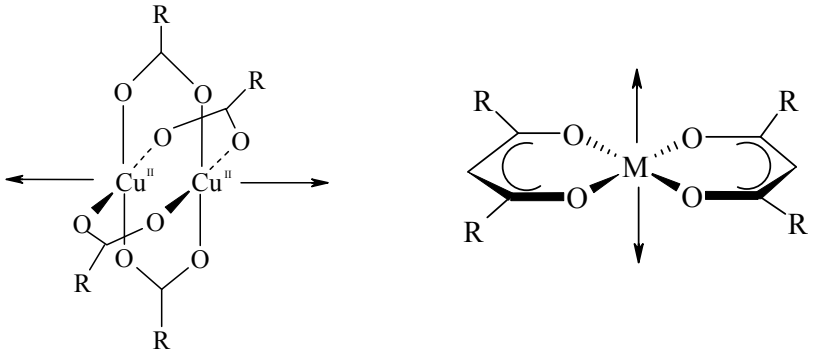


**Figure 5.1** Substituted M(II) "paddlewheel" and "acac" complexes with arrows showing the two axial coordination sites.

Additionally, copper(II) 1,1,1,5,5,5-hexafluoro-2,4-pentanedione [Cu(II) $(hfacac)_2$], cobalt(II) 1,3-diphenyl-1,3-propanedione [Co(II)$(DBM)_2$] and nickel(II) 1,3-diphenyl-1,3-propanedione [Ni(II)$(DBM)_2$] were also used in this study.[9] Complexes of this type are attractive due to the fact that two dione anions occupy four equatorial sites around the M(II) ion thereby producing an overall neutral metal-containing building block. The two remaining axial sites can be utilized for constructing extended linear supramolecular architectures with an appropriate bifunctional ligand, Figure 5.1b.

A structurally bifunctional ligand (a supramolecular linker) for this family of complex ions could combine a donor atom capable of effective metal-ion coordination with a functional group capable of forming self-complementary hydrogen bonds to a neighboring complex, thus extending the network. Four different ligands were designed and synthesized to fit these specific requirements, Figure 5.2.

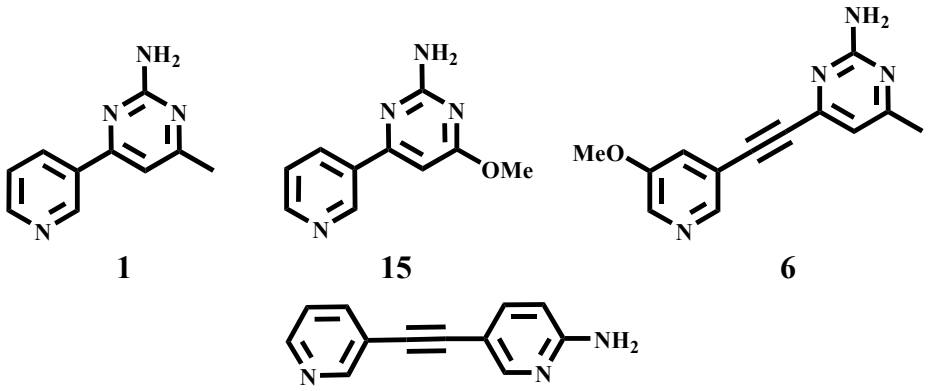


**Figure 5.2** A family of structurally bifunctional ligands; 3-(2-amino-4-methylpyrimidin-6-yl)pyridine **1**, 3-(2-amino-4-methoxypyrimidin-6-yl)pyridine **15**, 1-(2-amino-4-methylpyrimidin-6-yl)-2-(3-methoxypyridin-5-yl)ethyne **6**, 1-(2-aminopyrid-5-yl)-2-(pyrid-3-yl)ethyne **16**.

Ligands **1** and **15** have slightly dissimilar hydrogen-bonding moieties due to the differences in electronic and steric influences provided by the methyl and methoxy substituents, respectively. In contrast, ligands **6** and **16** contain an ethynyl linker between the two heterocyclic rings, allowing for greater separation between the metal-ions within each chain, which provides a handle for tuning some potentially important metrics of the resulting architecture. Ligand **16** contains an amino-pyridine fragment instead of an amino-pyrimidine unit but it is still capable of forming self-complementary hydrogen-bond interactions with ligands of neighboring complex ions.

Herein we outline a specific and predetermined supramolecular design strategy for the construction of 1-D chains from suitable bifunctional organic ligands **1, 15, 6,** and **16** and dinuclear copper(II) "paddlewheels" or M(II)$(acac)_2$ (M = Co, Cu, Ni) complex ions. We are particularly interested in:

- Attempting to control the coordination geometry around the metal center upon introduction of the bifunctional ligand;

- The reliability of the self-complementary amino-pyrimidine/amino-pyrimidine hydrogen bonds to propagate the metal complexes into infinite 1-D chains;
- Examining the effects on supramolecular assembly upon altering the steric influences (-Me vs. -OMe) around the hydrogen bonding moiety as well as length (-C-C- vs. -C-C≡C-C-) between the two functional groups; and
- Investigating functional group tolerance upon supramolecular assembly, by examining the effects of changing the hydrogen bonding moiety from an amino-pyrimidine to amino-pyridine.

The reliability of the overall assembly process is evaluated by an examination of thirteen crystal structures in the context of the desired supramolecular target and the primary intermolecular interactions.

## 5.2 Experimental

### *5.2.1 Synthesis*

All chemicals, unless otherwise noted, were purchased from Aldrich and used without further purification. The catalyst, *bis*(triphenylphosphine)palladium(II) dichloride, was purchased from Strem chemicals. 3-Pyridylboronic acid was synthesized according to previous literature.[10] Metal salts, copper(II) 1,1,1,5,5,5-hexafluoro-2,4-pentanedione, cobalt(II) 1,3-diphenyl-1,3-propanedione, nickel(II) 1,3-diphenyl-1,3-propanedione, and copper(II) 2-fluorobenzoate, were prepared according to the literature.[11] The synthesis of 3-(2-amino-4-methylpyrimidin-6-yl)pyridine **1** and 1-(2-amino-4-methylpyrimidin-6-yl)-2-(3-methoxypyridin-5-yl)ethyne **6** are described in Chapter 2. Column chromatography was carried out on silica gel (150 Å pore size) from Analtech Inc. Melting points were determined on a Fisher-Johns melting point apparatus and are uncorrected. $^{1}H$ and $^{13}C$ NMR spectra were recorded on a Varian Unity plus 400 MHz or 200 MHz spectrometer in $CDCl_3$. Compounds were prepared for infrared spectroscopic (IR) analysis as a mixture in KBr. Electrospray Ionization – Ion-Trap Mass Spectrometry (ESI-IT-MS) was carried out on a Bruker Daltonics Esquire 3000 Plus. MALDI-TOF / TOF-MS was carried out on a Bruker Daltonics Ultraflex TOF/TOF.

#### *5.2.1.1 Synthesis of 3-(2-amino-4-methoxypyrimidin-6-yl)pyridine, 15*

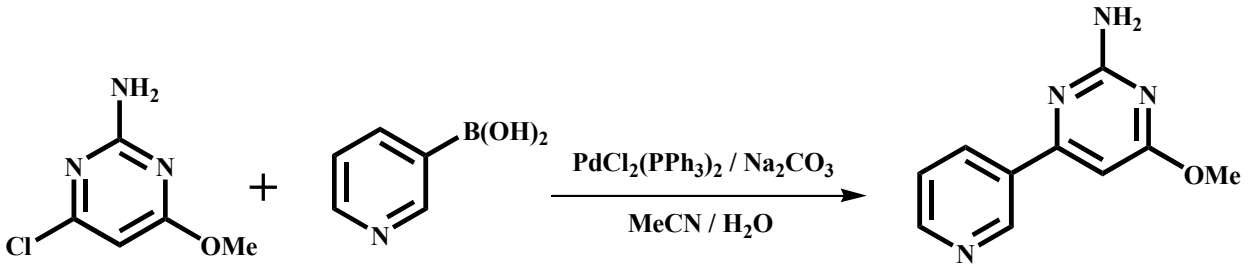


A mixture of 2-amino-4-chloro-6-methoxypyrimidine (1.50 g, 9.38 mmol), 3-pyridylboronic acid (1.58 g, 10.33 mmol), sodium carbonate (0.700 g, 6.6 mmol) *bis*(triphenylphosphine)palladium(II) dichloride (180 mg, 0.256 mmol, 2.7 mol %) was added to a round bottom flask. Acetonitrile (35 mL) and water (35 mL) were added and dinitrogen bubbled through the resultant mixture for 10 minutes. A condenser was attached and the mixture heated at 75 ˚C under a dinitrogen atmosphere. The reaction was monitored by TLC and allowed to cool to room temperature on completion (12 hours). The solution was then diluted with ethyl acetate (150 mL), washed with water (3 x 100 mL) then washed with saturated aqueous sodium chloride (2 x 100 mL). The organic layer was separated and dried over magnesium sulfate. The solvent was removed on a rotary evaporator and the residue chromatographed on silica with a hexanes/ethyl acetate mixture (1:1) as the eluant. The product was isolated as a white solid. The product **15** was then recrystallized from ethanol (200 proof) as colorless hair-shaped crystals, (1.44 g, 76 %). M.p. 138-140 ºC; $^{1}$H NMR ($\delta_H$; 400 MHz, $CDCl_3$): 9.15 (d, J = 2.4Hz, 1H), 8.68 (dd, J = 4Hz, J = 1Hz, 1H), 8.25 (dt, J = 8.8Hz, J = 2.4Hz, 1H), 7.38 (dd, J = 8Hz, J = 4.8Hz, 1H), 6.52 (s, 1H), 5.09 (s, 2H), 3.95 (s, 3H); $^{13}$C NMR ($\delta_C$; 400 MHz, $CDCl_3$): 171.61, 163.34, 163.21, 150.87, 148.38, 134.28, 133.15, 123.37, 94.387, 53.51; IR (KBr pellet): $\upsilon$ 3451, 3354, 1582, 1362 cm$^{-1}$, MALDI-TOF / TOF-MS *m/z* 187 ([**15** + H]$^{+}$).

### *5.2.1.2 Synthesis of 1-(2-aminopyrid-5-yl)-2-(pyrid-3-yl)ethyne, 16*

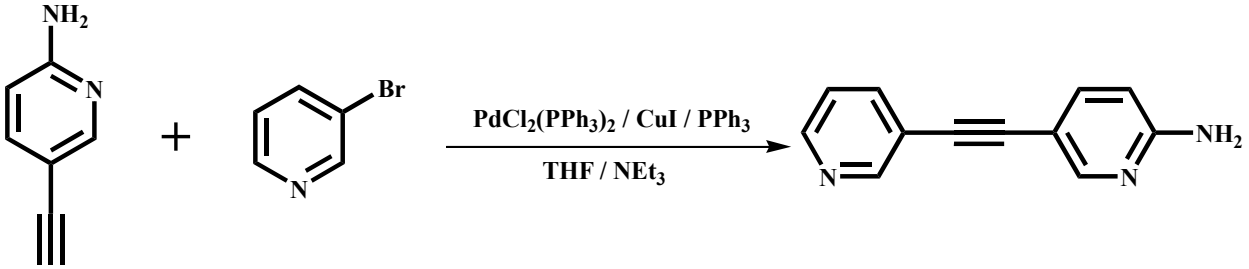

A mixture of 2-amino-5-ethynylpyridine (1.00 g, 8.70 mmol), 3-bromopyridine (1.60 g, 10.12 mmol), copper(I) iodide (0.050 g, 0.262 mmol), triphenylphosphine (0.220 g, 0.840 mmol), *bis*(triphenylphosphine)palladium(II) dichloride (0.220 g, 0.314 mmol) were added to a round bottom flask. Tetrahydrofuran (30 mL) and triethylamine (30 mL) were added and dinitrogen bubbled through the resultant mixture for 10 minutes. A condenser was attached and the mixture heated at 70 ˚C under a dinitrogen atmosphere. The reaction was monitored by TLC and allowed to cool to room temperature upon completion (36 hours). The solution was then diluted with ethyl acetate (100 mL), washed with water (3 x 100 mL) then washed with saturated aqueous sodium chloride (1 x 100 mL). The organic layer was separated and dried over magnesium sulfate. The solvent was removed on a rotary evaporator and the residue chromatographed on silica with a hexane/ethyl acetate mixture (1:1) as the eluant. The product **16** was isolated as a light brown solid and recrystallized from chloroform producing orange block-shaped crystals, (1.20 g, 79 %). M.p. 131-133 ºC; $^{1}$H NMR ($\delta_H$; 200 MHz, $CDCl_3$): 8.73 (d, J = 2.6Hz, 1H), 8.52 (dd, J = 4.9Hz, J = 1.7Hz, 1H), 8.28 (d, J = 2Hz, 1H), 7.77 (dt, J=8Hz, J=2Hz, 1H), 7.56 (dd, J=8.6Hz, J=2.4Hz, 1H), 7.27 (m, 1H), 6.49 (dd, J=8.4Hz, J=0.8Hz, 1H), 4.77 (s, 1H); $^{13}$C NMR ($\delta_C$; 200 MHz, $CDCl_3$): 157.79, 152.02, 151.50, 148.29, 140.39, 138.09, 122.96, 120.60, 109.08, 107.96, 90.37, 86.53; IR (KBr pellet): $\upsilon$ 3318, 3140, 2213, 1602, 1508, 1398 $cm^{-1}$, ESI-IT-MS *m/z* 197 ([**16** + H]$^{+}$).

### *5.2.2 Synthesis of coordination complexes*

#### *5.2.2.1 Synthesis of {tetrakis(μ-acetato-O,O')-bis(3-(2-amino-4-methylpyrimidin-6-yl)pyridine-N) dicopper(II)}, 1e*

A mixture of **1** (9 mg, 0.05 mmol) and copper(II) acetate (10 mg, 0.05 mmol) were added to a screw cap vial along with a methanol/acetonitrile mixture (2:1 mL). The mixture was heated gently until a clear homogeneous solution resulted. Without solvent evaporation, green block-shaped crystals were collected after one day. M.p. 210 - 212 °C. Anal. Calcd. for $C_{28}H_{32}N_8O_8Cu_2$: C, 45.77; H, 4.39; N, 15.26. Found: C, 45.72; H, 4.46; N, 15.09.

#### *5.2.2.2 Synthesis of {tetrakis(μ-2-fluorobenzoato-O,O')-bis(3-(2-amino-4-methylpyrimidin-6-yl)pyridine-N) dicopper(II)}, 1f*

A mixture of **1** (9 mg, 0.05 mmol) and copper(II)2-fluorobenzoate (16 mg, 0.02 mmol) were added to a screw cap vial along with a mixture of methanol/acetonitrile mixture (1:5 mL). The mixture was heated gently until a clear homogeneous solution resulted. Without solvent evaporation, green plate-shaped crystals were collected after one day. M.p. 224 - 226 °C. Anal. Calcd. for $C_{48}H_{36}N_8O_8F_4Cu_2 \cdot H_2O$: C, 53.75; H, 3.57; N, 10.45. Found: C, 53.69; H, 3.30; N, 10.45.

#### *5.2.2.3 Synthesis of {tetrakis(μ-acetato-O,O')-bis(3-(2-amino-4-methoxylpyrimidin-6-yl)pyridine-N) dicopper(II)}, 15a*

A mixture of **15** (10 mg, 0.05 mmol) and copper(II) acetate (10 mg, 0.05 mmol) were added to a screw cap vial along with a methanol/acetonitrile mixture (2:1 mL). The mixture was heated gently until a clear homogeneous solution resulted. Without solvent evaporation, green block-shaped crystals were harvested after one day. Dec. 212 °C. Anal. Calcd. for $C_{28}H_{32}N_8O_{10}Cu_2$: C, 43.86; H, 4.21; N, 14.62. Found: C, 43.62; H, 4.19; N, 14.57.

#### *5.2.2.4 Synthesis of {tetrakis(μ-2-fluorobenzoato-O,O')-bis(3-(2-amino-4-methoxypyrimidin-6-yl)pyridine-N) dicopper(II)}, 15b*

A mixture of **15** (9 mg, 0.05 mmol) and copper(II)2-fluorobenzoate (17 mg, 0.03 mmol) were added to a screw cap vial along with a mixture of methanol/acetonitrile mixture (1:5 mL). The mixture was heated gently until a clear homogeneous solution resulted. Without solvent evaporation, green plate-shaped crystals were collected after one day. M.p. 224 - 226 °C. Anal. Calcd. for $C_{48}H_{36}N_8O_{10}F_4Cu_2$: C, 53.03; H, 3.34; N, 10.31. Found: C, 52.92; H, 3.14; N, 10.22.

#### *5.2.2.5 Synthesis of {tetrakis(μ-acetato-O,O')-bis(1-(2-amino-4-methylpyrimidin-6-yl)-2-(3-methoxypyridin-5-yl-N)ethyne) dicopper(II)}, 6e*

A mixture of **6** (10 mg, 0.04 mmol) and copper(II)acetate (17 mg, 0.08 mmol) were added to a screw cap vial along with a 1:1:1 mixture of ethanol/acetonitrile/nitromethane. The mixture was heated gently until a clear homogeneous solution resulted. Without solvent evaporation, green block-shaped crystals were collected after two days. Dec. 160 °C. Anal. Calcd. for $C_{34}H_{36}N_8O_{10}Cu_2$: C, 48.45; H, 4.31; N, 13.30. Found: C, 48.11; H, 4.28; N, 13.28.

### *5.2.2.6 Synthesis of {tetrakis(μ-2-fluorobenzoato-O,O')-bis((2-aminopyrid-5-yl)-2-(pyrid-3-yl-N)ethyne) dicopper(II)}, 16a*

A mixture of **16** (11 mg, 0.06 mmol) and copper(II)2-fluorobenzoate (19 mg, 0.03 mmol) were added to a screw cap vial along with a mixture of methanol/acetonitrile mixture (3:5 mL). The mixture was heated gently until a clear homogeneous solution resulted. Without solvent evaporation, green plate-shaped crystals were collected after one day. Dec. 255 °C. Anal. Calcd. for $C_{40}H_{25}N_3O_8F_4Cu_2$: C, 54.73; H, 2.87; N, 4.79. Found: C, 54.65; H, 2.89; N, 4.96.

### *5.2.2.7 Synthesis of {tetrakis(μ-acetato-O,O')-bis((1-(2-aminopyrid-5-yl)-2-(pyrid-3-yl-N)ethyne) copper(II)}, 16b*

A mixture of **16** (13 mg, 0.07 mmol) and copper(II)acetate (26 mg, 0.13 mmol) were added to a screw cap vial along with a mixture of methanol/acetonitrile mixture (3:5 mL). The mixture was heated gently until a clear homogeneous solution resulted. Without solvent evaporation, green block-shaped crystals were collected after one day. Dec. 210 °C. Anal. Calcd. for $C_{20}H_{21}N_3O_8Cu_2$: C, 43.09; H, 3.80; N, 7.54. Found: C, 42.92; H, 3.77; N, 7.54.

### *5.2.2.8 Synthesis of {bis(1,1,1,5,5,5-hexafluoro-2,4-pentanedionato-O,O')-trans-bis(3-(2-amino-4-methoxypyrimidin-6-yl)pyridine-N) copper(II)}-chloroform, 15c*

A mixture of **15** (13 mg, 0.060 mmol) and copper(II)-1,1,1,5,5,5-hexafluoro-2,4-pentanedione (17 mg, 0.040 mmol) were added to a screw cap vial along with chloroform (3 mL). The mixture was heated gently until a clear homogeneous solution resulted. Green prism-shaped crystals were harvested after three days (13 mg, 46%). M.p. 143-145 °C.

### *5.2.2.9 Synthesis of {bis(1,3-diphenyl-1,3-propanedionato-O,O')-trans-bis(3-(2-amino-4-methoxypyrimidin-6-yl)pyridine-N) cobalt(II)}, 15d*

A mixture of **15** (12 mg, 0.060 mmol) and cobalt(II)-1,3-diphenyl-1,3-propanedione (16 mg, 0.030 mmol) were added to a screw cap vial along with a mixture of 1,2-dichloroethane/chloroform (7:3 mL). The mixture was heated gently until a clear homogeneous solution resulted. Orange prism-shaped crystals formed after one day (19 mg, 70%). Dec. 219 °C.

#### *5.2.2.10 Synthesis of {bis(1,1,1,5,5,5-hexafluoro-2,4-pentanedionato-O,O')-trans-bis(3-(2-amino-4-methylpyrimidin-6-yl)pyridine-N) copper(II)}-1,2-dichloroethane, 1g*

A mixture **1** (14 mg, 0.080 mmol) and copper(II)-1,1,1,5,5,5-hexafluoro-2,4-pentanedione (18 mg, 0.040 mmol) were added to a screw cap vial along with 1,2-dichloroethane (4 mL). The mixture was heated gently until a clear homogeneous solution resulted. Green block-shaped crystals were collected after two days (18 mg, 56%). M.p. 156-158 °C.

#### *5.2.2.11 Synthesis of {bis(1,1,1,5,5,5-hexafluoro-2,4-pentanedionato-O,O')-(1-(2-amino-4-methylpyrimidin-6-yl)-2-(3-methoxypyridin-5-yl-N)ethyne) copper(II)}, 6f*

A mixture of **6** (9.0 mg, 0.040 mmol) and copper(II)-1,1,1,5,5,5-hexafluoro-2,4-pentanedione (10 mg, 0.020 mmol) were added to a screw cap vial along with chloroform (2 mL). Green block-shaped crystals were collected after one day (14 mg, 52%). M.p. 164-166 °C.

#### *5.2.2.12 Synthesis of {bis(1,3-diphenyl-1,3-propanedionato-O,O')-trans-bis(1-(2-amino-4-methylpyrimidin-6-yl)-2-(3-methoxypyridin-5-yl-N)ethyne) cobalt(II)}, 6g*

A mixture of **6** (10 mg, 0.040 mmol) and cobalt(II)-1,3-diphenyl-1,3-propanedione (11 mg, 0.020 mmol) were added to a screw cap vial along with chloroform (2 mL). Orange block-shaped crystals were grown over a period of one day. (13 mg, 65 %). Dec. 215 °C.

#### *5.2.2.13 Synthesis of {bis(1,3-diphenyl-1,3-propanedionato-O,O')-trans-bis(1-(2-amino-4-methylpyrimidin-6-yl)-2-(3-methoxypyridin-5-yl-N)ethyne) nickel(II)}, 6h*

A mixture of **6** (10 mg, 0.04 mmol) and nickel(II)-1,3-diphenyl-1,3-propanedione (11 mg, 0.02 mmol) were added to a screw cap vial along with a mixture of nitromethane/dichloromethane (2:2 mL). Green plate-shaped crystals were grown over a period of two days. (12 mg, 36 %) Dec. 205 °C.

## 5.3 Results

A summary of the crystallographic information for **1e-1g**, **15a-15d**, **6e-6h**, and **16a-16b** is displayed in Tables B.4. Bond distances and angles for these compounds are given in Table 5.1 and hydrogen-bond geometries for **1e-1g**, **15a-15d**, **6e-6h**, and **16a-16b** are listed in Table 5.2.

**Table 5.1** Selected bond distances and angles for **1e-1g**, **15a-15d**, **6e-6h**, and **16a-16b**

| Compound | M(II)–N (Å) | < N–M(II)–N (°) | < N–M(II)–M(II) (°) |
|---|---|---|---|
| **1e** | Cu1–N21, 2.1743(11) | ----- | 177.68(3) |
| **1f** | Cu1–N11, 2.145(3) | ----- | 173.73(8) |
| | Cu2-N51, 2.149(2) | ----- | 178.71(8) |
| **15a** | Cu1–N21, 2.169(2) | ----- | 174.68(5) |
| **15b** | Cu1–N11, 2.149(3) | ----- | 176.24(8) |
| **6e** | Cu1–N21, 2.1813(18) | ----- | 176.17(5) |
| **16a** | Cu1–N11, 2.162(3) | ----- | 176.37(10) |
| **16b** | Cu1–N11, 2.1981(14) | ----- | 177.49(4) |
| **15c** | Cu1–N11, 2.0227(16) | 179.998(1) | ----- |
| **15d** | Co1–N41, 2.1514(14) | 180.0 | ----- |
| | Co1–N41, 2.1515(14) | 180.0 | ----- |
| **1g** | Cu1–N31, 2.0044(12) | 180.00(11) | ----- |
| **6f** | Cu1–N21, 2.2751(18) | ----- | ----- |
| **6g** | Co1–N21, 2.2083(11) | 180.0 | ----- |
| | Co1-N21, 2.2083(11) | 180.0 | ----- |
| **6h** | Ni1–N11, 2.142(2) | 180.0 | ----- |
| | Ni1-N11, 2.142(2) | 180.0 | ----- |

**Table 5.2** Hydrogen-bond geometries for **16**, **1e-1g**, **15a-15d**, **6e-6h**, and **16a-16b**

| Compound | D-H···A | D-H/ Å | H···A/Å | D···A/Å | <(DHA)/° | Generator for A |
|---|---|---|---|---|---|---|
| **16** | N12-H12A···N21 | 0.872(9) | 2.25(10) | 3.1183(9) | 175.8(8) | x+1,-y+1/2,z+3/2 |
| | N12-H12B···N11 | 0.88(10) | 2.17(10) | 3.0522(9) | 178.0(8) | -x+2,-y+1,-z+3 |
| **1e** | N12-H12···N11 | 0.87(2) | 2.17(2) | 3.043(17) | 175.2(2) | -x,-y+1,-z+1 |
| | N12-H12···O42 | 0.89(2) | 0.89(2) | 2.975(16) | 170.5(19) | -x+1, y-1/2,-z+1/2 |
| **1f** | N22-H22···N63 | 0.93(4) | 2.31(4) | 3.241(4) | 174(3) | -x+1,-y+1,-z+1 |
| | N22-H22···O78 | 0.95(4) | 2.26(4) | 3.206(4) | 173(3) | ----- |
| | N62-H62···N21 | 0.73(4) | 2.27(4) | 3.001(4) | 171(4) | -x+1,-y+1,-z+1 |
| | N62-H62···O48 | 0.83(4) | 2.27(4) | 3.055(4) | 159(3) | x-1,y,z |
| **15a** | N12-H12···N11 | 0.95(3) | 2.24(3) | 3.177(3) | 171(2) | -x+1,-y,-z+1 |
| | N12-H12···O41 | 0.91(3) | 2.29(3) | 3.185(3) | 170(3) | -x+1,-y,-z+1 |
| **15b** | N22-H22···N23 | 0.88 | 2.52 | 3.253(5) | 141.2 | -x+1,-y+1,-z |
| **6e** | N12-H12···N23 | 0.82(4) | 2.22(4) | 2.982(3) | 155(3) | x,y-1,z+1 |
| | N12-H12···O42 | 0.72(3) | 2.34(4) | 3.061(3) | 173(3) | -x,-y,-z+2 |
| **16a** | N12-H12…O38 | 0.88 | 2.43 | 3.295(8) | 168.3 | x+1,y,z |
| **16b** | N16-H16…O31 | 0.88 | 2.32 | 3.078(3) | 144.5 | -x+1,-y+1,-z+1 |
| **15c** | N27-H27···O34 | 0.88 | 2.25 | 3.112(2) | 165.5 | x,y-1,z |
| | N57-H57···O62 | 0.88 | 2.19 | 3.040(2) | 162.7 | x,y+1,z |
| **15d** | N52-H52···N51#2 | 0.86(2) | 2.37(2) | 3.203 | 164(2) | -x+1,-y,-z |
| | N52-H52···O13#3 | 0.88(2) | 2.16(2) | 3.033(18) | 171(2) | x,y,z-1 |
| **1g** | N22-H22···N21#3 | 0.80(3) | 2.28(3) | 3.085(19) | 174(2) | -x+2,-y+1,-z+1 |
| **6f** | N12-H12···N11#1 | 0.88 | 2.12 | 3.002(3) | 175.0 | -x+1,-y,-z+2 |
| | N12-H12···O42#2 | 0.88 | 2.27 | 3.044(2) | 147.5 | -x+1,-y+1,-z+1 |
| **6g** | N12-H12···O31#2 | 0.87(2) | 2.18(2) | 3.036(16) | 169.1(18) | -x+1,-y+2,-z+1 |
| | N12-H12···N11#3 | 0.81(2) | 2.26(2) | 3.065(17) | 173.1(18) | -x,-y+3,-z |
| **6h** | N22-H22···O31#2 | 0.78(3) | 2.29(3) | 3.058(3) | 168(3) | ----- |
| | N22-H22···N21#3 | 0.82(3) | 2.24(3) | 3.058(3) | 173(3) | 2-x,-y,-z |

### *5.3.1 Crystal structure of 1-(2-aminopyrid-5-yl)-2-(pyrid-3-yl)ethyne, 16*

The crystal structure of **16** displays one molecule within the asymmetric unit, orientated in a relatively planar fashion, Figure 5.3.

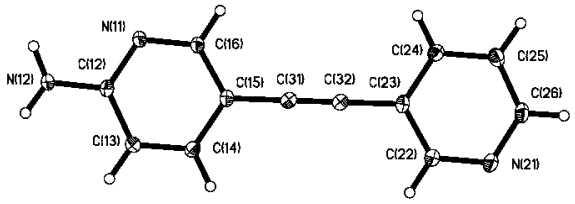


**Figure 5.3** Thermal-ellipsoids plot (50% probability level) of ligand **16**.

Extension of the architecture shows individual ligands forming a 2-D sheet through multiple N-H···N hydrogen bonds. The amino-pyridine moiety forms self-complementary N-H···N hydrogen bonds with a neighboring ligand producing a dimeric unit, which is further extended by secondary N-H···N hydrogen bonds from the *anti*-amino proton to the pyridyl nitrogen atom, Figure 5.4.

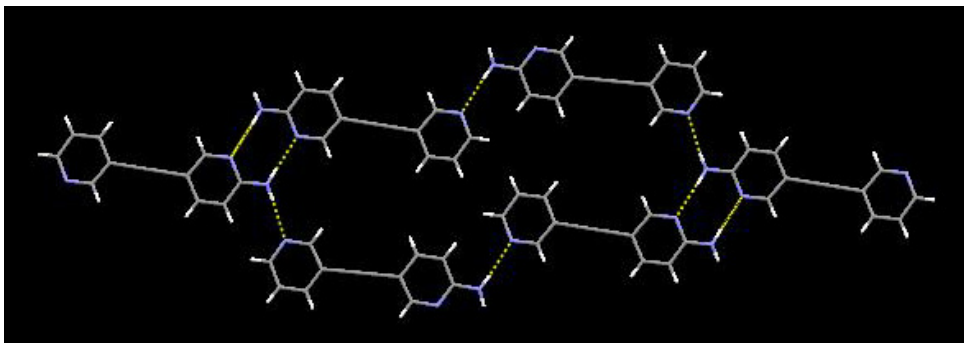

**Figure 5.4** Extended 2-D architecture formed through multiple N-H···N hydrogen bonds.

### *5.3.2 Crystal structure of {tetrakis(μ-acetato-O,O')-bis(3-(2-amino-4-methylpyrimidin-6-yl)pyridine-N) dicopper(II)}, 1e*

The complex-ion in the crystal structure of **1e** is composed of two ligands **1** bound at the axial positions of the dicopper tetraacetate complex, Figure 5.5. The symmetry-related Cu(II) ion displays a square-pyramidal coordination geometry and is assembled into infinite chains through self-complementary N-H···N hydrogen bonds, between the *syn*-amino proton and a pyrimidine nitrogen atom. Neighboring chains are organized into a 2-D sheet via N-H···O hydrogen bonds between the *anti*-amino proton and an acetate oxygen atom from an adjacent strand, Figure 5.6 (a) and (b).

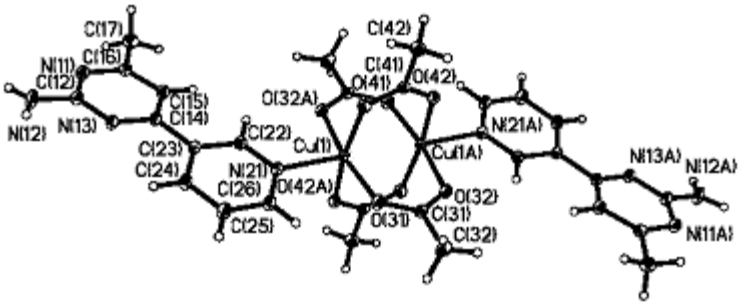


**Figure 5.5** Labeled thermal ellipsoids of **1e** (50% probability level).

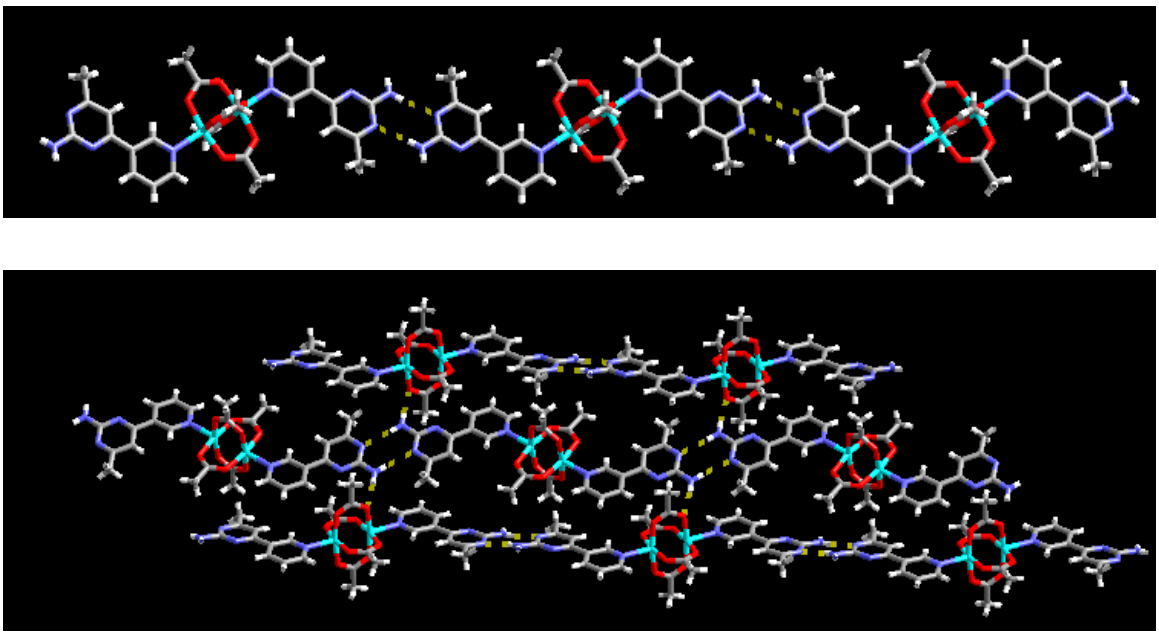

**Figure 5.6** (a) One-dimensional strand in **1e** formed by self-complementary N-H···N hydrogen bonds (top); (b) Two-dimensional sheet produced in **1e** from a combination of N-H···N and N-H···O hydrogen bonds (bottom).

### *5.3.3 Crystal structure of {tetrakis(μ-2-fluorobenzoato-O,O')-bis(3-(2-amino-4-methylpyrimidin-6-yl)pyridine-N) dicopper(II)}, 1f*

The crystal structure of **1f** contains two crystallographically unique Cu(II)-complexes, Figure 5.7. Within each complex the copper atoms are arranged in the familiar "paddle-wheel" motif in which two copper atoms are bridged by four acetate groups, thus leaving two axial sites for further coordination. The two ligands **1** are coordinated axially through the nitrogen atom of the pyridyl moiety to the Cu(II) ions, each with a square-pyramidal geometry. The two unique

complexes are connected in a zig-zag manner through self-complementary N-H···N hydrogen bonds, produced from the *syn*-amino proton and a pyrimidine nitrogen atom, Figure 5.8

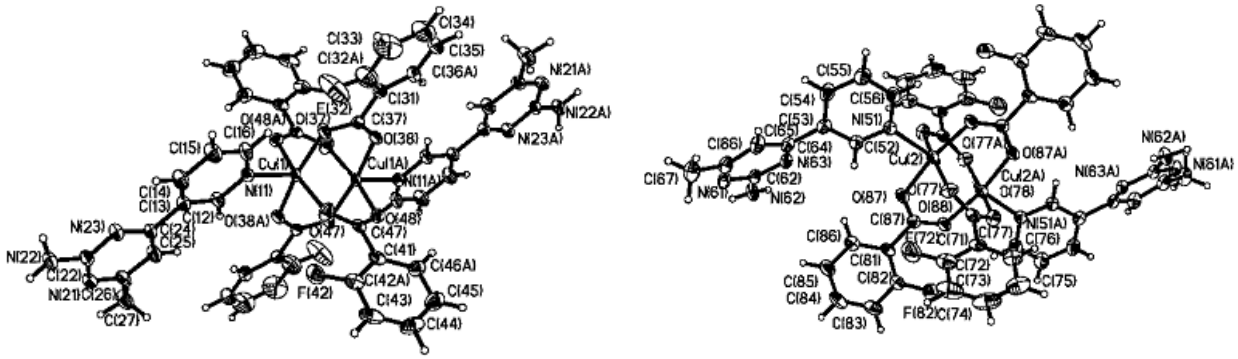


**Figure 5.7** Labeled thermal ellipsoids of **1f** (50% probability level).

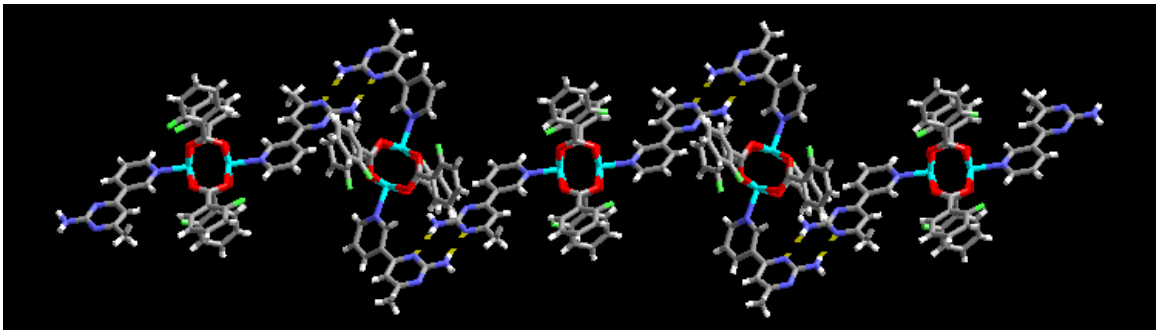

**Figure 5.8** 1-D zig-zag chain in **1f** produced through self-complementary N-H···N hydrogen bonds.

The 1-D zig-zag rows are then extended into a 2-D sheet through N-H···O hydrogen bonds from the *anti*-amino proton to an adjacent acetate oxygen atom from an adjacent strand, Figure 5.9

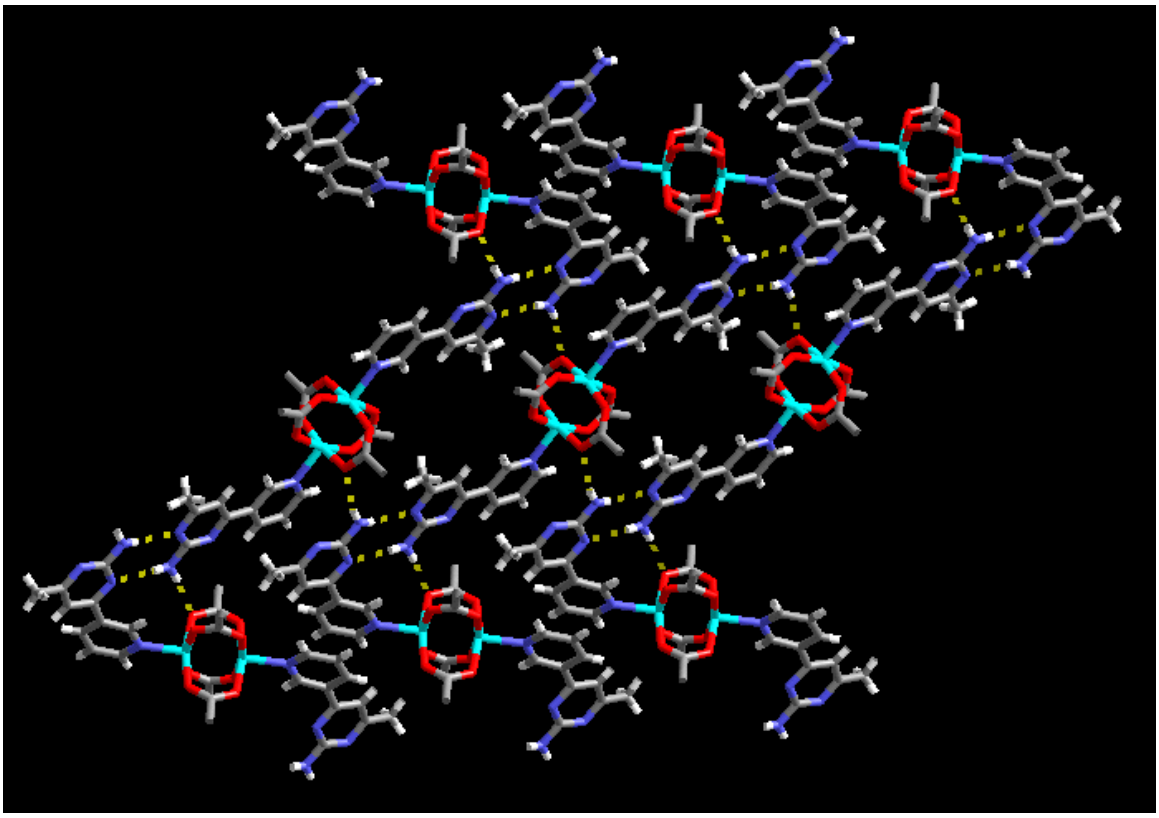

**Figure 5.9** Extended network of **1f** through a series of N-H···N and N-H···O hydrogen bonds (the fluoro-phenyl rings have been omitted for clarity).

### *5.3.4 Crystal structure of {tetrakis(μ-acetato-O,O')-bis(3-(2-amino-4-methoxylpyrimidin-6-yl)pyridine-N) dicopper(II)}, 15a*

The complex-ion in the crystal structure of **15a** contains two ligands **15** bound axially through their pyridyl nitrogen atoms to the dicopper tetraacetate dimer affording a five-coordinate square-pyramidal geometry around each Cu(II) ion, Figure 5.10. Discrete 1-D chains are formed from self-complementary N-H···N hydrogen bonds between the *syn*-amino proton and a pyrimidine nitrogen atom, whilst the *anti*-amino proton hydrogen bonds with a neighboring acetate oxygen atom through N-H···O interactions, Figure 5.11. The second nitrogen atom of the pyrimidine ring is blocked by the adjacent methoxy substituent and does not act as a hydrogen-bond acceptor.

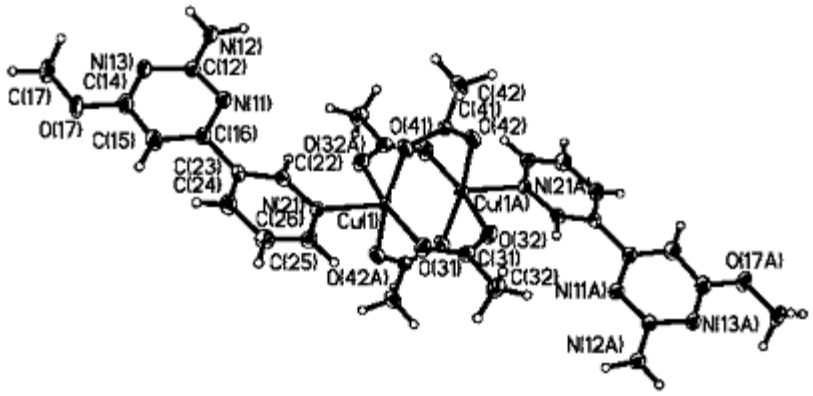


**Figure 5.10** Labeled thermal ellipsoids of **15a** (50% probability level).

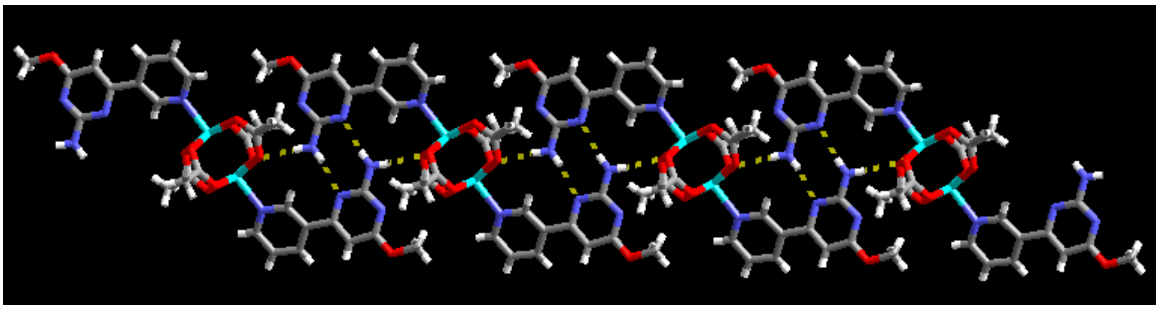

**Figure 5.11** Infinite chain in **15a** formed from Cu(II)-py coordination bonds and self-complementary N-H···N and heteromeric N-H···O hydrogen bonds.

### *5.3.5 Crystal structure of {tetrakis(μ-2-fluorobenzoato-O,O')-bis(3-(2-amino-4-methoxypyrimidin-6-yl)pyridine-N) dicopper(II)}, 15b*

The complex ion in the structure of **15b** contains two ligands **15** bound axially via the pyridyl nitrogen atoms to the "paddle-wheel" copper dimer unit, furnishing each Cu(II) ion with a square-pyramidal coordination geometry, Figure 5.12. Similar to structure **15a**, 1-D chains are produced from self-complementary N-H···N hydrogen bonds from the *syn*-amino proton to a pyrimidine nitrogen atom, and N-H···O interactions from the *anti*-amino proton to an acetate oxygen atom of a neighboring strand, Figure 5.13. Additional stabilization is provided by π–π stacking between the fluoro-substituted phenyl rings and the amino-pyrimidine rings with a centroid-centroid distance of 3.28 Å, which is consistent (< 3.5 Å) with reported values when molecules are π-stacked in a slip-stacked fashion.[12]

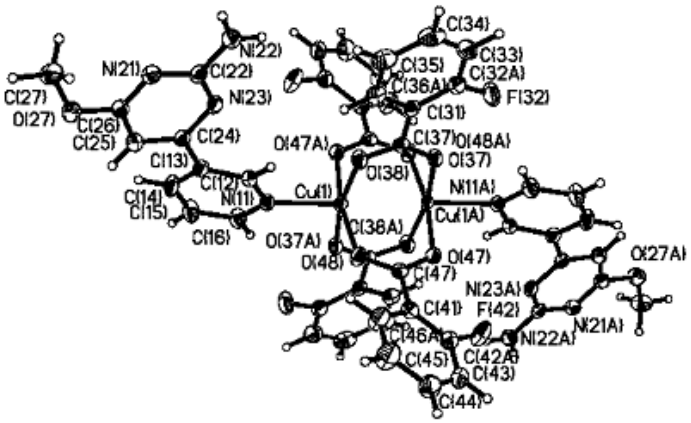


**Figure 5.12** Labeled thermal ellipsoids of **15b** (50% probability level).

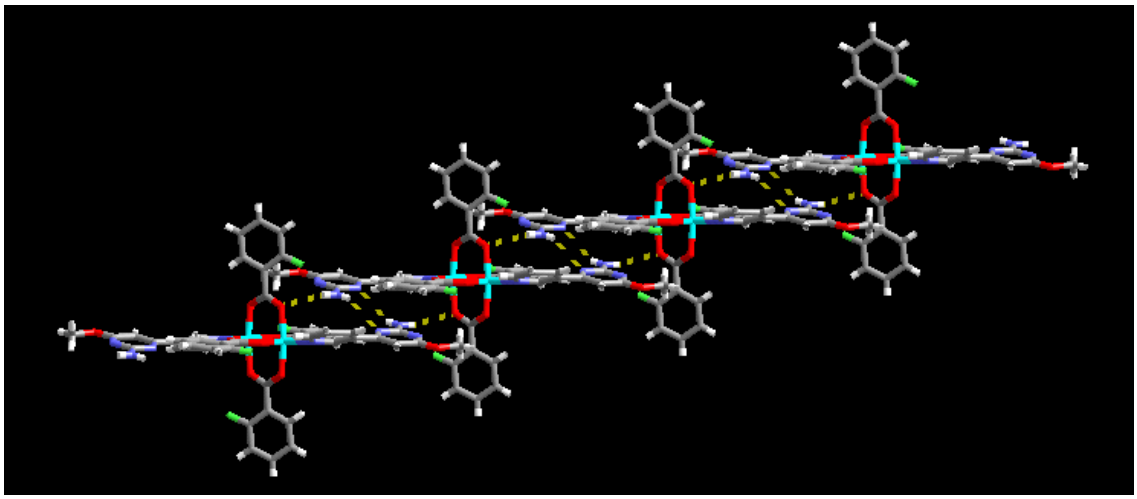

**Figure 5.13** 1-D stair-step architecture stabilized by a combination of hydrogen bonds and π-π-stacking in **15b**.

### *5.3.6 Crystal structure of {tetrakis(μ-acetato-O,O')-bis(1-(2-amino-4-methylpyrimidin-6-yl)-2-(3-methoxypyridin-5-yl-N)ethyne) dicopper(II)}, 6e*

The crystal structure of **6e** contains two ligands **6** bound in the axial positions of the two Cu(II) ions contained within the tetraacetate "paddlewheel" unit, creating a square-pyramidal coordination geometry around each copper ion, Figure 5.14. Infinite 1-D chains are produced from self-complementary N-H···N hydrogen bonds between the *syn*-amino proton and a pyrimidine nitrogen atom, Figure 5.15. Neighboring chains are subsequently organized into a 2-

D sheet via N-H···O hydrogen bonds between the *anti*-amino proton and an acetate oxygen atom from an adjacent strand, similar to what was observed in the structure of **1e**.

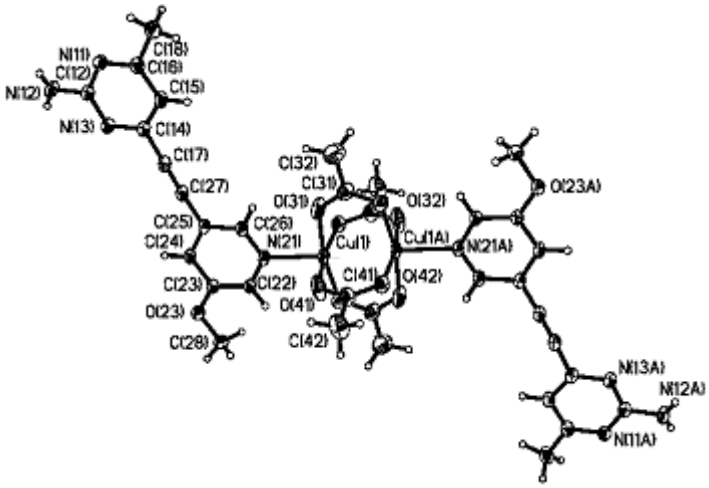


**Figure 5.14** Labeled thermal ellipsoids of **6e** (50% probability level).

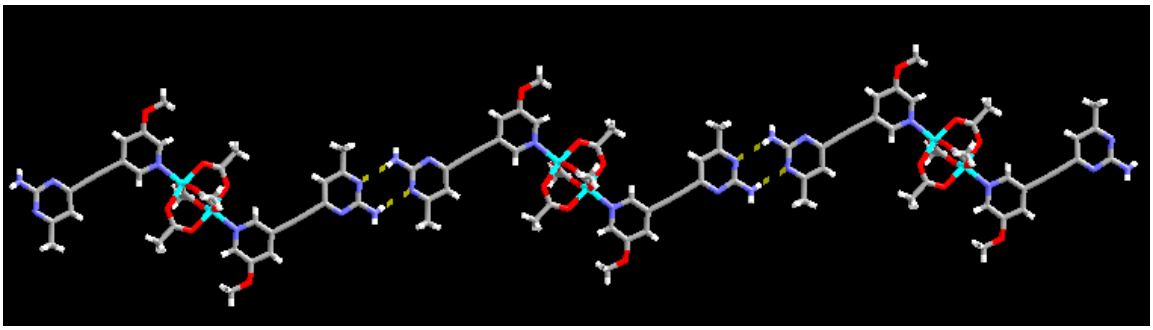

**Figure 5.15** 1-D strand in **6e** formed through self-complementary amino-pyrimidine N-H···N hydrogen bonds.

### *5.3.7 Crystal structures of {tetrakis(μ-2-fluorobenzoato-O,O')-bis((2-aminopyrid-5-yl)-2-(pyrid-3-yl-N)ethyne) dicopper(II)}, 16a*

In the crystal structures of **16a** there are two ligands **16** bound axially, through the pyridyl nitrogen atoms to the "paddle-wheel" copper dimer unit, creating a square-pyramidal coordination geometry. The ligand **16** is essentially located on an inversion center, with–$NH_2$ and –H randomly disordered with 50% occupancy. Thus, the complex ions are shown with both ends of the ligand containing an amino group, Figure 5.16. Although the ligand contains a potential self-complementary N-H···N hydrogen bonding moiety, no hydrogen bonds are formed between adjacent ligands. Instead, both pyridyl moieties coordinate to two different "paddle-wheel" units which, in effect, creates 1-D coordination polymers within the lattice of **16a**.

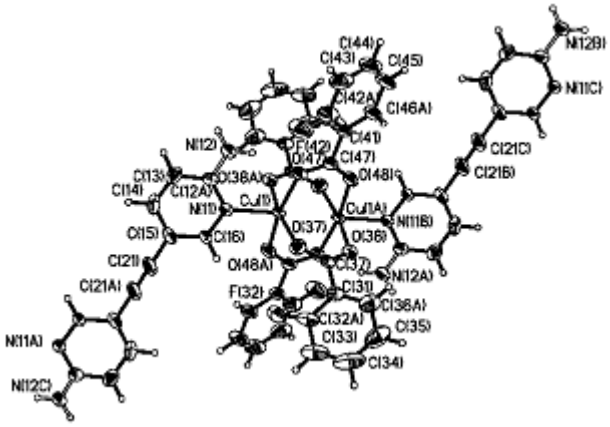

**Figure 5.16** Labeled thermal ellipsoids of **16a** at 50% probability level.

### *5.3.8 Crystal structure of {tetrakis(μ-acetato-O,O')-bis((1-(2-aminopyrid-5-yl)-2-(pyrid-3-yl-N)ethyne) copper(II)}, 16b*

In the crystal structures of **16b** there are two ligands **16** bound axially, through the pyridyl nitrogen atoms to the "paddle-wheel" copper dimer unit, creating a square-pyramidal coordination geometry. The ligand **16** is essentially located on an inversion center, with–$NH_2$ and –H randomly disordered with 50% occupancy. Thus, the complex ions are shown with both ends of the ligand containing an amino group, Figure 5.17. Although the ligand contains a potential self-complementary N-H···N hydrogen bonding moiety, no hydrogen bonds are formed between adjacent ligands. Instead, both pyridyl moieties coordinate to two different "paddle-wheel" units which, in effect, creates 1-D coordination polymers within the lattice of **16b**.

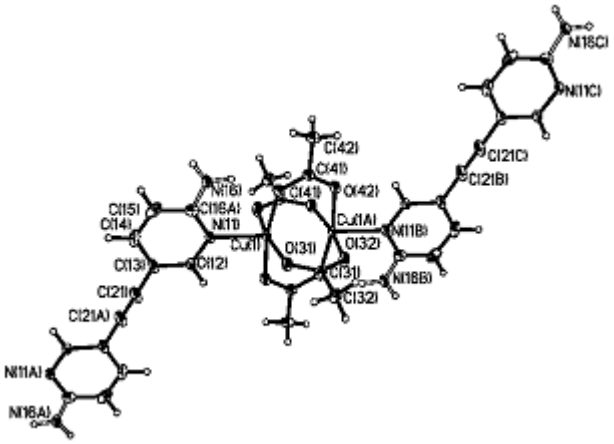

**Figure 5.17** Labeled thermal ellipsoids of **16b** (right) at 50% probability level.

### *5.3.9 Crystal structure of {bis(1,1,1,5,5,5-hexafluoro-2,4-pentanedionato-O,O')-trans-bis(3-(2-amino-4-methoxypyrimidin-6-yl)pyridine-N) copper(II)}-chloroform, 15c*

The crystal structure of **15c** contains two crystallographically unique complexes (A & B), Figure 5.18. The two ligands **15** reside perpendicular to the [$(hfac)_2$Cu(II)] complex resulting in an octahedral coordination geometry around the copper center. The ligands are coordinated through the pyridyl nitrogen atoms and due to the close similarities of the supramolecular assembly of A and B, only one will described in detail. Neighboring complex ions are held together in a head-to-tail motif where the *syn*-amino proton forms a N-H···O hydrogen bond with an oxygen atom from an adjacent acac complex, producing an infinite ribbon, Figure 5.19. The *anti*-amino proton and the pyrimidine nitrogen atoms are participating in extending the networks. In addition, two molecules of chloroform are incorporated into the crystal lattice.

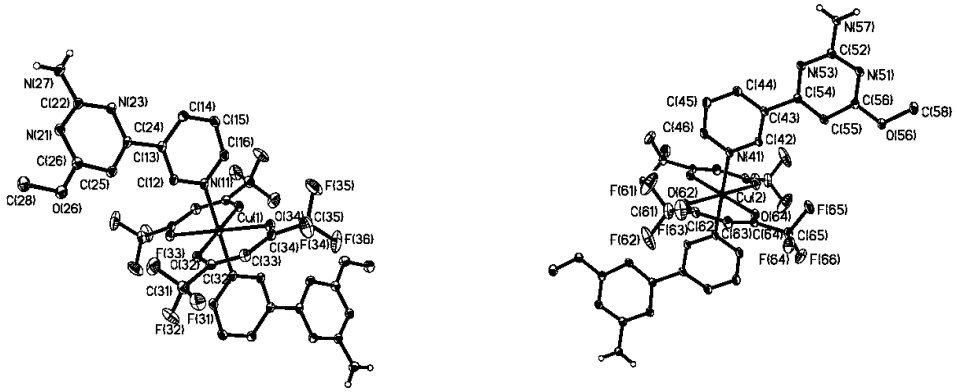


**A** **B**

**Figure 5.18** Labeled thermal ellipsoids (50 % probability level) of the two asymmetric complex ions in the crystal structure of **15c**. Two molecules of chloroform are omitted for clarity.

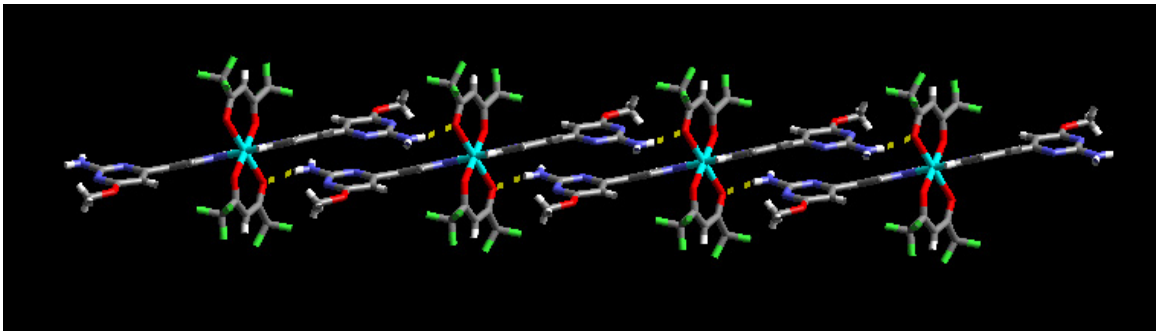

**Figure 5.19** Adjacent complex ions in **15c** organized into an extended chain held together by head-to-tail N-H···O hydrogen bonds. Two molecules of chloroform are omitted for clarity.

### *5.3.10 Crystal structure of {bis(1,3-diphenyl-1,3-propanedionato-O,O')-trans-bis(3-(2-amino-4-methoxypyrimidin-6-yl)pyridine-N) cobalt(II)}, 15d*

The metal-complex in the crystal structure of **15d** is composed of two ligands **15** bound at the axial positions of the [$(DBM)_2Co(II)$] complex, Figure 5.20. The Co(II) ion displays an octahedral coordination geometry and the extended network exhibits a connectivity in which head-to-tail N-H···O hydrogen bonds are formed between the *anti*-amino proton and an oxygen atom from a neighboring acac complex. Additionally there are self-complementary N-H···N hydrogen bonds, between the *syn*-amino proton and a pyrimidine nitrogen atom, Figure 5.21.

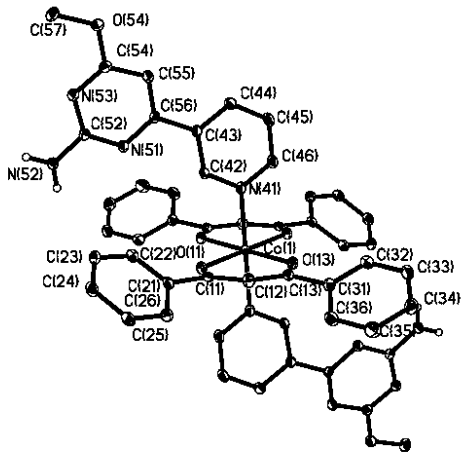


**Figure 5.20** Labeled thermal ellipsoids in the crystal structure of **15d** drawn at 50% probability level (hydrogen atoms, apart from $-NH_2$, omitted for clarity).

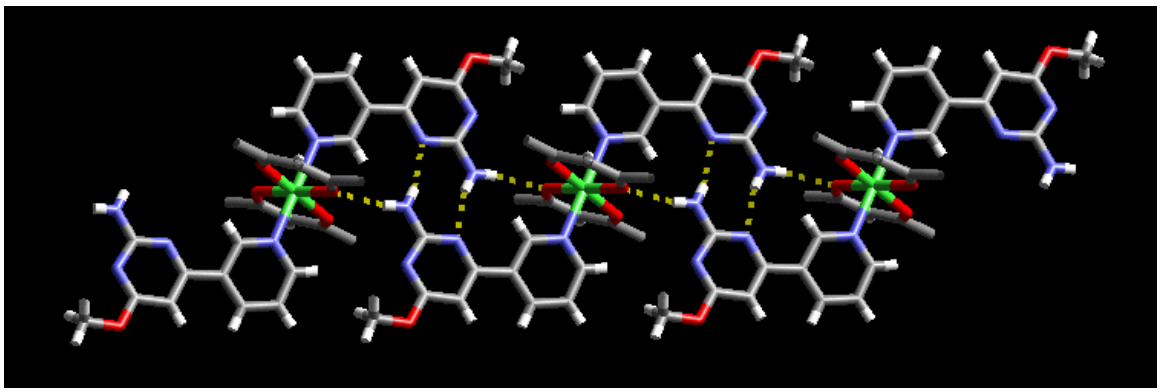

**Figure 5.21** Infinite chain in the crystal structure of **15d** produced from N-H···O and N-H···N hydrogen bonds. Acac phenyl rings have been omitted for clarity.

### *5.3.11 Crystal structure of {bis(1,1,1,5,5,5-hexafluoro-2,4-pentanedionato-O,O')-trans-bis(3-(2-amino-4-methylpyrimidin-6-yl)pyridine-N) copper(II)}-1,2-dichloroethane, 1g*

The metal-complex in **1g** is composed of two ligands **1** bound to a $[(hfac)_2Cu(II)]$ complex. The orientation and arrangement of the ligands **1** with respect to the $[(hfac)_2Cu(II)]$ complex is similar to that shown in the structure of **15c**, where coordination to the axial positions of the metal ion takes place via the pyridyl moieties thus creating an octahedral metal environment, Figure 5.22. Within this arrangement the amino-pyrimidine functionality is suitable for self-complementary hydrogen bonds with neighboring complexes. Thus the *syn*-amino protons form N-H···N hydrogen bonds with pyrimidine nitrogen atoms resulting in a 1-D infinite ribbon, Figure 5.23. The extended structures of **15c** and **15d** are possibly different due to a subtle change of the substituents on the organic counterpart. Ligand **15** has a methoxy substituent ortho- to the pyrimidine nitrogen atom sterically congesting that binding site, thus blocking the interactions to the neighboring amino- protons. The second pyrimidine nitrogen atom and *anti*-amino proton are not involved in extending the network. Furthermore a solvent molecule of 1,2-dichloroethane is incorporated in the crystal lattice, without disrupting any self-complementary hydrogen bonds.

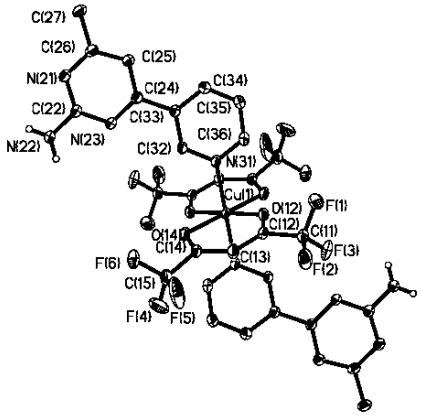


**Figure 5.22** Numbered thermal ellipsoids in the crystal structure of **1g** drawn at 50% probability level. One molecule of 1,2-dichloroethane and the hydrogen atoms (apart from $-NH_2$) have been omitted for clarity).

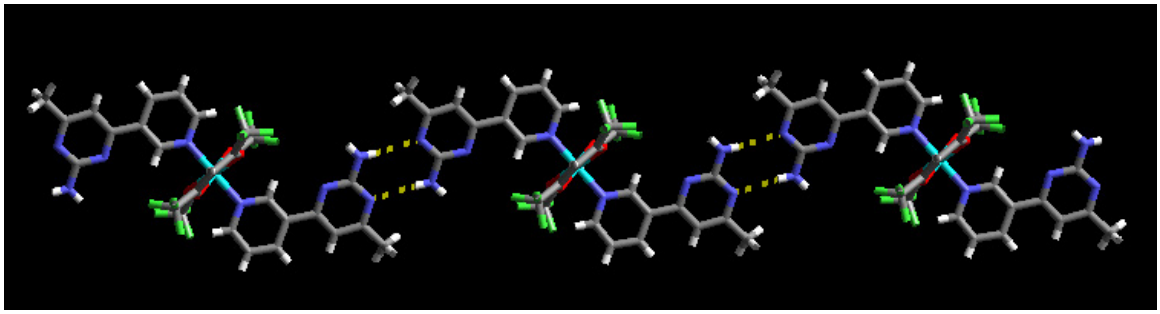

**Figure 5.23** Infinite ribbon held together by self-complementary N-H···N amino-pyrimidine interactions in the crystal structure of **1g**.

### *5.3.12 Crystal structure of {bis(1,1,1,5,5,5-hexafluoro-2,4-pentanedionato-O,O')-(1-(2-amino-4-methylpyrimidin-6-yl)-2-(3-methoxypyridin-5-yl-N)ethyne) copper(II)}, 6f*

The crystal structure of **6f** includes only one ligand **6** coordinated to a $[(hfac)_2Cu(II)]$ complex in the axial position, Figure 5.24. Coordination occurs through the pyridyl nitrogen atom of the ligand to the copper center resulting in a square pyramidal metal coordination geometry. The ligand:metal complexes form head-to-tail N-H···O hydrogen bonded dimers through the *anti*-amino proton to the oxygen atom of an adjacent metal acac complex. Further extension of the network is fashioned by N-H···N hydrogen bonds from the *syn*-amino proton to a nitrogen atom of the pyrimidine ring, Figure 5.25. The second pyrimidine nitrogen atom is aligned to coordinate at the axial position of a neighboring acac complex, although the Cu-N distance is approximately 2.70 Å.

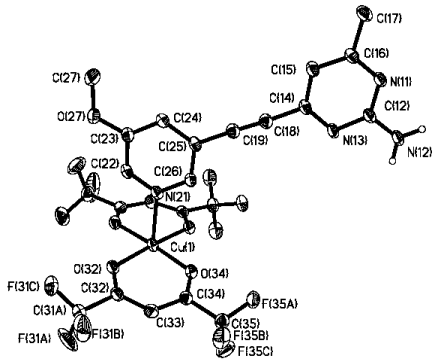


**Figure 5.24** Labeled thermal ellipsoids (drawn at 50% probability level) of crystal structure **6f** with the hydrogen atoms (apart from $-NH_2$) omitted for clarity.

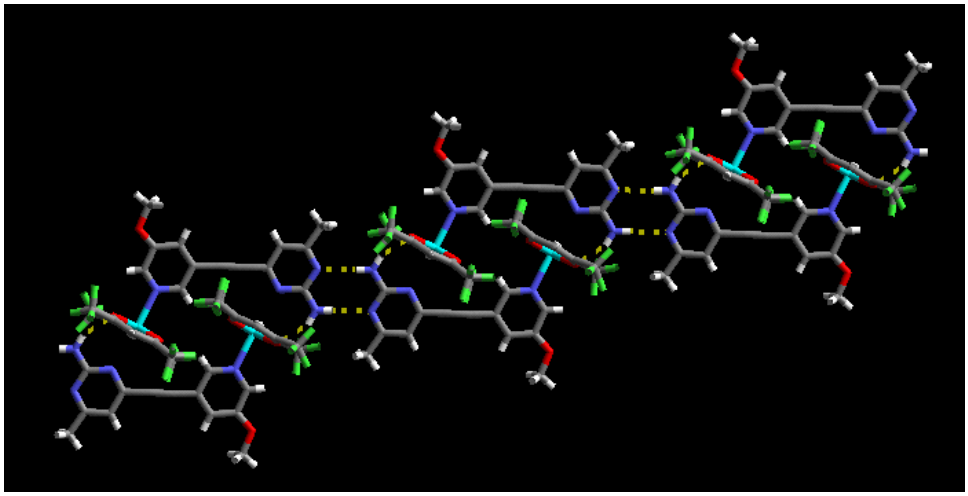

**Figure 5.25** Extended network in the crystal structure of **6f** showing the N-H···N and N-H···O hydrogen bonds.

### *5.3.13 Crystal structure of {bis(1,3-diphenyl-1,3-propanedionato-O,O')-trans-bis(1-(2-amino-4-methylpyrimidin-6-yl)-2-(3-methoxypyridin-5-yl-N)ethyne) cobalt(II)}, 6g*

The metal complex in **6g** contains two symmetry related ligands **6** bound axially to a $[(DBM)_2Co(II)]$ complex creating an octahedral cobalt coordination geometry, Figure 5.26. The network forms an infinite sheet by self-complementary N-H···N hydrogen bonds from the *syn*-amino protons to a nitrogen atom of the pyrimidine ring and by N-H···O hydrogen bonds from the *anti*-amino protons to an oxygen atom of the adjacent acac complex, Figure 5.27

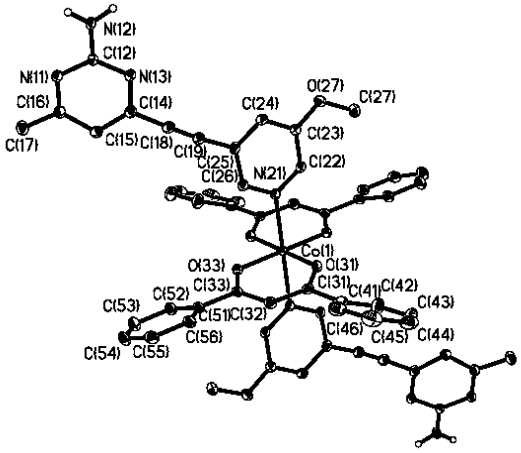


**Figure 5.26** Labeled thermal ellipsoids of structure **6g** with the hydrogen atoms (apart from $-NH_2$) omitted for clarity drawn at 50% probability level.

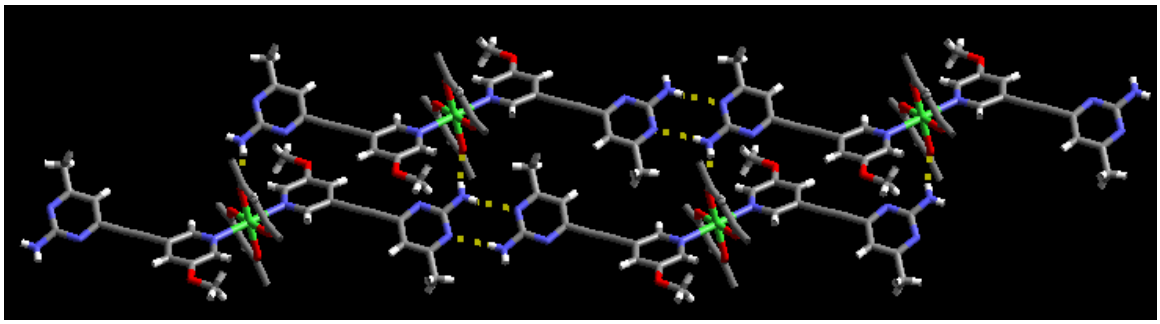

**Figure 5.27** Extended network in the crystal structure of **6g** with the phenyl rings omitted from the metal acac complex for clarity.

### *5.3.14 Crystal structure of {bis(1,3-diphenyl-1,3-propanedionato-O,O')-trans-bis(1-(2-amino-4-methylpyrimidin-6-yl)-2-(3-methoxypyridin-5-yl-N)ethyne) nickel(II)}, 6h*

The crystal structure of **6h** is isostructural with the crystal structure of **6g**. Two ligands **6** are coordinate axially to the $[(DBM)_2Ni(II)]$ complex with creating an octahedral coordination geometry around the nickel center, Figure 5.28. The overall structure is extended through self-complementary N-H···N hydrogen bonds from the *syn*-amino protons to a nitrogen atom of the pyrimidine ring and by N-H···O hydrogen bonds from the *anti*-amino protons to an oxygen atom of an adjacent acac complex, Figure 5.29.

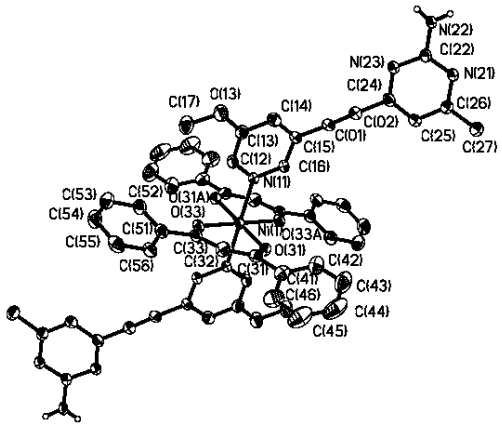


**Figure 5.28** Labeled thermal ellipsoids for the crystal structure of **6h** with the hydrogen atoms (apart from $-NH_2$) omitted for clarity drawn at 50% probability level.

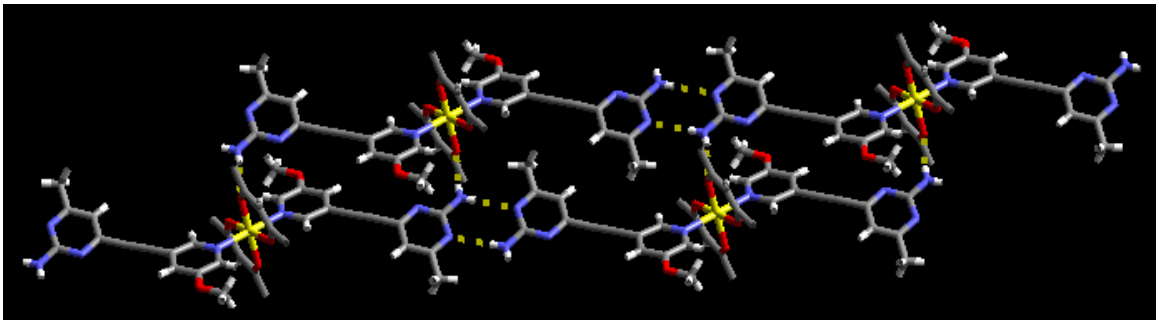

**Figure 5.29** Extended network in the crystal structure of **6h** with the phenyl rings omitted from the metal acac complex for clarity.

## 5.4 Discussion

### *5.4.1 Controlling the M(II) coordination geometry*

In twelve of the thirteen crystal structures obtained in this effort, the desired coordination environment around each M(II) ion was achieved resulting in rigid neutral metal-containing acac complexes or dicopper(II) tetracarboxylate complexes, while structure **6f** displays a five-coordinate square-pyramidal coordination geometry around the copper ion. A search through the CSD resulted in 109 hits when the search criteria consisted of Cu(II)(hfacac)$_2$ and an N-donor ligand.[13] Of the 109 structures, 88 posses an octahedral six-coordinate geometry, while 21 have a five-coordinate geometry. Although the majority of the structures favor an octahedral environment (~81 %), five-coordinate structures do exist (~19 %), with **6f** being the first five-coordinate pyridine/amino-pyrimidine-containing Cu(II)(hfacac)$_2$ complex reported.[6f] The next phase in the supramolecular synthesis requires some means for aligning and connecting these complex ions in such a way that the inherent geometry of the metal complex is propagated into extended metal-containing networks. We therefore examined the ability of four different bifunctional ligands **1**, **6**, **15**, and **16** to act as supramolecular reagents for the construction of 1-D motifs. In all seven structures containing dicopper(II) tetracarboxylate complexes **1e-1f**, **6e**, **15a-15b**, and **16a-16b** and five out of six structures containing M(II)-acac complexes **1g**, **6g-6h**, **15c-15d** the pyridyl moiety provides a robust and reliable binding site for attaching the supramolecular bifunctional ligand to the open, axial coordination sites on the M(II) ion, Figure 5.30.

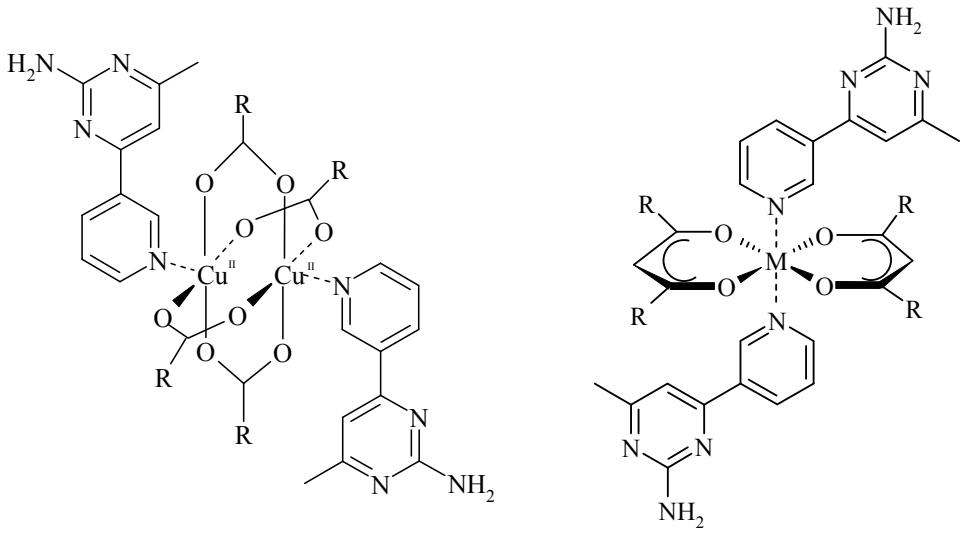

**Figure 5.30** Pictoral representation of the desired coordination chemistry around the M(II) centers after SR binding. SR **1**, is only used in this example, however the other SR's also display the observed coordination chemistry.

### *5.4.2 Attempts at controlling the supramolecular assembly*

With a remarkable success rate, each time a bifunctional ligand with a pyrimidine component was employed (10/11 structures, 91 %) neighboring ligands were connected via a dimeric N-H···N motif. The desired supramolecular chemistry failed in **15c**, and the assembly is generated through an N-H···O hydrogen bond, from the *syn*-amino proton to an oxygen atom from an adjacent acac complex. The exact directional and structural consequence of this interaction is, however, complicated by the fact that the 2-aminopyrimidine moieties, employed in this study, are asymmetric about the C1-C4 vector, Figure 5.31. Consequently, each bifunctional ligand, **1**, **6**, and **15** has two different ways of producing a self-complementary N-H···N/N···H-N motif. If the hydrogen bonds between adjacent 2-aminopyrimidine moieties serve to maximize the through-space separation between metal ions, Figure 5.31a, the result is a diverging assembly, whereas if the N-H···N/N···H-N synthon brings the complex ions closer together, Figure 5.31b, the assembly is converging.

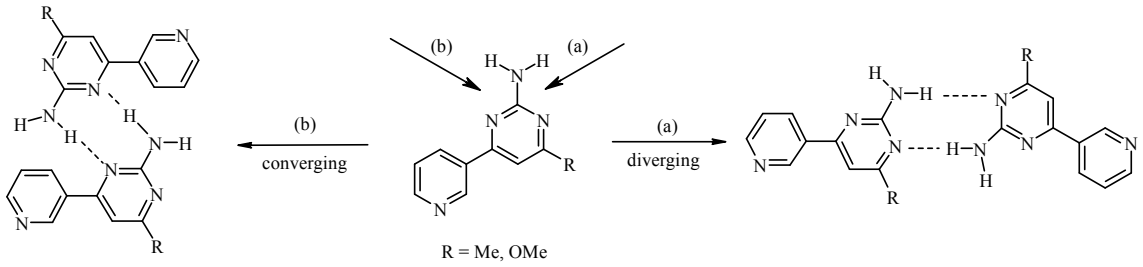


**Figure 5.31** Pictorial description of converging or diverging structural motifs.

Another variable that needs to be taken into consideration is the fact that the pyridyl moiety and the 2-amino substituent can be arranged either *cis*- or *trans* with respect to each other, Figure 5.32.

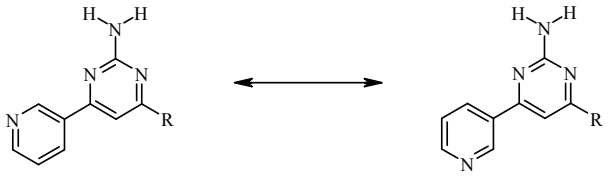


**Figure 5.32** Possible *cis*- or *trans* isomers based on the arrangement of the pyridine nitrogen atom and the 2-amino substituent.

Steric considerations dictate that only one of the two arrangements is possible in any given structure but, from a supramolecular synthetic viewpoint, it would be of interest to establish whether or not a suitable molecular substitution can provide a tool for guiding this particular assembly process in a rational manner.

### *5.4.2.1 Effects of sterics and SR length on supramolecular assembly*

The five crystal structures **1e**, **1g**, **6e**, **6g**, and **6h** posses diverging motifs, Figure 5.31a, and in all cases the 2-amino moiety is *trans* to the pyridyl nitrogen. The methyl substituent present on the pyrimidine ring does not seem large enough to control the relative interplanar orientation in the bifunctional ligands and it is not clear if a specific interaction is responsible for the observed orientation.

However, the three crystal structures **15a**, **15b**, and **15d** display converging motifs, Figure 5.31b, and in all cases a *cis* arrangement exists. The converging motif is due to the fact that the –OMe substituent blocks the adjacent cyclic nitrogen atom, and thus prevents it from

participating as an acceptor in a self-complementary N-H···N/N···H-N motif. In fact, a search of the CSD showed that a methoxy-substituent *ortho*- to a pyridine nitrogen atom is very likely to reside co-planar with the ring and face the adjacent nitrogen atom, which does limit its availability as a potential hydrogen-bond acceptor.[14] Furthermore, relevant literature shows when a –OMe substituent is *ortho*- to the amino-pyrimidine nitrogen atoms, N-H···N/N···H-N interactions are possible, but occurring only 43 % of the time (3 out of 7).[15]

The crystal structure of **1f** provides a good example of the difficulties that can be encountered when trying to establish clear structural patterns and/or intermolecular preferences. In this structure there are two crystallographically unique metal-containing building blocks: one with a *cis* and one with a *trans* orientation of the 2-amino functionality with respect to the pyridyl moiety. The former ligand gives rise to a converging assembly, whereas the latter produces a divergent motif.

As stated earlier, another way of minimizing steric crowding (that could prevent or disrupt intended supramolecular assembly) would be to increase the separation between the two different binding sites on the bifunctional ligand. Consequently, an ethynyl bridge was incorporated into ligand **6** in an attempt to facilitate access to the hydrogen-bonding site and this strategy worked very well as exemplified by the crystal structure determinations of **6e** and **6f-6h**. Despite the fact that the coordination chemistry is different, square-pyramidal vs. octahedral, respectively, each contains the *trans* arrangement as well as self-complementary N-H···N/N···H-N hydrogen bonds between adjacent amino-pyrimidine sites that act as the principle driving forces for the supramolecular assembly.

### *5.4.3 Amino-pyrimidine or amino-pyridine; does it matter?*

For the extension of the metal:ligand complex, three of the ligands utilize an amino-pyrimidine moiety, whereas one ligand, **16**, relies on the amino-pyridine functionality. For the two structures, **16a** and **16b**, were the latter ligand was employed, the desired intermolecular interactions failed to materialize. Surprisingly, the disordered bipyridine-type ligands acted as ditopic linkers between adjacent Cu(II)-ions resulting in 1-D coordination polymers. The reason for the failure of **16** to act in the desired manner is not obvious, but it is possible that the pyridyl moiety, which is an integral part of the hydrogen-bonding functionality, is simply too good of a ligand to give up a Cu(II) ion in exchange for acting as an acceptor in an N-H···N hydrogen

bond. This interpretation is supported by the fact that when a pyridyl moiety is replaced with a less effective ligand, a pyrimidine heterocycle, a dimeric hydrogen-bond motif is favored over a pyrimidine-Cu, ligand-metal, interaction.

The principle supramolecular target for this study, M(II)-containing 1-D assemblies was realized in a reasonable supramolecular yield (10/13, 77 %) using a combination of new bifunctional ligands and the well-known μ-O,O'coordinating mode of the carboxylate functionality or vacant axial sites of the M(II)-acac complex. In 12 out of 13 cases, we successfully controlled the coordination geometry around the often M(II) ion. The exact nature of the assembly, convergent or divergent, is determined by the relative orientation of the two aromatic components of our bifunctional ligands, which, in turn, can be represented by the rather soft potential energy curve typically associated with aryl-aryl torsion angles.

In a sense, our supramolecular success mirrors quite closely the relative strengths of the interactions that are responsible for the different recognition and binding events that take place in the course of these reactions: metal-ligand 13/13 (100%) and N-H···N hydrogen-bonds 10/13 (77 %).

## References:


[1] (a) Chi, K.-W.; Addicott, C.; Arif, A. M.; Stang, P. J. *J. Am. Chem. Soc*. **2004**, *126*, 16569. (b) Chatterjee, B.; Noveron, J. C.; Resendiz, M. J. E.; Liu, J.; Yamamoto, T.; Parker, D.; Cinke, M.; Nguyen, C. V.; Arif, A. M.; Stang, P. J. *J. Am. Chem. Soc*. **2004**, *126*, 10645. (c) Nakabayashi, K.; Kawano, M.; Yoshizawa, M.; Ohkoshi, S.; Fujita, M. *J. Am. Chem. Soc*. **2004**, *126*, 16694. (d) Braga, D.; Desiraju, G. R.; Miller, J. S.; Orpen, A. J.; Price, S. L. *CrystEngComm* **2002**, 500. (e) Tashiro, S.; Tominaga, M.; Kusukawa, T.; Kawano, M.; Sakamoto, S.; Yamaguchi, K.; Fujita, M. *Angew. Chem., Int. Ed*. **2003**, *42*, 3267-3270. (f) Natarajan, R.; Savitha, G.; Moorthy, J. N. *Cryst. Growth Des*. **2005**, 5, 69.

[2] (a) Yoshizawa, M.; Miyagi, S.; Kawano, M.; Ishiguro, K.; Fujita, M. *J. Am. Chem. Soc*. **2004**, *126,* 9172. (b) Fujita, M.; Tominaga, M.; Hori, A.; Therrien, B. *Acc. Chem. Res.* **2005**, *38*, 369. (c) Yoshizawa, M.; Takeyama, Y.; Okano, T.; Fujita, M. *J. Am. Chem. Soc.* **2003**, *125*, 3243. (d) Rowsell, J. L. C.; Yaghi, O. M. *Microporous and Mesoporous Materials* **2004**, *73*, 3. (e) Rowsell, J. L. C.; Millward, A. R.; Park, K. S.; Yaghi, O. M. *J. Am. Chem. Soc*. **2004**, *126*, 5666. (f) Atwood, J. L.; Barbour, L. J.; Dalgarno, S. J.; Hardie, M. J.; Raston, C. L.; Webb, H. R. *J. Am. Chem. Soc.* **2004**, *126*, 13170.

[3] (a) Hill, R. J.; Long, D.-L.; Champness, N. R.; Hubberstey, P.; Schroder, M. *Acc. Chem. Res*. **2005**, *38*, 335. (b) Campbell, K.; Kuehl, C. J.; Ferguson, M. J.; Stang, P. J.; Tykwinski, R. R. *J. Am. Chem. Soc*. **2002**, *124*, 7266. (c) Braga, D.; Giaffreda, S. L.; Grepioni, F.; Polito, M. *CrystEngComm* **2004**, *6*, 458. (d) Berry, J. F.; Cotton, F. A.; Fewox, C. S.; Lu, T.; Murillo, C. A.; Wang, X. *Dalton Trans*. **2004**, *15*, 2297. (e) McManus, G. J.; Wang, Z.; Zaworotko, M. J. *Cryst. Growth Des*. **2004**, *4*, 11. (f) Braga, D.; Brammer, L.; Champness, N. R. *CrystEngComm* **2005**, 7, 1. (g) Schultheiss, N.; Barnes, C. L.; Bosch, E. *Cryst. Growth Des.* **2003**, *3*, 573. (h) Oh, M.; Stern, C. L.; Mirkin, C. A. *Inorg. Chem.* **2005**, *44*, 2647.

[4] (a) *Supramolecular Assembly via Hydrogen Bonds II. Structure and Bonding*, eds. D. M. P. Mingos, St. Edmund Hall, Oxford, UK, Springer-Verlag: Berlin, Heidelberg, New York. 2004. (b) Desiraju, G. R. *Acc. Chem. Res*. **1996**, *29*, 441. (c) Aakeröy, C. B.; Beatty, A. M.; Helfrich, B. A. *J. Am. Chem. Soc.* **2002**, *124,* 14425. (d) Raymo, F. M.; Bartberger, M. D.; Houk, K. N.; Stoddart, J. F. *J. Am. Chem. Soc*. **2001**, *123*, 9264. (e) Fournier, J.–H.; Maris, T.; Wuest, J. D.;

Guo, W.; Galoppini, E. *J. Am. Chem. Soc*. **2003**, *125*, 1002. (f) Braga, D.; Polito, M.; D'Addario, D.; Grepioni, F. *Cryst. Growth Des.* **2004**, *4*, 1109.

[5] (a) Ohmori, O.; Kawano, M.; Fujita, M. *CrystEngComm* **2005**, *7*, 255. (b) Sundararaman, A.; Zakharov, L. N.; Rheingold, A. L.; Jaekle, F. *Chem. Commun*. **2005**, *13*, 1708. (c) Garcia-Baez, E. V.; Martinez-Martinez, F. J.; Hoepfl, H.; Padilla-Martinez, I. I. *Cryst. Growth Des.* **2003**, *3*, 35. (d) Blake, A. J.; Champness, N. R.; Khlobystov, A. N.; Lemenovskii, D. A.; Li, W.-S.; Schroder, M. *Chem. Commun*. **1997**, *15*, 1339. (e) Oren, A. B.; Curtis, M. D.; Kampf, J. W. *Chem. Mat*. **2000**, *12*, 1519.

[6] (a) Aakeröy, C. B.; Beatty, A. M.; Lorimer, K. R. J. *Chem. Soc., Dalton Trans*. **2000**, *21*, 3869. (b) Aakeröy, C. B.; Beatty, A. M.; Leinen, D. S.; Lorimer, K. R. J. *Chem. Commun.* **2000**, *11*, 935. (c) Aakeröy, C. B.; Beatty, A. M.; Desper, J.; O'Shea, M.; Valdés-Martínez, J. *Dalton Trans*. **2003**, *20*, 3956. (d) Bose, D.; Banerjee, J.; Rahaman, S. H.; Mostafa, G.; Fun, H.-K.; Bailey Walsh, R. D.; Zaworotko, M. J.; Ghosh, B. K. *Polyhedron* **2004**, *23*, 2045. (e) Burchell, T. J.; Eisler, D. J.; Puddephatt, R. J. *Inorg. Chem*. **2004**, *43*, 5550. (f) Aakeröy, C. B.; Schultheiss, N.; Desper, J. *Inorg. Chem*. **2005**, 44, 4983. (g) Aakeröy, C. B.; Schultheiss, N.; Desper, J. *Dalton Trans.* **2006**, 1627.

[7] (a) Thompson, D. W. *On Growth and Form*, Cambridge University Press, 1942. (b) Mann, S. J. *Chem. Soc., Dalton, Trans*. **1997**, *21*, 3953. (c) Li, M.; Mann, S. *J. Mater. Chem*. **2004**, *14*, 2260. (d) Mann, S. *Chem. Commun*. **2004**, *1*, 1.

[8] (a) Wu, P.; Bhamidipati, M.; Coles, M.; Roa, D. V. G. L. N. *Chem. Physics Let*. **2004**, *400*, 506. (b) Kooi, B. J.; M DeHosson, J. Th. *J. of Applied Phys*. **2004**, 95, 4714. (c) Okumura, H.; Twisselmann, D. J.; McMichael, R. D.; Huang, M. Q.; Hsu, Y. N.; Laughlin, D. E.; McHenry, M. E. *J. of Applied Phys*. **2003**, 93, 6528.

[9] (a) Panthou, F. L.; Luneau, D.; Musin, R.; Öhrström, L.; Grand, A.; Turek, P.; Rey, P. *Inorg. Chem*. **1996**, *35*, 3484. (b) Sano, Y.; Tanaka, M.; Koga, N.; Matsuda, K.; Iwamura, H.; Rabu, P.; Drillon, M. *J. Am. Chem. Soc*. **1997**, *119*, 8246.

[10] Li, W.; Nelson, D. P.; Jensen, M. S.; Hoerner, R. S.; Cai, D.; Larsen, R. D.; Reider, P. J. *J. Org. Chem*. **2002**, *67*, 5394.

[11] Soldatov, D. V.; Ripmeester, J. A. *Chem. Eur. J.* **2001**, *7*, 2979.

[12] Hunter, C. A.; Sanders, J. K. M. *J. Am. Chem. Soc.* **1990**, *112*, 5525.

[13] 109 hits on CSD as of March 2007, when searching for Cu(II)(hfacac)$_2$ and a N-donor ligand.

[14] A CSD search resulted in 30 crystal structures showing a methoxy substituent *ortho* to the pyridine nitrogen. In all 30 structures the methoxy substituent is bent towards the nitrogen atom.

[15] A CSD search displayed the following structures exhibiting N-H···N/ N···H-N interactions; AFUYIJ, LUPWAU, LUPWOI while CUWHOR, GUKTOV, IHEPIU, LUPXAV do not.

# CHAPTER 6 - Formation of hydrogen-bonded heterodimeric cavitand-based molecular capsules

## 6.1 Introduction

Molecular recognition, a central concept within supramolecular chemistry, is the result of a fine-balance between shape, size, and functional complementarity, which allows for the assembly of individual entities into multi-component aggregates.[1] These reversible intermolecular forces are the synthetic tools for the supramolecular chemist, just as the making and breaking of covalent bonds provide the tools for the synthetic organic chemist.

Utilizing directed-assembly to bring together two concave bowl-shaped supramolecular hosts into discrete nano-sized capsules is of considerable importance. Upon formation, the interior of the capsule offers a nano-sized reaction chamber where a range of important chemical transformations can be carried out with an unprecedented degree of control. Due to the restricted and isolated nature of the inner-cavity, properties differ (within the capsule) drastically compared to those of the bulk phase environment. This leads to potential practical applications including, molecular sensing,[2] stabilization of reactive intermediates,[3] increased chemical reaction rates,[4] molecular catalysis,[5] and detection of various isomers.[6] Furthermore, individual molecules coming together to form larger aggregates, which contain enforced cavities, play vital roles in many biological molecular recognition processes such as a concave receptor or enzyme site recognizing and binding to a convex substrate surface.[7] More specifically, the protein shell or coat of a virus is made up of hundreds of subunits that self-assemble into a cage arrangement, surrounding, then transporting, viral nucleic acids. Many efforts have been made to mimick the function of various cage-like protein coats, which provide great promise for the pharmaceutical industry in hopes of advancing drug delivery systems.[8]

The construction of molecular capsules has been primarily achieved through complementary ionic[9] or non-covalent interactions (*i.e.*, hydrogen bonds[10] with the formation of either homodimeric- or heterodimeric-based assemblies). Incorporation of two or more different guests within a cavity of a homodimeric/symmetric capsule is unusual and only achievable if the guests preferentially engage in heteromeric interactions, independent of the host, before entering the cavity.[11] However, within a heterodimeric-based assembly, if both halves of the capsule are

different and capable of incorporating its own guest selectively, then upon capsule formation two different reactive guests could reside within the same cavity, Figure 6.1

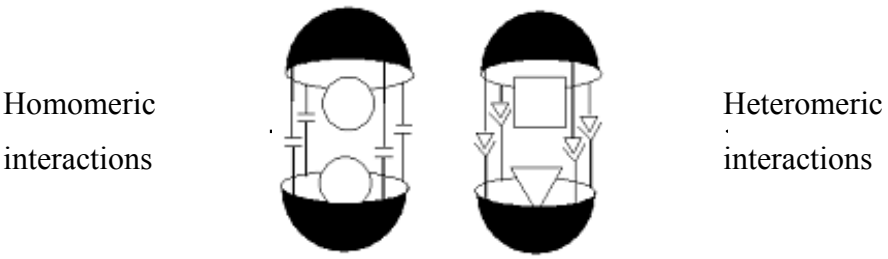


**Figure 6.1** A cartoon representation of a homodimeric capsule encapsulating two of the same guests (left) and a heterodimeric capsule incorporating two different guests (right).

Cavitands were originally defined by D. J. Cram, as "synthetic organic compounds with enforced cavities large enough to complex complementary organic compounds or ions."[12] Through the years, two types of bowl-shaped hosts, resorcin[4]arene-based and cyclotriveratrylenes (CTV's), have received particular attention, Figure 6.2. Both of these cavity-bearing frameworks are constructed from multiple aromatic rings tethered together by methylene bridges, constricting the overall arrangement to a rigid bowl-shaped curvature. This Chapter will discuss resorcin[4]arene-based cavitands in greater detail, while Chapter 7 will focus solely on the CTV's.

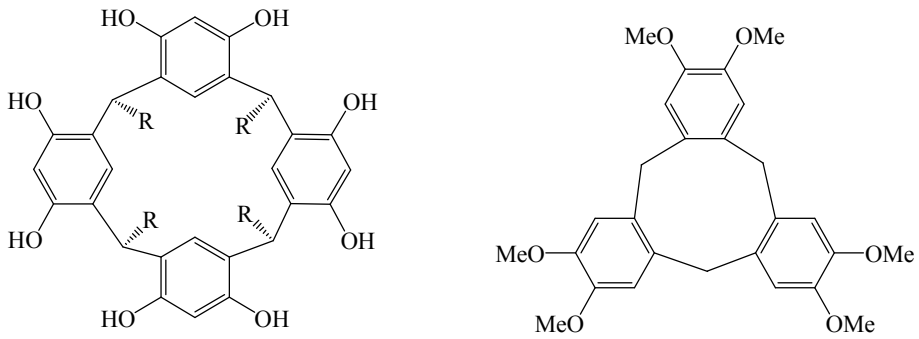


**Figure 6.2** Two types of cavitands; resorcin[4]arene-based (left) and cyclotriveratrylene (right).

Resorcin[4]arene-based cavitands are attractive molecules due the large variation of covalent modifications that can be achieved in three general positions, without compromising the overall structural integrity of the cavity-bearing framework, Figure 6.3.

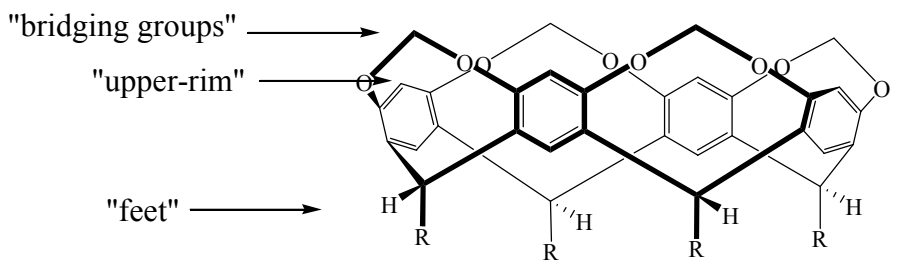


**Figure 6.3** A resorcin[4]arene-based cavitand outlining the location of its functionalizable parts.

Although modifications to the 'feet',[13] usually to improve solubility, have been reported, most alterations occur at the 'upper-rim'[14] or 'bridging groups'[15] producing a multitude of functionalized products. Our efforts will focus on covalent modifications to the upper-rim (labeled X) of resorcin[4]arene-based cavitands, while the bridging groups (-$CH_2$-) and feet (-pentyl) will not be altered, Figure 6.4.

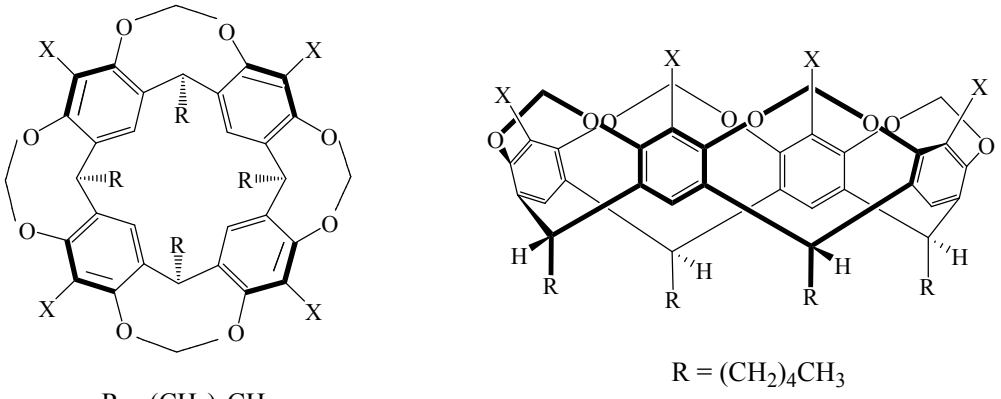


**Figure 6.4** Double-rimmed resorcinarene-based cavitands; top-view (left) and side-view (right).

In order to rationally design and build heterodimeric hydrogen-bonded cavitand-based capsules, it is necessary to have access to a wide range of cavitands that posess functional groups that complement each other such that heteromeric hydrogen-bonds are favored over homomeric intermolecular interactions.[16] Based upon extensive results from recent efforts in design and synthesis of co-crystals,[17] it is clear that the pyridine moiety is an effective hydrogen-bond acceptor that can form intermolecular interactions of sufficient strength to drive the formation of binary and ternary co-crystals. Consequently, a pyridyl functionalized cavitand can, in principle, act as one half of numerous hydrogen-bonded capsules where the complementary cavitand is decorated with hydrogen-bond donors such as –OH, -COOH, $–NH_2$, or –C(R)=NOH moieties.

Herein we present our recent efforts in resorcin[4]arene-based cavitand design and synthesis, with the construction of various hydrogen-bond donor and acceptor appended cavitands. These functionalized cavitands will be utilized in the directed-assembly of heterodimeric capsules.

## 6.2 Experimental

### *6.2.1 Synthesis*

All chemicals were purchased from Aldrich and used without further purification. Melting points were determined on a Fisher-Johns melting point apparatus and are uncorrected. $^{1}H$ and $^{13}C$ NMR spectra were recorded on a Varian Unity plus 400 MHz or 200 MHz spectrometer in $CDCl_3$ or $D_6$-DMSO. Compounds were prepared for infrared spectroscopic (IR) analysis as a mixture in KBr. Elemental Analysis was carried out by Atlantic Microlab Inc. Electrospray Ionization – Ion-Trap Mass Spectrometry (ESI-IT-MS) was carried out on a Bruker Daltonics Esquire 3000 Plus. MALDI-TOF / TOF-MS was carried out on a Bruker Daltonics Ultraflex TOF/TOF.

#### *6.2.1.1 Synthesis of C-pentylcalix[4]resorcinarene, 17*[18]

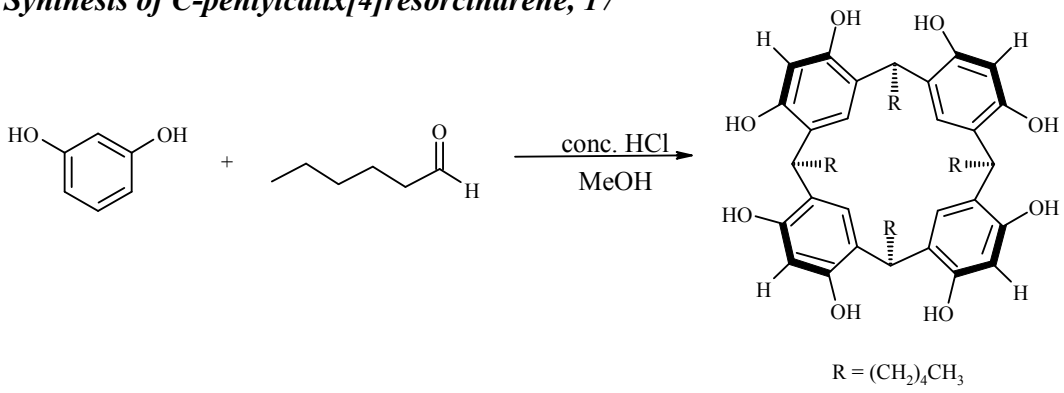


**17**

To a solution of resorcinol (10.0 g, 0.09 mol) and hexanal (9.10 g, 0.09 mol) in ethanol (90 mL) was added conc. HCl (14.5 mL) at 0 ºC under a dinitrogen atmosphere. A condenser was attached and the mixture heated to 70 ˚C for 10 hours. The reaction was monitored by TLC and allowed to cool to room temperature upon completion, then diluted with water. A white precipitate formed which was filtered and dried, (15.1 g, 86 %). M.p. >280 ˚C; $^{1}H$ NMR ($\delta_H$; 400 MHz, $D_6$-DMSO): 8.86 (s, 8H), 7.15 (s, 4H), 6.14 (s, 4H), 4.21 (t, J = 7.6Hz, 4H), 2.00 – 2.02

(m, 8H), 1.16 – 1.25 (m, 24H), 0.83 (t, J = 6.4Hz, 12H); $^{13}$C NMR ($\delta_H$; 200 MHz, $D_6$-DMSO): 151.68, 124.92, 123.08, 102.37, 33.99, 33.07, 31.51, 27.49, 22.27, 13.99; IR (KBr pellet): *v* 3276, 2955, 2859, 1617, 1502, 1457, 1293, 1170, 1084, 841 cm$^{-1}$; MALDI-TOF / TOF-MS *m/z* 791 ([**17** + Na]$^+$).

### *6.2.1.2 Synthesis of C-pentyltetrabromocalix[4]resorcinarene, 18*[19]

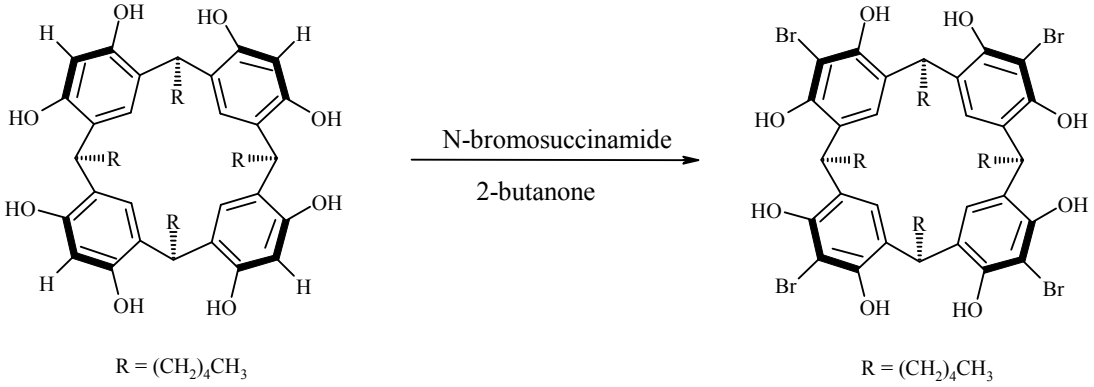


**17** **18**

A mixture of *C*-pentylcalix[4]resorcinarene **17** (10.0 g, 0.013 mol) and *N*-bromosuccinamide (13.8 g, 0.078 mol) were added to a round bottom flask. 2-Butanone (75 mL) was added and stirred at room temperature for 12 hours. The precipitate from the reaction was filtered and washed with cold 2-butanone (50 mL) then cold water (3 x 100 mL). Product **18** was dried in the oven overnight producing a pure white solid, (10.2 g, 72 %). M.p. >280 ˚C; $^1$H NMR ($\delta_H$; 400 MHz, $D_6$-DMSO): 9.10 (s, 8H), 7.35 (s, 4H), 4.35 (t, J = 7.6Hz, 4H), 2.15 – 2.17 (m, 8H), 1.18 – 1.32 (m, 24H), 0.84 (t, J = 7Hz, 12H); $^{13}$C NMR ($\delta_H$; 200 MHz, $D_6$-DMSO): 148.60, 125.48, 123.64, 101.29, 35.46, 33.48, 31.35, 27.38, 22.25, 13.94; IR (KBr pellet): *v* 3397, 2929, 2853, 1614, 1472, 1306, 1168, 1081, 768 cm$^{-1}$; MALDI-TOF / TOF-MS *m/z* 1107 ([**18** + Na]$^+$).

### *6.2.1.3 Synthesis of C-pentyltetrabromocavitand, 19*[19]

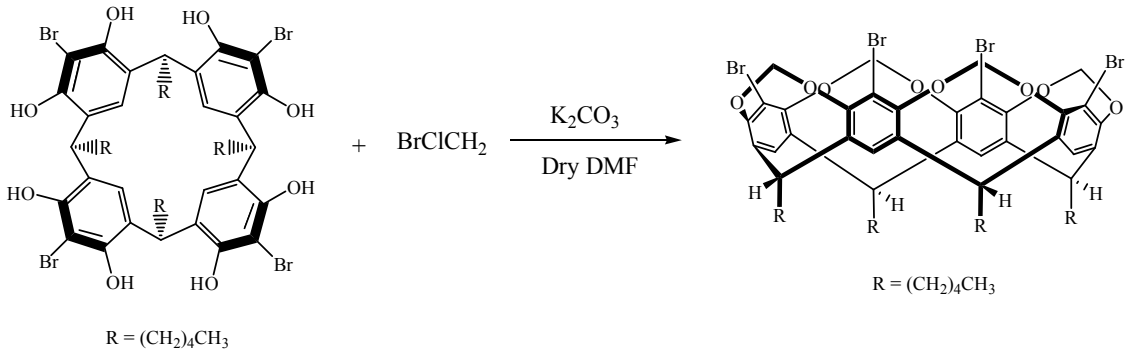


**18** **19**

A mixture of *C*-pentyltetrabromocalix[4]resorcinarene **18** (1.0 g, 1.30 mmol), potassium carbonate (3.8 g, 27.7 mmol) and bromochloromethane (1.2 mL, 9.3 mmol) were added to a round bottom flask. Dry DMF (27 mL) was added and dinitrogen bubbled through the resultant mixture for 10 minutes. A condenser was attached and the mixture heated to 65 ˚C under a dinitrogen atmosphere for 4 days. Every 24 hours, more bromochloromethane (0.3 mL, 2.3 mmol) was added. The DMF was removed under vacuo to give a dark brown solid. Chloroform (20 mL) was added to the reaction mixture along with 2M HCl (30 mL). The aqueous phase was separated and extracted with more chloroform (3 x 50 mL). The organic separations were combined then washed with water (3 x 100 mL) then washed with saturated aqueous sodium chloride (1 x 100 mL) and dried over magnesium sulfate. The solvent was removed on a rotary evaporator and the residue chromatographed on silica with a hexane/dichloromethane (1/2) mixture as the eluant. Product **19** was isolated as a white solid, (720 mg, 49 %). M.p. >280 ˚C; $^{1}$H NMR ($\delta_H$; 400 MHz, $CDCl_3$): 7.04 (s, 4H), 5.97 (d, J = 7.2Hz, 4H), 4.86 (t, J = 8.2Hz, 4H), 4.40 (d, J = 7.2Hz, 4H), 2.18 – 2.24 (m, 8H), 1.32 – 1.43 (m, 24H), 0.87 – 0.94 (m, 12H); $^{13}$C NMR ($\delta_H$; 400 MHz, $CDCl_3$): 152.04, 139.26, 119.01, 113.50, 98.45, 37.66, 31.84, 29.80, 27.39, 22.60, 14.03; IR (KBr pellet): *v* 2919, 2858, 1460, 1404, 1296, 1086, 1015, 948, 789 cm$^{-1}$; ESI-IT-MS *m/z* 1167 ([**19** + Cl]$^-$).

### *6.2.1.4 Synthesis of C-pentyltetra(3-pyridyl)cavitand, 20*

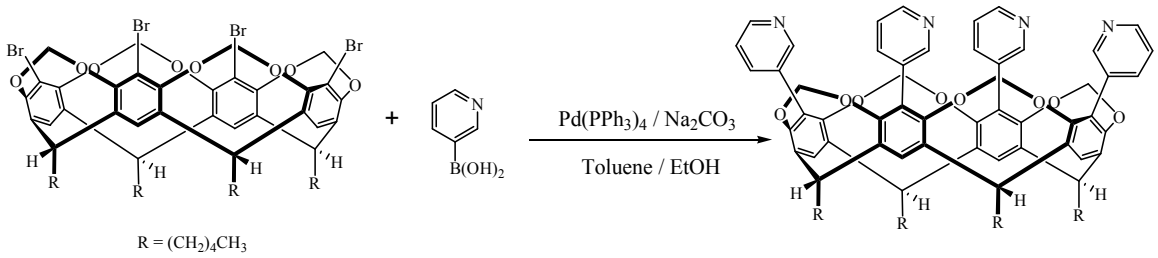


**19** **20**

A mixture of *C*-pentyltetrabromocavitand **19** (2.0 g, 1.77 mmol) and *tetrakis*-triphenylphosphine palladium (II) (420 mg, 0.362 mmol) were added to a round bottom flask under a stream of dinitrogen. Toluene (30 mL), ethanol (20 mL) and aqueous sodium bicarbonate (100 mg, 5 mL) were all purged with dinitrogen, then added to the round bottom flask along with 3-pyridylboronic acid (2.8 g, 22.76 mmol). The reaction mixture was refluxed for 72 hours under a dinitrogen atmosphere. Upon completion the reaction was cooled to room temperature and diluted with water (100 mL). The aqueous phase was washed with dichloromethane (3 x 100 mL) and dried with magnesium sulfate. The solvent was removed on a rotary evaporator and the residue purified by column chromatography using an ethanol/ethyl acetate (1:2) mixture as the eluant. The product **20** was isolated as a white crystalline solid, (1.72 g, 87 %). M.p. >280 ˚C; $^{1}$H NMR ($\delta_H$; 400 MHz, $CDCl_3$): 8.35 (br s, 4H), 8.21 (br s, 4H), 7.39 (br s, 4H), 7.33 (br s, 4H), 7.12 (s, 4H), 5.18 (s, 4H), 4.86 (t, J = 8Hz, 4H), 4.20 (s, 4H), 2.39 – 2.34 (m, 8H), 1.50 – 1.38 (m, 24H), 0.95 (t, J = 7Hz, 12 H); $^{13}$C NMR ($\delta_H$; 200 MHz, $CDCl_3$): 152.61, 150.16, 148.24, 138.58, 137.56, 129.52, 125.90, 122.70, 120.60, 100.21, 37.13, 31.99, 30.32, 17.61, 22.66, 14.09; IR (KBr pellet): *v* 2929, 2859, 1583, 1450, 1408, 1160, 1084, 975, 716 cm$^{-1}$; ESI-IT-MS *m/z* 1125 ([**20** + H]$^{+}$); Anal. Calcd. for $C_{72}H_{76}N_4O_8 \cdot H_2O$: C, 75.66; H, 6.83; N, 4.90. Found: C, 75.50; H, 6.78; N, 4.89.

### *6.2.1.5 Synthesis of C-pentyltetra(4-carboxyphenyl)cavitand, 21*

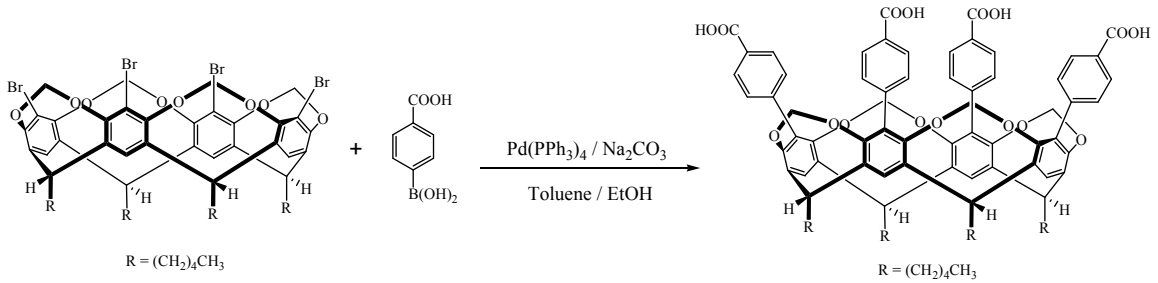


**19** **21**

A mixture of *C*-pentyltetrabromocavitand **19** (1.00 g, 0.883 mmol), 4-carboxyphenylboronic acid (1.47 g, 8.86 mmol), and *tetrakis*-triphenylphosphine palladium (II) (210 mg, 0.181 mmol) were added to a round bottom flask under a stream of dinitrogen. Toluene (20 mL), ethanol (15 mL) and aqueous sodium bicarbonate (1.0 g, in 5 mL $H_2O$) were all purged with dinitrogen, then added to the round bottom flask. The reaction mixture was refluxed for 72 hours under a dinitrogen atmosphere. Upon completion the reaction was cooled to room temperature and diluted with water (100 mL). The aqueous phase was washed with chloroform (3 x 100 mL) then precipitated with concentrated hydrochloric acid. Upon acidification a white precipitate formed, which was filtered and dried. The product **21** was isolated as a white crystalline solid, (900 mg, 79 %). M.p. >280 °C; $^1$H NMR ($\delta_H$; 200 MHz, $CDCl_3$): 8.35 (s, 4H), 8.21 (s, 4H), 7.39 (s, 4H), 7.33 (s, 4H), 7.12 (s, 4H), 5.18 (s, 4H), 4.86 (t, J = 8Hz, 4H), 4.20 (s, 4H), 2.39 – 2.34 (m, 8H), 1.50 – 1.38 (m, 24H), 0.95 (t, J = 7Hz, 12 H).

### *6.2.1.6 Synthesis of C-pentyltetraboronic acid pinacolyl ester cavitand, 22*

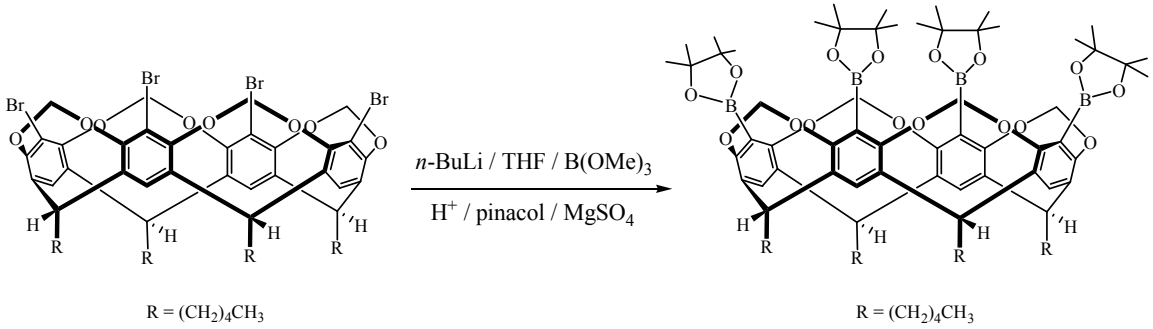


**19** **22**

*C*-Pentyltetrabromocavitand **19** (1.00g, 0.883 mmol) was dissolved in dry tetrahydrofuran (10 mL), and the solution was then evaporated and dried at 130 °C (0.1 mmHg) for 2 h under an

argon atmosphere. This procedure was repeated until all the water and residual solvents were removed from the sample. The resulting cavitand was dissolved in dry tetrahydrofuran (70 mL) and cooled to –78 °C (dry ice/acetone bath), under a dinitrogen atmosphere. *N*-butyllithium (1.6 M in hexanes, 2.54 mL, 4.06 mmol) was added dropwise over 10 minutes and stirred for an additional 0.5h. Trimethoxyborane (0.60 mL, 5.3 mmol) was added dropwise over 10 minutes and the resulting solution was stirred at –78 °C for 0.5h, at which time the dry ice/acetone bath was removed and the reaction mixture was allowed to reach room temperature. Upon reaching room temperature, the reaction mixture was quenched with a 1M hydrochloric acid solution (100 mL) and stirred for 0.5h. The mixture was extracted with dichloromethane (3 x 100 mL), the organic portions collected and dried over magnesium sulfate. The solvent was removed via rotary evaporator and the resulting residue dissolved in dichloromethane (100 mL). Excess pinacol (750 mg, 6.30 mmol) and magnesium sulfate (2.25 g) were added to the mixture, which was stirred for 12 h and then filtered and brought to dryness via a rotary evaporator. The residue was dissolved in dichloromethane and added to a beaker of acetone, in which a white precipitate formed and was filtered resulting in pure product **22,** (800 mg, 70 %). M.p. >280 ˚C; $^{1}$H NMR ($\delta_H$; 400 MHz, $CDCl_3$): 7.10 (s, 4H), 5.59 (d, J = 6.8Hz, 4H), 4.75 (t, J = 7.2Hz, 4H), 4.54 (d, J = 7.6Hz, 4H), 2.17-2.15 (m, 8H), 1.40-1.29 (m, 72H), 0.90-0.88 (m, 12H); $^{13}$C NMR ($\delta_H$; 200 MHz, $CDCl_3$); 157.72, 137.77, 122.37, 99.42, 83.53, 36.11, 31.91, 30.89, 29.88, 27.54, 24.70, 22.65, 14.02; IR (KBr pellet): *v* 2977, 2931, 1705, 1592, 1442, 1358, 1316, 1145, 978, 851, 582 cm$^{-1}$; MALDI-TOF / TOF-MS *m/z* 1344 ([**22** + H + (Na)23]$^{+}$); Anal. Calcd. for $C_{76}H_{108}O_{16}B_4$: C, 69.09; H, 8.18. Found: C, 69.24; H, 8.44.

### *6.2.1.7 Synthesis of C-pentyltetraiodocavitand, 23*

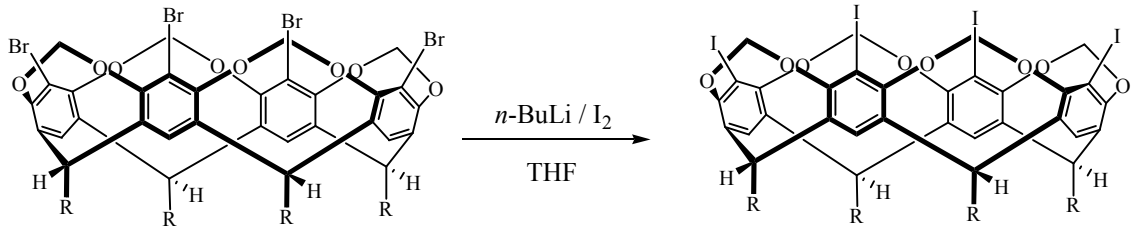


**19** **23**

*C*-pentyltetrabromocavitand **19** (2.0 g, 1.77 mmol) was added to a round-bottomed flask containing dry, freshly distilled THF (40 mL). The solution was cooled to –78 °C (dry ice/acetone bath temperature) and *n*-butyllithium (6.0 equiv., 6.63 mL, ca. 1.6 M solution in hexanes) was rapidly added. After stirring for 1h, iodine (3.6 g, 14.2 mmol, solution in THF (5 mL)) was added and the cooling bath removed allowing the reaction mixture to warm to room temperature. After 2 hours the reaction mixture was cooled to 0 ºC and quenched with a saturated aqueous sodium thiosulfate solution. The aqueous phase was extracted with ethyl acetate (3 x 75 mL), the portions washed with brine and dried with magnesium sulfate. The solvent was removed on a rotary evaporator and the residue purified by column chromatography using a hexanes/dichloromethane (4:1) mixture as the eluent. The product was further purified by reprecipitation (dichloromethane:hexanes) yielding a white powder **23**, (1.46 g, 63 %). M.p. >280 ˚C; $^{1}$H NMR ($\delta_H$; 200 MHz, $CDCl_3$): 7.07 (s, 4H), 5.98 (d, J = 7.4Hz, 4H), 4.86 (t, J = 8Hz, 4H), 4.33 (d, 7.8Hz, 4H), 2.20 – 2.19 (m, 8H), 1.39 (m, 24H), 0.92 (t, J = 7Hz, 12 H); $^{13}$C NMR ($\delta_H$; 200 MHz, $CDCl_3$): 154.86, 138.69, 120.65, 98.70, 93.02, 37.94, 31.84, 30.04, 27.40, 22.61, 14.03.

### *6.2.1.8 Synthesis of C-pentyltetra(3-ethynylpyridine)cavitand, 24*

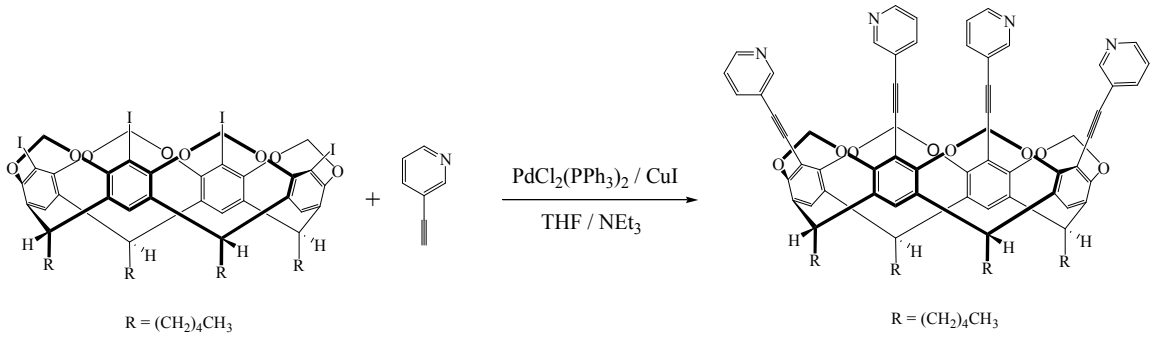


**23** **24**

A mixture of *C*-pentyltetraiodocavitand **23** (400 mg, 0.303 mmol), 3-ethynylpyridine (480 mg, 4.29 mmol), *bis*(triphenylphosphine)palladium (II) dichloride (50 mg, 0.07 mmol), triphenylphosphine (20 mg, 0.08 mmol), and copper(I) iodide (12 mg, 0.06 mmol) was added to a round bottom flask. Tetrahydrofuran (25 mL) and triethylamine (25 mL) were added and dinitrogen bubbled through the resultant mixture for 10 minutes. A condenser was attached and the mixture heated at 65 ºC under a dinitrogen atmosphere. The reaction was

monitored by TLC and allowed to cool to room temperature upon completion (72 hours). The solution was diluted with chloroform (100 mL), washed with water (3 x 100 mL), and washed with brine (2 x 100 mL). The organic layer was separated and dried over magnesium sulfate. The solvent was removed on a rotary evaporator and the residue chromatographed on silica with an ethyl acetate/ethanol mixture (2:1) containing 1% triethylamine as the eluant. The product was isolated as an off-white solid. The product **24** was then recrystallized from chloroform and hexanes, (250 mg, 67 %). M.p. >280 ˚C; $^{1}$H NMR ($\delta_H$; 400 MHz, $CDCl_3$): 8.69 (m, 4H), 8.55 (dd, J = 4.8Hz, J = 1.6Hz, 4H), 7.71 (dt, J = 8Hz, J = 1.6Hz, 4 H), 7.29 (m, 4H), 6.03 (d, J = 7.2Hz, 4H) 4.88 (t, J = 8Hz, 4H), 4.62 (d, 6.8Hz, 4H), 2.28 – 2.45 (m, 8H), 1.46 – 1.35 (m, 24H), 0.96 – 0.92 (m, 12 H); $^{13}$C NMR ($\delta_H$; 200 MHz, $CDCl_3$): 155.40, 152.23, 148.93, 138.52, 138.39, 123.11, 120.65, 120.03, 112.60, 98.36, 94.07, 84.25, 36.50, 31.81, 29.46, 27.38, 22.63, 14.03.

### *6.2.1.9 Synthesis of C-pentyltetra(2-amino-5-ethynylpyridine)cavitand, 25*

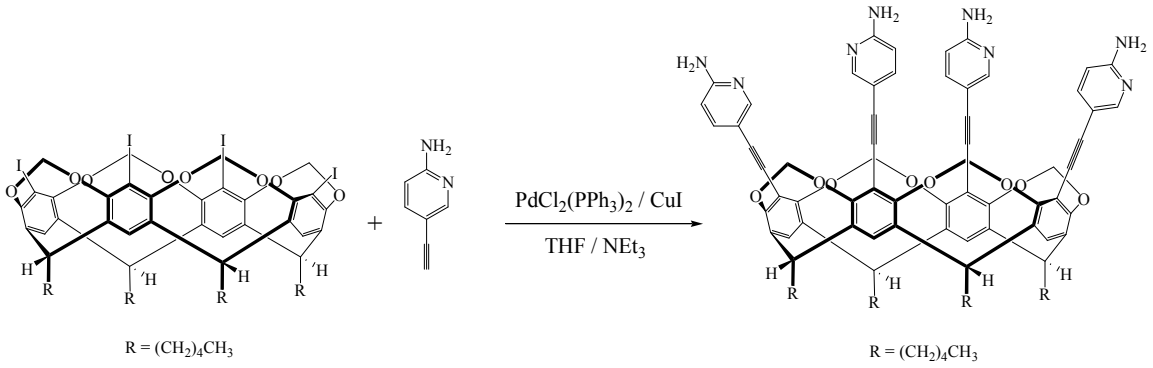


**23** **25**

A mixture of *C*-pentyltetraiodocavitand **23** (250 mg, 0.189 mmol), 2-amino-5-ethynylpyridine (217 mg, 1.89 mmol), *bis*(triphenylphosphine)palladium (II) dichloride (30 mg, 0.04 mmol), triphenylphosphine (10 mg, 0.04 mmol), and copper(I) iodide (7 mg, 0.04 mmol) were added to a round bottom flask. Tetrahydrofuran (15 mL) and triethylamine (15 mL) were added and dinitrogen bubbled through the resultant mixture of 10 minutes. A condenser was attached and the mixture heated at 50 ºC under a dinitrogen atmosphere. The reaction was monitored by TLC and allowed to cool to room temperature upon completion (72 hours). The solution was diluted with chloroform (100 mL), washed with water (3 x 100 mL), and washed with brine (2 x 100 mL). The organic layer was separated and dried over magnesium sulfate.

The solvent was removed on a rotary evaporator and the residue chromatographed on silica with an ethyl acetate/ethanol mixture (2:1) containing 1% triethylamine as the eluant. The product was isolated as a yellow solid. The product **25** was then reprecipitated, as a white solid, from dissolving in chloroform and adding to hexanes, (178 mg, 74 %). M.p. >285 ˚C; $^{1}$H NMR ($\delta_H$; 400 MHz, $CDCl_3$): 8.16 (d, J = 2Hz, 4H), 7.47 (dd, J = 8.4Hz, J = 2Hz, 4H), 7.06 (s, 4 H), 6.45 (d, J = 8.8Hz, 4H), 5.98 (d, J = 7.2Hz, 4H), 4.84 (t, J = 8Hz, 4H), 4.75 (s, 8H), 4.59 (d, 7.2 Hz, 4H), 2.28 – 2.21 (m, 8H), 1.44 – 1.36 (m, 24H), 0.98 – 0.90 (m, 12 H); $^{13}$C NMR ($\delta_H$; 200 MHz, $CDCl_3$): 157.64, 155.08, 151.53, 140.36, 138.38, 119.77, 113.32, 109.64, 107.94, 98.41, 95.32, 81.62, 36.52, 31.85, 29.52, 27.43, 22.67, 14.07; IR (KBr pellet): *v* 3380, 3196, 2930, 2853, 2203, 1608, 1445, 1086, 1020, 974, 697 cm$^{-1}$.

### *6.2.1.10 Synthesis of C-pentyltetra(4-formyl)cavitand, 26*

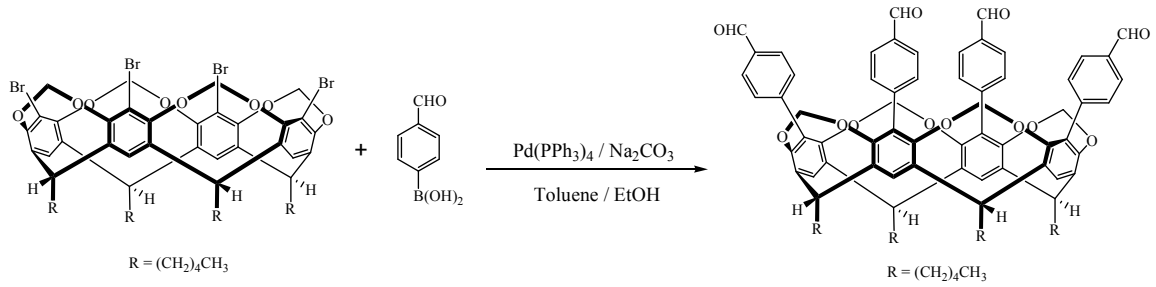


**19** **26**

A mixture of *C*-pentyltetrabromocavitand **19** (1.0 g, 0.883 mmol) and *tetrakis*-triphenylphosphine palladium (II) (210 mg, 0.181 mmol) were added to a round bottom flask under a stream of dinitrogen. Toluene (20 mL), ethanol (15 mL), and aqueous sodium bicarbonate (1.00 g) were all purged with dinitrogen, then added to the round bottom flask along with 4-formylphenyl boronic acid (1.32 g, 8.80 mmol). The reaction mixture was refluxed for 72 hours under a dinitrogen atmosphere. Upon completion the reaction was cooled to room temperature and diluted with water (100 mL). The aqueous phase was extracted with chloroform (3 x 100 mL) and dried with magnesium sulfate. The solvent was removed on a rotary evaporator and the residue purified by column chromatography using a hexanes/ethyl acetate (1:1) mixture as the eluant. The product was further purified by reprecipitation (chloroform:hexanes). The product **26** was isolated as a white crystalline solid, (900 mg, 83 %). M.p. >270 ˚C; $^{1}$H NMR ($\delta_H$; 400 MHz, $CDCl_3$): 10.00 (s, 4H), 7.85 (d, J = 8.4Hz, 8H), 7.38 (s,

4H), 7.20 (d, J = 8.4Hz, 8H), 5.16 (d, J = 6.8Hz, 4H), 4.86 (t, J = 8Hz, 4H), 4.23 (d, 6.8 Hz, 4H), 2.39 – 2.34 (m, 8H), 1.50 – 1.38 (m, 24H), 0.95 (t, J = 7Hz, 12 H); $^{13}$C NMR ($\delta_H$; 200 MHz, $CDCl_3$): 191.68, 152.37, 140.44, 138.55, 135.22, 130.58, 129.26, 128.44, 120.62, 100.43, 37.08, 32.02, 30.31, 27.63, 22.69, 14.12.

### *6.2.1.11 Synthesis of C-pentyltetra(3-methoxy-5-ethynylpyridine)cavitand, 27*

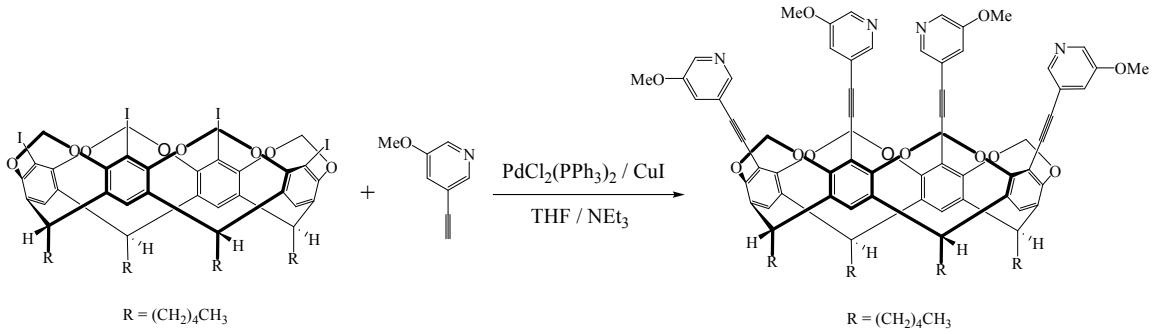


**23** **27**

A mixture of *C*-pentyltetraiodocavitand **23** (250 mg, 0.189 mmol), 3-methoxy-5-ethynylpyridine (310 mg, 2.30 mmol), *bis*(triphenylphosphine)palladium (II) dichloride (25 mg, 0.04 mmol), triphenylphosphine (10 mg, 0.04 mmol), and copper(I) iodide (7 mg, 0.04 mmol) were added to a round bottom flask. Tetrahydrofuran (15 mL) and triethylamine (15 mL) were added and dinitrogen bubbled through the resultant mixture of 10 minutes. A condenser was attached and the mixture heated at 50 ºC under a dinitrogen atmosphere. The reaction was monitored by TLC and allowed to cool to room temperature upon completion (72 hours). The solution was diluted with chloroform (100 mL), washed with water (3 x 100 mL), and washed with brine (2 x 100 mL). The organic layer was separated and dried over magnesium sulfate. The solvent was removed on a rotary evaporator and the residue chromatographed on silica with an ethyl acetate/ethanol mixture (2:1) containing 1% triethylamine as the eluant. The product was isolated as an off-white solid. The product **27** was then recrystallized, as colorless rods, from chloroform and then addition of hexanes, (105 mg, 41 %). M.p. 240-242 ˚C; $^1$H NMR ($\delta_H$; 200 MHz, $CDCl_3$): 8.28 (d, J = 1.6Hz, 4H), 8.25 (d, J = 3Hz, 4H), 7.23 (dd, J = 1.6Hz, J = 2.8Hz, 4 H), 7.14 (s, 4H), 6.03 (d, J = 7.4Hz, 4H), 4.88 (t, J = 8Hz, 4H), 4.62 (d, 7.4Hz, 4H), 2.28 – 2.35 (m, 8H), 1.43 – 1.36 (m, 24H), 0.98 – 0.91 (m, 12 H); $^{13}$C NMR ($\delta_H$; 200 MHz, $CDCl_3$): 155.46,

155.05, 144.59, 138.54, 137.48, 122.44, 120.69, 120.13, 112.63, 98.43, 94.09, 84.00, 55.67, 36.53, 31.84, 29.50, 27.42, 22.66, 14.07.

### *6.2.2 Synthetic challenges*

An optimum yield was achieved in the synthesis of **23**, when precursor **19** was totally free of solvent or moisture. Accordingly, precursor **19** was kept under high vacuum for 24 hours while being heated ~125 °C, to remove excess moisture, before it was added to the reaction mixture. Additionally, new sure-seal bottles of *n*-butyl lithium and molecular iodine where used immediately upon opening.

### *6.2.3 Crystallizations*

#### *6.2.3.1 C-pentyltetrabromocavitand, 19; C-pentyltetrabromocavitand 19(1); C-pentyltetra(3-pyridyl)cavitand, 20; C-pentyltetra(3-pyridyl)cavitand, 20(1)*

Crystals suitable for single-crystal X-ray crystallography, of **19** were grown by slow evaporation of an acetonitrile solution at room temperature over one day. Crystals suitable for single-crystal X-ray crystallography, of **19(1)** were grown by slow evaporation of a dichloromethane solution at room temperature over one day. Crystals suitable for single-crystal X-ray crystallography, of **20** were grown by slow evaporation of an acetonitrile solution at room temperature over one day. Crystals suitable for single-crystal X-ray crystallography, of **20(1)** were grown by slow evaporation of a methanol solution at room temperature over two days.

#### *6.2.3.2 C-pentyltetra(3-pyridyl)cavitand:4-cyanobenzoic acid, 20a*

*C*-pentyltetra(3-pyridyl)cavitand (10 mg, 0.05 mmol) and 4-cyanobenzoic acid (63 mg, 0.30 mmol) were placed in a beaker containing ethanol (10 mL) and heated until a clear homogeneous solution was obtained. After one day of slow evaporation, yellowish/orange prism-shaped crystals were obtained. M.p. 155-157 °C; IR (KBr pellet) $\upsilon$ 3331 and 3198 $cm^{-1}$ ($NH_2$, m), 2442 and 1912 $cm^{-1}$ (O-H···N, br), 1635 $cm^{-1}$ (C=O, m).

#### *6.2.3.3 C-pentyltetra(3-pyridyl)cavitand:C-pentyltetra(4-carboxyphenyl)cavitand:1,4-diiodobenzene, 20b*

*C*-pentyltetra(3-pyridyl)cavitand (10 mg, 0.01 mmol), *C*-pentyltetra(4-carboxyphenyl)cavitand (15 mg, 0.01 mmol), and 1,4-diiodobenzene (40 mg, 0.12 mmol)

were placed in a beaker containing ethanol and heated until a clear homogeneous solution was obtained. After five days of slow evaporation, colorless block-shaped crystals were obtained. M.p. > 285 °C; IR (KBr pellet) $\upsilon$ 2925, 2853, 2510, 1931, 1696, 1465, 1408, 1276, 1081, 973. Anal. Calcd. for $C_{152}H_{156}N_4O_{24}I_2$: C, 68.21; H, 5.83; N, 2.09. Found: C, 69.18; H, 5.99; N, 2.2

#### *6.2.3.4 C-pentyltetra(4-carboxyphenyl)cavitand, 21; C-pentyltetraboronic acid pinacolyl ester cavitand, 22; C-pentyltetraiodocavitand, 23; C-pentyltetra(3-ethynylpyridine)cavitand, 24*

Crystals suitable for single-crystal X-ray crystallography, of **21** were grown by slow evaporation of an ethanol solution at room temperature over one day. Crystals suitable for single-crystal X-ray crystallography, of **22** were grown by slow evaporation of a hexanes/dichloromethane solution at room temperature over one day. Crystals suitable for single-crystal X-ray crystallography, of **23** were grown by slow evaporation of an acetronitrile solution at room temperature over one day. Crystals suitable for single-crystal X-ray crystallography, of **24** were grown by slow evaporation of an acetonitrile solution at room temperature over one day.

#### *6.2.3.5 C-pentyltetra(2-amino-5-ethynylpyridine)cavitand:3,5-dinitrobenzoic acid, 25a*

*C*-pentyltetra(2-amino-5-ethynylpyridine)cavitand (10 mg, 0.05 mmol) and 3,5-dinitrobenzoic acid (21 mg, 0.10 mmol) were placed in a beaker containing a solution of acetonitrile, ethanol, *p*-xylenes and nitrobenzene (5:10:1:1 mL) and heated until a clear yellow homogeneous solution was obtained. After one day of slow evaporation, yellowish/orange prism-shaped crystals were obtained. M.p. 155-157 °C; IR (KBr pellet) $\upsilon$ 3331 and 3198 $cm^{-1}$ ($NH_2$, m), 2442 and 1912 $cm^{-1}$ (O-H···N, br), 1635 $cm^{-1}$ (C=O, m).

#### *6.2.3.6* C*-pentyltetra(2-amino-5-ethynylpyridine)cavitand:glutaric acid, 25b*

*C*-pentyltetra(2-amino-5-ethynylpyridine)cavitand (10 mg, 0.05 mmol) and glutaric acid (21 mg, 0.10 mmol) were placed in a beaker containing a solution of ethanol, *p*-xylenes and nitrobenzene (10:1:1 mL) and heated until a clear yellow homogeneous solution was obtained. After one day of slow evaporation, yellowish/orange prism-shaped crystals were obtained. M.p. 155-157 °C; IR (KBr pellet) $\upsilon$ 3331 and 3198 $cm^{-1}$ ($NH_2$, m), 2442 and 1912 $cm^{-1}$ (O-H···N, br), 1635 $cm^{-1}$ (C=O, m).

## 6.3 Results and Discussion

### *6.3.1 Cross-coupling reaction precursors and their tetra-functionalized products*

Crystallographic information for **19**, **19(1)**, **20**, **20(1)**, **20a-20b**, **21-24**, **25a-25b** is displayed in Tables B.5.

The synthesis of cavitand precursor **19** was achieved in good yields following three well-established steps beginning with the acid-catalyzed cyclocondensation of resorcinol and hexanal generating the calix[4]resorcinarene molecule.[18] This compound is then brominated with N-bromosuccinamide, forming the tetrabrominated calix[4]resorcinarene.[19] The tetrabrominated calix[4]resorcinarene is then deepened and rigidified by 4-fold cyclizations with treatments of bromochloromethane, producing the final bromo-functionalized cavitand precursor **19**.[18]

The structure determination of **19**, Figure 6.5, shows that one guest molecule of acetonitrile is positioned at the lower-rim of the cavitand, surrounded by the pentyl-feet.

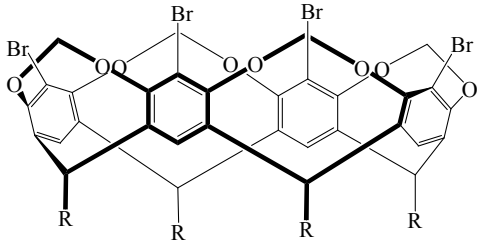


$R = (CH_2)_4CH_3$

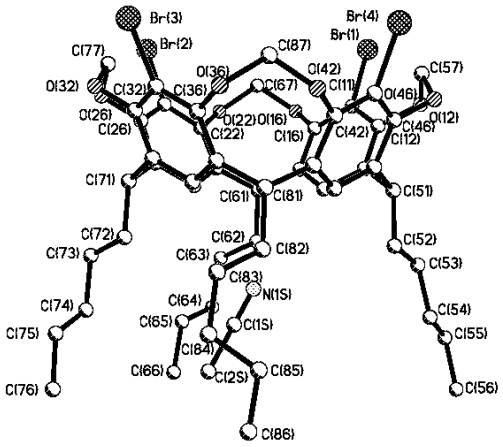


**Figure 6.5** Molecular structure and thermal ellipsoids (50% probility level) of the tetrabromo cavitand in the crystal structure of **19**.

The cavitands are organized into 1-dimensional strands as a result of the interaction between one of the pentyl-feet and the upper-rim of a neighboring cavitand, Figure 6.6a, furthermore, cavitands in neighboring strands are arranged in anti-parallel dimers organized via a pair of very short and symmetry related Br···Br interactions, 3.470 Å, Figure 6.6b.

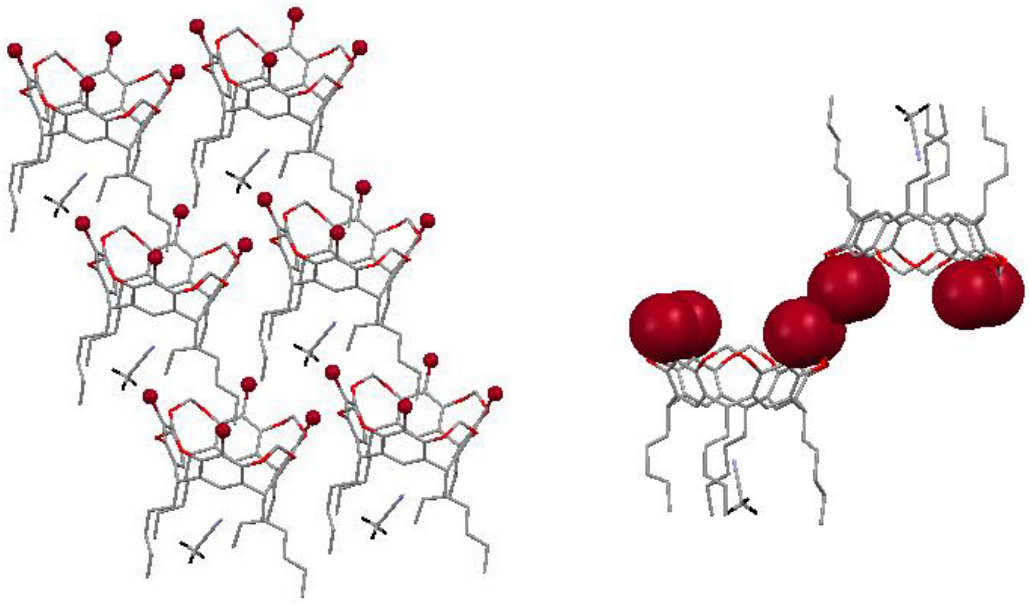

**(a)** **(b)**

**Figure 6.6** (a) Packing of cavitand **19**; (b) Neighboring cavitands linked through short Br···Br interactions in cavitand **19**. The hydrogen atoms have been removed, except on the acetonitrile solvent molecules, for clarity.

If **19** is recrystallized from dichloromethane instead of acetonitrile however, a cavitate **19(1)** is formed where the guest molecule resides outside the host-cavitand framework. However, regardless of the location of the guest, neighboring hosts are arranged into 1-dimensional strands where one of the pentyl-feet is dipping into the upper-rim of a neighboring cavitand, Figure 6.7a. One of the "feet" of the cavitand in **19(1)** does display a gauche conformation, but although unusal, such configurations are not rare,[20] and it is difficult to point directly at what may cause this geometry. The crystallographic screw axis is essentially perpendicular to the two 1-D strands shown in Figure 6.7, which means that the cavitands are not all pointing in the same direction. Furthermore, two symmetry-related pairs of Br···Br interactions, 3.349 Å and 3.676 Å, respectively, also play an important role in positioning adjacent cavitands into an extended up-and-down arrangement (running parallel with *a*), Figure 6.7b.

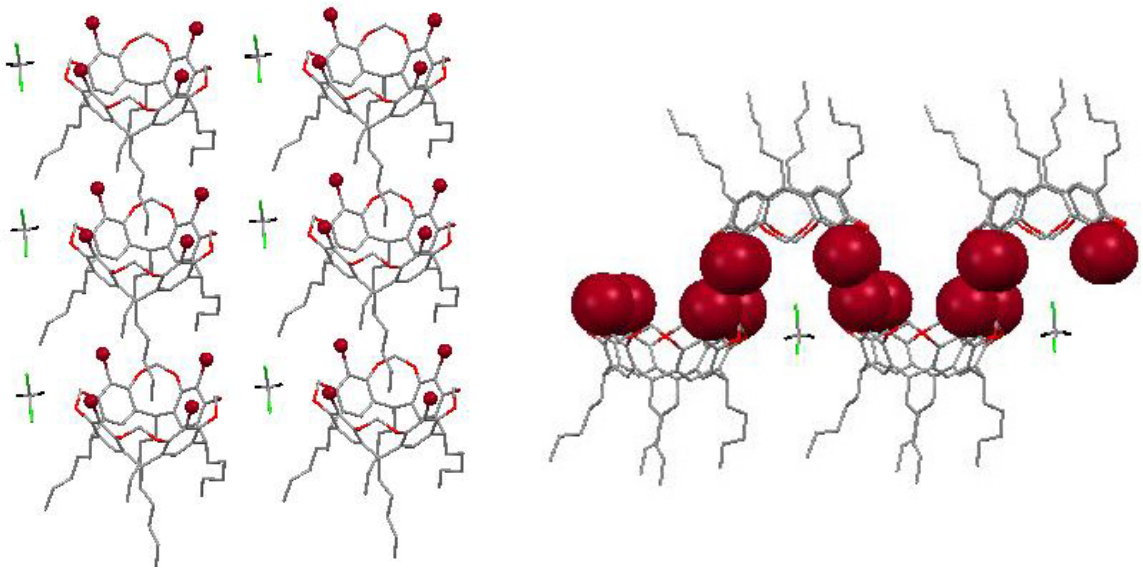

**(a)** **(b)**

**Figure 6.7** (a) Packing of cavitand **19(1);** (b) Adjacent hosts in cavitand **19(1)** linked via multiple Br···Br interactions. The hydrogen atoms have been omitted, except from the dichloromethane solvent molecules, for clarity.

Within the last five years, the palladium-catalyzed Suzuki-Miyaura cross-coupling reaction, has been utilized multiple times in the synthesis of functionalized resorcinarene-based cavitand receptor molecules.[16a, 21] In all reports, except one, the cavitand was tetrahalogenated (I or Br) and cross-coupled with a substituted (*e.g.* pyridyl, benzonitrile, or methoxyphenyl) aryl boronic acid or ester. In the one exception, the tetraboronic acid cavitand was formed and cross-coupled with 3-bromopyridine.

With the tetra-bromo cavitand precursor **19** synthesized and fully characterized, multiple Suzuki-Miyaura cross-coupling reactions were carried out.[22] The desired pyridyl-functionalized cavitand was synthesized by cross-coupling cavitand **19** and excess 3-pyridyl boronic acid under a basic media, Figure 6.8.

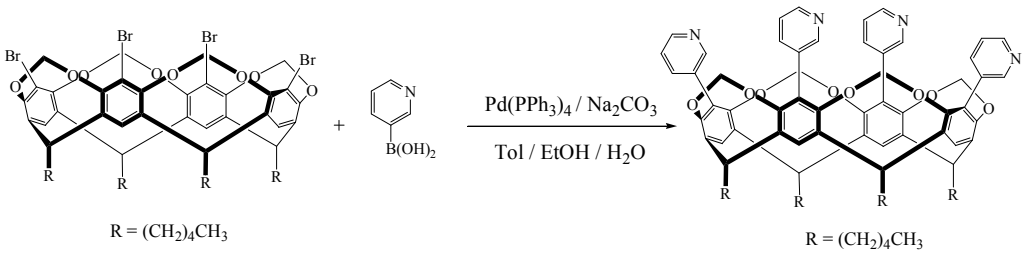


**Figure 6.8** Synthesis of *C*-pentyltetra(3-pyridyl)cavitand **20**.

It should be noted that cavitands similar to **20**, *C*-heptyltetra(3-pyidyl) and *C*-phenylethyltetra(3-pyridyl)cavitands, have been reported in the literature[16a] however, overall yields of these cavitands were 23% and 20%, respectively. In those cases, the synthesis was achieved by converting a tetra-bromo cavitand to the desired tetraboronic acid followed by reaction with 3-bromopyridine.

The structure determination of **20**, Figure 6.9, shows one py-cavitand and three acetonitrile molecules, although the asymmetric unit contains only one-half of a cavitand and three-half solvent molecules.

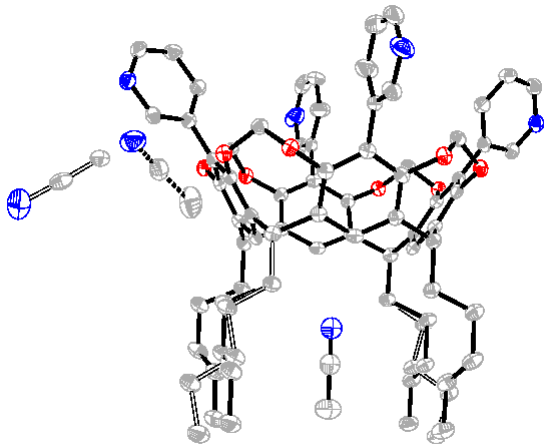

**Figure 6.9** Thermal ellipsoid plot (50% probability level) of py-cavitand **20**. The blue spheres represent nitrogen atoms, while the red spheres are oxygen atoms. The hydrogen atoms have been removed for clarity.

Suitable crystals were also obtained when cavitand **20** was recrystallized from methanol instead of acetonitrile. The asymmetric unit **20(1)** contains two py-cavitands and seven methanol solvent molecules, Figure 6.10.

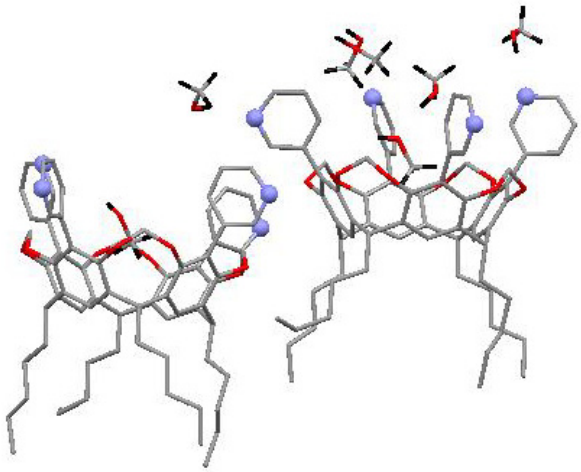

**Figure 6.10** Asymmetric unit of **20(1)** with the hydrogen atoms removed, except on the methanol solvent molecules, for clarity. The pyridyl nitrogen atoms are represented as light-blue spheres.

To complement the existing tetra-pyridyl functionalized cavitand, a tetra-substituted carboxyphenyl-derivatized cavitand was generated, following similar reaction conditions, Figure 6.11.

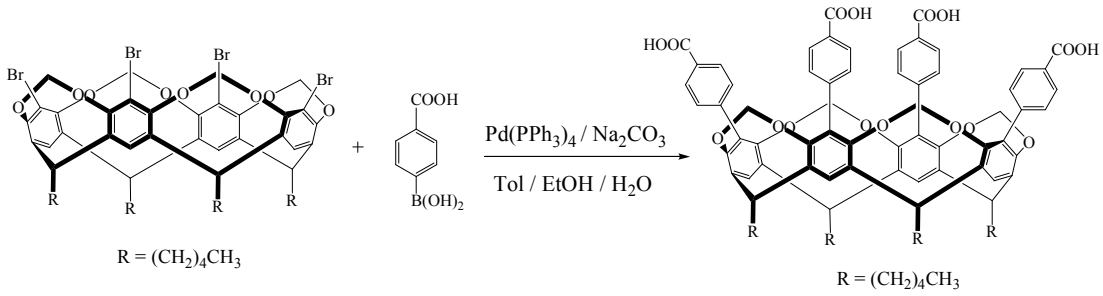


**Figure 6.11** Synthesis of *C*-pentyltetra(4-carboxyphenyl)cavitand **21**.

The structure determination of **21**, Figure 6.12, displays the tetra-carboxyphenyl functionalized cavitand. Due to poor quality diffraction data and heavy disorder around the ethanol solvent molecules, exact location of the carboxylic acid protons and solvent molecules cannot be determined.

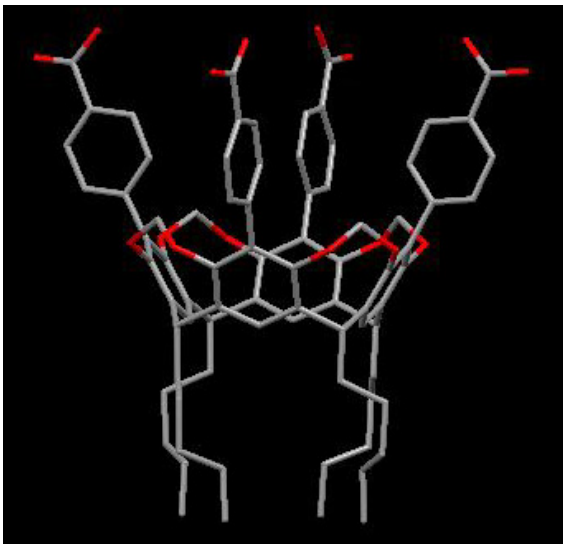

**Figure 6.12** Tetra-carboxyphenyl functionalized cavitand **21** with the alkyl and aromatic hydrogens omitted for clarity.

Extension of the architecture, reveals the multiple acid···acid homomeric dimers (O···O distance, 2.610 Å) produced from each carboxylic acid moiety, which links the neighboring cavitands in a 2-dimensional sheet through an up-down-up-down repeating pattern, Figure 6.13.

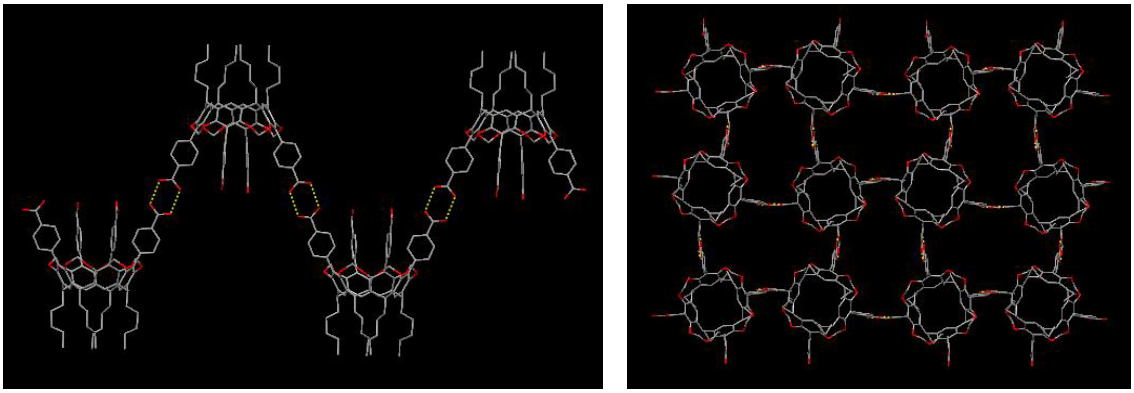

**Figure 6.13** Linking of neighboring cavitands through acid···acid dimers to produce a 2-D wave-like sheet.

The formation of polymeric capsules arises, upon stacking two sheets on top of one another. One sheet has the cavitands arranged in an up-down-up fashion, while the second sheet stacks in a down-up-down arrangement, Figure 6.14.

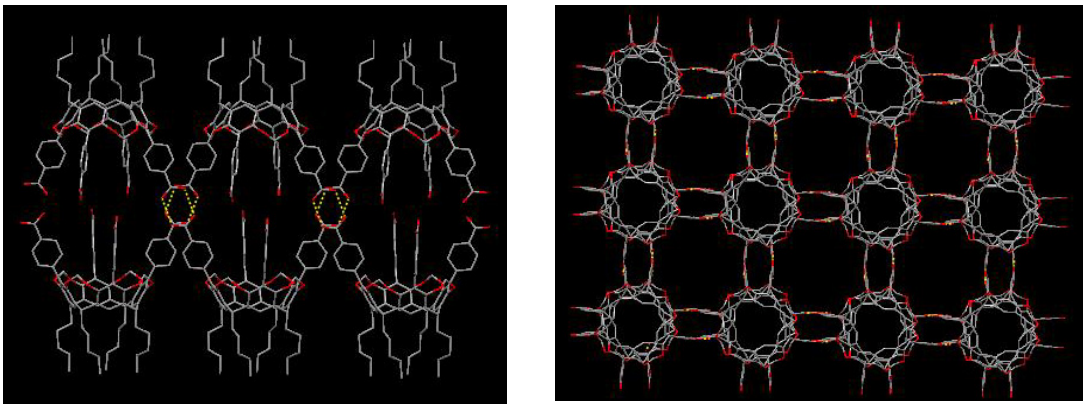

**Figure 6.14** Side-view of the polymeric network (left) and a top-view of the two independent sheets forming the polymeric capsules (right).

So far we have described the synthesis and characterization of tetrahalogenated cavitands and examined their ability to act as palladium catalyzed cross-coupling reactants with aryl boronic acids. We believe the limited number of functional groups appended to various cavitands, can be attributed to the relatively small number of inexpensive boronic acids and esters commercially available. However, if the cavitand was appended with the corresponding boronic acid or ester moiety, then a wider range of functionalized halogenated species are available for cross-coupling.

The synthesis of cavitand **22** was achieved in good yields ~70%, following a modified procedure.[23] It should be noted, in that case, the goal was to only convert two of the four bromine atoms into the pinacolyl borornate derivatives. In our case, *C*-pentyltetrabromo cavitand was allowed to react with 4.6 eq. of *n*-butyllithium at –78 °C for 0.5h resulting in a tetra lithium-halogen exchange. To this reaction 6 eq. of trimethoxyborane was added and the reaction was allowed to reach room temperature after 0.5h. The mixture was acidified with hydrochloric acid, producing the tetraboronic acid cavitand, which was converted to the desired tetraboronic pinacolyl ester cavitand **22**, by addition of excess pinacol and magnesium sulfate, Figure 6.15. Purification was carried out by dissolving the reaction mixture in dichloromethane and adding excess acetone, in which a white precipitate formed and was isolated.

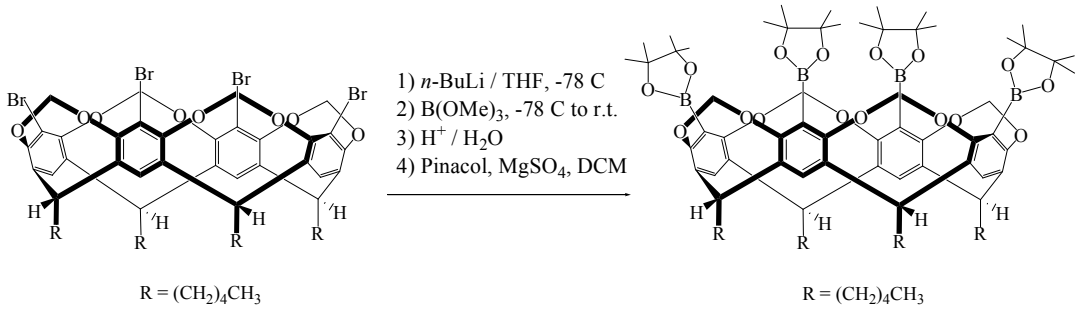


**Figure 6.15** Synthesis of tetraboronic pinacolyl ester cavitand **22**.

The structure determination of **22**, shows one tetraboronic pinacolyl ester cavitand and two hexanes molecules. The disorder around one boronic pinacolyl ester and both hexanes molecules has been omitted for clarity. One hexanes solvent molecule resides within the 'upper-cavity', while the second solvent molecule resides outside the cavitand, filling space within the crystalline lattice. Additionally, each of the pinacolyl ester fragments resides almost perpendicularly to the periphery of the upper-rim, due to electron-electron repulsion from the bridging oxygens of the cavitand, Figure 6.16a-b.

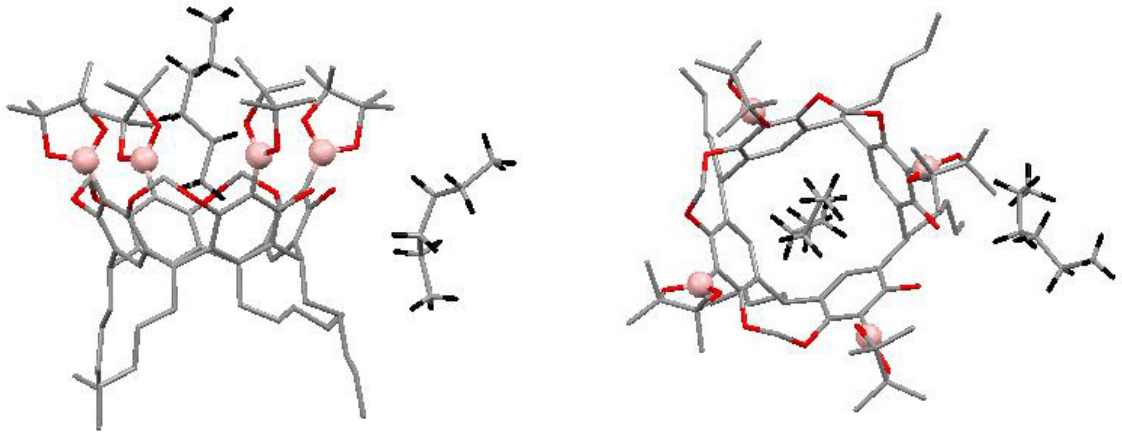

**Figure 6.16** (a) Side view of the asymmetric unit of **22**; (b) Top view displaying one hexane solvent molecule residing in the cavity of cavitand **22**, while one resides outside. Both pictures are with the hydrogen atoms removed, except on the hexane solvent molecules, for clarity. The boron atoms are represented as light-pink spheres.

Multiple palladium catalyzed cross-coupling reactions were carried out between tetraboronic pinacolyl ester cavitand, **22** and halogenated heterocyles, however, at this time,

successful coupling has not been achieved and further investigation into the reaction conditions *i.e.* catalyst, solvent, temperature, duration is needed.

In order to advance the synthesis of other functionalized cavitands, through palladium-catalyzed cross-coupling reactions, some additional covalent modifications needed to be carried out. We found no success in cross-coupling *C*-pentyltetrabromocavitand **19** and mono-ethynylated species under the Sonogashira reaction conditions, however improved coupling was achieved upon exchange of the bromine atoms for iodine atoms. Furthermore, the tetraiodo cavitand **23**, was synthesised by treating its tetrabromo analog with *n*-BuLi followed by addition of iodine.[24] Purificiation was carried out by silica-gel column chromatography and recrystallization from acetonitrile.

The crystal structure determination of **23**, Figure 6.17, reveals that one molecule of acetonitrile is located between the 'feet' of the host, with the nitrile end pointing up towards the equator of the host.

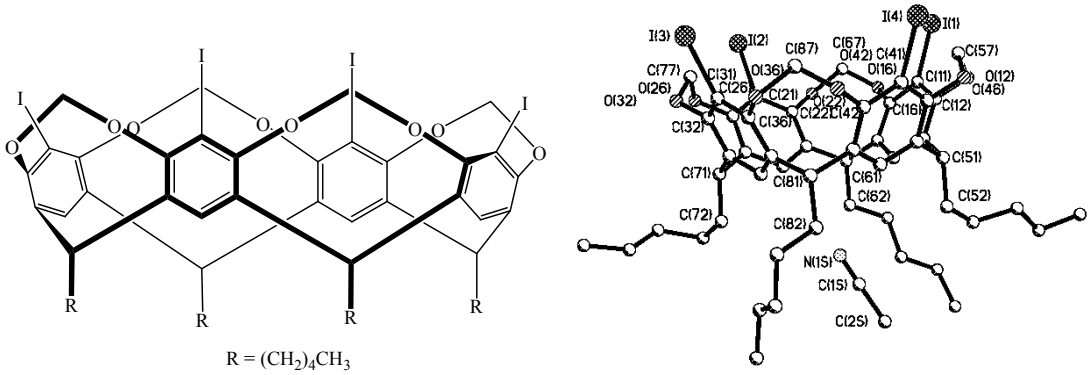


**Figure 6.17** Molecular structure and labeled thermal ellipsoids (50% probability level) of tetraiodo cavitand in the crystal structure of **23**.

The extended architecture of **23**, displays a 'foot-in-mouth' type of arrangement, where one of the pentyl-feet is resting in the upper-rim of an adjacent molecule, Figure 6.18.

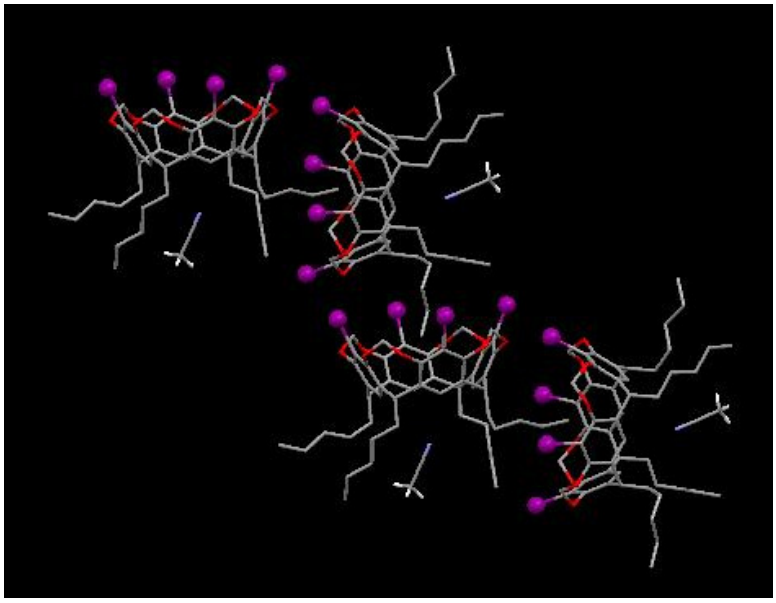

**Figure 6.18** Packing of molecule **23**. The hydrogen atoms have been removed, except on the acetonitrile solvent molecules, for clarity. The iodine atoms are represented as purple spheres.

To date, there are only six reported crystal structures,[25] of similar neutral host molecules where the upper-rim is tetra-substituted with halogen atoms and a lower-rim comprising of alkyl chains. However, none of these, except our previous examples, pack in a fashion where a 'foot' of one cavitand resides in the 'mouth' of a neighboring cavitand molecule. A search through the CSD reveled twenty-three hits when including cavitands with any type of tetra-substituted upper rim in combination with an alkyl-substituted lower-rim. However, none of these display the 'foot-in-mouth' arrangement observed in the crystal structures **19**, **19(1)**, and **23**. In one case, however, the upper-rim substituents interact with the 'mouth' of an adjacent cavitand molecule.[26]

With the complete synthesis and full characterization of the tetraiodo cavitand **23**, several palladium-catalyzed Sonogashira cross-coupling reactions were carried out. The desired pyridyl-functionalized cavitand **24** was synthesized under conventional palladium-catalyzed Sonogashira reaction conditions between **23** and 3-ethynylpyridine under basic media. Purification was achieved by silica-gel column chromatography. Recrystallization from a mixture of chloroform and hexanes yielded 67% of pure cavitand **24**.

The structure determination of **24**, shows the presence of one disordered molecule of acetonitrile (located within cavity), and two water molecules, which engage in multiple hydrogen bonds with the pyridyl-nitrogen atoms on the upper rim of the host, Figure 6.19.

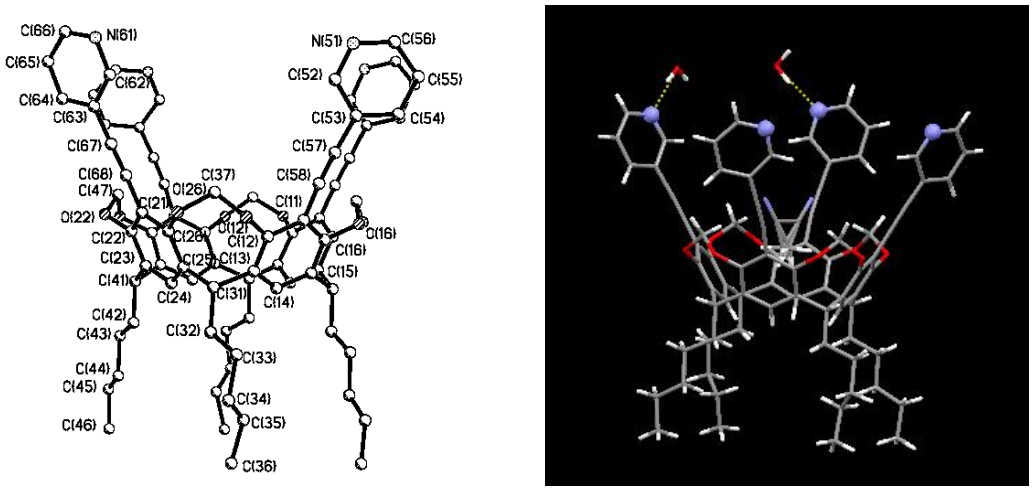


**Figure 6.19** Labeled molecular structure and molecular structure **24** displaying the disordered acetonitrile molecule in the center of the host and the two water molecules forming O-H···N hydrogen bonds to the pyridyl rings (blue spheres).

One of the water molecules in the crystal structure of **24** is responsible for linking the cavitands into one-dimensional rows, via symmetry related O-H···N hydrogen bonds, (O···N 2.8644(15) Å), Figure 6.20a. The second water molecule provides a bridge between the 1-D strands through symmetry-related O-H···N hydrogen bonds (O···N 2.912(2) Å), resulting in a two-dimensional "wavy" network, Figure 6.20b.

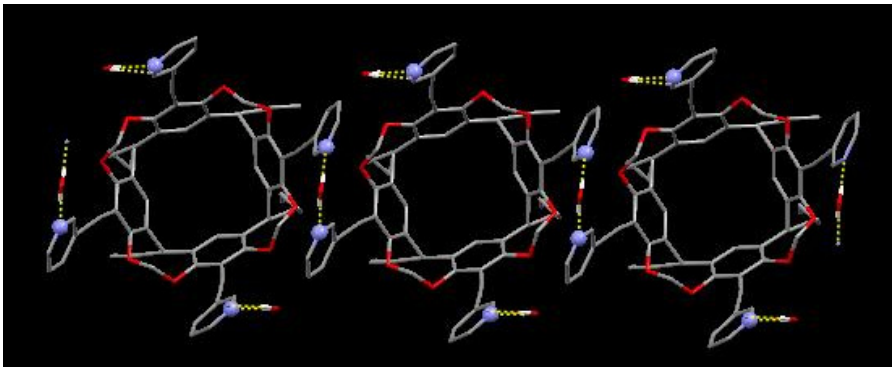

**(a)**

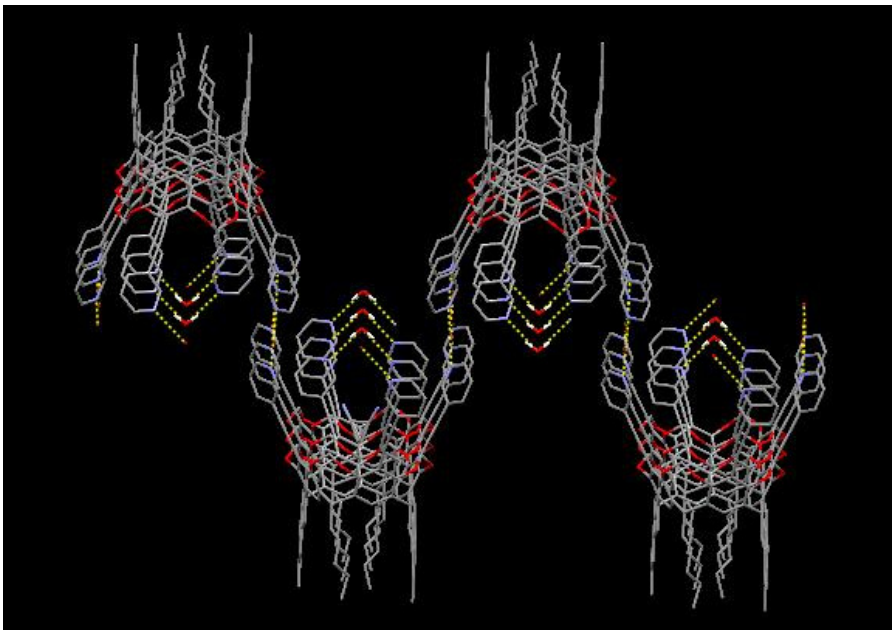

**(b)**

**Figure 6.20** (a) One-dimensional strands of **24** formed through O-H···N hydrogen bonds from bridging water molecules. (b) Side-on view of the extended architecture. Both pictures are displayed with the solvent and hydrogen atoms omitted for clarity, except on the water molecules.

Another potentially useful and versatile building block for the construction of a wide range of heterodimeric hydrogen-bond based capsules, is *C*-pentyltetra(2-amino-5-ethynylpyridine)cavitand. Once again, under palladium-catalyzed Sonogashira cross-coupling conditions, 5-ethynyl-2-aminopyridine and *C*-pentyltetraiodo cavitand **23** coupled smoothly to generate **25** in moderate to good yields ~ 74%, Figure 6.21.

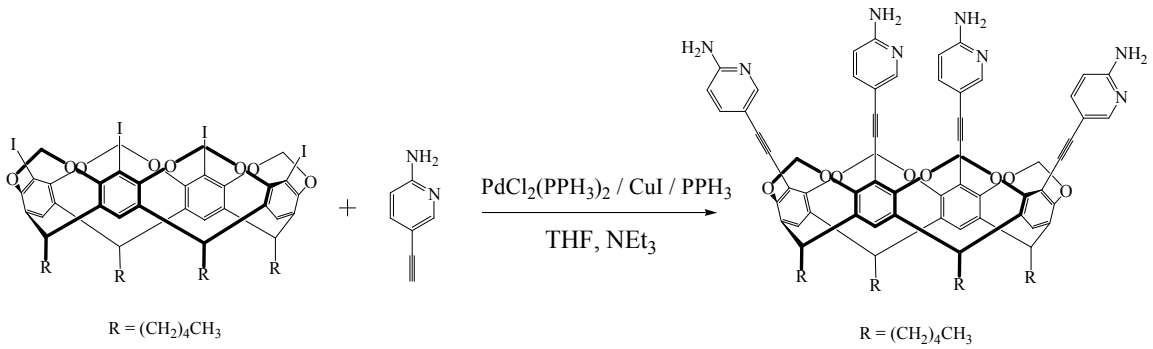


**Figure 6.21** *C*-pentyltetra(2-amino-5-ethynylpyridine)cavitand **25** synthesized through conventional Sonogashira reaction conditions.

Unfortunately, single-crystals of cavitand **25** were not obtained, however the amino-pyridine substituted cavitand will be used in the assembly process to form heteromeric-driven supermolecules with suitably functionalized counterparts.

### *6.3.2 Heteromeric-synthon driven multi-component cavitand-based supermolecules*

In order to design heteromeric multi-component hosts where hydrogen bonds are employed as the synthetic avenues for organizing individual building blocks into the appropriate configurations, we allowed our functionalized cavitands to self-assemble with the corresponding hydrogen-bond counterparts. We were initially interested in the versatility and strength of the pyridyl-functionalized cavitands to form heteromeric hydrogen bonds with mono-carboxylic acids through each of the pyridyl moieties. Thus, we allowed excess 4-cyanobenzoic acid to react with the pyridyl-functionalized cavitand **20**. Crystals of **20a** suitable for X-ray single-crystal diffraction were grown by slow evaporation from a saturated solution of ethanol at room temperature. Surprisingly, only one 4-cyanobenzoic acid molecule forms hydrogen bonds (O···O, 2.546 Å), through acid···pyridine interactions, to a pyridyl moiety of the tetrapyridyl cavitand, Figure 6.22a. Due to low quality of the data, from solvent disorder and crystal size, exact hydrogen atom location on the carboxylic acid cannot be determined. The extended network is comprised of 1-D columns, with the cyano-benzyl fragment resting in the feet region of the above cavitand, Figure 6.22b.

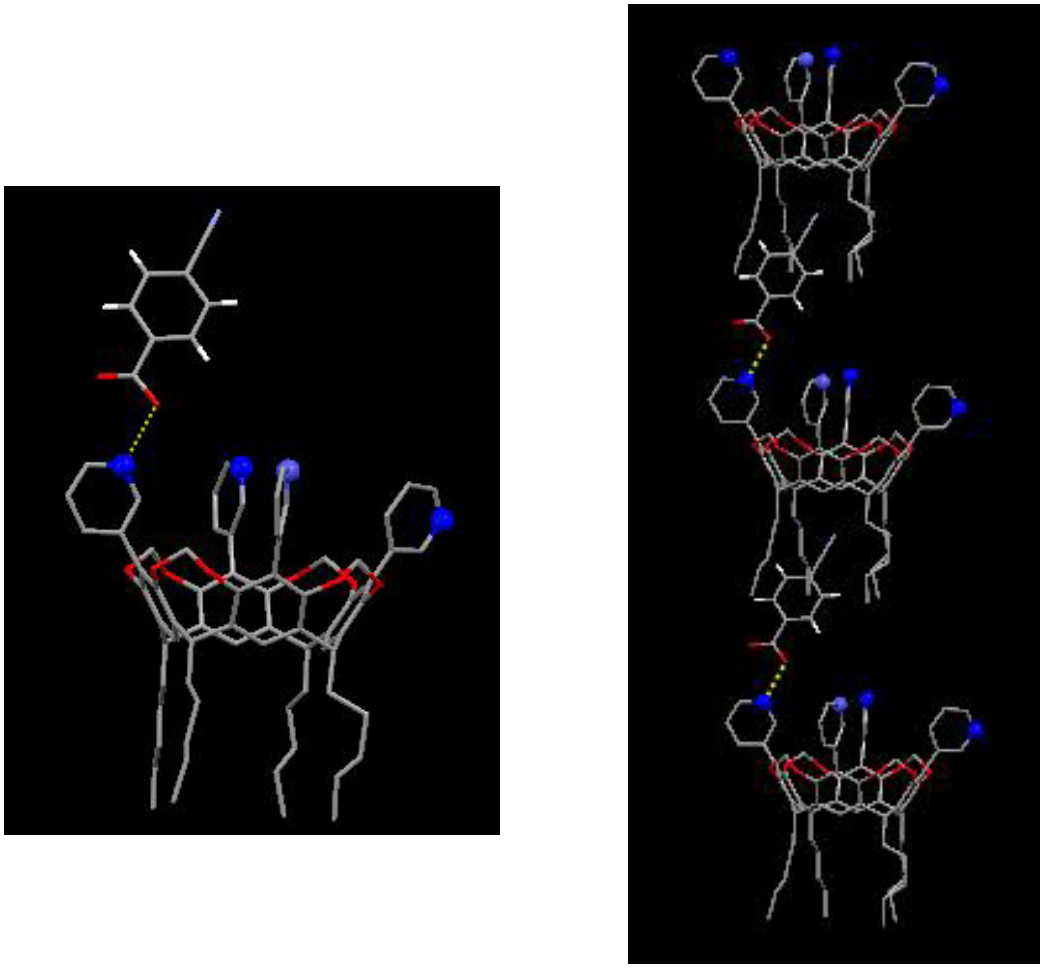

**(a)** **(b)**

**Figure 6.22** (a) Two-component supermolcule formed through a carboxylic acid/pyridine heteromeric synthon (hydrogen atoms on the cavitand have been omitted for clarity); (b) Molecular packing of neighboring 1:1 pyridyl-cavitand/acid complexes.

Although the overall result was not exactly as expected, we realized that the introduction of a moiety, in which strong complementary interactions could proceed, might be necessary in order to bring multiple components into a single crystalline lattice.

Thus, to explore the versatility and hydrogen-bonding capabilities of the four 2-aminopyridine moieties appended to **25**, an excess of 3,5-dintrobenzoic acid was presented to the cavitand in order to ensure that all four binding sites were simultaneously engaged by a complementary chemical functionality. Suitable single crystals were grown by slow evaporation from a mixture of solvents including acetonitrile, ethanol, nitrobenzene, and *p*-xylene (5:10:1:1).

The crystal lattice of **25a** contains four 3,5-dinitrobenzoic acid molecules and three molecules of acetonitrile for every cavitand **25**. Each 2-aminopyridine moiety participates in a pair of O-H···N/N-H···O hydrogen-bonds with a neighboring carboxylic acid, Figure 6.23. The O-H···N and N-H···O hydrogen bonding distances are 2.558 (8) Å, 2.582 (10) Å, 2.703 (8) Å, 2.579 (9) Å and 2.765 (9) Å, 2.863 (12) Å, 2.724 (9) Å, 2.878 (9) Å, respectively.

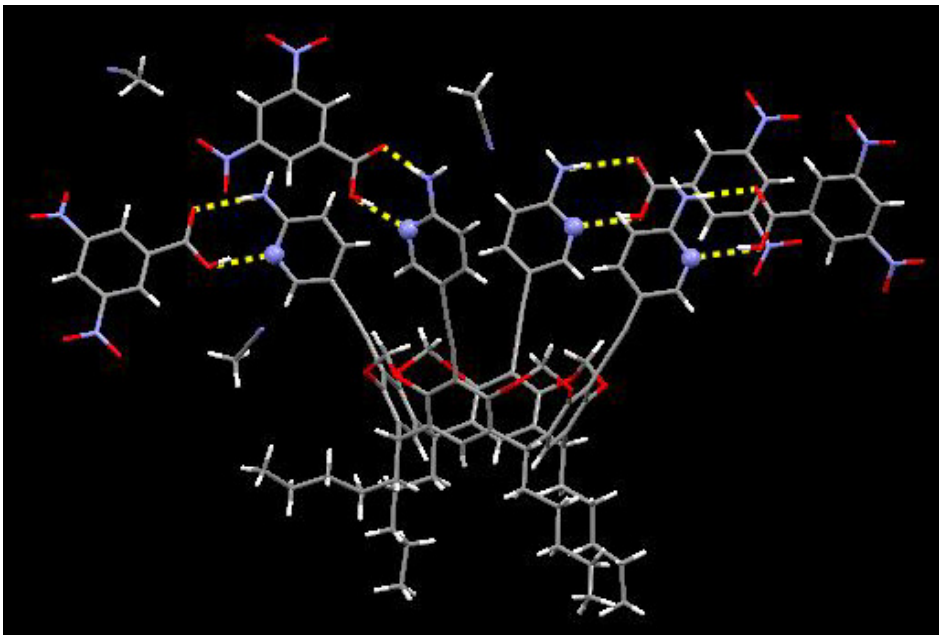

**Figure 6.23** A pentameric supermolecule in **25a** produced by four 3,5-dinitrobenzoic acid molecules forming O-H···N and N-H···O hydrogen bonds with each cavitand **25** (three acetonitrile molecules are also shown). Blue spheres indicate the pyridyl-nitrogen atoms.

This result displayed the versatility and strength of the amino-pyridine functionality in its ability to attract and bond multiple carboxylic acid moieties, compared to the pyridine moiety.

**Table 6.1** Hydrogen bonds for **25a** [Å and °].

| D-H...A | d(D-H) | d(H...A) | d(D...A) | <(DHA) |
|---|---|---|---|---|
| O411-H411...N211 | 0.84 | 1.74 | 2.558(8) | 164.2 |
| O412-H412...N212 | 0.84 | 1.75 | 2.582(10) | 170.6 |
| O413-H413...N213 | 0.84 | 1.88 | 2.703(8) | 168.0 |
| O414-H414...N214 | 0.84 | 1.76 | 2.579(9) | 163.5 |
| N221-H22A1...O421 | 0.88 | 1.89 | 2.765(9) | 176.8 |
| N222-H22A2...O422 | 0.88 | 2.06 | 2.863(12) | 151.7 |
| N223-H22A3...O423 | 0.88 | 1.85 | 2.724(9) | 169.7 |
| N224-H22A4...O424 | 0.88 | 2.01 | 2.878(9) | 171.1 |

It seemed reasonable, due to the increased hydrogen-bonding strength and directionality between the amino-pyridine and carboxylic acid moieties, that upon mixing cavitand **25** with a dicarboxylic acid, a molecular capsule composed of two cavitands (top and bottom) and four dicarboxylic acids (equatorial-belt) could assemble through multiple heteromeric N-H···O/O-H···N hydrogen bonds. Some elegant examples exist of molecular capsules, in which two individual cavity bearing hosts and four linking units, are brought together into discrete entities through hydrogen bonding. One such effort employed two carboxylic acid functionalized cavitands and four 2-aminopyrimidine molecules through sixteen complementary O-H···N/N-H···O hydrogen bonds[27], while another utilized O-H···N hydrogen bonds in order to assemble *C*-methylcalix[4]resorcinarene and 4,4'-bipyridine into a molecular capsule[28], Figure 6.24.

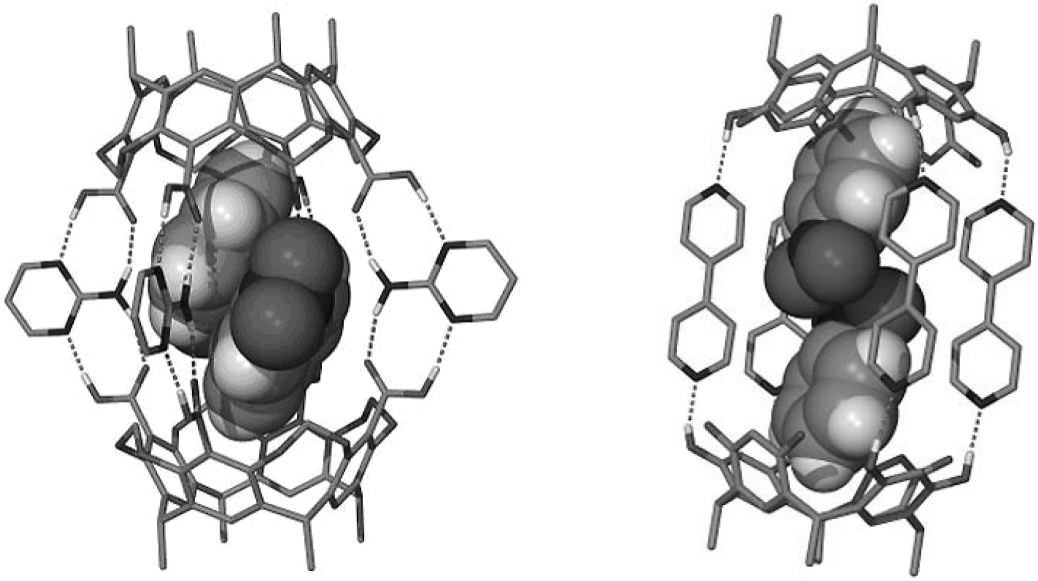

**(a)** **(b)**

**Figure 6.24** (a) Molecular capsule assembled through multiple hydrogen bonds between two carboxylic acid cavitands and four 2-aminopyrimidine molecules; (b) Multi-component system composed of a resorcinarene derivative and 4,4'-bipyridine.[29]

Our design strategy consists of linking two cavitand **25** molecules and four alkyl dicarboxylic acids through eight complementary heteromeric O-H···N/N-H···O hydrogen bonds. Thus cavitand **25** was allowed to self-assemble with a variety of alkyl dicarboxylic acids, in which one sample containing glutaric acid produced suitable crystals **25b** for X-ray diffraction.

The crystal structure determination of **25b** shows that the product contains two glutaric acid molecules and several solvent molecules (*p*-xylene and acetonitrile) for each cavitand **25**. Each ethynyl 2-aminopyridine arm is engaged in a heteromeric O-H···N/N-H···O motif with an adjacent carboxylic acid moiety, Figure 6.25a. The acid···pyridine hydrogen bonds do not produce a discrete hexameric assembly, instead a polymeric network is formed through multiple carboxylic acid···amino-pyridine hydrogen bonds, Figure 6.25b.

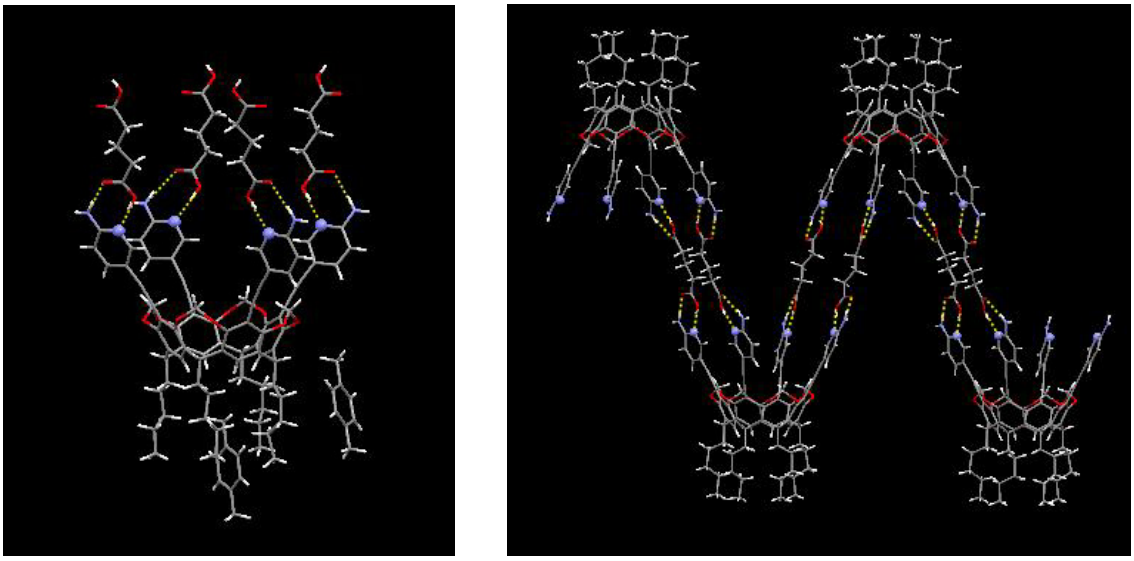

**(a)** **(b)**

**Figure 6.25** (a) Each binding site on **25b** forms a heteromeric interaction with a carboxylic acid moiety. Picture shows both *p*-xylenes solvent molecules; (b) Side-on view of the polymeric network of **25b**. Solvent molecules (*p*-xylene and acetonitrile) have been omitted for clarity.

One-dimensional strands, Figure 6.25b, are linked to neighboring strands via N-H···O hydrogen bonds (2.847 (4) Å), from the *anti*-amino proton to the carbonyl oxygen of the acid to form a two-dimensional wave-like sheet, Figure 6.26a. The two-dimensional sheets stack on top of one another, with one *p*-xylene molecule and the pentyl-feet of a neighboring cavitand residing in the upper-cavity of the cavitand beneath it, Figure 6.26b.

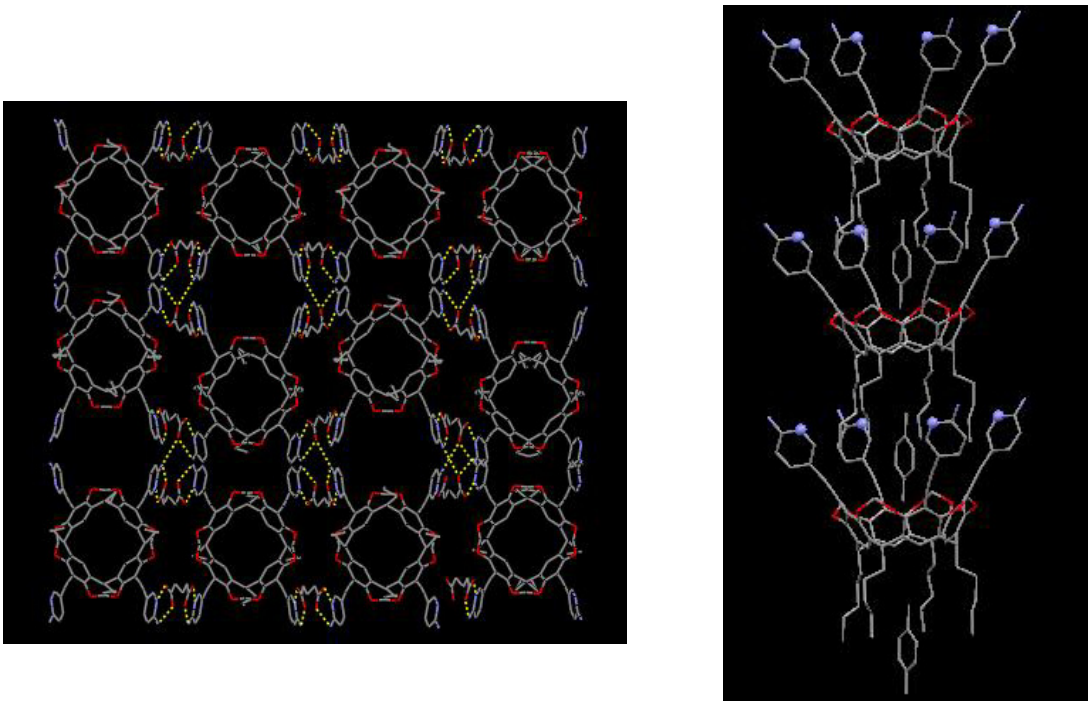

**(a)** **(b)**

**Figure 6.26** (a) Molecular packing diagram of **25b**, displaying the extensive hydrogen bonding between 1-D rows. Solvent molecules and hydrogen atoms have been removed for clarity; (b) Molecular packing of the cavitands in structure **25b**. The hydrogen atoms have been removed for clarity and the blue spheres represent the pyridyl nitrogen atoms.

**Table 6.2** Hydrogen bonds for **25b** [Å and °]

| D-H...A | d(D-H) | d(D-H) | d(D...A) | <(DHA) |
|---|---|---|---|---|
| O(1)-H(1)...N(61) | 0.84 | 1.82 | 2.652(4) | 169.0 |
| O(5)-H(5)...N(71)#2 | 0.84 | 1.84 | 2.664(4) | 165.7 |
| N(62)-H(62A)...O(2) | 0.88 | 1.94 | 2.815(4) | 173.4 |
| N(62)-H(62B)...O(6)#3 | 0.88 | 2.15 | 2.847(4) | 136.1 |
| N(72)-H(72A)...O(6)#2 | 0.88 | 2.01 | 2.878(4) | 168.6 |
| #2) -x+3,-y+1,-z+1 #3 x-1/2,y,-z+1/2 | | | | |

The question as to whether these assemblies **25a** and **25b** are held together, to some extent, by charge assisted, N-$H^{+}\cdots^{-}$OOC hydrogen bonds in the solid state is not possible to answer unambiguously. For the strucure of **25b**, it seems that all participating species are neutral as indicated by the C-N-C angle[30] of the two unique pyridyl rings (118.5 (3) and 118.0 (3) and by the C-O bond distances of the carboxylic acids (C1-O1, 1.303 (4) Å; C1-O2, 1.213 (5) Å and C5-O5, 1.304 (4) Å; C5-O6, 1.209 (4) Å). The large difference in C-O bond lengths ~ 0.09-0.095 Å and a smaller bond angle (< 120) supports the existence of a carboxylic acid moiety rather than a carboxylate.[31] Structure **25a**, is not as clear since the C-N-C angles of the pyridyl rings range from 116 to 120° and the difference betweeen the two C-O bond distances span 0.012 to 0.09 Å. A search of relevant structures in the CSD[32] show that when an amino-pyridine moiety is engaged in a heteromeric hydrogen-bond interaction with a carboxylic acid, protonation occurs (8/10) times.[31]

Surprisingly, only a handful of examples exist, in the literature, of hydrogen-bonded heterodimeric capsules composed of resorcinarene-based cavitands,[16a, 33] while only one has been characterized through single-crystal diffraction.[16a]

To expand upon previously reported data, we dissolved a 1:1 mixture of *C*-pentyltetra(3-pyridyl)cavitand and *C*-pentyltetra(4-carboxyphenyl)cavitand, with an excess of 1,4-diiodobenzene (10x) to aid as a template, in ethanol. After five days of slow evaporation crystals suitable for single-crystal X-ray diffraction **20b** were obtained. The crystalline product was intially characterized by melting point, elemental analysis and infrared spectroscopy, all confirming a 1:1 hydrogen bonded heterodimeric species. X-ray diffraction proved that the two components had indeed formed a 1:1 heteromeric molecular capsule, Figure 6.28.

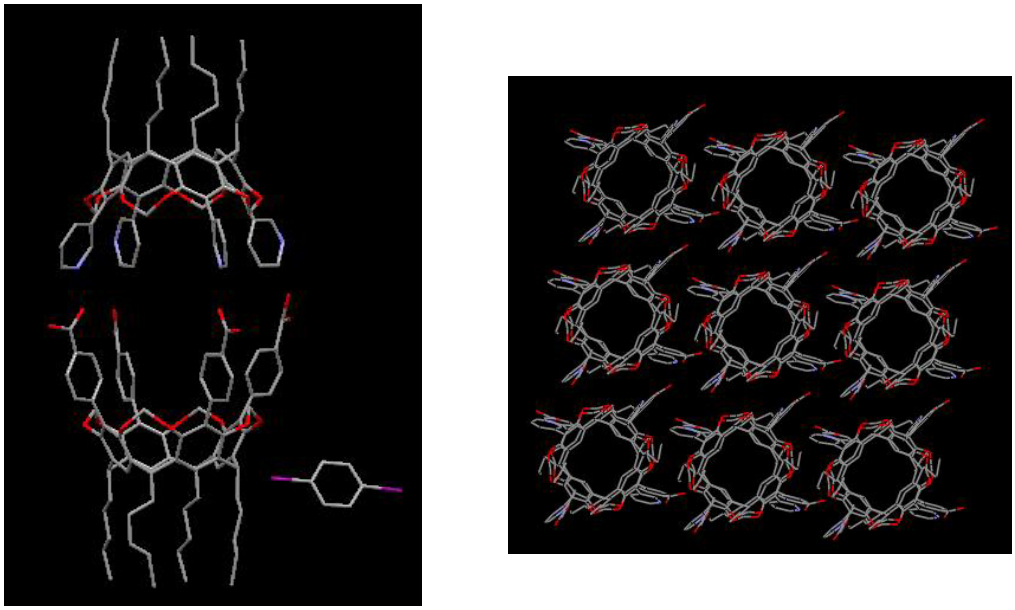

**Figure 6.27** Heterodimeric molecular capsule **20b** formed through O-H···N carboxylic acid/pyridine hydrogen bonds. The hydrogen atoms and solvent molecules have been removed for clarity.

Unfortunately, due to solvent disorder and the diiodobenzene residing on a crystallographic inversion center, refinement of the structure is not well-behaved. Furthermore, exact location of the carboxylic acid protons can not be established exactly, however short O···N contacts are observed for three of the four carboxylic acid/pyridine hydrogen bonds (027-4···N21-8, 2.921 Å; 027-2···N21-6, 2.476 Å; 027-3···N21-7, 2.545 Å). The diiodobenzene actually resides outside of the inner-cavity of the resorcinarene-based capsule. Attempts were carried out to grow crystalline materials without introducing the guest, however all were unsuccessful.

## 6.4 Conclusions

The study provides a basis for new reliable methods for the assembly of discrete molecular capsules. A variety of functionalized resorcinarene-based cavitands have been synthesized, in good yields, through either the palladium-catalyzed Suzuki-Miyaura or Sonogashira cross-coupling reaction.

The readily available pyridine and amino-pyridine decorated cavitands **21**, **24**, **25**, and **27** offer many opportunities for preparing asymmetric dimeric capsules using complementary

hydrogen-bond functionalities on different host molecules. Furthermore, the ethynyl moieties linking the rim to the pyridyl-substituents, produce increased size and depth as well as a more electron rich interior that can be utilized for selectively capturing electron poor.

The amino-pyridine appended cavitand demonstrated its usefulness and versatility in forming hydrogen bonds to either mono- or di-carboxylic acids. Cavitand **25** represents a very useful and versatile building block for the construction of a wide range of heterodimeric capsules and by combining **25** with a suitably functionalized counterpart, a series of heterodimeric capsules capable of capturing and and organizing two different guests within their interior, may be constructed.

Finally, upon mixing a pyridyl-functionalized cavitand along with a phenyl-carboxylic acid-coupled cavitand a 1:1 heterodimeric capsule is produced through complementary O-H···N hydrogen bonds. This example clearly demonstrates that heterotopic assembly can be achieved under suitable reaction conditions.

## References:


[1] (a) Lehn, J.-M.; Atwood, J. L.; Davies, J. E. D.; MacNicol, D. D.; Vögtle, F. Ed.; *Comprehensive Supramolecular Chemistry*, Pergamon: New York, 1996. (b) Lehn, J.-M. *Supramolecular Chemistry: concepts and perspectives*, VCH: Weinheim, 1995. (c) Steed, J. W.; Atwood, J. L. *Supramolecular Chemistry*, John Wiley and Sons: Ltd., Chichester, 2000.

[2] James, T. D.; Hartly, J. H.; Ward, C. J. *J. Chem. Soc, Perkin Trans. 1* **2000**, 3155.

[3] (a) Körner, S. K.; Tucci, F. C.; Rudkevich, D. M.; Heinz, T.; Rebek, J. *Chem. Eur. J*. **2000**, *6*, 187. (b) Yoshizawa, M.; Kumazawa, K.; Fujita, M. *J. Am. Chem. Soc*. **2005**, *127*, 13456. (c) Ziegler, M.; Brumaghim, J. L.; Raymond, K. N. *Angew. Chem., Int. Ed*. **2004**, *43*, 6748. (d) Yoshizawa, M.; Kusukawa, T.; Fujita, M.; Yamaguchi, K. *J. Am. Chem. Soc*. **2000**, *122*, 6311. (e) Ziegler, M.; Brumaghim, J. L.; Raymond, K. N. *Angew. Chem., Int. Ed*. **2000**, *39*, 4119.

[4] (a) Cohn, M. M.; Rebek, J. *Chem. Rev*. **1997**, *97*, 1647. (b) Yoshizawa, M.; Takeyama, Y.; Kusukawa, T.; Fujita, M. *Angew. Chem., Int. Ed*. **2002**, *41*, 1347.

[5] Fiedler, D.; Leung, D. H.; Bergman, R. G.; Raymond, K. N. *Acc. Chem. Res*. **2005**, *38*, 351. (b) Purse, B. W.; Ballester, P.; Rebek, J. *J. Am. Chem. Soc*. **2003**, *125*, 14682. (c) Cram, D. J. *Nature* **1992**, *356*, 29.

[6] (a) Yamanaka, M.; Rebek, J. *Chem. Commun*. **2004**, 1690. (b) Shivanyuk, A.; Rebek, J. *Angew. Chem*. **2003**, *115*, 708. (c) Shivanyuk, A.; Rebek, J. *Angew. Chem. Int. Ed*. **2003**, *42*, 684. (d) Scarso, A.; Shivanyuk, A.; Rebek, J. *J. Am. Chem. Soc*. **2003**, *125*, 13981.

[7] Douglas, T.; Young, M. *Nature* **1998**, *393*, 152.

[8] (a) Vögtle, F.; Stoddart, J. F.; Shibasaki, M. *Stimulating Concepts in Chemistry*, Wiley-VCH: Weinheim, 2000. (b) Rebek, J. *Chem*. *Commun*. **2000**, 637.

[9] (a) Fujita, M.; Umemoto, K.; Yoshizawa, M.; Fujita, N.; Kusukawa, T.; Biradha, K. *Chem. Commun*. **2001**, 509. (b) Olenyuk, B.; Whiteford, J. A.; Fechtenkotter, A.; Stang, P. J. *Nature* **1999**, *398*, 796. (c) Baxter, P. N. W.; Lehn, J.-M.; Baum, G.; Fenske, D. *Chem. Eur. J.* **1999**, *5*, 102. (d) Baxter, P. N. W.; Lehn, J.-M.; Kneisel, B. O.; Baum, G.; Fenske, D. *Chem. Eur. J*. **1999**, *5*, 113. (e) Fox, O. D.; Dalley, N. K.; Harrison, R. G. *J. Am. Chem. Soc*. **1998**, *120*, 7111.

[10] (a) MacGillivray, L. R.; Diamente, P. R.; Reid, J. L.; Ripmeester, J. A. *Chem. Commun*. **2000**, 359. (b) Kobayashi, K.; Shirasaka, T.; Yamaguchi, K.; Sakamoto, S.; Horn, E.; Furukawa, N.

*Chem. Commun*. **2000**, 41. (c) Cave, G. W. V.; Hardie, M. J.; Roberts, B. A.; Raston, C. L. *Eur. J. Org. Chem*. **2001**, 3227. (d) MacGillivray, L. R.; Atwood, J. L. *Nature* **1997**, *389*, 469. (e) Shivanyuk, A.; Paulus, E. F.; Rissanen, K.; Kolehmainen, E.; Bohmer, V. *Chem. Eur. J*. **2001**, *7*, 1944. (f) Prins, L. J.; Reinhoudt, D. N.; Timmerman, P. *Angew. Chem., Int. Ed.* **2001**, *40*, 2382. (g) Shivanyuk, A.; Paulus, F. E.; Böhmer, V. *Angew. Chem., Int. Ed*. **1999**, *38*, 2906. (h) Corbellini, F.; Knegtel, R. M. A.; Grootenhuis, P. D. J.; Crego-Calame, M.; Reinhoudt, D. N. *Chem.-Eur. J*. **2005**, *11*, 298.

[11] (a) Chen, J.; Rebek, J. *Org. Lett.* **2002**, *4*, 327. (b) Ebbing, M. H. K.; Villa, M. –J.; Valpuesta, J. –M.; Prados, P.; de Mendoza, J. *Proc. Natl. Acad. Sci. U. S. A*. **2002**, *99*, 4962.

[12] Cram, D. J.; Cram, J. M. *Container Molecules and Their Guests*; Royal Society of Chemistry: Cambridge, 1994.

[13] (a) Tunstad, L. M.; Tucker, J. A.; Dalcanale, E.; Weiser, J.; Bryant, J. A.; Sherman, J. C.; Helgeson, R. C.; Knobler, C. B.; Cram, D. J. *J. Org. Chem*. **1989**, *54*, 1305. (b) Mezo, A. R.; Sherman, J. C. *J. Org. Chem.* **1998**, *63*, 6824.

[14] (a) Högberg, A. C. S. *J. Am. Chem. Soc.* **1980**, *102*, 6046. (b) Högberg, A. C. S. *J. Org. Chem.* **1980**, *45*, 4498. (c) Moran, J. R.; Karbach, S.; Cram, D. J. *J. Am. Chem. Soc*. **1982**, *104*, 5826. (d) Cram, D. J.; Stewart, K. D.; Goldberg, I.; Trueblood, K. N. *J. Am. Chem. Soc.* **1985**, *107*, 2574. (e) Barrett, E. S.; Irwin, J. L.; Turner, P.; Sherburn, M. S. *J. Org. Chem.* **2001**, *66*, 8227.

[15] (a) Moran, J. R.; Ericson, J. L.; Dalcanale, E.; Bryant, J. A.; Knobler, C. B.; Cram, D. J. *J. Am. Chem. Soc*. **1991**, *113*, 5707. (b) Cram, D. J.; Choi, H.- J.; Bryant, J. R.; Knobler, C. B. *J. Am. Chem. Soc*. **1992**, *114*, 7748. (c) Hooley, R. J.; Van Anda, H. J.; Rebek, J. *J. Am. Chem. Soc*. **2006**, *128*, 3894. (d) Hooley, R. J.; Biros, S. M.; Rebek, J. *Angew. Chem., Int. Ed*. **2006**, *45*, 3517.

[16] (a) Kobayashi, K.; Ishii, K.; Shirasaka, T.; Yamaguchi, K. *J. Am. Chem. Soc*. **2003**, *125*, 10615. (b) Higler, I.; Grave, L.; Breuning, E.; Verboom, W.; de Jong, F.; Fyles, T. M.; Reinhoudt, D. N. *Eur. J. Org. Chem*. **2000**, 1727. (c) Kobayashi, K.; Ishii, K.; Yamanaka, M. *Chem. Eur. J*. **2005**, *11*, 4725.

[17] (a) Aakeröy, C. B.; Beatty, A. M.; Helfrich, B. A. *J. Am. Chem. Soc.* **2002**, *124*, 14425. (b) Aakeröy, C. B.; Desper, J.; Urbina, J. F. *Chem. Commun.* **2005**, *22*, 2820. (c) Aakeröy, C. B.; Desper, J.; Elisabeth, E.; Helfrich, B. A.; Levin, B.; Urbina, J. F. *Zeit Krist.* **2005**, *220*, 325. (d)

Aakeröy, C. B.; Desper, J.; Helfrich, B. A. *CrystEngComm.* **2004**, *6*, 19. (e) Aakeröy, C. B.; Beatty, A. M.; Helfrich, B. A.; Nieuwenhuyzen, M. *Cryst. Growth Des.* **2003**, *3*, 159.

[18] Aoyama, Y.; Tanaka, Y.; Sugahara, S. *J. Am. Chem. Soc.* **1989**, *111,* 2167.

[19] Bryant, J. A; Blanda, M. T.; Vincenti, M.; Cram, D. J. *J. Am. Chem. Soc.* **1991**, *113,* 2167.

[20] See CSD refcodes, e.g. FEBVUE, FESMEW, FEXFIY, LIFNUJ, and TUTYEM.

[21] (a) Aakeröy, C. B.; Schultheiss, N.; Desper, J. *Org. Lett*. **2006**, *8*, 2607. (b) Yamanaka, M.; Ishii, K.; Yamada, Y.; Kobayashi, K. *J. Org. Chem*. **2006**, *71*, 8800. (c) Kobayashi, K.; Yamada, Y.; Yamanaka, M.; Sei, Y.; Yamaguchi, K. *J. Am. Chem. Soc*. **2004**, *126*, 13896. (d) Haino, T.; Kobayashi, M.; Chikaraishi, M.; Fukazawa, Y. *Chem. Commun*. **2005**, 2321.

[22] (a) Miyaura, N.; Yanagi, T.; Suzuki, A. *Synth. Commun*. **1981**, *11*, 513. (b) Suzuki, A. *J. Organomet. Chem*. **1999**, *576*, 147 and references therein.

[23] Jude, H.; Sinclair, D. J.; Das, N.; Sherburn, M. S.; Stang, P. J. *J. Org. Chem*. **2006**, *71*, 4155.

[24] (a) Barrett, E. S.; Irwin, J. L.; Turner, P.; Sherburn, M. S.; *J. Org. Chem*. **2001**, *66*, 8227. (b) Haino, T.; Kobayashi, M.; Chikaraishi, M.; Fukazawa, Y. *Chem. Commun*. **2005**, *18*, 2321.

[25] CSD Refcodes: GEDKUV, GEDLAC, GEDLOQ, JILZEJ, KAWGAQ and TENLIH. Search parameters: Starting with a molecular framework as shown in Figure 6.17 with the upper-rim aromatic carbon substituted as 'Any halogen', lower-rim bridge carbons set as 'Any' and the upper-rim bridge set to 'containing only C and H'. The upper-rim bridge length was varied from $–CH_2-$ to $–CH_2CH_2-$ to $–CH_2CH_2CH_2-$.

[26] CSD Refcode: GIYWUG.

[27] Kobayashi, K.; Shirasaka, T.; Yamaguchi, K.; Sakamoto, S.; Horn, E.; Furukawa, N. *Chem. Commun*. **2000**, 41.

[28] MacGillivray, L. R.; Diamente, P. R.; Reid, J. L.; Ripmeester, J. A. *Chem. Commun*. **2000**, 359.

[29] Turner, D. R.; Pastor, A.; Alajarin, M.; Steed, J. W. *Structure and Bonding*, **2004**, *108*, 97.

[30] Cowan, J. A.; Howard, J. A. K.; McIntyre, G. J.; Lo, S. M. -F.; Williams, I. D. *Acta. Cryst.* **2003***, B59*, 794.

[31] CSD Refcodes of structures containing an amino-pyridine moiety interacting with a carboxylic acid moiety: Salts – IJISUP, PEBFIL, XEGNUS, XINRUH, XINSES, LAPNUM, LAPPAU and LAQGOA. Neutral – NUHMEI and TETXUL

[32] Allen, F. H. *Acta Cryst*. **2002**, *B58*, 380.

[33] (a) Higler, I.; Grave, L.; Breuning, E.; Verboom, W.; Jong, F. D.; Fyles, T. M.; Reinhoudt, D. N. *Eur. J. Org. Chem.* **2000**, 1727; (b) Kobayashi, K.; Ishii, K.; Yamanaka, M. *Chem. Eur. J.* **2005**, *11*, 4725.

# CHAPTER 7 - Cyclotriveratrylene-based molecular building blocks for hydrogen-bonded capsules

## 7.1 Introduction

Cyclotriveratrylene's (CTV's) belond to a class of cyclic oligomers, which form through condensation of the veratryl cation, under acidic conditions, in good yields, Figure 7.1. Numerous functionalized CTV's have been synthesized and characterized,[1] however our focus will be on the conventional tri-methoxy (R=Me) / tri-hydroxy (R'=H) molecular scaffold.[2]

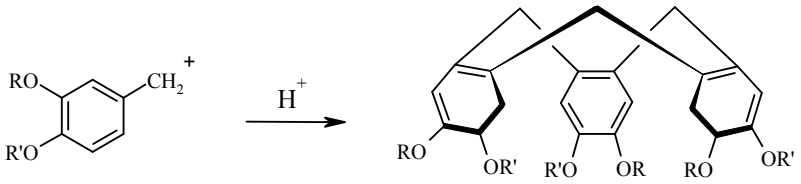


**Figure 7.1** General schematic displaying the cyclo-condensation of the veratryl cation.

CTV's possess a saucer-shape configuration, in which three aromatic rings are tethered together through methylene bridges. Although considerably shallower than their resorcinarene-based counterpart, CTV's can bind or encapsulate large organic molecules *i.e.* fullerenes,[3] *o*-carborane,[4] and organometallic complexes[5] within their cavity bearing framework. Extending the walls of the CTV through covalent synthesis has been explored, although only a small number of examples exist to date.[1,6] Furthermore, there has only been one report on hydrogen-bonded dimeric CTV capsules, where a carboxylate functionalized CTV was allowed to react with an ammonium functionalized CTV through charge-assisted interactions.[7] Herein we present our initial synthetic endeavors for generating a library of neutral hydrogen bond donor/acceptor appended CTV's, with the long-term goal of producing heterodimeric capsules through hydrogen bonds. However, we display some preliminary results in producing deep-walled CTV's through heteromeric acid···pyridine hydrogen bonds.

## 7.2 Experimental

### *7.2.1 Synthesis*

All chemicals, unless otherwise noted, were purchased from Aldrich and used without further purification. Column chromatography was carried out on silica gel (150 Å pore size) from Analtech Inc. Melting points were determined on a Fisher-Johns melting point apparatus and are uncorrected. $^{1}H$ and $^{13}C$ NMR spectra were recorded on a Varian Unity plus 400 MHz or 200 MHz spectrometer in $CDCl_3$ or $D_6$-DMSO. Compounds were prepared for infrared spectroscopic (IR) analysis as a mixture in KBr. Electrospray Ionization – Ion-Trap Mass Spectrometry (ESI-IT-MS) was carried out on a Bruker Daltonics Esquire 3000 Plus. MALDI-TOF / TOF-MS was carried out on a Bruker Daltonics Ultraflex TOF/TOF.

#### *7.2.1.1 Synthesis of 3-methoxy-4-(2-propenyloxy)benzene, 28[2a]*

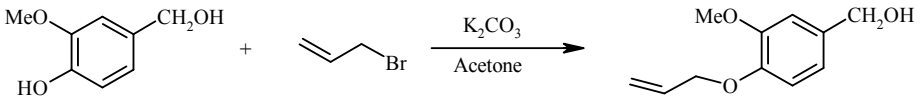


**28**

A mixture of vanillyl alcohol (50.0 g, 0.32 mol), allyl bromide (31.5 ml, 0.36 mol) and potassium carbonate (45.0 g, 0.32 mol) were added to a round bottom flask. Acetone (75 mL) was added and dinitrogen was bubbled through the resultant mixture for 10 minutes. A condenser was attached and the mixture was heated to reflux under a dinitrogen atmosphere. The reaction was monitored by TLC and allowed to cool to room temperature on completion, 4 h. The solution was then diluted with dichloromethane (150 mL), washed with water (3 x 100 mL) and dried over magnesium sulfate. The solvent was removed on a rotary evaporator producing a yellow oil. The product **28** was recrystallized from diethyl ether yielding a pure white solid, (44.6 g, 71 %). M.p. 66-68 ˚C; $^{1}H$ NMR ($\delta_H$; 400 MHz, $CDCl_3$): 6.89 (s, 1H), 6.82 (s, 2H), 6.01 – 6.10 (m, 1H), 5.25 – 5.40 (m, 2H), 4.56 (s + m, 4H), 3.84 (s, 3H), 2.31 (s, 1H).

#### *7.2.1.2 Synthesis of tris-methoxy-(2-propenyloxy) cyclotriveratrylene, 29[2a]*

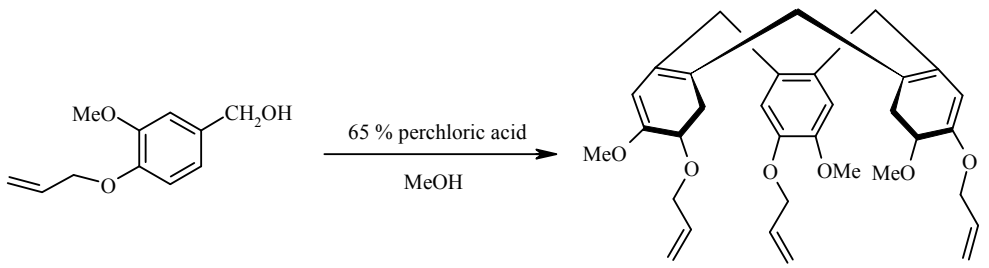


**28** **29**

A suspension of **28** (20.6 g, 0.11 mol) in methanol (125 mL) was cooled to 0 ˚C in an ice bath with magnetic stirring. Perchloric acid 65 % (60 mL) was added dropwise to the mixture, and then stirred under a dinitrogen atmosphere for 18 h at room temperature. Upon completion, the solution was diluted with dichloromethane (100 mL), washed with water (3 x 150 mL) and dried over magnesium sulfate. The solvent was removed on a rotary evaporator, which produced a white solid, that was further purified by recrystallization from diethyl ether (200 mL). Product **29** was isolated as a white powder, (8.3 g, 44 %). M.p. 176-178 ˚C; $^1$H NMR ($\delta_H$; 200 MHz, $CDCl_3$): 6.86 (s, 3H), 6.81 (s, 3H), 5.98 – 6.14 (m, 3H), 5.22 – 5.43 (m, 6H), 4.75 (d, J = 14Hz, 3H), 4.58 – 4.61 (m, 6H), 3.84 (s, 9H), 3.52 (d, J = 14Hz, 3H).

### *7.2.1.3 Synthesis of tris-methoxy-(2-hydroxy) cyclotriveratrylene, 30[2b]*

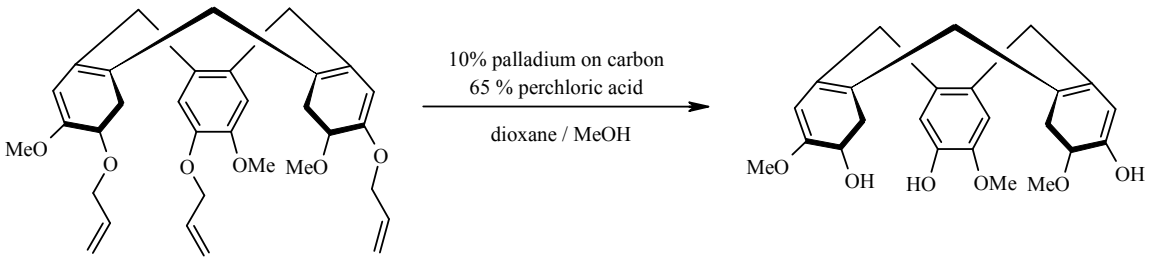


**29** **30**

In a round-bottom flask **29** (3.00 g, 5.68 mmol) was dissolved in hot dioxane (15 mL). To this solution was added ethanol (27 mL), 10% palladium on carbon (600 mg), and dropwise 65% perchloric acid (0.60 mL). A condenser was attached and the mixture was heated to 55 – 60 ˚C, in an oil bath, for 20 h. Upon completion, the reaction was allowed to cool to room temperature and the catalyst filtered off and washed with dioxane (10 mL) and then dichloromethane (50 mL). The organic layer was washed with water (3 x 100 mL) and dried

over magnesium sulfate. The solution was concentrated to 25 mL and allowed to crystallize overnight. The product **30** was collected by suction filtration as a white solid, (1.75 g, 72 %). M.p. >280 ˚C; $^{1}$H NMR ($\delta_H$; 200 MHz, $CDCl_3$): 6.89 (s, 3H), 6.80 (s, 3H), 5.41 (s, 3H), 4.72 (d, J = 14Hz, 3H), 3.86 (s, 9H), 3.51 (d, J = 14Hz, 3H).

### *7.2.1.4 Synthesis of tris(3-pyridylmethyl) cyclotriveratrylene, 31*

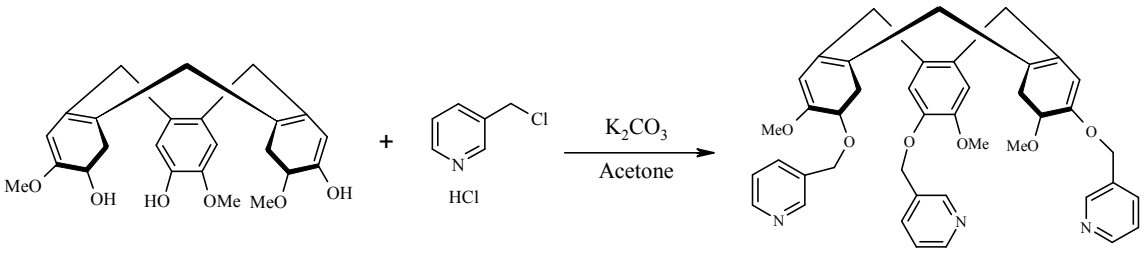


**30** **31**

A mixture of **30** (410 mg, 1.00 mmol) and potassium carbonate (1.39 g, 10.1 mmol) were refluxed under a dinitrogen atmosphere in acetone (60 mL) for 0.5 h. 3-picolylchloride hydrochloride (574 mg, 3.50 mmol) was added and the reaction refluxed for 96 h. Upon cooling, the acetone was removed by rotary evaporator, water (100 mL) added and extracted with dichloromethane (3 x 100 mL). The organic layer was dried over magnesium sulfate and the solvent removed on a rotary evaporator, producing a brown oil. The residue was chromatographed on silica using ethyl acetate/ethanol (10:1) as the eluant. The product **31** was further purified by trituration with methanol producing a white solid, (410 mg, 60 %). M.p. 120-122 °C; $^{1}$H NMR ($\delta_H$; 200 MHz, $CDCl_3$): 8.68 (d, J = 1.6Hz, 3H), 8.57 (dd, J = 4.8Hz, J = 1.8Hz, 3H), 7.76 (dt, J = 8Hz, 1.8Hz, 3H), 7.33 – 7.26 (m, 3H), 6.87 (s, 3H), 6.74 (s, 3H), 5.10 (s, 6H), 4.72 (d, J = 13.8Hz, 3H), 3.77 (s, 9 H), 3.50 (d, J = 14Hz, 3H); $^{13}$C NMR ($\delta_H$; 400 MHz, $CDCl_3$): 149.3, 148.9, 148.8, 146.8, 135.1, 133.4, 133.0, 131.8, 123.5, 117.2, 114.1, 69.6, 56.2, 36.4; IR (KBr): 2925, 1608, 1577, 1510, 1261, 1087; ESI-IT-MS *m/z* 681 ([**31** + H]$^{+}$).

### *7.2.1.5 Synthesis of tris(3-methoxycarbonylbenzyloxy) cyclotriveratrylene, 32*

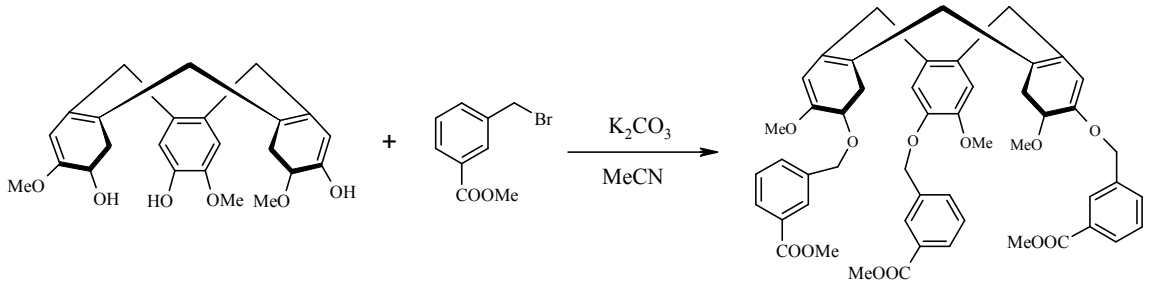


**30** **32**

A mixture of **30** (300 mg, 0.732 mmol) and potassium carbonate (625 mg, 4.54 mmol) were refluxed under a dinitrogen atmosphere in acetonitrile (25 mL) for 0.5 h. Methyl-3-(bromomethyl)benzoate (1.0 g, 4.37 mmol) was added and the reaction refluxed for 96 h. Upon cooling, acetonitrile was removed by rotary evaporator, water (100 mL) added and extracted with dichloromethane (3 x 100 mL). The organic layer was dried over magnesium sulfate and the solvent removed on a rotary evaporator, producing a yellow oil. The residue was chromatographed on silica using hexanes/ethyl acetate (3:1) as the eluant, affording **32** as a yellow oil, (410 mg, 66 %). $^{1}$H NMR ($\delta_H$; 200 MHz, $CDCl_3$): 8.10 (s, 1H), 8.57 (dt, J = 4.8Hz, J = 1.8Hz, 3H), 7.76 (dt, J = 8Hz, 1.8 Hz, 3H), 7.33 – 7.26 (m, 3H), 6.87 (s, 3H), 6.74 (s, 3H), 5.10 (s, 6H), 4.72 (d, J = 13.8Hz, 3H), 3.77 (s, 9 H), 3.50 (d, J = 14Hz, 3H); $^{13}$C NMR ($\delta_H$; 200 MHz, $CDCl_3$): 166.81, 148.51, 146.86, 137.98, 132.87, 131.64, 131.55, 130.39, 129.00, 128.73, 128.04, 116.35, 113.73, 71.21, 56.11, 52.13, 36.42.

### *7.2.1.6 Synthesis of tris(3-phenylcarboxymethyl)cyclotriveratrylene, 33*

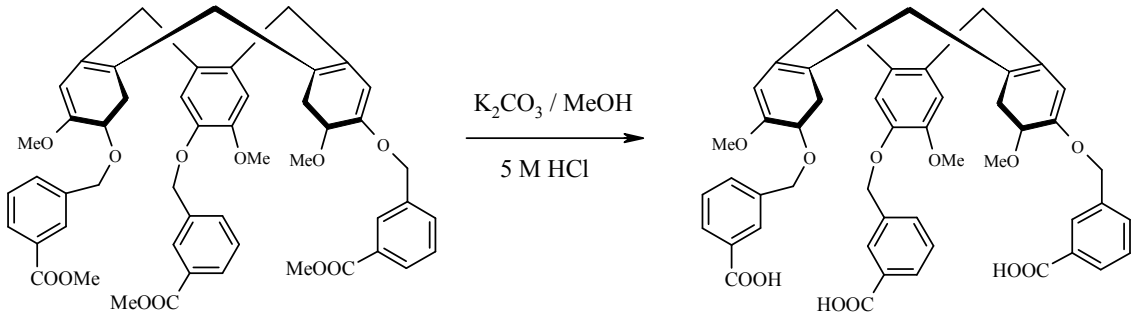


**32** **33**

A mixture of **30** (400 mg, 0.450 mmol) and potassium carbonate (625 mg, 4.06 mmol) was refluxed in an aqueous methanol solution ($MeOH/H_2O$ = 7:1, acetone, 60 mL) for 24 h. Upon cooling the solvent was removed on a rotary evaporator, water (30 mL) added along with 5 M HCl (10 mL). The suspension was stirred overnight and filtered, yielding an off-white precipitate, **33**, (380 mg, 80 %). Dec. 150 °C; $^1$H NMR ($\delta_H$; 200 MHz, DMSO-$d_6$): 8.01 (s, 3H), 7.88 (d, J = 7.4Hz, 3H), 7.64 (d, J = 7.6Hz, 3H), 7.49 (t, J = 7.6Hz, 3H), 7.18 (s, 3H), 7.02 (s, 3H), 5.11 (q, J = 12.6Hz, J = 16.8Hz, 6H), 4.70 (d, J = 13.8Hz, 3H), 3.66 (s, 9 H), 3.49 (d, J = 14.2Hz, 3H); IR (KBr pellet): 2930, 1696, 1609, 1511, 1445, 1265, 1184, 1081, 743; ESI-IT-MS *m/z* 811 (**33** + H]$^+$).

## 7.2.2 *Infrared spectroscopy*

### *7.2.2.1 Synthesis of tris(3-pyridylmethyl) cyclotriveratrylene:4-cyanobenzoic acid*

A mixture of **31** (10 mg, 0.015 mmol) and 4-cyanobenzoic acid (7 mg, 0.05 mmol) were placed on a watch glass. The watch glass was heated until a homogeneous mixture was formed. IR (KBr pellet) υ 2551 and 1936 cm$^{-1}$ (O-H···N, br), 1706 cm$^{-1}$ (C=O, m).

### *7.2.2.2 Synthesis of tris(3-pyridylmethyl) cyclotriveratrylene:4-nitrobenzoic acid*

A mixture of **31** (10 mg, 0.015 mmol) and 4-nitrobenzoic acid (8 mg, 0.05 mmol) were placed on a watch glass. The watch glass was heated until a homogeneous mixture was formed. IR (KBr pellet) υ 2551 and 1957 cm$^{-1}$ (O-H···N, br), 1696 cm$^{-1}$ (C=O, m).

### *7.2.2.3 Synthesis of tris(3-pyridylmethyl) cyclotriveratrylene:3,5-dinitrobenzoic acid*

A mixture of **31** (10 mg, 0.015 mmol) and 3,5-dinitrobenzoic acid (10 mg, 0.05 mmol) were placed on a watch glass. The watch glass was heated until a homogeneous mixture was formed. IR (KBr pellet) υ 2525 and 1921 cm$^{-1}$ (O-H···N, br), 1706 cm$^{-1}$ (C=O, m).

### *7.2.2.4 Synthesis of tris(3-pyridylmethyl) cyclotriveratrylene:pentamethylbenzoic acid*

A mixture of **31** (10 mg, 0.015 mmol) and pentamethylbenzoic acid (9 mg, 0.05 mmol) were placed on a watch glass. The watch glass was heated until a homogeneous mixture was formed. IR (KBr pellet) υ 2561 and 1931 cm$^{-1}$ (O-H···N, br), 1701 cm$^{-1}$ (C=O, m).

### *7.2.2.5 Synthesis of tris(3-pyridylmethyl) cyclotriveratrylene:3-N,N-dimethylaminobenzoic acid*

A mixture of **31** (10 mg, 0.015 mmol) and 3-*N,N*-dimethylaminobenzoic acid (8 mg, 0.05 mmol) were placed on a watch glass. The watch glass was heated until a homogeneous mixture was formed. IR (KBr pellet) υ 2535 and 1926 $cm^{-1}$ (O-H···N, br), 1675 $cm^{-1}$ (C=O, m).

## 7.3 Results and discussion

### *7.3.1 Characterization of tris-substituted CTV's*

Functionalized CTV's **31** and **32** were prepared in good yields ~ 60 % under basic conditions with the appropriate electrophile. For both molecules, purification proceeded smoothly through silica-gel column chromatography. Conversion of the three ester-groups of **32**, to carboxylic acids was achieved in good yields, *i.e.* 80%, under acidic conditions. Crystals suitable for single-crystal X-ray crystallography of **31** were grown by slow evaporation of a saturated toluene solution at room temperature over 36 h, Figure 7.2.

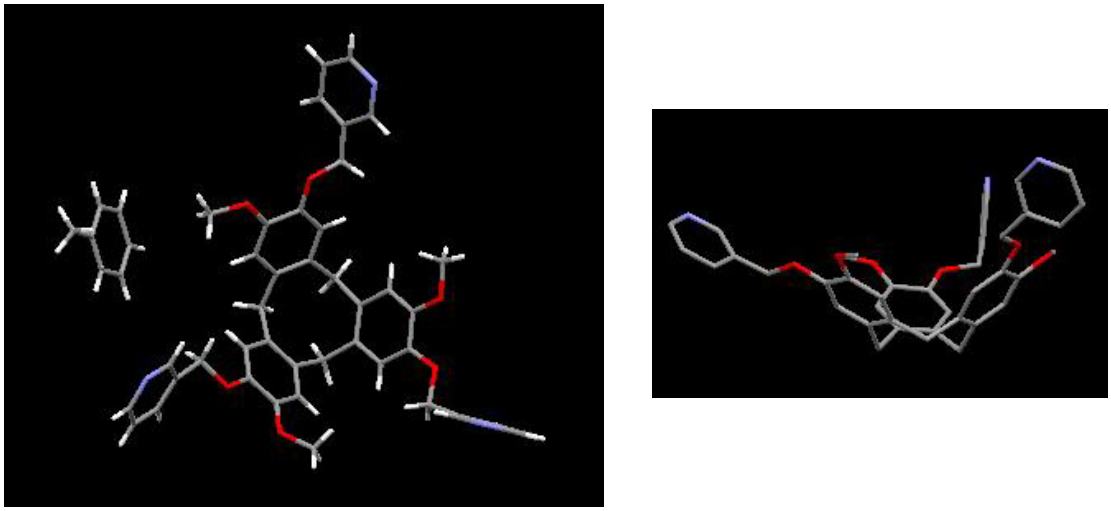

**Figure 7.2** (left) Top-view of CTV **31** along with one toluene solvent molecule. (right) Side-view of CTV **31**, displaying the shallow cavity. The hydrogen atoms and the toluene molecule have been omitted for clarity.

The crystal structure determination confirms that CTV **31** has undergone a three-fold substitution with methylene extended pyridyl rings, in which each of the pyridyl nitrogen atoms

are facing upwards. The packing diagram of **31** shows the toluene solvate residing outside the cavity (Figure 7.2), while adjacent molecules stack in a cup-like fashion, Figure 7.3.

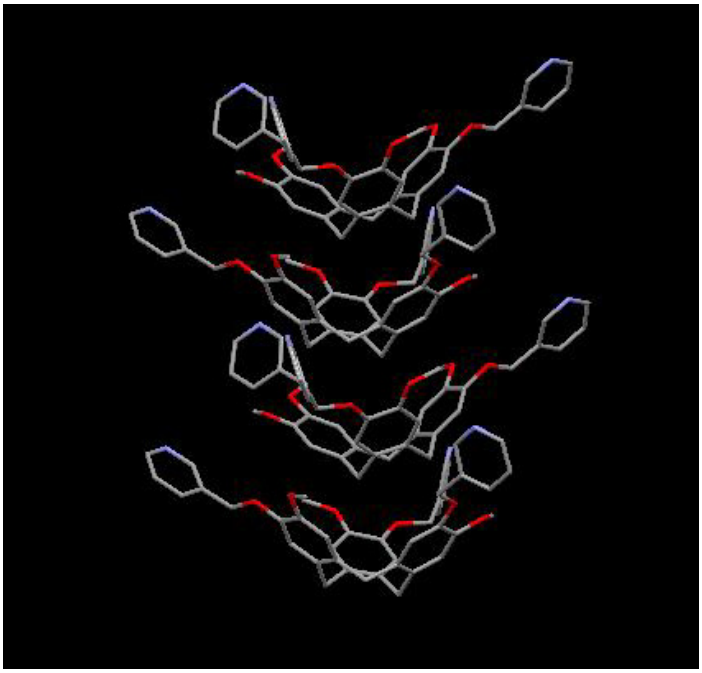

**Figure 7.3** Packing arrangement of adjacent CTV molecules within the solid state structure of **31**.

Unfortunately, crystals suitable for X-ray diffraction were not obtained for compounds **32** or **33**, however combinations of $^{1}$H NMR, $^{13}$C NMR and mass spectrometry confirm the resulting tri-substituted product.

As previously outlined in Chapter 6, the idea is to utilize self-complementary hydrogen bonding moieties to direct and align multiple components into discrete heteromeric complexes or capsules. Suitable single crystals of asymmetric complexes and capsules could not be obtained however the desired hydrogen bond interactions were detected using infrared spectroscopy.

### *7.3.2 Characterization through IR spectroscopy*

To determine if CTV **31** and aromatic acids form O-H···N hydrogen bonds, melt experiments were conducted, in which stoichiometric amounts of each component is mixed and heated until melting occurs. Melt experiments were carried out with CTV **31** and five different aromatic mono-carboxylic acids.[8] Each sample was analyzed by IR and O-H···N stretches were observed in all 5 cases, proving that hydrogen bonds are forming between the pyridyl rings of

CTV **31** and the carboxylic acid moieties. These very distinct, relatively broad stretches occur in the regions of 2500 and 1900 $cm^{-1}$, Table 7.1.

**Table 7.1** O-H···N stretches formed between CTV **31** and five benzoic acids

| Benzoic acids | 4-cyano | 4-nitro | 3,5-dinitro | pentamethyl | 4-*N,N*-dimethylamino |
|---|---|---|---|---|---|
| O-H···N ($cm^{-1}$) | 1936 | 1957 | 1921 | 1931 | 1926 |
| | 2551 | 2551 | 2525 | 2561 | 2535 |

Displayed in Figure 7.4 are IR spectra of CTV **31** and the product obtained between CTV **31** and 4-cyanobenzoic acid. Spectrum (b) reveals distinct O-H···N stretches at 2550 and 1938 $cm^{-1}$, while these stretches are absent in spectrum (a).

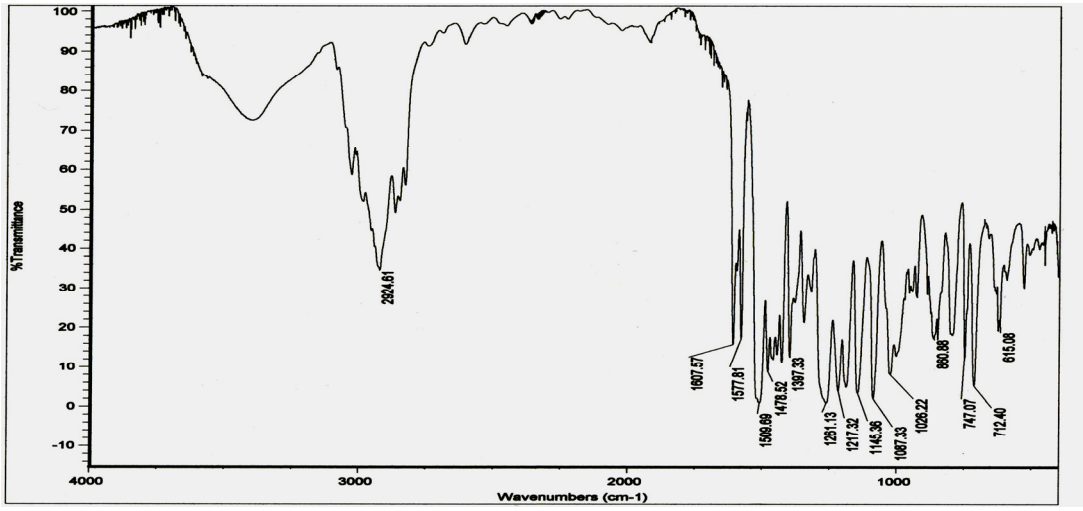


**(a)**

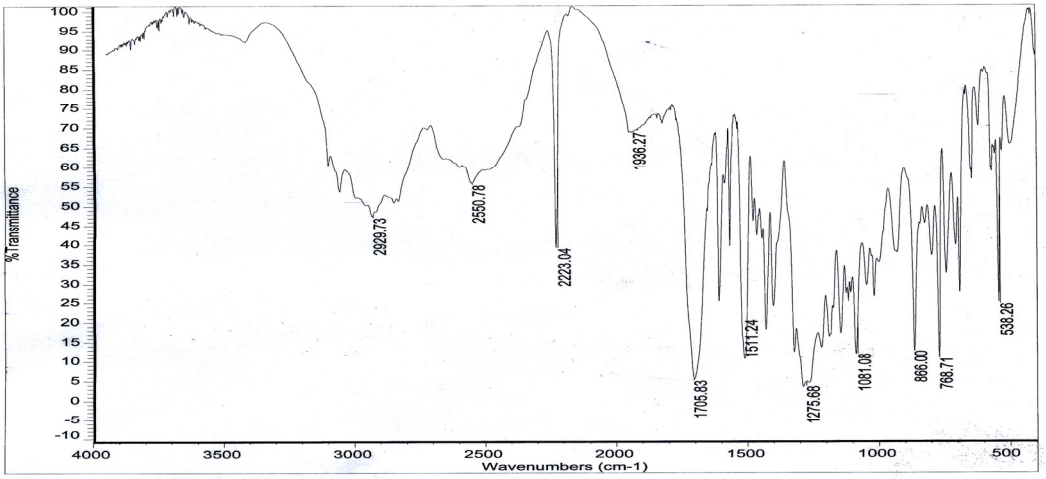


**(b)**

**Figure 7.4** (a) IR spectrum of CTV **31**, and (b) IR spectrum of CTV **31**:4-cyanobenzoic acid after the melt experiment.

Even though it is impossible to determine how many benzoic acid molecules bind to the pyridyl-fucntionalized CTV the IR data does show that the two components form heteromeric O-H···N hydrogen bonds. Continuing in our quest of detecting O-H···N hydrogen bonds through IR, a melt experiment with two individual CTV's *i.e.* **31** and **33** containing self-complementary moieties was conducted. Displayed in Figure 7.5 are IR spectra of CTV **33** and the product formed between **31** and **33** after the melt experiment was conducted. Unfortunately, the spectra of compounds **31** and **33**; (a) and (c) contain stretches in the regions where O-H···N interactions appear, furthermore spectra (c) and (d) display similar bands, making it difficult to determine if both CTV's are interacting through O-H···N hydrogen bonds or not.

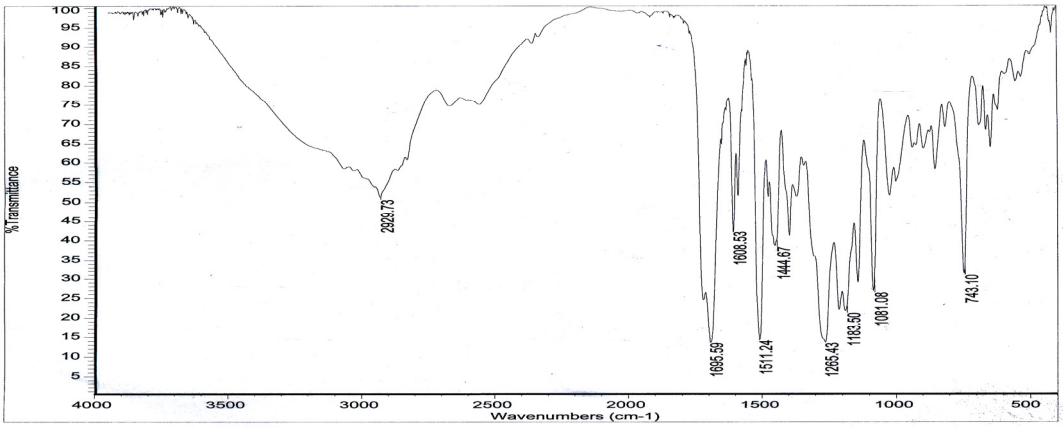


**(c)**

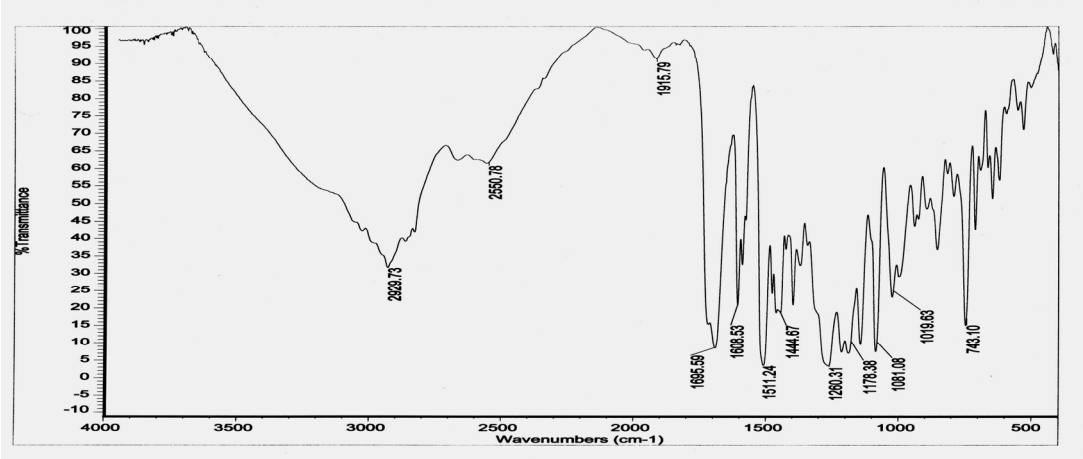


**(d)**

**Figure 7.5** (c) IR spectrum of CTV **33**, and (d) IR spectrum of CTV **31**:CTV **36** after the melt experiment.

We have demonstrated that CTV's containing either hydrogen bond donor or acceptor moieties can be easily prepared in good yields from the trimethoxy/trihydroxy molecular scaffold. Although single crystals were not obtained between reactions of CTV **31** and various benzoic acids, hydrogen bonds were detected using IR spectrometry. This project is still in the preliminary stages, however a foundation has been set for a variety of new functionalized CTV's to be produced alongwith initial studies in detecting and characterizing hydrogen bonding interactions between multiple components.

Future work will be centered around growing the number of CTV's with suitable hydrogen-bond moieties appended to the scaffold for the construction of homomeric and heterodimeric capsules, Figure 7.6.

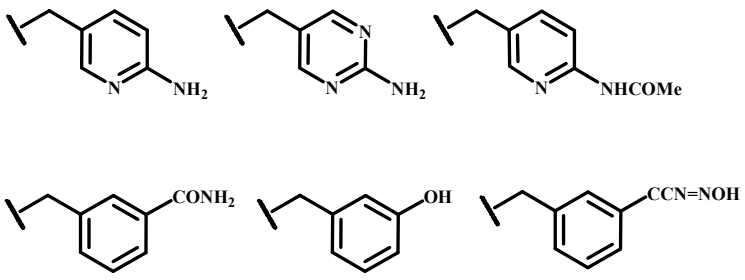


**Figure 7.6** Hydrogen bond donor/acceptor moieties to be substituted onto the CTV scaffold.

Attempts will be made to obtain suitable crystals, for single crystal X-ray crystallography, of the individual hydrogen bond appended CTV's (especially ones in which

self-complementry hydrogen bonds would exist) as well as combining suitable CTV's for the construction of heterodimeric capsules.

# References:


[1] (a) Collet, A. *Tetrahedron* **1987**, *43*, 5725. (b) Cram, D. J. *Science* **1983**, *219*, 1177. (c) Steed, J. W.; Zhang, H.; Atwood, J. L. *Supramol. Chem*. **1996**, *7*, 37. (d) Hardie, M. J.; Mills, R. M.; Sumby, C. *J. Org. Biomol. Chem*. **2004**, *2*, 2958.

[2] (a) Canceill, J.; Collet, A.; Gottarelli, G. *J. Am. Chem. Soc*. **1984**, *106*, 5997. (b) Collet, A.; Gabard, J. *J. Org. Chem*. **1980**, *45*, 5400.

[3] (a) Atwood, J. L.; Barnes, M. J.; Burkhalter, R. S.; Junk, P. C.; Steed, J. W.; Raston, C. L. *J. Am. Chem. Soc*. **1994**, *116*, 10346. (b) Atwood, J. L.; Barnes, M. J.; Gardiner, M. G.; Raston, C. L. *Chem. Commun*. **1996**, 1449. (c) Matsubara, H.; Hasegawa, A.; Shiwaku, K.; Asano, K.; Uno, M.; Takahashi, S.; Yamamoto, K. *Chem. Lett*. **1998**, *27*, 923. (d) Matsubara, H.; Oguri, S.; Yamamoto, K. *Chem. Lett.* **1999**, *28*, 431.

[4] (a) Hardie, M. J.; Godfrey, P. D.; Raston, C. L. *Chem. Eur. J*. **1999**, *5*, 1828. (b) Hardie, M. J.; Raston, C. L.; Wells, B. *Chem. Eur. J*. **2000**, *6*, 3293.

[5] Holman, K. T.; Steed, J. W.; Atwood, J. L. *Angew. Chem. Int. Ed*. **1997**, *36*, 1736.

[6] (a) Arduini, A.; Calzavacca, F.; Demuru, D.; Pochini, A.; Secchi, A. *J. Org. Chem*. **2004**, *69*, 1386. (b) Cram, D. J.; Weiss, J.; Helgeson, R. C.; Knobler, C. B.; Dorigo, A. E.; Houk, K. N. *J. Chem. Soc., Chem. Commun.* **1998**, 407. (c) Bohle, Bohle, D. S.; Stasko, D. J. *Inorg. Chem*. **2000**, *39*, 5768. (d) Zhan, H.-Q.; Jiang, X.-K.; Li, Z.-T.; *Chin. J. Chem*. **2001**, *19*, 147. (e) Ahmad, R.; Hardie, M. J. *Supramolecular Chem*. **2006**, *18*, 29. (f) Brotin, T.; Roy, V.; Dutasta, J.-P. *J. Org. Chem*. **2005**, *70*, 6187. (f) Zhang, S.; Echogoyen, L. *J. Am. Chem. Soc*. **2005**, *127*, 2006.

[7] Lee, S. B.; Hong, J.-I. *Tetrahedron Lett.* **1996**, *37*, 8501.

[8] Five different acids were tested, 4-cyanobenzoic acid, 4-nitrobenzoic acid, 3,5-dinitrobenzoic acid, pentamethylbenzoic acid, and 4-*N*,*N*-dimethylaminobenzoic acid.

# CHAPTER 8 - Summary

Supramolecular chemists have at their disposal a variety of reliable complementary intermolecular interactions e.g. hydrogen bonds, halogen···donor (N or O), and π-π interactions through which to synthesize supermolecules. Within supramolecular synthesis, desired product formation and isolation must be achieved from a single reaction, due to the freely reversible nature of non-covalent intermolecular interactions that hold the individual components together. This differs substantially from organic synthesis in which much stronger covalent bonds are broken and formed, allowing for reaction intermediates to be isolated, purified, and subjected to additional chemical transformations. However, the ability to carry out sequential supramolecular synthesis, to form higher-ordered products with predictable connectivities and stiochiometries, is achievable (although rare!) within one reaction pot by relying on an established hierarchy of reliable intermolecular interactions.

We designed and synthesized three supramolecular reactants (SR's) containing two distinct hydrogen bonding donor/acceptor sites (pyridine/amino-pyrimidine) to establish competitive intermolecular interactions during co-crystal assembly. These SR's were allowed to react with various aromatic carboxylic acids producing nine 1:1 molecular co-crystals and four 1:1 ionic salts through heteromeric O-H···N/N-H···O or charge-assisted $N\text{-}H^{+}\cdots O^{-}$/N-H···$O^{-}$ hydrogen bonds with the amino-pyrimidine binding site, Figure 8.1.

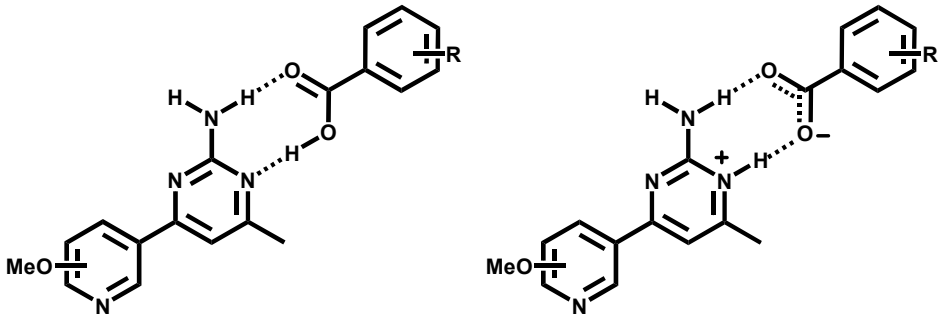


**Figure 8.1** Summary of primary hydrogen bonding motifs between 3-pyridine/amino-pyrimidine SR's and aromatic carboxylic acids.

Attempts to quantify the strengths of both hydrogen bond acceptor sites *i.e.* pyridine or amino-pyrimidine were carried out using semi-emperical AM1 electrostatic potential surfaces. By simply subtracting the negative potential of the hydrogen-bond acceptor from the positive potential of the hydrogen-bond donor in each binding site, a numerical value, Q, which represents the overall hydrogen-bond capability is obtained, Figure 8.2.

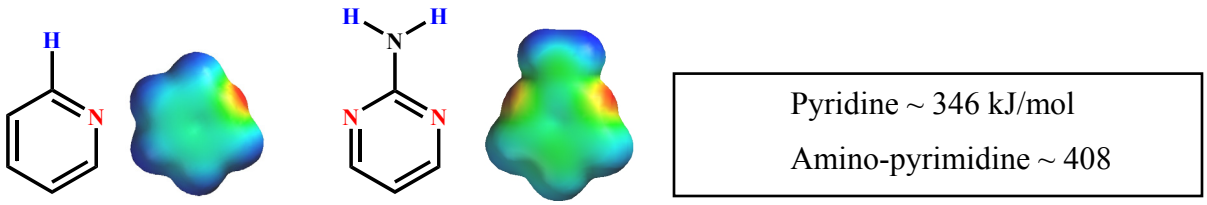


**Figure 8.2** Calculated Q-values for pyridine and amino-pyrimidine.

A comparison of the two binding sites indicated that the amino-pyrimidine moiety was a superior hydrogen-bond acceptor for an incoming carboxylic acid. This ranking in binding sites was also supported in the crystal structures that we obtained in which all thirteen structures (100% supramolecular yield) based upon SR's **1**, **2**, and **6** display the carboxylic acid/amino-pyrimidine synthon.

We allowed the same family of pyridine/amino-pyrimidine SR's to react with halogenated benzoic acids in which the amino-pyrimidine/carboxylic acid synthon formed 7/7 times (100% supramolecular yield) and halogen bonds (N···I or N···Br) extended the SR/acid dimers into polymeric networks 4/7 times (57% supramolecular yield), Figure 8.3.

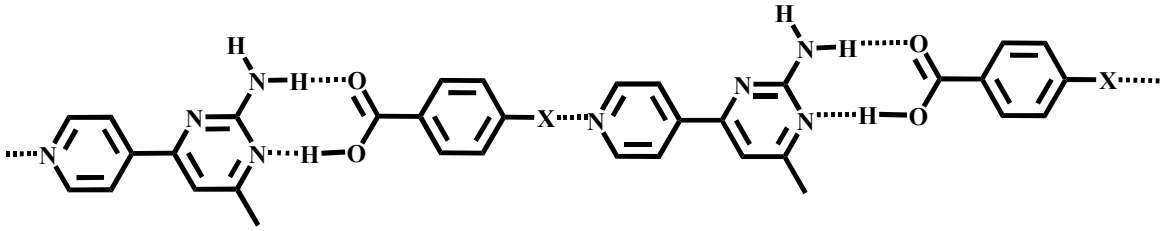

**Figure 8.3** A postulated network formed through a series of hydrogen and halogen bonds (X = I, Br).

These results were rationalized through a hierarchical view of intermolecular interactions consisting of both hydrogen and halogen bonds.

The construction of M(II)-containing (M = Cu, Co and Ni) supramolecular chains was achieved by combining suitable anionic ligands (for controlling the coordination geometry and

for creating a neutral building block) with three bifunctional ligands *i.e.* 3-pyridine/amino-pyrimidine SR's containing a metal-coordinating pyridyl site and a self-complementary hydrogen-bonding pyrimidine moiety. Eleven crystal structures are presented and in each case, the metal complex displays a neutral overall charge, with anionic ligands occupying the equatorial sites leaving room for the bifunctional ligand to coordinate in the axial positions 10/11 times (91% coordinate-covalent yield), Figure 8.4.

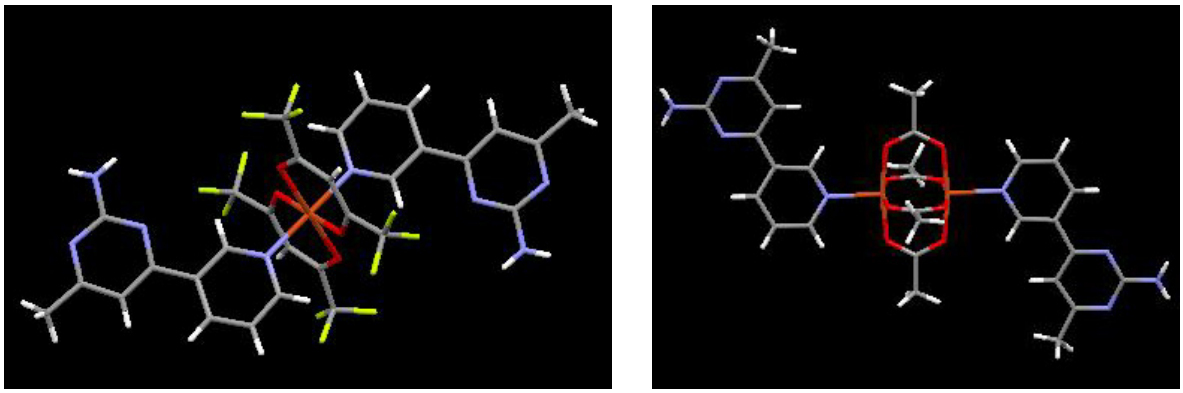

**Figure 8.4** The desired coordination chemistry around the metal center; (left) octahedral and (right) square-based pyramidal. The supramolecular chemistry, which organizes the coordination-complexes into the desired infinite 1-D chains, was driven by a combination of N-H···N amino-pyrimdine···amino-pyrimidine hydrogen bonds 10/13 times (77 % supramolecular yield), Figure 8.5.

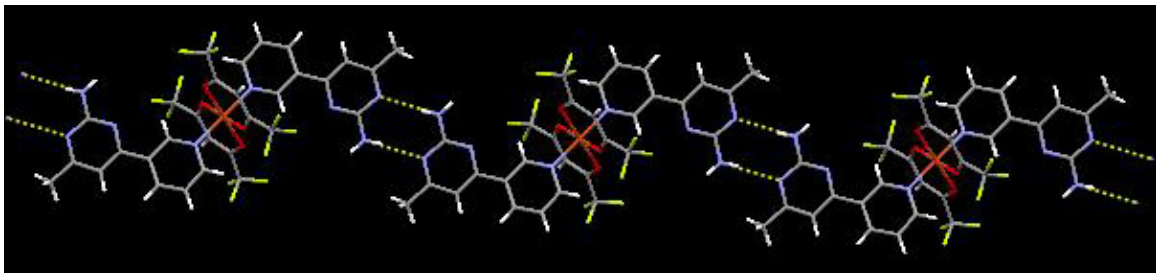

**Figure 8.5** Extension of the ligand:metal complex through self-complementary N-H···N hydrogen bonds

Finally, we utilized hydrogen-bonding interactions to organize and construct larger supermolecules. Accordingly, we synthesized and characterized a series of tetra-halogenated and tetra-substituted hydrogen bond donor and acceptor functionalized, *i.e.* pyridyl, amino-pyridine, carboxylic acid, resorcinarene-based cavitands, Figure 8.6.

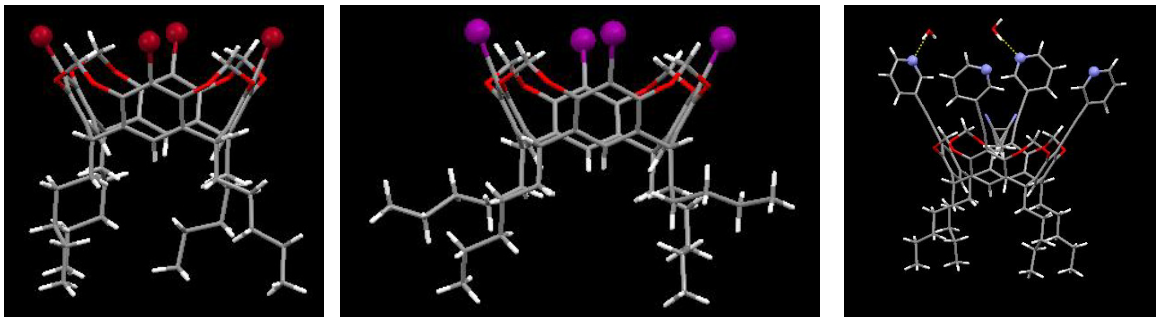

**(a)** **(b)** **(c)**

**Figure 8.6** (a) Tetra-bromo; (b) Tetra-iodo; (c) Tetra-ethynylpryidyl functionalized cavitands.

Our efforts produced deep-walled cavitands through amino-pyridine···carboxylic acid heteromeric synthons and a heterodimeric molecular capsule through pyridyl···carboxylic acid hydrogen bonds, Figure 8.7. The heterodimeric capsule is only one of three, of its type, characterized crystallographically.

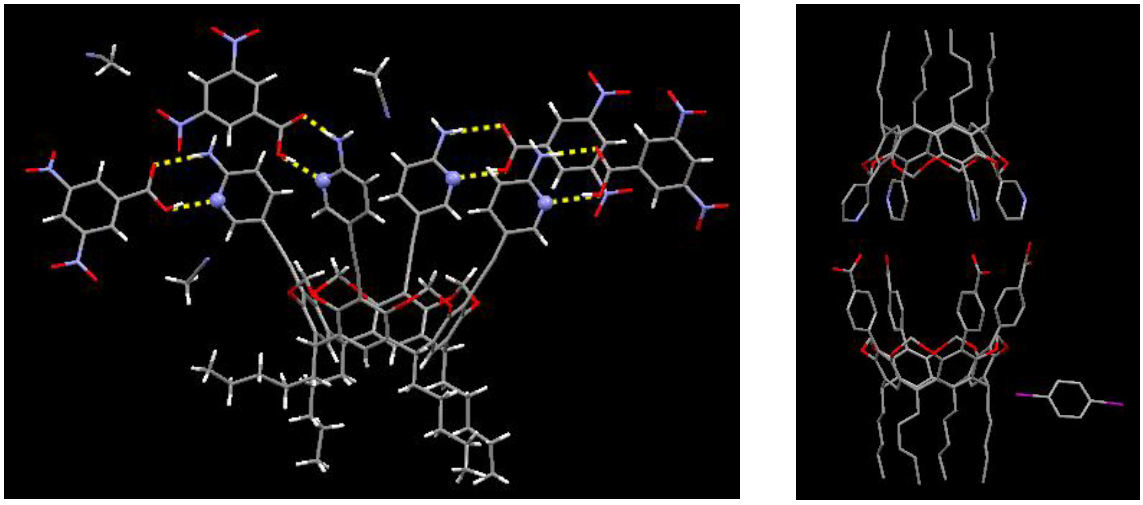

**Figure 8.7** A pentameric supermolecule produced by four 3,5-dinitrobenzoic acid molecules forming O-H···N and H-H···O hydrogen bonds with each cavitand (left); A 1:1 heterodimeric molecular capsule constructed through multiple pyridine···carboxylic acid hydrogen bonds (right)

Due to the restricted and isolated nature of the inner-cavity, properties differ (within the capsule) drastically compared to those of the bulk phase environment. This phenomenon leads to potential practical applications including, but not limited to, molecular sensing, stabilization of reactive intermediates, increase chemical reaction rates, molecular catalysis, drug delivery systems, and detection of various isomers.

# Appendix A - Crystallographic Experimental Data

## Chapter 2

Datasets for **1**, **2**, **6**, **1c-1d**, **2a-2e**, and **6b-6d** were collected on a SMART APEX. Data for **1a-1b** and **6a** were collected on a SMART 1000. All datasets were collected using Mo-$K_\alpha$ radiation and were uncorrected for absorption.

Data were collected using SMART.[1] Initial cell constants were found by small widely separated "matrix" runs. An entire hemisphere of reciprocal space was collected. Scan speed and scan width were chosen based on scattering power and peak rocking curves.

Unit cell constants and orientation matrix were improved by least-squares refinement of reflections thresholded from the entire dataset. Integration was performed with SAINT,[2] using this improved unit cell as a starting point. Precise unit cell constants were calculated in SAINT from the final merged dataset. Lorenz and polarization corrections were applied, and data were corrected for absorption

Data were reduced with SHELXTL.[3] All structures were solved by direct methods. In general, hydrogen atoms were assigned to idealized positions and were allowed to ride. Where possible, the coordinates of hydrogen-bonding hydrogens were allowed to refine. Where appropriate, weighting schemes were optimized based on the recommendations from SHELXL. Heavy atoms were refined with anisotropic thermal parameters. For all structures *except* **6a**, positional coordinates for carboxylic acid hydrogens (labelled H31 except for **2c**, where it is labelled H41) and amine hydrogens (H12A and H12B for all structures) were allowed to refine. Coordinates for the phenolic hydrogen atom H34 of **1c** were allowed to refine.

## Chapter 3

All datasets were collected on a SMART APEX at -120 °C using MoKα radiation. Data were collected using SMART.[1] Initial cell constants were found by small widely separated "matrix" runs. An entire hemisphere of reciprocal space was collected. Scan speed and scan width were chosen based on scattering power and peak rocking curves.

Unit cell constants and orientation matrix were improved by least-squares refinement of reflections thresholded from the entire dataset. Integration was performed with SAINT,[2] using

this improved unit cell as a starting point. Precise unit cell constants were calculated in SAINT from the final merged dataset. Lorenz and polarization corrections were applied. Absorption corrections were not applied.

Data were reduced with SHELXTL.[3] The structures were solved in all cases by direct methods without incident. Unless otherwise noted, hydrogen atoms were assigned to idealized positions and were allowed to ride. All non-hydrogen atoms were given anisotropic thermal parameters.

**7** The compound crystallized in the noncentrosymmetric orthorhombic space group $P2_12_12_1$. Friedel opposites were merged; no attempt was made to determine handedness of the lattice. Coordinates for the -NH2 protons (H12A&B) were allowed to refine.

**7(1)** The compound crystallized in the monoclinic crystal system and exhibited pseudo-merohedral twinning emulating the orthorhombic lattice; β=90.246, refined batch scale factor 0.157(1). The $–NH_2$ protons (H12A&B) were placed in calculated positions and were allowed to ride.

**7a** Coordinates for the $–NH_2$ protons (H12A&B), and carboxylic acid and phenol protons (H31 and H34, respectively) were allowed to refine.

**7b** Coordinates for the $–NH_2$ protons (H12A&B), and carboxylic acid and phenol protons (H31 and H33, respectively) were allowed to refine.

**7c** Proton transfer from acid to pyrimidine was observed. All protons, including pyrimdinium and amine protons, were placed in calculated positions and were allowed to ride. The compound crystallized in the centrosymmetric space group $P2_12_12_1$. Friedel opposites were merged and absolute stereochemistry was indeterminate.

**7d** All protons, including carboxylic acid and amine protons, were placed in calculated positions and were allowed to ride. The molecule crystallized in the polar space group P2(1) and was refined as a racemic twin.

**7e** Proton transfer from acid to pyrimidine was observed. Coordinates for the pyrimidinium proton H11, the $–NH_2$ protons (H12A&B), and the protonated carboxylic acid proton H31 were allowed to refine.

**7f** Proton transfer from acid to pyrimidine was observed. Coordinates for the pyrimidinium proton H11, the $–NH_2$ protons (H12A&B), and the protonated carboxylic acid proton H51 were allowed to refine.

## Chapter 4

Datasets were collected on a SMART APEX or a SMART 1000 as noted. All datasets were collected using MoKα radiation and, where noted, were corrected for absorption using the multi-scan procedure implemented by SADABS.

Data were collected using SMART.[1] Initial cell constants were found by small widely separated "matrix" runs. An entire hemisphere of reciprocal space was collected. Scan speed and scan width were chosen based on scattering power and peak rocking curves.

Unit cell constants and orientation matrix were improved by least-squares refinement of reflections thresholded from the entire dataset. Integration was performed with SAINT,[2] using this improved unit cell as a starting point. Precise unit cell constants were calculated in SAINT from the final merged dataset. Lorenz and polarization corrections were applied, and data were corrected for absorption.

Data were reduced with SHELXTL.[3] The structures were solved in all cases by direct methods without incident. Unless otherwise noted, hydrogens were assigned to idealized positions and were allowed to ride. All non-hydrogen atoms were given anisotropic thermal parameters.

**8a** Data were collected on a SMART APEX at -120 °C. Coordinates of the amine hydrogens H12A and H12B and carboxylic acid hydrogen H31 were allowed to refine.

**13a** Data were collected on a SMART 1000 at -100 °C.

**8b** Data were collected on a SMART APEX at -120 °C.

**13b** Data were collected on a SMART APEX at -120 °C. Proton transfer from acid to amine was clearly observed, and the coordinates of the ammonium hydrogen H11 were allowed to refine.

**14a** Data were collected on a SMART APEX at -120 °C. Proton transfer from acid to amine was clearly observed, and the coordinates of the ammonium hydrogen H11 and amine hydrogens H12A and H12B were allowed to refine.

**8c** Data were collected on a SMART APEX at -120 °C. Coordinates of the carboxylic acid hydrogen H31 were allowed to refine.

**14b** Data were collected on a SMART APEX at -120 °C. Proton transfer from acid to amine was clearly observed, and the coordinates of the ammonium hydrogen H11 and amine hydrogens H12A and H12B were allowed to refine.

## Chapter 5

Unless otherwise noted, X-ray data were collected on a Bruker SMART APEX three-circle CCD diffractometer using molybdenum Kα radiation. Data were collected using SMART.[1] Initial cell constants were found by small widely separated "matrix" runs. An entire hemisphere of reciprocal space was collected. Scan speed and scan width were chosen based on scattering power and peak rocking curves. Unless otherwise noted, data was collected at -173 °C, using 0.3° scan width.

Unit cell dimensions and orientation matrix were improved by least-squares refinement of reflections "thresholded" from the entire dataset. Integration was performed with SAINT,[2] using this improved unit cell as a starting point. Precise unit cell dimensions were calculated in SAINT from the final merged dataset. Lorenz and polarization corrections were applied, and data were corrected for absorption.

Data were reduced with SHELXTL.[3] The structures were solved in all cases by direct methods without incident. In general, hydrogen atoms were assigned to idealized positions and were allowed to ride. Where possible, the coordinates of hydrogen-bonding hydrogen atoms were allowed to refine. Heavy atoms, other than those of the guests, were refined with anisotropic thermal parameters.

**1e** Data were collected on a SMART APEX at 100 K. The copper complex sits on a crystallographic inversion center. Coordinates for the amine hydrogen atoms, H12A and H12B, were allowed to refine.

**1f** Data were collected on a SMART 1000 at 100 K. The lattice contains two independent copper complexes, each sitting on a crystallographic inversion center. Two of the four 2-fluorobenzoates existed in two nearly superimposable rotamers, differing in the relative placement of the fluorine substituent. Coordinates for the amine hydrogen atoms, H22A, H22B, H62A, and H62B, were allowed to refine.

**15a** Data were collected on a SMART 1000 at 100 K. The copper complex sits on a crystallographic inversion center. Coordinates for the amine hydrogen atoms, H12A and H12B, were allowed to refine.

**15b** Data were collected on a SMART 1000 at 100 K. The copper complex sits on a crystallographic inversion center. Both 2-fluorobenzoates existed in two nearly superimposable rotamers, differing in the relative placement of the fluorine substituent. The two amine hydrogen atoms, H22A and H22B, were placed in idealized positions and were allowed to ride.

**6e** Data were collected on a SMART APEX at 100 K. The copper complex sits on a crystallographic inversion center. The asymmetric unit contains a nearly superimposed disordered solvent pair of ethanol and acetonitrile. Occupancies for these two species were allowed to refine during initial model refinement and were fixed at 0.3 and 0.4 for final cycles. Coordinates for the amine hydrogen atoms, H12A and H12B, were allowed to refine.

**16a** Data were collected on a SMART 1000 at 100 K. The copper complex sits on a crystallographic inversion center. Both 2-fluorobenzoates existed in two nearly superimposable rotamers, differing in the relative placement of the fluorine substituent. The (nonsymmetric) acetylene molecule sits on a crystallographic inversion center, with the 2-amino substituent having 50% site occupancy. The amino hydrogen atoms were located in calculated positions and were allowed to ride.

**16b** Data were collected on a SMART APEX at 100 K. The copper complex sits on a crystallographic inversion center. The (nonsymmetric) acetylene molecule sits on a crystallographic inversion center, with the 2-amino substituent having 50% site occupancy. The amino hydrogen atoms were located in calculated positions and were allowed to ride.

**15c** Two disordered chloroform sites were identified in the difference Fourier map. Two conformers were included for each site, with occupancy for each site set to sum to 1, with the minor conformer constrained to approximate the geometry of the major conformer, and with thermal parameters for similarly located atoms tied to each other. The lattice contains two complexes, each located on a crystallographic inversion center. Amine hydrogen atoms H27A, H27B, H57A, and H57B were included at calculated positions. Although the placement of these two species on special positions suggested the possibility of a sublattice, the chloroform molecules were not similarly positioned.

**15d** The cobalt complex sits on a crystallographic inversion center. Coordinates for the amine hydrogen atoms, H52A and H52B, were allowed to refine.

**1g** The asymmetric unit contains a copper complex, located on an inversion center, and a disordered 1,2-dichloroethane species. The latter species contained two conformers (in an approximately 85:15 mixture), both of which straddled an inversion center. The unique carbon on both species was refined isotropically. For purposes of connectivity tables, two chlorine atoms, sharing atomic coordinates and thermal parameters, were included in the atom list. Atomic coordinates for the two amine hydrogen atoms, H22A and H22B, were allowed to refine.

**6f** The copper complex sits on a general position. A slight bit of $-CF_3$ disorder was modeled with two conformers (90:10 ratio). Geometry of the minor species was constrained to that of the major species, the isotropic thermal parameters of the two carbons were tied, and a free variable was employed to model isotropic thermal motion for the fluorine atoms on the minor conformer. Amine hydrogen atoms H12A and H12B were included in calculated positions.

**6g** The cobalt complex sits on a crystallographic inversion center. Amine hydrogen atoms H12A and H12B were allowed to refine.

**6h** Data were collected on a SMART 1000 CCD diffractometer at -100 °C, using a 0.2 ° scan width. The nickel complex sits on a crystallographic inversion center. Amine hydrogen atoms H22A and H22B were allowed to refine.

## Chapter 6

X-ray data were collected, except **20b**, using a fine-focus molybdenum Kα tube. Data were collected using SMART.[1] Initial cell constants were found by small widely separated "matrix" runs. Preliminary Laué symmetry was determined from axial images. For all structures an entire hemisphere of reciprocal space was collected. Scan speed and scan width were chosen based on scattering power and peak rocking curves.

Unit cell constants and orientation matrix were improved by least-squares refinement of reflections thresholded from the entire dataset. Integration was performed with SAINT,[2] using this improved unit cell as a starting point. Precise unit cell constants were calculated in SAINT

from the final merged dataset. Lorenz and polarization corrections were applied. Laué symmetry, space group, and unit cell contents were found with XPREP.

Data were reduced with SHELXTL.[3] The structures were solved in all cases by direct methods without incident. Hydrogen atoms were assigned to idealized positions and were allowed to ride, except as noted. Heavy atoms were refined with anisotropic thermal parameters.

**19** Data were collected at 173 K on a Bruker SMART 1000 diffractometer.

**19(1)** Data were collected at 100 K on a Bruker SMART 1000 diffractometer.

**20** Data were collected at 100 K on a Bruker SMART APEX 1000 diffractometer.

**20(1)** Data were collected at 153 K on a Bruker SMART APEX 1000 diffractometer.

**20a** The compound crystallizes in the tetragonal space groupP4/nnc. The cavitand molecule sits on a 4-fold special position and was fully ordered. The lattice also contained four molecules modelled as ethanol, with partial overlap among three of these four molecules. Site occupancy for these three molecules was restrained to sum to 1.0 by use of a SUMP command. Also present in the lattice were two partially occupied water sites. All solvent molecules were given isotropic thermal parameters.

**20b** The X-ray intensity data were measured at 95(2) K on a Bruker SMART APEX II system equipped with Montel mirrors and a Cu Kα fine-focus sealed tube (λ = 1.54178 Å) operated at 1.5 kW power (50 kV, 30 mA). The detector was placed at a distance of 5.1321 cm. from the crystal.

A total of 5288 frames were collected with a scan width of 0.5º in ω or ϕ and an exposure time of 10.0 sec/frame. The total data collection time was 17.62 hours. The frames were integrated with the Bruker SAINT software package using a narrow-frame integration algorithm. The integration of the data using a triclinic unit cell yielded a total of 35498 reflections to a maximum θ angle of 64.94° (0.85 Å resolution), of which 19633 were independent (average redundancy 1.808, completeness = 94.7%, $R_{int}$= 2.07%, $R_{sig}$ = 3.14%) and 18891 (96.22%) were greater than $2\sigma(F^2)$. The final cell constants of a = 12.4743(2) Å, b = 15.3416(2) Å, c = 21.9472(3) Å, α = 84.7880(10)°, β = 79.0650(10)°, γ = 83.7960(10)°, volume = 4089.09(10)Å$^3$, are based upon the refinement of the XYZ-centroids of 9763 reflections above20 σ(I) with 9.708°< 2θ < 129.243°. Analysis of the data showed negligible decay during data collection. Data were corrected for absorption effects using the multi-scan technique (SADABS). The ratio

of minimum to maximum apparent transmission was 0.4377. The calculated minimum and maximum transmission coefficients (based on crystal size) are 0.2989 and 0.6762.

The structure was solved and refined using the Bruker SHELXTL (Version 6.1) Software Package, using the space group P1, with Z = 1 for the formula unit, $C_{162}H_{166}N_4O_{26}I_2$. The final anisotropic full-matrix least-squares refinement on $F^2$with 1845 variables converged at R1 = 5.64%, for the observed data and wR2 = 16.47% for all data. The goodness-of-fit was 1.028. The largest peak on the final difference electron density synthesis was 1.112 $e^-/Å^3$ and the largest hole was -0.579 $e^-/Å^3$with an RMS deviation of 0.136 $e^-/Å^3$. On the basis of the final model, the calculated density was 1.153 $g/cm^3$ and F(000), 1480 $e^-$.

**21** The cavitand molecule was divided into four RESI parts for ease of labelling. Two of the four residues showed disorder for the two possible orientations of the 3-pyridyl fragment. One alkyl chain showed disorder and was modelled as two fragments, with occupancies summing to 1.0 and with the minor species (80% occupancy) given isotropic thermal parameters. The lattice contained a fully occupied 4-cyanobenzoic acid molecule, a partially occupied benzene molecule, and eight partially occupied methanol molecules. The benzene molecule was treated as an ideal hexagon with a common isotropic thermal parameter. All eight methanol molecules were idealized with DFIX commands and were given isotropic thermal parameters. Overlap among the solvent molecules was handled with SAME instructions.

**22** Data were collected on a SMART 1000 using MoKα radiation at 173 K and were uncorrected for absorption. Thermal parameters for the hydrogen atoms were constrained to 150% (methyl groups) or 120% (all others) of their parent atom. Ordered heavy atoms on the cavitand molecule were refined with anisotropic thermal parameters. Disordered atoms, including those in solvent, were given isotropic thermal parameters.

The cavitand molecule has chemical, but not crystallographical, 4-fold symmetry and was treated as four residues using the SHELXTL RESI command. One of the four borandioxolane fragments (in RESI 3) was disordered and was treated as three PARTs, each with four unique atoms (all ring atoms save the boron). The occupancies for these fragments converged to 58:27:15; these values were constrained for the final refinement cycles. Isotropic thermal parameters were constrained with sets of threefold EADP instructions, and geometries were restrained with SAME instructions.

Another borandioxolane fragment (in RESI 4) exhibited disorder that was modeled by splitting a single ring atom (C24A/B) and its two riding methyl groups. Isotropic thermal parameters were constrained with sets of twofold EADP instructions, and relative occupancy was allowed to refine with a free variable. Geometries were restrained with DFIX commands.

The pentyl chain in RESI 3 was disordered and was modeled with two species. Isotropic thermal parameters were constrained with sets of twofold EADP instructions, and relative occupancy was allowed to refine with a free variable. Geometries were restrained with DFIX commands.

Hexane solvent molecules were contained in two sites in the asymmetric unit. The first site contained two species. Isotropic thermal parameters were constrained with sets of twofold EADP instructions, and relative occupancy was allowed to refine with a free variable. Geometries were restrained with DFIX commands. The second site contained three species. The occupancies for these fragments converged to 35:22:43; these values were constrained for the final refinement cycles. A single free variable was used to model the isotropic thermal motion for all carbon atoms in the three molecules.

**23** Data were collected at 173 K on a SMART 1000, and were corrected for absorption ($\mu$=2.45 $mm^{-1}$; $R_{merge}$ before / after = 5.75 % / 4.00 %; trans min/max = 0.704 / 1.000). All hydrogen atoms were included in idealized positions, and their geometries were not optimized. After initial atom assignment, a feature in the difference density map was assigned as acetonitrile, which was refined successfully with full occupancy and anisotropic thermal motion.

**24** Data were collected at 100 K on a SMART APEX, and were corrected for absorption ($\mu$=0.08 $mm^{-1}$; $R_{merge}$ before / after = 4.55 % / 3.88 %; trans min/max = 0.853 / 1.000). After data collection, the unit cell was re-defined in order to obtain the standard setting of the orthorhombic space group Pnna. After initial atom assignment, a feature in the difference density map very close to a 2-fold axis was assigned as acetonitrile, which was refined successfully as a single species with half occupancy and anisotropic thermal motion. The SHELXL 'SPEC' command was required to prevent the C2S carbon from jumping to the nearby 2-fold axis. Its methyl group geometry was optimized with DFIX distance restraints, since the standard SHELXL 'AFIX 33' command for idealizing a methyl group failed in combination with the 'SPEC' command. Two other features, both located on 2-fold axes, were assigned as two water molecules and were

successfully refined with half occupancy for the water atoms. The positional coordinates of the individual unique hydrogen atom on each water molecule were allowed to refine.

**25a** One of the four alkyl chains was disordered and was treated with two PARTs with anisotropic thermal parameters constrained with pairwise EADP commands. The occupancies, which were constrained to 100%, refined to an ~55% / 45% ratio. The set of solvent molecules consisted of one fully-occupied isotropic acetonitrile, two superimposed acetonitriles with a single isotropic temperature factor (occupancies ~80% / 20% constrained to 100%), and a superimposed isotropic methanol / acetonitrile pair, with occupancies for each molecule fixed for the final refinement.

**25b** The molecule sits on a mirror plane bisecting two pairs of the saturated carbon atoms (C41/C47 and C51/C57) in the cavitand cylinder. These four atoms and the alkyl chains attached to them were all given half occupancy due to their location on a special position. One of these two alkyl chains showed signs of disorder and was treated as two isotropic PARTs, with total occupancy constrained to 50%, with idealized geometries enforced by DFIX commands. The remaining (fully occupied) alkyl chain also showed signs of disorder and was treated as two anisotropic PARTs, with total occupancy constrained to 100%, with idealized geometries enforced by DFIX commands. The set of solvent molecules consisted of two *p*-xylene molecules. The first was given an overall isotropic thermal parameter (which was allowed to refine) and was constrained to 35% occupancy. The second was given a fixed overall thermal parameter of 0.15, and was constrained to 25% occupancy. Because of their location near special positions, the PART -1 command was used to suppress bond generation between unique and equivalent species. As a result of this PART command, the standard AFIX 33 command for methyl hydrogen generation was unstable, and explicit bond length and angle constraints were imposed (using DFIX commands) to generate ideal methyl geometries. The latter *p*-xylene molecule was overlapped by two partially occupied isotropic acetonitrile molecules. Occupancy for these two molecules were constrained to 25%.

## Chapter 7

Single crystals were obtained as colorless plates and blades from toluene. For X-ray examination and data collection, a suitable crystal, approximate dimensions 0.16 x 0.10 x 0.07

mm, was mounted in a loop with paratone-N and transferred immediately to the goniostat bathed in a cold stream.

Intensity data were collected at 173K on a Kappa goniostat equipped with a Bruker Platinum200 CCD detector at Beamline 11.3.1 at the Advanced Light Source (Lawrence Berkeley National Laboratory) using synchrotron radiation tuned to λ=0.77500 Å. The detector was set at a distance of 7.4 cm from the crystal. A series of 1-s data frames measured at 0.2° increments of ω were collected to calculate a unit cell. For data collection frames were measured for a duration of 1-s at 0.3° intervals of ω with a maximum θ value of ~56°. The data frames were collected using the program APEX2 and processed using the program SAINT routine within APEX2. The data were corrected for absorption and beam corrections based on the multiscan technique as implemented in SADABS.

All hydrogens were included in calculated positions and were allowed to ride. All non-hydrogen atoms were given anisotropic thermal parameters with the exception of C87, which was refined isotropically.

A solvent toluene molecule was located in the difference Fourier map as two closely located species. The molecules were refined anisotropically using idealized hexagonal geometry for the benzene ring. Occupancies for the two species were constrained to sum to 1.0 with use of a free variable.

(1) Crystallographic data were collected through the SCrALS (Service Crystallography at Advanced Light Source) program at the Small-Crystal Crystallography Beamline 11.3.1 (developed by the Experimental Systems Group) at the Advanced Light Source (ALS). The ALS is supported by the U.S. Department of Energy, Office of Energy Sciences Materials Sciences Division, under contract DE-AC03-76SF00098 at Lawrence Berkeley National Laboratory.

(2) APEX2 v1.0-27 and SAINT v7.06A data collection and data processing programs, respectively. Bruker Analytical X-ray Instruments, Inc., Madison, WI; SADABS v2.10 semiempirical absorption and beam correction program. G.M. Sheldrick, University of Göttingen, Germany; SHELXTL v6.14 for structure solution, figures and tables, neutral-atom scattering factors as stored in this package. G.M. Sheldrick, University of Göttingen, Germany and Bruker Analytical X-ray Instruments, Inc., Madison, WI.

## References:

[1] SMART v5.060, © 1997 - 1999, Bruker Analytical X-ray Systems, Madison, WI.

[2] SAINT v6.02, © 1997 - 1999, Bruker Analytical X-ray Systems, Madison, WI.

[3] SHELXTL v5.10, © 1997, Bruker Analytical X-ray Systems, Madison, WI.

# Appendix B - Crystallographic Data Tables

**Table B.1** Crystal data and structure refinement for **1, 2, 6, 1a-1d, 2a-2e, and 6a-6d**

**1**

| | | |
|---|---|---|
| Identification code | ns0401 | |
| Empirical formula | C10 H10 N4 | |
| Formula weight | 186.22 | |
| Temperature | 203(2) K | |
| Wavelength | 0.71073 Å | |
| Crystal system | Triclinic | |
| Space group | P-1 | |
| Unit cell dimensions | a = 6.9426(4) Å | α= 92.459(4)°. |
| | b = 7.2048(5) Å | β= 91.380(4)°. |
| | c = 9.3201(6) Å | γ = 107.319(4)°. |
| Volume | 444.31(5) $Å^3$ | |
| Z | 2 | |
| Density (calculated) | 1.392 $g/cm^3$ | |
| Absorption coefficient | 0.090 $mm^{-1}$ | |
| F(000) | 196 | |
| Crystal size | 0.35 x 0.25 x 0.20 $mm^3$ | |
| Theta range for data collection | 2.19 to 27.86°. | |
| Index ranges | -9<=h<=9, -9<=k<=9, -11<=l<=10 | |
| Reflections collected | 3137 | |
| Independent reflections | 1937 [R(int) = 0.0454] | |
| Completeness to theta = 27.86° | 91.5 % | |
| Absorption correction | None | |
| Refinement method | Full-matrix least-squares on $F^2$ | |
| Data / restraints / parameters | 1937 / 0 / 133 | |
| Goodness-of-fit on $F^2$ | 1.119 | |
| Final R indices [I>2sigma(I)] | R1 = 0.0500, wR2 = 0.1507 | |
| R indices (all data) | R1 = 0.0625, wR2 = 0.1613 | |
| Largest diff. peak and hole | 0.258 and -0.284 $e.Å^{-3}$ | |

Crystal data and structure refinement for **2**

| | | |
|---|---|---|
| Identification code | ns0402 | |
| Empirical formula | C11 H12 N4 O | |
| Formula weight | 216.25 | |
| Temperature | 173(2) K | |
| Wavelength | 0.71073 Å | |
| Crystal system | Orthorhombic | |
| Space group | Pbca | |
| Unit cell dimensions | a = 11.6093(10) Å | $\alpha$= 90°. |
| | b = 7.2822(7) Å | $\beta$= 90°. |
| | c = 24.604(2) Å | $\gamma$ = 90°. |
| Volume | 2080.0(3) $Å^3$ | |
| Z | 8 | |
| Density (calculated) | 1.381 $g/cm^3$ | |
| Absorption coefficient | 0.094 $mm^{-1}$ | |
| F(000) | 912 | |
| Crystal size | 0.35 x 0.20 x 0.15 $mm^3$ | |
| Theta range for data collection | 2.41 to 28.28°. | |
| Index ranges | -15<=h<=15, -9<=k<=8, -32<=l<=32 | |
| Reflections collected | 14559 | |
| Independent reflections | 2469 [R(int) = 0.1334] | |
| Completeness to theta = 28.28° | 95.5 % | |
| Absorption correction | None | |
| Refinement method | Full-matrix least-squares on $F^2$ | |
| Data / restraints / parameters | 2469 / 0 / 153 | |
| Goodness-of-fit on $F^2$ | 0.941 | |
| Final R indices [I>2sigma(I)] | R1 = 0.0566, wR2 = 0.1229 | |
| R indices (all data) | R1 = 0.1229, wR2 = 0.1490 | |
| Extinction coefficient | 0.0068(13) | |
| Largest diff. peak and hole | 0.254 and -0.265 $e.Å^{-3}$ | |

Crystal data and structure refinement for **6**

| | | |
|---|---|---|
| Identification code | ns0414 | |
| Empirical formula | C13.50 H13 Cl N4 O | |
| Formula weight | 282.73 | |
| Temperature | 100(2) K | |
| Wavelength | 0.71073 Å | |
| Crystal system | Triclinic | |
| Space group | P-1 | |
| Unit cell dimensions | a = 7.2432(8) Å | α= 107.292(2)°. |
| | b = 7.7893(8) Å | β= 91.059(2)°. |
| | c = 12.6950(13) Å | γ = 98.566(2)°. |
| Volume | 674.75(12) $Å^3$ | |
| Z | 2 | |
| Density (calculated) | 1.392 $g/cm^3$ | |
| Absorption coefficient | 0.282 $mm^{-1}$ | |
| F(000) | 294 | |
| Crystal size | 0.42 x 0.32 x 0.10 $mm^3$ | |
| Theta range for data collection | 1.68 to 29.98°. | |
| Index ranges | -10<=h<=9, -10<=k<=10, -17<=l<=17 | |
| Reflections collected | 7714 | |
| Independent reflections | 3831 [R(int) = 0.0219] | |
| Completeness to theta = 29.98° | 97.6 % | |
| Absorption correction | Semi-empirical from equivalents | |
| Max. and min. transmission | 1.000 and 0.691 | |
| Refinement method | Full-matrix least-squares on $F^2$ | |
| Data / restraints / parameters | 3831 / 3 / 191 | |
| Goodness-of-fit on $F^2$ | 1.253 | |
| Final R indices [I>2sigma(I)] | R1 = 0.0677, wR2 = 0.1755 | |
| R indices (all data) | R1 = 0.0887, wR2 = 0.1922 | |
| Largest diff. peak and hole | 0.709 and -0.392 $e.Å^{-3}$ | |

Crystal data and structure refinement for **1a**

| | | |
|---|---|---|
| Identification code | ns0403 | |
| Empirical formula | C17 H15 N5 O4 | |
| Formula weight | 353.34 | |
| Temperature | 173(2) K | |
| Wavelength | 0.71073 Å | |
| Crystal system | Triclinic | |
| Space group | P-1 | |
| Unit cell dimensions | a = 6.8245(5) Å | $\alpha$= 77.174(4)°. |
| | b = 9.5538(7) Å | $\beta$= 84.400(4)°. |
| | c = 12.6278(9) Å | $\gamma$ = 82.637(4)°. |
| Volume | 794.13(10) Å$^3$ | |
| Z | 2 | |
| Density (calculated) | 1.478 g/cm$^3$ | |
| Absorption coefficient | 0.109 mm$^{-1}$ | |
| F(000) | 368 | |
| Crystal size | 0.30 x 0.25 x 0.10 mm$^3$ | |
| Theta range for data collection | 2.46 to 28.27°. | |
| Index ranges | -8<=h<=9, -12<=k<=12, -16<=l<=16 | |
| Reflections collected | 5974 | |
| Independent reflections | 3581 [R(int) = 0.0577] | |
| Completeness to theta = 28.27° | 90.9 % | |
| Absorption correction | None | |
| Refinement method | Full-matrix least-squares on F$^2$ | |
| Data / restraints / parameters | 3581 / 0 / 245 | |
| Goodness-of-fit on F$^2$ | 0.960 | |
| Final R indices [I>2sigma(I)] | R1 = 0.0506, wR2 = 0.1267 | |
| R indices (all data) | R1 = 0.0835, wR2 = 0.1485 | |
| Extinction coefficient | 0.017(4) | |
| Largest diff. peak and hole | 0.278 and -0.246 e.Å$^{-3}$ | |

Crystal data and structure refinement for **1b**

| | | |
|---|---|---|
| Identification code | ns0533m | |
| Empirical formula | C22 H26 N4 O2 | |
| Formula weight | 378.47 | |
| Temperature | 173(2) K | |
| Wavelength | 0.71073 Å | |
| Crystal system | Triclinic | |
| Space group | P-1 | |
| Unit cell dimensions | a = 8.2088(7) Å | α= 92.767(5)°. |
| | b = 8.7891(6) Å | β= 105.536(4)°. |
| | c = 15.3371(12) Å | γ = 115.332(4)°. |
| Volume | 946.59(13) $Å^3$ | |
| Z | 2 | |
| Density (calculated) | 1.328 $g/cm^3$ | |
| Absorption coefficient | 0.087 $mm^{-1}$ | |
| F(000) | 404 | |
| Crystal size | 0.40 x 0.40 x 0.20 $mm^3$ | |
| Theta range for data collection | 1.40 to 27.90°. | |
| Index ranges | -9<=h<=10, -10<=k<=11, -19<=l<=19 | |
| Reflections collected | 6992 | |
| Independent reflections | 4181 [R(int) = 0.0957] | |
| Completeness to theta = 27.90° | 92.3 % | |
| Absorption correction | None | |
| Refinement method | Full-matrix least-squares on $F^2$ | |
| Data / restraints / parameters | 4181 / 0 / 271 | |
| Goodness-of-fit on $F^2$ | 1.325 | |
| Final R indices [I>2sigma(I)] | R1 = 0.0738, wR2 = 0.1959 | |
| R indices (all data) | R1 = 0.0915, wR2 = 0.2100 | |
| Extinction coefficient | 0.040(9) | |
| Largest diff. peak and hole | 0.471 and -0.391 $e.Å^{-3}$ | |

Crystal data and structure refinement for **1c**

| | | |
|---|---|---|
| Identification code | ns0617 | |
| Empirical formula | C17 H16 N4 O3 | |
| Formula weight | 324.34 | |
| Temperature | 153(2) K | |
| Wavelength | 0.71073 Å | |
| Crystal system | Triclinic | |
| Space group | P-1 | |
| Unit cell dimensions | a = 8.3089(6) Å | α= 85.733(4)°. |
| | b = 8.9991(7) Å | β= 69.174(4)°. |
| | c = 11.1671(7) Å | γ = 77.699(5)°. |
| Volume | 762.52(9) $Å^3$ | |
| Z | 2 | |
| Density (calculated) | 1.413 $g/cm^3$ | |
| Absorption coefficient | 0.100 $mm^{-1}$ | |
| F(000) | 340 | |
| Crystal size | 0.370 x 0.280 x 0.220 $mm^3$ | |
| Theta range for data collection | 1.95 to 26.43°. | |
| Index ranges | -10<=h<=10, -11<=k<=11, -13<=l<=13 | |
| Reflections collected | 22047 | |
| Independent reflections | 3129 [R(int) = 0.1494] | |
| Completeness to theta = 26.43° | 99.5 % | |
| Absorption correction | None | |
| Refinement method | Full-matrix least-squares on $F^2$ | |
| Data / restraints / parameters | 3129 / 0 / 229 | |
| Goodness-of-fit on $F^2$ | 1.161 | |
| Final R indices [I>2sigma(I)] | R1 = 0.0863, wR2 = 0.2031 | |
| R indices (all data) | R1 = 0.1129, wR2 = 0.2161 | |
| Largest diff. peak and hole | 0.590 and -0.683 $e.Å^{-3}$ | |

Crystal data and structure refinement for **1d**

| | | |
|---|---|---|
| Identification code | ns0611 | |
| Empirical formula | C17 H14 F2 N4 O2 | |
| Formula weight | 344.32 | |
| Temperature | 100(2) K | |
| Wavelength | 0.71073 Å | |
| Crystal system | Monoclinic | |
| Space group | P2(1)/n | |
| Unit cell dimensions | a = 7.7430(8) Å | $\alpha$= 90°. |
| | b = 26.469(3) Å | $\beta$= 108.8810(10)°. |
| | c = 7.7443(8) Å | $\gamma$ = 90°. |
| Volume | 1501.8(3) $Å^3$ | |
| Z | 4 | |
| Density (calculated) | 1.523 $g/cm^3$ | |
| Absorption coefficient | 0.120 $mm^{-1}$ | |
| F(000) | 712 | |
| Crystal size | 0.30 x 0.17 x 0.09 $mm^3$ | |
| Theta range for data collection | 2.88 to 28.28°. | |
| Index ranges | -9<=h<=10, -34<=k<=34, -10<=l<=10 | |
| Reflections collected | 13073 | |
| Independent reflections | 3590 [R(int) = 0.0291] | |
| Completeness to theta = 28.28° | 96.6 % | |
| Absorption correction | None | |
| Refinement method | Full-matrix least-squares on $F^2$ | |
| Data / restraints / parameters | 3590 / 0 / 236 | |
| Goodness-of-fit on $F^2$ | 1.064 | |
| Final R indices [I>2sigma(I)] | R1 = 0.0487, wR2 = 0.1241 | |
| R indices (all data) | R1 = 0.0558, wR2 = 0.1286 | |
| Largest diff. peak and hole | 0.429 and -0.218 $e.Å^{-3}$ | |

Crystal data and structure refinement for **2a**

| | | |
|---|---|---|
| Identification code | ns0533 | |
| Empirical formula | C22 H26 N4 O2 | |
| Formula weight | 378.47 | |
| Temperature | 173(2) K | |
| Wavelength | 0.71073 Å | |
| Crystal system | Triclinic | |
| Space group | P-1 | |
| Unit cell dimensions | a = 8.2088(7) Å | α= 92.767(5)°. |
| | b = 8.7891(6) Å | β= 105.536(4)°. |
| | c = 15.3371(12) Å | γ = 115.332(4)°. |
| Volume | 946.59(13) $Å^3$ | |
| Z | 2 | |
| Density (calculated) | 1.328 $g/cm^3$ | |
| Absorption coefficient | 0.087 $mm^{-1}$ | |
| F(000) | 404 | |
| Crystal size | 0.40 x 0.40 x 0.20 $mm^3$ | |
| Theta range for data collection | 1.40 to 27.90°. | |
| Index ranges | -9<=h<=10, -10<=k<=11, -19<=l<=19 | |
| Reflections collected | 6992 | |
| Independent reflections | 4181 [R(int) = 0.0957] | |
| Completeness to theta = 27.90° | 92.3 % | |
| Absorption correction | None | |
| Refinement method | Full-matrix least-squares on $F^2$ | |
| Data / restraints / parameters | 4181 / 0 / 271 | |
| Goodness-of-fit on $F^2$ | 1.325 | |
| Final R indices [I>2sigma(I)] | R1 = 0.0738, wR2 = 0.1959 | |
| R indices (all data) | R1 = 0.0915, wR2 = 0.2100 | |
| Extinction coefficient | 0.040(9) | |
| Largest diff. peak and hole | 0.471 and -0.391 $e.Å^{-3}$ | |

Crystal data and structure refinement for **2b**

| | | |
|---|---|---|
| Identification code | ns0604 | |
| Empirical formula | C18 H16 F2 N4 O3 | |
| Formula weight | 374.35 | |
| Temperature | 293(2) K | |
| Wavelength | 0.71073 Å | |
| Crystal system | Monoclinic | |
| Space group | C2/c | |
| Unit cell dimensions | a = 33.158(4) Å | $\alpha$= 90°. |
| | b = 7.3848(7) Å | $\beta$= 106.439(6)°. |
| | c = 14.1634(16) Å | $\gamma$ = 90°. |
| Volume | 3326.4(6) Å$^3$ | |
| Z | 8 | |
| Density (calculated) | 1.495 g/cm$^3$ | |
| Absorption coefficient | 0.119 mm$^{-1}$ | |
| F(000) | 1552 | |
| Crystal size | 0.310 x 0.140 x 0.080 mm$^3$ | |
| Theta range for data collection | 2.56 to 27.18°. | |
| Index ranges | -42<=h<=41, -9<=k<=9, -18<=l<=18 | |
| Reflections collected | 68430 | |
| Independent reflections | 3690 [R(int) = 0.2039] | |
| Completeness to theta = 27.18° | 99.2 % | |
| Absorption correction | None | |
| Refinement method | Full-matrix least-squares on F$^2$ | |
| Data / restraints / parameters | 3690 / 0 / 260 | |
| Goodness-of-fit on F$^2$ | 0.876 | |
| Final R indices [I>2sigma(I)] | R1 = 0.0558, wR2 = 0.1233 | |
| R indices (all data) | R1 = 0.1522, wR2 = 0.1514 | |
| Largest diff. peak and hole | 0.259 and -0.229 e.Å$^{-3}$ | |

Crystal data and structure refinement for **2c**

| | | |
|---|---|---|
| Identification code | ns0610 | |
| Empirical formula | C23 H28 N4 O3 | |
| Formula weight | 408.49 | |
| Temperature | 100(2) K | |
| Wavelength | 0.71073 Å | |
| Crystal system | Triclinic | |
| Space group | P-1 | |
| Unit cell dimensions | a = 5.3534(5) Å | α= 87.7550(10)°. |
| | b = 12.6941(12) Å | β= 82.9210(10)°. |
| | c = 15.1880(14) Å | γ = 87.542(2)°. |
| Volume | 1022.72(17) $Å^3$ | |
| Z | 2 | |
| Density (calculated) | 1.327 $g/cm^3$ | |
| Absorption coefficient | 0.090 $mm^{-1}$ | |
| F(000) | 436 | |
| Crystal size | 0.42 x 0.14 x 0.06 $mm^3$ | |
| Theta range for data collection | 2.06 to 28.31°. | |
| Index ranges | -7<=h<=7, -16<=k<=16, -20<=l<=19 | |
| Reflections collected | 8494 | |
| Independent reflections | 4648 [R(int) = 0.0204] | |
| Completeness to theta = 28.31° | 91.4 % | |
| Absorption correction | None | |
| Refinement method | Full-matrix least-squares on $F^2$ | |
| Data / restraints / parameters | 4648 / 0 / 280 | |
| Goodness-of-fit on $F^2$ | 1.041 | |
| Final R indices [I>2sigma(I)] | R1 = 0.0519, wR2 = 0.1352 | |
| R indices (all data) | R1 = 0.0711, wR2 = 0.1483 | |
| Largest diff. peak and hole | 0.397 and -0.263 $e.Å^{-3}$ | |

Crystal data and structure refinement for **2d**

| | | |
|---|---|---|
| Identification code | ns0514 | |
| Empirical formula | C18 H16 N6 O7 | |
| Formula weight | 428.37 | |
| Temperature | 203(2) K | |
| Wavelength | 0.71073 Å | |
| Crystal system | Monoclinic | |
| Space group | P2(1)/n | |
| Unit cell dimensions | a = 9.5040(9) Å | $\alpha$= 90°. |
| | b = 21.8091(17) Å | $\beta$= 111.671(5)°. |
| | c = 9.9770(8) Å | $\gamma$ = 90°. |
| Volume | 1921.8(3) Å$^3$ | |
| Z | 4 | |
| Density (calculated) | 1.481 g/cm$^3$ | |
| Absorption coefficient | 0.117 mm$^{-1}$ | |
| F(000) | 888 | |
| Crystal size | 0.30 x 0.20 x 0.10 mm$^3$ | |
| Theta range for data collection | 1.87 to 28.27°. | |
| Index ranges | -12<=h<=12, -28<=k<=28, -13<=l<=13 | |
| Reflections collected | 25722 | |
| Independent reflections | 4447 [R(int) = 0.2018] | |
| Completeness to theta = 28.27° | 93.0 % | |
| Absorption correction | None | |
| Refinement method | Full-matrix least-squares on F$^2$ | |
| Data / restraints / parameters | 4447 / 0 / 289 | |
| Goodness-of-fit on F$^2$ | 0.928 | |
| Final R indices [I>2sigma(I)] | R1 = 0.0659, wR2 = 0.1451 | |
| R indices (all data) | R1 = 0.1673, wR2 = 0.1951 | |
| Largest diff. peak and hole | 0.314 and -0.408 e.Å$^{-3}$ | |

Crystal data and structure refinement for **2e**

| | | |
|---|---|---|
| Identification code | ns0601 | |
| Empirical formula | C18 H16 Cl2 N4 O3 | |
| Formula weight | 407.25 | |
| Temperature | 100(2) K | |
| Wavelength | 0.71073 Å | |
| Crystal system | Monoclinic | |
| Space group | P2(1)/c | |
| Unit cell dimensions | a = 7.0311(6) Å | $\alpha$= 90°. |
| | b = 28.119(2) Å | $\beta$= 99.5930(10)°. |
| | c = 9.0170(8) Å | $\gamma$ = 90°. |
| Volume | 1757.8(3) Å$^3$ | |
| Z | 4 | |
| Density (calculated) | 1.539 g/cm$^3$ | |
| Absorption coefficient | 0.398 mm$^{-1}$ | |
| F(000) | 840 | |
| Crystal size | 0.36 x 0.30 x 0.19 mm$^3$ | |
| Theta range for data collection | 2.40 to 28.27°. | |
| Index ranges | -7<=h<=9, -37<=k<=37, -11<=l<=11 | |
| Reflections collected | 11408 | |
| Independent reflections | 4125 [R(int) = 0.0316] | |
| Completeness to theta = 28.27° | 94.7 % | |
| Absorption correction | Semi-empirical from equivalents | |
| Max. and min. transmission | 1.000 and 0.758 | |
| Refinement method | Full-matrix least-squares on F$^2$ | |
| Data / restraints / parameters | 4125 / 0 / 255 | |
| Goodness-of-fit on F$^2$ | 1.196 | |
| Final R indices [I>2sigma(I)] | R1 = 0.0444, wR2 = 0.1085 | |
| R indices (all data) | R1 = 0.0560, wR2 = 0.1131 | |
| Largest diff. peak and hole | 0.448 and -0.359 e.Å$^{-3}$ | |

Crystal data and structure refinement for **6a**

| | | |
|---|---|---|
| Identification code | ns0523 | |
| Empirical formula | C20 H16 N6 O7 | |
| Formula weight | 452.39 | |
| Temperature | 173(2) K | |
| Wavelength | 0.71073 Å | |
| Crystal system | Triclinic | |
| Space group | P-1 | |
| Unit cell dimensions | a = 7.374(11) Å | $\alpha$= 93.51(10)°. |
| | b = 8.385(13) Å | $\beta$= 96.29(7)°. |
| | c = 17.56(3) Å | $\gamma$ = 104.50(11)°. |
| Volume | 1040(3) $Å^3$ | |
| Z | 2 | |
| Density (calculated) | 1.444 $Mg/m^3$ | |
| Absorption coefficient | 0.113 $mm^{-1}$ | |
| F(000) | 468 | |
| Crystal size | 0.40 x 0.15 x 0.10 $mm^3$ | |
| Theta range for data collection | 2.34 to 27.14°. | |
| Index ranges | -9<=h<=9, -10<=k<=10, -20<=l<=22 | |
| Reflections collected | 7011 | |
| Independent reflections | 4228 [R(int) = 0.2098] | |
| Completeness to theta = 27.14° | 91.7 % | |
| Absorption correction | None | |
| Refinement method | Full-matrix least-squares on $F^2$ | |
| Data / restraints / parameters | 4228 / 0 / 301 | |
| Goodness-of-fit on $F^2$ | 1.042 | |
| Final R indices [I>2sigma(I)] | R1 = 0.1139, wR2 = 0.2495 | |
| R indices (all data) | R1 = 0.2841, wR2 = 0.3299 | |
| Extinction coefficient | 0.057(12) | |
| Largest diff. peak and hole | 0.607 and -0.723 $e.Å^{-3}$ | |

Crystal data and structure refinement for **6b**

| | | |
|---|---|---|
| Identification code | ns0602 | |
| Empirical formula | C20 H17 N5 O5 | |
| Formula weight | 407.39 | |
| Temperature | 100(2) K | |
| Wavelength | 0.71073 Å | |
| Crystal system | Triclinic | |
| Space group | P-1 | |
| Unit cell dimensions | a = 6.9157(12) Å | α= 87.646(3)°. |
| | b = 6.9405(12) Å | β= 80.636(3)°. |
| | c = 19.854(4) Å | γ = 81.138(3)°. |
| Volume | 928.9(3) $Å^3$ | |
| Z | 2 | |
| Density (calculated) | 1.457 $g/cm^3$ | |
| Absorption coefficient | 0.108 $mm^{-1}$ | |
| F(000) | 424 | |
| Crystal size | 0.23 x 0.16 x 0.01 $mm^3$ | |
| Theta range for data collection | 2.08 to 26.02°. | |
| Index ranges | -8<=h<=8, -8<=k<=7, -23<=l<=24 | |
| Reflections collected | 4809 | |
| Independent reflections | 3438 [R(int) = 0.0277] | |
| Completeness to theta = 26.02° | 93.9 % | |
| Absorption correction | None | |
| Refinement method | Full-matrix least-squares on $F^2$ | |
| Data / restraints / parameters | 3438 / 0 / 282 | |
| Goodness-of-fit on $F^2$ | 1.001 | |
| Final R indices [I>2sigma(I)] | R1 = 0.0532, wR2 = 0.1136 | |
| R indices (all data) | R1 = 0.1084, wR2 = 0.1382 | |
| Largest diff. peak and hole | 0.307 and -0.250 $e.Å^{-3}$ | |

Crystal data and structure refinement for **6c**

| | | |
|---|---|---|
| Identification code | ns0609 | |
| Empirical formula | C22 H23 N5 O3 | |
| Formula weight | 405.45 | |
| Temperature | 293(2) K | |
| Wavelength | 0.71073 Å | |
| Crystal system | Monoclinic | |
| Space group | P2(1)/c | |
| Unit cell dimensions | a = 10.5742(19) Å | α= 90°. |
| | b = 14.599(3) Å | β= 102.453(11)°. |
| | c = 13.519(3) Å | γ = 90°. |
| Volume | 2037.9(7) $Å^3$ | |
| Z | 4 | |
| Density (calculated) | 1.322 $g/cm^3$ | |
| Absorption coefficient | 0.091 $mm^{-1}$ | |
| F(000) | 856 | |
| Crystal size | ? x ? x ? $mm^3$ | |
| Theta range for data collection | 2.42 to 27.22°. | |
| Index ranges | -13<=h<=13, -18<=k<=17, -17<=l<=17 | |
| Reflections collected | 44586 | |
| Independent reflections | 4534 [R(int) = 0.1870] | |
| Completeness to theta = 27.22° | 99.4 % | |
| Absorption correction | None | |
| Refinement method | Full-matrix least-squares on $F^2$ | |
| Data / restraints / parameters | 4534 / 0 / 280 | |
| Goodness-of-fit on $F^2$ | 1.019 | |
| Final R indices [I>2sigma(I)] | R1 = 0.0773, wR2 = 0.1753 | |
| R indices (all data) | R1 = 0.1809, wR2 = 0.2304 | |
| Largest diff. peak and hole | 0.268 and -0.375 $e.Å^{-3}$ | |

Crystal data and structure refinement for **6d**

| | | |
|---|---|---|
| Identification code | ns0526 | |
| Empirical formula | C20 H13 F5 N4 O3 | |
| Formula weight | 452.34 | |
| Temperature | 100(2) K | |
| Wavelength | 0.71073 Å | |
| Crystal system | Triclinic | |
| Space group | P-1 | |
| Unit cell dimensions | a = 6.9203(7) Å | α= 79.868(2)°. |
| | b = 7.3200(8) Å | β= 84.1760(10)°. |
| | c = 19.283(2) Å | γ = 77.8480(10)°. |
| Volume | 937.90(17) $Å^3$ | |
| Z | 2 | |
| Density (calculated) | 1.602 $g/cm^3$ | |
| Absorption coefficient | 0.143 $mm^{-1}$ | |
| F(000) | 460 | |
| Crystal size | 0.32 x 0.30 x 0.12 $mm^3$ | |
| Theta range for data collection | 2.15 to 28.28°. | |
| Index ranges | -8<=h<=8, -9<=k<=9, -25<=l<=25 | |
| Reflections collected | 10218 | |
| Independent reflections | 4358 [R(int) = 0.0182] | |
| Completeness to theta = 28.28° | 93.7 % | |
| Absorption correction | None | |
| Refinement method | Full-matrix least-squares on $F^2$ | |
| Data / restraints / parameters | 4358 / 0 / 300 | |
| Goodness-of-fit on $F^2$ | 1.031 | |
| Final R indices [I>2sigma(I)] | R1 = 0.0388, wR2 = 0.1010 | |
| R indices (all data) | R1 = 0.0466, wR2 = 0.1060 | |
| Largest diff. peak and hole | 0.323 and -0.235 $e.Å^{-3}$ | |

**Table B.2** Crystal data and structure refinement for **7, 7a-7f**

**7**

| | | |
|---|---|---|
| Identification code | ns0603 | |
| Empirical formula | C10 H10 N4 | |
| Formula weight | 186.22 | |
| Temperature | 100(2) K | |
| Wavelength | 0.71073 Å | |
| Crystal system | Orthorhombic | |
| Space group | P2(1)2(1)2(1) | |
| Unit cell dimensions | a = 5.5629(4) Å | $\alpha$= 90°. |
| | b = 7.4679(6) Å | $\beta$= 90°. |
| | c = 22.1080(18) Å | $\gamma$ = 90°. |
| Volume | 918.44(12) $Å^3$ | |
| Z | 4 | |
| Density (calculated) | 1.347 $Mg/m^3$ | |
| Absorption coefficient | 0.087 $mm^{-1}$ | |
| F(000) | 392 | |
| Crystal size | 0.10 x 0.24 x 0.25 $mm^3$ | |
| Theta range for data collection | 1.84 to 28.29°. | |
| Index ranges | -7<=h<=7, -9<=k<=9, -29<=l<=29 | |
| Reflections collected | 8151 | |
| Independent reflections | 1333 [R(int) = 0.0259] | |
| Completeness to theta = 28.29° | 98.2 % | |
| Absorption correction | None | |
| Refinement method | Full-matrix least-squares on $F^2$ | |
| Data / restraints / parameters | 1333 / 0 / 134 | |
| Goodness-of-fit on $F^2$ | 1.050 | |
| Final R indices [I>2sigma(I)] | R1 = 0.0365, wR2 = 0.1003 | |
| R indices (all data) | R1 = 0.0383, wR2 = 0.1022 | |
| Absolute structure parameter | 1(3) | |
| Largest diff. peak and hole | 0.291 and -0.172 $e.Å^{-3}$ | |

Crystal data and structure refinement for **7(1)**

| | | |
|---|---|---|
| Identification code | ns0641 | |
| Empirical formula | C10 H10 N4 | |
| Formula weight | 186.22 | |
| Temperature | 293(2) K | |
| Wavelength | 0.71073 Å | |
| Crystal system | Monoclinic | |
| Space group | P2(1)/c | |
| Unit cell dimensions | a = 12.7944(9) Å | α= 90°. |
| | b = 12.9712(9) Å | β= 90.246(4)°. |
| | c = 23.1035(15) Å | γ = 90°. |
| Volume | 3834.2(5) $Å^3$ | |
| Z | 16 | |
| Density (calculated) | 1.290 $g/cm^3$ | |
| Absorption coefficient | 0.083 $mm^{-1}$ | |
| F(000) | 1568 | |
| Crystal size | 0.560 x 0.440 x 0.220 $mm^3$ | |
| Theta range for data collection | 1.57 to 26.58°. | |
| Index ranges | -16<=h<=16, -16<=k<=16, -29<=l<=29 | |
| Reflections collected | 81780 | |
| Independent reflections | 7976 [R(int) = 0.1643] | |
| Completeness to theta = 26.58° | 99.6 % | |
| Absorption correction | None | |
| Refinement method | Full-matrix least-squares on $F^2$ | |
| Data / restraints / parameters | 7976 / 0 / 510 | |
| Goodness-of-fit on $F^2$ | 1.260 | |
| Final R indices [I>2sigma(I)] | R1 = 0.1079, wR2 = 0.2650 | |
| R indices (all data) | R1 = 0.1495, wR2 = 0.3066 | |
| Largest diff. peak and hole | 1.030 and -0.680 $e.Å^{-3}$ | |

Crystal data and structure refinement for **7a**

| | | |
|---|---|---|
| Identification code | ns0625 | |
| Empirical formula | C17 H16 N4 O3 | |
| Formula weight | 324.34 | |
| Temperature | 153(2) K | |
| Wavelength | 0.71073 Å | |
| Crystal system | Monoclinic | |
| Space group | P2(1)/n | |
| Unit cell dimensions | a = 9.3896(7) Å | α= 90°. |
| | b = 9.5195(7) Å | β= 93.833(4)°. |
| | c = 17.5881(12) Å | γ = 90°. |
| Volume | 1568.6(2) $Å^3$ | |
| Z | 4 | |
| Density (calculated) | 1.373 $g/cm^3$ | |
| Absorption coefficient | 0.097 $mm^{-1}$ | |
| F(000) | 680 | |
| Crystal size | 0.450 x 0.410 x 0.260 $mm^3$ | |
| Theta range for data collection | 2.39 to 27.19°. | |
| Index ranges | -12<=h<=12, -12<=k<=12, -22<=l<=22 | |
| Reflections collected | 39361 | |
| Independent reflections | 3480 [R(int) = 0.1389] | |
| Completeness to theta = 27.19° | 99.8 % | |
| Absorption correction | None | |
| Refinement method | Full-matrix least-squares on $F^2$ | |
| Data / restraints / parameters | 3480 / 0 / 229 | |
| Goodness-of-fit on $F^2$ | 1.093 | |
| Final R indices [I>2sigma(I)] | R1 = 0.0678, wR2 = 0.1705 | |
| R indices (all data) | R1 = 0.0830, wR2 = 0.1794 | |
| Largest diff. peak and hole | 0.591 and -0.515 $e.Å^{-3}$ | |

Crystal data and structure refinement for **7b**

| | | |
|---|---|---|
| Identification code | ns0628 | |
| Empirical formula | C17 H16 N4 O3 | |
| Formula weight | 324.34 | |
| Temperature | 173(2) K | |
| Wavelength | 0.71073 Å | |
| Crystal system | Triclinic | |
| Space group | P-1 | |
| Unit cell dimensions | a = 8.1179(5) Å | α= 63.121(4)°. |
| | b = 10.2654(6) Å | β= 78.189(4)°. |
| | c = 10.3655(6) Å | γ = 80.757(4)°. |
| Volume | 751.86(8) $Å^3$ | |
| Z | 2 | |
| Density (calculated) | 1.433 $g/cm^3$ | |
| Absorption coefficient | 0.101 $mm^{-1}$ | |
| F(000) | 340 | |
| Crystal size | 0.340 x 0.160 x 0.120 $mm^3$ | |
| Theta range for data collection | 3.10 to 27.53°. | |
| Index ranges | -10<=h<=10, -13<=k<=13, -13<=l<=12 | |
| Reflections collected | 18176 | |
| Independent reflections | 3442 [R(int) = 0.2027] | |
| Completeness to theta = 27.54° | 99.3 % | |
| Absorption correction | None | |
| Refinement method | Full-matrix least-squares on $F^2$ | |
| Data / restraints / parameters | 3442 / 0 / 230 | |
| Goodness-of-fit on $F^2$ | 0.857 | |
| Final R indices [I>2sigma(I)] | R1 = 0.0707, wR2 = 0.1392 | |
| R indices (all data) | R1 = 0.1771, wR2 = 0.1749 | |
| Largest diff. peak and hole | 0.304 and -0.339 $e.Å^{-3}$ | |

Crystal data and structure refinement for **7c**

| | | |
|---|---|---|
| Identification code | ns0614 | |
| Empirical formula | C17 H14 N6 O6 | |
| Formula weight | 398.34 | |
| Temperature | 153(2) K | |
| Wavelength | 0.71073 Å | |
| Crystal system | Orthorhombic | |
| Space group | P2(1)2(1)2(1) | |
| Unit cell dimensions | a = 6.2321(14) Å | $\alpha$= 90°. |
| | b = 11.369(2) Å | $\beta$= 90°. |
| | c = 25.320(5) Å | $\gamma$ = 90°. |
| Volume | 1794.0(7) $Å^3$ | |
| Z | 4 | |
| Density (calculated) | 1.475 $g/cm^3$ | |
| Absorption coefficient | 0.115 $mm^{-1}$ | |
| F(000) | 824 | |
| Crystal size | 0.500 x 0.220 x 0.170 $mm^3$ | |
| Theta range for data collection | 2.41 to 26.35°. | |
| Index ranges | -7<=h<=7, -14<=k<=14, -31<=l<=30 | |
| Reflections collected | 22642 | |
| Independent reflections | 2119 [R(int) = 0.1936] | |
| Completeness to theta = 26.35° | 99.2 % | |
| Absorption correction | None | |
| Refinement method | Full-matrix least-squares on $F^2$ | |
| Data / restraints / parameters | 2119 / 0 / 263 | |
| Goodness-of-fit on $F^2$ | 0.891 | |
| Final R indices [I>2sigma(I)] | R1 = 0.0637, wR2 = 0.1529 | |
| R indices (all data) | R1 = 0.1287, wR2 = 0.1739 | |
| Absolute structure parameter | -5(3) | |
| Largest diff. peak and hole | 0.259 and -0.295 $e.Å^{-3}$ | |

Crystal data and structure refinement for **7d**

| | | |
|---|---|---|
| Identification code | ns0607 | |
| Empirical formula | C24 H18 N8 O12 | |
| Formula weight | 610.46 | |
| Temperature | 100(2) K | |
| Wavelength | 0.71073 Å | |
| Crystal system | Triclinic | |
| Space group | P-1 | |
| Unit cell dimensions | a = 7.7509(6) Å | α= 98.7900(10)°. |
| | b = 11.8158(8) Å | β= 102.3690(10)°. |
| | c = 14.5927(10) Å | γ = 101.4610(10)°. |
| Volume | 1252.46(15) $Å^3$ | |
| Z | 2 | |
| Density (calculated) | 1.619 $g/cm^3$ | |
| Absorption coefficient | 0.133 $mm^{-1}$ | |
| F(000) | 628 | |
| Crystal size | 0.36 x 0.32 x 0.27 $mm^3$ | |
| Theta range for data collection | 1.80 to 28.28°. | |
| Index ranges | -10<=h<=10, -15<=k<=15, -18<=l<=19 | |
| Reflections collected | 11132 | |
| Independent reflections | 5761 [R(int) = 0.0172] | |
| Completeness to theta = 28.28° | 92.7 % | |
| Absorption correction | None | |
| Refinement method | Full-matrix least-squares on $F^2$ | |
| Data / restraints / parameters | 5761 / 0 / 409 | |
| Goodness-of-fit on $F^2$ | 1.027 | |
| Final R indices [I>2sigma(I)] | R1 = 0.0394, wR2 = 0.1028 | |
| R indices (all data) | R1 = 0.0464, wR2 = 0.1078 | |
| Largest diff. peak and hole | 0.322 and -0.389 $e.Å^{-3}$ | |

Crystal data and structure refinement for **7e**

| | | |
|---|---|---|
| Identification code | ns0612 | |
| Empirical formula | C26 H24 Br2 N4 O4 | |
| Formula weight | 616.31 | |
| Temperature | 153(2) K | |
| Wavelength | 0.71073 Å | |
| Crystal system | Monoclinic | |
| Space group | P2(1) | |
| Unit cell dimensions | a = 8.8985(15) Å | $\alpha$= 90°. |
| | b = 12.542(2) Å | $\beta$= 93.343(10)°. |
| | c = 11.395(2) Å | $\gamma$ = 90°. |
| Volume | 1269.6(4) Å$^3$ | |
| Z | 2 | |
| Density (calculated) | 1.612 Mg/m$^3$ | |
| Absorption coefficient | 3.233 mm$^{-1}$ | |
| F(000) | 620 | |
| Crystal size | 0.460 x 0.200 x 0.140 mm$^3$ | |
| Theta range for data collection | 2.42 to 27.33°. | |
| Index ranges | -11<=h<=11, -16<=k<=16, -14<=l<=14 | |
| Reflections collected | 65470 | |
| Independent reflections | 5645 [R(int) = 0.1296] | |
| Completeness to theta = 27.33° | 98.8 % | |
| Absorption correction | None | |
| Refinement method | Full-matrix least-squares on F$^2$ | |
| Data / restraints / parameters | 5645 / 1 / 329 | |
| Goodness-of-fit on F$^2$ | 0.952 | |
| Final R indices [I>2sigma(I)] | R1 = 0.0620, wR2 = 0.1494 | |
| R indices (all data) | R1 = 0.1436, wR2 = 0.1809 | |
| Absolute structure parameter | 0.191(18) | |
| Largest diff. peak and hole | 1.053 and -0.479 e.Å$^{-3}$ | |

Crystal data and structure refinement for **7f**

| | | |
|---|---|---|
| Identification code | ns0621 | |
| Empirical formula | C29 H27 F5 N4 O4 | |
| Formula weight | 590.55 | |
| Temperature | 293(2) K | |
| Wavelength | 0.71073 Å | |
| Crystal system | Triclinic | |
| Space group | P-1 | |
| Unit cell dimensions | a = 8.7406(5) Å | $\alpha$= 97.769(3)°. |
| | b = 9.2684(5) Å | $\beta$= 92.821(4)°. |
| | c = 17.1083(9) Å | $\gamma$ = 106.978(3)°. |
| Volume | 1307.63(12) Å$^3$ | |
| Z | 2 | |
| Density (calculated) | 1.500 g/cm$^3$ | |
| Absorption coefficient | 0.125 mm$^{-1}$ | |
| F(000) | 612 | |
| Crystal size | 0.250 x 0.140 x 0.120 mm$^3$ | |
| Theta range for data collection | 2.45 to 27.15°. | |
| Index ranges | -11<=h<=11, -11<=k<=11, -21<=l<=21 | |
| Reflections collected | 50487 | |
| Independent reflections | 5737 [R(int) = 0.2262] | |
| Completeness to theta = 27.15° | 99.1 % | |
| Absorption correction | None | |
| Refinement method | Full-matrix least-squares on F$^2$ | |
| Data / restraints / parameters | 5737 / 0 / 398 | |
| Goodness-of-fit on F$^2$ | 0.980 | |
| Final R indices [I>2sigma(I)] | R1 = 0.0829, wR2 = 0.1694 | |
| R indices (all data) | R1 = 0.1913, wR2 = 0.2177 | |
| Largest diff. peak and hole | 0.405 and -0.376 e.Å$^{-3}$ | |

**Table B.3** Crystal data and structure refinement for **14, 8a, 13a, 8b, 13b, 14a, 8c, 14b**

**14**

| | | |
|---|---|---|
| Identification code | ns0624 | |
| Empirical formula | C7 H Br F4 O2 | |
| Formula weight | 272.99 | |
| Temperature | 173(2) K | |
| Wavelength | 0.71073 Å | |
| Crystal system | Monoclinic | |
| Space group | P2(1)/n | |
| Unit cell dimensions | a = 4.3494(5) Å | α= 90°. |
| | b = 15.8920(18) Å | β= 100.463(8)°. |
| | c = 11.3932(14) Å | γ = 90°. |
| Volume | 774.41(16) $Å^3$ | |
| Z | 4 | |
| Density (calculated) | 2.341 $g/cm^3$ | |
| Absorption coefficient | 5.347 $mm^{-1}$ | |
| F(000) | 520 | |
| Crystal size | 0.45 x 0.40 x 0.15 $mm^3$ | |
| Theta range for data collection | 2.22 to 28.22°. | |
| Index ranges | -5<=h<=5, -20<=k<=20, -15<=l<=14 | |
| Reflections collected | 8772 | |
| Independent reflections | 1811 [R(int) = 0.0767] | |
| Completeness to theta = 28.22° | 94.9 % | |
| Absorption correction | Semi-empirical from equivalents | |
| Max. and min. transmission | 1.000 and 0.267 | |
| Refinement method | Full-matrix least-squares on $F^2$ | |
| Data / restraints / parameters | 1811 / 0 / 127 | |
| Goodness-of-fit on $F^2$ | 1.072 | |
| Final R indices [I>2sigma(I)] | R1 = 0.0547, wR2 = 0.1333 | |
| R indices (all data) | R1 = 0.0949, wR2 = 0.1670 | |
| Largest diff. peak and hole | 1.449 and -1.031 $e.Å^{-3}$ | |

Crystal data and structure refinement for **8a**

| | | |
|---|---|---|
| Identification code | ns0636 | |
| Empirical formula | C41 H38 I2 N8 O4 | |
| Formula weight | 960.59 | |
| Temperature | 293(2) K | |
| Wavelength | 0.71073 Å | |
| Crystal system | Triclinic | |
| Space group | P-1 | |
| Unit cell dimensions | a = 6.5689(2) Å | $\alpha$= 102.542(2)°. |
| | b = 9.5508(4) Å | $\beta$= 99.117(2)°. |
| | c = 16.4413(6) Å | $\gamma$ = 96.534(2)°. |
| Volume | 982.34(6) Å$^3$ | |
| Z | 1 | |
| Density (calculated) | 1.624 g/cm$^3$ | |
| Absorption coefficient | 1.653 mm$^{-1}$ | |
| F(000) | 478 | |
| Crystal size | 0.200 x 0.180 x 0.160 mm$^3$ | |
| Theta range for data collection | 3.18 to 27.50°. | |
| Index ranges | -8<=h<=8, -12<=k<=12, -21<=l<=21 | |
| Reflections collected | 38388 | |
| Independent reflections | 4495 [R(int) = 0.0384] | |
| Completeness to theta = 27.50° | 99.5 % | |
| Absorption correction | Semi-empirical from equivalents | |
| Max. and min. transmission | 1.000 and 0.930 | |
| Refinement method | Full-matrix least-squares on F$^2$ | |
| Data / restraints / parameters | 4495 / 0 / 290 | |
| Goodness-of-fit on F$^2$ | 1.056 | |
| Final R indices [I>2sigma(I)] | R1 = 0.0216, wR2 = 0.0517 | |
| R indices (all data) | R1 = 0.0241, wR2 = 0.0532 | |
| Largest diff. peak and hole | 0.873 and -0.772 e.Å$^{-3}$ | |

Crystal data and structure refinement for **13a**

| | | |
|---|---|---|
| Identification code | ns0626 | |
| Empirical formula | C17 H11 F4 I N4 O2 | |
| Formula weight | 506.20 | |
| Temperature | 173(2) K | |
| Wavelength | 0.71073 Å | |
| Crystal system | Monoclinic | |
| Space group | P2(1)/n | |
| Unit cell dimensions | a = 6.6313(15) Å | α= 90°. |
| | b = 34.494(8) Å | β= 103.151(16)°. |
| | c = 7.6535(18) Å | γ = 90°. |
| Volume | 1704.8(7) $Å^3$ | |
| Z | 4 | |
| Density (calculated) | 1.972 $g/cm^3$ | |
| Absorption coefficient | 1.943 $mm^{-1}$ | |
| F(000) | 984 | |
| Crystal size | 0.45 x 0.15 x 0.05 $mm^3$ | |
| Theta range for data collection | 1.18 to 28.76°. | |
| Index ranges | -8<=h<=8, -44<=k<=45, -10<=l<=9 | |
| Reflections collected | 12690 | |
| Independent reflections | 4007 [R(int) = 0.1594] | |
| Completeness to theta = 28.76° | 90.6 % | |
| Absorption correction | None | |
| Refinement method | Full-matrix least-squares on $F^2$ | |
| Data / restraints / parameters | 4007 / 0 / 254 | |
| Goodness-of-fit on $F^2$ | 0.944 | |
| Final R indices [I>2sigma(I)] | R1 = 0.0664, wR2 = 0.1606 | |
| R indices (all data) | R1 = 0.0999, wR2 = 0.1768 | |
| Largest diff. peak and hole | 1.721 and -3.059 $e.Å^{-3}$ | |

Crystal data and structure refinement for **8b**

| | | |
|---|---|---|
| Identification code | ns0618 | |
| Empirical formula | C17 H15 I N4 O2 | |
| Formula weight | 434.23 | |
| Temperature | 153(2) K | |
| Wavelength | 0.71073 Å | |
| Crystal system | Triclinic | |
| Space group | P-1 | |
| Unit cell dimensions | a = 7.9304(7) Å | $\alpha$= 109.850(3)°. |
| | b = 10.0937(9) Å | $\beta$= 96.640(4)°. |
| | c = 11.1149(10) Å | $\gamma$ = 96.096(4)°. |
| Volume | 821.10(13) Å$^3$ | |
| Z | 2 | |
| Density (calculated) | 1.756 Mg/m$^3$ | |
| Absorption coefficient | 1.968 mm$^{-1}$ | |
| F(000) | 428 | |
| Crystal size | 0.460 x 0.300 x 0.280 mm$^3$ | |
| Theta range for data collection | 1.97 to 27.48°. | |
| Index ranges | -10<=h<=10, -12<=k<=13, -14<=l<=14 | |
| Reflections collected | 25406 | |
| Independent reflections | 3768 [R(int) = 0.0787] | |
| Completeness to theta = 27.48° | 99.7 % | |
| Absorption correction | None | |
| Refinement method | Full-matrix least-squares on F$^2$ | |
| Data / restraints / parameters | 3768 / 0 / 218 | |
| Goodness-of-fit on F$^2$ | 1.076 | |
| Final R indices [I>2sigma(I)] | R1 = 0.0360, wR2 = 0.0947 | |
| R indices (all data) | R1 = 0.0385, wR2 = 0.0966 | |
| Largest diff. peak and hole | 1.103 and -0.868 e.Å$^{-3}$ | |

Crystal data and structure refinement for **13b**

| | | |
|---|---|---|
| Identification code | ns0629 | |
| Empirical formula | C17 H11 F4 I N4 O2 | |
| Formula weight | 506.20 | |
| Temperature | 153(2) K | |
| Wavelength | 0.71073 Å | |
| Crystal system | Monoclinic | |
| Space group | P2(1)/c | |
| Unit cell dimensions | a = 3.9153(3) Å | $\alpha$= 90°. |
| | b = 24.016(2) Å | $\beta$= 92.995(4)°. |
| | c = 18.1909(15) Å | $\gamma$ = 90°. |
| Volume | 1708.1(2) $Å^3$ | |
| Z | 4 | |
| Density (calculated) | 1.968 $g/cm^3$ | |
| Absorption coefficient | 1.939 $mm^{-1}$ | |
| F(000) | 984 | |
| Crystal size | 0.580 x 0.140 x 0.080 $mm^3$ | |
| Theta range for data collection | 2.78 to 27.13°. | |
| Index ranges | -5<=h<=5, -30<=k<=29, -23<=l<=22 | |
| Reflections collected | 40104 | |
| Independent reflections | 3737 [R(int) = 0.1383] | |
| Completeness to theta = 27.13° | 99.7 % | |
| Absorption correction | None | |
| Refinement method | Full-matrix least-squares on $F^2$ | |
| Data / restraints / parameters | 3737 / 0 / 257 | |
| Goodness-of-fit on $F^2$ | 1.019 | |
| Final R indices [I>2sigma(I)] | R1 = 0.0433, wR2 = 0.1079 | |
| R indices (all data) | R1 = 0.0599, wR2 = 0.1189 | |
| Largest diff. peak and hole | 0.796 and -0.991 $e.Å^{-3}$ | |

Crystal data and structure refinement for **14a**

| | | |
|---|---|---|
| Identification code | ns0639 | |
| Empirical formula | C17 H11 Br F4 N4 O2 | |
| Formula weight | 459.21 | |
| Temperature | 293(2) K | |
| Wavelength | 0.71073 Å | |
| Crystal system | Monoclinic | |
| Space group | P2(1)/c | |
| Unit cell dimensions | a = 3.79850(10) Å | $\alpha$= 90°. |
| | b = 24.2190(7) Å | $\beta$= 93.6890(10)°. |
| | c = 18.1436(5) Å | $\gamma$ = 90°. |
| Volume | 1665.68(8) Å$^3$ | |
| Z | 4 | |
| Density (calculated) | 1.831 Mg/m$^3$ | |
| Absorption coefficient | 2.534 mm$^{-1}$ | |
| F(000) | 912 | |
| Crystal size | 0.500 x 0.210 x 0.140 mm$^3$ | |
| Theta range for data collection | 3.36 to 27.12°. | |
| Index ranges | -4<=h<=4, -31<=k<=30, -23<=l<=23 | |
| Reflections collected | 42293 | |
| Independent reflections | 3662 [R(int) = 0.0370] | |
| Completeness to theta = 27.12° | 99.7 % | |
| Absorption correction | Semi-empirical from equivalents | |
| Max. and min. transmission | 1.000 and 0.882 | |
| Refinement method | Full-matrix least-squares on F$^2$ | |
| Data / restraints / parameters | 3662 / 0 / 263 | |
| Goodness-of-fit on F$^2$ | 1.050 | |
| Final R indices [I>2sigma(I)] | R1 = 0.0243, wR2 = 0.0628 | |
| R indices (all data) | R1 = 0.0304, wR2 = 0.0655 | |
| Largest diff. peak and hole | 0.356 and -0.353 e.Å$^{-3}$ | |

Crystal data and structure refinement for **8c**

| | | |
|---|---|---|
| Identification code | ns0633 | |
| Empirical formula | C20 H17 I N4 O3 | |
| Formula weight | 488.28 | |
| Temperature | 293(2) K | |
| Wavelength | 0.71073 Å | |
| Crystal system | Triclinic | |
| Space group | P-1 | |
| Unit cell dimensions | a = 6.7820(5) Å | $\alpha$= 103.905(4)°. |
| | b = 8.9813(7) Å | $\beta$= 95.254(4)°. |
| | c = 16.6932(11) Å | $\gamma$ = 100.313(5)°. |
| Volume | 961.37(12) $Å^3$ | |
| Z | 2 | |
| Density (calculated) | 1.687 $g/cm^3$ | |
| Absorption coefficient | 1.695 $mm^{-1}$ | |
| F(000) | 484 | |
| Crystal size | 0.380 x 0.120 x 0.080 $mm^3$ | |
| Theta range for data collection | 2.39 to 27.62°. | |
| Index ranges | -8<=h<=8, -11<=k<=11, -21<=l<=21 | |
| Reflections collected | 39877 | |
| Independent reflections | 4426 [R(int) = 0.2269] | |
| Completeness to theta = 27.62° | 98.8 % | |
| Absorption correction | Semi-empirical from equivalents | |
| Max. and min. transmission | 1.000 and 0.671 | |
| Refinement method | Full-matrix least-squares on $F^2$ | |
| Data / restraints / parameters | 4426 / 0 / 258 | |
| Goodness-of-fit on $F^2$ | 1.017 | |
| Final R indices [I>2sigma(I)] | R1 = 0.0745, wR2 = 0.1835 | |
| R indices (all data) | R1 = 0.0954, wR2 = 0.1928 | |
| Largest diff. peak and hole | 1.095 and -1.139 $e.Å^{-3}$ | |

Crystal data and structure refinement for **14b**

| | | |
|---|---|---|
| Identification code | ns0632 | |
| Empirical formula | C20 H13 Br F4 N4 O3 | |
| Formula weight | 513.25 | |
| Temperature | 293(2) K | |
| Wavelength | 0.71073 Å | |
| Crystal system | Triclinic | |
| Space group | P-1 | |
| Unit cell dimensions | a = 6.8878(2) Å | $\alpha$= 80.331(2)°. |
| | b = 7.4613(2) Å | $\beta$= 88.064(2)°. |
| | c = 19.6275(7) Å | $\gamma$ = 77.591(2)°. |
| Volume | 971.13(5) Å$^3$ | |
| Z | 2 | |
| Density (calculated) | 1.755 g/cm$^3$ | |
| Absorption coefficient | 2.187 mm$^{-1}$ | |
| F(000) | 512 | |
| Crystal size | 0.360 x 0.290 x 0.100 mm$^3$ | |
| Theta range for data collection | 2.11 to 27.10°. | |
| Index ranges | -8<=h<=8, -9<=k<=9, -25<=l<=25 | |
| Reflections collected | 24991 | |
| Independent reflections | 4292 [R(int) = 0.0374] | |
| Completeness to theta = 27.10° | 99.9 % | |
| Absorption correction | Semi-empirical from equivalents | |
| Max. and min. transmission | 1.000 and 0.921 | |
| Refinement method | Full-matrix least-squares on F$^2$ | |
| Data / restraints / parameters | 4292 / 0 / 300 | |
| Goodness-of-fit on F$^2$ | 1.213 | |
| Final R indices [I>2sigma(I)] | R1 = 0.0246, wR2 = 0.0765 | |
| R indices (all data) | R1 = 0.0293, wR2 = 0.0968 | |
| Largest diff. peak and hole | 0.396 and -0.370 e.Å$^{-3}$ | |

**Table B.4** Crystal data and structure refinement for **16, 1e, 1f, 15a, 15b, 6e, 16a, 16b, 15c, 15d, 1g, 6f, 6g, and 6h**

**16**

| | | |
|---|---|---|
| Identification code | ns0413 | |
| Empirical formula | C12 H9 N3 | |
| Formula weight | 195.22 | |
| Temperature | 100(2) K | |
| Wavelength | 0.71073 Å | |
| Crystal system | Monoclinic | |
| Space group | P2(1)/c | |
| Unit cell dimensions | a = 8.6286(6) Å | α= 90°. |
| | b = 15.3249(10) Å | β= 115.5070(10)°. |
| | c = 8.1780(6) Å | γ = 90°. |
| Volume | 976.00(12) $Å^3$ | |
| Z | 4 | |
| Density (calculated) | 1.329 $g/cm^3$ | |
| Absorption coefficient | 0.083 $mm^{-1}$ | |
| F(000) | 408 | |
| Crystal size | 0.56 x 0.50 x 0.24 $mm^3$ | |
| Theta range for data collection | 2.62 to 30.02°. | |
| Index ranges | -12<=h<=12, -21<=k<=21, -11<=l<=11 | |
| Reflections collected | 11007 | |
| Independent reflections | 2834 [R(int) = 0.0195] | |
| Completeness to theta = 30.02° | 99.3 % | |
| Absorption correction | Semi-empirical from equivalents | |
| Max. and min. transmission | 1.000 and 0.832 | |
| Refinement method | Full-matrix least-squares on $F^2$ | |
| Data / restraints / parameters | 2834 / 0 / 142 | |
| Goodness-of-fit on $F^2$ | 1.464 | |
| Final R indices [I>2sigma(I)] | R1 = 0.0563, wR2 = 0.1780 | |
| R indices (all data) | R1 = 0.0624, wR2 = 0.1887 | |
| Largest diff. peak and hole | 0.381 and -0.505 $e.Å^{-3}$ | |

Crystal data and structure refinement for **1e**

| | | |
|---|---|---|
| Identification code | ns0409 | |
| Empirical formula | C28 H32 Cu2 N8 O8 | |
| Formula weight | 735.70 | |
| Temperature | 100(2) K | |
| Wavelength | 0.71073 Å | |
| Crystal system | Monoclinic | |
| Space group | P2(1)/c | |
| Unit cell dimensions | a = 8.0282(5) Å | $\alpha$= 90°. |
| | b = 10.6399(7) Å | $\beta$= 99.3600(10)°. |
| | c = 18.9041(13) Å | $\gamma$ = 90°. |
| Volume | 1593.27(18) $Å^3$ | |
| Z | 2 | |
| Density (calculated) | 1.534 $g/cm^3$ | |
| Absorption coefficient | 1.396 $mm^{-1}$ | |
| F(000) | 756 | |
| Crystal size | 0.16 x 0.28 x 0.38 $mm^3$ | |
| Theta range for data collection | 2.18 to 30.00°. | |
| Index ranges | -11<=h<=11, -14<=k<=14, -26<=l<=26 | |
| Reflections collected | 17891 | |
| Independent reflections | 4630 [R(int) = 0.0237] | |
| Completeness to theta = 30.00° | 99.8 % | |
| Absorption correction | None | |
| Refinement method | Full-matrix least-squares on $F^2$ | |
| Data / restraints / parameters | 4630 / 0 / 217 | |
| Goodness-of-fit on $F^2$ | 1.052 | |
| Final R indices [I>2sigma(I)] | R1 = 0.0276, wR2 = 0.0751 | |
| R indices (all data) | R1 = 0.0301, wR2 = 0.0767 | |
| Largest diff. peak and hole | 0.553 and -0.315 $e.Å^{-3}$ | |

Crystal data and structure refinement for **1f**

| | | |
|---|---|---|
| Identification code | ns0426 | |
| Empirical formula | C48 H36 Cu2 F4 N8 O8 | |
| Formula weight | 1055.93 | |
| Temperature | 173(2) K | |
| Wavelength | 0.71073 Å | |
| Crystal system | Monoclinic | |
| Space group | P2(1)/c | |
| Unit cell dimensions | a = 21.3553(18) Å | $\alpha$= 90°. |
| | b = 17.9389(15) Å | $\beta$= 90.742(5)°. |
| | c = 11.4887(9) Å | $\gamma$ = 90°. |
| Volume | 4400.8(6) $Å^3$ | |
| Z | 4 | |
| Density (calculated) | 1.594 $g/cm^3$ | |
| Absorption coefficient | 1.050 $mm^{-1}$ | |
| F(000) | 2152 | |
| Crystal size | 0.40 x 0.20 x 0.10 $mm^3$ | |
| Theta range for data collection | 1.48 to 28.30°. | |
| Index ranges | -26<=h<=27, -23<=k<=23, -15<=l<=14 | |
| Reflections collected | 31431 | |
| Independent reflections | 9998 [R(int) = 0.0734] | |
| Completeness to theta = 28.30° | 91.3 % | |
| Absorption correction | None | |
| Refinement method | Full-matrix least-squares on $F^2$ | |
| Data / restraints / parameters | 9998 / 0 / 658 | |
| Goodness-of-fit on $F^2$ | 0.984 | |
| Final R indices [I>2sigma(I)] | R1 = 0.0470, wR2 = 0.1060 | |
| R indices (all data) | R1 = 0.0965, wR2 = 0.1240 | |
| Largest diff. peak and hole | 0.486 and -0.534 e.$Å^{-3}$ | |

Crystal data and structure refinement for **15a**

| | | |
|---|---|---|
| Identification code | ns0405 | |
| Empirical formula | C28 H32 Cu2 N8 O10 | |
| Formula weight | 767.70 | |
| Temperature | 173(2) K | |
| Wavelength | 0.71073 Å | |
| Crystal system | Triclinic | |
| Space group | P-1 | |
| Unit cell dimensions | a = 8.2800(6) Å | $\alpha$= 71.144(4)°. |
| | b = 9.3983(6) Å | $\beta$= 81.585(4)°. |
| | c = 11.2233(7) Å | $\gamma$ = 79.240(4)°. |
| Volume | 808.49(9) Å$^3$ | |
| Z | 1 | |
| Density (calculated) | 1.577 g/cm$^3$ | |
| Absorption coefficient | 1.383 mm$^{-1}$ | |
| F(000) | 394 | |
| Crystal size | 0.40 x 0.15 x 0.10 mm$^3$ | |
| Theta range for data collection | 2.32 to 28.24°. | |
| Index ranges | -10<=h<=9, -12<=k<=12, -13<=l<=14 | |
| Reflections collected | 6060 | |
| Independent reflections | 3638 [R(int) = 0.0224] | |
| Completeness to theta = 28.24° | 91.2 % | |
| Absorption correction | Semi-empirical from equivalents | |
| Refinement method | Full-matrix least-squares on F$^2$ | |
| Data / restraints / parameters | 3638 / 0 / 223 | |
| Goodness-of-fit on F$^2$ | 1.300 | |
| Final R indices [I>2sigma(I)] | R1 = 0.0376, wR2 = 0.0935 | |
| R indices (all data) | R1 = 0.0482, wR2 = 0.0999 | |
| Largest diff. peak and hole | 0.371 and -0.707 e.Å$^{-3}$ | |

Crystal data and structure refinement for **15b**

| | | |
|---|---|---|
| Identification code | ns0425 | |
| Empirical formula | C48 H36 Cu2 F4 N8 O10 | |
| Formula weight | 1087.93 | |
| Temperature | 173(2) K | |
| Wavelength | 0.71073 Å | |
| Crystal system | Triclinic | |
| Space group | P-1 | |
| Unit cell dimensions | a = 10.1310(9) Å | α= 64.853(5)°. |
| | b = 10.5499(8) Å | β= 86.149(5)°. |
| | c = 12.2936(9) Å | γ = 67.896(4)°. |
| Volume | 1095.24(15) $Å^3$ | |
| Z | 1 | |
| Density (calculated) | 1.649 $g/cm^3$ | |
| Absorption coefficient | 1.061 $mm^{-1}$ | |
| F(000) | 554 | |
| Crystal size | 0.20 x 0.15 x 0.10 $mm^3$ | |
| Theta range for data collection | 2.18 to 27.85°. | |
| Index ranges | -13<=h<=13, -13<=k<=13, -16<=l<=15 | |
| Reflections collected | 7872 | |
| Independent reflections | 4793 [R(int) = 0.0785] | |
| Completeness to theta = 27.85° | 91.9 % | |
| Absorption correction | None | |
| Refinement method | Full-matrix least-squares on $F^2$ | |
| Data / restraints / parameters | 4793 / 4 / 335 | |
| Goodness-of-fit on $F^2$ | 1.043 | |
| Final R indices [I>2sigma(I)] | R1 = 0.0580, wR2 = 0.1523 | |
| R indices (all data) | R1 = 0.0725, wR2 = 0.1635 | |
| Largest diff. peak and hole | 0.736 and -0.759 $e.Å^{-3}$ | |

Crystal data and structure refinement for **6e**

| | | |
|---|---|---|
| Identification code | ns0509 | |
| Empirical formula | C36.80 H41.40 Cu2 N8.80 O10.60 | |
| Formula weight | 903.67 | |
| Temperature | 95.2(2) K | |
| Wavelength | 1.54178 Å | |
| Crystal system | Triclinic | |
| Space group | P-1 | |
| Unit cell dimensions | a = 12.4743(2) Å | $\alpha$= 84.7880(10)°. |
| | b = 15.3416(2) Å | $\beta$= 79.0650(10)°. |
| | c = 21.9472(3) Å | $\gamma$ = 83.7960(10)°. |
| Volume | 4089.09(10) $Å^3$ | |
| Z | 1 | |
| Density (calculated) | 1.153 $g/cm^3$ | |
| Absorption coefficient | 3.538 $mm^{-1}$ | |
| F(000) | 1480 | |
| Crystal size | 0.45 x 0.45 x 0.12 $mm^3$ | |
| Theta range for data collection | 3.83 to 64.94°. | |
| Index ranges | -13<=h<=14, -17<=k<=17, -25<=l<=25 | |
| Reflections collected | 35498 | |
| Independent reflections | 19633 [R(int) = 0.0207] | |
| Completeness to theta | 94.7 % | |
| Absorption correction | empirical multi-scans (SADABS) | |
| Max. and min. transmission | 0.6762 and 0.2989 | |
| Refinement method | Full-matrix least-squares on $F^2$ | |
| Data / restraints / parameters | 19633 / 3031 / 1845 | |
| Goodness-of-fit on $F^2$ | 0.967 | |
| Final R indices [I>2sigma(I)] | R1 = 0.0564, wR2 = 0.1617 | |
| R indices (all data) | R1 = 0.0579, wR2 = 0.1647 | |
| Largest diff. peak and hole | 1.112 and -0.579 $e.Å^{-3}$ | |

Crystal data and structure refinement for **16a**

| | | |
|---|---|---|
| Identification code | ns0428 | |
| Empirical formula | C40 H25 Cu2 F4 N3 O8 | |
| Formula weight | 878.71 | |
| Temperature | 173(2) K | |
| Wavelength | 0.71073 Å | |
| Crystal system | Monoclinic | |
| Space group | P2(1)/c | |
| Unit cell dimensions | a = 9.3471(9) Å | α= 90°. |
| | b = 15.5850(15) Å | β= 104.714(7)°. |
| | c = 12.9025(11) Å | γ = 90°. |
| Volume | 1817.9(3) $Å^3$ | |
| Z | 2 | |
| Density (calculated) | 1.605 $g/cm^3$ | |
| Absorption coefficient | 1.250 $mm^{-1}$ | |
| F(000) | 888 | |
| Crystal size | 0.15 x 0.15 x 0.05 $mm^3$ | |
| Theta range for data collection | 2.09 to 28.30°. | |
| Index ranges | -12<=h<=12, -19<=k<=18, -14<=l<=16 | |
| Reflections collected | 12614 | |
| Independent reflections | 4188 [R(int) = 0.1368] | |
| Completeness to theta = 28.30° | 92.4 % | |
| Absorption correction | None | |
| Refinement method | Full-matrix least-squares on $F^2$ | |
| Data / restraints / parameters | 4188 / 0 / 271 | |
| Goodness-of-fit on $F^2$ | 0.894 | |
| Final R indices [I>2sigma(I)] | R1 = 0.0598, wR2 = 0.1275 | |
| R indices (all data) | R1 = 0.1077, wR2 = 0.1457 | |
| Extinction coefficient | 0.0081(10) | |
| Largest diff. peak and hole | 0.703 and -0.653 $e.Å^{-3}$ | |

Crystal data and structure refinement for **16b**

| | | |
|---|---|---|
| Identification code | ns0508 | |
| Empirical formula | C20 H21 Cu2 N3 O8 | |
| Formula weight | 558.48 | |
| Temperature | 100(2) K | |
| Wavelength | 0.71073 Å | |
| Crystal system | Triclinic | |
| Space group | P-1 | |
| Unit cell dimensions | a = 8.1368(11) Å | α= 86.244(3)°. |
| | b = 8.3062(11) Å | β= 80.480(3)°. |
| | c = 8.7490(12) Å | γ = 80.539(3)°. |
| Volume | 574.79(13) $Å^3$ | |
| Z | 1 | |
| Density (calculated) | 1.613 $g/cm^3$ | |
| Absorption coefficient | 1.900 $mm^{-1}$ | |
| F(000) | 284 | |
| Crystal size | 0.09 x 0.10 x 0.30 $mm^3$ | |
| Theta range for data collection | 2.36 to 30.08°. | |
| Index ranges | -11<=h<=11, -11<=k<=11, -12<=l<=12 | |
| Reflections collected | 11035 | |
| Independent reflections | 11035 [R(int) = 0.0000] | |
| Completeness to theta = 30.08° | 96.3 % | |
| Absorption correction | None | |
| Refinement method | Full-matrix least-squares on $F^2$ | |
| Data / restraints / parameters | 11035 / 0 / 155 | |
| Goodness-of-fit on $F^2$ | 0.969 | |
| Final R indices [I>2sigma(I)] | R1 = 0.0553, wR2 = 0.1354 | |
| R indices (all data) | R1 = 0.0655, wR2 = 0.1398 | |
| Largest diff. peak and hole | 1.186 and -0.576 $e.Å^{-3}$ | |

Crystal data and structure refinement for **15c**

| | | |
|---|---|---|
| Identification code | ns0411 | |
| Empirical formula | C32 H24 Cl6 Cu F12 N8 O6 | |
| Formula weight | 1120.83 | |
| Temperature | 100(2) K | |
| Wavelength | 0.71073 Å | |
| Crystal system | Triclinic | |
| Space group | P-1 | |
| Unit cell dimensions | a = 10.4149(6) Å | α= 105.6980(10)°. |
| | b = 12.1682(7) Å | β= 105.8970(10)°. |
| | c = 18.2488(10) Å | γ = 93.1160(10)°. |
| Volume | 2120.6(2) $Å^3$ | |
| Z | 2 | |
| Density (calculated) | 1.755 $g/cm^3$ | |
| Absorption coefficient | 1.000 $mm^{-1}$ | |
| F(000) | 1118 | |
| Crystal size | 0.38 x 0.18 x 0.12 $mm^3$ | |
| Theta range for data collection | 1.76 to 30.00°. | |
| Index ranges | -14<=h<=14, -17<=k<=16, -25<=l<=25 | |
| Reflections collected | 24652 | |
| Independent reflections | 12133 [R(int) = 0.0257] | |
| Completeness to theta = 30.00° | 98.1 % | |
| Absorption correction | Semi-empirical from equivalents | |
| Max. and min. transmission | 1.000 and 0.840 | |
| Refinement method | Full-matrix least-squares on $F^2$ | |
| Data / restraints / parameters | 12133 / 36 / 615 | |
| Goodness-of-fit on $F^2$ | 1.046 | |
| Final R indices [I>2sigma(I)] | R1 = 0.0459, wR2 = 0.1182 | |
| R indices (all data) | R1 = 0.0572, wR2 = 0.1263 | |
| Largest diff. peak and hole | 1.594 and -0.565 $e.Å^{-3}$ | |

Crystal data and structure refinement for **15d**

| | | |
|---|---|---|
| Identification code | ns0410 | |
| Empirical formula | C50 H42 Co N8 O6 | |
| Formula weight | 909.85 | |
| Temperature | 100(2) K | |
| Wavelength | 0.71073 Å | |
| Crystal system | Triclinic | |
| Space group | P-1 | |
| Unit cell dimensions | a = 9.3368(7) Å | α= 85.536(2)°. |
| | b = 10.3686(8) Å | β= 79.677(2)°. |
| | c = 11.0609(8) Å | γ = 83.026(2)°. |
| Volume | 1043.95(14) $Å^3$ | |
| Z | 1 | |
| Density (calculated) | 1.447 $g/cm^3$ | |
| Absorption coefficient | 0.475 $mm^{-1}$ | |
| F(000) | 473 | |
| Crystal size | 0.04 x 0.09 x 0.38 $mm^3$ | |
| Theta range for data collection | 1.87 to 30.00°. | |
| Index ranges | -13<=h<=12, -14<=k<=14, -15<=l<=14 | |
| Reflections collected | 12145 | |
| Independent reflections | 5980 [R(int) = 0.0228] | |
| Completeness to theta = 30.00° | 98.1 % | |
| Absorption correction | Semi-empirical from equivalents | |
| Max. and min. transmission | 1.00 and 0.79 | |
| Refinement method | Full-matrix least-squares on $F^2$ | |
| Data / restraints / parameters | 5980 / 0 / 301 | |
| Goodness-of-fit on $F^2$ | 1.060 | |
| Final R indices [I>2sigma(I)] | R1 = 0.0462, wR2 = 0.1079 | |
| R indices (all data) | R1 = 0.0536, wR2 = 0.1121 | |
| Largest diff. peak and hole | 0.673 and -0.271 $e.Å^{-3}$ | |

Crystal data and structure refinement for **1g**

| | | |
|---|---|---|
| Identification code | ns0412 | |
| Empirical formula | C32 H26 Cl2 Cu F12 N8 O4 | |
| Formula weight | 949.05 | |
| Temperature | 100(2) K | |
| Wavelength | 0.71073 Å | |
| Crystal system | Triclinic | |
| Space group | P-1 | |
| Unit cell dimensions | a = 8.2843(4) Å | α= 113.0810(10)°. |
| | b = 10.8750(5) Å | β= 94.4120(10)°. |
| | c = 11.7573(6) Å | γ = 103.8330(10)°. |
| Volume | 928.75(8) $Å^3$ | |
| Z | 1 | |
| Density (calculated) | 1.697 $g/cm^3$ | |
| Absorption coefficient | 0.843 $mm^{-1}$ | |
| F(000) | 477 | |
| Crystal size | 0.20 x 0.36 x 0.53 $mm^3$ | |
| Theta range for data collection | 2.13 to 30.03°. | |
| Index ranges | -11<=h<=11, -15<=k<=15, -16<=l<=15 | |
| Reflections collected | 10734 | |
| Independent reflections | 5322 [R(int) = 0.0160] | |
| Completeness to theta = 30.03° | 97.9 % | |
| Absorption correction | Semi-empirical from equivalents | |
| Max. and min. transmission | 1.000 and 0.816 | |
| Refinement method | Full-matrix least-squares on $F^2$ | |
| Data / restraints / parameters | 5322 / 0 / 274 | |
| Goodness-of-fit on $F^2$ | 1.036 | |
| Final R indices [I>2sigma(I)] | R1 = 0.0376, wR2 = 0.1055 | |
| R indices (all data) | R1 = 0.0405, wR2 = 0.1077 | |
| Largest diff. peak and hole | 0.866 and -0.358 $e.Å^{-3}$ | |

Crystal data and structure refinement for **6f**

| | | |
|---|---|---|
| Identification code | ns0415 | |
| Empirical formula | C23 H14 Cu F12 N4 O5 | |
| Formula weight | 717.92 | |
| Temperature | 100(2) K | |
| Wavelength | 0.71073 Å | |
| Crystal system | Triclinic | |
| Space group | P-1 | |
| Unit cell dimensions | a = 9.6243(11) Å | α= 85.905(2)°. |
| | b = 10.4481(12) Å | β= 86.300(2)°. |
| | c = 13.8822(15) Å | γ = 74.690(2)°. |
| Volume | 1341.4(3) $Å^3$ | |
| Z | 2 | |
| Density (calculated) | 1.777 $g/cm^3$ | |
| Absorption coefficient | 0.941 $mm^{-1}$ | |
| F(000) | 714 | |
| Crystal size | 0.32 x 0.28 x 0.18 $mm^3$ | |
| Theta range for data collection | 2.02 to 30.08°. | |
| Index ranges | -13<=h<=13, -14<=k<=14, -17<=l<=19 | |
| Reflections collected | 15237 | |
| Independent reflections | 7644 [R(int) = 0.0260] | |
| Completeness to theta = 30.08° | 96.9 % | |
| Absorption correction | Semi-empirical from equivalents | |
| Max. and min. transmission | 1.000 and 0.698 | |
| Refinement method | Full-matrix least-squares on $F^2$ | |
| Data / restraints / parameters | 7644 / 6 / 420 | |
| Goodness-of-fit on $F^2$ | 1.029 | |
| Final R indices [I>2sigma(I)] | R1 = 0.0467, wR2 = 0.1261 | |
| R indices (all data) | R1 = 0.0583, wR2 = 0.1333 | |
| Largest diff. peak and hole | 1.243 and -0.649 $e.Å^{-3}$ | |

Crystal data and structure refinement for **6g**

| | | |
|---|---|---|
| Identification code | ns0416 | |
| Empirical formula | C56 H46 Co N8 O6 | |
| Formula weight | 985.94 | |
| Temperature | 100(2) K | |
| Wavelength | 0.71073 Å | |
| Crystal system | Triclinic | |
| Space group | P-1 | |
| Unit cell dimensions | a = 10.5076(5) Å | α= 68.9160(10)°. |
| | b = 10.7568(6) Å | β= 82.6200(10)°. |
| | c = 11.9544(6) Å | γ = 69.1900(10)°. |
| Volume | 1178.48(10) $Å^3$ | |
| Z | 1 | |
| Density (calculated) | 1.389 $g/cm^3$ | |
| Absorption coefficient | 0.427 $mm^{-1}$ | |
| F(000) | 513 | |
| Crystal size | 0.35 x 0.20 x 0.10 $mm^3$ | |
| Theta range for data collection | 2.07 to 30.02°. | |
| Index ranges | -14<=h<=14, -15<=k<=15, -16<=l<=16 | |
| Reflections collected | 13759 | |
| Independent reflections | 6762 [R(int) = 0.0238] | |
| Completeness to theta = 30.02° | 98.2 % | |
| Absorption correction | Semi-empirical from equivalents | |
| Max. and min. transmission | 1.000 and 0.823 | |
| Refinement method | Full-matrix least-squares on $F^2$ | |
| Data / restraints / parameters | 6762 / 0 / 328 | |
| Goodness-of-fit on $F^2$ | 1.037 | |
| Final R indices [I>2sigma(I)] | R1 = 0.0429, wR2 = 0.1081 | |
| R indices (all data) | R1 = 0.0470, wR2 = 0.1111 | |

Crystal data and structure refinement for **6h**

| | | |
|---|---|---|
| Identification code | ns0429 | |
| Empirical formula | C56 H46 N8 Ni O6 | |
| Formula weight | 985.72 | |
| Temperature | 173(2) K | |
| Wavelength | 0.71073 Å | |
| Crystal system | Triclinic | |
| Space group | P-1 | |
| Unit cell dimensions | a = 10.4666(7) Å | $\alpha$= 68.678(4)°. |
| | b = 10.6669(7) Å | $\beta$= 82.626(4)°. |
| | c = 11.9828(8) Å | $\gamma$ = 69.230(3)°. |
| Volume | 1165.27(13) $Å^3$ | |
| Z | 1 | |
| Density (calculated) | 1.405 $g/cm^3$ | |
| Absorption coefficient | 0.480 $mm^{-1}$ | |
| F(000) | 514 | |
| Crystal size | 0.45 x 0.20 x 0.10 $mm^3$ | |
| Theta range for data collection | 1.82 to 27.84°. | |
| Index ranges | -13<=h<=12, -13<=k<=13, -15<=l<=15 | |
| Reflections collected | 11668 | |
| Independent reflections | 5170 [R(int) = 0.1241] | |
| Completeness to theta = 27.84° | 93.4 % | |
| Absorption correction | None | |
| Refinement method | Full-matrix least-squares on $F^2$ | |
| Data / restraints / parameters | 5170 / 0 / 329 | |
| Goodness-of-fit on $F^2$ | 0.982 | |
| Final R indices [I>2sigma(I)] | R1 = 0.0570, wR2 = 0.1355 | |
| R indices (all data) | R1 = 0.0788, wR2 = 0.1470 | |
| Extinction coefficient | 0.022(3) | |
| Largest diff. peak and hole | 0.427 and -0.495 $e.Å^{-3}$ | |

**Table B.5** Crystal data and structure refinement for **19, 19(1), 20, 20(1), 20a, 20b, 21-24, 25a and 25b**

**19**

| | | |
|---|---|---|
| Identification code | ns0501 | |
| Empirical formula | C54 H63 Br4 O8 N | |
| Formula weight | 1173.69 | |
| Temperature | 100(2) K | |
| Wavelength | 0.71073 Å | |
| Crystal system | Triclinic | |
| Space group | $P\bar{1}$ | |
| Unit cell dimensions | a = 10.7767(7) Å | $\alpha$= 80.392(4)°. |
| | b = 11.6740(7) Å | $\beta$= 97.977(3)°. |
| | c = 20.8192 Å | $\gamma$ = 76.503(3)°. |
| Volume | 2510.8(3) $Å^3$ | |
| Z | 2 | |
| Density (calculated) | 1.552 $g/cm^3$ | |
| Absorption coefficient | 3.261 $mm^{-1}$ | |
| Crystal size | 0.30 x 0.25 x 0.20 $mm^3$ | |
| Theta range for data collection | 1.82 to 28.28°. | |
| Reflections collected | 18907 | |
| Independent reflections | 9466 | |
| Absorption correction | None | |
| Refinement method | Full-matrix least-squares on $F^2$ | |
| Goodness-of-fit on $F^2$ | 1.097 | |
| Final R indices [I>2sigma(I)] | R1 = 0.0287 | |
| R indices (all data) | R1 = 0.0330, wR2 = 0.0877 | |

Crystal data and structure refinement for **19(1)**

| | | |
|---|---|---|
| Identification code | ns0510 | |
| Empirical formula | C53 H62 Br4 Cl2 O8 | |
| Formula weight | 1217.57 | |
| Temperature | 100(2) K | |
| Wavelength | 0.71073 Å | |
| Crystal system | Monoclinic | |
| Space group | P2(1) | |
| Unit cell dimensions | a = 10.4432(15) Å | $\alpha$= 90°. |
| | b = 15.049(2) Å | $\beta$= 97.977(3)°. |
| | c = 16.320(2) Å | $\gamma$ = 90°. |
| Volume | 2540.0(6) $Å^3$ | |
| Z | 2 | |
| Density (calculated) | 1.592 $g/cm^3$ | |
| Absorption coefficient | 3.328 $mm^{-1}$ | |
| F(000) | 1236 | |
| Crystal size | 0.22 x 0.19 x 0.02 $mm^3$ | |
| Theta range for data collection | 2.39 to 30.09°. | |
| Index ranges | -14<=h<=14, -21<=k<=21, -22<=l<=22 | |
| Reflections collected | 22914 | |
| Independent reflections | 13646 [R(int) = 0.0610] | |
| Completeness to theta = 30.09° | 98.2 % | |
| Absorption correction | None | |
| Refinement method | Full-matrix least-squares on $F^2$ | |
| Data / restraints / parameters | 13646 / 7 / 602 | |
| Goodness-of-fit on $F^2$ | 0.735 | |
| Final R indices [I>2sigma(I)] | R1 = 0.0447, wR2 = 0.0596 | |
| R indices (all data) | R1 = 0.1046, wR2 = 0.0674 | |
| Absolute structure parameter | -0.011(6) | |
| Largest diff. peak and hole | 0.790 and -0.656 $e.Å^{-3}$ | |

Crystal data and structure refinement for **20**

| | | |
|---|---|---|
| Identification code | ns0605 | |
| Empirical formula | C78 H85 N7 O8 | |
| Formula weight | 1248.53 | |
| Temperature | 100(2) K | |
| Wavelength | 0.71073 Å | |
| Crystal system | Tetragonal | |
| Space group | P4(3)2(1)2 | |
| Unit cell dimensions | a = 18.3708(7) Å | α= 90°. |
| | b = 18.3708(7) Å | β= 90°. |
| | c = 19.8745(15) Å | γ = 90°. |
| Volume | 6707.4(6) $Å^3$ | |
| Z | 4 | |
| Density (calculated) | 1.236 $g/cm^3$ | |
| Absorption coefficient | 0.080 $mm^{-1}$ | |
| F(000) | 2664 | |
| Crystal size | 0.24 x 0.10 x 0.10 $mm^3$ | |
| Theta range for data collection | 1.87 to 28.31°. | |
| Index ranges | -22<=h<=23, -11<=k<=24, -25<=l<=26 | |
| Reflections collected | 30563 | |
| Independent reflections | 4615 [R(int) = 0.0582] | |
| Completeness to theta = 28.31° | 97.8 % | |
| Absorption correction | None | |
| Refinement method | Full-matrix least-squares on $F^2$ | |
| Data / restraints / parameters | 4615 / 34 / 486 | |
| Goodness-of-fit on $F^2$ | 1.059 | |
| Final R indices [I>2sigma(I)] | R1 = 0.0514, wR2 = 0.1234 | |
| R indices (all data) | R1 = 0.0744, wR2 = 0.1353 | |
| Absolute structure parameter | 1.1(16) | |
| Largest diff. peak and hole | 0.362 and -0.219 $e.Å^{-3}$ | |

Crystal data and structure refinement for **20(1)**

| | | |
|---|---|---|
| Identification code | ns0608 | |
| Empirical formula | C151 H180 N8 O23 | |
| Formula weight | 2475.03 | |
| Temperature | 100(2) K | |
| Wavelength | 0.71073 Å | |
| Crystal system | Monoclinic | |
| Space group | P2(1)/n | |
| Unit cell dimensions | a = 23.4463(17) Å | α= 90°. |
| | b = 22.2094(16) Å | β= 94.2510(10)°. |
| | c = 25.5712(19) Å | γ = 90°. |
| Volume | 13279.0(17) $Å^3$ | |
| Z | 4 | |
| Density (calculated) | 1.238 $g/cm^3$ | |
| Absorption coefficient | 0.083 $mm^{-1}$ | |
| F(000) | 5304 | |
| Crystal size | 0.32 x 0.30 x 0.23 $mm^3$ | |
| Theta range for data collection | 1.26 to 28.29°. | |
| Index ranges | -31<=h<=30, -28<=k<=28, -32<=l<=34 | |
| Reflections collected | 117595 | |
| Independent reflections | 31461 [R(int) = 0.0306] | |
| Completeness to theta = 28.29° | 95.4 % | |
| Absorption correction | None | |
| Refinement method | Full-matrix least-squares on $F^2$ | |
| Data / restraints / parameters | 31461 / 9 / 1628 | |
| Goodness-of-fit on $F^2$ | 1.025 | |
| Final R indices [I>2sigma(I)] | R1 = 0.0628, wR2 = 0.1609 | |
| R indices (all data) | R1 = 0.0835, wR2 = 0.1771 | |
| Largest diff. peak and hole | 1.504 and -0.847 $e.Å^{-3}$ | |

Crystal data and structure refinement for **20a**

| | | |
|---|---|---|
| Identification code | ns0524 | |
| Empirical formula | C84.75 H93.05 N5 O14.15 | |
| Formula weight | 1408.09 | |
| Temperature | 100(2) K | |
| Wavelength | 0.71073 Å | |
| Crystal system | Monoclinic | |
| Space group | P2(1)/n | |
| Unit cell dimensions | a = 17.9287(15) Å | α= 90°. |
| | b = 22.5778(18) Å | β= 110.3500(10)°. |
| | c = 20.4821(17) Å | γ = 90°. |
| Volume | 7773.5(11) $Å^3$ | |
| Z | 4 | |
| Density (calculated) | 1.203 $g/cm^3$ | |
| Absorption coefficient | 0.082 $mm^{-1}$ | |
| F(000) | 2999 | |
| Crystal size | 0.08 x 0.44 x 0.48 $mm^3$ | |
| Theta range for data collection | 2.91 to 26.78°. | |
| Index ranges | -21<=h<=21, -25<=k<=28, -25<=l<=25 | |
| Reflections collected | 52203 | |
| Independent reflections | 15450 [R(int) = 0.0414] | |
| Completeness to theta = 26.78° | 93.2 % | |
| Absorption correction | Semi-empirical from equivalents | |
| Max. and min. transmission | 1.000 and 0.719 | |
| Refinement method | Full-matrix least-squares on $F^2$ | |
| Data / restraints / parameters | 15450 / 18 / 935 | |
| Goodness-of-fit on $F^2$ | 1.664 | |
| Final R indices [I>2sigma(I)] | R1 = 0.0902, wR2 = 0.2577 | |
| R indices (all data) | R1 = 0.1534, wR2 = 0.2835 | |
| Largest diff. peak and hole | 0.796 and -1.187 $e.Å^{-3}$ | |

Crystal data and structure refinement for **20b**

| | | |
|---|---|---|
| Empirical formula | C162 H166 N4 O26 I2 | |
| Formula weight | 2752.70 | |
| Temperature | 100(2) K | |
| Wavelength | 0.71073 Å | |
| Crystal system | Monoclinic | |
| Space group | P2(1)/n | |
| Unit cell dimensions | a = 23.4463(17) Å | α= 90°. |
| | b = 22.2094(16) Å | β= 94.2510(10)°. |
| | c = 25.5712(19) Å | γ = 90°. |
| Volume | 13279.0(17) $Å^3$ | |
| Z | 4 | |
| Density (calculated) | 1.238 $g/cm^3$ | |
| Absorption coefficient | 0.083 $mm^{-1}$ | |
| F(000) | 5304 | |
| Crystal size | 0.32 x 0.30 x 0.23 $mm^3$ | |
| Theta range for data collection | 1.26 to 28.29°. | |
| Index ranges | -31<=h<=30, -28<=k<=28, -32<=l<=34 | |
| Reflections collected | 117595 | |
| Independent reflections | 31461 [R(int) = 0.0306] | |
| Completeness to theta = 28.29° | 95.4 % | |
| Absorption correction | None | |
| Refinement method | Full-matrix least-squares on $F^2$ | |
| Data / restraints / parameters | 31461 / 9 / 1628 | |
| Goodness-of-fit on $F^2$ | 1.025 | |
| Final R indices [I>2sigma(I)] | R1 = 0.0628, wR2 = 0.1609 | |
| R indices (all data) | R1 = 0.0835, wR2 = 0.1771 | |
| Largest diff. peak and hole | 1.504 and -0.847 $e.Å^{-3}$ | |

Crystal data and structure refinement for **21**

| | | |
|---|---|---|
| Identification code | ns0511 | |
| Empirical formula | C45 H50.50 O11.10 | |
| Formula weight | 768.95 | |
| Temperature | 100(2) K | |
| Wavelength | 0.71073 Å | |
| Crystal system | Tetragonal | |
| Space group | P4/nnc | |
| Unit cell dimensions | a = 13.7676(6) Å | α= 90°. |
| | b = 13.7676(6) Å | β= 90°. |
| | c = 47.476(4) Å | γ = 90°. |
| Volume | 8999.0(10) $Å^3$ | |
| Z | 8 | |
| Density (calculated) | 1.135 $Mg/m^3$ | |
| Absorption coefficient | 0.081 $mm^{-1}$ | |
| F(000) | 3274 | |
| Crystal size | 0.26 x 0.30 x 0.36 $mm^3$ | |
| Theta range for data collection | 1.54 to 25.70°. | |
| Index ranges | -16<=h<=16, -16<=k<=15, -57<=l<=57 | |
| Reflections collected | 51431 | |
| Independent reflections | 4198 [R(int) = 0.0429] | |
| Completeness to theta = 25.70° | 97.4 % | |
| Absorption correction | None | |
| Refinement method | Full-matrix least-squares on $F^2$ | |
| Data / restraints / parameters | 4198 / 13 / 262 | |
| Goodness-of-fit on $F^2$ | 3.653 | |
| Final R indices [I>2sigma(I)] | R1 = 0.1638, wR2 = 0.4419 | |
| R indices (all data) | R1 = 0.1835, wR2 = 0.4497 | |
| Largest diff. peak and hole | 1.541 and -0.858 $e.Å^{-3}$ | |

Crystal data and structure refinement for **22**

| | | |
|---|---|---|
| Identification code | ns0627 | |
| Empirical formula | C88 H136 B4 O16 | |
| Formula weight | 1493.21 | |
| Temperature | 173(2) K | |
| Wavelength | 0.71073 Å | |
| Crystal system | Monoclinic | |
| Space group | P2(1)/n | |
| Unit cell dimensions | a = 15.0290(12) Å | $\alpha$= 90°. |
| | b = 21.2864(17) Å | $\beta$= 102.322(5)°. |
| | c = 28.579(2) Å | $\gamma$ = 90°. |
| Volume | 8932.2(13) Å$^3$ | |
| Z | 4 | |
| Density (calculated) | 1.110 g/cm$^3$ | |
| Absorption coefficient | 0.074 mm$^{-1}$ | |
| F(000) | 3248 | |
| Crystal size | 0.40 x 0.35 x 0.10 mm$^3$ | |
| Theta range for data collection | 1.20 to 27.53°. | |
| Index ranges | -19<=h<=18, -26<=k<=27, -37<=l<=36 | |
| Reflections collected | 64051 | |
| Independent reflections | 20283 [R(int) = 0.1710] | |
| Completeness to theta = 27.53° | 98.5 % | |
| Absorption correction | None | |
| Refinement method | Full-matrix least-squares on F$^2$ | |
| Data / restraints / parameters | 20283 / 125 / 958 | |
| Goodness-of-fit on F$^2$ | 0.953 | |
| Final R indices [I>2sigma(I)] | R1 = 0.0970, wR2 = 0.2583 | |
| R indices (all data) | R1 = 0.2082, wR2 = 0.3080 | |
| Largest diff. peak and hole | 0.565 and -0.578 e.Å$^{-3}$ | |

Crystal data and structure refinement for **23**

| | | |
|---|---|---|
| Identification code | ns0503 | |
| Empirical formula | C54 H63 I4 N O8 | |
| Formula weight | 1361.65 | |
| Temperature | 173(2) K | |
| Wavelength | 0.71073 Å | |
| Crystal system | Monoclinic | |
| Space group | P2(1)/c | |
| Unit cell dimensions | a = 19.045(3) Å | $\alpha$= 90°. |
| | b = 16.627(2) Å | $\beta$= 118.047(8)°. |
| | c = 18.618(3) Å | $\gamma$ = 90°. |
| Volume | 5203.3(13) $Å^3$ | |
| Z | 4 | |
| Density (calculated) | 1.738 $g/cm^3$ | |
| Absorption coefficient | 2.449 $mm^{-1}$ | |
| F(000) | 2680 | |
| Crystal size | 0.40 x 0.10 x 0.10 $mm^3$ | |
| Theta range for data collection | 1.72 to 28.38°. | |
| Index ranges | -24<=h<=23, -21<=k<=20, -24<=l<=24 | |
| Reflections collected | 38563 | |
| Independent reflections | 12203 [R(int) = 0.0585] | |
| Completeness to theta = 28.38° | 93.5 % | |
| Absorption correction | Semi-empirical from equivalents | |
| Max. and min. transmission | 1.000 and 0.704 | |
| Refinement method | Full-matrix least-squares on $F^2$ | |
| Data / restraints / parameters | 12203 / 0 / 604 | |
| Goodness-of-fit on $F^2$ | 1.013 | |
| Final R indices [I>2sigma(I)] | R1 = 0.0449, wR2 = 0.0956 | |
| R indices (all data) | R1 = 0.1000, wR2 = 0.1200 | |
| Largest diff. peak and hole | 0.860 and -1.547 $e.Å^{-3}$ | |

Crystal data and structure refinement for **24**

| | | |
|---|---|---|
| Identification code | ns0515 | |
| Empirical formula | C82 H83 N5 O10 | |
| Formula weight | 1298.53 | |
| Temperature | 100(2) K | |
| Wavelength | 0.71073 Å | |
| Crystal system | Orthorhombic | |
| Space group | Pnna | |
| Unit cell dimensions | a = 25.359(2) Å | $\alpha$= 90°. |
| | b = 22.2099(19) Å | $\beta$= 90°. |
| | c = 12.1129(10) Å | $\gamma$ = 90°. |
| Volume | 6822.2(10) $Å^3$ | |
| Z | 4 | |
| Density (calculated) | 1.264 $g/cm^3$ | |
| Absorption coefficient | 0.083 $mm^{-1}$ | |
| F(000) | 2760 | |
| Crystal size | 0.34 x 0.32 x 0.20 $mm^3$ | |
| Theta range for data collection | 2.44 to 29.29°. | |
| Index ranges | -33<=h<=34, -30<=k<=30, -15<=l<=16 | |
| Reflections collected | 59454 | |
| Independent reflections | 8904 [R(int) = 0.0420] | |
| Completeness to theta = 29.29° | 95.3 % | |
| Absorption correction | None | |
| Refinement method | Full-matrix least-squares on $F^2$ | |
| Data / restraints / parameters | 8904 / 9 / 467 | |
| Goodness-of-fit on $F^2$ | 1.076 | |
| Final R indices [I>2sigma(I)] | R1 = 0.0558, wR2 = 0.1338 | |
| R indices (all data) | R1 = 0.0638, wR2 = 0.1401 | |
| Largest diff. peak and hole | 0.519 and -0.239 $e.Å^{-3}$ | |

Crystal data and structure refinement for **25a**

| | | |
|---|---|---|
| Identification code | ns0616 | |
| Empirical formula | C114 H106.10 N18.45 O32.55 | |
| Formula weight | 2255.37 | |
| Temperature | 143(2) K | |
| Wavelength | 0.71073 Å | |
| Crystal system | Triclinic | |
| Space group | P-1 | |
| Unit cell dimensions | a = 14.636(3) Å | α= 76.787(10)°. |
| | b = 17.062(3) Å | β= 85.972(12)°. |
| | c = 25.079(4) Å | γ = 64.566(9)°. |
| Volume | 5503.3(16) $Å^3$ | |
| Z | 2 | |
| Density (calculated) | 1.361 $g/cm^3$ | |
| Absorption coefficient | 0.102 $mm^{-1}$ | |
| F(000) | 2359 | |
| Crystal size | 0.30 x 0.15 x 0.10 $mm^3$ | |
| Theta range for data collection | 1.35 to 27.65°. | |
| Index ranges | -18<=h<=19, -20<=k<=22, -32<=l<=29 | |
| Reflections collected | 41304 | |
| Independent reflections | 24410 [R(int) = 0.1944] | |
| Completeness to theta = 27.65° | 95.2 % | |
| Absorption correction | None | |
| Refinement method | Full-matrix least-squares on $F^2$ | |
| Data / restraints / parameters | 24410 / 22 / 1471 | |
| Goodness-of-fit on $F^2$ | 0.762 | |
| Final R indices [I>2sigma(I)] | R1 = 0.1084, wR2 = 0.2468 | |
| R indices (all data) | R1 = 0.3967, wR2 = 0.3484 | |
| Largest diff. peak and hole | 0.700 and -0.489 $e.Å^{-3}$ | |

Crystal data and structure refinement for **25b**

| | | |
|---|---|---|
| Identification code | ns0619 | |
| Empirical formula | C101.60 H111 N9 O16 | |
| Formula weight | 1714.19 | |
| Temperature | 85(2) K | |
| Wavelength | 0.71073 Å | |
| Crystal system | Orthorhombic | |
| Space group | Pnma | |
| Unit cell dimensions | a = 12.7783(9) Å | $\alpha$= 90°. |
| | b = 24.5634(18) Å | $\beta$= 90°. |
| | c = 29.317(2) Å | $\gamma$ = 90°. |
| Volume | 9202.1(11) $Å^3$ | |
| Z | 4 | |
| Density (calculated) | 1.237 $g/cm^3$ | |
| Absorption coefficient | 0.084 $mm^{-1}$ | |
| F(000) | 3646 | |
| Crystal size | 0.14 x 0.19 x 0.38 $mm^3$ | |
| Theta range for data collection | 1.39 to 28.37°. | |
| Index ranges | -16<=h<=16, -32<=k<=30, -24<=l<=37 | |
| Reflections collected | 48646 | |
| Independent reflections | 11429 [R(int) = 0.0618] | |
| Completeness to theta = 28.37° | 97.1 % | |
| Absorption correction | None | |
| Refinement method | Full-matrix least-squares on $F^2$ | |
| Data / restraints / parameters | 11429 / 86 / 651 | |
| Goodness-of-fit on $F^2$ | 1.020 | |
| Final R indices [I>2sigma(I)] | R1 = 0.0945, wR2 = 0.2654 | |
| R indices (all data) | R1 = 0.1589, wR2 = 0.3114 | |
| Largest diff. peak and hole | 1.222 and -0.659 $e.Å^{-3}$ | |

**Table B.6** Crystal data and structure refinement for **31**

| | | |
|---|---|---|
| Identification code | ns0535 | |
| Empirical formula | C49 H47 N3 O6 | |
| Formula weight | 773.90 | |
| Temperature | 293(2) K | |
| Wavelength | 0.71073 Å | |
| Crystal system | Monoclinic | |
| Space group | P2(1)/n | |
| Unit cell dimensions | a = 14.985(2) Å | α= 90°. |
| | b = 9.9790(16) Å | β= 90.627(4)°. |
| | c = 26.990(4) Å | γ = 90°. |
| Volume | 4035.8(11) $Å^3$ | |
| Z | 4 | |
| Density (calculated) | 1.274 $Mg/m^3$ | |
| Absorption coefficient | 0.084 $mm^{-1}$ | |
| F(000) | 1640 | |
| Crystal size | 0.16 x 0.10 x 0.07 $mm^3$ | |
| Theta range for data collection | 1.51 to 28.45°. | |
| Index ranges | -19<=h<=19, -13<=k<=13, -34<=l<=35 | |
| Reflections collected | 37766 | |
| Independent reflections | 9832 [R(int) = 0.0678] | |
| Completeness to theta = 28.45° | 96.6 % | |
| Absorption correction | None | |
| Refinement method | Full-matrix least-squares on $F^2$ | |
| Data / restraints / parameters | 9832 / 6 / 546 | |
| Goodness-of-fit on $F^2$ | 1.331 | |
| Final R indices [I>2sigma(I)] | R1 = 0.0690, wR2 = 0.1988 | |
| R indices (all data) | R1 = 0.1047, wR2 = 0.2225 | |
| Extinction coefficient | 0.0142(15) | |
| Largest diff. peak and hole | 0.627 and -0.340 $e.Å^{-3}$ | |

# Appendix C - $^{1}H$ and $^{13}C$ NMR

400 MHz

$_{D6}$-DMSO

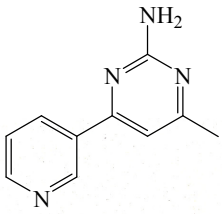


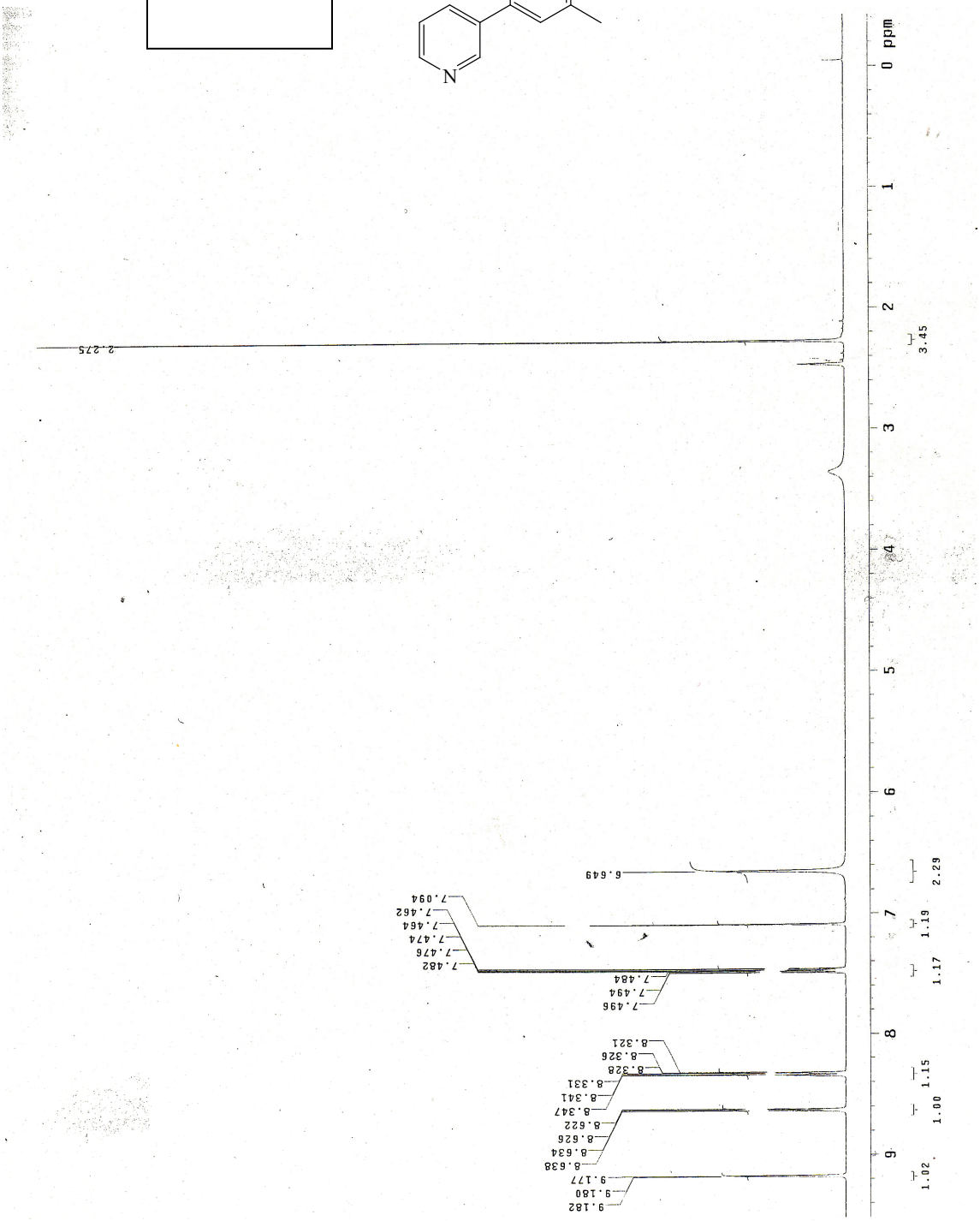

400 MHz

$D_6$-DMSO

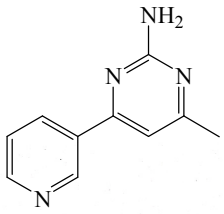


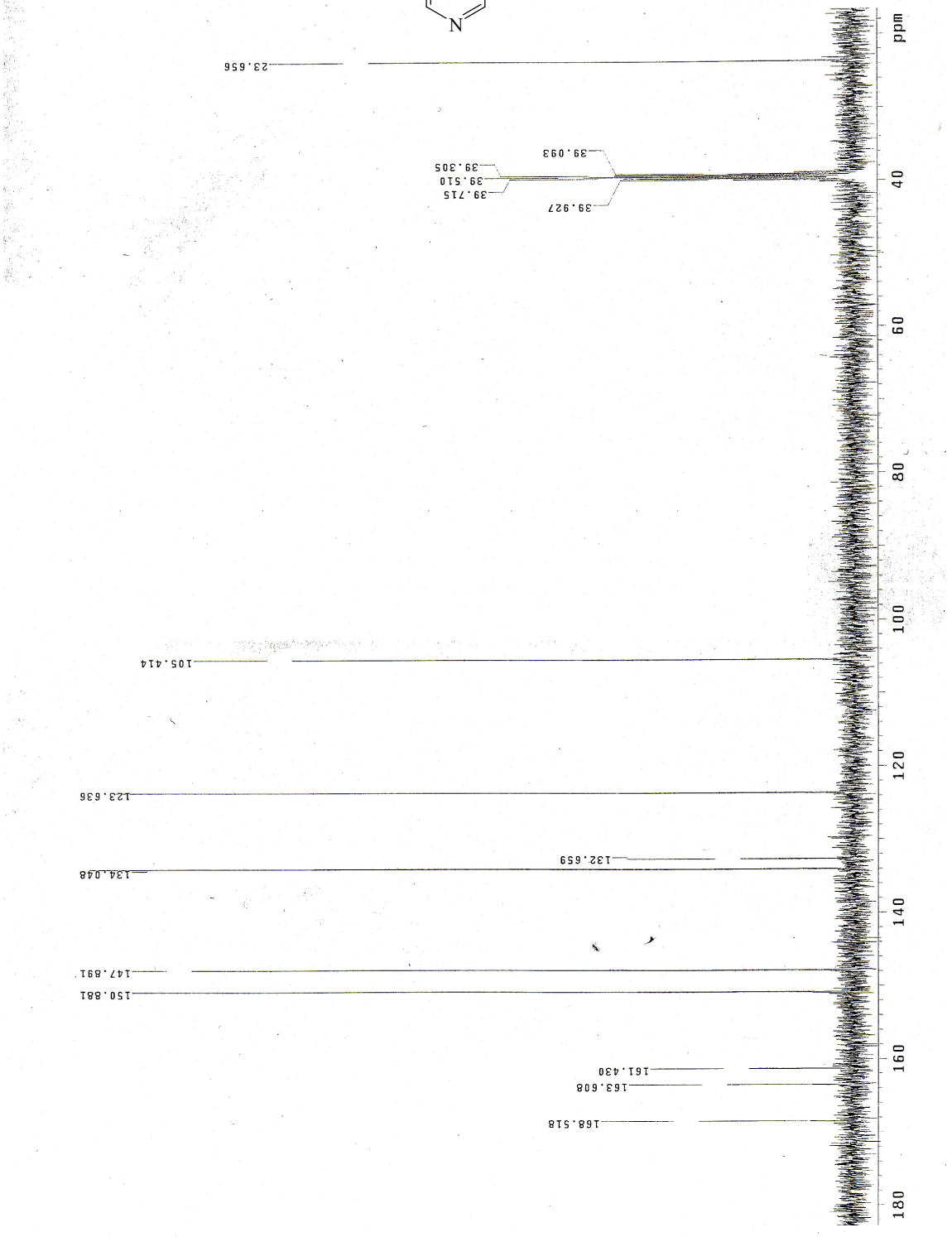

400 MHz

$CDCl_3$

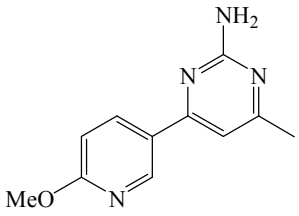


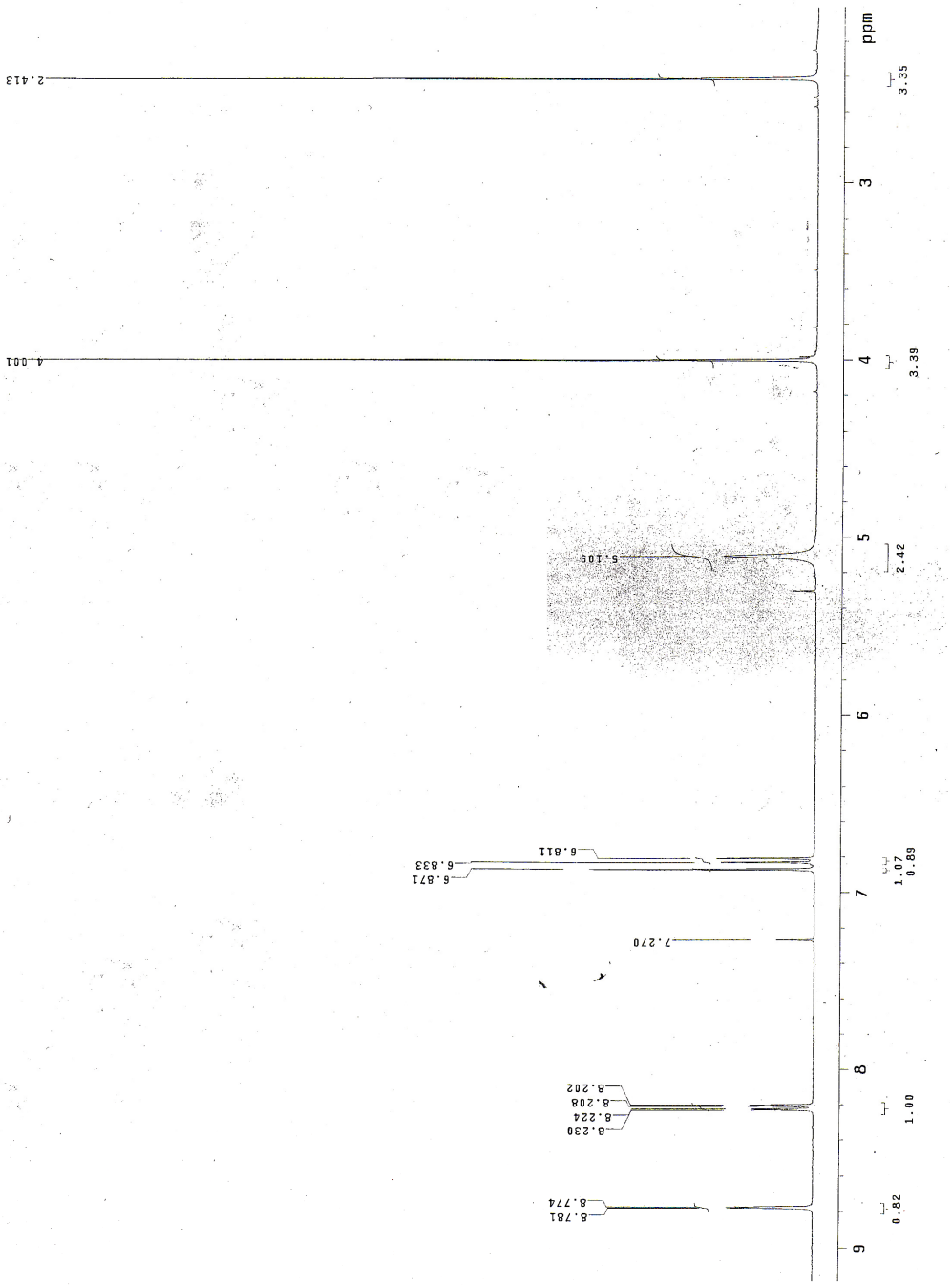

400 MHz

$CDCl_3$

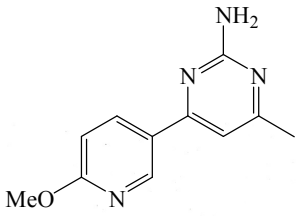


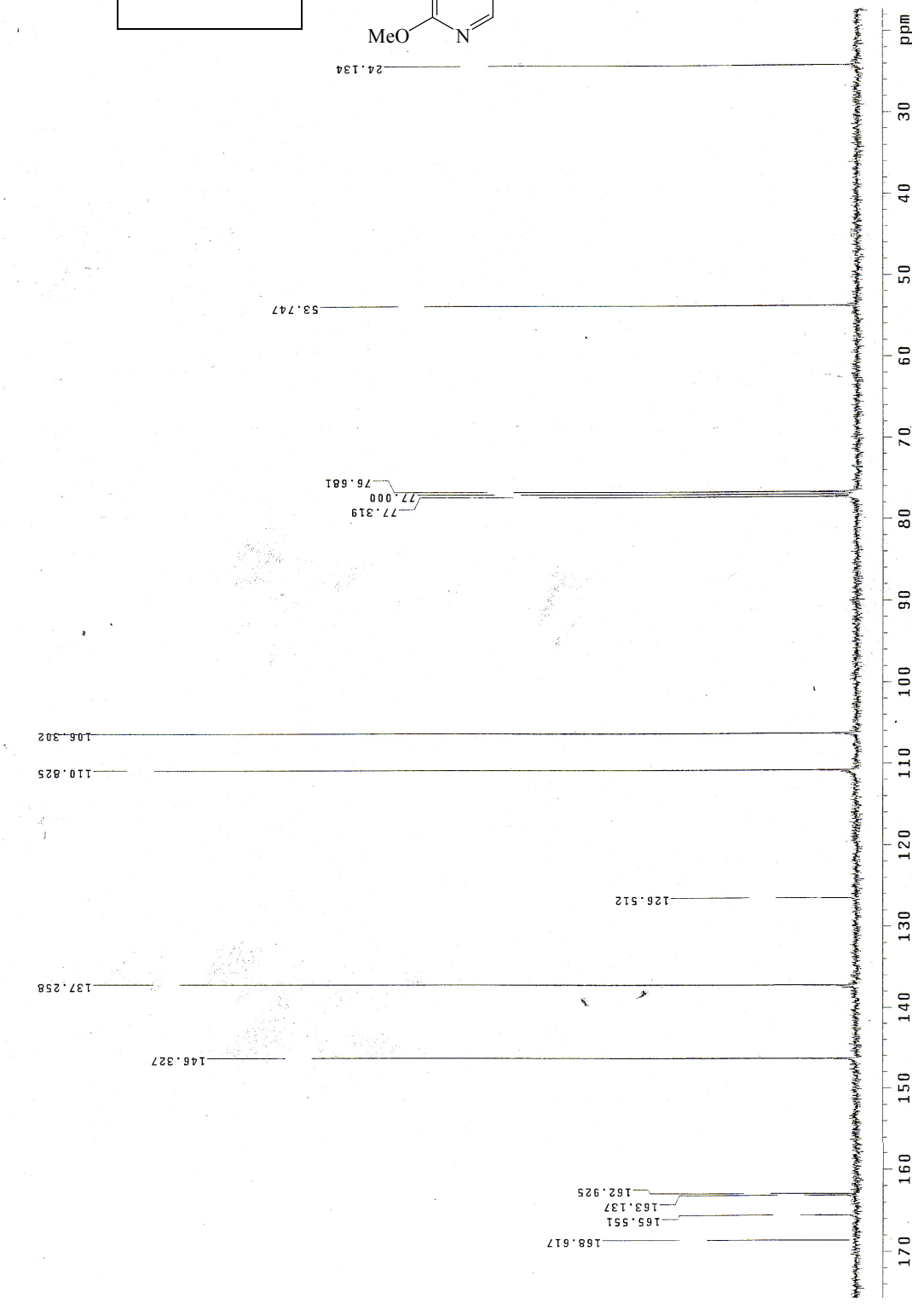

400 MHz

$CDCl_3$

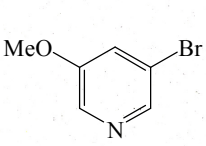

400 MHz

$CDCl_3$

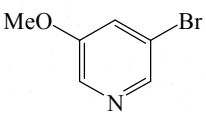

200 MHZ

$CDCl_3$

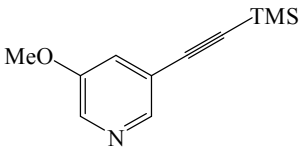


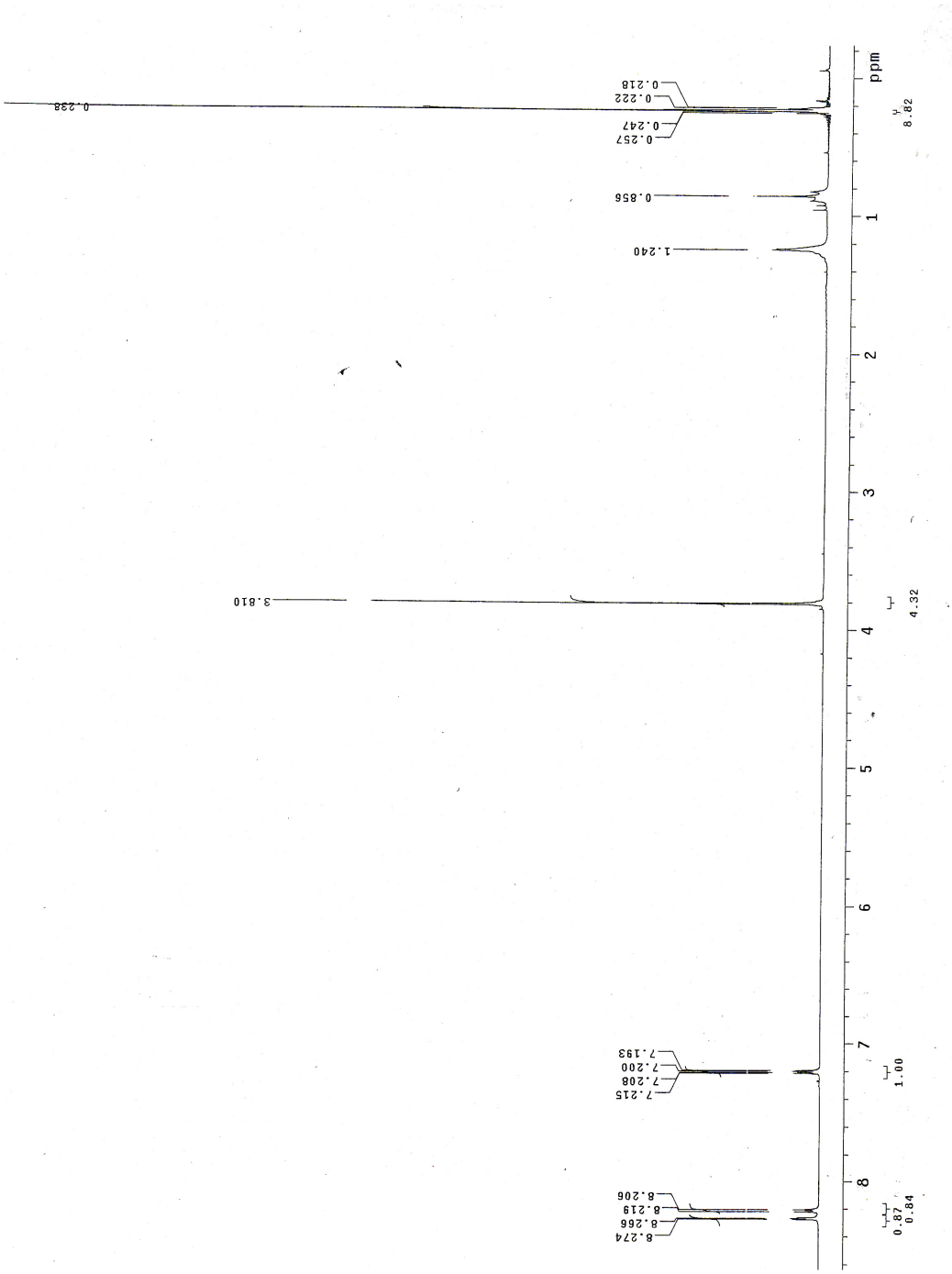

200 MHZ

$CDCl_3$

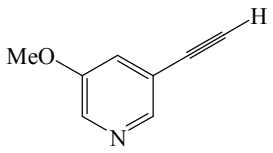


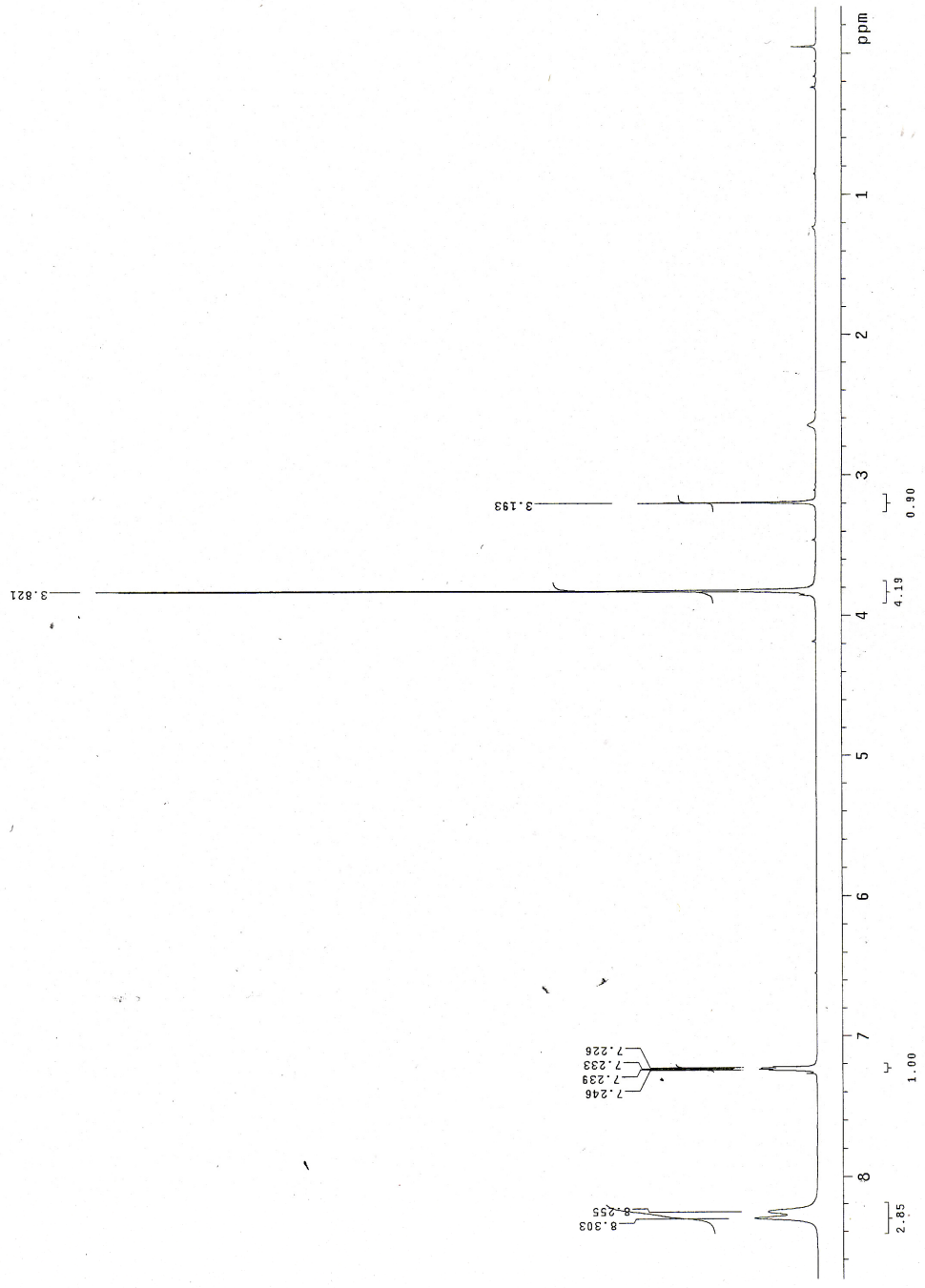

400 MHZ

$CDCl_3$

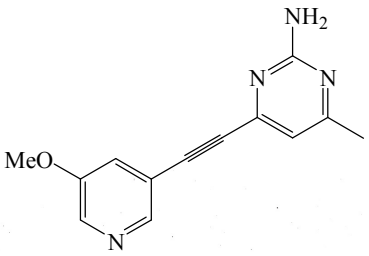


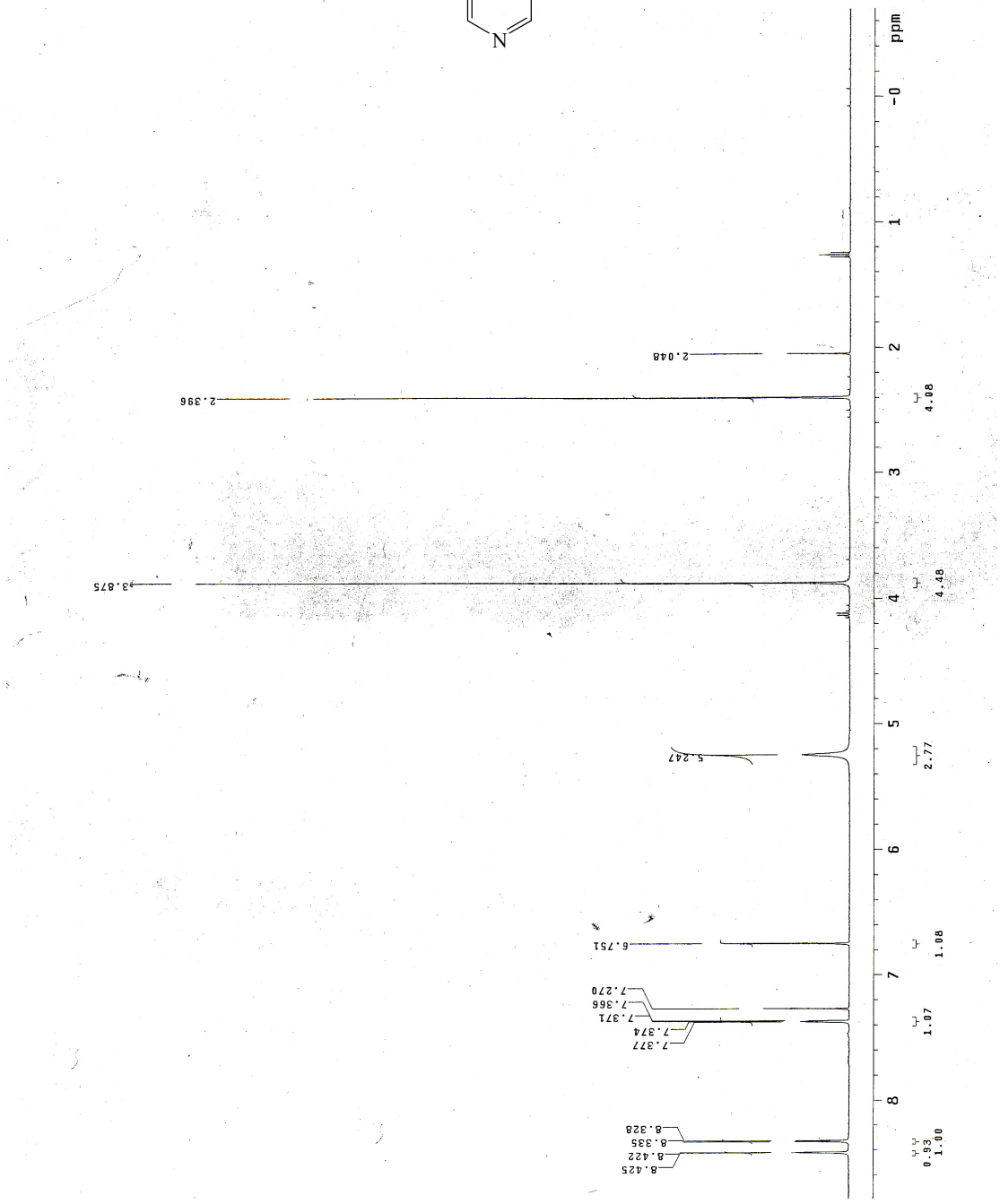

400 MHZ

$CDCl_3$

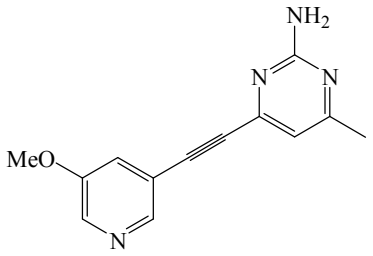


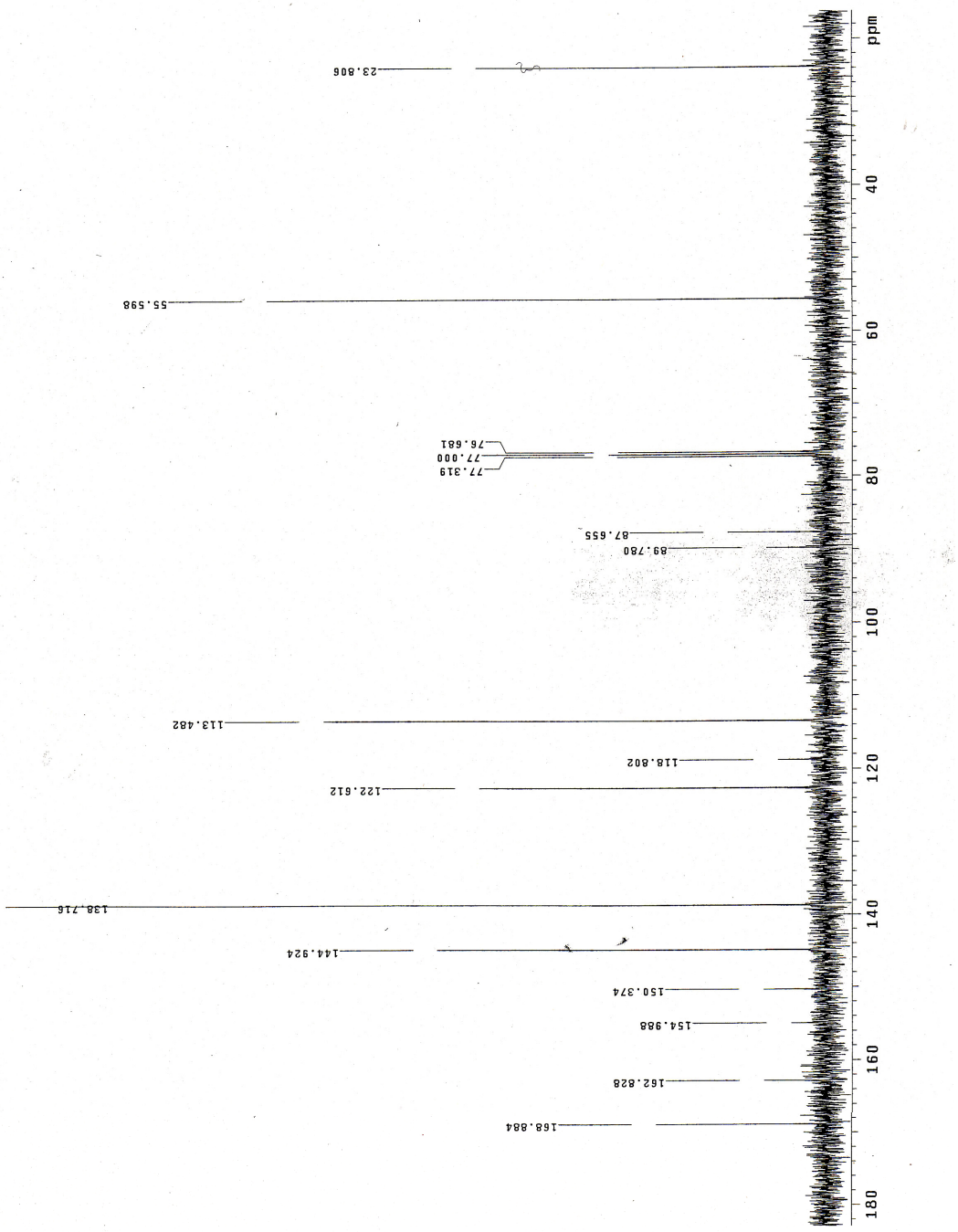

200 MHZ

$CDCl_3$

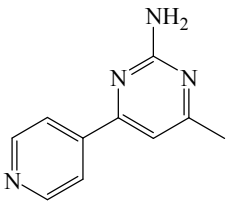


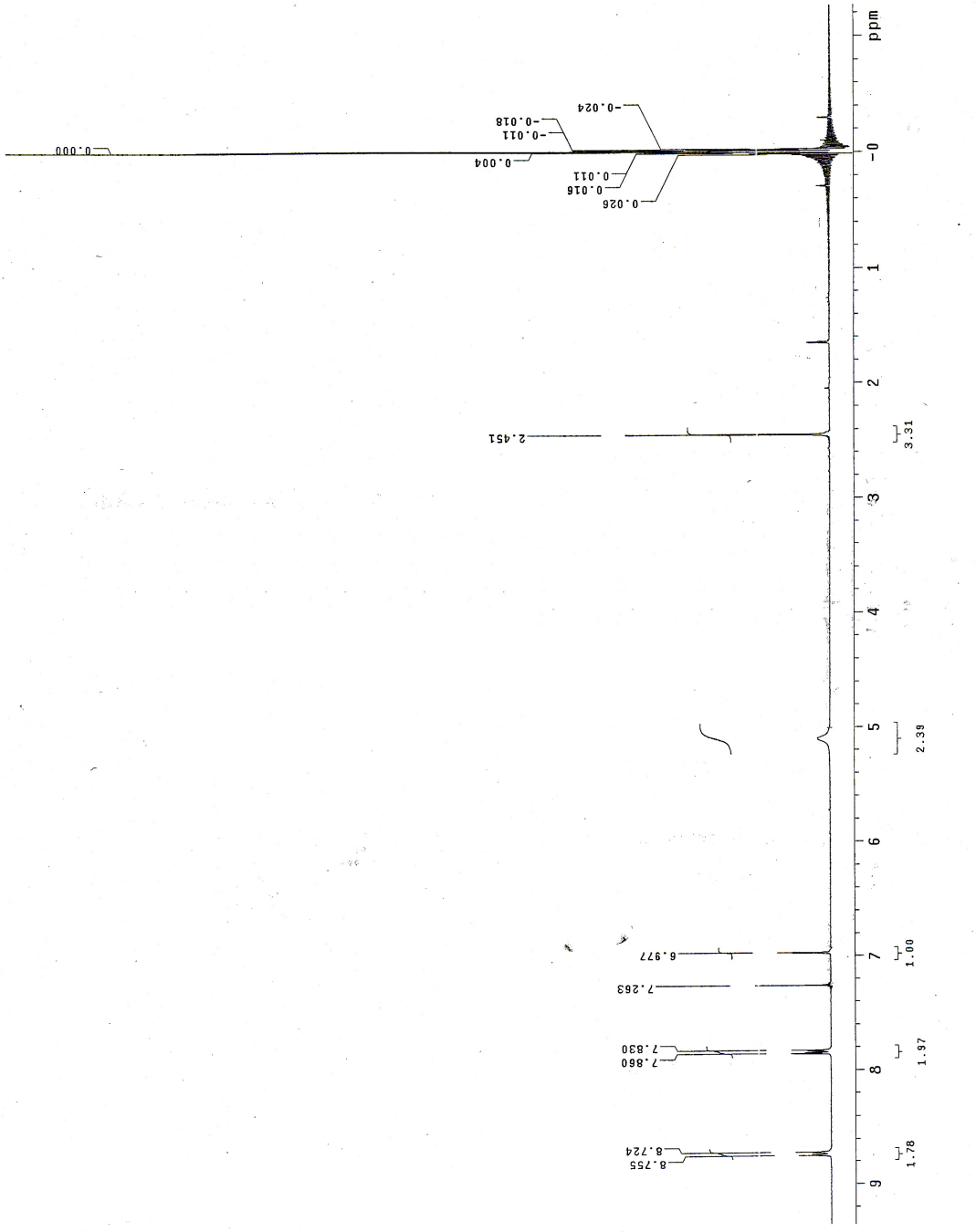

200 MHZ

$CDCl_3$

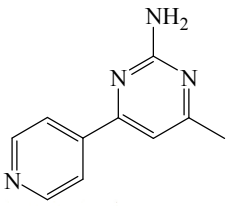


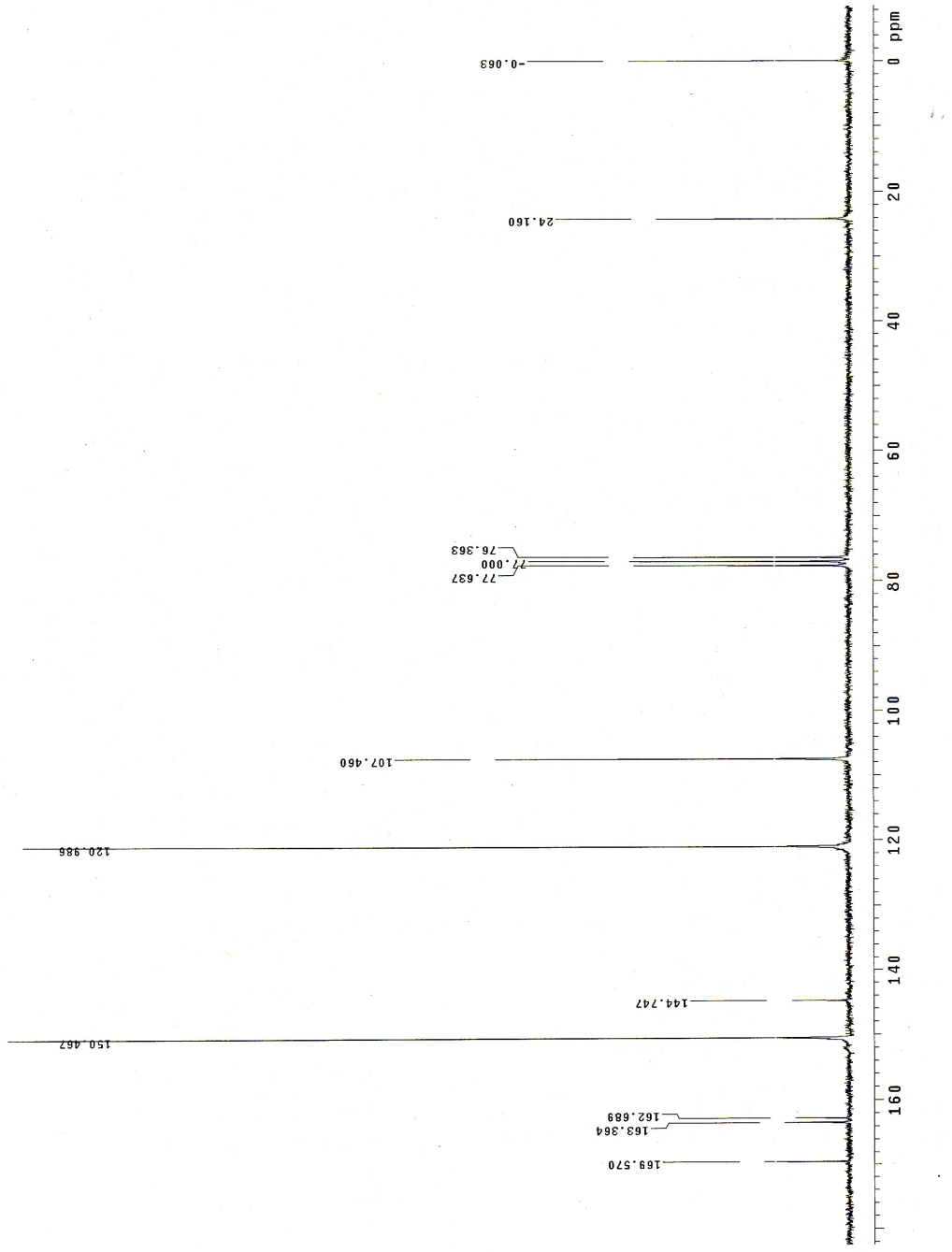

200 MHZ

$CDCl_3$

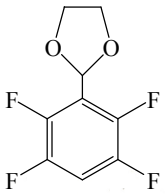


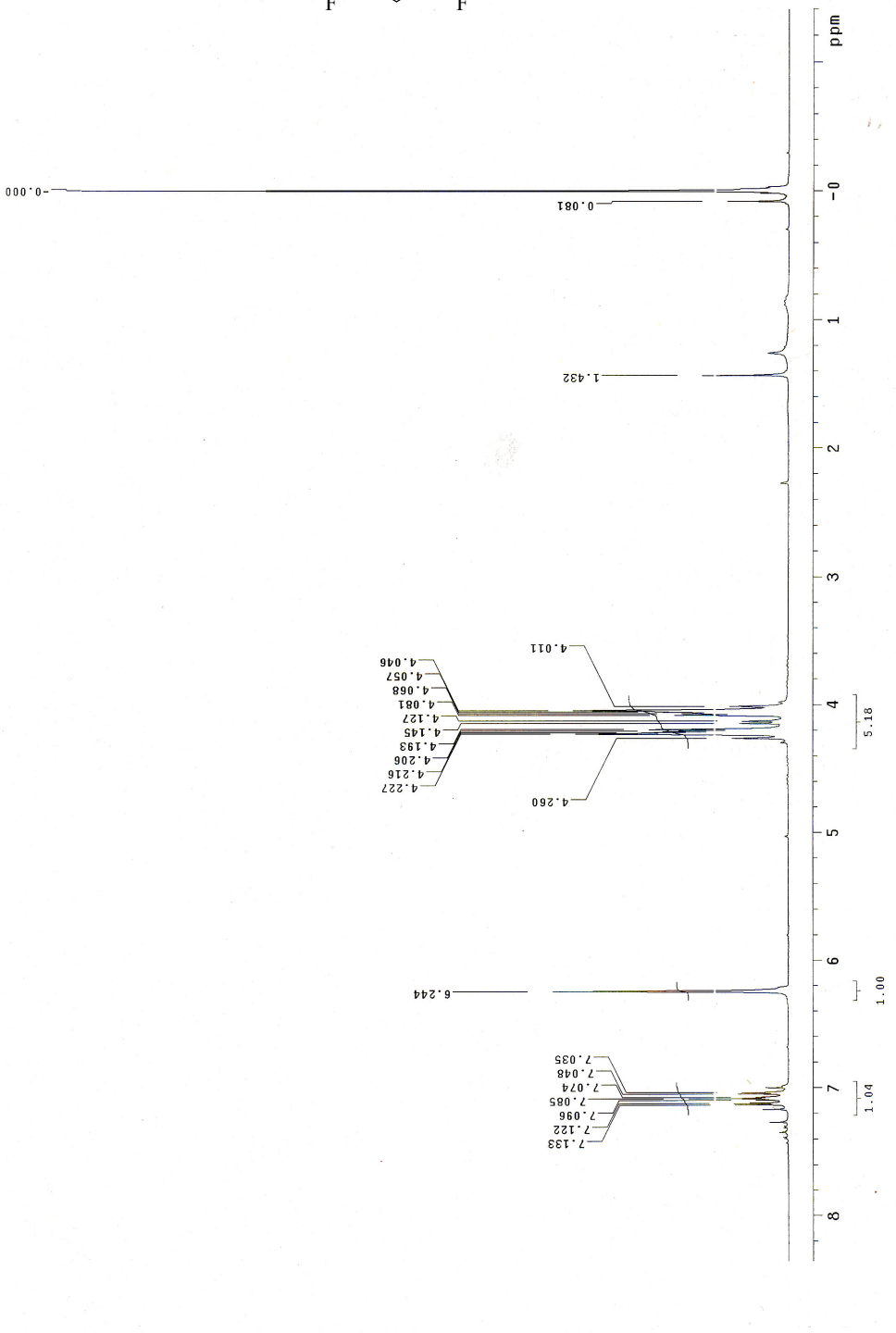

200 MHZ

$CDCl_3$

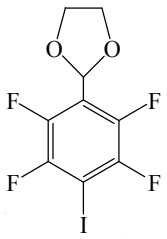


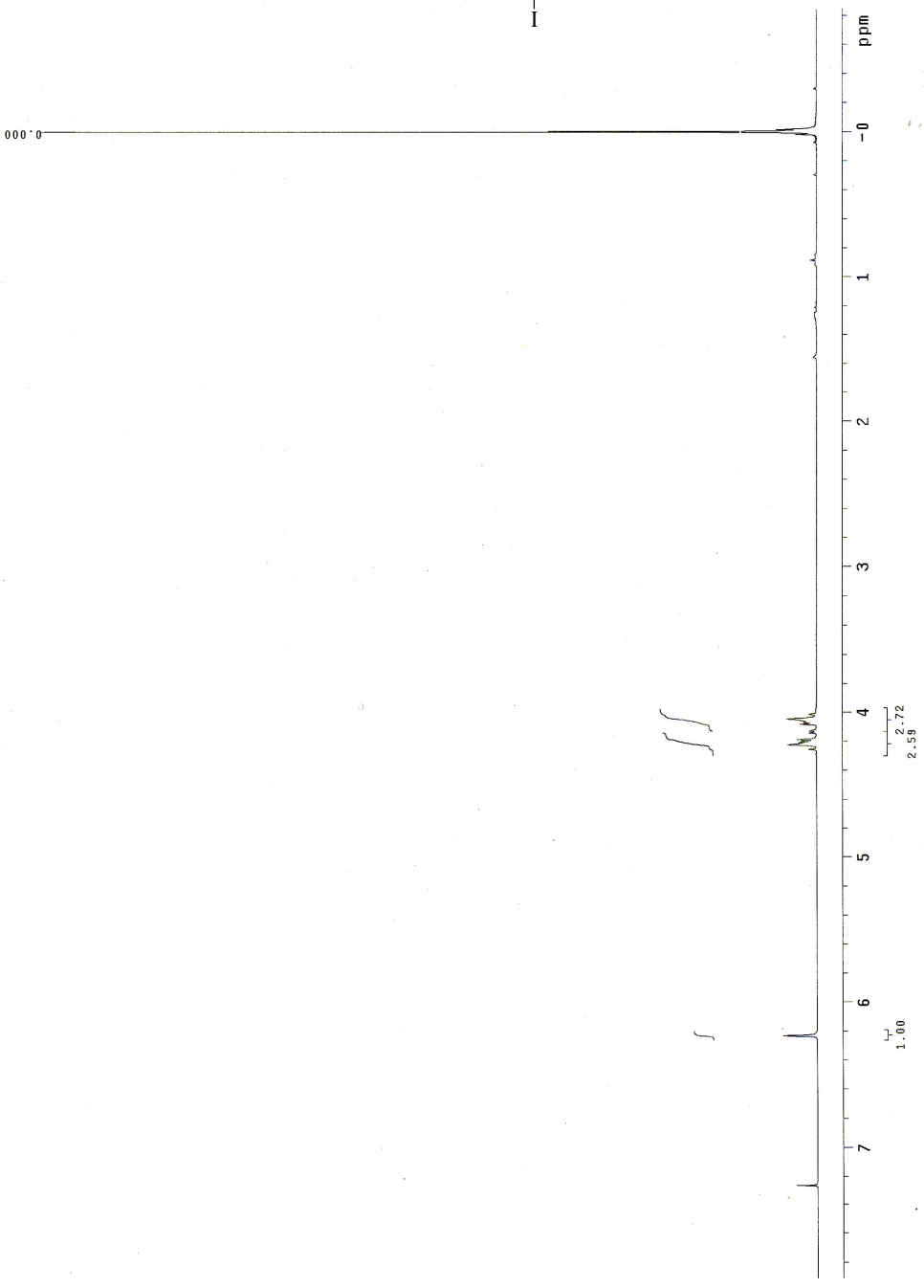

200 MHZ

$CDCl_3$

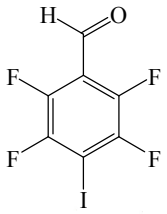


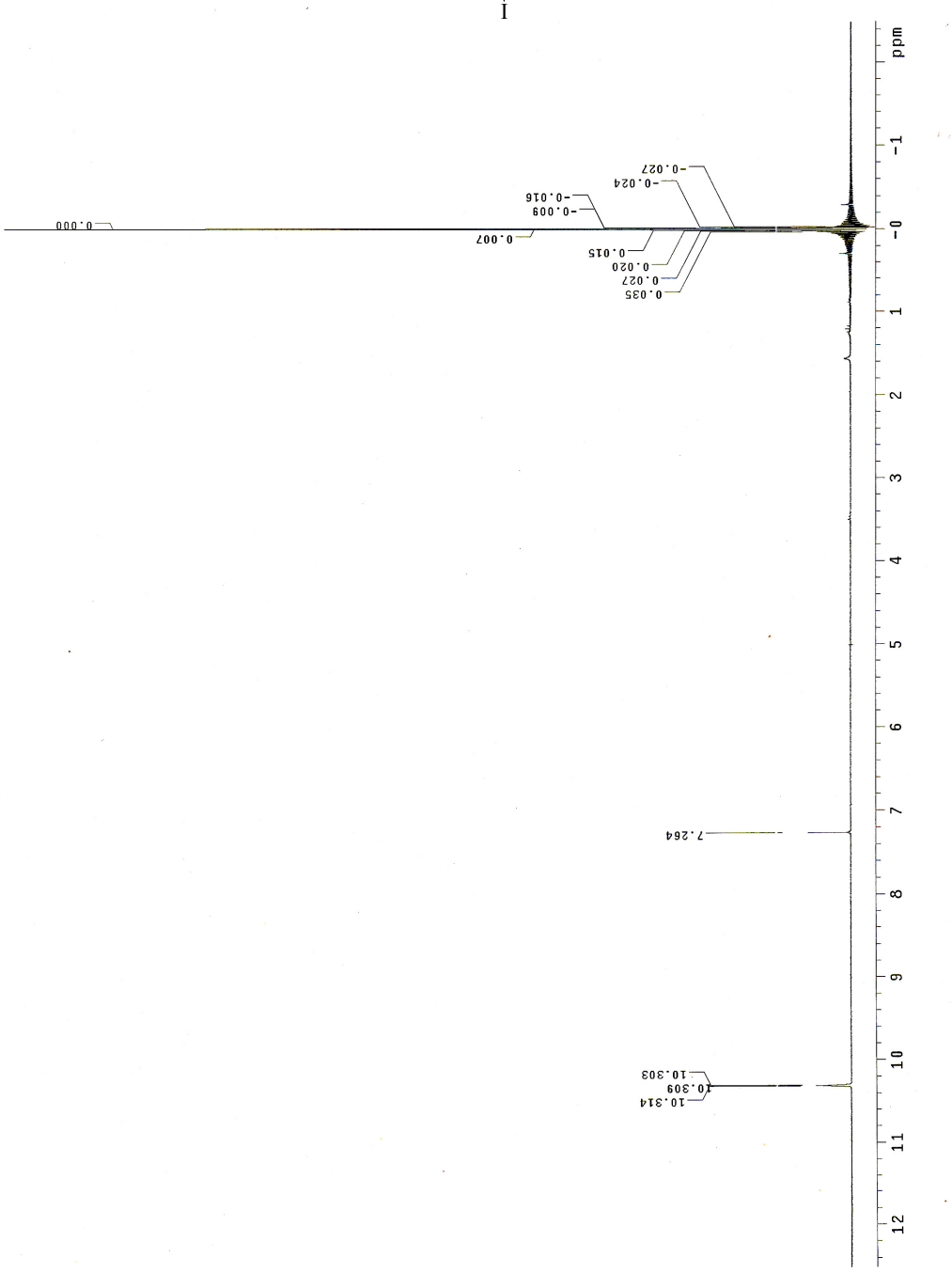

200 MHZ

$CDCl_3$

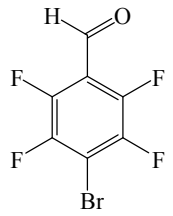


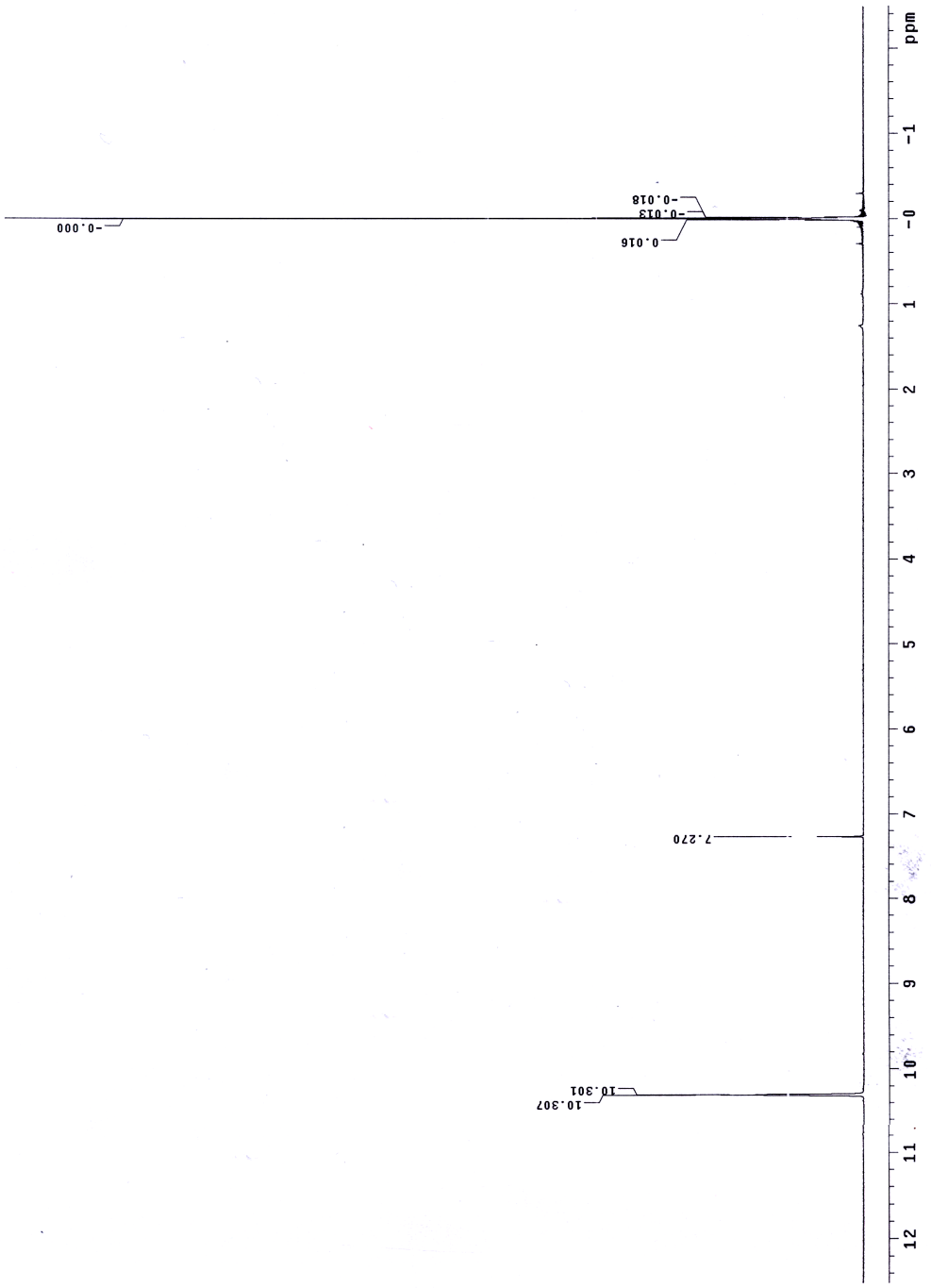

200 MHZ

$CDCl_3$

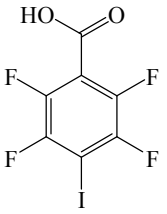


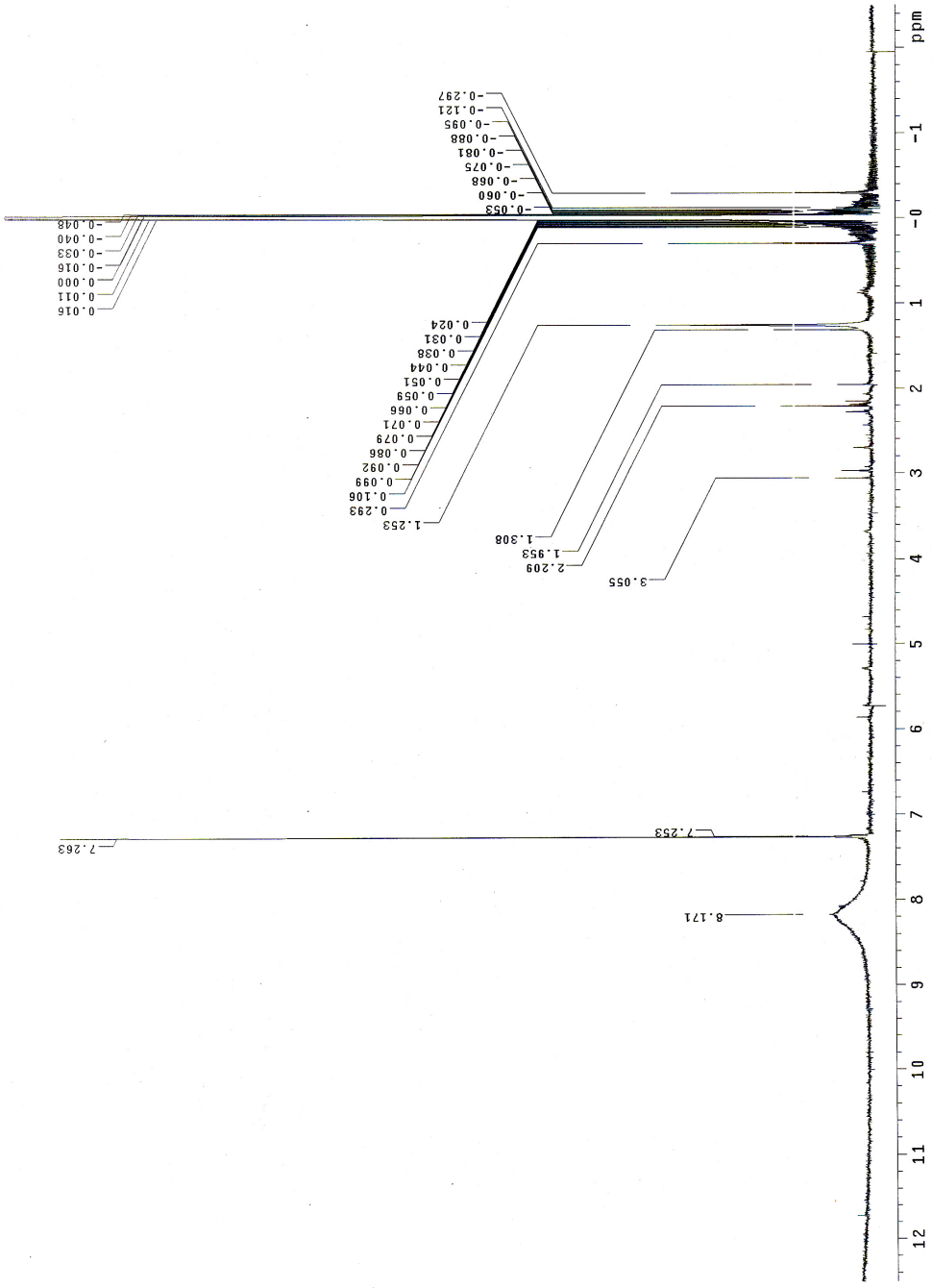

200 MHZ

$CDCl_3$

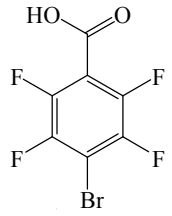


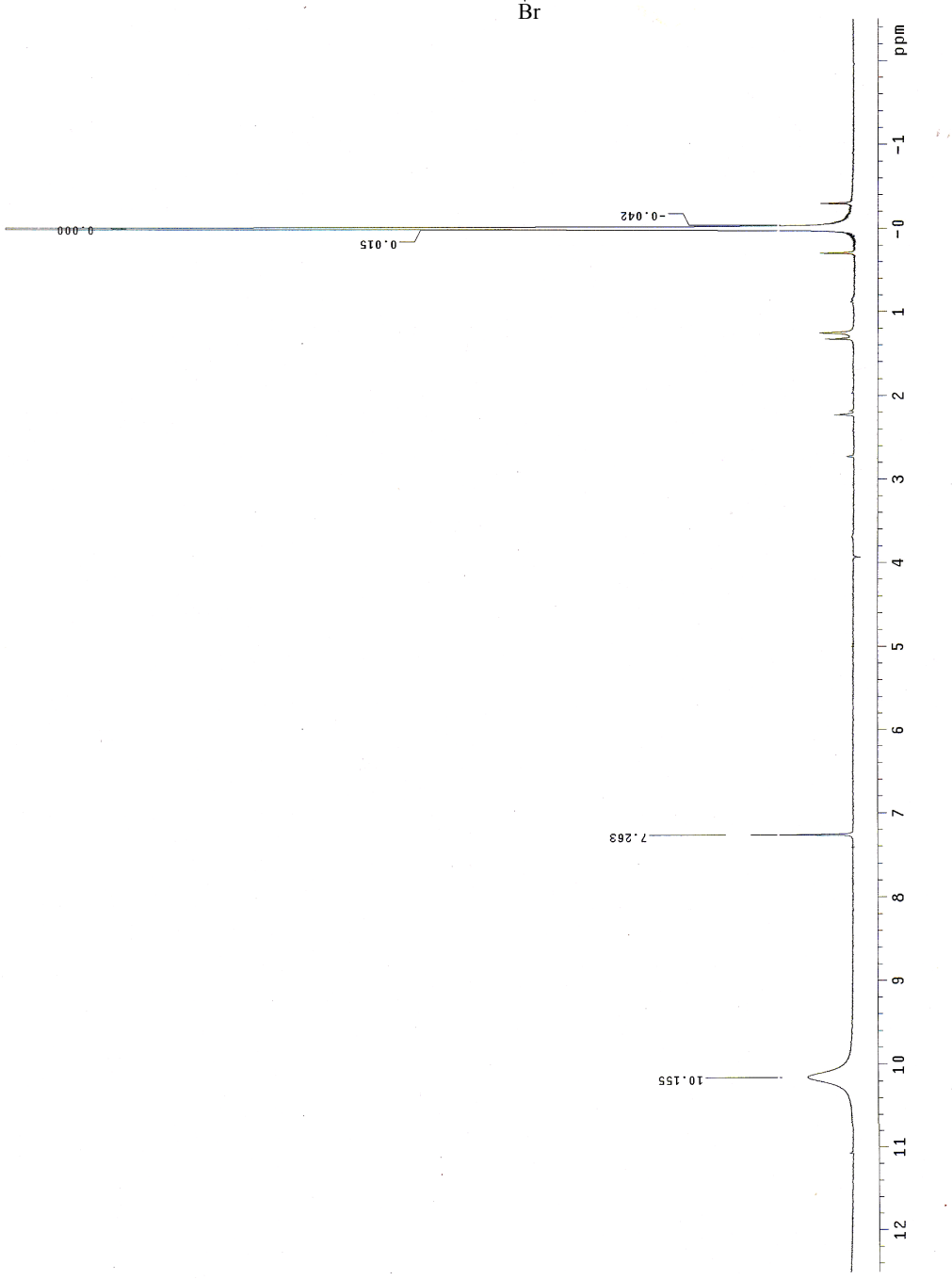

400 MHZ

$CDCl_3$

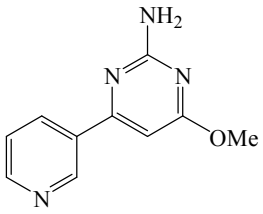


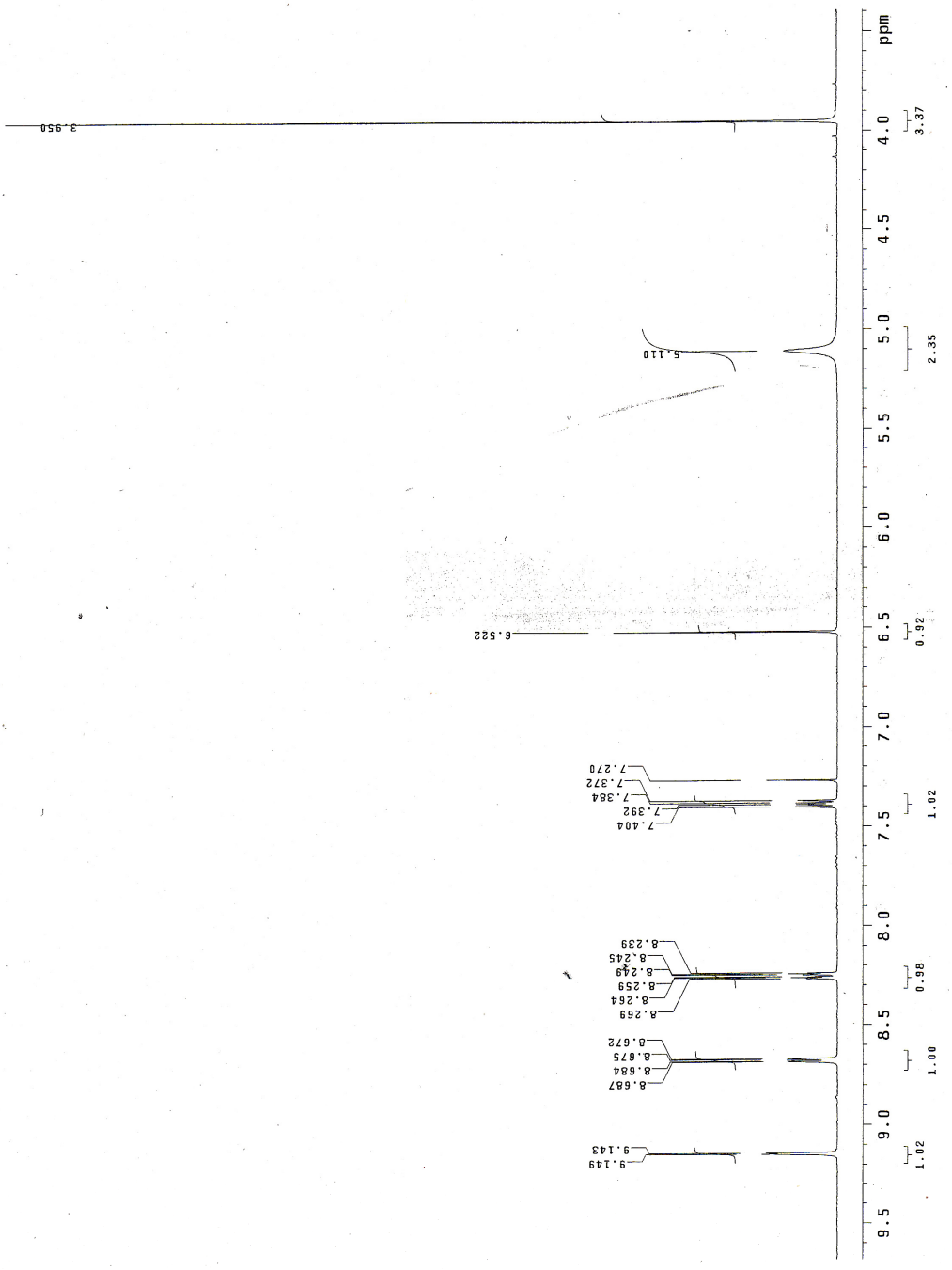

400 MHZ

$CDCl_3$

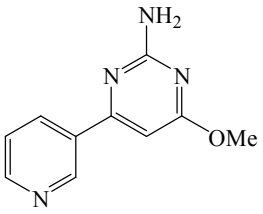


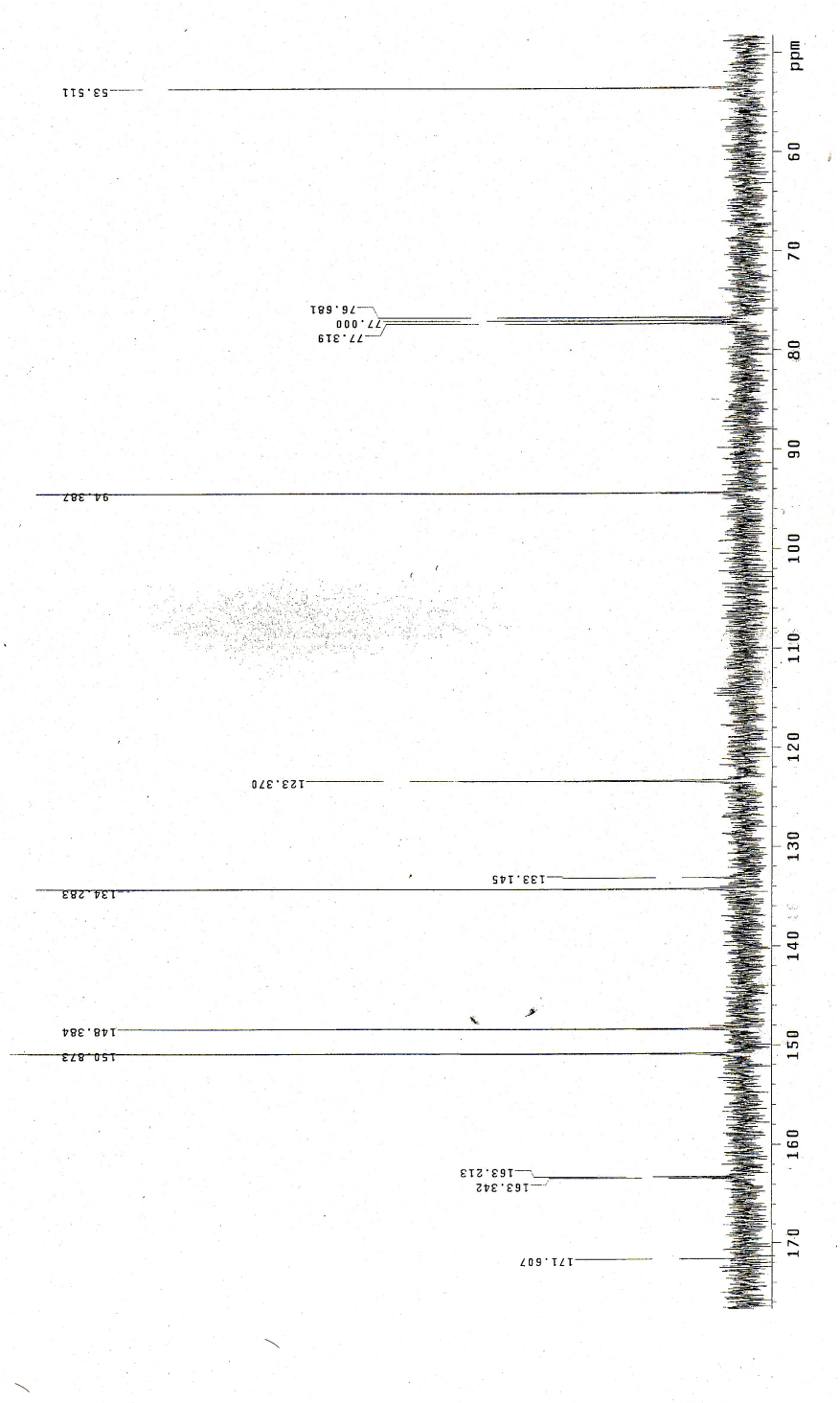

200 MHZ

CDCl3

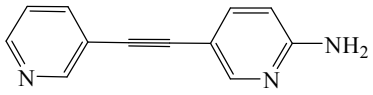


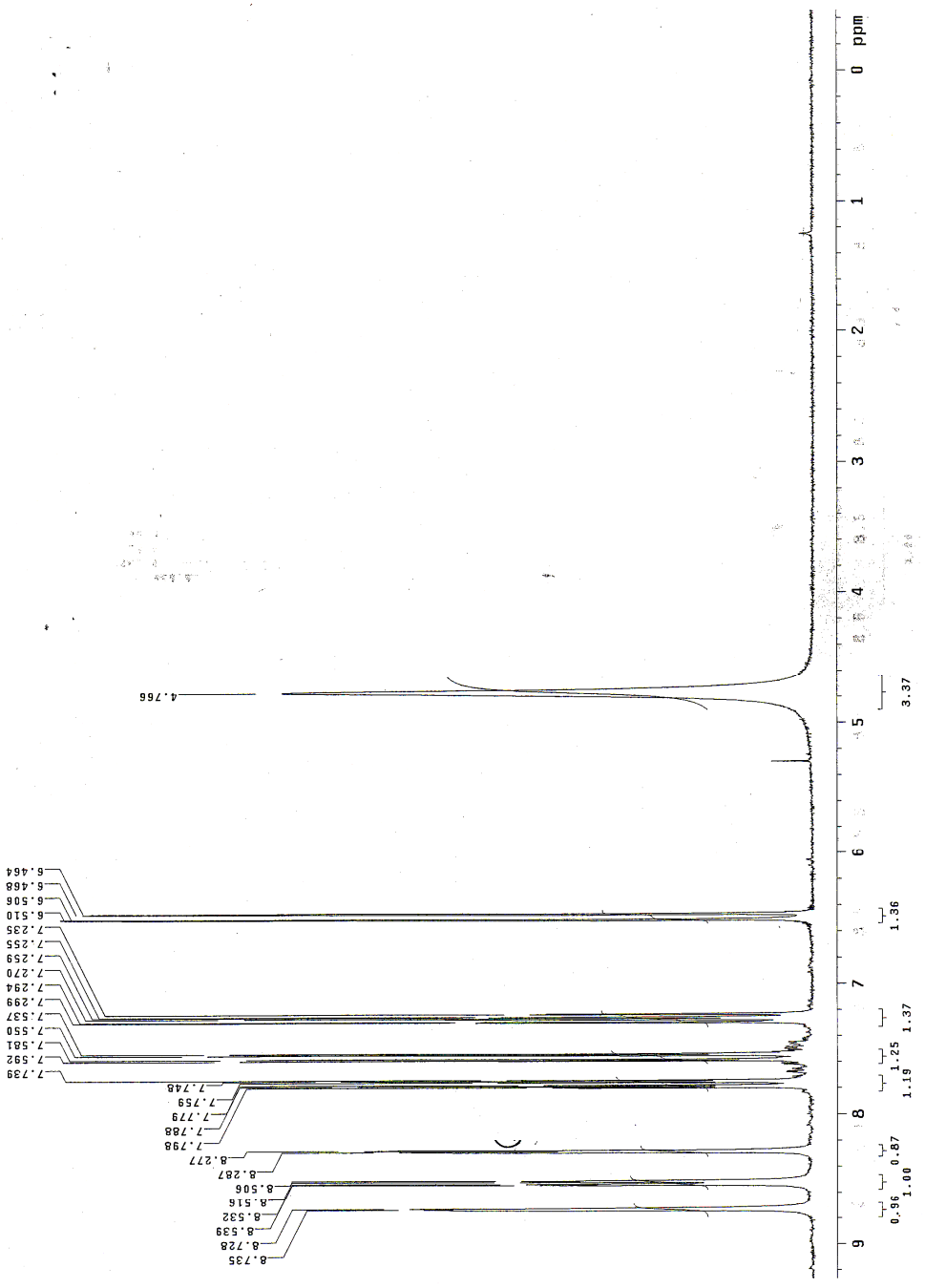

400 MHZ

CDCl3

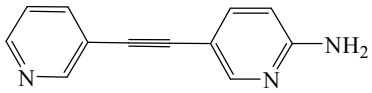


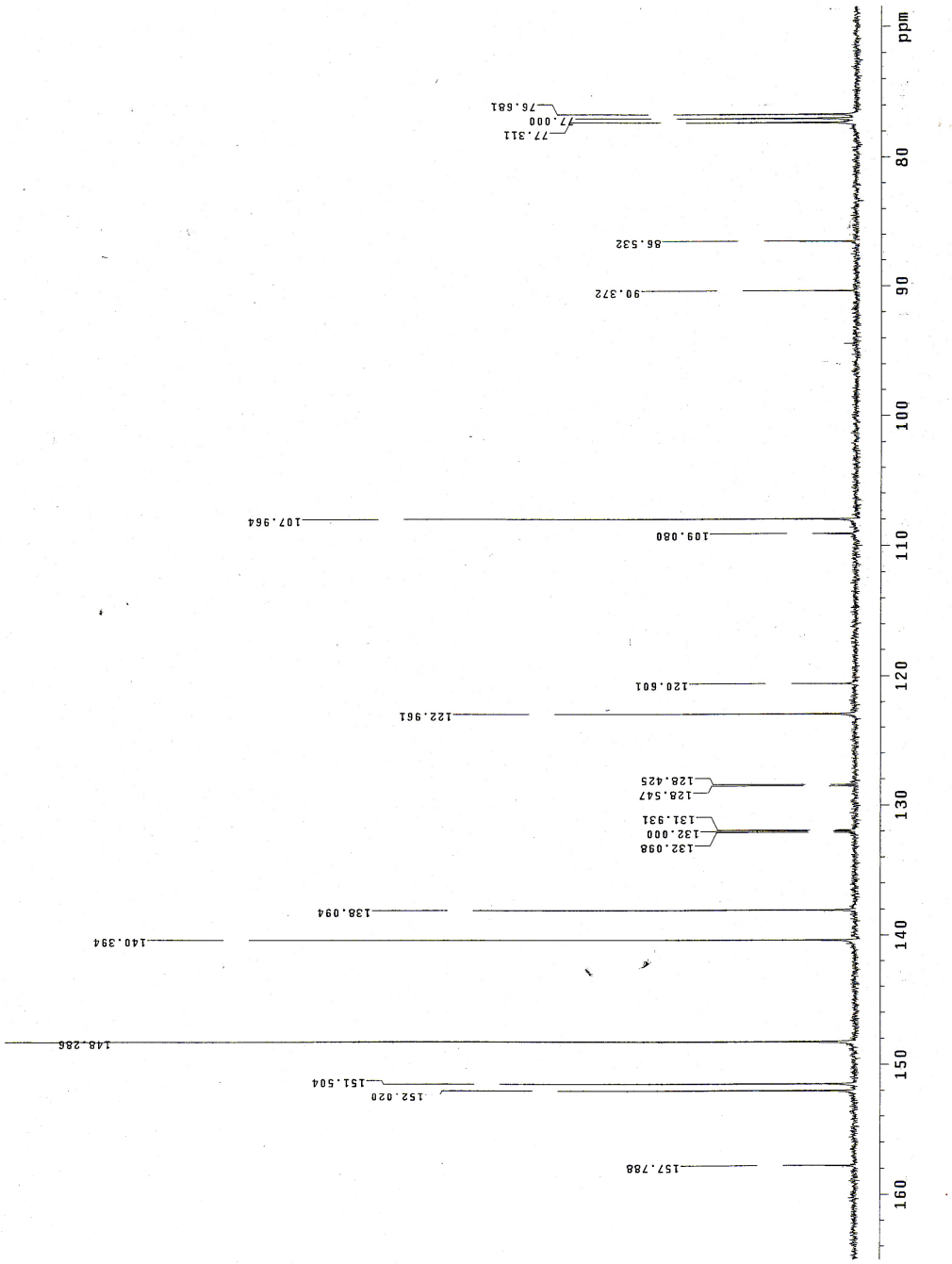

400 MHZ

$D_6$-DMSO

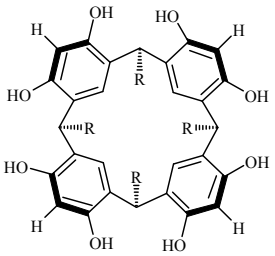

R = $(CH_2)_4CH_3$

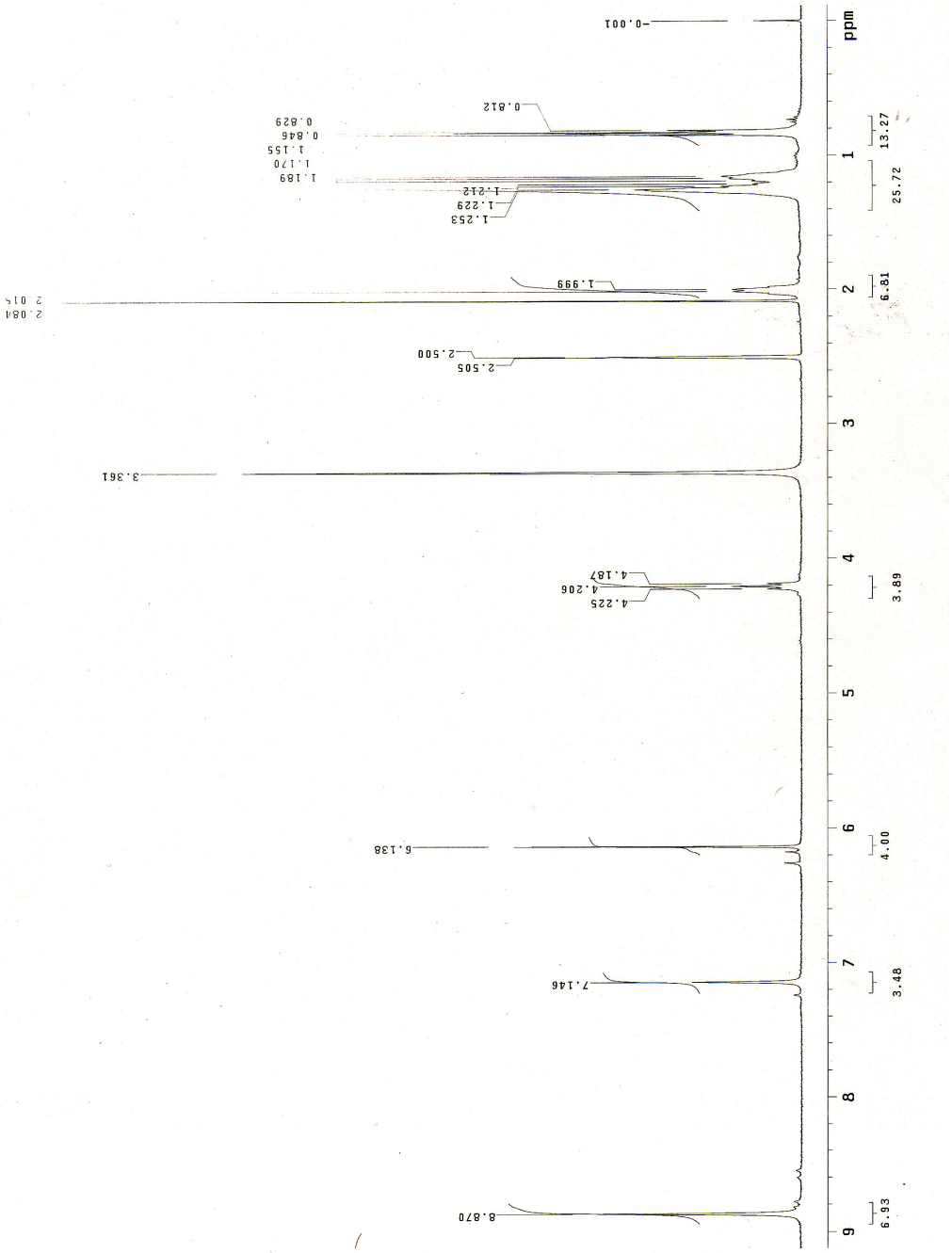

400 MHZ

$D_6$-DMSO

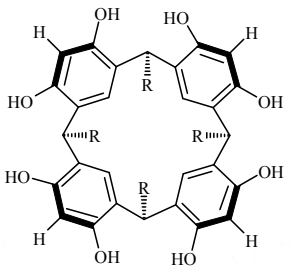


R = $(CH_2)_4CH_3$

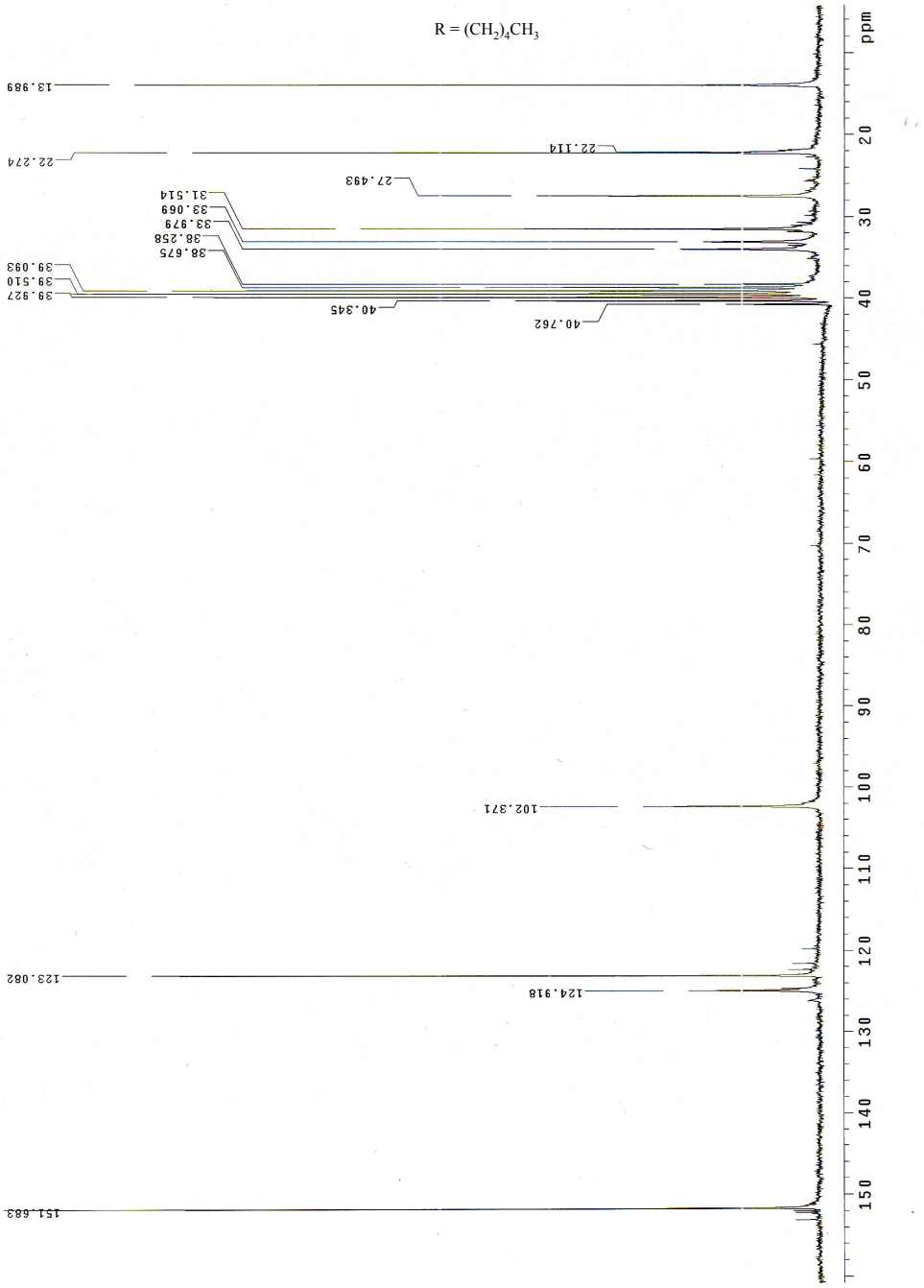

400 MHZ

$D_6$-DMSO

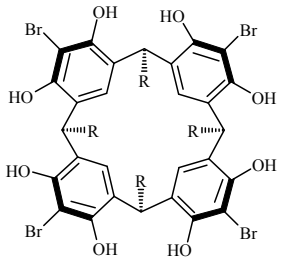


$R = (CH_2)_4CH_3$

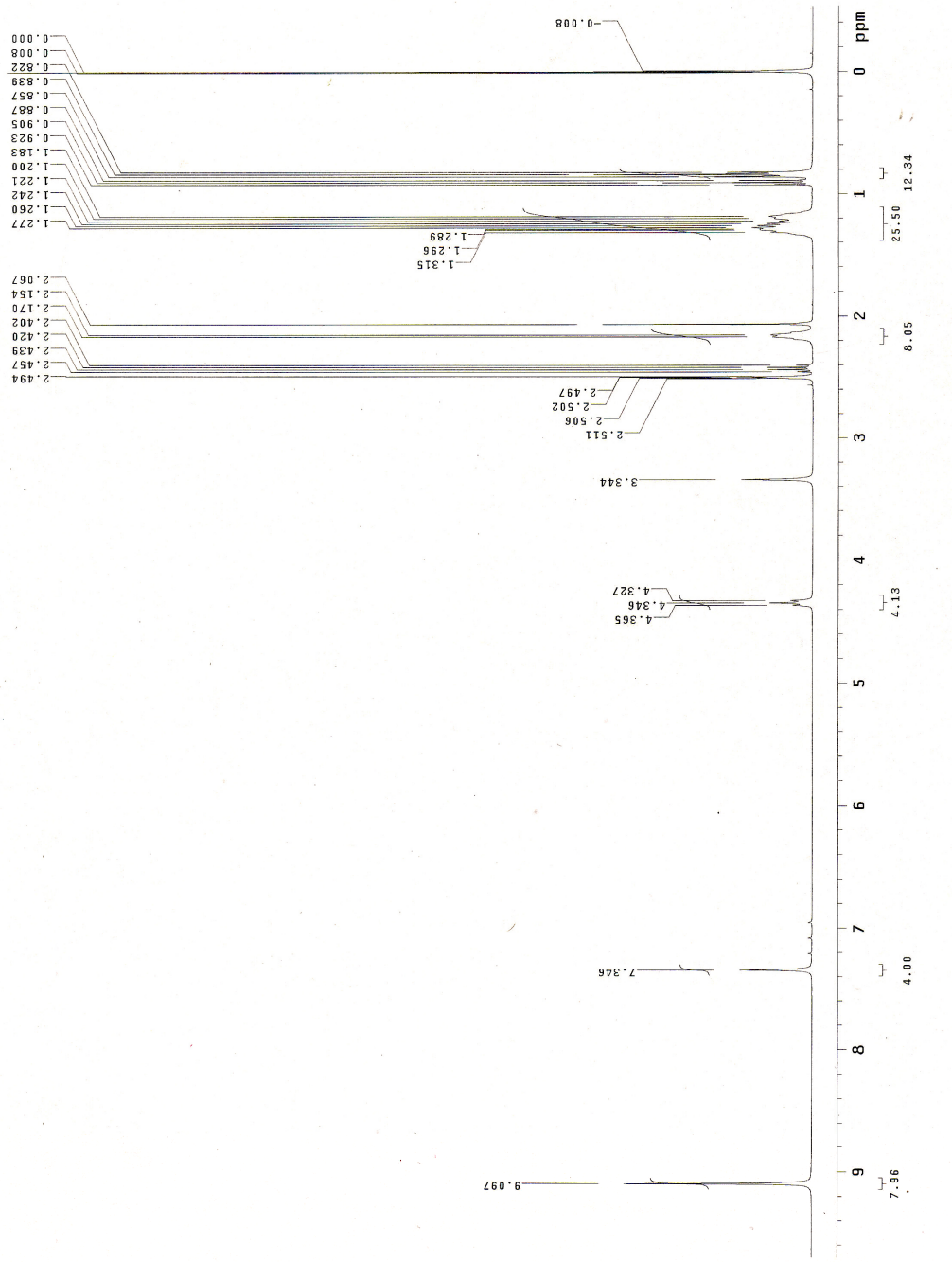

400 MHZ

$D_6$-DMSO

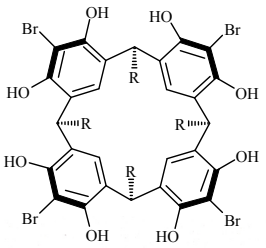


$R = (CH_2)_4CH_3$

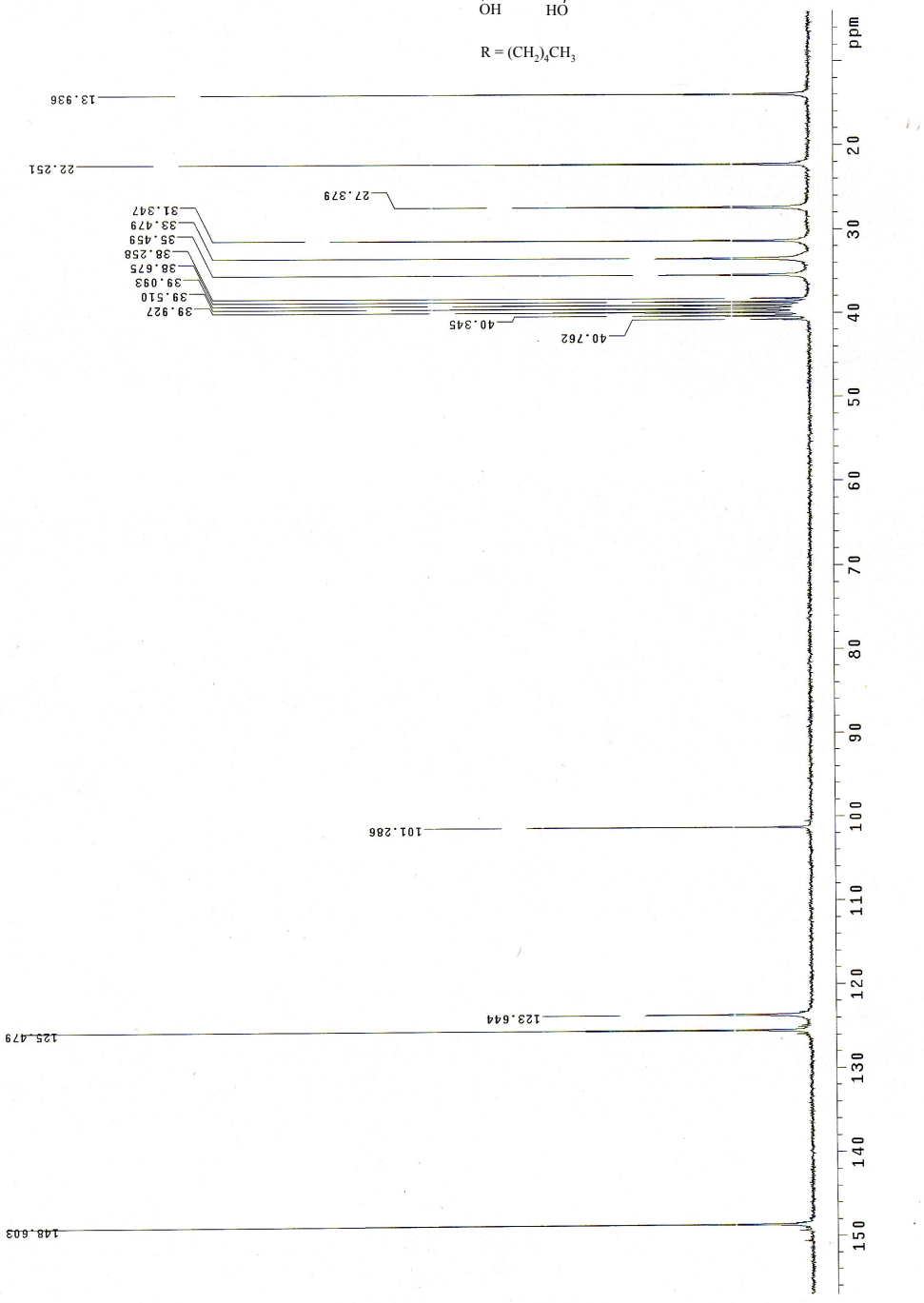

400 MHZ

$CDCl_3$

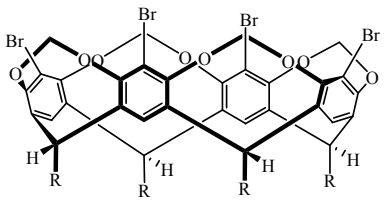


R = $(CH_2)_4CH_3$

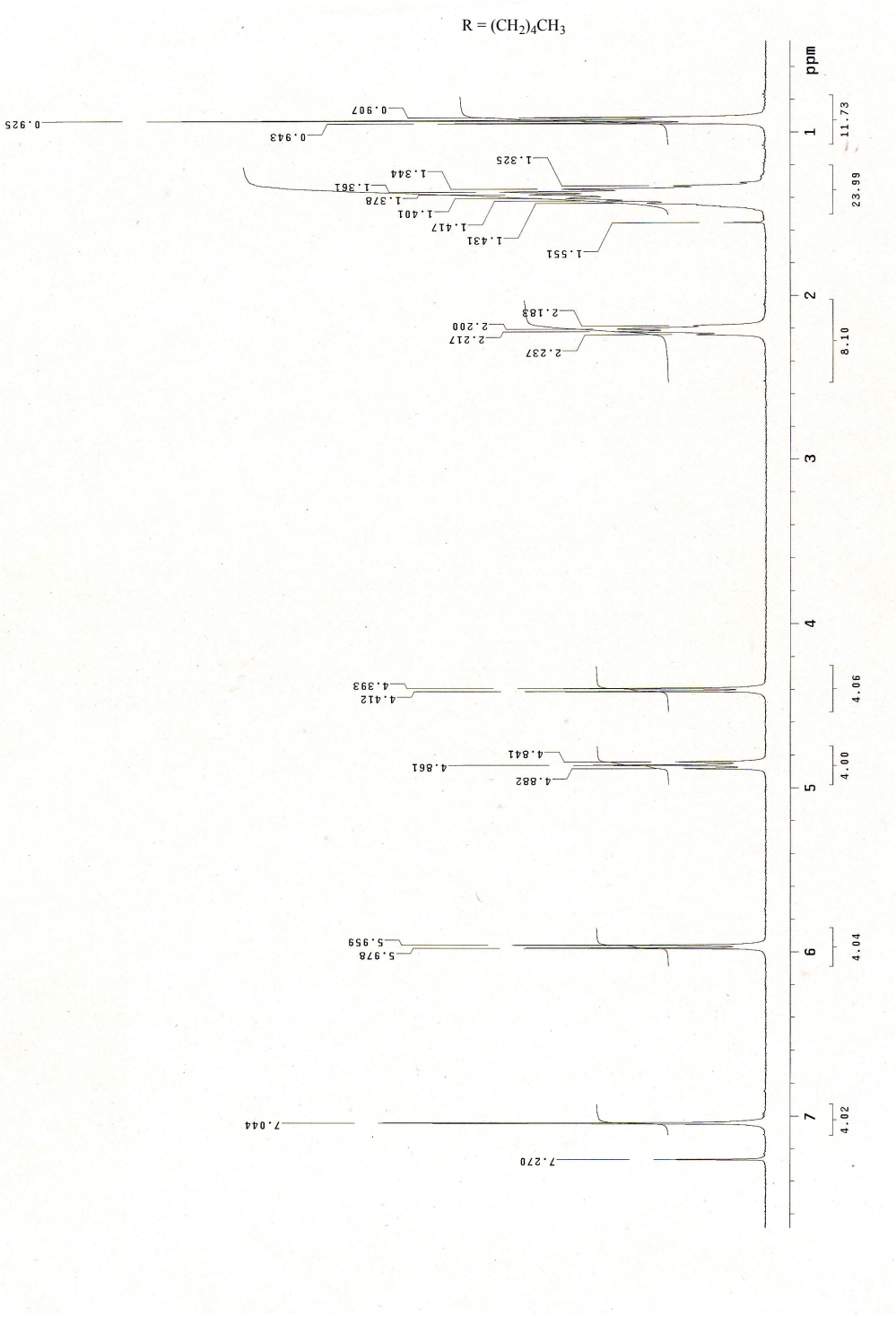

400 MHZ

$CDCl_3$

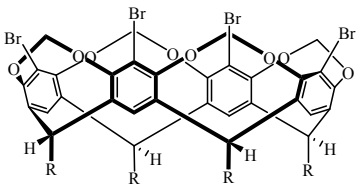

R = $(CH_2)_4CH_3$

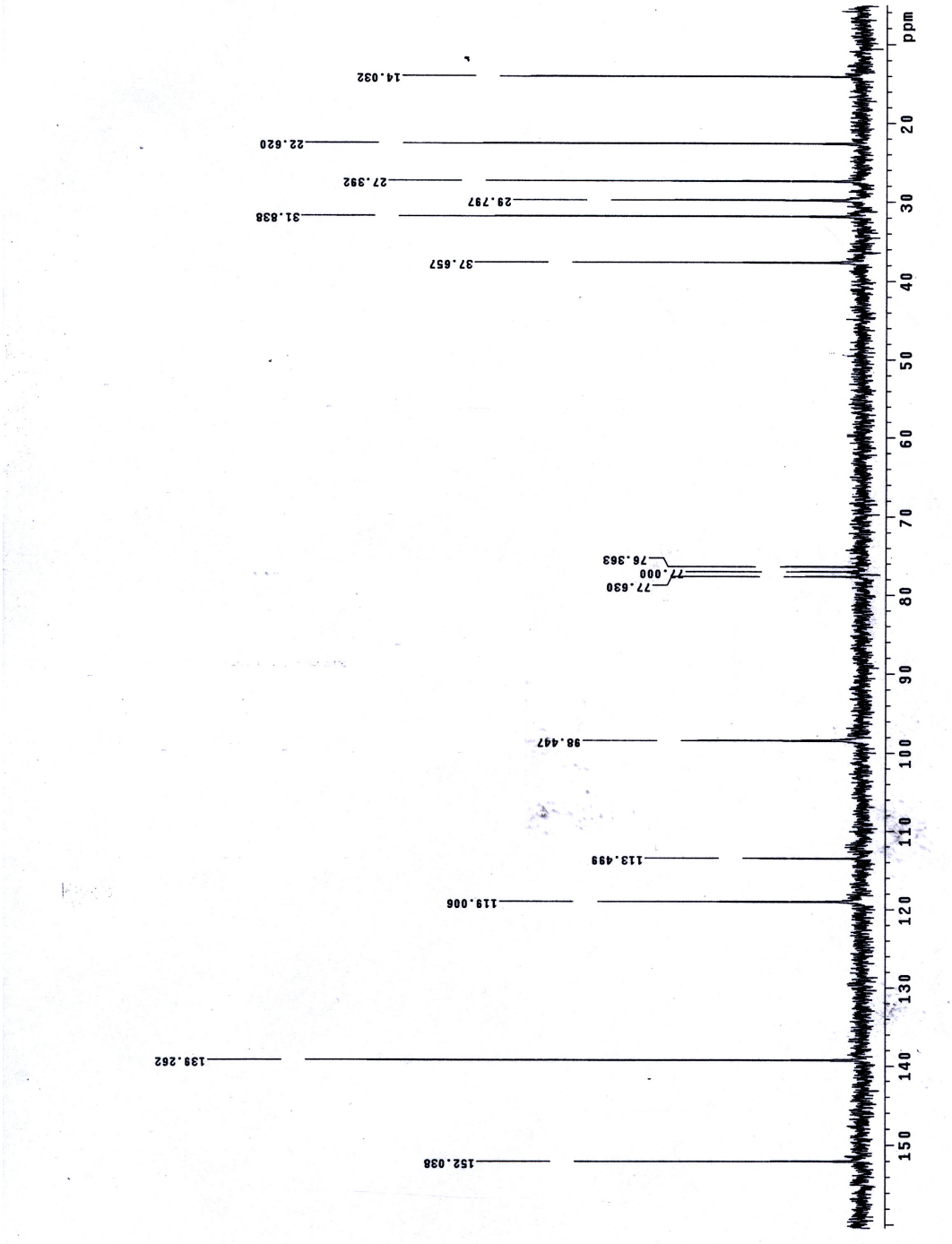

400 MHZ

$CDCl_3$

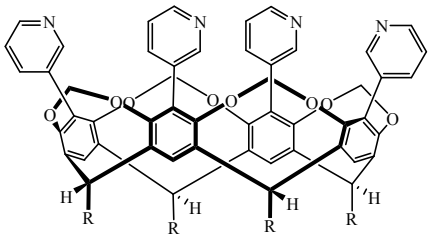

$R = (CH_2)_4CH_3$

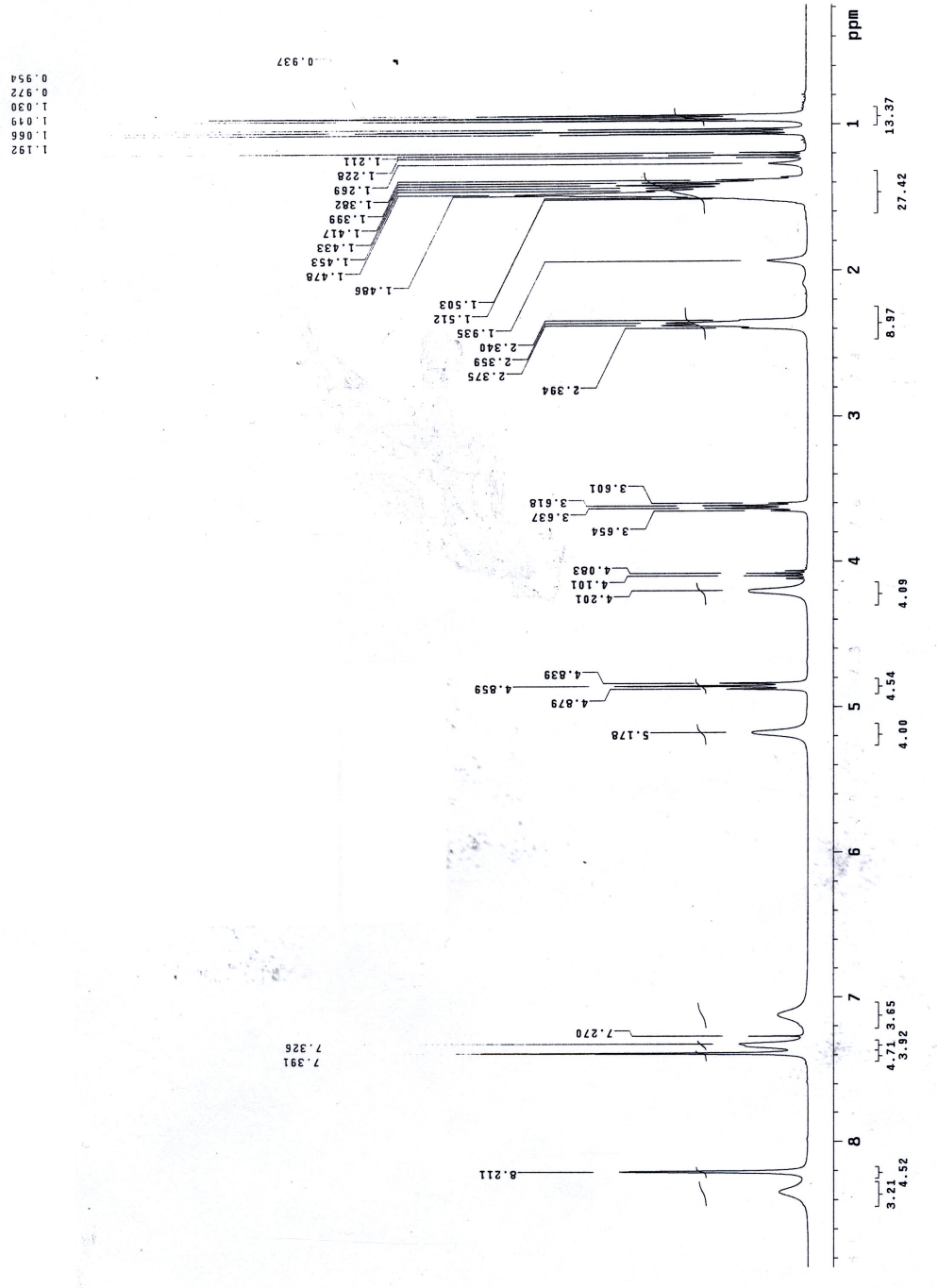

200 MHZ

$CDCl_3$

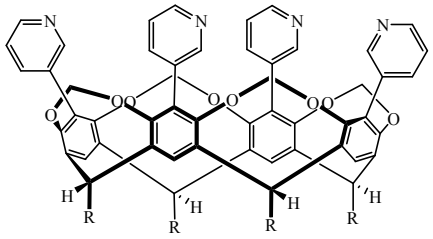

R = $(CH_2)_4CH_3$

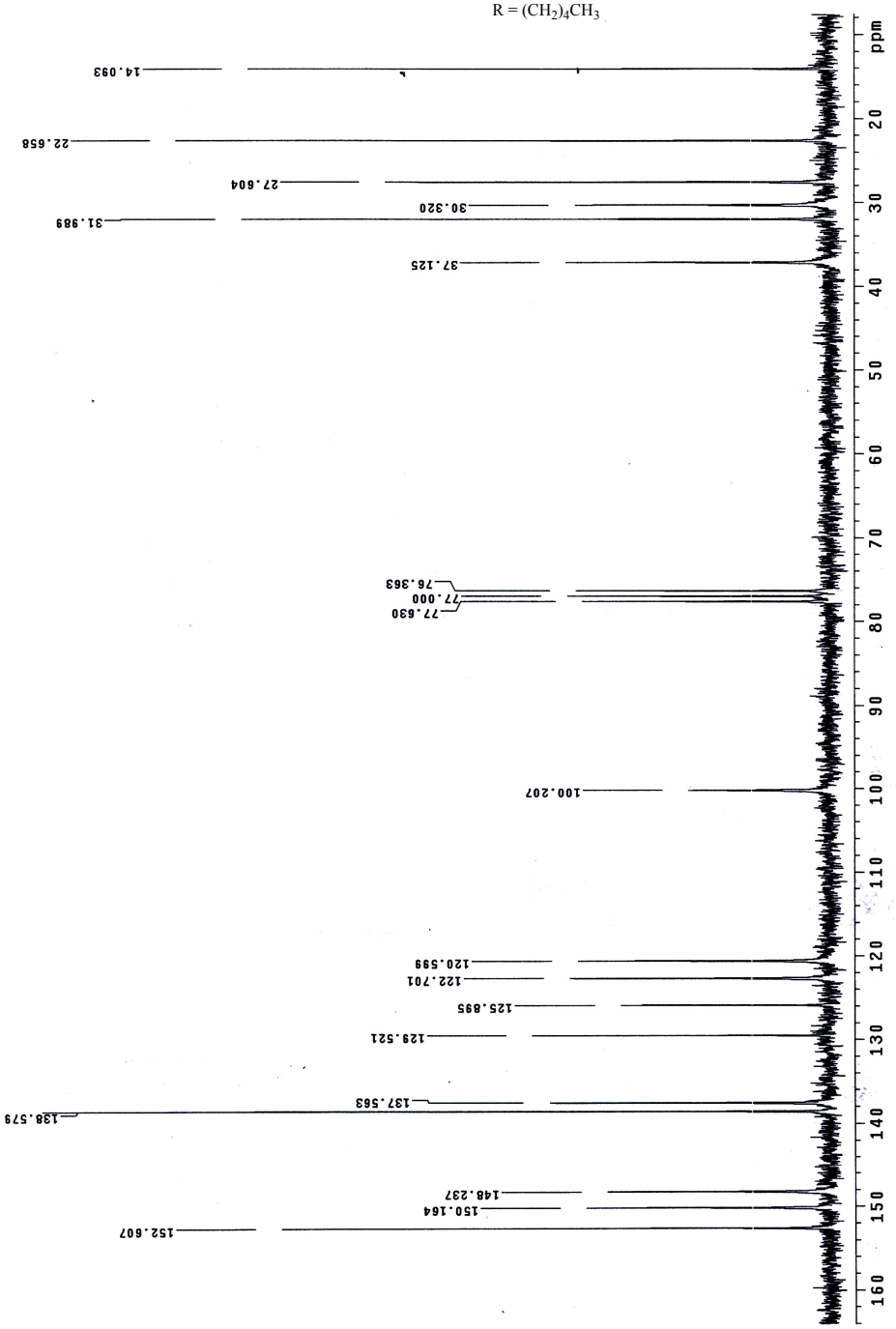

200 MHZ

$D_6$-DMSO

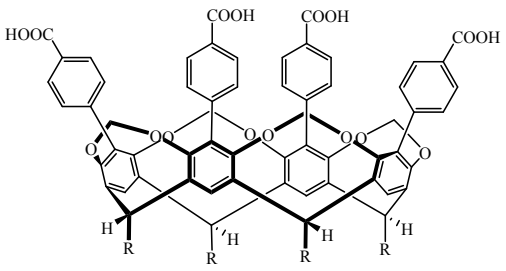


$R = (CH_2)_4CH_3$

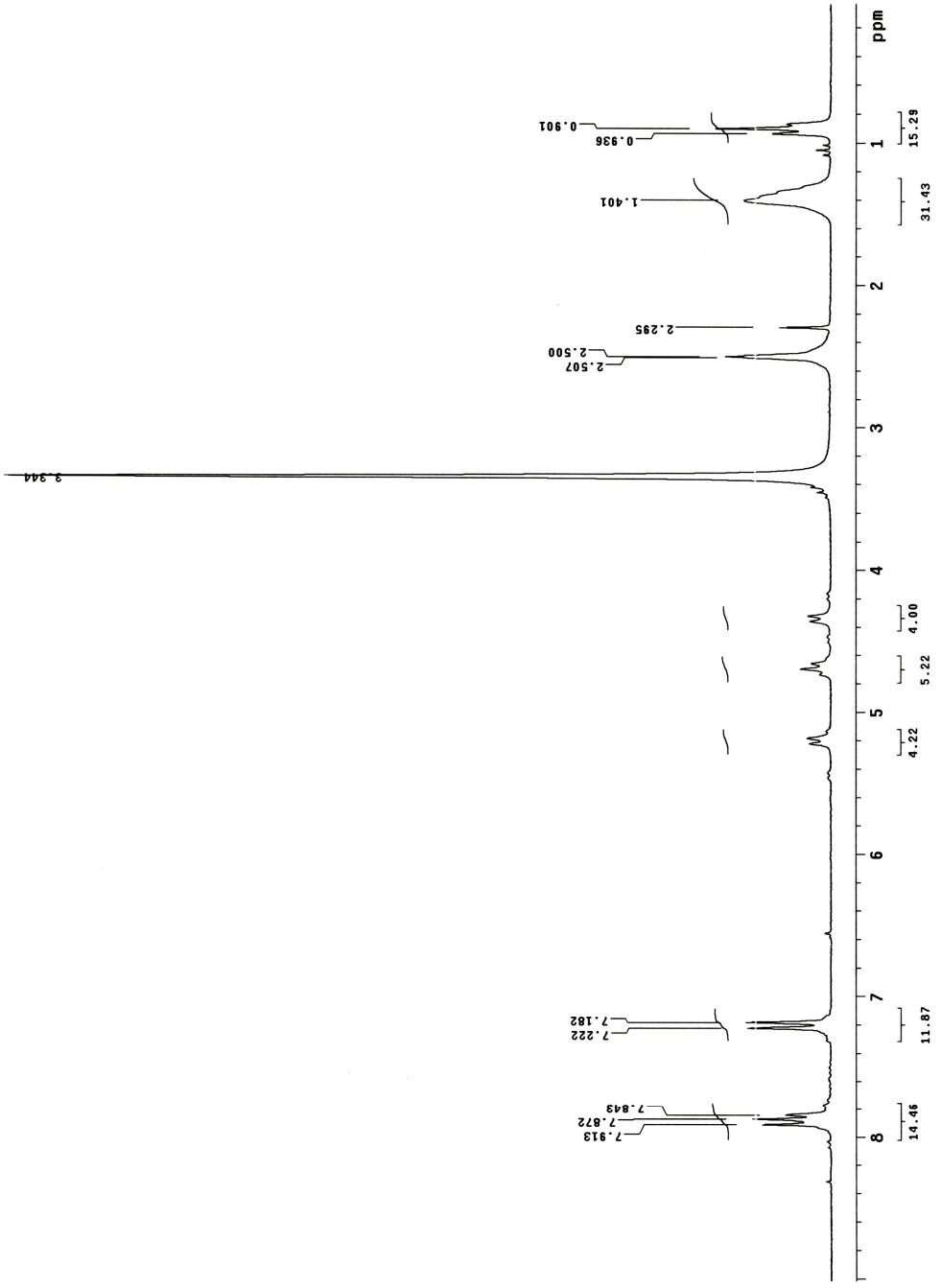

400 MHZ

$CDCl_3$

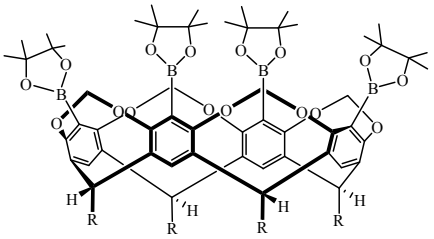

$R = (CH_2)_4CH_3$

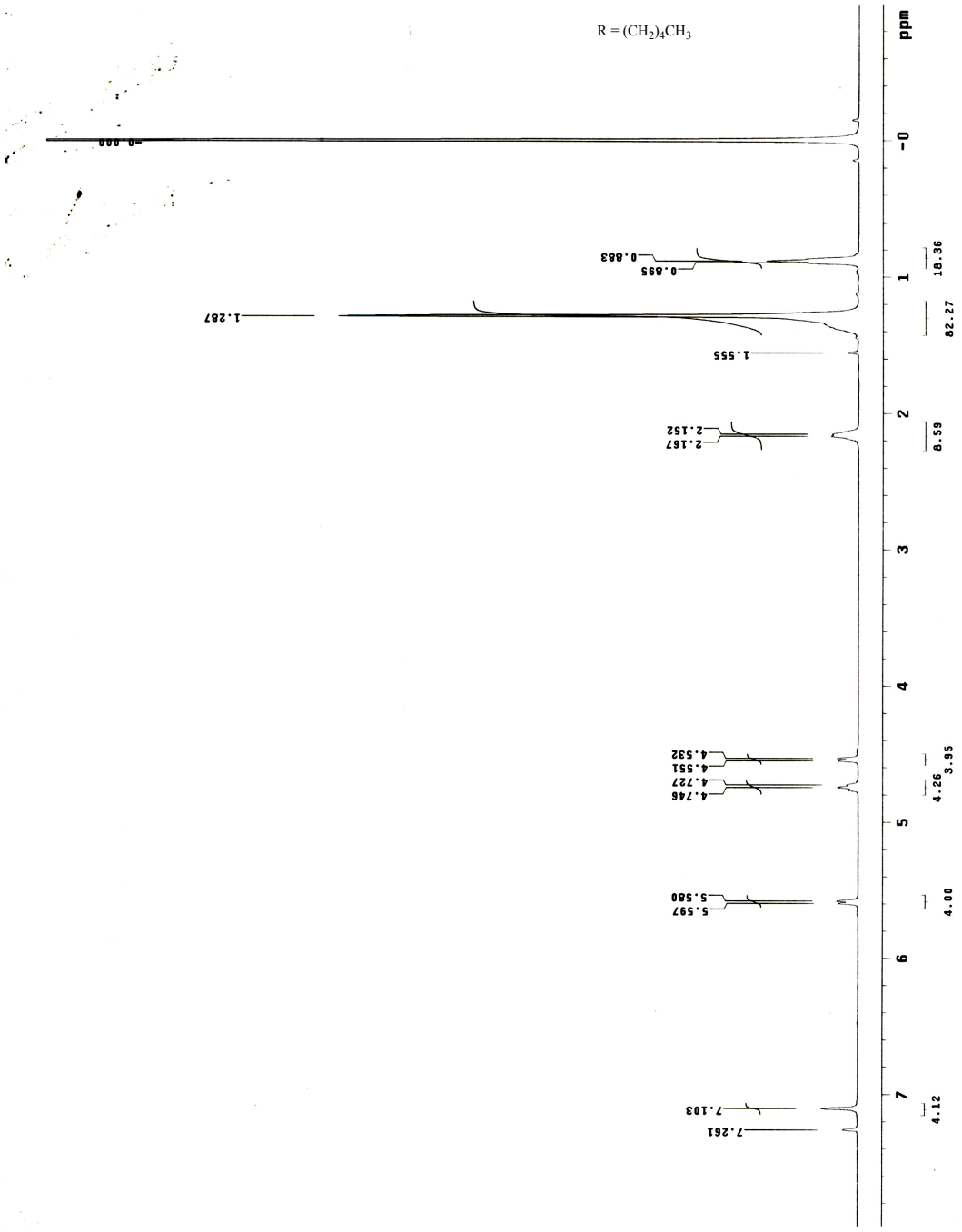

200 MHZ

$CDCl_3$

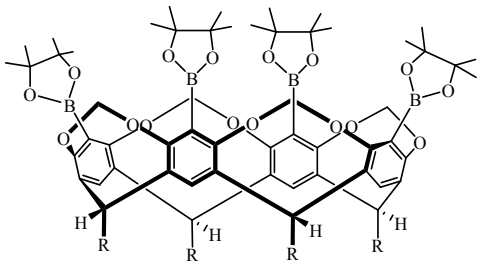

$R = (CH_2)_4CH_3$

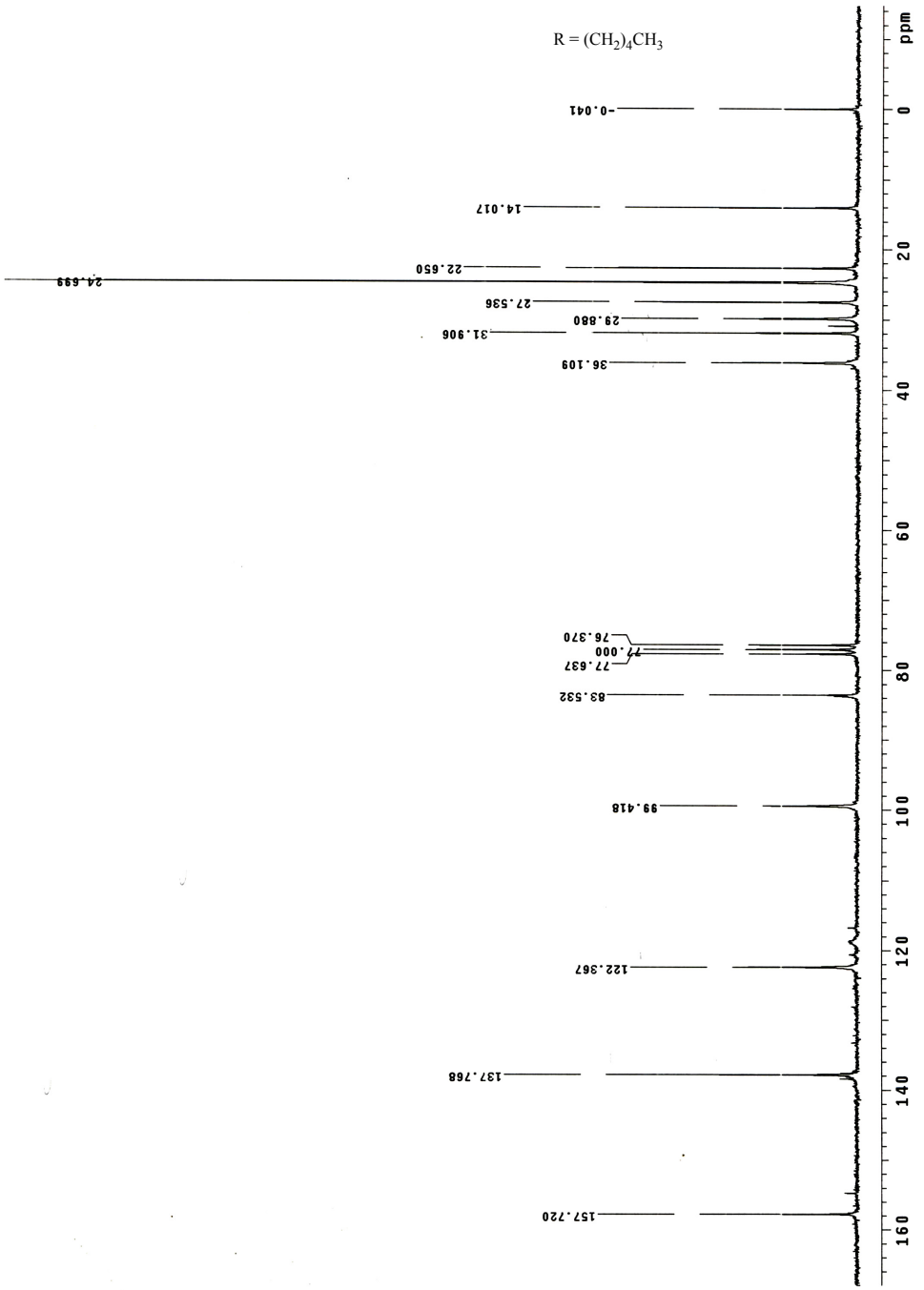

200 MHZ

$CDCl_3$

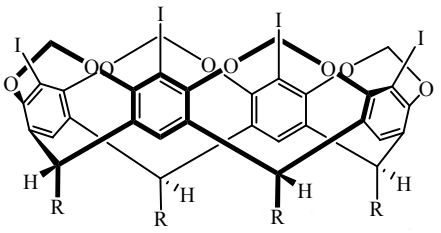

R = $(CH_2)_4CH_3$

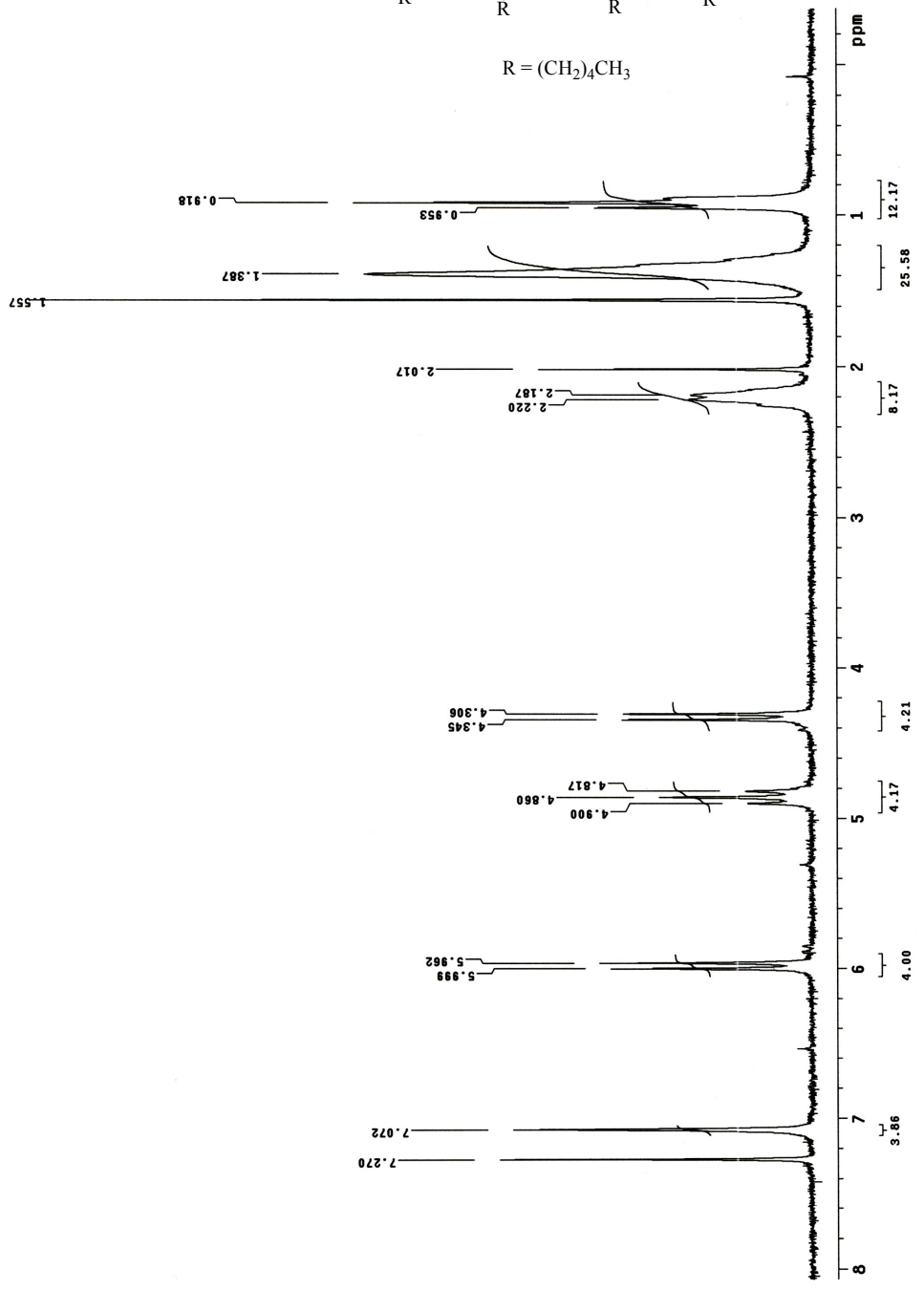

200 MHZ

$CDCl_3$

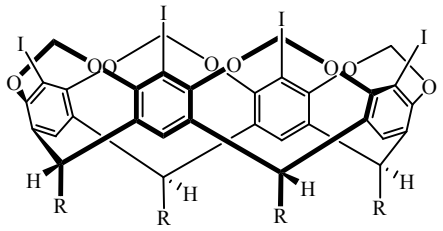

R = $(CH_2)_4CH_3$

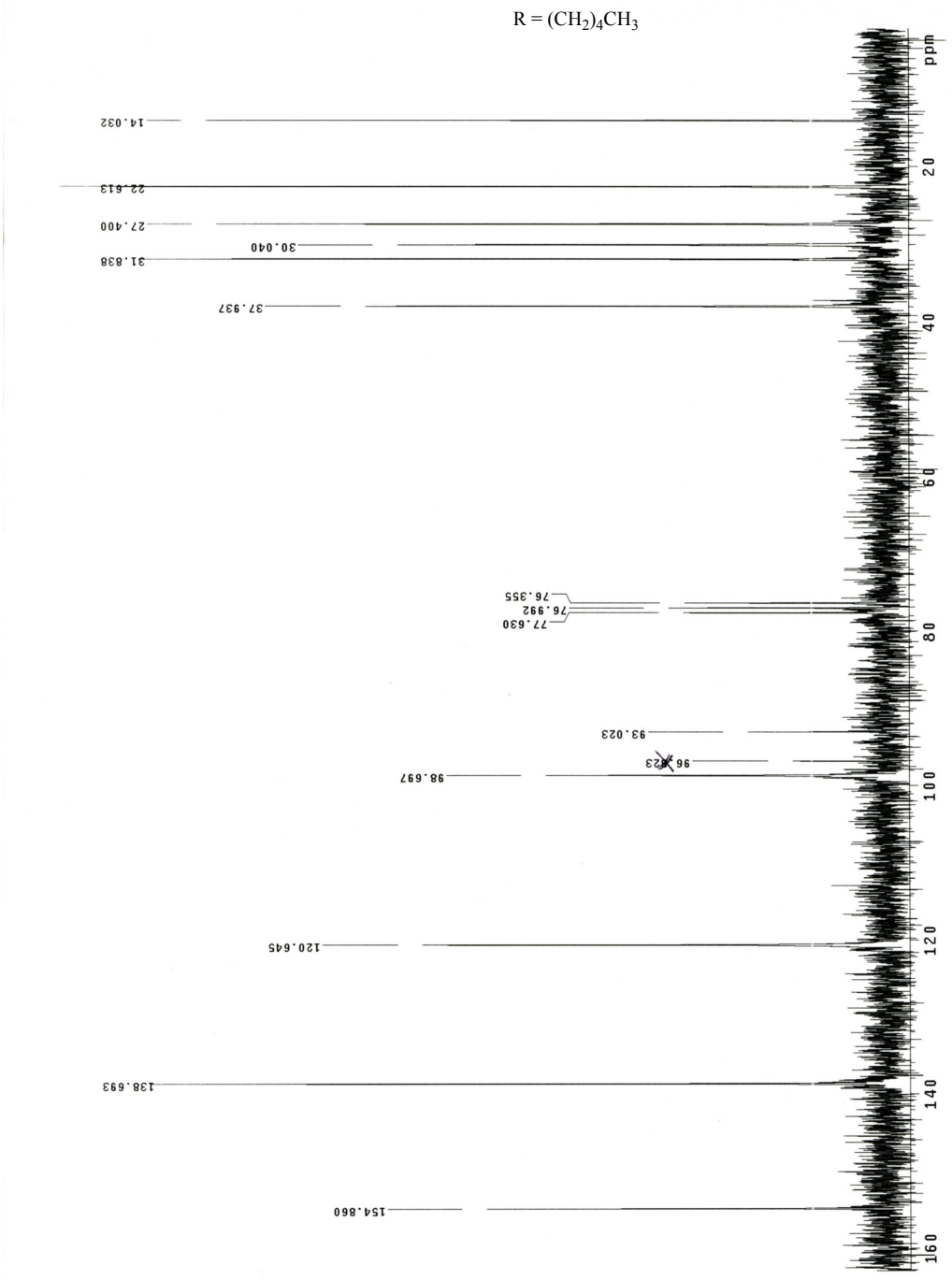

400 MHZ

$CDCl_3$

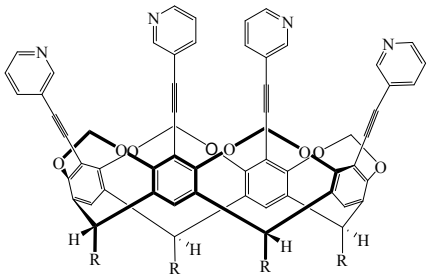

R = $(CH_2)_4CH_3$

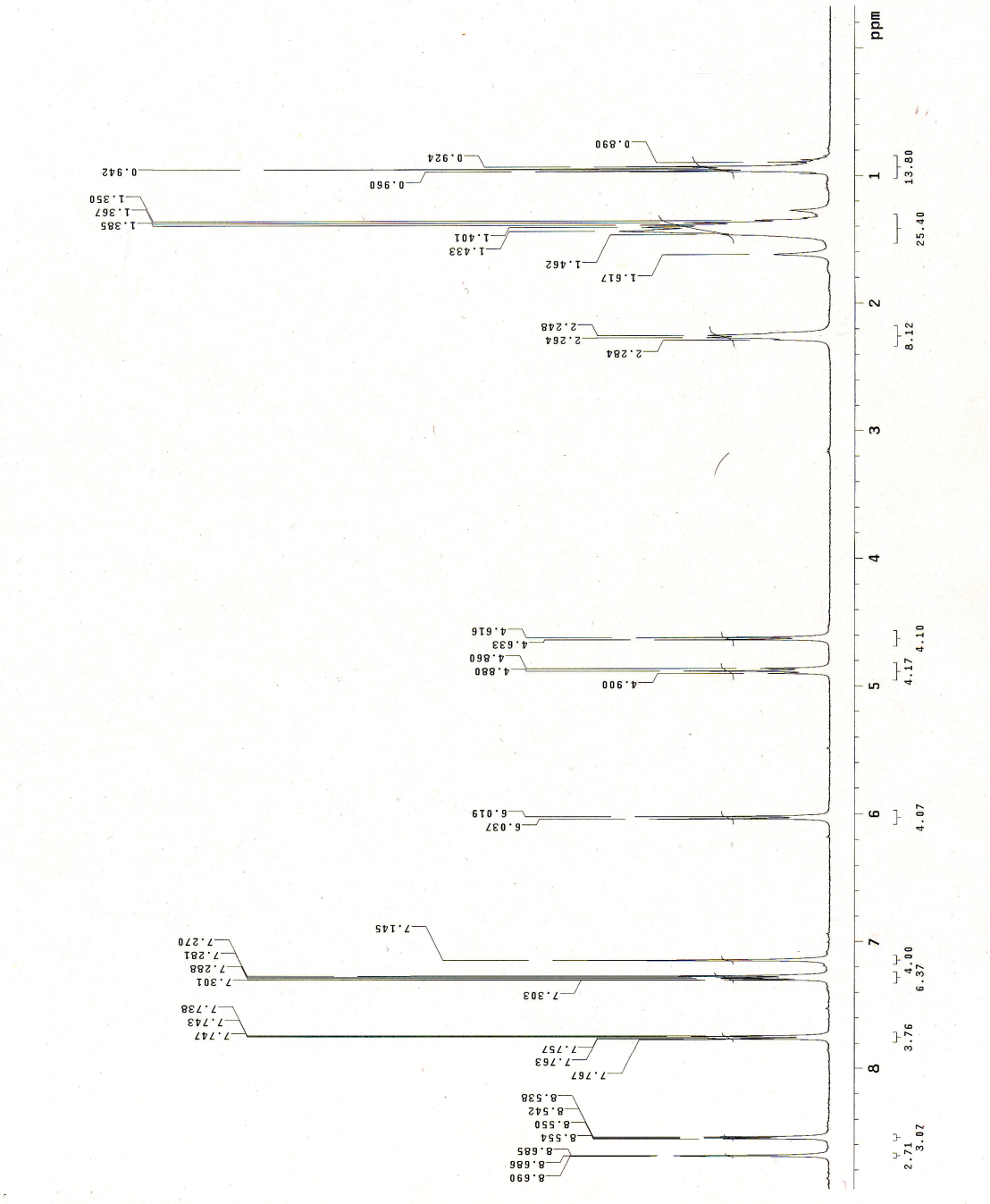

200 MHZ

$CDCl_3$

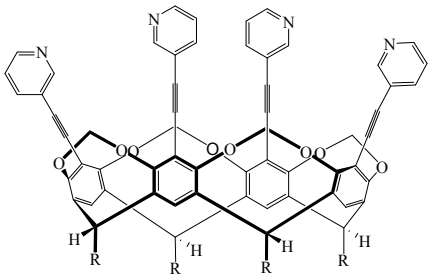

R = $(CH_2)_4CH_3$

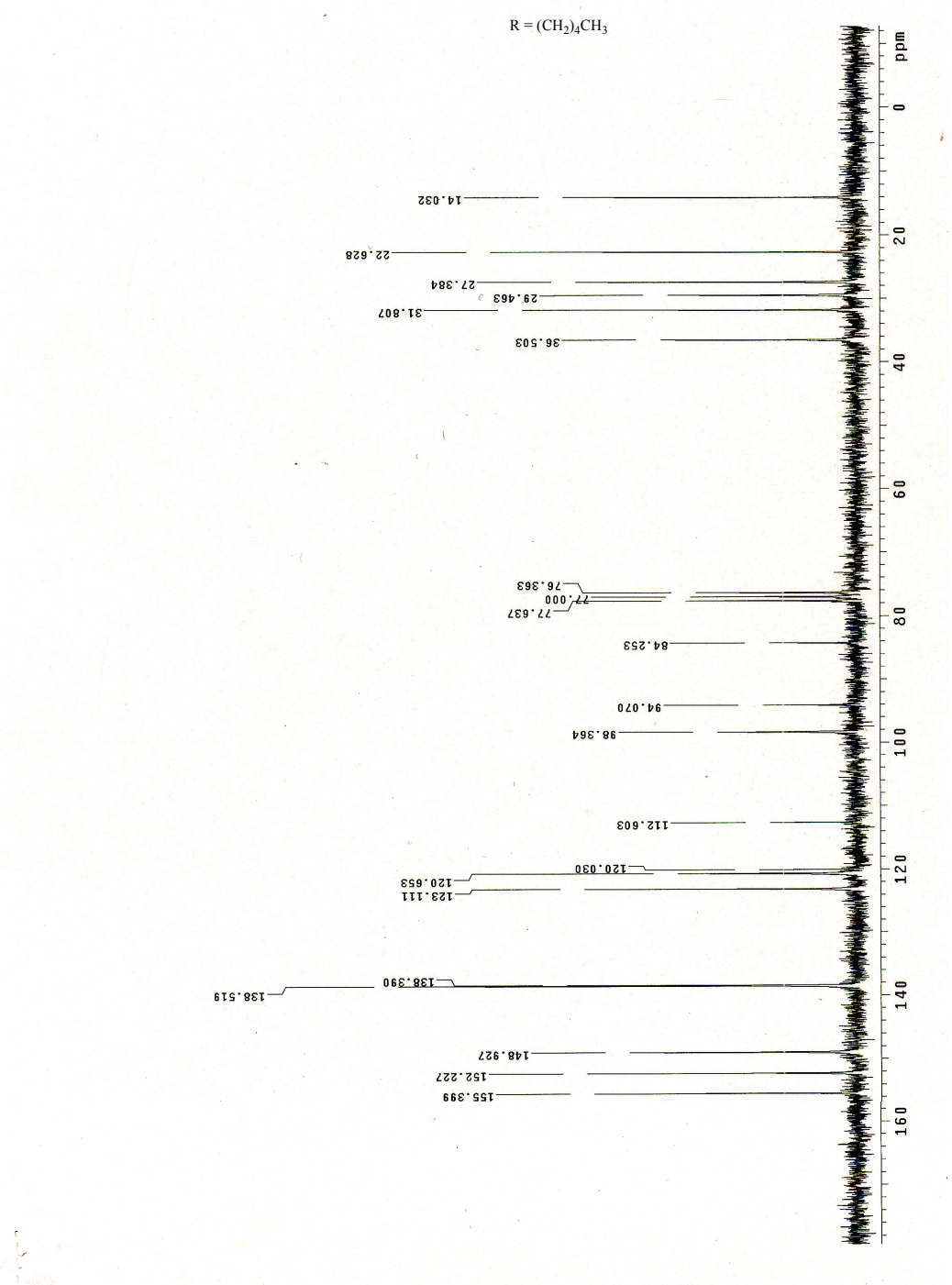

200 MHZ

$CDCl_3$

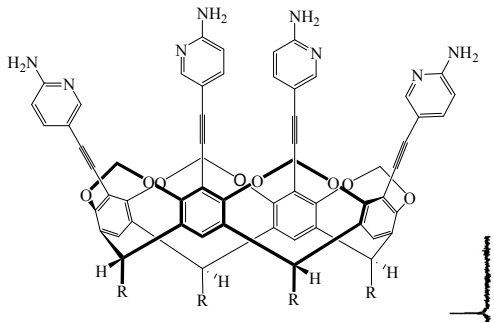

$R = (CH_2)_4CH_3$

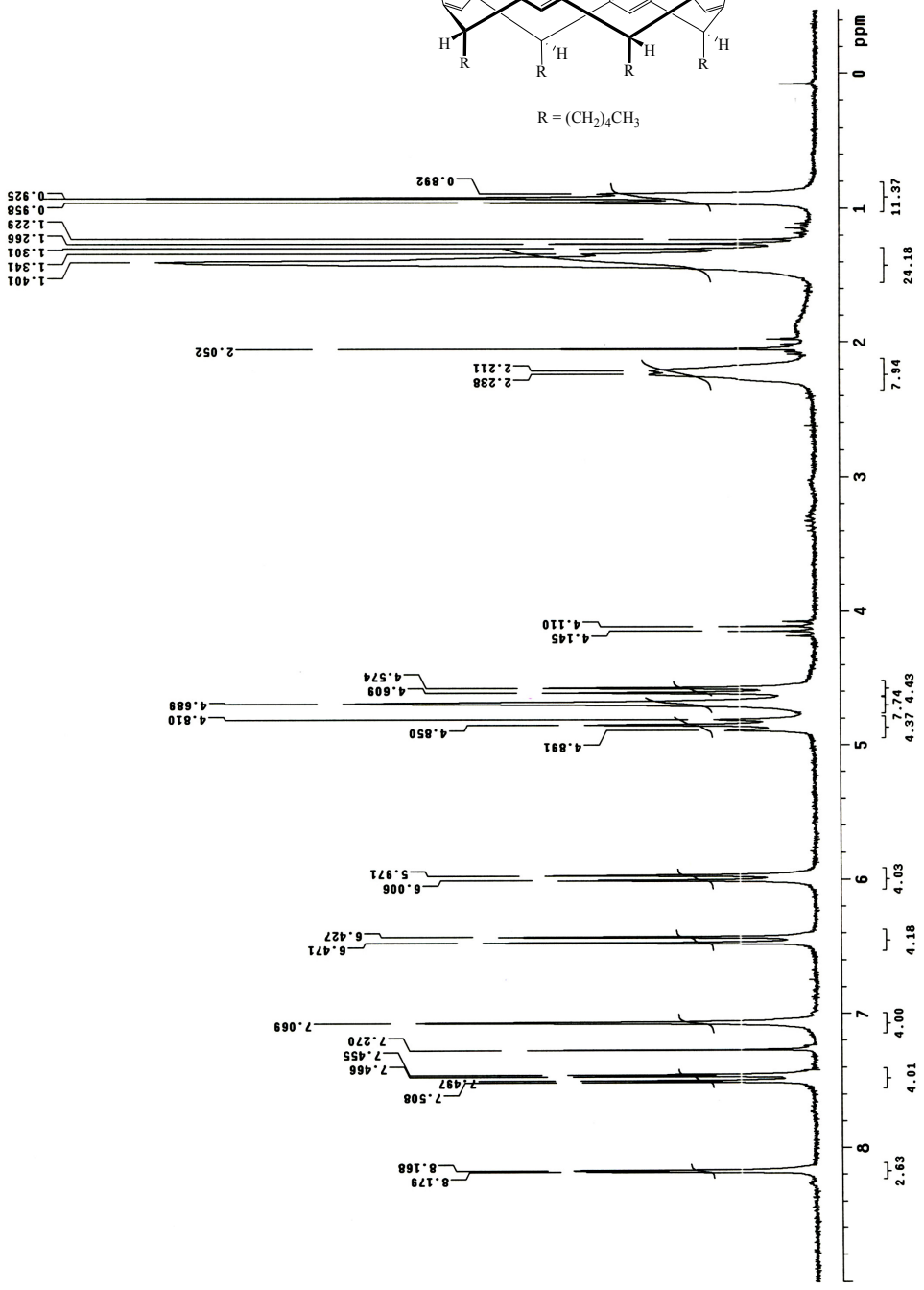

200 MHZ

$CDCl_3$

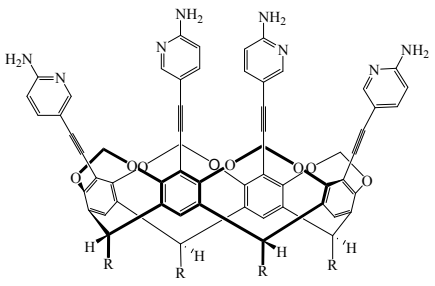

R = $(CH_2)_4CH_3$

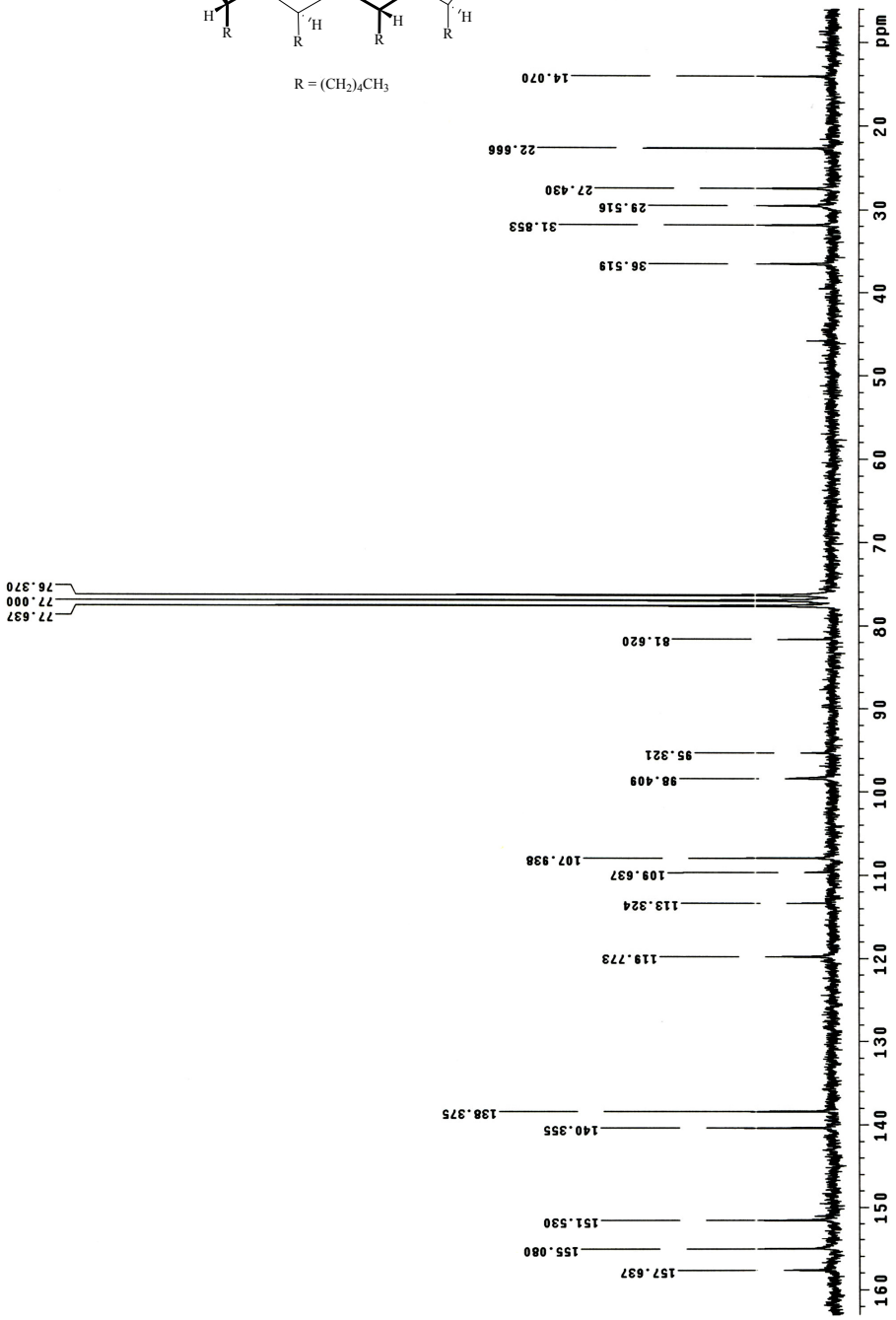

200 MHZ

$CDCl_3$

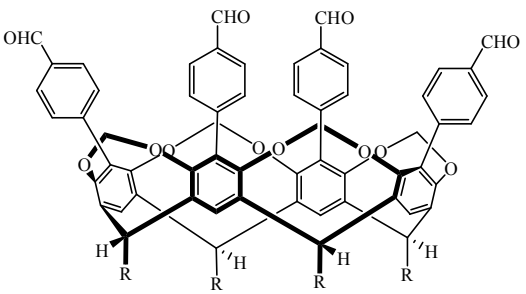


$R = (CH_2)_4CH_3$

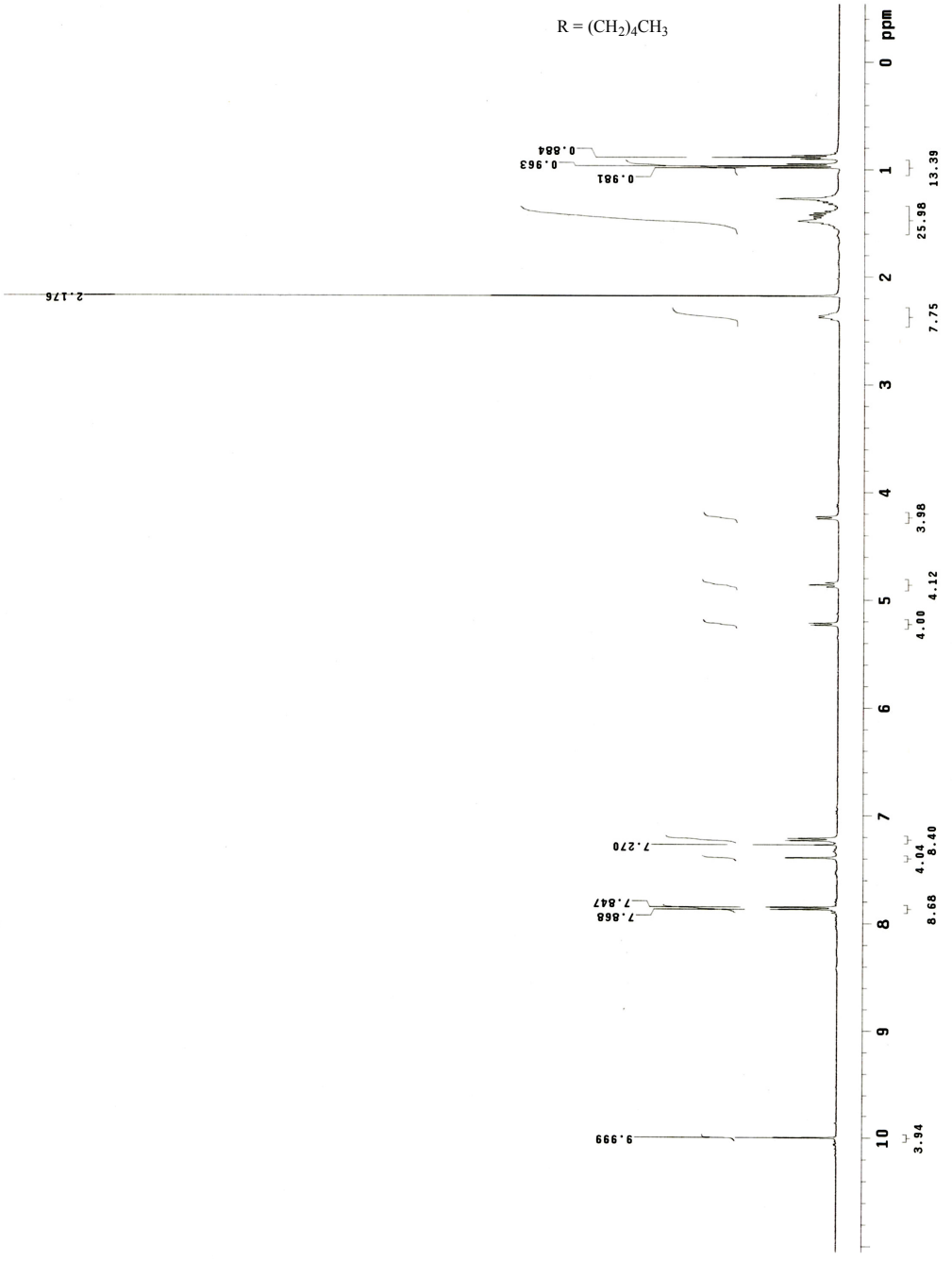

200 MHZ

$CDCl_3$

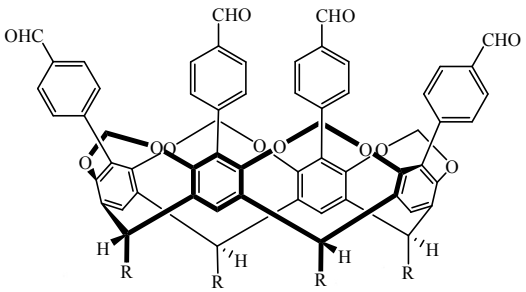


R = $(CH_2)_4CH_3$

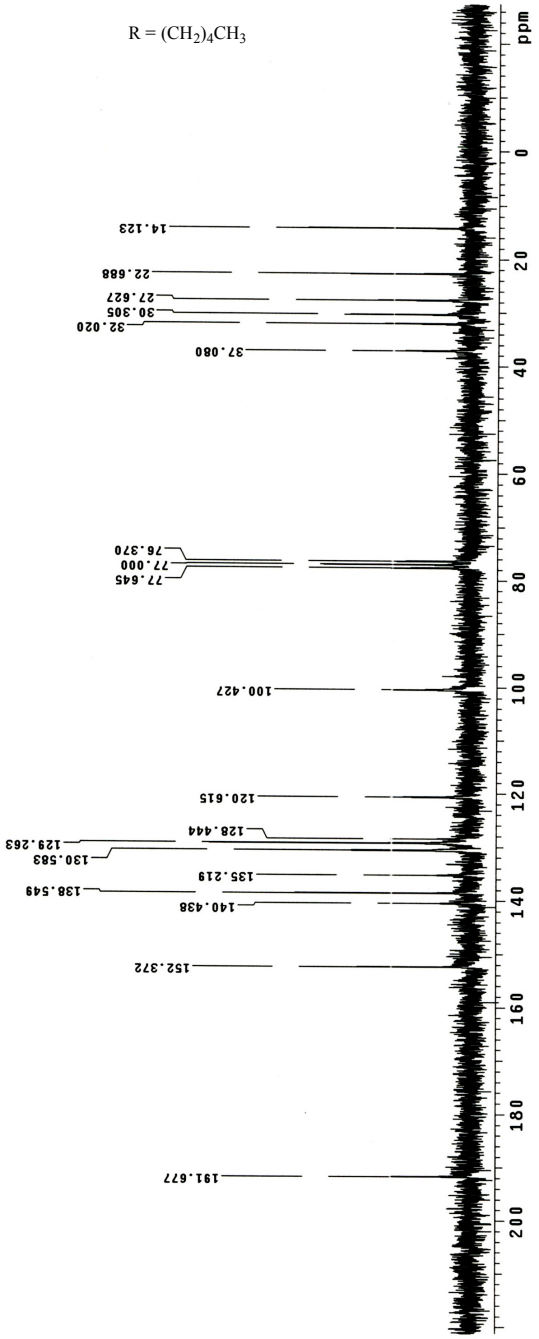

200 MHZ

$CDCl_3$

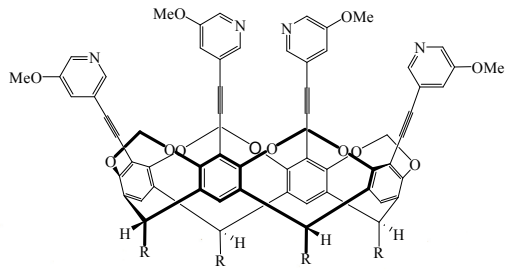


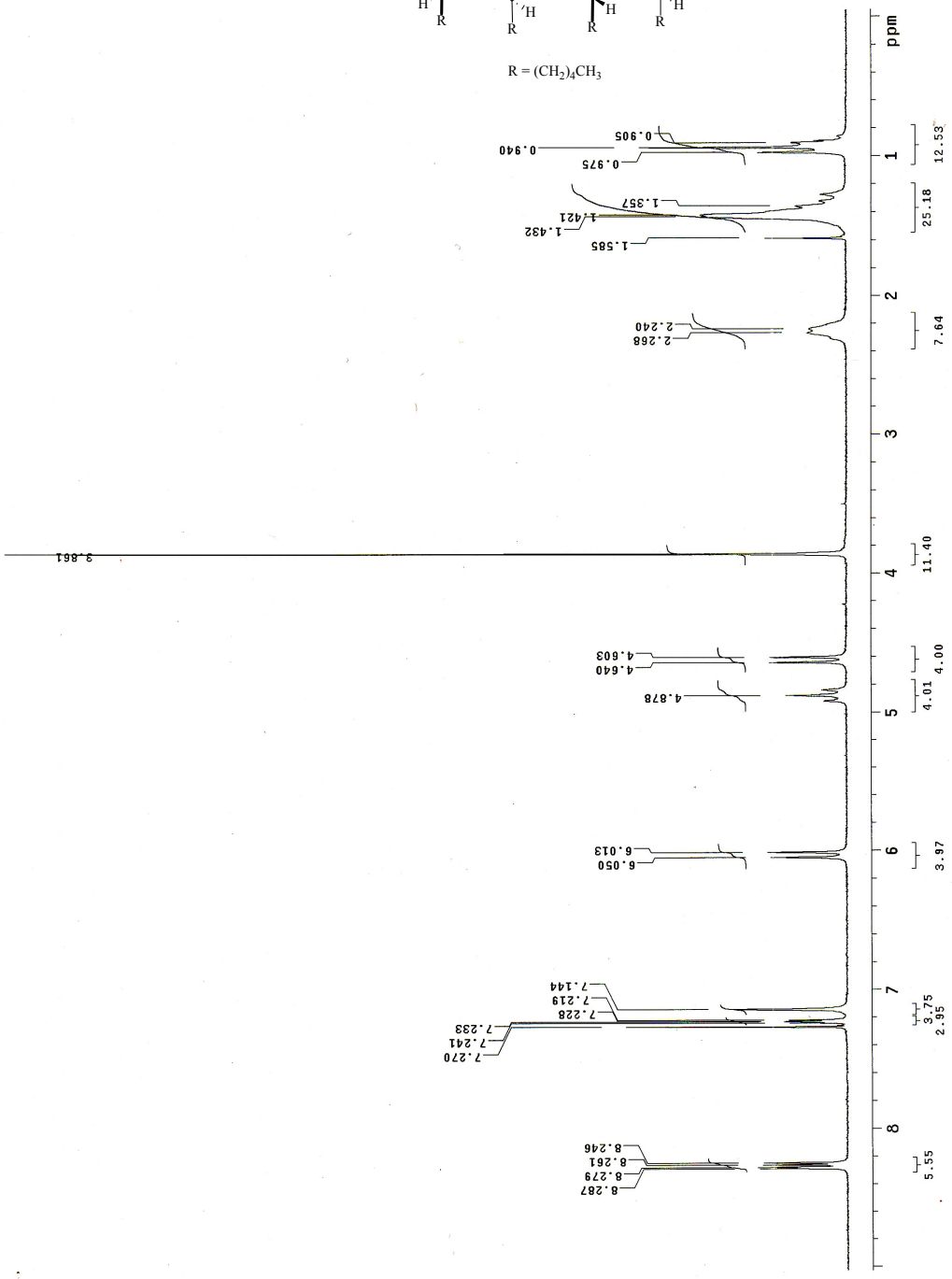

200 MHZ

$CDCl_3$

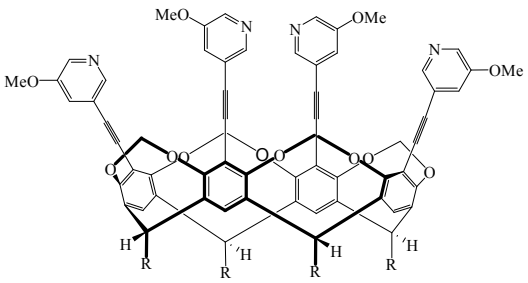


$R = (CH_2)_4CH_3$

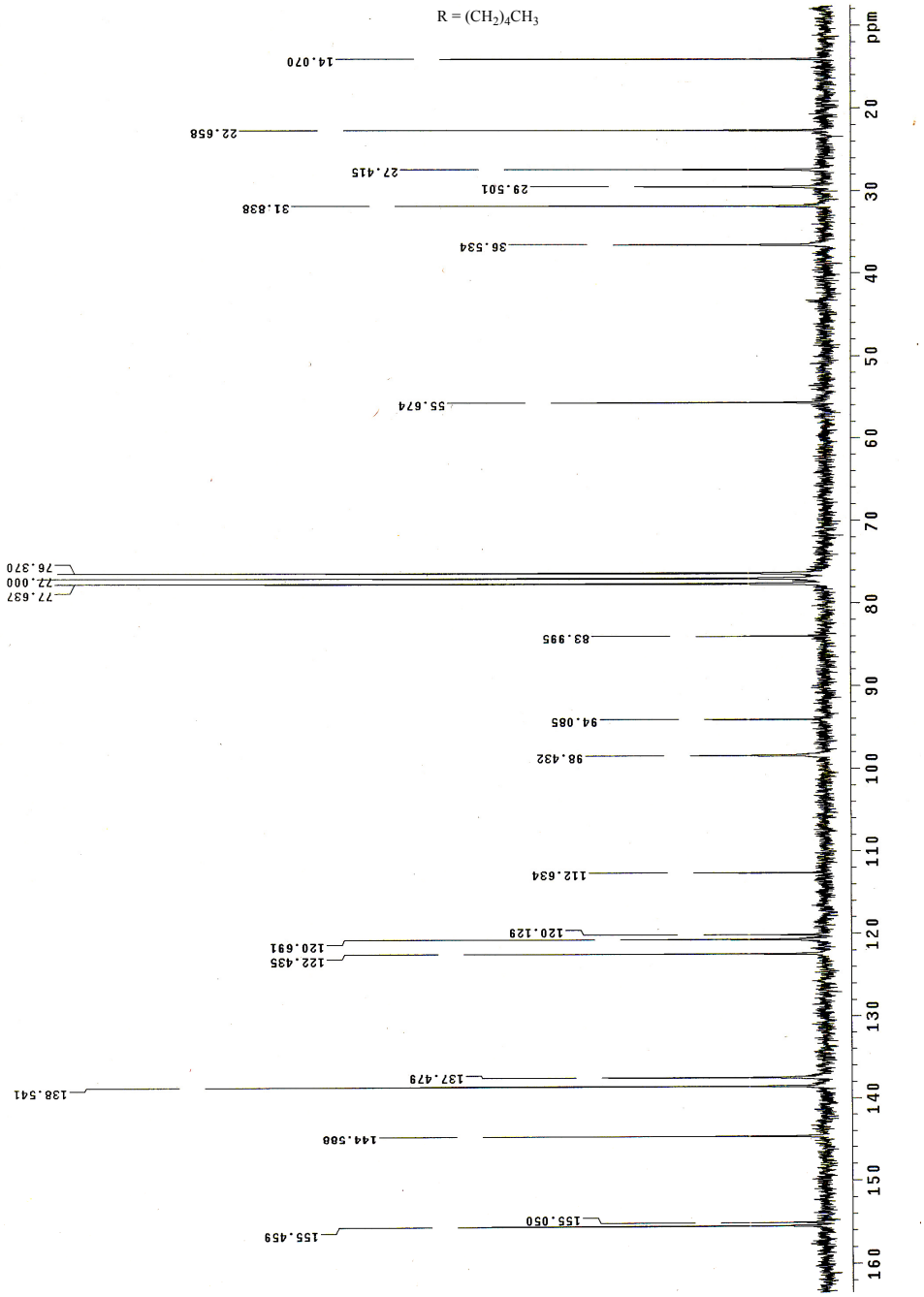

400 MHz

$CDCl_3$

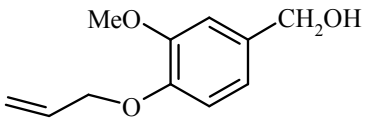


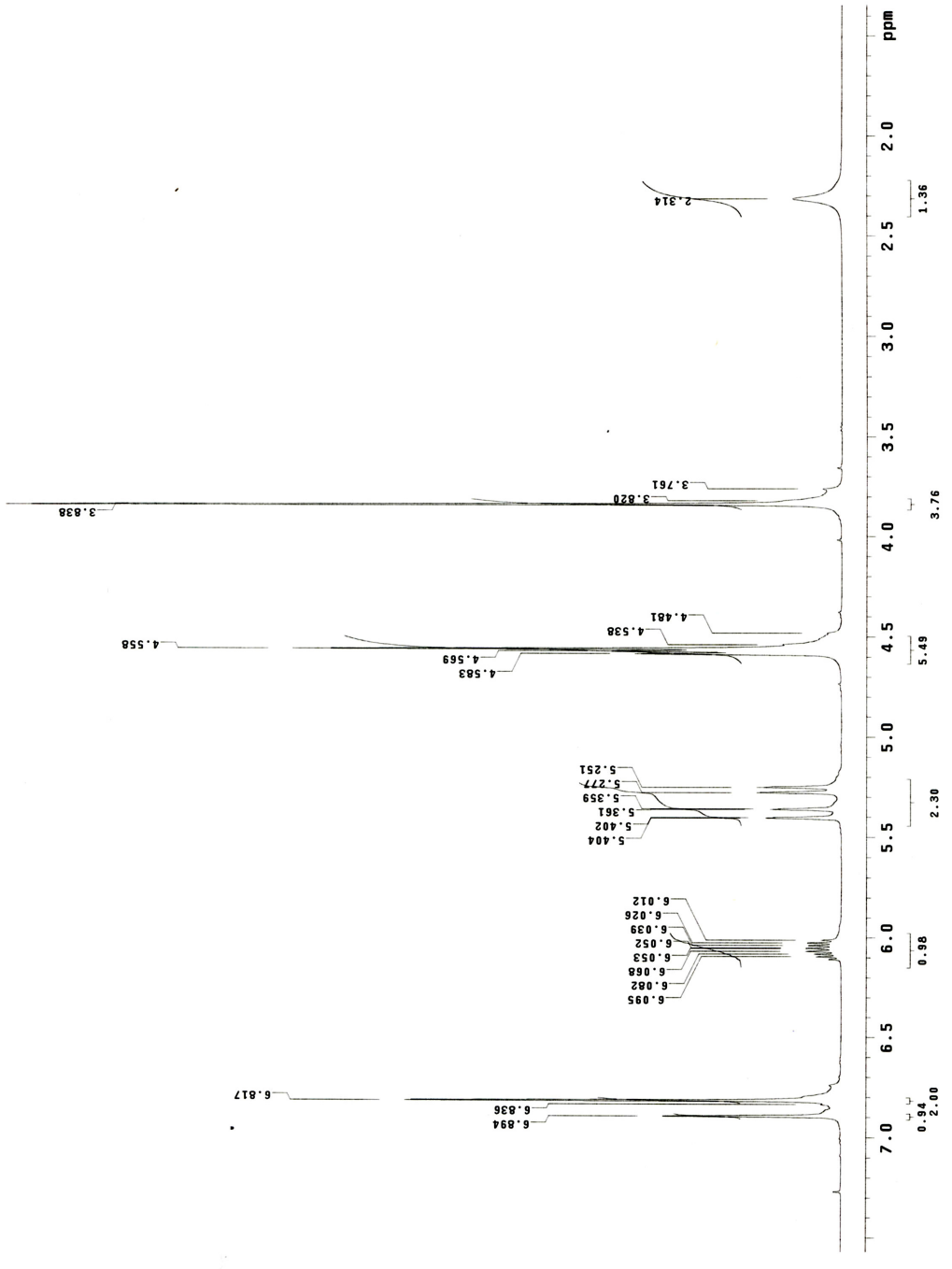

200 MHz

$CDCl_3$

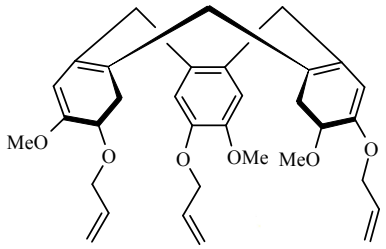


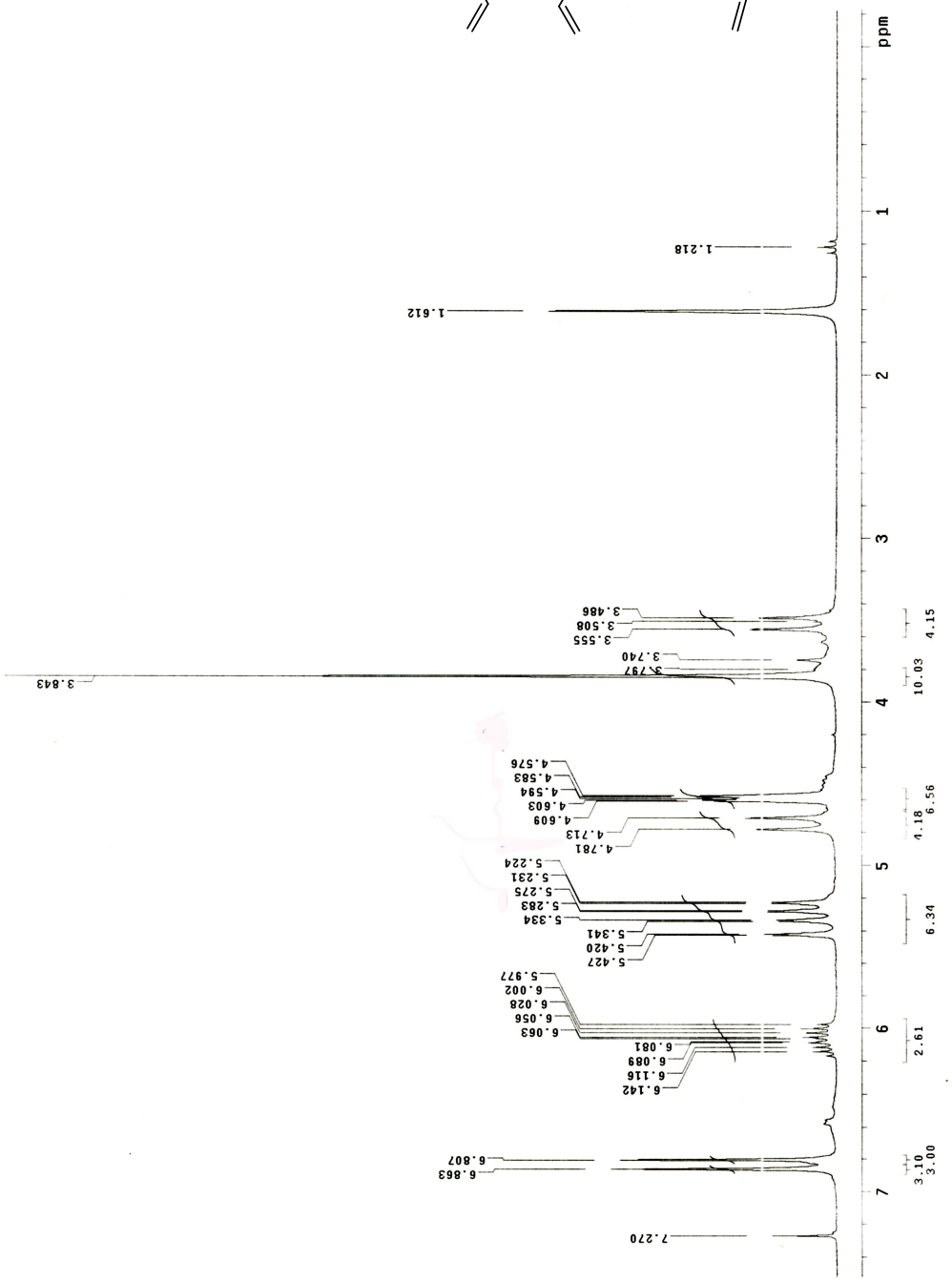

200 MHz

$CDCl_3$

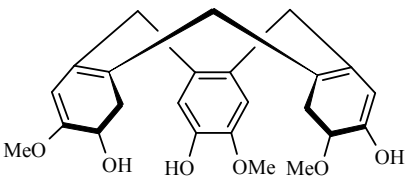


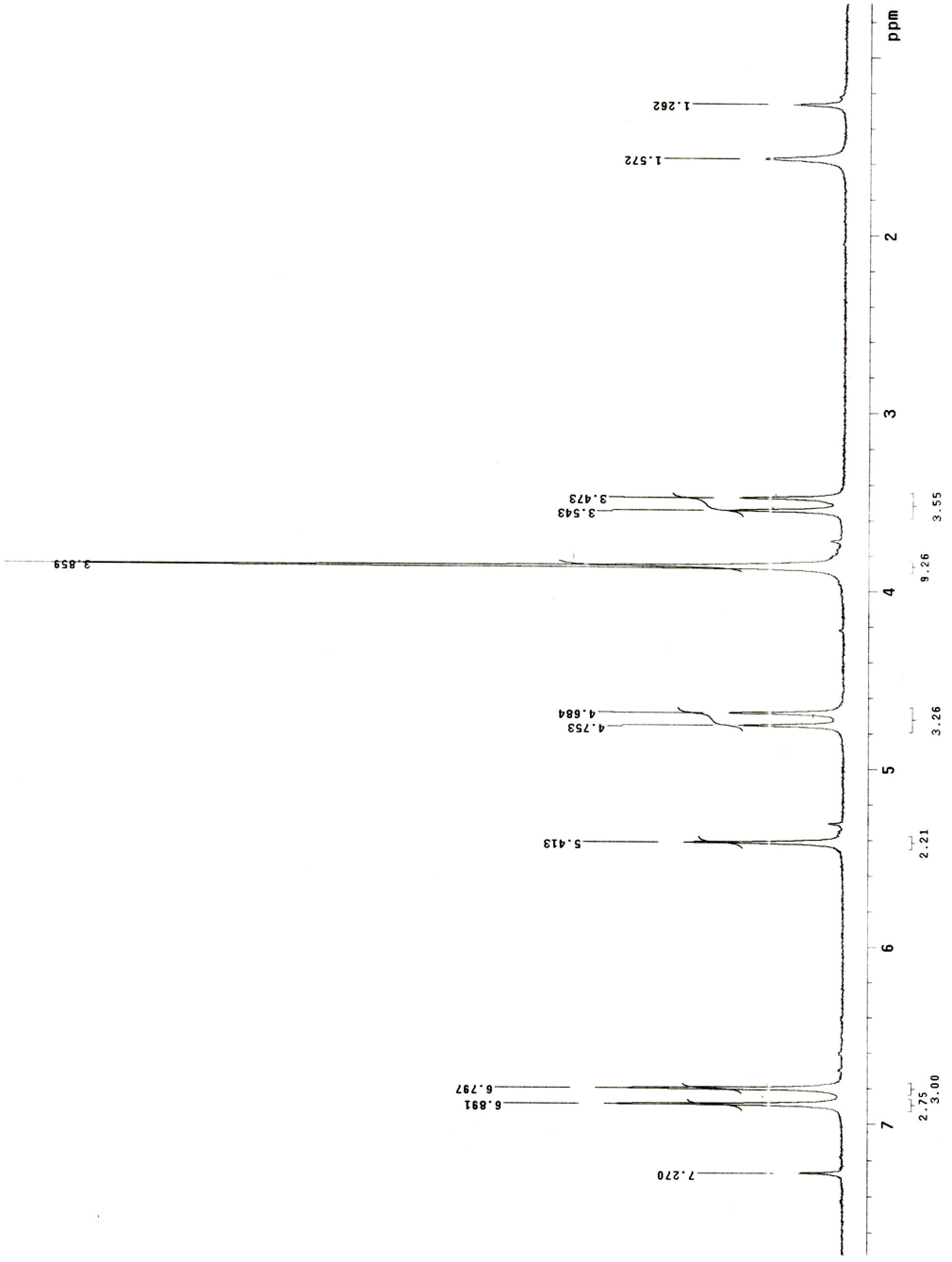

200 MHZ

$CDCl_3$

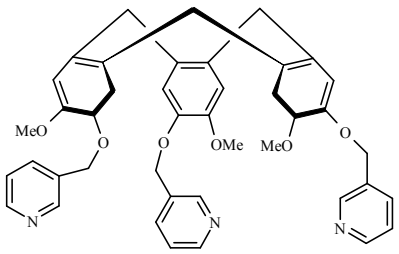


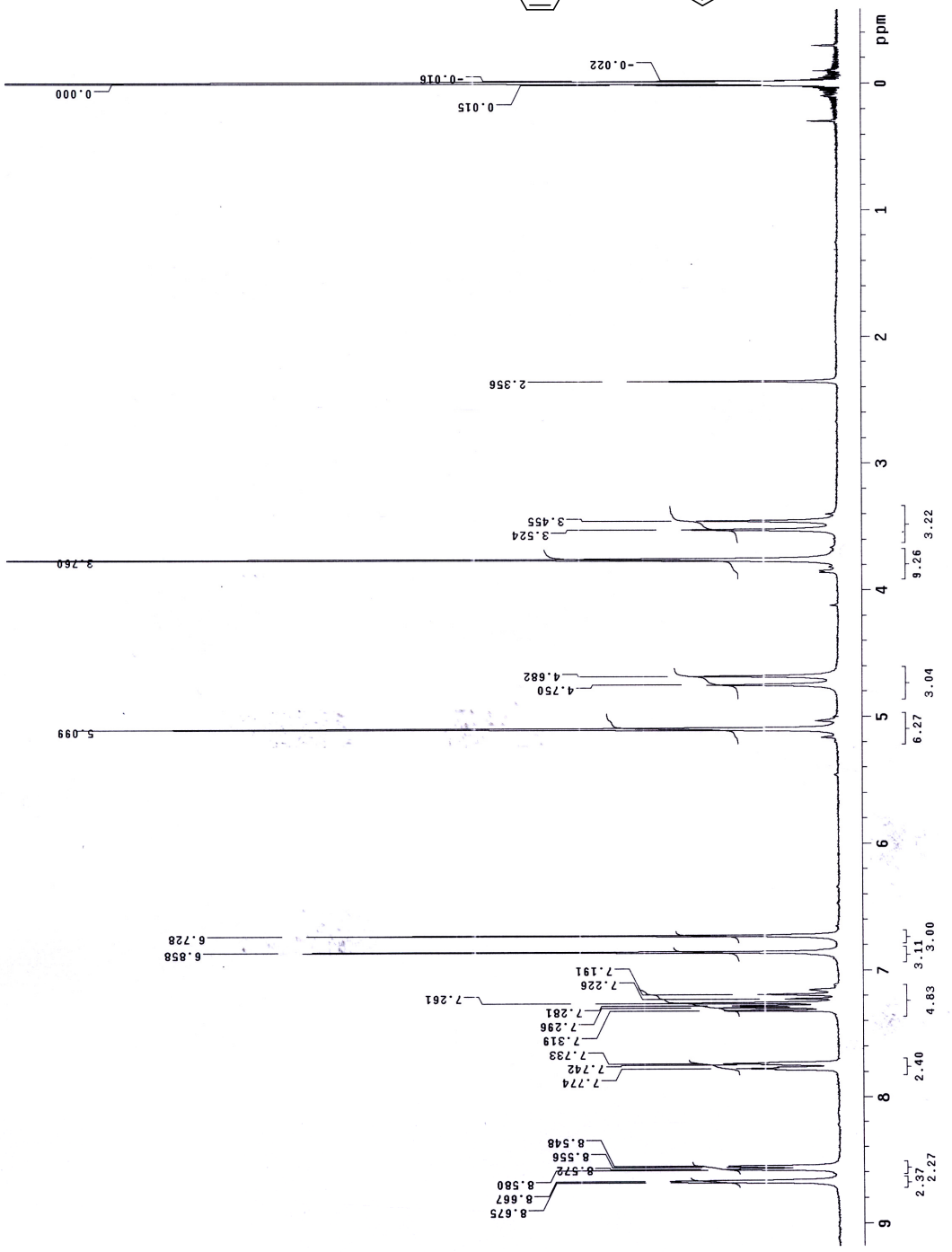

400 MHz

$CDCl_3$

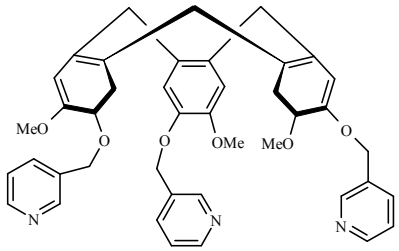


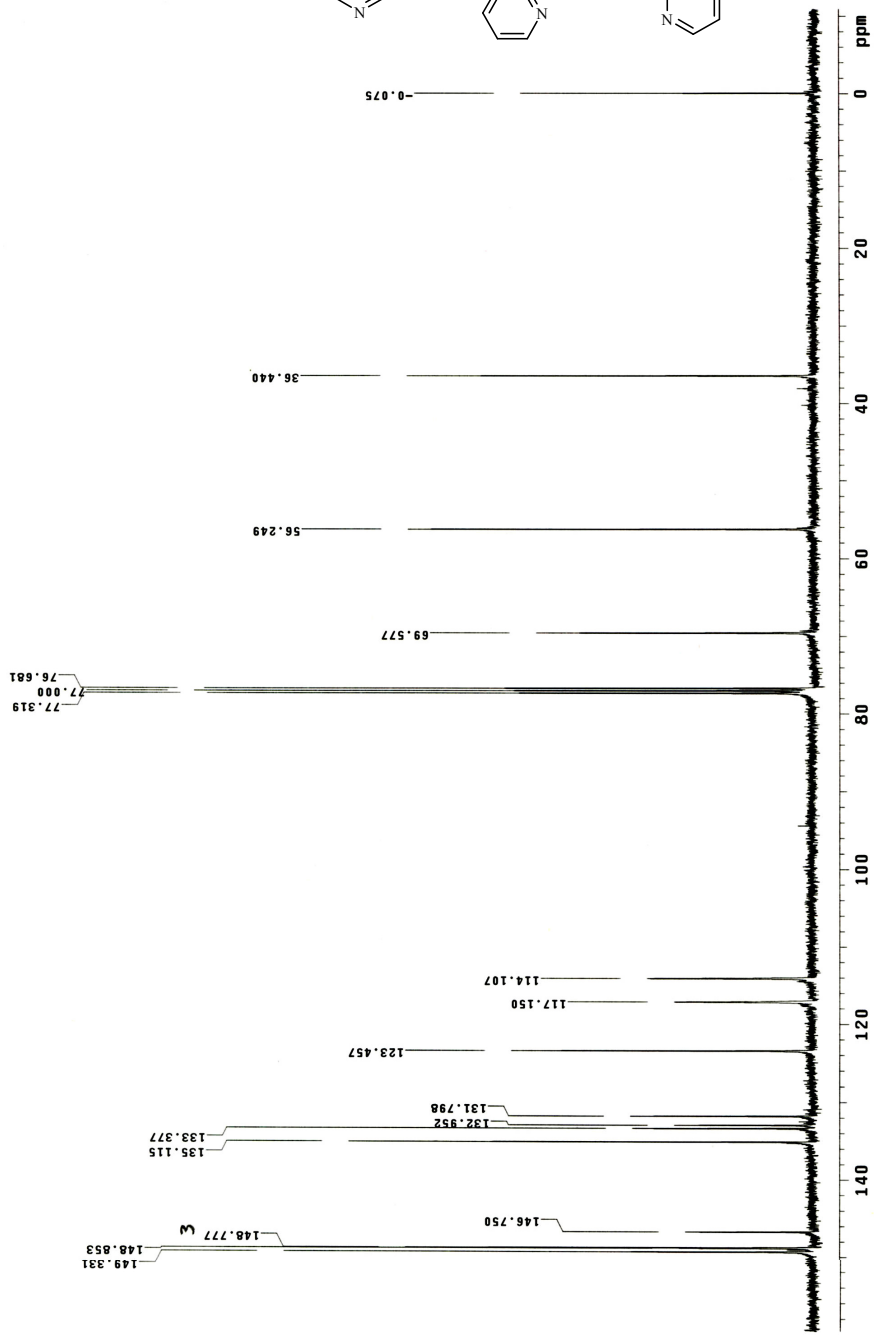

200 MHz

$CDCl_3$

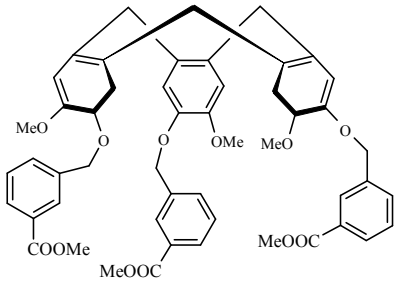


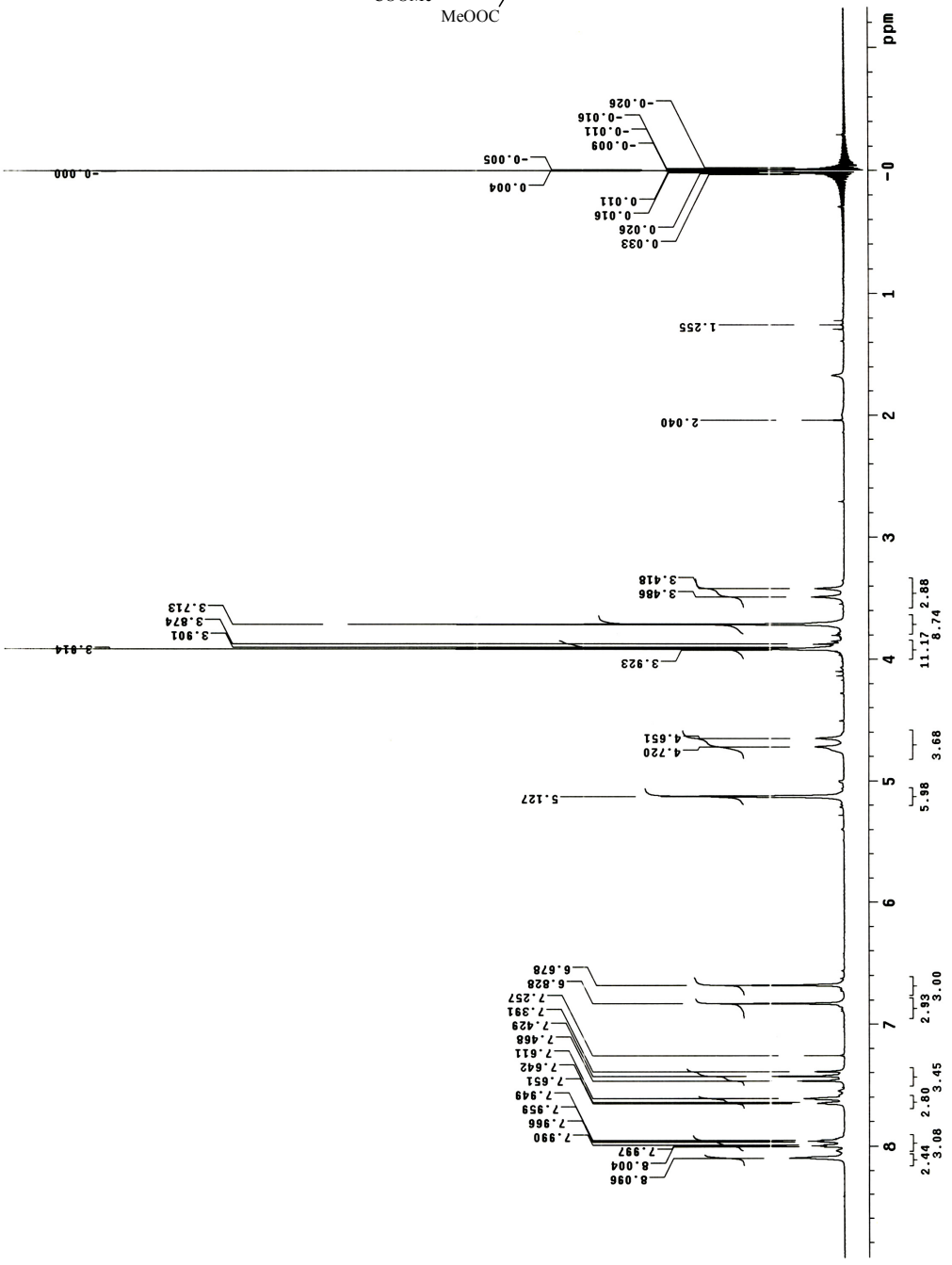

200 MHz

$CDCl_3$

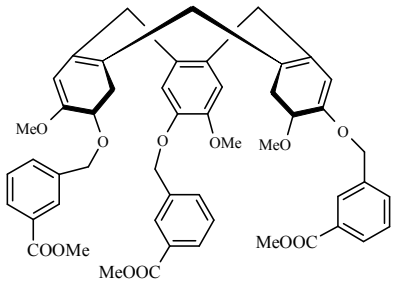


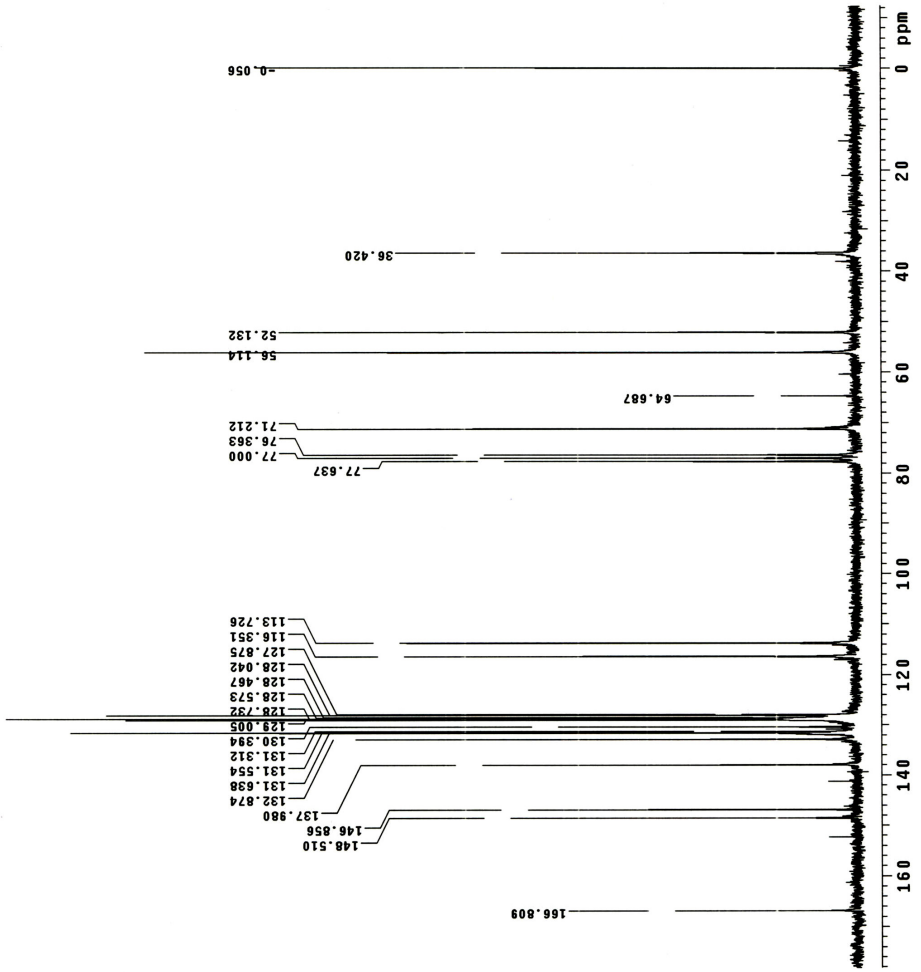

200 MHZ

$D_6$-DMSO